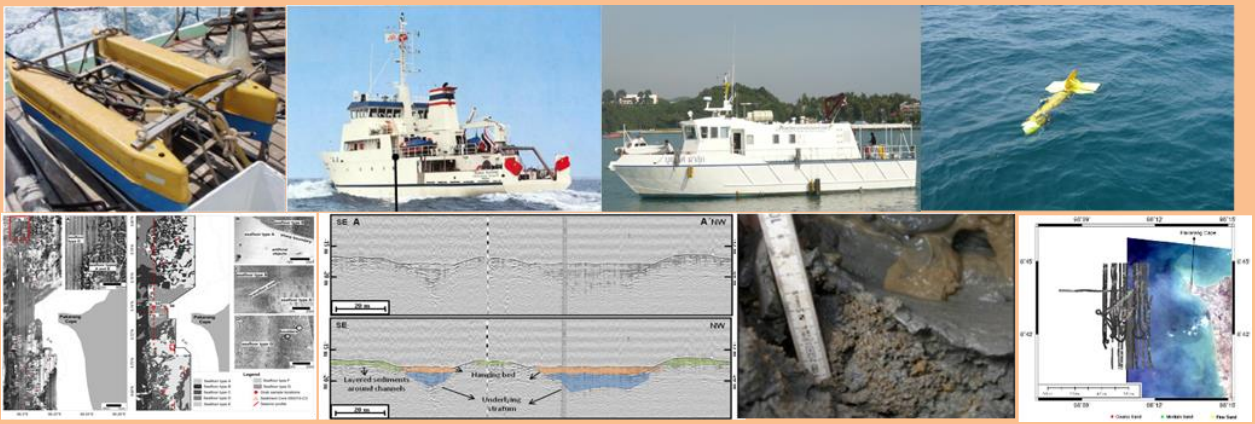
รายงานการวิจัยฉบับสมบูรณ์

การเปลี่ยนแปลงของชั้นตะกอนทะเลและร่องรอยการเกิดสึนามิในอดีต จากตะกอนชายฝั่งทะเลอันดามัน

Changing of Sediment Stratigraphy and Historical Tsunami Tracing by Nearshore Sediment of the Andaman Sea



ตามโครงการความร่วมมือไทย – เยอรมัน

โดย

1) ภาควิชาวิทยาศาสตร์ทางทะเล คณะวิทยาศาสตร์ จุฬาลงกรณ์มหาวิทยาลัย

2) ศูนย์เครือข่ายงานวิเคราะห์วิจัยและฝึกอบรมการเปลี่ยนแปลงของโลกฯ จุฬาลงกรณ์มหาวิทยาลัย

3) สถาบันวิจัยและพัฒนาทรัพยากรทางทะเล ชายฝั่งทะเล และป่าชายเลน กระทรวงทรัพยากรธรรมชาติและสิ่งแวดล้อม

4) Christian-Albrechts University of Kiel สหพันธรัฐเยอรมนี

ได้รับทุนอุดหนุนการวิจัยจากสำนักงานคณะกรรมการวิจัยแห่งชาติ

มิถุนายน พ.ศ. 2557

รายงานการวิจัยฉบับสมบูรณ์

การเปลี่ยนแปลงของชั้นตะกอนทะเลและร่องรอยการเกิดสึนามิในอดีต จากตะกอนชายฝั่งทะเลอันดามัน

Changing of Sediment Stratigraphy and Historical Tsunami Tracing by Nearshore Sediment of the Andaman Sea

ตามโครงการโครงการวิจัยภายใต้ความร่วมมือ ไทย-เยอรมัน
เพื่อการศึกษาวิจัยทะเลอันดามัน:ธรณีศาสตร์ นิเวศวิทยาและวิศวกรรมศาสตร์เพื่อการจัดการภัยพิบัติทางธรรมชาติและการใช้ทรัพยากรทางทะเลอย่างยั่งยืน
Thai-German Cooperative Research and Capacity Building: Ocean Geosciences, Marine Ecology and Natural Hazard Management

โดย

ภาควิชาวิทยาศาสตร์ทางทะเล คณะวิทยาศาสตร์ จุฬาลงกรณ์มหาวิทยาลัย
ศูนย์เครือข่ายงานวิเคราะห์วิจัยและฝึกอบรมการเปลี่ยนแปลงของโลกฯ จุฬาลงกรณ์มหาวิทยาลัย
คณะพัฒนาสังคมและสิ่งแวดล้อม สถาบันบัณฑิตพัฒนบริหารศาสตร์
สถาบันวิจัยและพัฒนาทรัพยากรทางทะเล ชายฝั่งทะเล และป่าชายเลน
Christian-Albrechts University of Kiel สหพันธรัฐเยอรมนี

ได้รับทุนอุดหนุนการวิจัยจากสำนักงานคณะกรรมการวิจัยแห่งชาติ
มิถุนายน พ.ศ. 2557

กิตติกรรมประกาศ

โครงการ “การเปลี่ยนแปลงของชั้นตะกอนทะเลและร่องรอยการเกิดสึนามิในอดีตจากตะกอนชายฝั่งทะเลอันดามัน” ได้รับทุนอุดหนุนการวิจัยจากสำนักงานคณะกรรมการวิจัยแห่งชาติ ประจำปีงบประมาณพ.ศ. 2553 2554 และ 2557 จึงใคร่ขอขอบคุณสำนักงานคณะกรรมการวิจัยแห่งชาติ ที่สนับสนุนเงินงบประมาณเพื่อการวิจัยในครั้งนี้อย่างต่อเนื่องเป็นเวลา 3 ปี และขอขอบคุณผู้วิจัยร่วมทุกท่าน ตลอดจน DFG ที่ให้การสนับสนุนและทุ่มเทกำลังในการทำงานจนสามารถทำให้งานวิจัยฯ นี้สำเร็จลุล่วงอย่างดียิ่ง

โครงการฯ หวังเป็นอย่างยิ่งว่าผลงานวิจัยเล่มนี้จะเป็นประโยชน์ต่อการศึกษาวิจัยและการพัฒนาทะเลอันดามันเพื่อนำไปสู่การจัดการภัยพิบัติทางธรรมชาติและการใช้ทรัพยากรทางทะเลอย่างยั่งยืน หากผลงานชิ้นนี้มีข้อบกพร่องหรือข้อผิดพลาด คณะนักวิจัยฯ ขอน้อมรับไว้และจะนำไปพิจารณาปรับปรุงในการวิจัยต่อไป

คณะนักวิจัยฯ

สิงหาคม 2558

บทสรุปผู้บริหาร
[Executive Summary]

1. รายละเอียดเกี่ยวกับโครงการวิจัย

1.1 ชื่อเรื่อง

(ภาษาไทย) การเปลี่ยนแปลงของชั้นตะกอนทะเลและร่องรอยการเกิดสึนามิในอดีตจากตะกอนชายฝั่งทะเลอันดามัน

(ภาษาอังกฤษ) Changing of sediment stratigraphy and historical tsunami tracing by nearshore sediment of the Andaman Sea

1.2 ชื่อคณะผู้วิจัย

1) ผศ. ดร.เพ็ญใจ สมพงษ์ชัยกุล
   - ภาควิชาวิทยาศาสตร์ทางทะเล คณะวิทยาศาสตร์ จุฬาลงกรณ์มหาวิทยาลัย
   - ศูนย์เครือข่ายงานวิเคราะห์วิจัยและฝึกอบรมการเปลี่ยนแปลงของโลก จุฬาลงกรณ์มหาวิทยาลัย
2) ผศ. ดร.อานนท์ สนิทวงศ์ ณ อยุธยา
   - สำนักงานพัฒนาเทคโนโลยีอวกาศและภูมิสารสนเทศ (องค์การมหาชน)
   - ศูนย์เครือข่ายงานวิเคราะห์วิจัยและฝึกอบรมการเปลี่ยนแปลงของโลก จุฬาลงกรณ์มหาวิทยาลัย
3) รศ. ดร.ศิวัช พงษ์เพียจันทร์
   คณะพัฒนาสังคมและสิ่งแวดล้อม สถาบันบัณฑิตพัฒนบริหารศาสตร์
4) ดร.สมเกียรติ ขอเกียรติวงศ์
   สถาบันวิจัยและพัฒนาทรัพยากรทางทะเล ชายฝั่งทะเล และป่าชายเลน
5) นางสาวสุรัตตา บุญสมบูรณ์สกุล
   - นิสิตดุษฎีบัณฑิต ภาควิชาวิทยาศาสตร์ทางทะเล คณะวิทยาศาสตร์ จุฬาลงกรณ์มหาวิทยาลัย
   - ศูนย์เครือข่ายงานวิเคราะห์วิจัยและฝึกอบรมการเปลี่ยนแปลงของโลก จุฬาลงกรณ์มหาวิทยาลัย

6) Dr. Klaus Schwarzer
Institute of Geosciences, Sedimentology, Coastal and Shelf Geology,
Christian-Albrechts-Universität zu Kiel, Germany

7) รศ. ดร.ชัยยุทธ ขันธปราบ (ที่ปรึกษา)
ผู้อำนวยการโครงการพัฒนาบัณฑิตศึกษาและวิจัยด้านวิทยาศาสตร์และเทคโนโลยี
สำนักงานคณะกรรมการการอุดมศึกษา

1.3 งบประมาณและระยะเวลาทำวิจัย

ได้รับงบประมาณ ประจำปีงบประมาณ พ.ศ. 2552, 2554 และ 2557 งบประมาณที่ได้รับรวม 3,283,000 บาท ระยะเวลาทำวิจัย ตั้งแต่

ปีที่ 1 ได้รับทุนอุดหนุนการวิจัยประเภท ทุนอุดหนุนการวิจัย ประจำปี 2552
จำนวนเงิน 1,100,000 บาท
ระยะเวลาทำการวิจัย 1 ปี ตั้งแต่ พ.ศ. 2552 ถึง พ.ศ. 2553

ปีที่ 2 ได้รับทุนอุดหนุนการวิจัยประเภท แบบสัญญาจ้างที่ปรึกษา ประจำปี 2554
จำนวนเงิน 1,000,000 บาท
ระยะเวลาทำการวิจัย 1 ปี ตั้งแต่ พ.ศ. 2554 ถึง พ.ศ. 2555

ปีที่ 3 ได้รับทุนอุดหนุนการวิจัยประเภท ทุนอุดหนุนการวิจัย ประจำปี 2557
จำนวนเงิน 1,183,000 บาท
ระยะเวลาทำการวิจัย 1 ปี ตั้งแต่ พ.ศ. 2557 ถึง พ.ศ. 2558

2. สรุปโครงการวิจัย

คลื่นสึนามิ นอกจากจะมีศักยภาพสูงในการเปลี่ยนแปลงชายฝั่ง ยังมีอิทธิพลต่อการสะสมตัวของตะกอนทั้งบนชายฝั่ง (onshore) และนอกชายฝั่ง (offshore) หนึ่งในปรากฏการณ์ที่เป็นผลกระทบจากการเกิดสึนามิที่มีนัยสำคัญมากที่สุด ได้แก่ การเคลื่อนย้ายของตะกอนในปริมาณมากออกจากชายฝั่ง ตามด้วยการทับถมของทรายจากทะเลในพื้นที่ราบต่ำชายฝั่ง (coastal lowland) นอกจากนี้คลื่นสึนามิที่ไหลเข้าฝั่ง (incoming flow) และไหลย้อนกลับออกสู่ทะเล (returning flow หรือ backwash) ยังทำให้เกิดการกวน (resuspend) และเคลื่อนย้าย (transport) ตะกอน นำพาไปตกตะกอนใหม่ (redeposit) ไปสะสมบนพื้นท้องทะเลที่อื่น

งานวิจัยนี้มีวัตถุประสงค์เพื่อศึกษาหลักฐานทางธรณีสัณฐาน ตะกอนวิทยา ธรณีเคมี และธรณีวิทยา นอกชายฝั่งอันดามันบริเวณหน้าฝั่งด้านบน (upper shoreface) ที่ได้รับผลกระทบโดยตรงกระแสไหลย้อนของสึนามิ เพื่อประเมินผลกระทบจากคลื่นสึนามิที่มีต่อการเปลี่ยนแปลง และ/หรือ รูปแบบการแพร่กระจายของตะกอนบริเวณใกล้และนอกฝั่ง โดยเฉพาะอย่างยิ่งผลที่เกิดจากกระแสไหลย้อนของสึนามิที่ไปสะสมนอกฝั่งและการพัฒนาบุคลากรไทยให้มีความรู้เพียงพอที่จะทำการศึกษาวิจัย

ผลของการศึกษาในพื้นที่นอกชายฝั่งแหลมปะการัง จังหวัดพังงา ระหว่างอ่าวทับละมุและเกาะพระทอง โดยสรุปพบว่า

1) ธรณีสัณฐานทั่วไปของพื้นที่ศึกษา มีความลาดเอียงจากฝั่งออกไปและความชันของพื้นทะเลจะเพิ่มขึ้นอย่างรวดเร็วตั้งแต่ความลึกน้ำ 25 เมตรขึ้นไป ที่ระดับความลึก 10-20 เมตร นอกชายฝั่งแหลมปะการัง มีแนวร่องธรรมชาติ 3 แนว วางตัวตามแนวตะวันตกเฉียงเหนือ-ตะวันออกเฉียงใต้ (NW-SE) ลักษณะร่องไม่สมมาตร แต่ละร่องความกว้างประมาณ 150-300 เมตร แต่มีความยาวหลายกิโลเมตร เมื่อเกิดสึนามิจึงเป็นร่องที่มีดินตะกอนมาสะสมตัวมากกว่าบริเวณอื่น การศึกษาชั้นตะกอนในบริเวณนี้ จึงเป็นตัวแทนที่ดีในการศึกษาตะกอนสึนามิ

2) การกระจายตัวและรูปแบบการสะสมตัวของดินตะกอนจากใกล้ฝั่งไปถึงนอกฝั่ง มีลักษณะดังนี้ คือ พื้นท้องทะเลที่ความลึก 7-15 เมตร ปกคลุมด้วยดินตะกอนละเอียดและมีหย่อมโคลนบริเวณใกล้ฝั่ง ที่ระดับความลึก 10-16 เมตร พบแนวร่องที่มีการสะสมตัวของเศษซากพืช เศษเปลือกหอย เป็นชั้นสลับกับชั้นโคลน และมีลักษณะที่ถูกเติมตะกอนใหม่ลงไปในร่อง ระดับความลึกตั้งแต่ 15 เมตรไปถึงนอกชายฝั่ง มีลักษณะเป็นสันเขาสูงประมาณ 2 เมตร จากพื้นทะเลที่มีผลต่อการสะสมตัวของตะกอนสึนามิ นอกจากนี้ ยังพบร่องรอยจากการทำเหมืองแร่ดีบุกในพื้นที่หน้าเขาหลัก ที่ความลึกน้ำ 20-25 เมตร และที่ความลึกน้ำ 30-35 เมตร มีลานหินเล็ก ๆ ซึ่งจะมีการทับถมของตะกอนที่ถูกพามากับกระแสไหลย้อนลงทะเล

3) จากสัดส่วน Ti/Ca ในแต่ละชั้นของแท่งตะกอน ซึ่งแตกต่างกันตามความลึก แสดงถึงความแตกต่างของแหล่งที่มาของตะกอนที่มาสะสมและจำแนกชนิดของชั้นตะกอนได้ ดินตะกอนในแนวร่องมีสัดส่วน Ti/Ca แตกต่างกับดินตะกอนนอกแนวร่อง แสดงว่าถึงความแตกต่างของโครงสร้างชั้นตะกอนอย่างชัดเจน

4) ตัวอย่างแท่งดินตะกอน 2 แท่ง ที่เก็บตัวอย่างจากแนวร่องที่ระดับความลึกน้ำเดียวกัน คือ ประมาณ 9 เมตร มีร่องรอยการสะสมของตะกอนสึนามิหนา 18 เซนติเมตรเท่ากัน ซึ่งเป็นหลักฐานที่ดีในการศึกษาชั้นตะกอนสึนามิและอัตราการสะสมตัวของตะกอนไหลย้อน

5) จากการหาอายุของดินตะกอนด้วยไอโซโทป Pb-210 พบว่าอัตราการสะสมตัวของดินตะกอนบริเวณนี้อยู่ระหว่าง 1.3 ถึง 5.7 เซนติเมตรต่อปี และสามารถระบุชี้ชนิดของชั้นตะกอนได้

6) จากรูปแบบการกระจายตัวของ PAHs ในดินตะกอน และการใช้สถิติขั้นสูงวิเคราะห์ค่า PAH isomer ratios บ่งชี้ว่าแหล่งกำเนิดของ PAHs ที่มาสะสมในดินตะกอนในพื้นที่ศึกษามีแหล่งที่มาอยู่ 2 กลุ่มหลัก คือ กลุ่มแรกมีค่า PAHs สูง ซึ่งเป็นกลุ่มที่ถูกพามากับกระแสไหลย้อนของคลื่นสึนามิ จากแหลมปะการังออกไปสะสมนอกชายฝั่ง ไกลถึง 25 กิโลเมตร กับกลุ่มที่เป็นการสะสมตัวแบบปกติ

โครงการนี้ยังได้พัฒนาบุคลากรเพื่อต่อยอดการทำงานวิจัยร่วมกับทางนักวิจัยเยอรมนี โดยมีนักวิจัยและนักศึกษา เข้ารับการฝึกอบรม ร่วมวิจัย และศึกษาระดับปริญญาโทและเอก ทั้งทางฝ่ายไทยและฝ่ายเยอรมนี ซึ่งประสบผลสำเร็จอย่างดียิ่ง

งานวิจัยครั้งนี้ เป็นการวิเคราะห์ข้อมูลหลายด้านประกอบกันแบบ multi-method และ multi-proxy เพื่อการแปลผลให้แม่นยำ แม้ว่าจะมีปัญหาอุปสรรคในการวิจัย มีข้อจำกัดในเรื่องอุปกรณ์ งบประมาณ และบุคลากร อีกทั้งการวิเคราะห์ข้อมูลยังต้องอาศัยโปรแกรมและเครื่องมือที่เฉพาะ และขาดข้อมูลก่อนเกิดเหตุการณ์สึนามิที่จะนำมาเปรียบเทียบ แต่การวิจัยครั้งนี้ก็ยังสามารถตอบวัตถุประสงค์ที่ตั้งไว้ ซึ่งนักวิจัยคาดหวังว่าบุคลากรที่ได้พัฒนาขึ้นภายใต้โครงการนี้ทั้งทางตรงและทางอ้อม จะเป็นกำลังสำคัญในการศึกษาขยายองค์ความรู้ในด้านนี้ต่อไปในอนาคต

3. บทคัดย่อภาษาไทยและบทคัดย่อภาษาอังกฤษ (Abstract)

บทคัดย่อ

สึนามิเป็นหนึ่งในพิบัติภัยทางธรรมชาติที่มีความรุนแรงมากที่สุดในเขตพื้นที่ราบต่ำชายฝั่งและชุมชนในพื้นที่นั้น เนื่องจากอานุภาพของมันและการที่ไม่สามารถทำนายได้ว่าจะเกิดเมื่อใด สึนามิที่เกิดขึ้นเมื่อปี พ.ศ. 2547 นอกจากจะสร้างความเสียหายแล้ว ยังก่อให้เกิดการเปลี่ยนแปลงที่ภูมิสัณฐานที่เห็นได้ชัดทั้งบนบกและนอกชายฝั่ง แต่เหตุการณ์ซึ่งบันทึกอยู่ที่พื้นท้องทะเล ยังขาดองค์ความรู้ทางวิทยาศาสตร์ที่จะอธิบาย จากการสร้างแผนที่พื้นท้องทะเลความละเอียดสูง ในพื้นที่นอกชายฝั่งแหลมปะการัง จังหวัดพังงา ระหว่างอ่าวทับละมุและเกาะพระทอง โดยการสำรวจทางธรณีฟิสิกส์ด้วยคลื่นเสียงหลายวิธี และเก็บตัวอย่างดินตะกอนผิวหน้าและแท่งตะกอนตามความลึก ตามตำแหน่งที่บ่งชี้ในแผนที่ว่าน่าจะมีตะกอนที่ถูกพามาสะสมโดยสึนามิ วิเคราะห์ตัวอย่างดินตะกอนโดยใช้วิธีการทางตะกอนวิทยา ธรณีเคมี จุลบรรพชีวิน เคมี และฟิสิกส์ ผลการศึกษาพบว่าพื้นทะเลมีความลาดเอียงจากฝั่งออกไปและความชันเพิ่มขึ้นอย่างรวดเร็วตั้งแต่ความลึกน้ำ

25 เมตรขึ้นไป พื้นท้องทะเลบริเวณใกล้ฝั่ง ที่ความลึก 7-15 เมตร เป็นดินตะกอนละเอียดและมีหย่อมโคลน ที่ระดับความลึก 10-16 เมตร พบแนวร่องธรรมชาติ 3 แนว กว้าง 150-300 เมตร ยาวหลายกิโลเมตร วางตัวในแนวตะวันตกเฉียงเหนือ-ตะวันออกเฉียงใต้ (NW-SE) ร่องดังกล่าวมีลักษณะไม่สมมาตร ผลการศึกษาแท่งตะกอนพบว่ามีเศษซากพืช เศษเปลือกหอย เป็นชั้นสลับกับชั้นโคลน และมีลักษณะของตะกอนใหม่ที่ถูกเติมลงไปในร่อง ที่ระดับความลึกตั้งแต่ 15 เมตรไปถึงนอกชายฝั่ง มีลักษณะเป็นสันเขาสูงจากพื้นทะเลประมาณ 2 เมตร โดยด้านตะวันตกเฉียงใต้จะชันกว่าด้านตะวันออกเฉียงเหนือ ที่ความลึกน้ำ 20-25 เมตร ทางตะวันตกเฉียงเหนือของแหลมปะการัง พบร่องหลุมบนพื้นทะเล ซึ่งบางหลุมลึกถึง 7 เมตร คาดว่าน่าจะเป็นร่องรอยจากการทำเหมืองแร่ดีบุกในอดีต และที่ความลึกน้ำ 30-35 เมตร มีลานหินเล็ก ๆ ที่ถูกพามาทับถม จากการวิเคราะห์ตัวอย่างดินตะกอนทางตะกอนวิทยา หาสัดส่วน Ti/Ca และหาอายุด้วยไอโซโทป Pb-210 สามารถบ่งชี้ชั้นตะกอนที่เกิดจากการทับถมจากพายุและสึนามิในอดีต โดยอัตราการสะสมตัวของดินตะกอนบริเวณนี้อยู่ระหว่าง 1.3 ถึง 5.7 เซนติเมตรต่อปี ขณะที่คลื่นไหลย้อนของสึนามิก่อให้เกิดการสะสมตะกอนที่ผิดปกติในบางพื้นที่ได้หนาถึง 12-39 เซนติเมตร จากการใช้เฟอรามินิเฟอราในการแยกตะกอนที่เกิดจากการไหลเข้าและไหลย้อนกลับของคลื่นสึนามิได้ พบว่าอิทธิพลของกระแสไหลเข้ามีผลที่ความลึกน้ำไม่เกิน 20 เมตร และเมื่อวิเคราะห์ผลร่วมกับรูปแบบการกระจายตัวของ PAHs และค่า PAH isomer ratios ในดินตะกอน จะพบว่าดินตะกอนในพื้นที่ศึกษามีแหล่งที่มา 2 กลุ่มหลัก คือ กลุ่มที่เป็นการสะสมตัวแบบปกติ และกลุ่มที่มีค่า PAHs สูง ซึ่งเป็นกลุ่มที่ถูกพามากับกระแสไหลย้อนของคลื่นสึนามิ จากแหลมปะการังออกไปสะสมนอกชายฝั่งไกลถึง 25 กิโลเมตร

Abstract

Tsunami symbolizes one of the most harmful natural disasters for low-lying coastal zones and their residents, due to both its destructive power and irregularity. The 2004 tsunami caused in extreme alterations of both onshore and offshore coastal morphology. However, there are many missing scientific knowledge to deal with the recorded events deposited on the seafloor. Following high resolution mapping with different hydroacoustic methods along offshore of cape Pakarang, Phangnga province (between Thap Lamu and Phra thong island), positions for grab sampling and coring were identified, where

tsunami deposits were supposed to occur. The sampled material was analyzed using a wide range of sedimentological, geochemical, micropalaeontological, chemical, and physical methods. The results reveal that the seafloor slope on over 25 m water depth is rising towards the shoreline. Close to the coast, a patchy cover of fine grained sediments (mud with small amount of sand) exists in water depths between 7 to 15 m. In water depths between 10 to 16 m, asymmetric natural channel structures appear in 3 lines in the NW-SE striking features, 150-300 m width and a few kilometer length. Towards the base of the core, muddy sand with few shells is found and below this layer, coarse sand containing complete shells and shell fragments is deposited. Generally, the ridge structures are observed in approximately 15 m water depth to offshore, with a steep NW and a gently dipping SE side reaches heights of about 2 m above the seafloor. Remnants of tin mining activities can be found in water depths of about 20 to 25 m northwest of Cape Pakarang, visible in form of up to 7 m deep holes. In water depths between 30 and 35 meters, elongated fields of stones and boulders appear in the survey mapping. According to sedimentological, Ti/Ca ratio and Pb-210 isotope studies, storm and tsunami event layers could be identified and distinguished. In this area, natural annually accumulation rates of sediments was found to be around 1.3 to 5.7 cm. Individual layers, ranging from 12–39 cm in thickness, were interpreted as tsunami deposits. Run-up and backwash deposits could be distinguished. Based on foraminiferal transfer functions and textural analyses re-suspension of sediment during run-up seemed to be restricted to about 20 m water depth. On the other hand it could be shown by using PAHs distribution in sediments and PAH isomer ratios as chemical proxies to discriminate tsunami related that the loaded backwash extends up to 25 km offshore.

สารบัญ

		หน้า
กิตติกรรมประกาศ (Acknowledgement)		ก
บทสรุปผู้บริหาร บทคัดย่อภาษาไทยและบทคัดย่อภาษาอังกฤษ (Abstract)		ข
สารบัญ (Table of Contents)		ฌ
สารบัญรูป (List of Illustrations)		ญ
สารบัญตาราง (List of Tables)		ณ
บทที่ 1	บทนำ	1-1
	1.1 ความสำคัญและที่มาของปัญหา	1-1
	1.2 วัตถุประสงค์	1-4
	1.3 ขอบเขตการวิจัย	1-7
	1.4 ประโยชน์ที่คาดว่าจะได้รับ	1-7
	1.5 แผนการถ่ายทอดเทคโนโลยีหรือผลการวิจัยสู่กลุ่มเป้าหมายเมื่อสิ้นสุดการวิจัย	1-10
	1.6 ผลงานตีพิมพ์ในวารสารวิชาการ	1-10
บทที่ 2	วิธีการดำเนินการวิจัยและสถานที่ทำการทดลอง/เก็บข้อมูล	2-1
	2.1 วิธีการดำเนินการวิจัย	2-2
	2.2 การทบทวนวรรณกรรม / งานวิจัยที่เกี่ยวข้อง	2-3
	2.3 ระยะเวลาทำการวิจัย และแผนการดำเนินงานตลอดโครงการวิจัย	2-4
	2.4 รายละเอียดการดำเนินงานตามแผนงานวิจัย	2-5
บทที่ 3	ผลการวิจัยและการวิเคราะห์ข้อมูล	3-1
	3.1 ผลการสำรวจทางธรณีฟิสิกส์	3-1
	3.2 จัดทำแผนที่พื้นท้องทะเลรายละเอียดสูง	3-14
	3.3 การเก็บตัวอย่างดินตะกอนจากพื้นทะเล	3-19
	3.4 การวิเคราะห์ในห้องปฏิบัติการ	3-20
	3.5 การวิเคราะห์ผล	3-27
	3.6 การพัฒนาบุคลากร	3-57
บทที่ 4	สรุปผลการวิจัยและข้อวิจารณ์	4-1
	4.1 ธรณีสัณฐาน การกระจายตัวและรูปแบบการสะสมตัวของดินตะกอน	4-1
	4.2 ธรณีเคมีของดินตะกอน	4-3
	4.3 การพัฒนาบุคลากร	4-5
เอกสารอ้างอิง		
ภาคผนวก		

สารบัญรูป

		หน้า
รูปที่ 1.1	พื้นที่ศึกษานอกชายฝั่งจังหวัดพังงา ในรูปแสดงตำแหน่งการเก็บตัวอย่างตะกอนผิวหน้าและตัวอย่างตะกอนตามความลึกของทั้งโครงการฯ โดยพื้นที่ในกรอบสี่เหลี่ยมแสดงตำแหน่งที่ตัวอย่างแท่งตะกอนตามความลึกที่นำมาศึกษาทางธรณีเคมีและอายุตะกอนโดยละเอียดบนแผนภาพยังแสดงพื้นที่และเส้นทางการสำรวจด้วยเครื่องมือทางธรณีฟิสิกส์	1-8
รูปที่ 1.2	แหลมปะการังซึ่งอยู่ใกล้เขาหลัก ภาพบนเป็นภาพถ่ายดาวเทียมแสดงให้เห็นการเปลี่ยนแปลงของแหลมปะการังโดยคลื่นยักษ์สึนามิเมื่อวันที่ 26 ธันวาคม พ.ศ. 2547 และภาพล่างแสดงสภาพบนพื้นดิน	1-9
รูปที่ 2-1	เรือสำรวจจักรทอง ทองใหญ่ ของสถาบันวิจัยและพัฒนาทรัพยากรทางทะเล ชายฝั่งทะเลและป่าชายเลน จังหวัดภูเก็ต กรมทรัพยากรทางทะเลและชายฝั่ง กระทรวงทรัพยากร-ธรรมชาติและสิ่งแวดล้อม	2-4
รูปที่ 2-2	เครื่องหยั่งความลึกด้วยเสียงสะท้อนชนิดหลายลำคลื่น (multibeam echo sounder) และการติดตั้งทางกาบเรือด้านขวา	2-8
รูปที่ 2-3	ความเร็วเสียงตามความลึกที่ตรวจวัดได้จากหัวอ่าน CTD (CTD sound velocity profile) ในวันที่ 7 ธันวาคม พ.ศ. 2550 เส้นสีฟ้าแสดงข้อมูลความเร็วเสียงขณะหย่อนหัวอ่านลงตามความลึกน้ำและเส้นสีแดงแสดงข้อมูลความเร็วเสียงขณะดึงหัวอ่านขึ้นจากตามความลึกน้ำ	2-9
รูปที่ 2-4	ระหว่างบันทึก profile 20071125145631018 หน่วยควบคุมการป้อน heave data เกิดการขัดข้องชื่อไฟล์ที่ใช้เก็บข้อมูลจากเครื่องหยั่งความลึกด้วยเสียงสะท้อนชนิดหลายลำคลื่นอยู่ในรูปแบบ "day-month-year-number-subsample" เช่น 05120747B ตัวเลขจะเพิ่มขึ้นเป็นลำดับตลอดช่วงการปฏิบัติการ	2-9
รูปที่ 2-5	เครื่องโซนาร์กวาดทางข้าง (Side Scan Sonar) และปฏิบัติการขณะปล่อยลงทะเลเพื่อลากสำรวจ	2-11
รูปที่ 2-6	ระบบวัดการสะท้อนของคลื่นไหวสะเทือน (Boomer System) บนชุดลากจูงและปฏิบัติการขณะปล่อยลงทะเลเพื่อลากสำรวจ	2-12
รูปที่ 2-7	การเก็บตัวอย่างดินตะกอนโดย Van-Veen Grab Sampler และการตรวจสอบลักษณะทั่วไปของดินตะกอน	2-16
รูปที่ 2-8	การเก็บตัวอย่างดินตะกอนโดย Rumohr Gravity Corer (ซ้าย) และการเก็บรักษาแท่งดินตะกอนให้อยู่ในแนวตั้ง (ขวา)	2-17

		หน้า
รูปที่ 2-9	แนวที่ทำการสำรวจด้วยเครื่องโซนาร์กวาดทางข้าง (Side Scan Sonar) และเครื่องหยั่งความลึกด้วยเสียงสะท้อนชนิดหลายลำคลื่น (Multibeam echo-sounder) (รูปบน) และแนวที่ทำการสำรวจด้วยเครื่อง Multibeam echo-sounder (รูปล่าง)	2-18
รูปที่ 2-10	ตำแหน่งเก็บตัวอย่างดินตะกอนผิวหน้า (surface sediment) ในพื้นที่สำรวจ (รูปบน) และตำแหน่งเก็บตัวอย่างดินตะกอนผิวหน้าในกรอบประของรูปบน (รูปล่าง)	2-19
รูปที่ 2-11	ตำแหน่งเก็บตัวอย่างดินตะกอน (core sediment) ตามความลึกในพื้นที่สำรวจ (รูปบน) และตำแหน่งเก็บตัวอย่างดินตะกอนตามความลึกในกรอบประของรูปบน (รูปล่าง)	2-20
รูปที่ 2-12	ห้องประมวลผลข้อมูลทางธรณีฟิสิกส์ภายใน เรือสำรวจจักรทอง ทองใหญ่	2-21
รูปที่ 3-1	ภาพแสดงข้อมูลจากเครื่องหยั่งความลึกด้วยเสียงสะท้อนชนิดหลายลำคลื่น (Multibeam echo-sounder)	3-3
รูปที่ 3-2	ข้อมูลพื้นท้องทะเล (Bathymetric data) ทางตะวันออกเฉียงเหนือของแหลมปะการัง จะเห็นร่องรอยการทำเหมืองดีบุกได้ชัดเจน ในลักษณะเป็นหลุมลึกที่เกิดขึ้นเป็นหย่อมๆ นพื้นที่ตอนเหนือของพื้นที่ทำการสำรวจ (กรอบสีขาวในรูปทางด้านขวา)	3-4
รูปที่ 3-3	ข้อมูลจากเครื่องหยั่งความลึกด้วยเสียงสะท้อนชนิดหลายลำคลื่น (multibeam echo-sounder) ในพื้นที่นอกชายฝั่งใกล้แหลมปะการัง ในรูปเล็กด้านขวาบนแสดงภาพตัดขวางในแนว A-B จะเห็นว่ามีลักษณะเป็นร่องที่มีความไม่สมมาตร	3-5
รูปที่ 3-4	ภาพแสดงลักษณะข้อมูลที่ได้จากเครื่องโซนาร์กวาดทางข้าง (Side Scan Sonar) ภาพ (1) แสดงลักษณะที่เป็นร่องลึก (channel) ที่เกิดขึ้นบริเวณพื้นทะเล ในบริเวณ 8° 43’ เหนือ 98° 11’ ตะวันออก; ภาพ (2) แสดงลักษณะที่เป็นหลุมเล็ก ๆ (pock-like depressions) ในบริเวณ 8° 43’ เหนือ 98° 03’ ตะวันออก; ภาพ (3) และ (4) แสดงลักษณะท้องทะเลในเขตน้ำลึกที่มีก้อนหินขนาดใหญ่ บริเวณ 8° 44’ เหนือ 98° 05’ ตะวันออก และ 8° 30’ เหนือ 98° 02’ ตะวันออก	3-6
รูปที่ 3-5	ข้อมูลจากเครื่องหยั่งความลึกด้วยเสียงสะท้อนชนิดหลายลำคลื่น (multibeam echo-sounder) ในพื้นที่นอกชายฝั่งใกล้แหลมปะการัง ทับซ้อนกับภาพถ่ายจากดาวเทียม IKONOS ที่ถ่ายภาพกระแสไหลย้อนของคลื่นสึนามิ (backwash of tsunami) เมื่อเดือนธันวาคม 2543	3-7
รูปที่ 3-6	ตัวอย่างดินตะกอนใกล้ฝั่งจากแนว 02120712 พบว่ามีซากพืชที่มีลักษณะคล้ายหญ้าบนบก ซึ่งหญ้าดังกล่าวถูกตะกอนขนาดหยาบปนละเอียดทับถมอยู่ลึกประมาณ 3 เซนติเมตร	3-8
รูปที่ 3.7	เศษทรายหยาบและชิ้นส่วนศิลาแลง (laterite) ในตัวอย่างดินตะกอนผิวหน้าหมายเลข 061208-11 ซึ่งอยู่ห่างออกไป 3.5 กิโลเมตร นอกชายฝั่งแหลมปะการัง	3-8

		หน้า
รูปที่ 3-8	ภาพแสดงลักษณะตะกอนหยาบปนละเอียดในตัวอย่างดินตะกอนที่เก็บตามความลึก (Core sediment sample)	3-9
รูปที่ 3.9	ข้อมูลจากเครื่องโซนาร์กวาดทางข้าง (Scan Sonar data) ในพื้นที่ใกล้ชายฝั่ง (ใกล้กับ 8° 40’ เหนือ 98° 12’ ตะวันออก) ตำแหน่ง (a) เป็นลักษณะพื้นท้องทะเลบริเวณที่มีก้อนหินขนาดใหญ่สะสม; ตำแหน่ง (b) เป็นลักษณะพื้นท้องทะเลที่เป็นระลอกคลื่น; และตำแหน่ง (c) เป็นลักษณะพื้นท้องทะเลที่มีตะกอนละเอียดสะสมตัวอยู่	3-9
รูปที่ 3-10	ข้อมูลจากระบบวัดการสะท้อนของคลื่นไหวสะเทือนในน้ำตื้น (boomer) แนว 28110706 แสดงสัณฐานพื้นท้องทะเลในแนวตั้งฉากกับฝั่ง และข้อมูลจากเครื่องโซนาร์กวาดทางข้าง (side scan sonar) ณ ความลึกน้ำต่างระดับ ภาพ (1) ลักษณะพื้นทะเลเป็นตะกอนละเอียด; ภาพ (2) แนวกองหินที่พบเห็นได้ทั่วไปในข้อมูลจากรระบบวัดการสะท้อนของคลื่นไหวสะเทือนในน้ำตื้นที่ลากสำรวจในแนวตั้งฉากกับฝั่ง และภาพ (3) บริเวณที่พื้นท้องทะเลต่ำกว่าพื้นที่ข้างเคียง	3-10
รูปที่ 3-11	ข้อมูลจากระบบวัดการสะท้อนของคลื่นไหวสะเทือนในน้ำตื้น (boomer) แนว 01120706 แสดงสัณฐานพื้นท้องทะเลในแนวตั้งฉากกับฝั่ง และข้อมูลจากเครื่องโซนาร์กวาดทางข้าง (side scan sonar) ณ ความลึกน้ำต่างระดับ ภาพ (1) หย่อมตะกอนละเอียดที่พบได้ทั่วไปในพื้นท้องทะเลบริเวณใกล้ฝั่ง; ภาพ (2) บริเวณรอยต่อระหว่างบริเวณที่เป็นตะกอนละเอียดกับบริเวณที่ตะกอนมีขนาดหยาบขึ้น; ภาพ (3) แนวกองหินที่พบเห็นได้ทั่วไปในข้อมูลจากรระบบวัดการสะท้อนของคลื่นไหวสะเทือนในน้ำตื้นที่ลากสำรวจในแนวตั้งฉากกับฝั่ง และภาพ (4) บริเวณที่พื้นท้องทะเลต่ำกว่าพื้นที่ข้างเคียง	3-11
รูปที่ 3-12	เรือสำรวจจักรทอง ทองใหญ่ และเรือสำรวจบุญเลิศ ผาสุก ของสถาบันวิจัยและพัฒนาทรัพยากรทางทะเล ชายฝั่งทะเล และป่าชายเลน จังหวัดภูเก็ต	3-13
รูปที่ 3-13	การติดตั้งเครื่องมือทางธรณีฟิสิกส์บนเรือสำรวจบนเรือสำรวจบุญเลิศ ผาสุก	3-15
รูปที่ 3-14	เส้นทางการสำรวจโดยใช้เครื่องมือทางธรณีฟิสิกส์และตำแหน่งจุดเก็บตัวอย่างดินตะกอนผิวหน้า และตัวอย่างดินตะกอนตามความลึก จากการสำรวจ 2 รอบเรือ (พฤศจิกายน – ธันวาคม พ.ศ. 2550 และพฤศจิกายน – ธันวาคม พ.ศ. 2551)	3-17
รูปที่ 3-15	เครื่อง Multi sensor core logger (MSCL) ณ Christian-Albrechts-University of Kiel ประเทศเยอรมนี	3-23
รูปที่ 3-16	การวิเคราะห์สมบัติทางกายภาพ (physical properties) แบบ (core loggers)	3-24

		หน้า
รูปที่ 3-17	เครื่องกวาดตรวจเอกซ์ฟลูออเรสเซน (X-ray Fluorescence scanner หรือ XRF scanner) ณ Christian-Albrechts-University of Kiel ประเทศเยอรมนีและการหาสัดส่วนของธาตุ (Ti/Ca)	3-24
รูปที่ 3-18	ภาพถ่ายรังสีเอกซ์ (X-radiography images) ของแท่งตะกอน	3-25
รูปที่ 3-19	ตัวอย่าง X-ray Diffraction Peak ของแร่ดินเหนียว	3-25
รูปที่ 3-20	ชุดสกัด Soxhlet extraction และเครื่อง Varian Saturn 2200 Gas Chromatography/Mass Spectrometric detector–Ion–Trap (GC/MS–Ion-Trap)	3-26
รูปที่ 3.21	ตัวอย่าง Chromatograms ของ (ก) สารละลายมาตรฐาน, (ข) ตัวอย่างจากสถานี และ (ค) สารอ้างอิงมาตรฐาน	3-26
รูปที่ 3-22	ภาพบน: ภาพที่ได้จากการปะติดปะต่อข้อมูลภาพจากเครื่องโซนาร์กวาดทางข้าง (side scan sonar) แสดงสภาพนอกชายฝั่งแหลมปะการัง (ข้อมูลจากการสำรวจปี พ.ศ. 2551) สีเข้มแสดงพื้นที่ที่มีลักษณะเป็นทราย ส่วนพื้นที่ที่มีสีอ่อนเป็นพื้นที่ที่ปกคลุมด้วยตะกอนละเอียด (พื้นที่ a ในภาพ) พาดไปตามแนว SW-NE และยังปรากฏให้เห็นแม้ว่าจะห่างฝั่งออกไปไกล (พื้นที่ b ในภาพ) และภาพล่าง: ภาพตัดขวางความลึก (bathymetric profiles) แสดงสัณฐานของหย่อมโคลน ตามแนว A – A', B – B' และ C – C' ในภาพบน	3-30
รูปที่ 3-23	ภาพแสดงหย่อมของตะกอนที่เป็นทรายแห้งและที่เป็นโคลน (a) นอกฝั่ง 3 ถึง 7 กิโลเมตร ความลึกน้ำ 7 ถึง 15 เมตร ไกลออกไปนอกฝั่งลักษณะเช่นนี้จะเห็นเป็นแนวแคบลง (b) ที่ยังคงเชื่อมต่อ (c) กับหย่อมโคลนใกล้ฝั่ง Profile A – A´ (รูปที่ 3-22 แสดงตำแหน่งการสำรวจ)	3-31
รูปที่ 3-24	Seismic profile ตัดพาดร่องโคลน (profile A-A´ ในรูปที่ 3-23) ในภาพจะเห็นร่อง 2 ร่องที่ถูกเติมเต็ม (ส่วนที่เป็นสีส้มและสีฟ้าในรูป) โครงสร้างของพื้นท้องทะเลโดยรอบเห็นเป็นชั้น ๆ เช่นกัน (ส่วนที่เป็นสีเขียว)	3-31
รูปที่ 3-25	ก้อนกรวด (clasts) ขนาดทรายหยาบประกอบไปด้วยเศษลูกรัง (laterite) ที่พบในตัวอย่างดินตะกอนผิวหน้าหมายเลข GRAB 061208-11 ที่เก็บที่ 3.5 กิโลเมตร นอกฝั่งแหลมปะการัง (ตำแหน่งเก็บตัวอย่างแสดงในรูปที่ 3-22)	3-32
รูปที่ 3-26	ตัวอย่างตะกอนผิวหน้าหมายเลข GRAB 021207-12 จากพื้นที่ใกล้ฝั่ง พบว่ามีซากพืชที่มีลักษณะคล้ายหญ้าบนบก ซึ่งหญ้าดังกล่าวถูกตะกอนขนาดหยาบปนละเอียดทับถมอยู่ลึกประมาณ 3 เซนติเมตร	3-32
รูปที่ 3-27	แท่งตะกอนหมายเลข CORE 051207-32 ที่เก็บในพื้นที่ที่เป็นร่อง ที่ความลึกน้ำ 14.4 เมตร (ตำแหน่งเก็บตัวอย่างแสดงในรูปที่ 3-22)	3-33

		หน้า
รูปที่ 3-28	ภาพปะต่อจากข้อมูลที่ได้จากเครื่องโซนาร์กวาดทางข้าง (side scan sonar image) ของแนวสันเขาที่พบในชุดข้อมูลความลึก (bathymetric dataset)	3-34
รูปที่ 3-29	Seismic profile ตัดขวางแนวสันเขา (ตำแหน่งพื้นที่แสดงในรูปที่ 3.22) จะเห็นลักษณะที่ไม่สมมาตร (asymmetric form) ของสันเขา ซึ่งบ่งชี้ว่าการเคลื่อนย้ายตะกอนในแนวจากทิศใต้ไปทิศเหนือ ยิ่งไปกว่านั้นใต้สันเขายังเห็นแยกเป็นชั้น ๆ	3-35
รูปที่ 3-30	แท่งตะกอนหมายเลข CORE 051207-37 ที่เก็บจากบริเวณลาดเอียง (slope) ของสันเขา ด้านซ้าย: ภาพถ่ายแสดงลักษณะตะกอนในแท่งตะกอน ตรงกลาง: กราฟแสดงสัดส่วน Ti/Ca และ Fe/Ca ที่ระดับความลึกต่าง ๆ ในแท่งตะกอน และด้านขวา: ภาพถ่ายรังสีเอกซ์ (X-radiography images)	3-35
รูปที่ 3-31	ข้อมูลพื้นท้องทะเล (Bathymetric data) ทางตะวันออกเฉียงเหนือของแหลมปะการัง (PC) เมื่อครั้งการสำรวจในปี 2550 จะเห็นร่องรอยการทำเหมืองดีบุกได้ชัดเจน ในลักษณะเป็นหลุมลึกที่เกิดขึ้นเป็นหย่อมๆ ในพื้นที่ตอนเหนือของพื้นที่ทำการสำรวจ (ในรูปทางด้านขวา)	3-37
รูปที่ 3-32	รูป A: บริเวณ (a) ในรูป เป็นลานหิน (Stone fields) ที่พบที่ความลึกน้ำ 30 ถึง 35 เมตร รูป B: บริเวณ (b) ในรูป เป็นหลุมเล็กๆ (small depressions) พบทั่วไปที่ความลึกน้ำ 35 เมตร (ตำแหน่งที่พบแสดงในรูปที่ 3-31)	3-38
รูปที่ 3-33	ภาพถ่ายรังสีเอกซ์ (X-radiography images), ขนาดเฉลี่ยของตะกอน และโครงสร้างอายุ (age model) ของแท่งตะกอนหมายเลข CORE 021207-18 ซึ่งเก็บตัวอย่างจากนอกชายฝั่ง 24 กิโลเมตร ที่ระดับความลึกน้ำ 52 เมตร บริเวณที่มีการกระจายขนาดของตะกอนจากหยาบมาละเอียดขึ้นเป็นลำดับ ซึ่งมีอยู่ 2 ชุด แสดงไว้โดยลูกศร	3-38
รูปที่ 3-34	ในเขตน้ำลึก ตะกอนสมุทรยุคปัจจุบัน (recent marine sediments) ดูเหมือนจะเกิดเป็นแนวบาง ๆ อยู่ปกคลุมอยู่ด้านบนและวางตัวอยู่ใต้ชั้นฐาน (underlying stratum) ในชั้นใต้ชั้นตะกอนสมุทรจะพบโครงสร้าง diffuse internal structures ซึ่งยังไม่รู้มูลเหตุกำเนิด	3-39
รูปที่ 3-35	ภาพถ่ายรังสีเอกซ์, รูปแท่งตะกอนและคุณลักษณะของแท่งตะกอน 030310-C3 โดยเทคนิคการวิเคราะห์ micropalaeontological, sedimentological and geochemical analyses โดยแท่งตะกอนนี้มีการแบ่งชั้นตะกอนออกเป็น 6 รูปแบบ	3-42
รูปที่ 3-36	ภาพถ่ายรังสีเอกซ์, รูปแท่งตะกอนและคุณลักษณะของแท่งตะกอน 050310-C6 โดยเทคนิคการวิเคราะห์ micropalaeontological, sedimentological and geochemical analyses โดยแท่งตะกอนนี้มีการแบ่งชั้นตะกอนออกเป็น 4 รูปแบบ	3-43

		หน้า
ปที่ 3-37	ตำแหน่งเก็บตัวอย่างตะกอนผิวหน้าสำหรับการวิเคราะห์หาสาร Polycyclic aromatic hydrocarbons (PAHs) จากการสำรวจปีที่ 1 พ.ศ. 2550 จำนวน 70 ตัวอย่าง	3-44
รูปที่ 3-38	รูปแบบการแพร่กระจายของ PAHs ในตะกอนผิวหน้านอกชายฝั่งเขาหลัก	3-48
รูปที่ 3-39	Cross-plot ระหว่าง B[a]A/(B[a]A+Chry) ratio กับ Ind/(Ind+B[g,h,i]P) ratio	3-50
รูปที่ 3-40	Hierarchical Cluster Analysis (HCA) ของตัวอย่างตะกอนดิน 70 ตัวอย่างจากนอกชายฝั่งเขาหลัก	3-51
รูปที่ 3-41	ภาพที่ได้จากการปะติดปะต่อข้อมูลภาพจากเครื่องโซนาร์กวาดทางข้าง (side scan sonar) แสดงสภาพนอกชายฝั่งแหลมปะการัง (ข้อมูลจากการสำรวจปี พ.ศ. 2551) (ซ้าย) และภาพจากการ interpretation ของพื้นท้องทะเลที่ความลึกน้ำประมาณ 15 เมตร โดยแบ่งเป็น 7 ประเภท คือ A, B, C, D, E, F, G จากการจำแนกโดยข้อมูลโซนาร์กวาดทางข้าง (ขวา)	3-54
รูปที่ 3-42	การจำแนกผิวพื้นท้องทะเลบริเวณนอกชายฝั่ง หน้าเขาหลัก ที่ความลึกน้ำประมาณ 35 เมตร จากการจำแนกโดยข้อมูลโซนาร์กวาดทางข้างและการวิเคราะห์จากตะกอนผิวหน้าดิน แสดงชนิดของผิวพื้นท้องทะเลชนิด B D E F H และแสดงพื้นที่เหมืองเก่าด้านบนของภาพ	3-55
รูปที่ 3-43	เปรียบเทียบแท่งตะกอนดิน 6 แท่ง ในเขตน้ำตื้น (ความลึกน้ำไม่เกิน 16 เมตร) ที่บันทึกเหตุการณ์ต่าง ๆ ได้แก่ ตะกอนสึนามิแบบ A, แบบ B และแบบ C ตะกอนที่การสะสมตัวในช่วงน้ำท่วม (flood) และตะกอนที่ถูกพามาโดยพายุ	3-56

สารบัญตาราง

		หน้า
ตารางที่ 1-1	ลักษณะบ่งชี้บางประการที่แสดงว่าเคยมีการเกิดสึนามิขึ้น	1-2
ตารางที่ 1-2	แผนการถ่ายทอดเทคโนโลยีหรือผลการวิจัยสู่กลุ่มเป้าหมายเมื่อสิ้นสุดการวิจัย	1-10
ตารางที่ 2-1	รายละเอียดงานส่วนของการวิเคราะห์ในห้องปฏิบัติการทั้งในประเทศเยอรมันและประเทศไทย	2-2
ตารางที่ 2-2	ขั้นตอนการดำเนินงานการศึกษาผลกระทบของคลื่นสึนามิต่อพื้นท้องทะเล	2-5
ตารางที่ 2-3	ภาระกิจในแต่ละวันระหว่างการสำรวจพื้นท้องทะเลฝั่งอันดามัน	2-14
ตารางที่ 3-1	ข้อมูลแท่งตะกอนจากบริเวณ offshore area	3-40
ตารางที่ 3-2	ปริมาณ PAHs แต่ละชนิดใน surface sediment	3-45
ตารางที่ 3-3	Characteristic values ของ selected diagnostic ratios สำหรับ petroleum และ single-source combustion	3-49
ตารางที่ 3-4	Rotated component matrix ของ PAHs 13 ชนิด จากตัวอย่างตะกอน 70 ตัวอย่างจากนอกชายฝั่งเขาหลัก	3-52

บทที่ 1
บทนำ

1.1 ความสำคัญและที่มาของปัญหา

"สึนามิ" (tsunami) จัดได้ว่าเป็นหนึ่งในวิบัติภัยจากธรรมชาติที่ส่งผลกระทบอย่างรุนแรง เมื่อสืบค้นประวัติศาสตร์ย้อนกลับไปในอดีตพบการจดบันทึกเหตุการณ์เอาไว้ และมีนักวิจัยจำนวนมากพยายามที่จะศึกษาเพื่อหาสาเหตุ เพื่อดูการแผ่กระจายของคลื่นสึนามิที่เกิดขึ้น ตลอดจนกระบวนการสลายของพลังงานเมื่อคลื่นสึนามิกระทบฝั่ง

เหตุการณ์แผ่นดินไหวขนาด 9.3 ริกเตอร์ ที่เกิดจากกระบวนการเทกโทนิก (tectonic) ที่ซับซ้อน โดยแผ่นเปลือกโลกอินโด-ออสเตรเลียน (Indo-Australian plate) เคลื่อนชนกับแผ่นเปลือกโลกซุนดรา (Sunda plate) ในทะเลนอกชายฝั่งด้านตะวันออกเฉียงเหนือของเกาะสุมาตรา เมื่อวันที่ 26 ธันวาคม พ.ศ. 2547 ก่อให้เกิดคลื่นสึนามิขนาดใหญ่ที่ส่งผลกระทบอย่างใหญ่หลวงต่อพื้นที่ชายฝั่งทะเลทั่วทั้งเอเชียตะวันออกเฉียงใต้ และยังส่งผลกระทบไปไกลถึงชายฝั่งด้านตะวันออกของทวีปแอฟริกา (LAY et al. 2005, WEISS & BAHLBURG 2006)

คลื่นสึนามิ นอกจากจะมีศักยภาพสูงในการเปลี่ยนแปลงชายฝั่ง ยังมีอิทธิพลต่อการสะสมตัวของตะกอนทั้งบนชายฝั่ง (onshore) และนอกชายฝั่ง (offshore) (BRYANT 2001, WIEGEL 2006a และ 2006b เป็นต้น ดูเพิ่มเติมได้ในสารสารวิชาการ Sedimentary Geology ฉบับที่ 200 ปี ค.ศ. 2007 และ Marine Geology ฉบับที่ 242 ปี ค.ศ. 2007) หนึ่งในปรากฏการณ์ที่เป็นผลกระทบจากการเกิดสึนามิที่มีนัยสำคัญมากที่สุด ได้แก่ การเคลื่อนย้ายของตะกอนในปริมาณมากออกจากชายฝั่ง ตามด้วยการทับถมของทรายจากทะเลในพื้นที่ราบต่ำชายฝั่ง (coastal lowland) (MINOURA & NAKAYA 1991) นอกจากนี้คลื่นสึนามิที่ไหลเข้าหาชายฝั่ง (incoming flow) และย้อนกลับออกจากชายฝั่ง (returning flow) ยังกวนให้ดินตะกอน (resuspend) เคลื่อนย้าย (transport) และตกกลับลงมาใหม่ (redeposit) บนพื้นท้องทะเล

อย่างไรก็ดี องค์ความรู้เกี่ยวกับการสะสมตะกอนในเขตพื้นที่น้ำตื้นนอกชายฝั่ง อันเป็นผลมาจากการเกิดสึนามินั้น มาจากหลักฐานที่ปรากฏบนแผ่นดิน (CANTALAMESSA & DI CELMA 2005, FUJIWARA & KAMATAKI 2007, DAWSON & STEWART 2008) MAMO et al. (2009) ได้รวบรวมลักษณะสำคัญที่ถูกบันทึกไว้ทางธรณี ซึ่งใช้บ่งชี้ได้ว่าเคยมีการเกิดสึนามิทั้งในยุคปัจจุบันและยุคดึกดำบรรพ์ หลักฐานเหล่านี้เกือบทั้งหมดอ้างอิงมาจากการศึกษาที่ดำเนินการบนแผ่นดิน ดังนั้นดัชนีบ่งชี้เหล่านี้จึงยังมีข้อจำกัดเมื่อนำมาใช้กับหลักฐานที่ถูกบันทึกไว้ในตะกอนในพื้นที่นอกชายฝั่ง ตารางที่ 1-1 เป็นตัวอย่างของหลักฐานบ่งชี้ที่อาจจะนำมาใช้กับพื้นที่นอกชายฝั่ง

ตารางที่ 1-1 ลักษณะบ่งชี้บางประการที่แสดงว่าเคยมีการเกิดสึนามิขึ้น (ดัดแปลงจาก MAMO et al., 2009)

ลักษณะบ่งชี้ที่แสดงว่ามีการสะสมเนื่องมาจากสึนามิ	คำอธิบาย
ชั้นฐานมีลักษณะรอยชั้นไม่ต่อเนื่อง (Basal unconformity)	มีความแตกต่างกันอย่างชัดเจน หรือไม่ต่อเนื่อง หรือมีการกร่อนระหว่างชั้นตะกอนเดิมกับชั้นตะกอนที่ถูกพามาโดยคลื่นสึนามิ
มีชั้นเศษหินภายใน (Intraclasts)	ส่วนฐานหรือด้านล่างของชั้นตะกอนสึนามิอาจประกอบไปด้วยกองเศษหินอยู่ภายใน หรือมีการกวนเอาตะกอนที่ตกอยู่ในส่วนล่างๆ ขึ้นมา
โครงสร้างของวัสดุที่ถูกพามาทับถม	ส่วนฐานหรือด้านล่างของชั้นตะกอนสึนามิอาจประกอบไปด้วยวัสดุที่ถูกพามาทับถม
แนวโน้มของตะกอนมาทางด้านบนมีขนาดอนุภาคละเอียดขึ้น	ชั้นตะกอนสึนามิจะมีขนาดอนุภาคละเอียดมาทางด้านบน
โครงสร้างของชั้นตะกอนที่ทับถมในพื้นที่มีลักษณะสลับไปมาของวัสดุที่มาสะสม (Cross bedding)	กระแสน้ำที่เข้าหาฝั่ง (landward) และออกจากฝั่ง (seaward) ทำให้เกิดการเรียนซ้อนกันของซากเปลือกหอย และ/หรือ ลิ่มของตะกอนแผ่ออกไป และ/หรือ สลับไปมา
ชั้นของหินกรวดมนใหญ่	ธรณีสัณฐานบริเวณชายฝั่งที่มีลักษณะเป็นสัน หรือเป็นกองหิน หรือเป็นร่องรอยการสะสมตัวของหินกรวดมนใหญ่ (boulders)
ชั้นของซากสิ่งมีชีวิต	บรรพชีวินขนาดเล็ก (microfossil) ที่พบประกอบไปด้วย ไดอะตอม (diatoms) และฟอรามินิเฟอรา (foraminifera) หรืออาจจะมีซากสิ่งมีชีวิตที่อยู่ในน้ำและ/หรือที่อาศัยอยู่หน้าดินบริเวณชายฝั่ง May be pelagic and/or benthic species in shallow water or coastal environments. Frustules/tests may be crushed or broken in significant percentages.
เศษซากของวัสดุจากแผ่นดิน	ชิ้นส่วนของหญ้าหรือพืชที่เคยขึ้นบนแผ่นดิน ได้แก่ ชิ้นส่วนศิลาแลง (laterite fragments) หรือชิ้นส่วนไม้ (wood fragments)
วัสดุที่มีแหล่งกำเนิดเนื่องมาจากมนุษย์	เศษอิฐ เศษซีเมนต์

ปัจจุบัน องค์ความรู้ในเรื่องการสะสมตัวของดินตะกอนพื้นทะเลบริเวณหน้าฝั่ง (shoreface)[1] ทั้งส่วนบน (upper) และส่วนล่าง (lower) และบริเวณ shelf (shoreface และ shelf นิยามตาม COWELL et al. 1999) ที่เกิดขึ้นจากการเหนี่ยวนำของกระแสไหลย้อนของสึนามิ ซึ่งอาจก่อให้เกิดเปื้อนดินตะกอน (sediment aprons) สันทรายใต้น้ำ (sand bars) หรือคลื่นตะกอน (sediment waves)

ที่ผ่านมามีการสำรวจศึกษาน้อยมาก ทั้งในเรื่องของดินตะกอนทะเลอายุเยาว์ (young marine deposits) (LE ROUX & VARGAS 2005, VARGAS et al. 2005, NODA et al. 2007) และในการหาหลักฐานที่จะใช้เป็นดัชนีบ่งชี้สาเหตุการสะสมตัวที่เกิดเนื่องมาจากสึนามิ โดยเฉพาะอย่างยิ่งที่เกิดจากกระแสไหลย้อน FUJIWARA & KAMATAKI (2007) ได้พยายามพัฒนาแบบจำลองการสะสมของดินตะกอนจากสึนามิ โดยศึกษาชั้นดินตะกอนสึนามิสมัยโฮโลซีน (Holocene tsunami deposits) ส่วน WEISS (2007) ทำการศึกษาใช้ทฤษฎีต่าง ๆ (theoretical approach) เพื่อประเมินผลของสึนามิต่อการตกทับถมของดินตะกอนในน้ำลึก (deep water sediments) ขณะที่ HAWKES et al. (2007) และ SUGAWARA et al. (2009) ใช้ซากฟอรามินิเฟอรา (assemblages of foraminifera) ในการแยกแยะระหว่างดินตะกอนที่สะสมก่อนเกิดสึนามิ (pre-tsunami deposits) และที่เกิดจากสึนามิ (tsunami deposits) ผลงานวิจัยของ SUGAWARA et al. (2009) มีหลักฐานที่แสดงว่าบรรพชีวินขนาดเล็ก (microfossils) มีการเคลื่อนย้ายจากหน้าฝั่งส่วนบน (upper shoreface) ไปยังหน้าฝั่งส่วนล่าง (lower shoreface) โดยกระแสไหลย้อนกลับลงทะเล (backwash flow) ของสึนามิ

องค์ความรู้ปัจจุบันเกี่ยวกับดินตะกอนในเขตน้ำตื้นนอกชายฝั่งทราบเพียงแต่ว่า หากเป็นดินตะกอนที่ถูกพามาโดยคลื่นสึนามิ จะประกอบไปด้วยพวกเศษหินเศษกรวดจากชั้นดินชั้นหินโบราณที่โผล่พ้นแผ่นดินในยุคนั้น (Cantalamessa & Di Celma, 2005) Le Roux & Vargas (2005) ระบุว่าดัชนีที่บ่งชี้ร่องรอยของกระแสไหลย้อนของสึนามิในดินตะกอนสมัย Miocene คือ ชั้นของพวกตะกอนหินและทรายซึ่งปะปนอยู่กับหินคาร์บอเนต รวมถึงพวกหินกรวดมนใหญ่ที่ถูกคลื่นขัดจนเรียบที่แทรกอยู่ใต้ชั้นดินตะกอน แต่องค์ความรู้ในเรื่องการสะสมของดินตะกอนบริเวณตอนบนและตอนล่างของหน้าฝั่ง (shoreface) ที่เกิดจากกระแสไหลย้อนกลับลงทะเลของคลื่นสึนามิยังมีอยู่น้อย ทั้งนี้เนื่องจากงานวิจัยในเรื่องการสะสมตัวของดินตะกอนสมัย Halocene ยังมีอยู่น้อยมาก (Le Roux & Vargas 2005; Vargas et al. 2005)

เนื่องจากไม่เคยมีการบันทึกมาก่อนว่า เคยมีสึนามิเกิดขึ้นในประเทศไทย ทำให้ไม่มีการเตรียมการเพื่อรับมือกับพิบัติภัยดังกล่าวอย่างเหมาะสม แต่เหตุการณ์ที่คลื่นสึนามิขึ้นฝั่งอันดามันเมื่อวันที่ 26 ธันวาคม พ.ศ. 2547 ทำให้ทัศนคติทั่วไปที่เคยเชื่อว่า ภูมิภาคนี้ปลอดจากคลื่นยักษ์สึนามิ ได้เปลี่ยนไปอย่างสิ้นเชิง อย่างไรก็ตาม การเตรียมการเพื่อรับมือกับพิบัติภัยดังกล่าว ก็มีข้อจำกัดที่สำคัญ ได้แก่ การขาดข้อมูลความรู้เกี่ยวกับปัจจัยทางธรณีวิทยาที่พื้นทะเล ซึ่งส่งผลต่อการยกตัวของคลื่นที่เข้าสู่บริเวณชายฝั่งทะเลอันดามันของประเทศไทย อีกทั้งคลื่นยักษ์สึนามิที่เกิดขึ้นนอกจากจะทำความเสียหายต่อสังคมและ

[1] พื้นหาดใต้น้ำทะเลตั้งแต่บริเวณที่น้ำลงต่ำสุดจนถึงแนวลึกสุดที่ได้รับอิทธิพลของระลอกคลื่นแบบปกติ

ระบบนิเวศบนบกแล้ว คลื่นสึนามิยังกวาดดินปริมาตรมหาศาลลงสู่ในทะเล ทำให้เกิดการเปลี่ยนแปลงทางธรณีวิทยาและระบบนิเวศที่พื้นทะเล แต่โดยเหตุที่ผลกระทบเหล่านี้ไม่สามารถมองเห็นได้โดยตรง จึงทำให้ยังไม่มีการศึกษาในเรื่องนี้มากนัก

ข้อมูลการอุบัติและการอุบัติซ้ำของสึนามิในอดีต มีความสำคัญต่อการประเมินความเสี่ยงของพื้นที่ชายฝั่งทะเล แต่เนื่องจากคลื่นยักษ์สึนามิเป็นภัยพิบัติทางธรรมชาติที่ไม่ได้เกิดขึ้นบ่อยในประเทศไทย ดังนั้นข้อมูลของการเกิดคลื่นดังกล่าวในอดีตจึงไม่สามารถศึกษาได้โดยตรง อย่างไรก็ดี คลื่นสึนามิที่เกิดขึ้นในอดีตแต่ละครั้ง มักจะทิ้งร่องรอยบันทึกไว้เป็นหลักฐานทางธรณีวิทยา เคมี และบรรพชีวินวิทยา ซึ่งสามารถแกะรอยได้ โดยใช้เทคโนโลยีและการวิเคราะห์ทางวิทยาศาสตร์ขั้นสูง ซึ่งศักยภาพนักวิจัยของไทยยังมีอยู่จำกัด จำเป็นที่จะต้องร่วมมือกับประเทศที่มีศักยภาพดังกล่าว เพื่อเป็นการเรียนรู้เทคนิควิธีการและประสบการณ์ พร้อมไปกับการพัฒนาบุคลากรและเครือข่าย ตั้งแต่ระดับปฏิบัติการจนถึงระดับงานวิจัยขั้นสูง ซึ่งสถาบันหลายแห่งในประเทศเยอรมันได้แสดงความสนใจที่จะมีความร่วมมือในด้านนี้โดยผ่านสำนักงานคณะกรรมการวิจัยแห่งชาติ

จากการประชุมร่วมไทย-เยอรมัน NRCT-DFG Cooperative Research and Capacity Building: Ocean Geosciences, Marine Ecology and Engineering for Natural Hazard Management and Sustainable Use of Marine Resources เมื่อวันที่ 27-29 กรกฎาคม พ.ศ. 2549 ที่ประชุมมีความเห็นตรงกันว่า การศึกษาปฏิสัมพันธ์ระหว่างคลื่นสึนามิและลักษณะการกายภาพของชั้นตะกอนชายฝั่งทั้งบนบกและในทะเลมีความสำคัญ และเป็นประเด็นที่ต้องศึกษาโดยเร่งด่วน เพื่อที่จะเป็นพื้นฐานของโครงการอื่น ๆ เนื่องจากข้อมูลและความรู้ดังกล่าวมีอยู่อย่างจำกัดมาก นักวิจัยฝ่ายเยอรมันจึงได้พัฒนาชุดโครงการ TRIAS (Tracing Tsunami Impacts in the Andaman Region) เพื่อทำการศึกษาวิจัยและพัฒนาบุคลากรให้กับทางฝ่ายไทย โดยมี DFG เป็นผู้สนับสนุนทุนวิจัยทางฝ่ายเยอรมัน และสำนักงานคณะกรรมการวิจัยแห่งชาติ (NRCT) เป็นผู้สนับสนุนทุนวิจัยแก่โครงการคู่ขนานทางฝ่ายไทย

โครงการ “การเปลี่ยนแปลงของชั้นตะกอนทะเลและร่องรอยการเกิดสึนามิในอดีตจากตะกอนชายฝั่งทะเลอันดามัน” เป็นโครงการคู่ขนานกับโครงการ TUNWAT (Tsunami Deposits in Near-Shore and Coastal Waters of Thailand) ซึ่งเป็นโครงการย่อยภายใต้ชุดโครงการ TRIAS

1.2 วัตถุประสงค์

ในงานวิจัยนี้ ทำการศึกษาหลักฐานทางธรณีสัณฐาน ตะกอนวิทยา ธรณีเคมี และธรณีวิทยานอกชายฝั่งอันดามันบริเวณหน้าฝั่งด้านบน (upper shoreface) ซึ่งได้รับผลกระทบโดยตรงกระแสไหลย้อนกลับลงทะเล (backwash flow) ของสึนามิ โครงการนี้นับเป็นครั้งแรกที่ทำการประเมินผลกระทบจากคลื่นสึนามิที่มีต่อการเปลี่ยนแปลง และ/หรือ รูปแบบการแผ่กระจายของดินตะกอนบริเวณไหล่ทวีปโดยเฉพาะอย่างยิ่ง ผลที่มาจากกระแสไหลย้อนของสึนามิ

นอกจากนี้ โครงการยังมีวัตถุประสงค์ที่จะพัฒนาบุคลากรไทยให้มีความรู้เพียงพอที่จะทำการศึกษาวิจัยด้านธรณีวิทยาทางทะเลของชายฝั่งและไหล่ทวีป โดยกระบวนการ “training on the job” ทั้งในภาคสนามและขั้นตอนการวิเคราะห์และแปลผล ซึ่งดำเนินการที่ Christian-Albrechts-Universität zu Kiel ประเทศเยอรมนี

โครงการนี้เป็นโครงการ 3 ปี โดยโครงการในปีที่ 1 ทำการวิเคราะห์ผลทางธรณีฟิสิกส์ของพื้นท้องทะเลในพื้นที่ศึกษา ซึ่งยังเป็นผลเบื้องต้น โครงการในปีที่ 2 ทำการสำรวจและเก็บข้อมูลทางธรณีฟิสิกส์เพิ่มเติม เพื่อนำมาวิเคราะห์ในรายละเอียด ให้เห็นลักษณะพื้นท้องที่ถูกต้อง ที่จะนำไปแปลผลร่วมกับผลการวิเคราะห์ทางธรณีเคมี และผลการวิเคราะห์ PAHs ซึ่งเริ่มวิเคราะห์ในโครงการปีที่ 2 และโครงการปีที่ 3 ศึกษา วิเคราะห์ ตรวจสอบ และสรุปผล

1.2.1 วัตถุประสงค์ของโครงการในปีที่ 1

1.2.1.1 ศึกษาการกระจายและการสะสมในภาพรวมของพื้นที่ เพื่อสำรวจหาพื้นทะเลบริเวณที่มีดินตะกอนที่ถูกพามาโดยคลื่นสึนามิ เมื่อปี พ.ศ. 2547 โดยใช้เครื่องมือทาง hydroacoustic ได้แก่ Multi-beam echo sounding, Side-scan sonar mapping และ Boomer system

1.2.1.2 เก็บตัวอย่างดินตะกอนพื้นผิวท้องทะเล (surface sediment) ในพื้นที่ศึกษา เพื่อนำไปวิเคราะห์ทางตะกอนวิทยาและทางธรณีเคมี เพื่อหาหลักฐานทางธรณีเคมีที่สามารถใช้เป็นตัวชี้วัดการเกิดสึนามิ ได้แก่ สารโพลีไซคลิอะโรมาติกไฮโดรคาร์บอน (polycyclic aromatic hydrocarbons; PAHs) และตรวจวัดอัตราการตกตะกอนโดยใช้ไอโซโทปกัมมันตรังสี (radio isotopes)

1.2.1.3 เก็บตัวอย่างดินตะกอนตามความลึก (core sediment) ในบางพื้นที่ที่น่าสนใจ เพื่อนำไปวิเคราะห์ทางตะกอนวิทยาและทางธรณีเคมีในปีที่ 2

1.2.1.4 พัฒนาบุคลากรไทยเพื่อทำงานด้านธรณีวิทยาทางทะเลในภาคสนาม และฝึกการแปลผล Hydroacoustic data ที่ Christian-Albrechts-Universität zu Kiel ประเทศเยอรมนี

1.2.2 วัตถุประสงค์ของโครงการในปีที่ 2

1.2.2.1 สำรวจพื้นที่ท้องทะเลเพิ่มเติมอย่างละเอียด โดยใช้เครื่องมือทาง hydroacoustic เพื่อดูการกระจายและการสะสมของตะกอนอย่างละเอียด ทั้งนี้เพื่อ

- แยกดินตะกอนที่มาจากกิจกรรมการทำเหมืองดีบุก โดยเฉพาะเรือดูดแร่ ซึ่งส่งผลต่อลักษณะพื้นท้องทะเลบริเวณนั้น การแปลผลจะต้องพิจารณาอย่างรอบคอบและหา

ข้อมูลเพิ่มเติมเพื่อแยกแยะให้ชัดเจน และเพื่อป้องกันการสับสนกับลักษณะที่เกิดจากสีนามิ

- ในโครงการปี 1 พบว่า พื้นทะเลบริเวณใกล้ฝั่งมีลักษณะเป็นหย่อมดินตะกอนละเอียดแตกต่างกับดินตะกอนข้างเคียง ซึ่งจะหยาบกว่า และเห็นได้ชัดโดยเครื่อง Side Scan Sonar โดยเฉพาะอย่างยิ่งบริเวณพื้นที่ตื้นนอกแหลมปะการัง แต่ก็ยังพบได้ในเขตน้ำลึกประมาณ 30–35 เมตร เป็นลักษณะที่น่าสนใจยิ่ง ซึ่งในโครงการปีที่ 1 ข้อมูลที่ระดับน้ำลึกกว่า 30 เมตร ยังไม่สมบูรณ์ ต้องการการสำรวจยืนยันในตำแหน่งที่มีลักษณะพิเศษและน่าสงสัย เพื่อจะได้ไม่แปลผลผิดพลาด

1.2.2.2 วิเคราะห์สาร PAHs ในตัวอย่าง surface sediment ที่เก็บตัวอย่างในปีที่ 1 เพื่อเป็นข้อมูลทางธรณีเคมีที่จะใช้ยืนยันผลที่ได้จากการแปลผลข้อมูลทาง hydroacoustic ซึ่งเป็นการสำรวจทางธรณีฟิสิกส์

1.2.2.3 วิเคราะห์ตรวจวิเคราะห์องค์ประกอบธาตุของ surface sediment และ core sediment ที่ได้จากปีที่ 1

1.2.2.4 เก็บตัวอย่าง core sediment เพิ่มเติมเพื่อนำไปวิเคราะห์ทางตะกอนวิทยาและทางธรณีเคมี

1.2.2.5 พัฒนาบุคลากรไทยเพื่อทำงานด้านธรณีวิทยาทางทะเลในภาคสนาม และฝึกการแปลผล Hydroacoustic data และวิเคราะห์องค์ประกอบธาตุของดินตะกอนที่ Christian-Albrechts-Universität zu Kiel ประเทศเยอรมนี

1.2.3 วัตถุประสงค์ของโครงการในปีที่ 3

1.2.3.1 วิเคราะห์สาร PAHs ในตัวอย่าง surface sediment ที่เก็บตัวอย่างในปีที่ 1 และ 2 ให้แล้วเสร็จทั้งหมด เพื่อเป็นข้อมูลทางธรณีเคมีที่จะใช้ยืนยันผลที่ได้จากการแปลผลข้อมูลทาง Hydroacoustic ซึ่งเป็นการสำรวจทางธรณีฟิสิกส์

1.2.3.2 วิเคราะห์ตรวจวิเคราะห์องค์ประกอบธาตุของ surface sediment และ core sediment ที่ได้จากปีที่ 1 และ 2 ให้แล้วเสร็จทั้งหมด

1.2.3.3 เก็บตัวอย่าง core sediment เพิ่มเติม และไปวิเคราะห์ทางตะกอนวิทยาและทางธรณีเคมีให้แล้วเสร็จทั้งหมด

1.2.3.4 พัฒนาบุคลากรไทยเพื่อทำงานด้านธรณีวิทยาทางทะเลในภาคสนาม และฝึกการแปลผล Hydroacoustic data และวิเคราะห์องค์ประกอบธาตุของตะกอนจากข้อมูลที่ได้โดยร่วมกับนักวิจัยจาก Christian-Albrechts-Universität zu Kiel ประเทศเยอรมนี

1.3 ขอบเขตการวิจัย

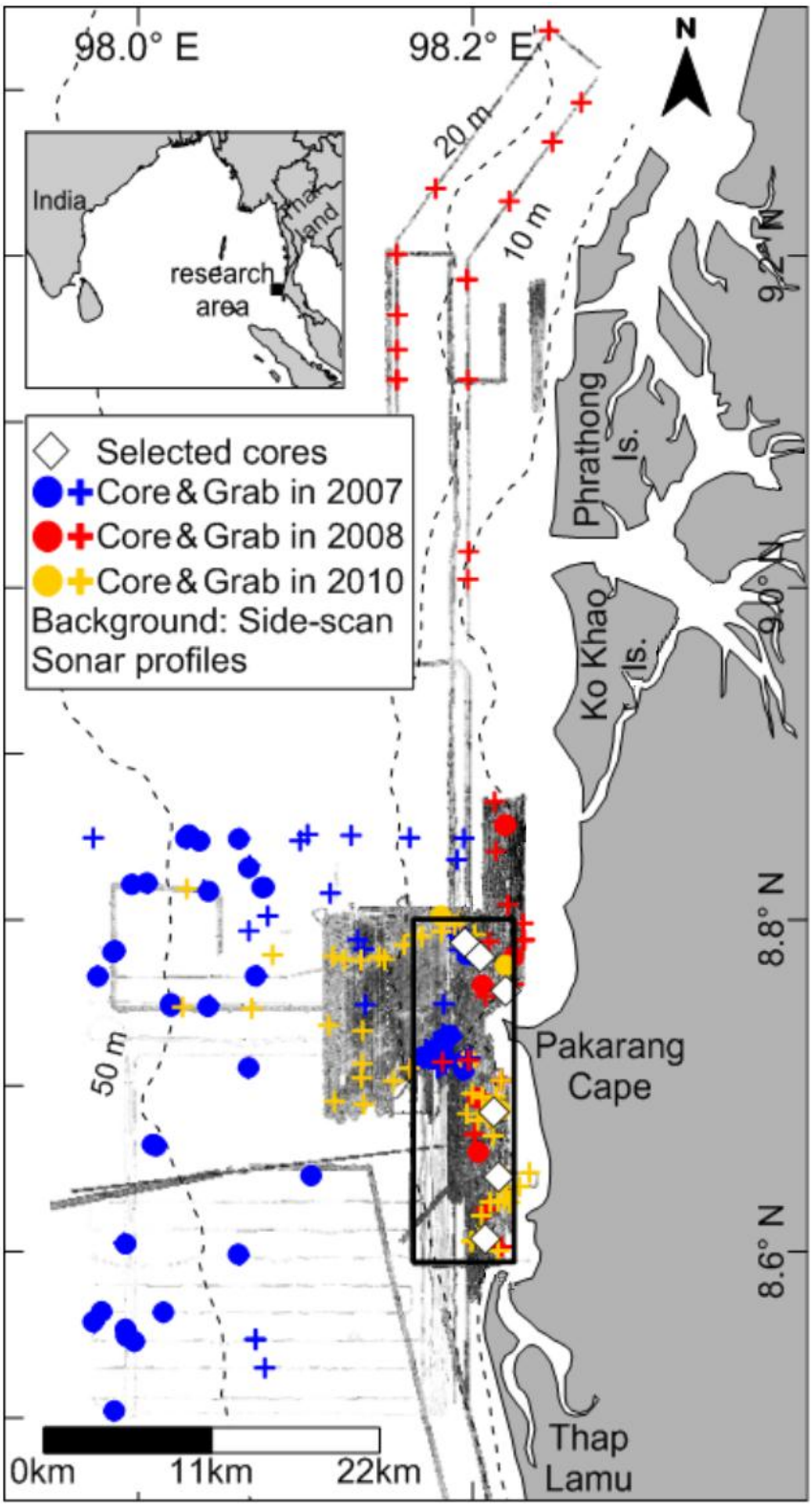
ไหล่ทวีปของทะเลอันดามันซึ่งเชื่อมต่อกับคาบสมุทรไทย-มาเลย์ (Thai-Malay Penninsula) มีลักษณะแคบและลาดเอียงสูง เส้นชั้นความลึกที่ 50 เมตรของทะเลอันดามันอยู่ห่างเพียงประมาณ 7 กิโลเมตรจากชายฝั่งจังหวัดภูเก็ต และประมาณ 30 กิโลเมตรจากชายฝั่งจังหวัดพังงา พื้นที่ชายฝั่งส่วนใหญ่เป็นผาหิน มีหาดทรายและอ่าวเป็นระยะ ๆ ลมมรสุมที่มีอิทธิพลต่อพื้นที่ศึกษา ได้แก่ ลมมรสุมตะวันออกเฉียงเหนือ ระหว่างเดือนตุลาคมถึงเดือนมีนาคม และลมมรสุมตะวันตกเฉียงใต้ ระหว่างเดือนพฤษภาคมถึงเดือนตุลาคม พายุที่รุนแรงเกิดค่อนข้างน้อย (อ้างถึงใน JANKAEW et al., 2008) น้ำขึ้นน้ำลงเป็นแบบผสม (mixed semidiurnal) อยู่ในช่วง 1.1 เมตร ถึง 3.6 เมตร (THAMPANYA et al., 2006)

พื้นที่ศึกษาอยู่นอกชายฝั่งจังหวัดพังงา ระหว่างอ่าวทับละมุและเกาะพระทอง มีพื้นที่รวมประมาณ 1,000 ตารางกิโลเมตร (25 กิโลเมตร ในแนวตะวันออก–ตะวันตก และ 40 กิโลเมตร ในแนวเหนือ–ใต้) พื้นที่ศึกษานี้เลือกจากข้อมูลที่ระบุว่าบริเวณนี้ถูกคลื่นสึนามิ เมื่อ พ.ศ. 2547 ซัดถล่มอย่างรุนแรง (รูปที่ 1-1) (BELL et al. 2005, TSUJI et al. 2006, THANAWOOD et al. 2006) มีคลื่นไหลท่วม (wave run-up) บ่าเข้าฝั่งลึกไปไกลจากแนวน้ำทะเลปกติ ถึง 15 กิโลเมตร ที่แหลมปะการัง (Pakarang Cape) (SIRIPONG 2006) และไกลถึง 20 กิโลเมตร บริเวณเกาะพระทอง (Phra Thong Island) (JANKAEW et al. 2008) พื้นที่แหลมปะการังถูกคลื่นกัดกร่อนหายไปถึงประมาณ 12,500 ตารางเมตร หรือเกือบ 8 ไร่ (รูปที่ 1-2) (SYNOLAKIS & KONG 2006) ปะการังจำนวนมากจากแนวปะการังใต้น้ำ ถูกคลื่นซัดทำลายและพาขึ้นมากองในเขตน้ำขึ้นน้ำลง (GOTO et al. 2007)

อย่างไรก็ดี ในอดีตจังหวัดพังงามีการทำเหมืองแร่ดีบุก ซึ่งมีทั้งที่ดำเนินการบนฝั่งและที่ดำเนินการนอกชายฝั่งไปจนถึงเขตน้ำลึกประมาณ 50 เมตร แต่เมื่อราคาดีบุกในตลาดโลกลดต่ำลงอย่างมาก ทำให้การทำเหมืองดีบุกในพื้นที่นี้หยุดลงมาประมาณ 20 กว่าปีแล้ว การแผ่กระจายของดินตะกอนตามพื้นท้องทะเลที่เกิดเนื่องจากการทำเหมืองแร่ดีบุกยังปรากฏเห็นได้ในบริเวณนี้ (SUWANWERAKAMTORN et al. 1990) ในพื้นที่นี้ดินตะกอนที่ถูกพามากับน้ำท่าจัดว่าน้อยมาก ดังนั้น ร่องรอยของวัสดุจากแผ่นดินที่ถูกสึนามิพาลงทับถมที่พื้นท้องทะเล จึงถูกรบกวนโดยตะกอนจากแผ่นดิน (ที่ถูกพาลงทะเลในช่วงฤดูฝน) น้อยมาก

1.4 ประโยชน์ที่คาดว่าจะได้รับ

1) แผนที่การกระจายตัวของตะกอนสึนามิบนพื้นทะเล
2) ร่องรอยและการอุบัติซ้ำของคลื่นสึนามิในอดีตบริเวณชายฝั่งทะเลอันดามัน เพื่อนำใช้ในการวางมาตรการการป้องกัน และการวางแผนเพื่อลดผลกระทบทั้งในระยะสั้นและระยะยาว
3) การพัฒนาบุคลากรวิจัยด้านธรณีวิทยาทางทะเลกระบวนการเกี่ยวกับภัยพิบัติในทะเลของประเทศ



รูปที่ 1-1 พื้นที่ศึกษานอกชายฝั่งจังหวัดพังงา ในรูปแสดงตำแหน่งการเก็บตัวอย่างตะกอนผิวหน้าและตัวอย่างตะกอนตามความลึกของทั้งโครงการฯ โดยพื้นที่ในกรอบสี่เหลี่ยมแสดงตำแหน่งที่ตัวอย่างแท่งตะกอนตามความลึกที่นำมาศึกษาทางธรณีเคมีและอายุตะกอนโดยละเอียด บนแผนภาพยังแสดงพื้นที่และเส้นทางการสำรวจด้วยเครื่องมือทางธรณีฟิสิกส์



ที่มา: Images acquired and processed by CRISP, National University of Singapore. IKONOS image © 2004. www.crisp.nus.edu.sg/tsunami/tsunami.ht

รูปที่ 1-2 แหลมปะการังซึ่งอยู่ใกล้เขาหลัก ภาพบนเป็นภาพถ่ายดาวเทียมแสดงให้เห็นการเปลี่ยนแปลงของแหลมปะการังโดยคลื่นยักษ์สึนามิเมื่อวันที่ 26 ธันวาคม พ.ศ. 2547 และภาพล่างแสดงสภาพบนพื้นดิน

1.5 การถ่ายทอดเทคโนโลยีหรือผลการวิจัยสู่กลุ่มเป้าหมายเมื่อสิ้นสุดการวิจัย

การถ่ายทอดเทคโนโลยีหรือผลการวิจัยสู่กลุ่มเป้าหมายเมื่อสิ้นสุดการวิจัย ได้วางแผนไว้ดังตารางที่ 1-2

ตารางที่ 1-2 แผนการถ่ายทอดเทคโนโลยีหรือผลการวิจัยสู่กลุ่มเป้าหมายเมื่อสิ้นสุดการวิจัย

ขั้นตอนการดำเนินงาน	ปีงบประมาณ		
	1	2	3
จัดทำระบบสารสนเทศและ Website ของโครงการวิจัย	✓	✓	✓
เผยแพร่ผลการศึกษาวิจัยแก่สาธารณะผ่านสื่อประเภทต่างๆ		✓	✓
ผลงานตีพิมพ์ในวารสารวิชาการ (จำนวนต่อปี)	1	1	1

การถ่ายทอดเทคโนโลยีได้ดำเนินการ

1) เผยแพร่ข้อมูลผ่านทาง http://www.start.or.th และ http://www.ifg.uni-kiel.de/1118.html

2) จัดทำระบบสารสนเทศเพื่อเผยแพร่ข้อมูลพื้นทะเล แต่ทั้งนี้เนื่องจากข้อมูลมีขนาดใหญ่จึงไม่สามารถนำขึ้นระบบ Website ได้ ทั้งนี้สามารถติดต่อโครงการฯ เพื่อขอรับข้อมูลเผยแพร่ได้ที่

   โครงการ “การเปลี่ยนแปลงของชั้นตะกอนทะเลและร่องรอยการเกิดสึนามิในอดีตจากตะกอนชายฝั่งทะเลอันดามัน”
   ศูนย์เครือข่ายงานวิเคราะห์วิจัยและฝึกอบรมการเปลี่ยนแปลงของโลกฯ
   จุฬาลงกรณ์มหาวิทยาลัย
   อาคารจุฬาวิชช์ 1
   ถนนอังรีดูนังต์ วังใหม่ ปทุมวัน กรุงเทพฯ 10330
   โทรศัพท์ 02-218-9465-7 โทรสาร 02-251-9416

3) ผลงานตีพิมพ์ในวารสารวิชาการ ดังรายละเอียดในหัวข้อ 1.6

1.6 ผลงานตีพิมพ์ในวารสารวิชาการ

ผลงานวิชาการจากโครงการ “การเปลี่ยนแปลงของชั้นตะกอนทะเลและร่องรอยการเกิดสึนามิในอดีตจากตะกอนชายฝั่งทะเลอันดามัน” ที่เผยแพร่ตั้งแต่เริ่มโครงการ ประกอบด้วย บทความในวารสารวิชาการ (Journal) 13 เรื่อง และบทความในการประชุมวิชาการ (Conference & Workshop) 12 เรื่อง บทความฉบับเต็มได้แนบไว้ในภาคผนวก ก

1.6.1 วารสารวิชาการ

พ.ศ. 2552 (ค.ศ. 2009)

ผลการศึกษาตอบวัตถุประสงค์ปีที่ 1 ข้อที่ 1.2.1.1

1) Feldens, P., Schwarzer, K., Szczuciński, W., Stattegger, K., Sakuna, D. and Somgpongchaiyakul, P. (2009) Impact of the 2004 Indian Ocean Tsunami on Seafloor Morphology and Sediments Offshore Pakarang Cape, Thailand. Polish J. of Environ. Stud. 18(1): 63-68.

พ.ศ. 2553 (ค.ศ. 2010)

ผลการศึกษาตอบวัตถุประสงค์ข้อที่ 1.2.1.2

1) Feldens, P., Sakuna, D., Sompongchaiyakul, P. and Schwarzer, K., (2010) Shallow water sediment structures in a tsunami-affected area (Pakarang Cape, Thailand). In Coastline Reports 2010-16 from Brazil to Thailand New Results in Coastal Research (Schwarzer, K., Schrottke, K. and Stattegger, K., eds.), p. 15-24. (ISBN: 978-3-9811839-9-3)

พ.ศ. 2555 (ค.ศ. 2012)

ผลการศึกษาตอบวัตถุประสงค์ปีที่ 1 ข้อที่ 1.2.1.2 – 1.2.1.3 และปีที่ 2 ข้อที่ 1.2.2.1 – 1.2.2.4

1) Tipmanee, D., Deelaman, W., Pongpiachan, S., Schwarzer, K. and Sompongchaiyakul, P. (2012). Using Polycyclic Aromatic Hydrocarbons (PAHs) as a Chemical Proxy to Indicate Tsunami 2004 Backwash in Khao Lak Coastal Area, Thailand. Natural Hazards and Earth System Sciences 12(5): 1441-1451.

2) Feldens, P., Schwarzer, K., Sakuna, D, Szczuciński, W. and Sompongchaiyakul, P. (2012) Sediment distribution on the inner continental shelf off Khao Lak (Thailand) after the 2004 Indian Ocean Tsunami. Earth, Planet and Space 64: 875-887.

3) Sakuna, D., Szczuciński, W., Feldens, P., Schwarzer, K., Khokiattiwong, S. (2012). "Sedimentary deposits left by the 2004 Indian Ocean tsunami on the inner continental shelf offshore Khao Lak, Andaman Sea (Thailand)", Earth Planets Space, 64, 931 - 943.

4) Pongpiachan, S., Thumanu, K., Kositanont, C., Schwarzer, K., Prietzel, J., Hirunyatrakul, P., and Kittikoon, I. (2012). “Parameters Influencing Sulfur Speciation in Environmental Samples Using Sulfur Kedge X-Ray Absorption Near-Edge Structure (XANES)”, J. Anal. Methods. Chem., Article ID 659858, 12 pages, doi: 10.1155/2012/659858

พ.ศ. 2556 (ค.ศ. 2013)

ผลการศึกษาตอบวัตถุประสงค์ปีที่ 2 ข้อที่ 1.2.2.1 และ 1.2.2.3

1) Pongpiachan, S., Thumanu, K.., Na Phatthalung, W., Tipmanee, D., Kanchai, P., Feldens, P., and Schwarzer, K. (2013) Using Fourier Transform Infrared (FTIR) to Characterize Tsunami Deposits in Near-shore and Coastal Waters of Thailand. Journal of Tsunami Society International 32(1): 39-57.

2) Pongpiachan, S., Thumanu, K.., Tanthanuch, W., Tipmanee, D., Kanchai, P., Schwarzer, K. and Tancharakorn, S. (2013) Sedimentary features of tsunami backwash deposits as assessed by micro-beam synchrotron X-ray fluorescence (μ-SXRF) at the Siam Photon Laboratory. Journal of Tsunami Society International 32(2): 96-115.

3) Pongpiachan S. and Schwarzer, K. (2013) A critical review and evaluation of applying Semi-Volatile Organic Compounds (SVOCS) as a geochemical tracer to indicate tsunami backwash: The Bilateral, Deutsche Forschungsgemeinschaft (DFG) and National Research council of Thailand (NRCT) Funded Project "Tsunami Deposits in Near-Shore- and Coastal Waters of Thailand (TUNWAT)". Journal of Tsunami Society International 32(4), 236-280.

4) Pongpiachan, S., Tipmanee, D., Deelaman, W., Muprasit, J., Feldens, P., and Schwarzer, K. (2013) Risk assessment of the presence of polycyclic aromatic hydrocarbons (PAHs) in coastal areas of Thailand affected by the 2004 tsunami. Marine Pollution Bulletin 76: 370-378.

พ.ศ. 2557 (ค.ศ. 2014)

ผลการศึกษาตอบวัตถุประสงค์ปีที่ 3 ข้อที่ 1.2.3.1 – 1.2.3.3

1) Sakuna-Schwartz, D., Feldens, P., Schwarzer, K., Khokiattiwong, S., Stattegger, K. (2014). "Internal structure of event layers preserved on the Andaman Sea continental shelf, Thailand: Tsunami vs. Storm and Flash Flood deposits", Nat. Hazards Earth Syst. Sci., Discuss., 2, 7225 – 7267, doi: 10.5194/nhessd-2-7225-2014.

2) Pongpiachan S. (2014), “Application of binary diagnostic ratios of polycyclic aromatic hydrocarbons for identification of Tsunami 2004 backwash sediments in Khao Lak, Thailand”, Scientific World Journal, volume 2014, article ID 485068, 14 pages, doi: 10.1155/2014/485068.

3) Milker, Y., Wilken, M., Schumann, J., Sakuna, D., Feldens, P., Schwarzer, K., Schmiedl, G. (2013). "Sediment transport on the inner shelf off Khao Lak Andaman Sea, Thailand) during the 2004 Indian Ocean tsunami and former storm events: evidence from foraminiferal transfer functions", Nat. Hazards Earth Syst. Sci. 13: 3113 – 3128.

1.6.2 การประชุมวิชาการ

พ.ศ. 2552 (ค.ศ. 2009)

ผลการศึกษาตอบวัตถุประสงค์ปีที่ 2 ข้อที่ 1.2.2.2

1) Pongpiachan, S., Klysubun, W., Thumanu, K., Sompongchaiyakul, P. and Bualert, S. (2009) Parameters influencing Analytical Reliability of Sulfur Speciations in Aerosol Samples Using Sulfur K-Edge X-Ray Absorption Near-Edge Structure. Asian Aerosol Conference AAC09, 24-27 Nov., 2009, Bangkok, Thailand.

2) Pongpiachan, S.; Sompongchaiyakul, P.; Deelaman, W.; Muprasit, J. and Schwarzer, K. (2009) Using PAHs as a proxy to investigate the impact of the tsunami on the distribution of terrestrial sediments in the recent deposits of the Andaman Sea. Presented in the TRIAS Workshop, 13 – 14 February 2009, Braunschweig, Germany.

3) Brückner, H.; Kelletat, D.; Vött, A.; Scheffers, A.; Scheffers, S.; Schmidt, J.-U.; Neubauer, N.-P.; Baukaew, Y. and Sompongchaiyakul, P. (2009) Tracing tsunami impacts in coastal geo and bio-archives along the west coast of Thailand – first results of the TRIAS-COAST project. Presented in the TRIAS Workshop, 13 – 14 February 2009, Braunschweig, Germany.

พ.ศ. 2553 (ค.ศ. 2010)

ผลการศึกษาตอบวัตถุประสงค์ปีที่ 1 ข้อที่ 1.2.1.1 – 1.2.1.2

1) Feldens, P., Sakuna, D., Schwarzer, K., Stattegger, K., Sompongchaiyakul, P. and Pongpiachan, S. (2010) Impacts of the 2004 Indian Ocean tsunami backwash offshore Pakarang Cape, Thailand. Paper presented at the 3rd International Tsunami Field Symposium: Science, Technology, and Disaster Mitigation, 10-11 April 2010, Tohoku University, Sendai, Japan.

2) Feldens, P., Sakuna, D., Schwarzer, K., Szczuciński, W., and Sompongchaiyakul, P. (2010) Geomorphological structures and sediment distribution offshore Pakarang Cape. Presented in the TRIAS Workshop, 26 February - 1 March 2010, Bangkok Thailand.

3) Pongpiachan, S., Sompongchaiyakul, P., Tipmanee, D., Thumanu, K., Klysubun, W., Feldens, P. and Schwarzer, K. (2010) Using Attenuated Total Reflectance Fourier Transform Infrared (ATR-FTIR) and sulfur K-edge X-ray absorption Near-Edge Structure (XANES) to characterize Tsunami deposits in near-shore and coastal waters of Thailand (TUNWAT). Presented in the TRIAS Workshop, 26 February – 1 March 2010, Bangkok Thailand.

พ.ศ. 2555 (ค.ศ. 2012)

ผลการศึกษาตอบวัตถุประสงค์ปีที่ 2 ข้อที่ 1.2.2.2 – 1.2.2.3

1) Bunsomboonsakul, S., Liu, Z.-F., Sompongchaiyakul, P., Snidvongs, A. and Krastel, S. (2012) Clay Mineralogical Records in Sediments along the Shelf Break of the Eastern Andaman Sea. (Abstract No. PP31C-2057). Paper presented at 2012 Fall Meeting, American Geological Union (AGU), 3-7 December 2012, San Francisco, California, USA.

2) Tipmanee, D., Sompongchaiyakul, P., Pongpiachan, S. and Schwarzers, K. (2012) Evidence of Land to Sea Transport caused by Tsunami 2004 backwash using Polycyclic Aromatic Hydrocarbons in Khao Lak Coastal Area of Thailand. Paper presented at the Fifth International Workshop on the Fluvial Sediment Supply to the South China Sea, November 13-16, 2012, Research Center for Geotechnology, Indonesian Institute of Sciences, Bandung, Indonesia.
3) Tipmanee, D., Pongpiachan, S., Schwarzer, K. and Sompongchaiyakul, P. (2012) Polycyclic Aromatic Hydrocarbons (PAHs) Biomarker as a Proxy for Tracing Tsunami 2004 in Khao Lak Coastal Area, Thailand. AOGS –AGU (WPGM) Joint Assembly 2012, 12-17 August 2012, Singapore.

พ.ศ. 2556 (ค.ศ. 2013)

ผลการศึกษาตอบวัตถุประสงค์ปีที่ 2 ข้อที่ 1.2.2.2 – 1.2.2.3 และปีที่ 3 ข้อที่ 1.2.3.1

1) Bunsomboonsakul, S., Liu, Z.F., Sompongchaiyakul, P., Shi, X.F., Khokiattiwong S. (2013), Clay mineralogical changes since the last glaciation in the eastern Andaman Sea and their paleoenvironmental implications, presented at the 5th National Conference of Sedimentology, Hangzhou, China.
2) Tipmanee, D., Pongpiachan, S., Schwarzer, K. and Sompongchaiyakul, P. (2013) Source Apportionment and Transport of Polycyclic Aromatic Hydrocarbons (PAHs) in Khao Lak Coastal Area, Thailand. International Conference on Environmental Pollution, Restoration and Management, 6-8 March 2013, Hanoi, Vietnam.

พ.ศ. 2558 (ค.ศ. 2015)

ผลการศึกษาตอบวัตถุประสงค์ปีที่ 3 ข้อที่ 1.2.3.1 – 1.2.3.3

1) Schwarzer, K., Feldens, P., Sakuna-Schwartz, D., Pongpiachan, S., Milker, Y., Tipmanee, D. (2015). “The Indian Ocean tsunami 2004: Identification of Tsunami Deposits in the Andaman Sea by Different Proxis”, Conference: Coastal Sediments 2015, SanDiego, DOI: 10.1142/9789814689977_0184

บทที่ 2
วิธีการดำเนินการวิจัยและสถานที่ทำการทดลอง/เก็บข้อมูล

เหตุแผ่นดินไหวเมื่อ 26 ธันวาคม พ.ศ. 2547 ที่เกิดขึ้นนอกชายฝั่งเกาะสุมาตรา ตามด้วยคลื่นยักษ์สึนามิที่เข้าถล่มแผ่นดินรอบชายฝั่งมหาสมุทรอินเดีย นับว่าเป็นเหตุการณ์คลื่นยักษ์สึนามีที่มีการบันทึกที่ดีที่สุดในประวัติศาสตร์ของมนุษย์ชาติ ณ ปัจจุบันองค์ความรู้ทางด้านนี้แทบไม่มี หรือมีก็น้อยมาก จึงเป็นโอกาสอันดีที่จะใช้บันทึกจากเหตุการณ์ครั้งนี้ในการจำแนกแจกแจงผลกระทบที่เกิดจากกระบวนการทางธรณีวิทยาในทะเล

ในงานวิจัยนี้ จึงศึกษาหลักฐานทั้งทางธรณีสัณฐาน ตะกอนวิทยา ธรณีเคมี และธรณีวิทยานอกชายฝั่งอันดามันบริเวณหน้าฝั่งด้านบน (upper shoreface) ซึ่งได้รับผลกระทบโดยตรงกระแสไหลย้อนของสึนามิ โครงการนี้นับเป็นครั้งแรกที่ทำการประเมินผลกระทบจากคลื่นสึนามิที่มีต่อการเปลี่ยนแปลงและ/หรือ รูปแบบการแพร่กระจายของตะกอนบริเวณไหล่ทวีป โดยเฉพาะอย่างยิ่งผลที่เกิดจากกระแสไหลย้อนของสึนามิ

โดยมีคำถามวิจัยเชิงวิทยาศาสตร์ของโครงการฯ ดังนี้

- คลื่นสึนามิขาเข้า (incoming tsunami) มีผลต่อรูปแบบของดินตะกอนและภูมิลักษณ์ของน่านน้ำใกล้ฝั่ง ต่อหน้าฝั่งด้านบนและด้านล่าง (upper and lower shoreface) และต่อพื้นทะเลบริเวณไหล่ทวีปอย่างไร?
- กระแสไหลย้อนของคลื่นสึนามิขาออกที่ไหลกลับลงสู่ทะเล มีผลต่อดินตะกอน รูปแบบของดินตะกอนและภูมิลักษณ์ของพื้นทะเล (sea bottom topography) ของน่านน้ำใกล้ฝั่ง หน้าฝั่ง และไหล่ทวีปอย่างไร?
- มีร่องรอยของดินตะกอนที่ถูกพาลงทะเลไปกับการไหลกลับของคลื่นสึนามิให้เห็นเด่นชัดหรือไม่?
- ดินตะกอนจะถูกคลื่นสึนามิที่ไหลกลับลงทะเลพาออกไปไกลจากชายฝั่งได้ไกลแค่ไหน?
- คลื่นสึนามิส่งผลต่อการเปลี่ยนแปลงด้านตะกอนวิทยาและโครงสร้างของตะกอนพื้นท้องทะเลได้จนถึงความลึกเท่าไรและไกลจากฝั่งออกไปเท่าไร?
- ดินตะกอนที่เกิดจากการพามาสะสมในพื้นที่นั้นโดยคลื่นสึนามิมีลักษณะเช่นไร?

นอกจากนี้ยังมีวัตถุประสงค์ที่จะพัฒนาลุคลากรไทยให้มีความรู้เพียงพอที่จะทำการศึกษาวิจัยด้านธรณีวิทยาทางทะเลของชายฝั่งและไหล่ทวีป โดยกระบวนการ “training on the job” ทั้งในภาคสนามและขั้นตอนการวิเคราะห์และแปลผลซึ่งดำเนินการที่ Kiel University ประเทศเยอรมนี

2.1 วิธีการดำเนินการวิจัย

1.2.1 วิเคราะห์ตัวอย่างและจำแนกความแตกต่างของตะกอนทะเลทางตะกอนวิทยา ธรณีเคมี และชีวเคมี

เก็บตัวอย่างตะกอน เพื่อนำมาวิเคราะห์ทางตะกอนวิทยา ธรณีเคมี และชีวเคมี เพื่อยืนยันเสริมกับแผนที่พื้นท้องทะเลทั้ง 3 รูปแบบ และผลสำรวจตัวแปรด้านตะกอนในคอลัมน์น้ำ

1) เก็บตัวอย่างตะกอนพื้นท้องทะเล โดย box-corer และ gravity-corer
2) วิเคราะห์โครงสร้าง (structure) และสมบัติทางกายภาพ (physical properties) ของตะกอน เพื่อตรวจหาร่องรอยของแร่ที่มีแหล่งที่มาจากแผ่นดิน (land derived tracer mineral) ซึ่งจะแตกต่างจากตะกอนที่มีแหล่งกำเนิดจากในทะเล
3) ถ่ายรูปตะกอนด้วยเทคนิค X-radiography เพื่อดูความแตกต่างของชั้นตะกอน เนื่องจากตะกอนไหล่ทวีปจะมีลักษณะ macroscopically uniform คือ จะมองไม่เห็นความแตกต่างหากดูด้วยตาเปล่า
4) หาอายุตะกอนโดยใช้ไอโซโทปกัมมันตรังสี ^{14}C, ^{210}Pb, ^{210}Po, ^{137}Cs และ ^{7}Be เพื่อให้ได้ข้อมูลการแบ่งชั้นของตะกอนที่แม่นยำ
5) วิเคราะห์หา PAHs (polycyclic aromatic hydrocarbons) และสัดส่วนของ PAHs ในดินตะกอน เพื่อใช้เป็น “organic tracer” ของตะกอนจากแผ่นดิน ซึ่งจะมี anthropogenic PAHs มากกว่า และยังมีสารประกอบอินทรีย์ประเภทสายตรง (aliphatics) จากพืชบก

งานวิเคราะห์ด้านตะกอนวิทยาและธรณีเคมี มีการแบ่งงานเพื่อวิเคราะห์ในห้องปฏิบัติการทั้งในประเทศเยอรมัน และประเทศไทย ดังตาราง 2-1

ตาราง 2-1 รายละเอียดงานส่วนของการวิเคราะห์ในห้องปฏิบัติการทั้งในประเทศเยอรมันและประเทศไทย

รายละเอียดงาน	ห้องปฏิบัติการ	
	ไทย	เยอรมัน
Sedimentology: Grain-size analysis, particle texture, physical properties, carbonate content, coarse-fraction components, X-radiography	✓	✓
(AMS) dating including stable isotope (C, O) analysis and U/Th dating*		✓
Radionuclide measurements (^{210}Pb, ^{210}Po, ^{137}Cs, ^{7}Be) and calculation of sedimentation rates*		✓
Carbon analytics	✓	✓
Clay mineralogy	✓	
Concentration of SVOCs and PAHs in the sediments	✓	
Data processing and analysis: multivariate statistics, GIS, geostatistics	✓	✓

1.2.2 การพัฒนาบุคลากร

เนื่องจากนักวิจัยไทยยังไม่มีประสบการณ์และความชำนาญในการใช้เครื่องมือและอุปกรณ์ดังที่กล่าวมาข้างต้นและยังขาดองค์ความรู้เพื่อประกอบการวิเคราะห์ข้อมูลเชิงธรณีฟิสิกส์และการวิเคราะห์ตะกอน ดังนั้น

1) ปีที่ 1 ได้จัดส่งบุคลากร 2 คน ไปฝึกอบรมเพื่อเรียนรู้เทคนิคและวิธีการตั้งแต่ระดับปฏิบัติการจนถึงระดับงานวิจัยขั้นสูง หลักสูตร “Introduction Marine Geophysics and Geology” นาน 4 สัปดาห์ โดยแบ่งการอบรมเป็น 2 เรื่อง คือ ความรู้เบื้องต้นเกี่ยวกับ Marine Geophysic ที่ Leibniz Institute of Marine Sciences (IFM-GEOMAR), Kiel และ Hydroacoustic ที่ Christian-Albrechts-University of Kiel
2) ปีที่ 2 ได้จัดส่งบุคลากร 1-2 คน เพื่อเรียนรู้เทคนิคการวิเคราะห์ข้อมูลทางธรณีฟิสิกส์และธรณีเคมี ที่ Christian-Albrechts-University of Kiel และสร้างความร่วมมือกันทั้งอย่างเป็นทางการและไม่เป็นทางการในการแลกเปลี่ยนความรู้ แนวความคิด และเทคโนโลยีด้านการวิจัยทางทะเลและชายฝั่ง ระหว่างนักวิจัยทั้งสองประเทศ
3) ปีที่ 3 บุคลากรที่ได้รับการพัฒนาในโครงการ 2 ปีแรก ได้จบการศึกษาแล้ว 1 คน จากจุฬาลงกรณ์มหาวิทยาลัย จะจบการศึกษา 1 คน ที่ Christian-Albrechts-University of Kiel และอีก 1 คน กำลังศึกษาระดับปริญญาเอกทางด้าน Marine Geology ซึ่งเป็นโครงการ JOINT DOCTORAL PROGRAM ภายใต้ความร่วมมือระหว่างภาควิชาวิทยาศาสตร์ทางทะเล จุฬาลงกรณ์มหาวิทยาลัย ประเทศไทย และ State Key Laboratory of Marine Geology และ School of Ocean and Earth Science, Tongji University ประเทศสาธารณรัฐประชาชนจีน โดยเป็นการพัฒนาบุคลากรทาง Marine Geology อย่างต่อเนื่องจากงานที่ดำเนินการภายใต้ความร่วมมือไทย-เยอรมัน

2.2 ทบทวนวรรณกรรม/งานวิจัยที่เกี่ยวข้อง

ที่ผ่านมาในการศึกษาร่องรอยการเกิดสึนามิ ส่วนใหญ่จะเน้นไปในด้านการวิเคราะห์ความแตกต่างของชั้นดินตะกอน (เช่น DAWSON et al. 1996, NANAYAMA et al. 2000, GOFF et al. 2001, MOORE et al. 2005, LIU et al. 2005, SUGAWARA et al. 2009) แต่การเก็บตัวอย่างดินตะกอนขึ้นมาวิเคราะห์มักไม่ได้ทำตามกระบวนการเก็บดินตะกอนเพื่อการศึกษาในเชิงตะกอนวิทยาและไม่มีการจัดทำแผนที่พื้นท้องทะเล (bathymetric map) ก่อนการเก็บตัวอย่าง แผนที่พื้นท้องทะเลและแผนที่แสดงการกระจายของตะกอน จะทำให้ระบุพื้นที่และขอบเขตของดินตะกอนที่ถูกพามากับกระแสไหลย้อนของคลื่นสึนามิ ลักษณะทางสัณฐานวิทยาของชายฝั่งนอกเขาหลัก อย่างไรก็ดี ในการวิเคราะห์ข้อมูลจำเป็นจะต้องพิจารณาอย่างถี่ถ้วน เพื่อจำแนกความแตกต่างของตะกอนที่ตกสะสมตามธรรมชาติ (natural) และที่เกิดจาก

มนุษย์ (anthropogenic) ทั้งนี้เนื่องจากในอดีตพื้นที่บริเวณนี้มีการทำเหมืองแร่ดีบุกกันมาก ดังนั้นในการจัดทำแผนที่พื้นท้องทะเลจึงมีความจำเป็น

โครงการนี้สำรวจภาคสนามและเก็บตัวอย่างตะกอนโดยเรือสำรวจจักรทอง ทองใหญ่ (รูปที่ 2-1) ของสถาบันวิจัยและพัฒนาทรัพยากรทางทะเล ชายฝั่งทะเล และป่าชายเลน จังหวัดภูเก็ต โดยใช้เครื่องมือทางธรณีฟิสิกส์ประเภทคลื่นเสียงในน้ำ (hydroacoustic) ได้แก่ เครื่องโซนาร์กวาดทางข้าง (Side Scan Sonar), ระบบวัดการสะท้อนของคลื่นไหวสะเทือนในน้ำตื้นชนิดความละเอียดสูง (Shallow Water High Resolution Reflection Seismic System หรือ Boomer System) และ เครื่องหยั่งความลึกด้วยเสียงชนิดหลายลำคลื่น (Multibeam System Echo Sounding) และสังเกตการณ์ด้วยวีดีโอใต้น้ำ (underwater-video observations) เพื่อจัดทำแผนที่พื้นท้องทะเลความละเอียดสูง จากนั้นจึงจะใช้ข้อมูลนี้ในการพิจารณาตำแหน่งเก็บตัวอย่างตะกอนดิน ทั้งแบบผิวหน้าและตามความลึกของชั้นตะกอน



รูปที่ 2-1 เรือสำรวจจักรทอง ทองใหญ่ ของสถาบันวิจัยและพัฒนาทรัพยากรทางทะเล ชายฝั่งทะเล และป่าชายเลน จังหวัดภูเก็ต กรมทรัพยากรทางทะเลและชายฝั่ง กระทรวงทรัพยากรธรรมชาติและสิ่งแวดล้อม

2.3 ระยะเวลาทำการวิจัย และแผนการดำเนินงานตลอดโครงการวิจัย

ระยะเวลาในการวิจัยทั้งหมดในโครงการ “การเปลี่ยนแปลงของชั้นตะกอนทะเลและร่องรอยการเกิดสึนามิในอดีตจากตะกอนชายฝั่งทะเลอันดามัน” รวม 3 ปี โดยพื้นที่ศึกษาผลกระทบจากคลื่นสึนามิต่อดินตะกอนพื้นทะเลจะเลือกบริเวณชายฝั่งเขาหลัก-น้ำเค็ม ซึ่งเป็นพื้นที่ที่คลื่นมีความรุนแรงสูงสุดเปรียบเทียบกับชายฝั่งหาดท้ายเหมืองซึ่งเป็นพื้นที่ที่คลื่นมีความรุนแรงไม่มาก

ทั้งนี้ตามวัตถุประสงค์ของโครงการฯ ได้ทำการสำรวจภาคสนามอย่างละเอียดในปีที่ 1 และ 2 ส่วนในปีที่ 3 ของโครงการจะเน้นการวิเคราะห์ในห้องปฏิบัติการซึ่งจะดำเนินการในห้องปฏิบัติการของภาควิชาวิทยาศาสตร์ทางทะเล จุฬาลงกรณ์มหาวิทยาลัย และ ที่ Christian-Albrechts-University of Kiel ประเทศเยอรมนี ขั้นตอนการดำเนินงานสรุปไว้ในตาราง 2-2

ตาราง 2-2 ขั้นตอนการดำเนินงานการศึกษาผลกระทบของคลื่นสึนามิต่อพื้นท้องทะเล

โครงการ/ขั้นตอนการดำเนินงาน	ปีงบประมาณ		
	1	2	3
การสำรวจโดยใช้เรือสำรวจจักรทอง ทองใหญ่			
– เก็บตัวอย่างพื้นทะเล	✓	✓	
– Multi-beam echo sounding	✓	✓	
– Side-scan sonar mapping	✓	✓	
– Boomer system	✓	✓	
การสำรวจโดยใช้เรือสำรวจขนาดเล็กเก็บตัวอย่างพื้นทะเลใกล้ชายฝั่ง			
– เก็บตัวอย่างพื้นทะเล	✓	✓	
– Echo sounding	✓	✓	
การวิเคราะห์ตัวชี้วัดทางธรณีวิทยาของตะกอนในห้องปฏิบัติการ	✓	✓	✓
การวิเคราะห์ตัวชี้วัดทางธรณีเคมีของตะกอนในห้องปฏิบัติการ		✓	✓

การทำการวิเคราะห์ตัวชี้วัดทางธรณีวิทยาของตะกอนในห้องปฏิบัติการและการวิเคราะห์ตัวชี้วัดทางธรณีเคมีของตะกอนในห้องปฏิบัติการทั้งในประเทศเยอรมันและประเทศไทย ดังรายละเอียดการปฏิบัติงานแสดงในตาราง 2-1

2.4 รายละเอียดการดำเนินงานตามแผนงานวิจัย

2.4.1 เครื่องมือสำรวจทางธรณีฟิสิกส์และเก็บตัวอย่างตะกอนที่ใช้ในเรือสำรวจ

1. เครื่องหยั่งความลึกด้วยเสียงชนิดหลายลำคลื่น (Multibeam System Echo Sounding)
   วัตถุประสงค์ สร้างแผนที่ท้องทะเล (bathymetric maps)
   ความถี่ที่ใช้ 180 kHz
   ยี่ห้อ-รุ่น SeaBeam 1185 (L3 Communication / ELAC Nautik)

2. เครื่องโซนาร์กวาดทางข้าง (Side Scan Sonar) ชนิดความละเอียดสูง

   วัตถุประสงค์ สร้างแผนที่การแพร่กระจายของตะกอน (ร่วมกับข้อมูลตะกอนวิทยา)

   ความถี่ที่ใช้ 384 kHz

   ยี่ห้อ-รุ่น KLEIN 595 towfish & control unit และ digital data acquisition พร้อมTRITON-software

3. ระบบวัดการสะท้อนของคลื่นไหวสะเทือนในน้ำตื้นชนิดความละเอียดสูง (Shallow Water High Resolution Reflection Seismic System หรือ Boomer System)

   วัตถุประสงค์ ข้อมูลด้านโครงสร้างของชั้นตะกอนด้านบน (Subsurface Structure)

   ความถี่ที่ใช้ 0.3 – 7 kHz

   ยี่ห้อ-รุ่น EG&G boomer system

4. Van-Veen-Grab-Sampler

   วัตถุประสงค์ เก็บตัวอย่างตะกอนดินที่ผิวหน้าพื้นท้องทะเล

5. RUMOHR gravity corer

   วัตถุประสงค์ เก็บตัวอย่างตะกอนดินพื้นท้องทะเลตามความลึก

2.4.2 ระบบนำร่องสำหรับเครื่องมือสำรวจ

ระบบนำร่องสำหรับเครื่องมือสำรวจทางธรณีฟิสิกส์ ปกติใช้ระบบกำหนดพิกัดบนพื้นโลก (GPS System) ที่ติดตั้งมากับเรือสำรวจ แต่ในการปฏิบัติงานในทะเลครั้งนี้ได้ใช้ระบบ GPS 2 ชุด โดยใช้ระบบที่ติดตั้งมากับเรือสำหรับการเดินเรือ ซึ่งจะเรียกว่า “Bridge-GPS” และใช้ระบบ GPS อีกชุดหนึ่งสำหรับเครื่องมือ ซึ่งจะเรียกว่า “Lab-GPS” ระบบ GPS ทั้ง 2 ชุดนี้ มีค่าแตกต่างกันเล็กน้อยดังสมการ

$$\text{Bridge-GPS} = \text{Lab-GPS} - 0^\circ\ 0.144'\ \text{N} + 0^\circ\ 0.260'\ \text{E}$$

ค่าความแตกต่างกันนี้คงที่ตลอดระยะเวลาการปฏิบัติการในทะเล ข้อมูลที่ได้จากการสำรวจและตำแหน่งการเก็บตัวอย่างจะรายงานโดยใช้พิกัดที่อ่านได้จาก Lab-GPS ทั้งนี้ยังไม่ทราบว่าเครื่องชุดใดที่ให้ค่าถูกต้องที่สุด จึงได้เทียบตำแหน่งที่ตั้งที่แน่นอนของท่าเทียบเรือสถาบันวิจัยและพัฒนาทรัพยากรทางทะเล ชายฝั่งทะเล และป่าชายเลน จ.ภูเก็ต เป็นจุดอ้างอิงในแผนที่

2.4.3 การปฏิบัติงานสำรวจทางธรณีฟิสิกส์บนเรือสำรวจ

ในการสำรวจภาคสนามในปีที่ 1 ของโครงการ ใช้เรือสำรวจจักรทอง ทองใหญ่ (รูปที่ 2-1) ของสถาบันวิจัยและพัฒนาทรัพยากรทางทะเล ชายฝั่งทะเล และป่าชายเลน จ.ภูเก็ต โดยต้องการที่จะเห็นลักษณะของพื้นท้องทะเลโดยรวม และรู้ถึงลักษณะทางตะกอนวิทยา ทางธรณีวิทยา และการแบ่งชั้นของชั้นตะกอนที่สะสมในบริเวณน้ำลึกตั้งแต่ 10 ถึง 80 เมตรโดยประมาณ การสำรวจเพื่อจัดทำแผนที่พื้นท้องทะเลติดตั้งและใช้เครื่องมือทางธรณีฟิสิกส์ดังนี้

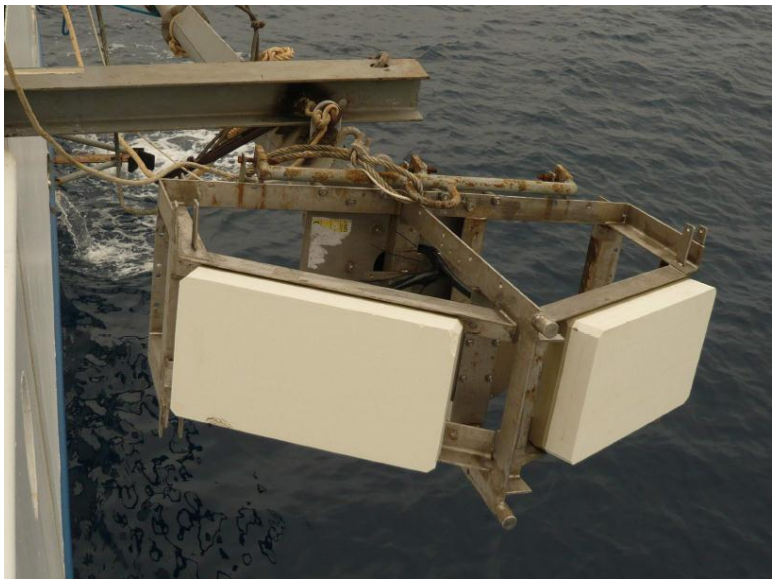
2.4.3.1 เครื่องหยั่งความลึกด้วยเสียงสะท้อนชนิดหลายลำคลื่น (Multibeam echo-sounder)

เครื่องหยั่งความลึกด้วยเสียงสะท้อนชนิดหลายลำคลื่น หรือ Multibeam echo-sounder จะเก็บข้อมูลพื้นท้องทะเลในพื้นที่ที่กว้างกว่าเครื่องส่งเสียงสะท้อน (echo-sounder) แบบปกติทั่วไปที่ใช้ลำคลื่นเดี่ยว (single beam) เนื่องจากวิจัยครั้งนี้อยู่ในเขตน้ำที่ค่อนข้างตื้น จึงเลือกใช้เครื่องหยั่งความลึกด้วยเสียงสะท้อนชนิดหลายลำคลื่นที่มีตัวแปรสัญญาณแบบที่ใช้ในน้ำตื้น ซึ่งมีความถี่ที่ 180 KHz โดยมีข้อมูล CTD (conductivity, temperature และ depth) เป็นตัวปรับเทียบกับความเร็วเสียงที่แท้จริงในน้ำ การติดตั้งทำโดยติดตั้งกับเสาที่ต่อยื่นออกไปข้างลำตัวเรือ (รูปที่ 2-2) และสามารถปรับลดระดับของเครื่องให้จมลงใต้ผิวน้ำได้เมื่อต้องการตรวจวัด และยกขึ้นระหว่างมีการเก็บตัวอย่างดินตะกอนหรือระหว่างเรือแล่นเป็นระยะทางยาว ดังนี้

- ตำแหน่งเครื่องรับสัญญาณการเคลื่อนไหว (motion sensor) เป็นตำแหน่งที่ใช้เป็นจุดอ้างอิง
- สายอากาศสำหรับเครื่องหาตำแหน่งบนพื้นโลก (GPS-antenna) ติดตั้งในตำแหน่ง 50 เซนติเมตร ทางด้านหน้า 210 เซนติเมตร ทางกาบขวาของเรือ และ 347 เซนติเมตร เหนือเครื่องรับ
- ตำแหน่งกึ่งกลางของตัวแปรสัญญาณตัวขวา (starboard transducer) อยู่ที่ตำแหน่ง 130 เซนติเมตร ไปทางด้านซ้าย และ 608 เซนติเมตร ต่ำกว่าเครื่องรับ
- ตำแหน่งกึ่งกลางของตัวแปรสัญญาณตัวซ้าย (port transducer) อยู่ที่ตำแหน่ง 178 เซนติเมตร ไปทางด้านซ้าย และ 608 เซนติเมตร ต่ำกว่าเครื่องรับ

ข้อมูลจากเครื่องหยั่งความลึกด้วยเสียงสะท้อนชนิดหลายลำคลื่น จะถูกบันทึกโดย software HydroStar ในระบบ non-proprietary XSE และ ELAC-Nautik specific DAT format

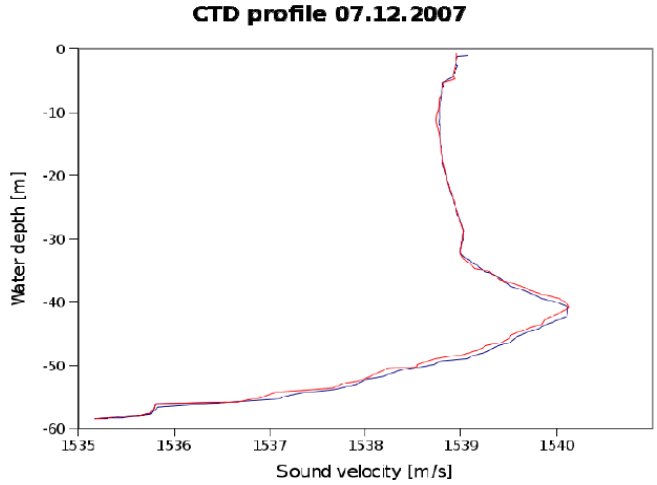
ในการปรับเทียบความเร็วของเสียงที่ผ่านน้ำสำหรับเครื่องหยั่งความลึกด้วยเสียงสะท้อนชนิดหลายลำคลื่น ใช้ข้อมูลความเร็วเสียงตามความลึก (sound velocity profile) ที่ได้จาก CTD ซึ่งเป็นข้อมูลความเร็วเสียงตามความลึกที่ตรวจวัดได้ขณะดำเนินการศึกษาครั้งนี้ รูปที่ 2-3 เป็นตัวอย่างข้อมูลความเร็วเสียงตามความลึกที่ได้จาก CTD ในสันที่ 7 ธันวาคม พ.ศ. 2550



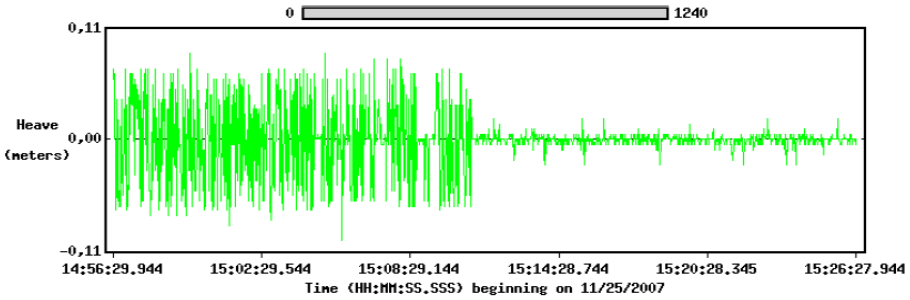


รูปที่ 2-2 เครื่องหยั่งความลึกด้วยเสียงสะท้อนชนิดหลายลำคลื่น (multibeam echo sounder) และการติดตั้งทางกาบเรือด้านขวา

อย่างไรก็ดี ข้อมูลจากเครื่องหยั่งความลึกด้วยเสียงสะท้อนชนิดหลายลำคลื่น ในช่วง 20071125145631018 พบว่าเกิดการขัดข้องในหน่วยควบคุมการป้อน heave data ซึ่งเป็นข้อมูลจากเครื่องรับสัญญาณการเคลื่อนไหว (motion sensor) ที่ใช้ปรับแก้ความคลาดเคลื่อนของข้อมูลความลึกน้ำ (bathymetric data) ซึ่งเกิดจากการรบกวนจากคลื่นอื่น (รูปที่ 2-4) ทำให้คุณภาพข้อมูลจากเครื่องหยั่งความลึกด้วยเสียงสะท้อนชนิดหลายลำคลื่นลดลง เนื่องจากทุกครั้งของการเคลื่อนเรือจะก่อให้เกิดคลื่นรบกวนและถูกบันทึกลงในข้อมูลความลึกน้ำ จึงได้ทำการแก้ไขโดยแยกการเก็บ heave data ด้วยเครื่องคอมพิวเตอร์อีกเครื่องหนึ่ง เนื่องจากเครื่องรับสัญญาณการเคลื่อนไหว (motion sensor) ยังทำงานเป็นปกติ เพื่อนำข้อมูลดังกล่าวมาปรับแก้ในภายหลัง



รูปที่ 2-3 ความเร็วเสียงตามความลึกที่ตรวจวัดได้จากหัวอ่าน CTD (CTD sound velocity profile) ในวันที่ 7 ธันวาคม พ.ศ. 2550 เส้นสีฟ้าแสดงข้อมูลความเร็วเสียงขณะหย่อนหัวอ่านลงตามความลึกน้ำ และเส้นสีแดงแสดงข้อมูลความเร็วเสียงขณะดึงหัวอ่านขึ้นจากตามความลึกน้ำ



รูปที่ 2-4 ระหว่างบันทึก profile 20071125145631018 หน่วยควบคุมการป้อน heave data เกิดการขัดข้องชื่อไฟล์ที่ใช้เก็บข้อมูลจากเครื่องหยั่งความลึกด้วยเสียงสะท้อนชนิดหลายลำคลื่น อยู่ในรูปแบบ "day-month-year-number-subsample" เช่น 05120747B ตัวเลขจะเพิ่มขึ้นเป็นลำดับตลอดช่วงการปฏิบัติการ

2.4.3.2 เครื่องโซนาร์กวาดทางข้าง (Side Scan Sonar)

การสำรวจด้วยเครื่องโซนาร์กวาดทางข้าง หรือ Side Scan Sonar (รูปที่ 2-5) ดำเนินการตรวจวัดพื้นท้องทะเลด้วยคลื่นเสียงความถี่สูง (high frequency acoustic waves) โดยตัวแปรสัญญาณ (transducer) จะปล่อยคลื่นเสียงความถี่สูงออกไปและรับคลื่นเสียงที่สะท้อนจากพื้นท้องทะเล ความเข้ม (intensity) ของสัญญาณที่สะท้อนกลับก็จะถูกแสดงผลออกมา

ข้อมูลที่ได้จากเครื่องโซนาร์กวาดทางข้าง จะนำไปแปลผลร่วมกับผลวิเคราะห์ทางตะกอนวิทยาและธรณีเคมีของตะกอนตัวอย่างที่เก็บกลับไปวิเคราะห์ในห้องปฏิบัติการ จึงจะสามารถสร้างแผนที่พื้นท้องทะเลออกมาได้ เนื่องจากเครื่องโซนาร์กวาดทางข้างจะให้เฉพาะข้อมูลสมบัติทางเสียง (acoustic properties) ของพื้นท้องทะเล ซึ่งเป็นข้อมูลทางกายภาพ แต่ยังไม่สามารถบ่งบอกประเภทของตะกอน ทั้งนี้เพราะว่าขนาดของพลังงานที่สะท้อนกลับมานั้นขึ้นกับปัจจัยอีกหลายประการ ปัจจัยที่สำคัญ ได้แก่ การกระจายขนาดของอนุภาค (grain size distribution) ความหยาบของพื้นท้องทะเล (seafloor roughness) และมุมลาดเอียง (slope angle)

ในการสำรวจอาจจะมีคลื่นเสียงใต้น้ำซึ่งเกิดจากการหมุนของตัวแปรสัญญาณหรือการเปลี่ยนความเร็วของเรือที่ลากเครื่องมือ ระบบที่ใช้ในการศึกษาครั้งนี้ คือ “Klein Dual Frequency Sonar System 595” ที่คลื่นความถี่ 384 KHz โดยลากทางด้านท้ายเรือ โดยเครื่องจะตั้งอยู่บนทุ่นลอยซึ่งจะด้านล่างถ่วงด้วยน้ำหนัก 90 กก. เพื่อทำให้ตัวเครื่องเสถียรและตัดสัญญาณรบกวนอันเนื่องมาจากการเครื่องที่ของเรือ ข้อมูลที่ได้บันทึกด้วย ISIS Sonar Software 4.5.4 ซึ่งพัฒนาขึ้นโดย Triton Elics จากนั้นประมวลผลด้วย ISIS Sonar-software 6.0.6 และ Delph Map 2.9 (Triton Elics)

ชื่อไฟล์ที่ใช้เก็บข้อมูลจากเครื่องโซนาร์กวาดทางข้างอยู่ในรูปแบบ "day-month-year-number" ปรับตั้งตัวเลขให้เริ่มต้นที่ 1 ในแต่ละวันใหม่ ในกรณีที่ระบบรวนหรือมีการเปลี่ยนระดับลึกของการลากเครื่องมือ ทำการบันทึกข้อมูลโดบใช้ไฟล์ใหม่ซึ่งใช้ชื่อเดิม แต่ให้เติม b หรือ c, d,... ต่อท้าย โดยจะตั้งชื่อไฟล์ของข้อมูลที่ได้จากเครื่องโซนาร์กวาดทางข้าง (Side Scan Sonar) และเครื่องวัดการสะท้อนของคลื่นไหวสะเทือน (Boomer) ให้อยู่ในชื่อเดียวกัน

2.4.3.3 ระบบวัดการสะท้อนของคลื่นไหวสะเทือน (Boomer System)

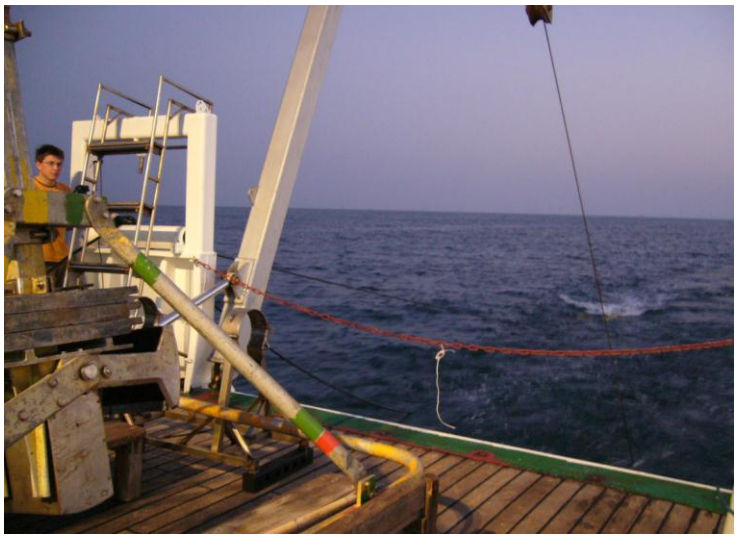
การสำรวจด้วยระบบวัดการสะท้อนของคลื่นไหวสะเทือนในน้ำตื้นชนิดความละเอียดสูง (shallow water high resolution reflection seismic system) หรือ Boomer system (รูปที่ 2-6) จะให้ข้อมูลชั้นตะกอนด้านบน (subsurface) ของพื้นท้องทะเล โดยตัวแปลงสัญญาณ 2 ชุด จะส่งคลื่นเสียงความถี่ต่ำที่ประมาณ 300 ถึง 7,000 Hz ออกไป คลื่นเสียงความถี่ต่ำนี้จะแทรกผ่านน้ำลงไปและสามารถทะลุผ่านชั้นตะกอนได้ลึกประมาณ 20 ถึง 60 เมตร ขึ้นกับลักษณะของตะกอนและพลังงานของสัญญาณเสียงที่ส่งออกไป ความเข้มสูงสุดของคลื่นเสียงที่ระบบวัดการสะท้อนของคลื่นไหวสะเทือนในน้ำสามารถส่งออกไปได้อยู่ที่ประมาณ 4,000 Hz



รูปที่ 2-5 เครื่องโซนาร์กวาดทางข้าง (Side Scan Sonar) และปฏิบัติการขณะปล่อยลงทะเลเพื่อลากสำรวจ







รูปที่ 2-6 ระบบวัดการสะท้อนของคลื่นไหวสะเทือน (Boomer System) บนชุดลากจูงและปฏิบัติการ ขณะปล่อยลงทะเลเพื่อลากสำรวจ

บริเวณรอยต่อระหว่างน้ำกับตะกอนคลื่นเสียงจะสะท้อนกลับ ขึ้นกับความต้านทานต่อการผ่านของเสียง (acoustic impedance) ที่แตกต่างกันของวัตถุที่ตกกระทบ โดยมีไฮโดรโฟนที่ลากเรียงกันเป็นแถว(hydrophone array) อยู่ด้านท้ายเรือ เป็นตัวรับสัญญาณคลื่นเสียงที่สะท้อนกลับ ข้อมูลเสียงสะท้อนจะถูกบันทึกโดย software NWC 1.4.1 (Nautic Seismic Recording System) ซึ่งพัฒนาโดย Nautik Nord GmBH

ชื่อไฟล์ที่ใช้เก็บข้อมูลจากระบบวัดการสะท้อนของคลื่นไหวสะเทือนในน้ำ อยู่ในรูปแบบ "day-month-year-number" ปรับตั้งตัวเลขให้เริ่มต้นที่ 1 ในแต่ละวันใหม่ ในกรณีที่ระบบรวน ทำการบันทึกข้อมูลโดบใช้ไฟล์ใหม่ซึ่งใช้ชื่อเดิม แต่ให้เติม b หรือ c, d,... ต่อท้าย โดยจะตั้งชื่อไฟล์ของข้อมูลให้อยู่ในชื่อเดียวกันกับที่ได้จากเครื่องโซนาร์กวาดทางข้าง

2.4.4 การเก็บตัวอย่างดินตะกอนเพื่อวิเคราะห์ทางตะกอนวิทยาและธรณีเคมี

ตำแหน่งในการเก็บตัวอย่างดินตะกอนทั้งดินตะกอนผิวหน้าและดินตะกอนตามความลึกเลือกโดยอาศัยข้อมูลพื้นท้องทะเลจากแผนที่พื้นท้องทะเลที่จัดทำขึ้น

2.4.4.1 การเก็บตัวอย่างดินตะกอนผิวหน้า

เก็บตัวอย่างดินตะกอนผิวหน้าพื้นท้องทะเลด้วยเครื่องมือเก็บตัวอย่างดินตะกอนแบบ Van-Veen Grab Sampler ในจุดเก็บตัวอย่างที่กำหนดจากข้อมูลที่ได้จากการสำรวจทางธรณีฟิสิกส์ เมื่อได้ตัวอย่างดินตะกอนผิวหน้าที่ได้จากแต่ละจุดเก็บตัวอย่าง ทำการบันทึกภาพ ตรวจสอบลักษณะทั่วไปของดินตะกอน (รูปที่ 2-7) และแบ่งตัวอย่างออกเป็น 4 ส่วน สำหรับวิเคราะห์ทางตะกอนวิทยาและธรณีเคมีในห้องปฏิบัติการ โดยส่วนที่จะนำไปวิเคราะห์ polycyclic aromatic hydrocarbons (PAHs) นำเก็บรักษาโดยการแช่แข็ง

2.4.4.2 การเก็บตัวอย่างดินตะกอนตามความลึก

เก็บตัวอย่างดินตะกอนผิวหน้าพื้นท้องทะเล ด้วยเครื่องมือเก็บตัวอย่างดินตะกอนแบบ Rumohr Gravity Corer ในจุดเก็บตัวอย่างที่กำหนดจากข้อมูลที่ได้จากการสำรวจทางธรณีฟิสิกส์ เพื่อดูโครงสร้างของชั้นดินตะกอน ความยาวของท่อดินตะกอนที่ได้ประมาณ 2 เมตร เก็บรักษาตัวอย่างโดยวางตัวอย่างในแนวตั้ง (รูปที่2-8) สำหรับวิเคราะห์ทางตะกอนวิทยาและธรณีเคมีในห้องปฏิบัติการ

ภาระกิจในการสำรวจแต่ละครั้ง (ตารางที่ 2-3) ประกอบด้วย เส้นทางสำรวจและตรวจวัดคลื่นเสียงใต้น้ำ โดยโซนาร์กวาดทางข้าง (Side Scan Sonar) เครื่องวัดคลื่นไหวสะเทือนในน้ำ (Boomer System) และเครื่องหยั่งความลึกด้วยเสียงสะท้อนชนิดหลายลำคลื่น (Multibeam echo-sounder) แสดงในรูปที่ 2-9 ตำแหน่งจุดเก็บตัวอย่างดินตะกอนผิวหน้าและดินตะกอนตามความลึก แสดงในรูปที่ 2-10 และ 2-11 ตามลำดับ ข้อมูลที่ได้จากสัญญาณที่ส่งกลับมายังเครื่องรับสัญญาณของเครื่องมือเหล่านี้จะถูกส่งเข้าเครื่องประมวลผลในห้องประมวลผลภายใน เรือสำรวจจักรทอง ทองใหญ่ (รูปที่ 2-12)

ตารางที่ 2-3 ภาระกิจในแต่ละวันระหว่างการสำรวจพื้นท้องทะเลฝั่งอันดามัน

วันสำรวจ	ภาระกิจ	หมายเหตุ	เครื่องมือที่ใช้
วันที่ 1	— ออกเดินทางจากท่าเทียบเรือสถาบันวิจัยและพัฒนาทรัพยากรทางทะเล ชายฝั่งทะเล และป่าชายเลน จ.ภูเก็ต — ทำการตรวจวัดทาง hydroacoustic		Side Scan Sonar, Boomer, Multibeam
วันที่ 2 - 6	ทำการตรวจวัดทาง hydroacoustic	พบโครงสร้างพื้นทะเลในบริเวณใกล้ฝั่ง มีลักษณะเป็นร่องๆ พาดยาวตลอดตะวันตกเฉียงเหนือ–ตะวันออกเฉียงใต้ (NW–SE) ภายในร่องมีตะกอนละเอียดสะสม โดยเฉพาะทางตอนเหนือของพื้นที่ศึกษา ซึ่งเคยมีการทำเหมืองแร่ดีบุกกันมาก	Side Scan Sonar, Boomer, Multibeam
วันที่ 7	• เก็บตัวอย่างดินตะกอนทางตอนเหนือของพื้นที่สำรวจ • ทำการตรวจวัดทาง hydroacoustic		Side Scan Sonar, Boomer, Multibeam, Grab Sampler, Gravity Corer
วันที่ 8	• เก็บตัวอย่างดินตะกอนทางตอนเหนือของพื้นที่สำรวจ • ทำการตรวจวัดทาง hydroacoustic • ปรับเทียบมาตรฐานระบบ multibeam	เติมน้ำเข้าถังเก็บน้ำในเรือ	Side Scan Sonar, Boomer, Multibeam, Grab Sampler, Gravity Corer
วันที่ 9	• เก็บตัวอย่างดินตะกอนทางตอนเหนือของพื้นที่สำรวจ • ทำการตรวจวัดทาง hydroacoustic	ตัวอย่างตะกอนจาก Grab รหัส 02120712 มีองค์ประกอบที่คาดว่าน่าจะเป็นหญ้าจากแผ่นดิน	Side Scan Sonar, Boomer, Multibeam, Grab Sampler, Gravity Corer
วันที่ 10	• ทำการสำรวจเต็มรูปแบบบริเวณแนวร่องใกล้แหลมปะการัง	ข้อมูล Side Scan Sonar ขัดข้อง	Side Scan Sonar, Boomer, Multibeam
วันที่ 11	• ทำการสำรวจเต็มรูปแบบบริเวณแนวร่องใกล้แหลมปะการัง • เก็บตัวอย่างตะกอนนอกแนวร่อง		Side Scan Sonar, Boomer, Multibeam, Grab Sampler, Gravity Corer
วันที่ 12	• ทำการตรวจวัดทาง hydroacoustic ในแนวตั้งฉากกับชายฝั่ง		Side Scan Sonar, Boomer, Multibeam

ตารางที่ 2-3 (ต่อ)

วันสำรวจ	ภาระกิจ	หมายเหตุ	เครื่องมือที่ใช้
วันที่ 13	• ทำการตรวจวัดทาง hydroacoustic ในแนวตั้งฉากกับชายฝั่ง • เก็บตัวอย่างตะกอนทางตอนใต้ของพื้นที่สำรวจ • ทำการตรวจวัด CTD (conductivity, temperature, depth)		Side Scan Sonar, Boomer, Multibeam, Grab Sampler, Gravity Corer
วันที่ 14	• ทำการสำรวจเต็มรูปแบบบริเวณแนวร่องใกล้แหลมปะการัง • เก็บตัวอย่างตะกอนใกล้แหลมปะการังนอกแนวร่องที่ 2 • บันทึกภาพวีดีทัศน์ใต้น้ำเหนือแนวร่อง	เกิดอุบัติเหตุถังน้ำอับเฉาเรือแตก	Side Scan Sonar, Boomer, Multibeam, Grab Sampler, Gravity Corer, underwater video camera
วันที่ 15	• เดินทางกลับและเทียบท่าที่ท่าเทียบเรือของสถาบันวิจัยและพัฒนาทรัพยากรทางทะเล ชายฝั่งทะเล และป่าชายเลน		

หมายเหตุ:

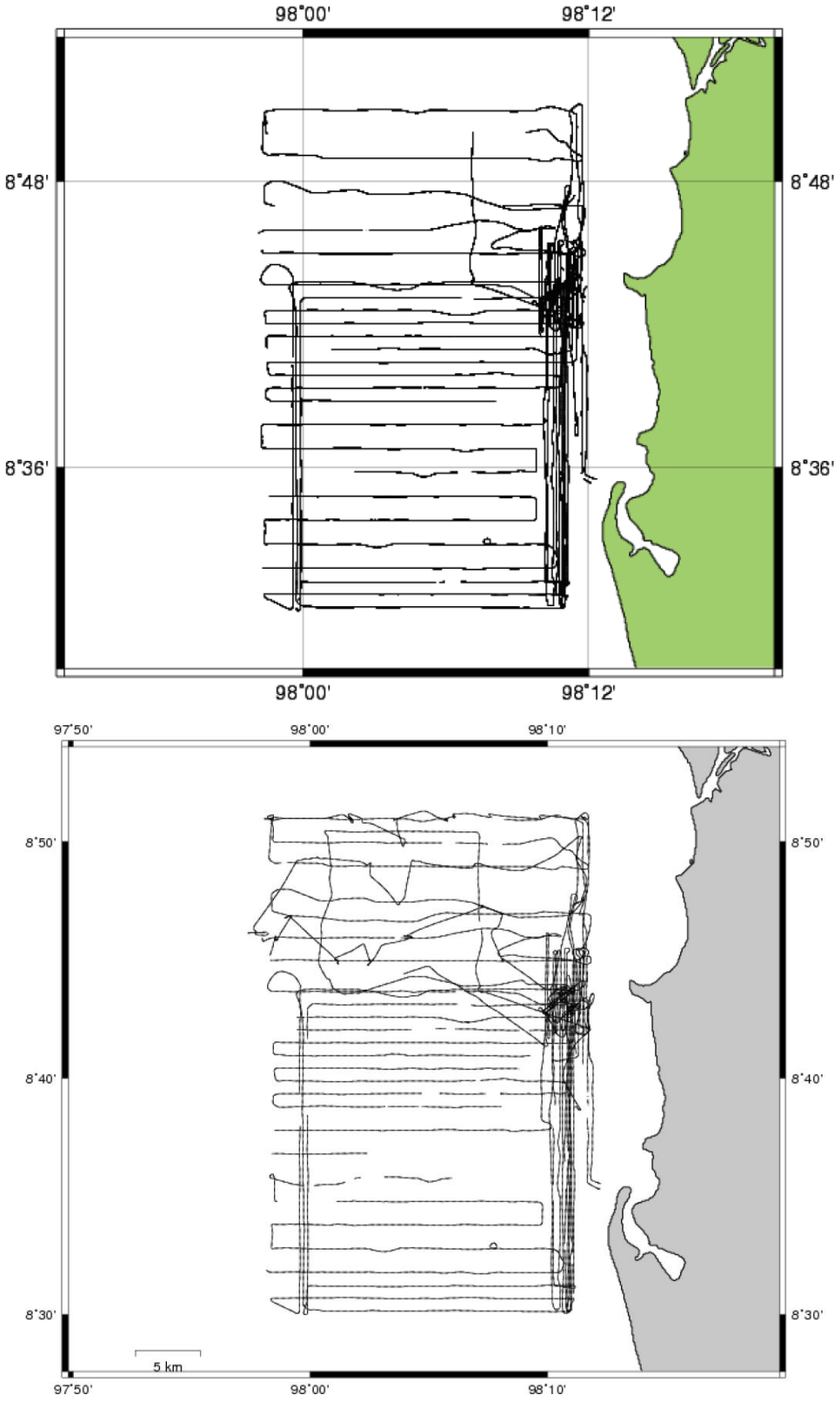
- เนื่องจากเรือสำรวจจักรทอง ทองใหญ่ มีขนาดค่อนข้างใหญ่ การตรวจวัดทาง hydroacoustic ในแนวใกล้ฝั่งจึงทำได้เฉพาะในช่วงเวลากลางวันเท่านั้น นอกจากนี้ในช่วงเวลากลางคืนยังมีเรือประมงขนาดเล็กมากมายทำให้ไม่สามารถทำการตรวจวัดได้ เนื่องจากมีความเสี่ยงสูงที่จะทำให้เครื่องมือเสียหาย หากลากจูงเครื่อง Side Scan Sonar และ Multibeam ผ่านเครื่องมือประมงในช่วงเวลากลางคืน
- แนวร่องในบริเวณใกล้ฝั่ง ซึ่งพาดในแนวตะวันตกเฉียงเหนือ–ตะวันออกเฉียงใต้ (NW–SE) ซึ่งตรวจพบในช่วง 2-3 วันแรกของการสำรวจ พบว่าตะกอนที่สะสมในร่องที่อยู่ทางด้านใต้มีลักษณะแตกต่างจากตะกอนบริเวณใกล้เคียงอย่างชัดเจน ดังนั้นจึงได้ทำการสำรวจเต็มรูปแบบบริเวณแนวร่องใกล้แหลมปะการัง นอกจากนี้ยังพบร่องลึกทางตอนเหนือของพื้นที่ศึกษา ซึ่งอาจเป็นร่องรอยของการทำเหมืองแร่ดีบุกในอดีต
- ตำแหน่งการเก็บตัวอย่างตะกอน กำหนดโดยใช้ข้อมูลที่ได้จาก Side Scan Sonar และ Boomer ในวันก่อนหน้าการเก็บตัวอย่าง
- ในวันที่ 14 เกิดอุบัติเหตุถังน้ำอับเฉาเรือแตก ทำให้เรือไม่สามารถควบคุมสมดุลได้ ด้วยเหตุผลในเรื่องความปลอดภัยจึงได้ตัดสินใจยุติการสำรวจ และเดินทางกลับสถาบันวิจัยและพัฒนาทรัพยากรทางทะเล ชายฝั่งทะเล และป่าชายเลน



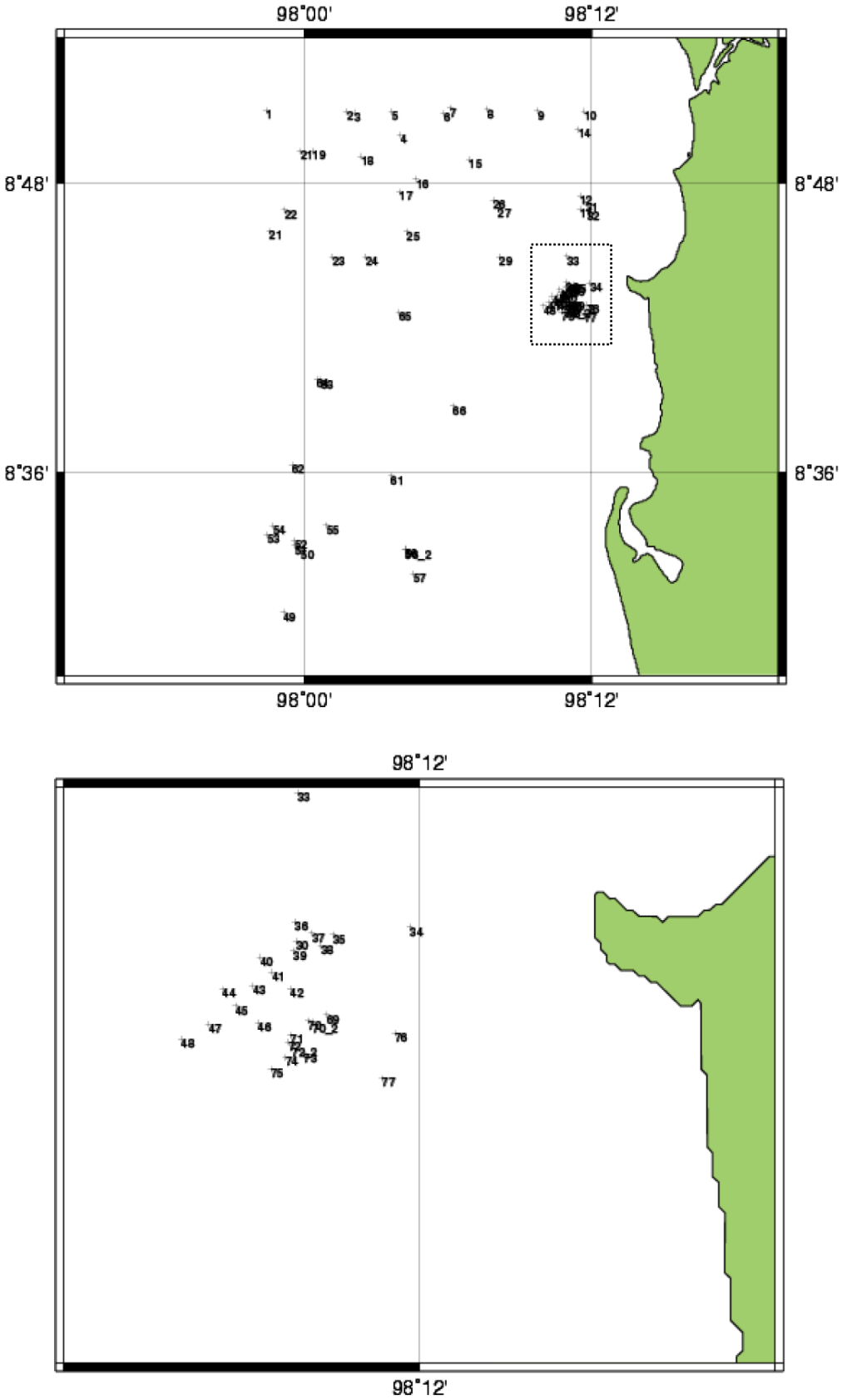
รูปที่ 2-7 การเก็บตัวอย่างดินตะกอนโดย Van-Veen Grab Sampler และการตรวจสอบลักษณะทั่วไปของดินตะกอน



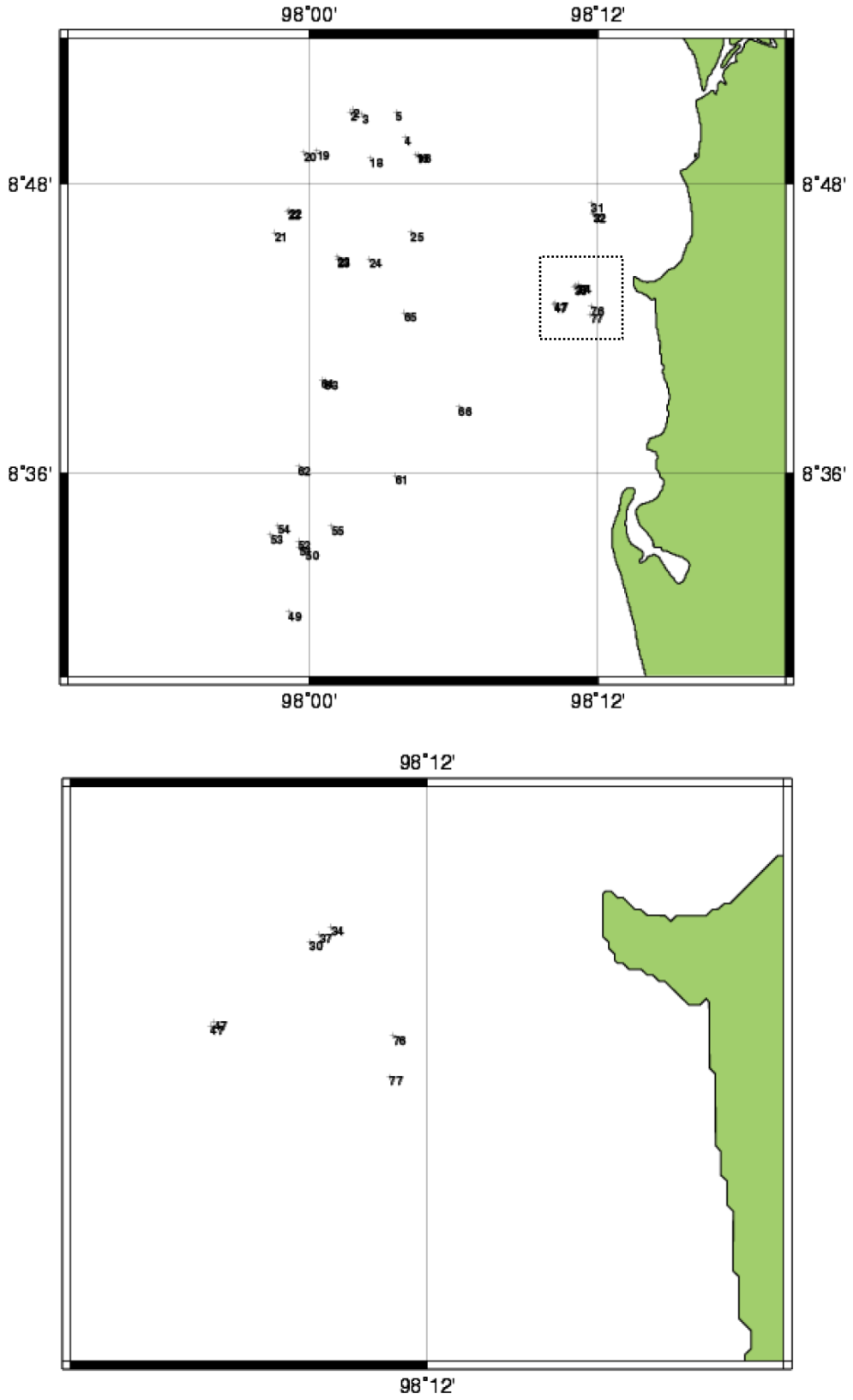
รูปที่ 2-8 การเก็บตัวอย่างดินตะกอนโดย Rumohr Gravity Corer (ซ้าย) และการเก็บรักษาแท่งดินตะกอนให้อยู่ในแนวตั้ง (ขวา)



รูปที่ 2-9 แนวที่ทำการสำรวจด้วยเครื่องโซนาร์กวาดทางข้าง (Side Scan Sonar) และเครื่องหยั่งความลึกด้วยเสียงสะท้อนชนิดหลายลำคลื่น (Multibeam echo-sounder) (รูปบน) และแนวที่ทำการสำรวจด้วยเครื่อง Multibeam echo-sounder (รูปล่าง)



รูปที่ 2-10 ตำแหน่งเก็บตัวอย่างดินตะกอนผิวหน้า (surface sediment) ในพื้นที่สำรวจ (รูปบน) และตำแหน่งเก็บตัวอย่างดินตะกอนผิวหน้าในกรอบประของรูปบน (รูปล่าง)



รูปที่ 2-11 ตำแหน่งเก็บตัวอย่างดินตะกอน (core sediment) ตามความลึกในพื้นที่สำรวจ (รูปบน) และตำแหน่งเก็บตัวอย่างดินตะกอนตามความลึกในกรอบประของรูปบน (รูปล่าง)



รูปที่ 2-12 ห้องประมวลผลข้อมูลทางธรณีฟิสิกส์ภายใน เรือสำรวจจักรทอง ทองใหญ่

2.4.5 การวิเคราะห์ในห้องปฏิบัติการ

การที่จะทราบได้ว่าพื้นที่ใดบนฝั่งได้รับอิทธิพลจากสึนามิ ทำโดยการเอาดินบนฝั่งหรือดินตะกอนในแหล่งน้ำบนฝั่งมาวิเคราะห์ หากพบว่ามีวัสดุหรือสสารใด ๆ ไม่ว่าจะเป็นอนินทรีย์สารหรืออินทรีย์สารที่มีแหล่งกำเนิดจากทะเล ก็แสดงว่าพื้นที่นั้นได้รับผลกระทบจากสึนามิ ในทางกลับกัน พื้นที่ในทะเลที่เป็นแหล่งทับถมของดินตะกอนที่สึนามิพามา ก็ควรที่จะประกอบไปด้วยวัสดุหรือสสารที่บ่งชี้ว่ามีแหล่งกำเนิดบนแผ่นดิน ซึ่งมากน้อยก็ขึ้นอยู่กับลักษณะสภาพพื้นที่และความแรงของคลื่นสึนามิที่เข้ากระทำต่อพื้นที่ชายฝั่งบริเวณนั้น (ABRANTES et al. 2008, CHOOWONG et al. 2008, FUJIWARA & KAMATAKI 2007, HAWKES et al. 2007) โดยการวิเคราะห์จะแบ่งเป็น 2 ส่วน คือ

แบ่งออกเป็น 2 ส่วน คือ

1) การวิเคราะห์ทางธรณีวิทยาของตะกอน เพื่อหาโครงสร้าง (structure) และคุณสมบัติทางกายภาพ (physical properties) ของตะกอน เพื่อตรวจหาร่องรอยของแร่ที่มีแหล่งที่มาจากแผ่นดิน (land derived tracer mineral) ซึ่งจะแตกต่างจากตะกอนที่มีแหล่งกำเนิดจากในทะเล โดยถ่ายรูปตะกอนด้วยเทคนิค X-radiography เพื่อดูความแตกต่างของชั้นตะกอน

2) การวิเคราะห์ทางธรณีเคมีของตะกอน โดยวิเคราะห์หา PAHs (polycyclic aromatic hydrocarbons) และสัดส่วนของ PAHs ในตะกอน เพื่อใช้เป็น “organic tracer” ของตะกอนจากแผ่นดิน และวิเคราะห์หาอายุตะกอนโดยใช้ไอโซโทปกัมมันตรังสีโดย 210Pb เพื่อให้ได้ข้อมูลอายุของตะกอนแต่ละชั้นของตะกอนที่แม่นยำ

2.4.5.1 การวิเคราะห์ขนาดอนุภาคตะกอน

วิเคราะห์หาขนาดอนุภาคที่เป็นองค์ประกอบในดินตะกอนผิวหน้าจากพื้นที่ศึกษา เพื่อที่ปรับเทียบมาตรฐาน (calibrate) ข้อมูลกับภาพที่ได้จากเครื่องโซนาร์กวาดทางข้าง (Side Scan Sonar) และสร้างแผนที่แสดงการกระจายตัวของดินตะกอนบนพื้นท้องทะเล โดยวิธีการร่อนและเครื่องเลเซอร์พาร์ทิเคิล-ไซเซอร์ (Laser Particle Sizer)

2.4.5.2 การวิเคราะห์สมบัติทางกายภาพและสมบัติด้านเสียงของดินตะกอน

การวิเคราะห์สมบัติทางกายภาพ (physical properties) และสมบัติเรื่องด้านเสียง (acoustical properties) ของดินตะกอน ด้วยใช้เครื่อง multi sensor core logger (MSCL) จะไม่ทำลายโครงสร้างของดินตะกอน เครื่อง MSCL ตรวจวัดโดยอาศัยสมบัติของดินตะกอน เช่น การลดทอนรังสีแกมมา (gamma-ray attenuation), ความหนาแน่นรวม (bulk-density), ความเร็วมของคลื่น P-wave (P-wave velocity) และความไวต่อคลื่นแม่เหล็ก (magnetic susceptibility) โดยตรวจวัดด้วยความละเอียดสูงที่ทุก ๆ 1 เซนติเมตร ตลอดความยาวของแท่งตะกอน (SCHULTTHEISS & WEAVER 1992, BEST & GUNN 1999)

เทคนิคนี้นิยมใช้ในการศึกษาในด้านสมุทรศาสตร์ดึกดำบรรพ์ (paleooceanographic), ภูมิอากาศดึกดำบรรพ์ (paleoclimatic) และศึกษาการแบ่งชั้นของหินเพื่อหาสหสัมพันธ์กับการลำดับชั้นตามลักษณะหิน (stratigraphic studies for lithostratigraphic correlation) (MIENERT et al. 1988, HERBERT & MEYER 1991, SHACKLETON et al. 1995) ซึ่งเทคนิคนี้สามารถประยุกต์มาใช้กับงานการศึกษาคลื่นสึนามิ โดยใช้ระบุการเปลี่ยนแปลงอย่างทันทีทันใด (abrupt change) ของสมบัติและสภาพของตะกอน (ABRANTES et al. 2008)

2.4.5.3 การวิเคราะห์องค์ประกอบธาตุ

ตรวจวิเคราะห์องค์ประกอบธาตุ โดยเครื่องกวาดตรวจเอกซ์ฟลูออเรสเซน (X-ray Fluorescence scanner หรือ XRF scanner) วิธีนี้เป็นวิธีการตรวจหาปริมาณสัมพัทธ์ขององค์ประกอบธาตุต่าง ๆ ในตะกอนโดยไม่ทำลายโครงสร้างของตะกอน การตรวจวัดทำโดยผ่าครึ่งแท่งตะกอน จากนั้นกวาดตรวจโดยตรงที่บริเวณผิวดินตะกอนจากด้านหนึ่งไปจนสุดความยาวแท่งดินตะกอนอีกด้านหนึ่ง เครื่องมือจะอ่านค่าความเข้มของธาตุ (element intensities) เป็นจำนวนนับต่อวินาที (count per second) ข้อมูลที่ได้สามารถใช้ระบุแหล่งของตะกอนได้ (sediment provenance identification)

(JANSEN et al. 1998, PÄLIKE et al. 2001, WELTJI & TJALLINGII 2008) โดย Al, K, Si, Ti และ Fe จะสมนัย (correspond) กับองค์ประกอบที่มาจากแผ่นดิน (terrigenous content) แต่ถ้าเป็น Ca มากจะบ่งบอกว่ามาจาก $CaCO_3$ ซึ่งเป็นลักษณะที่พบมาในตะกอนทะเล

ในดินตะกอนที่มีวัสดุจากแผ่นดินมาปะปนอยู่ในปริมาณสูงค่าสัมพันธ์ระหว่างสัดส่วนของธาตุ (Fe/Ca, Ti/Ca) จะจำแนกดินตะกอนส่วนที่มีแหล่งกำเนิดในทะเลออกได้ (BAHR et al., 2005, OHTA & ARAI, 2007) ดังนั้นจึงนำมาใช้ในการจำแนกความแตกต่างระหว่างดินตะกอนที่ถูกคลื่นสึนามิพามาสะสมในชั้นดินตะกอนทะเลที่มีองค์ประกอบจากแผ่นดินปะปนอยู่ อย่างไรก็ดี เปลือกหอยที่พบปะปนอยู่ในตะกอนที่เป็นตะกอนที่ถูกพามาจากแผ่นดิน จะเป็นตัวรบกวนการแปลผล เนื่องจากมันจะเปลี่ยน Ti/Ca ไปทาง Ca

2.4.5.4 การบันทึกภาพถ่ายรังสีเอกซ์

บันทึกภาพถ่ายรังสีเอกซ์ (X-radiography images) ของผิวหน้าของดินตะกอนในแท่งดินตะกอน เพื่อดูความแตกต่างของชั้นดินตะกอน เนื่องจากดินตะกอนไหล่ทวีปจะมีลักษณะ macroscopically uniform คือ จะมองไม่เห็นความแตกต่างหากดูด้วยตาเปล่า ซึ่งวิธีนี้เป็นวิธีที่แนะนำให้ปฏิบัติเสมอในการศึกษาดินตะกอนประเภท unconsolidated sediments เพื่อเป็นการวิเคราะห์ในเบื้องต้น (AXELSSON & HÄNDEL 1972, JACKSON et al. 1996)

2.4.5.5 การวิเคราะห์อายุดินตะกอน

วิเคราะห์อายุดินตะกอนเพื่อให้ได้ข้อมูลการแบ่งชั้นของดินตะกอนที่แม่นยำขึ้น โดยใช้เทคนิค Pb-210 ที่ Institute of Geology, Adam Mickiewicz University ในประเทศโปแลนด์ โดยนำตัวอย่างมาทำให้แห้ง บดละเอียด บรรจุลงในภาชนะพลาสติก และปิดผนึก ทิ้งไว้อย่างน้อย 3 สัปดาห์ เพื่อให้ ^{222}Rn สลายตัวอย่างสมบูรณ์ ตรวจวัดรังสีแกมมา (Gamma ray) ที่ปลดปล่อยจากเรดิโอนิวไคลน์ (^{210}Pb, ^{214}Pb, ^{214}Bi, ^{137}Cs) โดยใช้ตัวตรวจวัดแบบ high purity coaxial wide energy Germanium detector (Canberra GX2520 (relative efficiency 25%, resolution <2.0 keV) คู่กับ remote detector chamber option (RDC-6 inches) สำหรับตัดลด low energy background ปลายของตัวตรวจวัดประกอบด้วย low attenuated polycarbon window และอยู่ใน lead shield ซึ่งมีความหนาของผนัง 10 เซนติเมตร แสดงผลเป็นสเปคตรัม (spectrum) โดย DSA1000 MCA with digital signal processing

ตัวตรวจวัดจะ characterize ด้วยวิธี MCNP ที่เรียกว่า ISOCS/LabSOCS Characterization ประสิทธิภาพ (efficiency) การวัดในเชิง geometry ใช้ LabSOCS code ช่วงพลังงาน 45 - 3000 keV ในการปรับแก้ค่าทั้งหมดของ sample geometry, matrix และ container type วิเคราะห์ผลโดยใช้ซอฟท์แวร์ GENIE 2000 ซึ่งมี gamma analysis option ความแม่นยำ (precision) และค่า MDA (minimum detectable activity) ของการตรวจวัดหาโดย standard GENIE 2000 algorithms ซึ่งรายงานความไม่แน่นอนในการวิเคราะห์ (analytical uncertainties) ทั้งหมด ในรูปของ 2

sigma error เนื่องจากไอโซโทป (isotopes) ที่ตรวจวัดนี้เป็นแบบ low activities ดังนั้นจึงต้องใช้เวลาโดยเฉลี่ยในการตรวจวัดนานถึง 155 ชั่วโมง (6.5 วัน)

ในการศึกษาทางธรณีกาลวิทยา (geochronology) ของ ^{210}Pb จำเป็นที่จะต้องแยก ^{210}Pb supported (เกิดขึ้นอย่างต่อเนื่องในดินตะกอน) และ ^{210}Pb excess (เกิดเนื่องมาจากแหล่งภายนอก) ค่า ^{210}Pb supported หาได้จากการตรวจวัด ^{214}Pb, ^{226}Ra และ ^{214}Bi สำหรับค่า ^{210}Pb excess หาได้จากการเอาค่า ^{210}Pb supported (ค่า activities เฉลี่ยของ ^{214}Pb, ^{226}Ra และ ^{214}Bi) ไปลบออกจากค่า ^{210}Pb ทั้งหมดที่ตรวจวัดได้ นอกจากนี้โครงการนี้ยังได้ทำการตรวจวัด ^{137}Cs และ ^{40}K

2.4.5.6 การวิเคราะห์สารโพลีไซคลิอะโรมาติกไฮโดรคาร์บอน (polycyclic aromatic hydrocarbons; PAHs) ในตัวอย่างตะกอนพื้นผิวท้องทะเล (surface sediment)

ดินตะกอนส่วนหนึ่งแช่แข็งเพื่อจะนำไปวิเคราะห์ polycyclic aromatic hydrocarbons (PAHs) ซึ่งเป็นวิธีการใหม่วิธีหนึ่งที่ทางโครงการวิจัยนี้นำมาประยุกต์ในการจำแนกความแตกต่างของแหล่งกำเนิดประเภท anthropogenic และแหล่งกำเนิดประเภท biogenic เนื่องจากในการศึกษาด้านอื่นมีการประยุกต์ใช้ PAHs และ aliphatics เป็นตัวแทน หรือที่เรียกว่า “proxy” มาหลายทศวรรษแล้ว และพบว่ามีงานวิจัยจำนวนหนึ่งที่ใช้การวิเคราะห์หาสารประกอบอินทรีย์ในตะกอนประเภท semi-volatile organic compounds (SVOCs) ได้แก่ PAHs, hopanes และ cholestanes (WESTERHOM et al. 1992; YUNKER et al. 2002; KALAITZOGLOU et al. 2004) เพื่อจำแนกความแตกต่างระหว่างองค์ประกอบประเภทจากทะเล (marine) และจากแผ่นดิน (terrigenous) ในดินตะกอนทะเล

ข้อดีของการใช้ PAHs ก็คือ PAHs มีที่มาจากการเผาไหม้ที่ไม่สมบูรณ์ของอินทรีย์สาร ซึ่งสารอินทรีย์ที่ต่างกันจะมีสัดส่วนของ PAHs แต่ละชนิดที่แตกต่างกันไป ดังนั้นการใช้ specific binary ratios จึงเหมาะที่จะใช้บ่งชี้ว่าแหล่งกำเนิดของ PAHs ที่พบนั้นมาจากมนุษย์หรือมาจากธรรมชาติ ดินตะกอนทะเลที่ถูกพามาจากแผ่นดินอันเนื่องมาจากการกวาดกลับของคลื่นสึนามิย่อมต้องมีสัดส่วนขององค์ประกอบประเภท terrigenous มากกว่า กล่าวคือ สารอินทรีย์ประเภทที่มีแหล่งกำเนิดจากมนุษย์จะมีอยู่ในสัดส่วนที่สูงกว่าดินตะกอนปกติ

บทที่ 3
ผลการวิจัยและการวิเคราะห์ข้อมูล

3.1 ผลการสำรวจทางธรณีฟิสิกส์

การวิจัยนี้ ศึกษาตั้งแต่เขตน้ำตื้นใกล้ฝั่งจนถึงเขตน้ำลึกไกลฝั่งออกไป ความจำกัดของเครื่องมือที่ใช้จึงทำให้ภาพโครงสร้างต่าง ๆ ที่ได้จะชัดเจนในเขตน้ำตื้นแต่จะเลือนไปบ้างในเขตน้ำลึก ระดับอ้างอิง (reference level) ที่ใช้ในการปรับ (adjust) เครื่องหยั่งความลึกด้วยเสียงชนิดหลายลำคลื่น (Multibeam echo-sounder) เพื่อที่จะให้ได้ข้อมูลความลึกน้ำที่เชื่อถือได้ (reliable bathymetrical data) คือ ระดับน้ำต่ำสุดในช่วงน้ำเกิด (spring tide low water) โดยข้อมูลทั้งหมดจะปรับแก้กับค่าระดับน้ำต่ำสุดในช่วงน้ำเกิดจากสถานีตรวจวัดระดับน้ำที่อ่าวเขาหลัก โดยใช้โปรแกรม Wxtide32 (www.wxtide32.com)

จากข้อมูลเครื่องหยั่งความลึกด้วยเสียงสะท้อนชนิดหลายลำคลื่น (Multibeam echo-sounder) และระบบวัดการสะท้อนของคลื่นไหวสะเทือนในน้ำตื้น (Boomer System) พบว่าสัณฐานวิทยาทั่วไปของพื้นทะเลในพื้นที่สำรวจ มีลักษณะค่อย ๆ ลาดเอียงจากฝั่งออกไป แต่เมื่อถึงระดับความลึก 25-30 เมตร ความชันของพื้นทะเลจะเพิ่มขึ้นอย่างรวดเร็ว เห็นได้ชัดเจนจากข้อมูล Multibeam echo-sounder (รูปที่ 3-1) โดยเฉพาะอย่างยิ่งทางตอนใต้ของพื้นที่สำรวจ และบางส่วนทางตะวันออกเฉียงเหนือของแหลมปะการัง (รูปที่ 3-2) บางหลุมลึกถึง 7 เมตร คาดว่าน่าจะเป็นร่องรอยที่เกิดจากการทำเหมืองแร่ดีบุกซึ่งในอดีตมีอยู่มากในพื้นที่หน้าเขาหลัก และคาดว่าตะกอนที่มากลับกระแสไหลย้อนของคลื่นสึนามิอาจจะมาตกทับถมในบริเวณนี้ได้มาก

บริเวณใกล้ฝั่งนอกแหลมปะการัง ที่ระดับความลึก 10-20 เมตร พบว่าพื้นทะเลมีแนวร่อง (channel) อย่างน้อย 3 แนว ซึ่งเป็นร่องธรรมชาติที่พาดอยู่ในแนวตะวันตกเฉียงเหนือ-ตะวันออกเฉียงใต้ (แนว NW-SE) ดังรูปที่ 3-3 และพบว่าเป็นร่องที่ไม่สมมาตร ความลึกของร่องทางตะวันออกเฉียงใต้ (ลึกประมาณ 2 เมตร) จะลึกกว่าทางตะวันตกเฉียงเหนือ (ลึกประมาณ 1 เมตร) และความชันของร่องทางด้านตะวันออกเฉียงใต้จะมากกว่า

จากข้อมูลเครื่องโซนาร์กวาดทางข้าง (Side Scan Sonar) พบว่าพื้นท้องทะเลที่ระดับความลึกประมาณ 10-20 เมตร จะมีลักษณะแนวกว้าง 150-300 เมตร ยาวหลายกิโลเมตร พาดในแนว NW-SE และประกอบไปด้วยตะกอนที่ละเอียดกว่าพื้นทะเลรอบข้าง ดังตัวอย่างในรูปที่ 3-4 (1) จะเห็นแนวแบ่งลักษณะตะกอนหยาบกับตะกอนละเอียดอย่างชัดเจน นอกจากนี้บริเวณพื้นที่สำรวจยังพบลักษณะพื้นทะเลที่เป็นริ้ว คล้ายระลอกคลื่นได้ทั่วไปในบริเวณที่เป็นตะกอนหยาบ ขณะที่บนพื้นทะเลที่เป็นตะกอนละเอียดจะไม่เห็นริ้วคล้ายระลอกคลื่น เมื่อนำไปทับซ้อนกับภาพถ่ายจากดาวเทียม IKONOS ที่ถ่ายภาพกระแสไหล

ย้อนของคลื่นสึนามิ (backwash of tsunami) เมื่อเดือนธันวาคม พ.ศ. 2543 ในรูปที่ 3-5

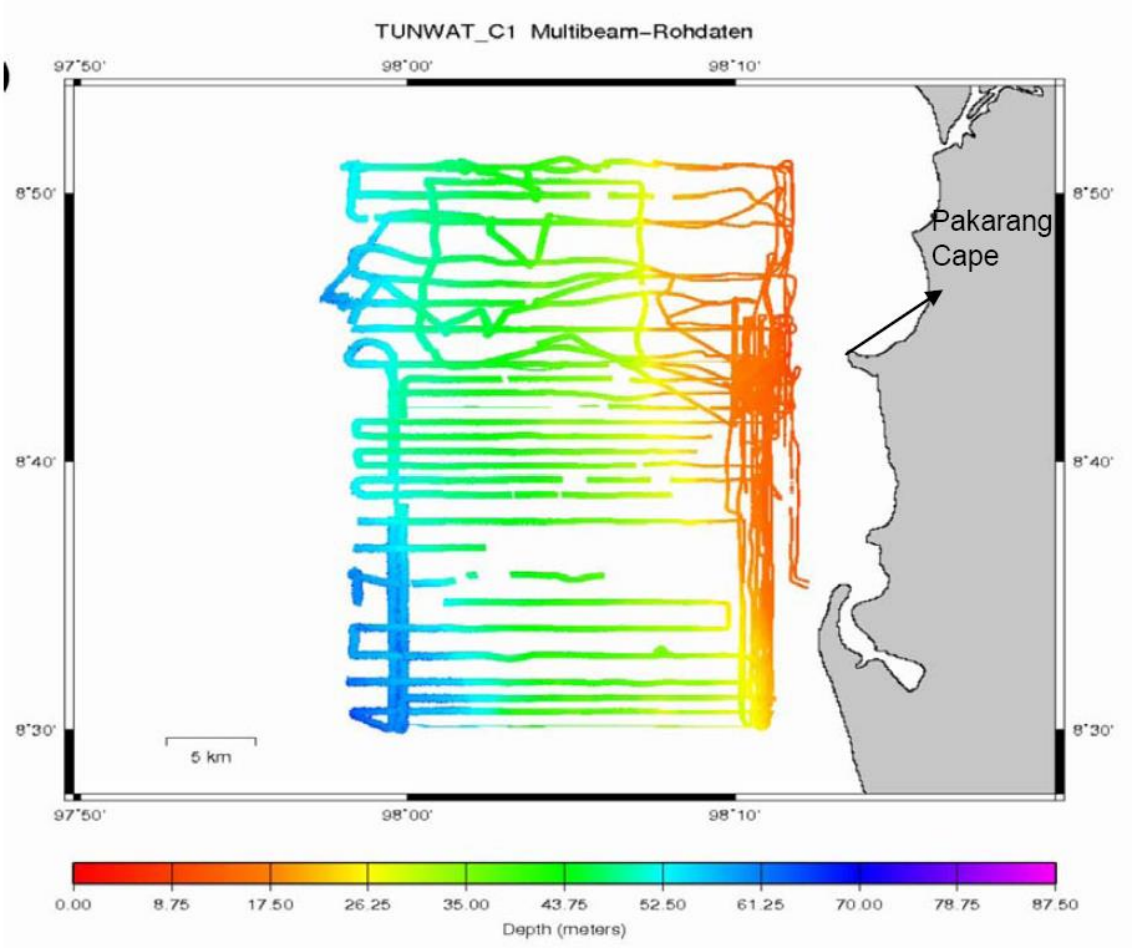
จุดสีต่าง ๆ ในรูปที่ 3-5 แสดงลักษณะดินตะกอนจากการวิเคราะห์ตัวอย่างที่เก็บจากพื้นที่ศึกษามาวิเคราะห์ทางตะกอนวิทยา ตัวอย่างดินตะกอนที่ได้จากแนว 02120712 ซึ่งอยู่ทางตะวันออกเฉียงเหนือของพื้นที่ศึกษา พบซากพืชที่น่าจะเป็นหญ้าจากบนบกปนอยู่กับดินตะกอนที่มีขนาดหยาบปนละเอียด (รูปที่ 3-6) ตัวอย่างดินตะกอนผิวหน้าหมายเลข 061208-11 ซึ่งอยู่นอกชายฝั่ง ห่างจากแหลมปะการัง 3.5 กิโลเมตร พบเศษชิ้นส่วนของศิลาแลง (laterite) (รูปที่ 3-7) ซึ่งเป็นวัสดุจากแผ่นดินปะปนอยู่เป็นจำนวนมาก รูปที่ 3-8 แสดงตัวอย่างดินตะกอนตามแนวลึก ที่พบเห็นดินตะกอนที่มีขนาดหยาบและละเอียดปะปนกัน ซึ่งพบได้ทั่วไปในพื้นที่ศึกษา

พื้นที่ใกล้ฝั่งจะเห็นตะกอนละเอียดเป็นหย่อม ๆ โดยดินตะกอนจะมีลักษณะแตกต่างกันกับดินตะกอนข้างเคียง ตัวอย่างดังรูปที่ 3-9 ซึ่งตะกอนหยาบขนาดใหญ่ (boulder) เห็นได้ทั่วไปจากข้อมูลที่ได้จากเครื่องโซนาร์กวาดทางข้าง (Side Scan Sonar) โดยเฉพาะอย่างยิ่งบริเวณพื้นที่ตื้นนอกแหลมปะการัง แต่ก็ยังพบเห็นได้ในเขตน้ำลึกประมาณ 30 – 35 เมตร ดังรูปที่ 3-4(3) และ 3-4(4) ซึ่งเป็นลักษณะที่น่าสนใจเป็นอย่างมาก

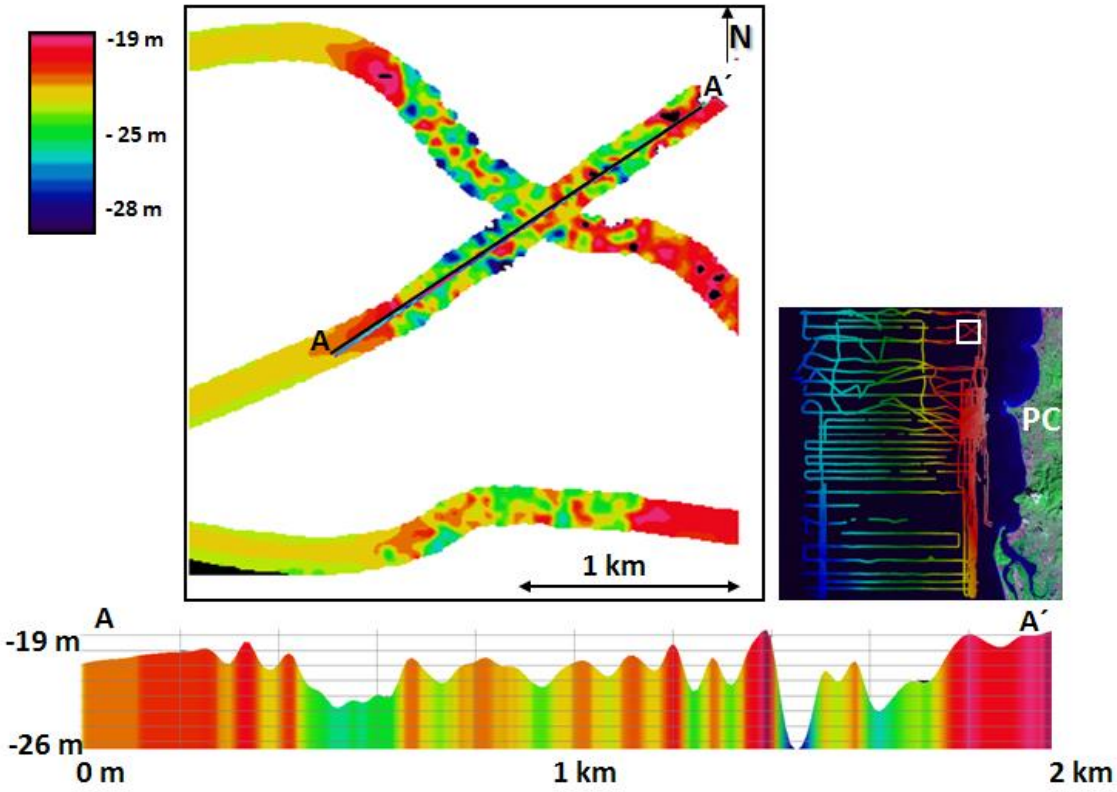
จากข้อมูลที่ได้จากระบบวัดการสะท้อนของคลื่นไหวสะเทือนในน้ำตื้น (boomer system) บ่งบอกว่าพื้นท้องทะเลที่เป็นกองหินที่พบเห็นในพื้นที่ใกล้ฝั่ง ไม่มีความสัมพันธ์กับกองหินที่พบในบริเวณไกลออกไปนอกชายฝั่ง ดังตัวอย่างในรูปที่ 3-9 ซึ่งคาดว่าก้อนหินขนาดใหญ่บริเวณพื้นท้องทะเลไกลออกไปทางนอกชายฝั่ง น่าจะเป็นก้อนหินที่ถูกคลื่นสึนามิที่เกิดขึ้นเมื่อเดือนธันวาคม พ.ศ. 2547 พาออกไปจากแหลมปะการังและไปตกสะสมในบริเวณนั้น ดังรายงานใน GOTO et al. (2007)

นอกจากนี้ข้อมูลจากระบบวัดการสะท้อนของคลื่นไหวสะเทือนในน้ำตื้น ซึ่งลากสำรวจตั้งฉากกับแนวชายฝั่ง พบว่าพื้นท้องทะเลมีแนวก้อนหินที่มีความสูง 3 – 4 เมตร ปรากฏอยู่ในบริเวณที่ความลึกของน้ำประมาณ 40 เมตร (รูปที่ 3-10 และ 3-11)

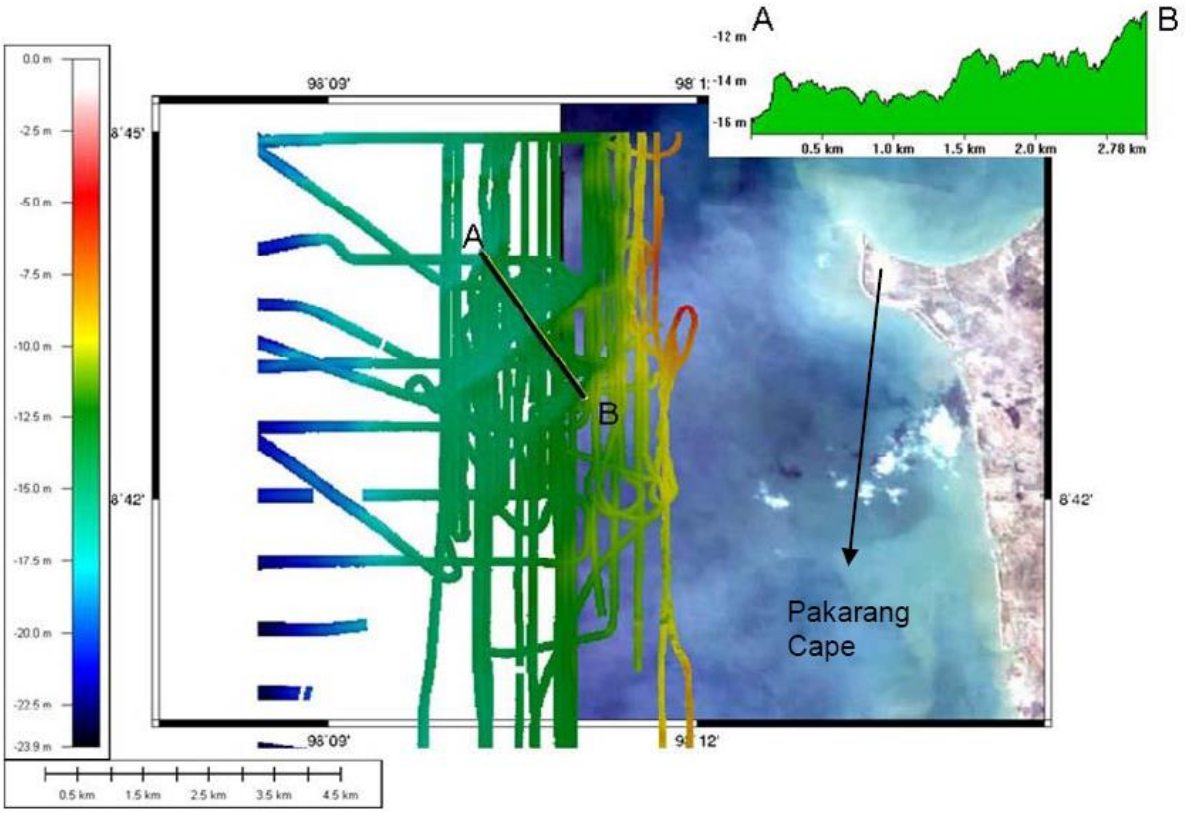
จากการวิเคราะห์ ^{210}Pb ในแท่งตะกอนที่เก็บตามความลึก (core) หมายเลข 021207-18 ซึ่งเก็บจากที่ความลึกน้ำ 52 เมตร อยู่ประมาณกึ่งกลางของไหล่ทวีปอันดามัน ข้อมูลขนาดอนุภาคและข้อมูลอายุตะกอนบ่งชี้ให้เห็นว่าชั้นบนสุดของแท่งตะกอนมีลักษณะเป็น laminated layer มีความหนาประมาณ 8 เซนติเมตร ซึ่งเห็นได้จากภาพถ่ายรังสีเอกซ์ (X-ray image) เช่นกัน จาก ^{210}Pb profile ในแบบจำลองอายุ (age-model) เห็นได้ชัดว่าแท่งตะกอนแบ่งออกเป็น 3 ส่วน ส่วนบนตั้งแต่ 0 ถึง 5 เซนติเมตร แสดงให้เห็นถึงการลดลงของ ^{210}Pb activities ตามความลึก ส่วนที่ 2 ที่ระดับ 5-8 เซนติเมตร ^{210}Pb activities เพิ่มเล็กน้อยตามความลึก และส่วนที่ 3 ตั้งแต่ระดับ 8 เซนติเมตรลงไป จะคล้ายคลึงกับส่วนบนสุด ลึกกว่า 30 เซนติเมตรลงไป ค่า excess ^{210}Pb ต่ำมาก



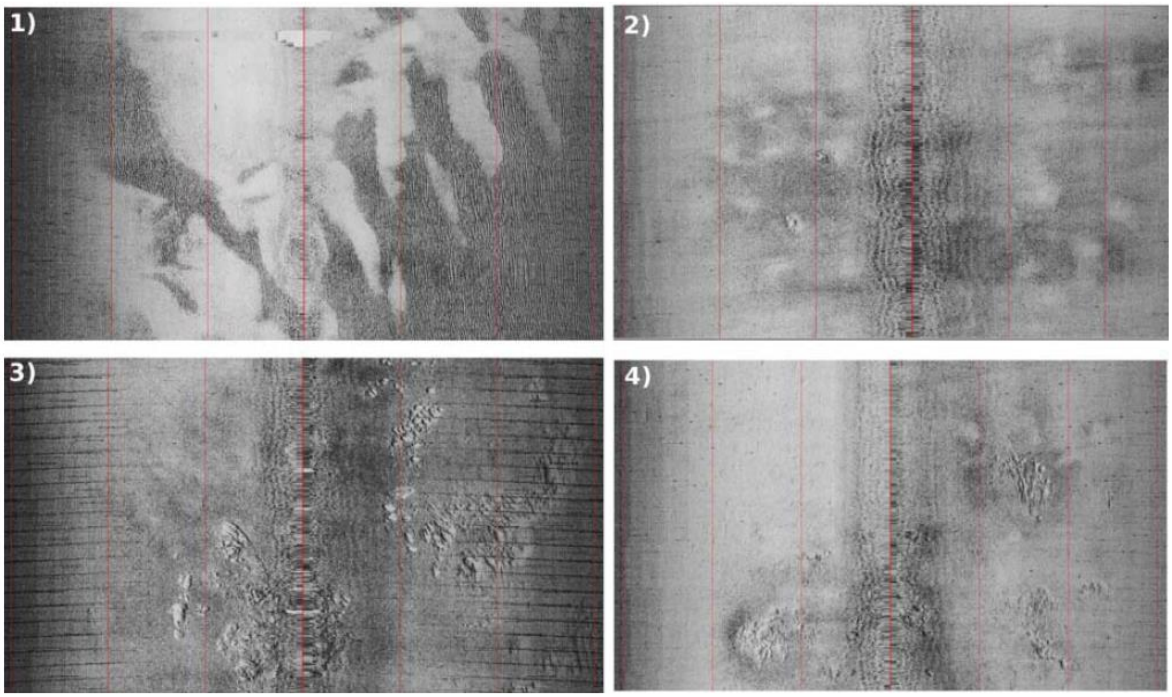
รูปที่ 3-1 ภาพแสดงข้อมูลจากเครื่องหยั่งความลึกด้วยเสียงสะท้อนชนิดหลายลำคลื่น (Multibeam echo-sounder)



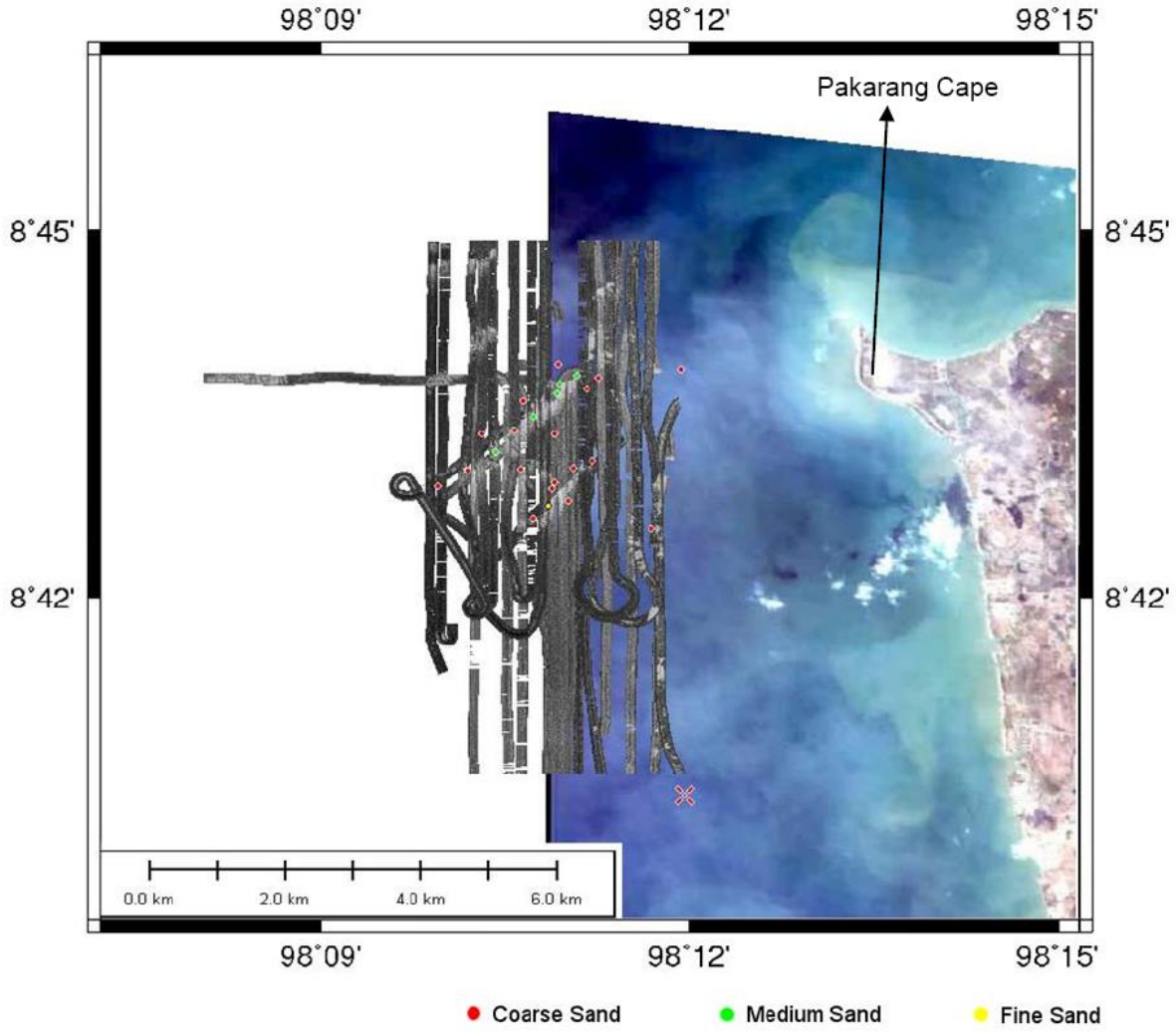
รูปที่ 3-2 ข้อมูลพื้นท้องทะเล (Bathymetric data) ทางตะวันออกเฉียงเหนือของแหลมปะการัง จะเห็นร่องรอยการทำเหมืองดีบุกได้ชัดเจน ในลักษณะเป็นหลุมลึกที่เกิดขึ้นเป็นหย่อม ๆ ในพื้นที่ตอนเหนือของพื้นที่ทำการสำรวจ (กรอบสีขาวในรูปทางด้านขวา)



รูปที่ 3-3 ข้อมูลจากเครื่องหยั่งความลึกด้วยเสียงสะท้อนชนิดหลายลำคลื่น (multibeam echo sounder) ในพื้นที่นอกชายฝั่งใกล้แหลมปะการัง ในรูปเล็กด้านขวาบนแสดงภาพตัดขวางในแนว A-B จะเห็นว่ามีลักษณะเป็นร่องที่มีความไม่สมมาตร

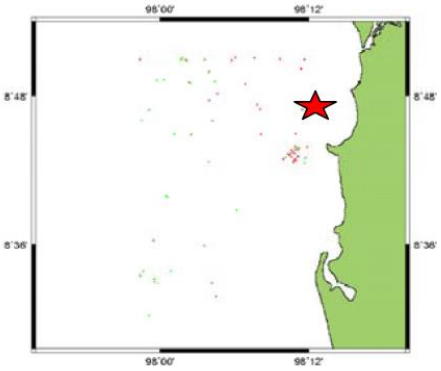


รูปที่ 3-4 ภาพแสดงลักษณะข้อมูลที่ได้จากเครื่องโซนาร์กวาดทางข้าง (Side Scan Sonar) ภาพ (1) แสดงลักษณะที่เป็นร่องลึก (channel) ที่เกิดขึ้นบริเวณพื้นทะเล ในบริเวณ 8° 43′ เหนือ 98° 11′ ตะวันออก; ภาพ (2) แสดงลักษณะที่เป็นหลุมเล็ก ๆ (pock-like depressions) ในบริเวณ 8° 43′ เหนือ 98° 03′ ตะวันออก; ภาพ (3) และ (4) แสดงลักษณะท้องทะเลในเขตน้ำลึกที่มีก้อนหินขนาดใหญ่ บริเวณ 8° 44′ เหนือ 98° 05′ ตะวันออก และ 8° 30′ เหนือ 98° 02′ ตะวันออก



รูปที่ 3-5 ข้อมูลจากเครื่องหยั่งความลึกด้วยเสียงสะท้อนชนิดหลายลำคลื่น (multibeam echo-sounder) ในพื้นที่นอกชายฝั่งใกล้แหลมปะการัง ทับซ้อนกับภาพถ่ายจากดาวเทียม IKONOS ที่ถ่ายภาพกระแสไหลย้อนของคลื่นสึนามิ (backwash of tsunami) เมื่อเดือนธันวาคม 2543 (ที่มา: IKONOS image @2004. www.crisp.nus.edu.sg/tsunami/tsunami.html)





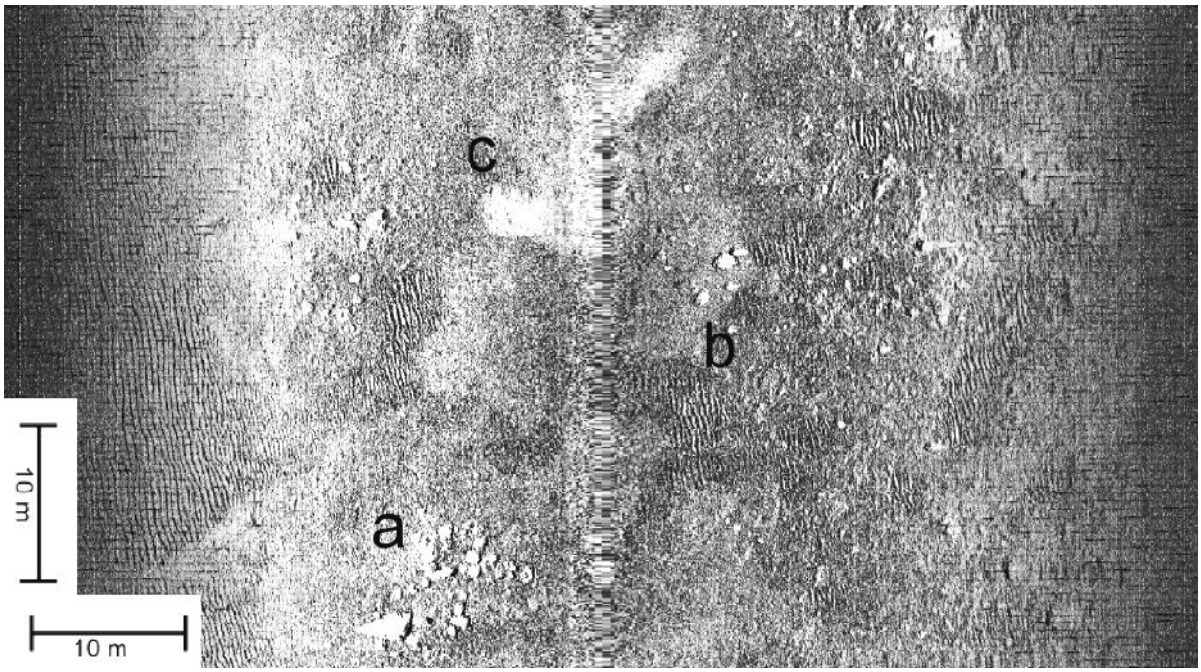
รูปที่ 3-6 ตัวอย่างดินตะกอนใกล้ฝั่งจากแนว 02120712 พบว่ามีซากพืชที่มีลักษณะคล้ายหญ้าบนบก ซึ่งหญ้าดังกล่าวถูกตะกอนขนาดหยาบปนละเอียดทับถมอยู่ลึกประมาณ 3 เซนติเมตร



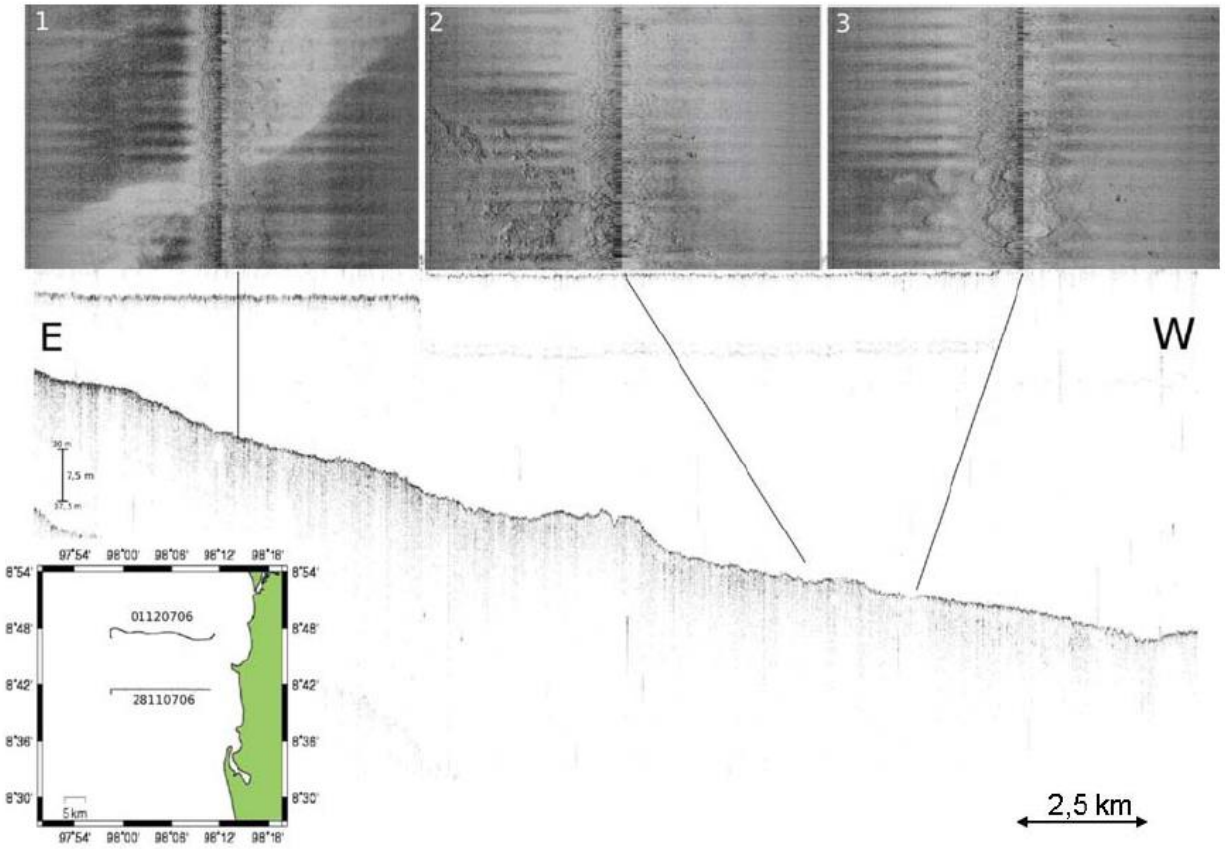
รูปที่ 3-7 เศษทรายหยาบและชิ้นส่วนศิลาแลง (laterite) ในตัวอย่างดินตะกอนผิวหน้าหมายเลข 061208-11 ซึ่งอยู่ห่างออกไป 3.5 กิโลเมตร นอกชายฝั่งแหลมปะการัง



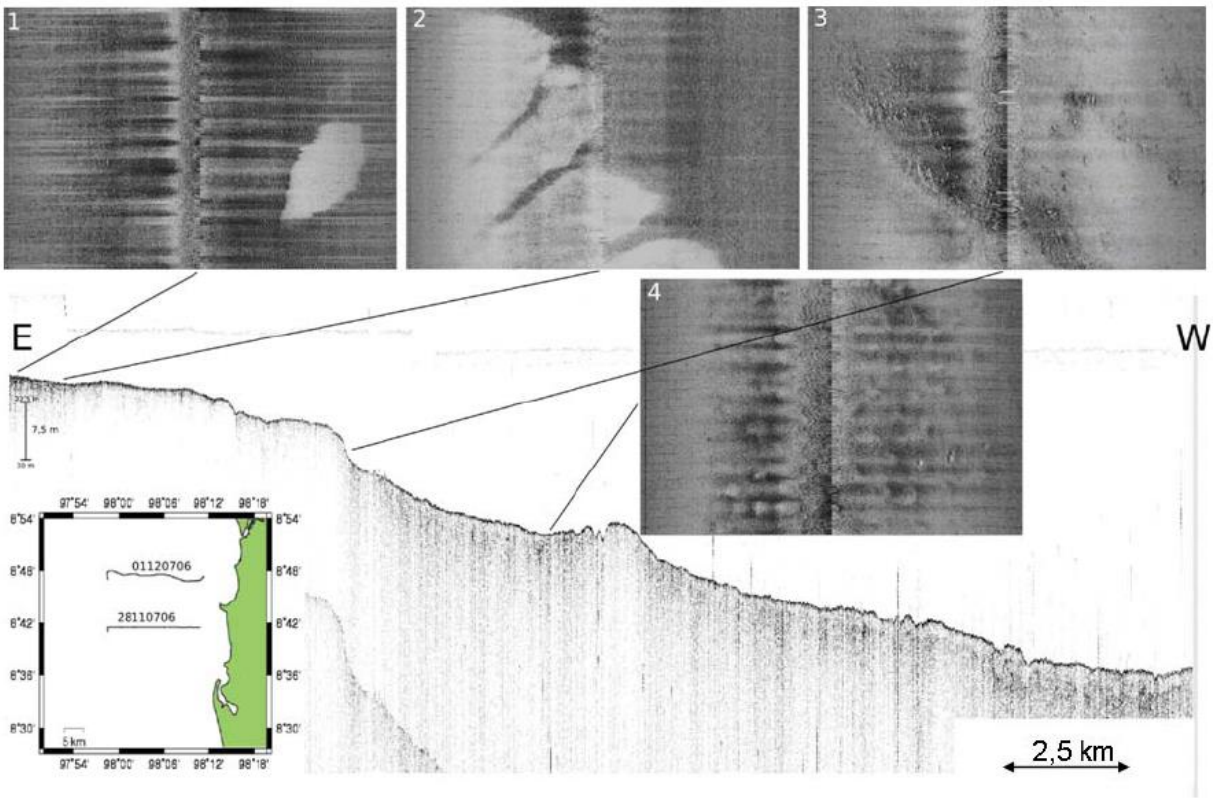
รูปที่ 3-8 ภาพแสดงลักษณะตะกอนหยาบปนละเอียดในตัวอย่างดินตะกอนที่เก็บตามความลึก (Core sediment sample)



รูปที่ 3-9 ข้อมูลจากเครื่องโซนาร์กวาดทางข้าง (Scan Sonar data) ในพื้นที่ใกล้ชายฝั่ง (ใกล้กับ 8° 40′ เหนือ 98° 12′ ตะวันออก) ตำแหน่ง (a) เป็นลักษณะพื้นท้องทะเลบริเวณที่มีก้อนหินขนาดใหญ่สะสม; ตำแหน่ง (b) เป็นลักษณะพื้นท้องทะเลที่เป็นระลอกคลื่น; และตำแหน่ง (c) เป็นลักษณะพื้นท้องทะเลที่มีตะกอนละเอียดสะสมตัวอยู่



รูปที่ 3-10 ข้อมูลจากระบบวัดการสะท้อนของคลื่นไหวสะเทือนในน้ำตื้น (boomer) แนว 28110706 แสดงสัณฐานพื้นท้องทะเลในแนวตั้งฉากกับฝั่ง และข้อมูลจากเครื่องโซนาร์กวาดทางข้าง (side scan sonar) ณ ความลึกน้ำต่างระดับ ภาพ (1) ลักษณะพื้นทะเลเป็นตะกอนละเอียด; ภาพ (2) แนวกองหินที่พบเห็นได้ทั่วไปในข้อมูลจากรระบบวัดการสะท้อนของคลื่นไหวสะเทือนในน้ำตื้นที่ลากสำรวจในแนวตั้งฉากกับฝั่ง และภาพ (3) บริเวณที่พื้นท้องทะเลต่ำกว่าพื้นที่ข้างเคียง



รูปที่ 3-11 ข้อมูลจากระบบวัดการสะท้อนของคลื่นไหวสะเทือนในน้ำตื้น (boomer) แนว 01120706 แสดงสัณฐานพื้นท้องทะเลในแนวตั้งฉากกับฝั่ง และข้อมูลจากเครื่องโซนาร์กวาดทางข้าง (side scan sonar) ณ ความลึกน้ำต่างระดับ ภาพ (1) หย่อมตะกอนละเอียดที่พบได้ทั่วไปในพื้นท้องทะเลบริเวณใกล้ฝั่ง; ภาพ (2) บริเวณรอยต่อระหว่างบริเวณที่เป็นตะกอนละเอียดกับบริเวณที่ตะกอนมีขนาดหยาบขึ้น; ภาพ (3) แนวกองหินที่พบเห็นได้ทั่วไปในข้อมูลจากรระบบวัดการสะท้อนของคลื่นไหวสะเทือนในน้ำตื้นที่ลากสำรวจในแนวตั้งฉากกับฝั่ง และภาพ (4) บริเวณที่พื้นท้องทะเลต่ำกว่าพื้นที่ข้างเคียง

ตะกอนส่วนที่ 1 และ 3 น่าจะเป็นการตกตะกอนสะสมแบบปกติในพื้นที่บริเวณนี้ เมื่อแปลผลข้อมูลโดยใช้แบบจำลอง CIC (constant initial concentration) พบว่าอัตราการสะสมของตะกอนอยู่ในอัตรา 0.3 เซนติเมตรต่อปี ส่วนที่ 2 แสดงให้เห็นว่ามีการตกตะกอนสะสมอย่างรวดเร็ว (rapid sedimentation) และ/หรือ มีการผสมผสาน (mixing) เกิดขึ้น ลักษณะตะกอนแบบส่วนที่ 2 ที่ปรากฏอยู่คั่นกลางระหว่างส่วนที่ 1 และส่วนที่ 3 บ่งชี้ว่าน่าจะมีเหตุการณ์บางอย่างเกิดขึ้น จากการหาอายุตะกอนพบว่ามีอายุอยู่ประมาณ ค.ศ. 1990 ซึ่งเมื่อเทียบย้อนเหตุการณ์ใหญ่ๆ ที่เกิดขึ้นในช่วงเวลานั้น พบว่าการสะสมของตะกอนในส่วนที่ 2 นั้นน่าจะมาจากอิทธิพลของไต้ฝุ่นเกย์ (Typhoon Gay) ในปี ค.ศ. 1989 ซึ่งเป็นไต้ฝุ่นลูกใหญ่ที่ถูกบันทึกว่าส่งผลกระทบต่อชายฝั่งทะเลแถบอันดามัน

จากการวิเคราะห์ข้อมูลที่ได้ในโครงการปีที่ 1 ซึ่งสำรวจโดยใช้เรือสำรวจจักรทอง ทองใหญ่ (รูปที่ 3-12ก) พบว่ามีความจำเป็นที่จะต้องขยายพื้นที่เก็บข้อมูลเพื่อจัดทำแผนที่พื้นท้องทะเลไปทางด้านทิศเหนือ แต่พื้นที่ด้านเหนือนั้นมีความลึกเพียง 5 เมตร เรือสำรวจจักรทอง ทองใหญ่ มีขนาดค่อนข้างใหญ่ และไม่สามารถเข้าทำการในเขตที่ความลึกน้ำน้อยกว่า 10 เมตร ในการสำรวจปีที่ 2 จึงได้ใช้เรือสำรวจบุญเลิศ ผาสุก (รูปที่ 3-12ข) ซึ่งมีขนาดเล็ก แทนเรือสำรวจจักรทอง ทองใหญ่ โดยทั้ง 2 ลำ อยู่ในความดูแลของสถาบันวิจัยและพัฒนาทรัพยากรทางทะเล ชายฝั่งทะเล และป่าชายเลน

ในการสำรวจทั้ง 2 ครั้ง ดำเนินการสำรวจพื้นท้องทะเลโดยใช้เครื่องมือทางธรณีฟิสิกส์ประเภทคลื่นเสียงในน้ำ (hydroacoustic) (ได้แก่ เครื่องโซนาร์กวาดทางข้าง (Side Scan Sonar), ระบบวัดการสะท้อนของคลื่นไหวสะเทือนในน้ำตื้นชนิดความละเอียดสูง (Shallow Water High Resolution Reflection Seismic System หรือ Boomer System) และ เครื่องหยั่งความลึกด้วยเสียงชนิดหลายลำคลื่น (Multibeam System Echo Sounding))และสังเกตการณ์ด้วยวีดีโอใต้น้ำ (underwater-video observations) เพื่อจัดทำแผนที่พื้นท้องทะเลความละเอียดสูง จากนั้นจึงจะใช้ข้อมูลนี้ในการพิจารณาตำแหน่งเก็บตัวอย่างตะกอนดิน ทั้งแบบผิวหน้าและตามความลึกของชั้นตะกอน อย่างไรก็ดี การใช้เรือสำรวจบุญเลิศ ผาสุก พบปัญหาอุปสรรค คือ พื้นที่ในการติดตั้งเครื่องมือลดน้อยลงมาก และกำลังไฟฟ้าสำหรับขับเคลื่อนเครื่องมือมีไม่เพียงพอ จึงต้องมีการปรับเปลี่ยนและดัดแปลงเครื่องมือบางชิ้น

ในปีที่ 2 เรือสำรวจบุญเลิศ ผาสุก เข้าทำการสำรวจตั้งต้นในพื้นที่แหลมปะการัง ซึ่งเป็นเขตน้ำตื้น ลึกประมาณ 5 เมตร ซึ่งเรือสำรวจจักรทอง ทองใหญ่ ไม่สามารถเข้าไปสำรวจได้ และทำการสำรวจซ้ำในพื้นที่ที่ผลการสำรวจในปีที่ 1 พบว่ามีรูปแบบการตกตะกอนที่น่าสนใจ การสำรวจในปีที่ 2 นี้ ยังได้ขยายพื้นที่สำรวจเข้าไปถึงบริเวณชายฝั่งนอกเกาะพระทอง ซึ่ง JANKAEW et al. (2008) รายงานว่าเป็นพื้นที่ที่ได้รับผลกระทบรุนแรงจากคลื่นสึนามิ

กิจกรรมสำรวจในโครงการปีที่ 2 ประกอบด้วย การจัดทำแผนที่พื้นท้องทะเลรายละเอียดสูง การสำรวจตัวแปรด้านตะกอนในคอลัมน์น้ำ การเก็บตัวอย่างตะกอนจากพื้นท้องทะเล และการถ่ายภาพวีดีโอใต้น้ำ



(ก) เรือสำรวจจักรทอง ทองใหญ่ ใช้ในการสำรวจปีที่ 1



(ข) เรือสำรวจบุญเลิศ ผาสุก ใช้ในการสำรวจปีที่ 2

รูปที่ 3-12 เรือสำรวจจักรทอง ทองใหญ่ และเรือสำรวจบุญเลิศ ผาสุก ของสถาบันวิจัยและพัฒนาทรัพยากรทางทะเล ชายฝั่งทะเล และป่าชายเลน จังหวัดภูเก็ต

งานหลักในการสำรวจปีที่ 2 คือ ข้อมูลสัณฐานวิทยาและตะกอนวิทยาที่ครอบคลุมพื้นที่นอกชายฝั่งจังหวัดพังงาด้านที่ติดต่อกับทะเลอันดามัน โดยเฉพาะอย่างยิ่งบริเวณรอบแหลมปะการัง โดยเริ่มตั้งแต่ความลึกน้ำ 5 เมตร เป็นต้นไป การที่มีความจำเป็นต้องได้แผนที่พื้นท้องทะเลในน้ำตื้นโดยทำ hydroacoustic mapping เนื่องจากอิทธิพลจากกระแสไหลย้อนของคลื่นสึนามิที่กลับลงสู่ทะเลมีมากในพื้นที่นี้ ซึ่งเป็นข้อมูลส่วนที่ไม่สามารถเก็บข้อมูลได้ในปีที่ 1 เพราะเรือสำรวจจักรทอง ทองใหญ่ ทำงานได้ที่ระดับน้ำลึกสุดแค่ 10 เมตร

ในการสำรวจปีที่ 2 จึงได้ย้อนกลับไปสำรวจในพื้นที่ที่ไม่สามารถเก็บข้อมูลได้ในปีที่ 1 บริเวณที่พบลักษณะพิเศษ เพื่อให้ได้ข้อมูลเพิ่มเติมด้านพลวัตรของตะกอน (sediment dynamics) เสถียรภาพของโครงสร้างที่ปรากฏ (stability of observed structures) และการเปลี่ยนแปลงสัณฐาน (changes in morphology) การสำรวจทางธรณีฟิสิกส์ในปีที่ 2 แม้จะใช้ SeaBeam 1185 (L3 Communication / ELAC Nautik) ในการตรวจวัดความลึกน้ำ แต่ transducer ต้องมีการย้ายไปติดตั้งที่หัวเรือ (รูปที่ 3-13ก) แล้วโยงดึงให้แน่นด้วย ประกอบกับเครื่องโซนาร์กวาดทางข้างเปลี่ยนเป็นแบบ dual-frequency Benthos 1645 side scan sonar system with chirp technology ซึ่ง chirp technology เป็นเทคโนโลยีที่ช่วยให้สามารถเก็บข้อมูลในพื้นที่น้ำตื้นโดยยังรายละเอียดสูงได้ โดยมีระยะกวาดไปทางด้านข้าง 100 เมตร ทั้งสองข้าง การวัดการสะท้อนของคลื่นไหวสะเทือน ได้ปรับเปลี่ยนไปใช้เครื่อง low voltage Boomer system (C-Boom, C-Products Europe Ltd) ซึ่งต้องการเพียง 0.6 KV ในการขับเคลื่อน ซึ่งต่างจาก EG&G Boomer system ที่ใช้ในปีที่ 1 ที่ต้องการกำลังไฟฟ้าสูงถึง 3.5 KV การถ่ายวีดีโอใต้น้ำทำโดยการลาก underwater MARISCOPE camera แต่การเก็บตัวอย่างตะกอนดินผิวหน้าพื้นทะเลยังคงใช้ Van-Veen Grab Sampler และเก็บตะกอนตามความลึกด้วย RUMOHR Gravity Corer เช่นเดียวกับปีที่ 1

อย่างไรก็ดี ด้วยงบประมาณที่จำกัดทำให้ระยะการทำงานไม่สามารถยืดออกไปได้ เนื่องจากไม่สามารถแบกรับภาระค่าใช้จ่ายในเรื่องค่าน้ำมันเรือ ในการสำรวจซ้ำเพื่อยืนยันและให้ได้รายละเอียดเพิ่มขึ้น จึงทำได้ค่อนข้างจำกัด นอกจากนี้ ได้ขยายพื้นที่ไปถึงแนวหน้าเกาะพระทอง เนื่องจากมีรายงานว่าพื้นที่นี้ได้รับผลกระทบรุนแรงจากคลื่นสึนามิ (JANKAEW et al., 2008)

3.2 จัดทำแผนที่พื้นท้องทะเลรายละเอียดสูง

ในการสำรวจทั้ง 2 รอบเรือของโครงการฯ เพื่อจัดทำแผนที่พื้นท้องทะเล ใช้เทคนิคการสำรวจทางทะเลด้วยคลื่นเสียง (marine acoustic techniques) ประกอบด้วย multibeam echo sounding, side-scan sonar mapping และ boomer system ทำการเก็บข้อมูลรายละเอียดสูงโดยการส่งสัญญาณจากเรือไปยังผิวพื้นท้องทะเล และรับสัญญาณที่ส่งสะท้อนกลับสู่เรือ ในขณะแล่นเรือไปในเส้นทางที่กำหนดด้วยความเร็วคงที่



รูปที่ 3-13 การติดตั้งเครื่องมือทางธรณีฟิสิกส์บนเรือสำรวจบนเรือสำรวจบุญเลิศ ผาสุก

(ก) ติดตั้งเครื่องหยั่งความลึกด้วยเสียงชนิดหลายลำคลื่น (Multibeam echo-sounder) ที่หัวเรือ

(ข) เครื่องโซนาร์กวาดทางข้าง (Side Scan Sonar) ก่อนปล่อยลงสู่ทะเล

(ค) ระบบวัดการสะท้อนของคลื่นไหวสะเทือนในน้ำตื้นชนิดความละเอียดสูง (Boomer System) ก่อนปล่อยลงสู่ทะเล

(ง) การเก็บตะกอนตามความลึกด้วยเครื่องมือเก็บตัวอย่างตะกอนดินแบบ Rumohr Gravity Corer

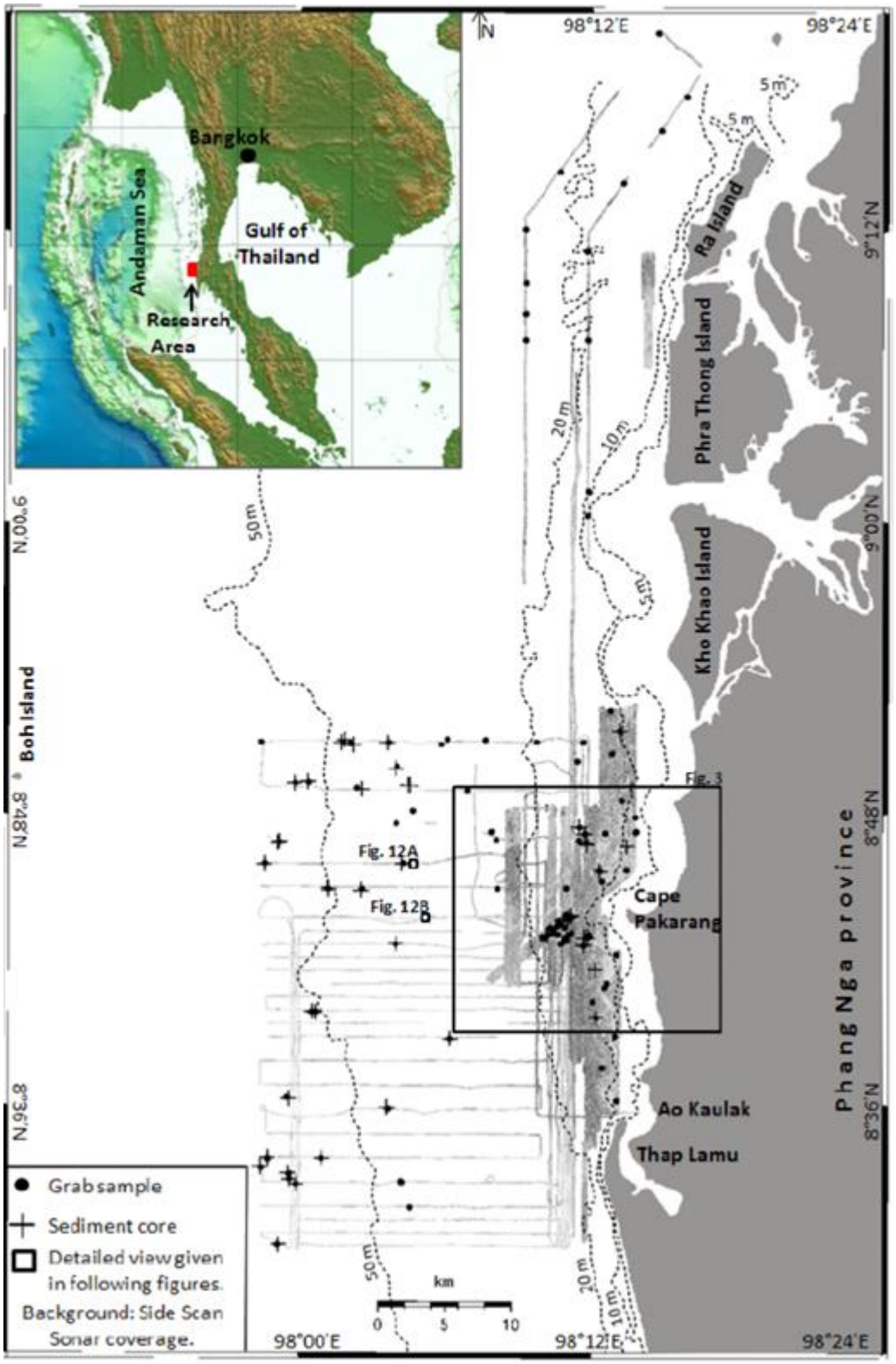
(จ) การเก็บตะกอนผิวท้องทะเลด้วยเครื่องมือเก็บตัวอย่างตะกอนดินแบบ Van-Veen Grab Sampler

รูปที่ 3-14 แสดงเส้นทางการสำรวจรวม ทั้ง 2 รอบเรือ คือ รอบที่ 1 เดือนพฤศจิกายน ถึง ธันวาคม พ.ศ. 2550 โดยเรือสำรวจจักรทอง ทองใหญ่ (โครงการปีที่ 1) และรอบที่ 2 เดือนพฤศจิกายน ถึง ธันวาคม พ.ศ. 2551 โดยเรือสำรวจบุญเลิศ ผาสุก (โครงการปีที่ 2) รวมระยะทางในการสำรวจพื้นทะเลด้วยเครื่องมือสำรวจทางธรณีฟิสิกส์ทั้งสิ้นประมาณ 1,500 ไมล์ทะเล (nautical mile) (หรือประมาณ 2,780 กิโลเมตร) รวมเวลาทั้งสิ้นกว่า 400 ชั่วโมง รูปที่ 3-13 แสดงการติดตั้งเครื่องมือสำรวจทางธรณีฟิสิกส์กับเรือสำรวจบุญเลิศ ผาสุก ในการปรับเทียบความเร็วของเสียงที่แท้จริงที่ผ่านน้ำสำหรับเครื่อง Multibeam Echo Sounding ใช้ข้อมูลความเร็วเสียงตามความลึก (sound velocity profile) ที่ได้จาก CTD

3.2.1 เครื่องหยั่งความลึกด้วยเสียงสะท้อนชนิดหลายลำคลื่น

เครื่องหยั่งความลึกด้วยเสียงสะท้อนชนิดหลายลำคลื่น หรือ Multibeam echo-sounder จะเก็บข้อมูลพื้นท้องทะเลในพื้นที่ที่กว้างกว่าเครื่องส่งเสียงสะท้อน (echo-sounder) แบบปกติทั่วไปที่ใช้เพียงลำคลื่นเดี่ยว (single beam) เนื่องจากวิจัยครั้งนี้อยู่ในเขตน้ำที่ค่อนข้างตื้น จึงเลือกใช้เครื่องหยั่งความลึกด้วยเสียงสะท้อนชนิดหลายลำคลื่นที่มีตัวแปรสัญญาณแบบที่ใช้ในน้ำตื้น ซึ่งมีความถี่ที่ 180 KHz โดยมีข้อมูล CTD (conductivity, temperature และ depth) เป็นตัวปรับเทียบกับความเร็วเสียงที่แท้จริงในน้ำ การติดตั้งทำโดยติดตั้งกับเสาที่ต่อยื่นออกไปนอกตัวเรือ (รูปที่ 3-13ก) และสามารถปรับลดระดับของเครื่องให้จมลงใต้ผิวน้ำได้เมื่อต้องการตรวจวัด และยกขึ้นระหว่างมีการเก็บตัวอย่างตะกอนหรือเดินเรือในระยะทางยาว

การปรับเทียบความเร็วของเสียงที่ผ่านน้ำสำหรับเครื่องหยั่งความลึกด้วยเสียงสะท้อนชนิดหลายลำคลื่น ใช้ข้อมูลความเร็วเสียงตามความลึก (sound velocity profile) ที่ได้จาก CTD ซึ่งข้อมูลความเร็วเสียงตามความลึกที่ตรวจวัดได้ขณะดำเนินการศึกษาครั้งนี้ เป็นข้อมูลตั้งต้นที่สำคัญมากในการศึกษาแบบคลื่นเสียง ทุกครั้งที่ทำการเริ่มออกสำรวจ จะต้องมีการวัดค่าความเร็วเสียงก่อนทุกครั้ง จากนั้นนำค่าความเร็วเสียงตั้งต้นนี้ไปหักลบกับข้อมูลตรวจวัด เพื่อความเป็นมาตราฐาน แต่ทั้งนี้โครงการฯ ได้เปรียบเทียบกับข้อมูลที่ตรวจวัดโดย Dr. W. Weinrebe (โครงการความร่วมมือภายใต้ชุดดครงการฯ) ซึ่งตรวจวัดในช่วงก่อนนี้ในพื้นที่ใกล้เคียงกันนี้แต่ห่างออกจากฝั่งมากกว่า พบว่าใกล้เคียงกันมาก แสดงว่าความเร็วเสียงในพื้นที่ศึกษาไม่แตกต่างกันมาก การเก็บข้อมูลความเร็วเสียงตามความลึกที่ได้จาก CTD ในวันที่ 7 ธันวาคม พ.ศ. 2550 ชื่อไฟล์ที่ใช้เก็บข้อมูลจากเครื่องหยั่งความลึกด้วยเสียงสะท้อนชนิดหลายลำคลื่น อยู่ในรูปแบบ "day-month-year-number-subsample" เช่น 05120747B ตัวเลขจะเพิ่มขึ้นเป็นลำดับตลอดช่วงการปฏิบัติการ



รูปที่ 3-14 เส้นทางการสำรวจโดยใช้เครื่องมือทางธรณีฟิสิกส์และตำแหน่งจุดเก็บตัวอย่างดินตะกอนผิวหน้าและตัวอย่างดินตะกอนตามความลึก จากการสำรวจ 2 รอบเรือ (พฤศจิกายน – ธันวาคม พ.ศ. 2550 และ พฤศจิกายน – ธันวาคม พ.ศ. 2551)

แต่พบว่าข้อมูลจากเครื่องหยั่งความลึกด้วยเสียงสะท้อนชนิดหลายลำคลื่นอาจจะมีการรบกวนจากปัจจัยภานนอกต่างๆ ได้ เช่ย ในช่วง 20071125145631018 เกิดการขัดข้องในหน่วยควบคุมการป้อน heave data ซึ่งเป็นข้อมูลจากเครื่องรับสัญญาณการเคลื่อนไหว (motion sensor) ซึ่งเกิดจากการรบกวนจากคลื่นอื่น ทำให้คุณภาพข้อมูลจากเครื่องหยั่งความลึกด้วยเสียงสะท้อนชนิดหลายลำคลื่นลดลง เนื่องจากทุกครั้งของการเคลื่อนเรือจะก่อให้เกิดคลื่นรบกวนและถูกบันทึกลงในข้อมูลความลึกน้ำรวมไปด้วย จึงต้องทำการแก้ไขโดยแยกการเก็บ heave data ด้วยเครื่องคอมพิวเตอร์อีกเครื่องหนึ่ง เนื่องจากเครื่องรับสัญญาณการเคลื่อนไหว (motion sensor) ยังทำงานเป็นปกติ เพื่อนำข้อมูลดังกล่าวมาปรับแก้ในภายหลัง

3.2.2 เครื่องโซนาร์กวาดทางข้าง

การสำรวจด้วยเครื่องโซนาร์กวาดทางข้าง หรือ Side Scan Sonar (รูปที่ 3-13ข) ดำเนินการตรวจวัดพื้นท้องทะเลด้วยคลื่นเสียงความถี่สูง (high frequency acoustic waves) โดยตัวแปรสัญญาณ (transducer) จะปล่อยคลื่นเสียงความถี่สูงออกไปและรับคลื่นเสียงที่สะท้อนจากพื้นท้องทะเล ความเข้ม (intensity) ของสัญญาณที่สะท้อนกลับก็จะถูกแสดงผลออกมา

ข้อมูลที่ได้จากเครื่องโซนาร์กวาดทางข้าง จะนำไปแปลผลร่วมกับผลวิเคราะห์ทางตะกอนวิทยาและธรณีเคมีของตะกอนตัวอย่างที่เก็บกลับไปวิเคราะห์ในห้องปฏิบัติการ จึงจะสามารถสร้างแผนที่พื้นท้องทะเลออกมาได้ เนื่องจากเครื่องโซนาร์กวาดทางข้างจะให้เฉพาะข้อมูลสมบัติทางเสียง (acoustic properties) ของพื้นท้องทะเล ซึ่งเป็นข้อมูลทางกายภาพ แต่ยังไม่สามารถบ่งบอกประเภทของตะกอน ทั้งนี้เพราะว่าขนาดของพลังงานที่สะท้อนกลับมานั้นขึ้นกับปัจจัยอีกหลายประการ ปัจจัยที่สำคัญ ได้แก่ การกระจายขนาดของอนุภาค (grain size distribution) ความหยาบของพื้นท้องทะเล (seafloor roughness) และมุมลาดเอียง (slope angle)

ในการสำรวจอาจจะมีคลื่นเสียงใต้น้ำซึ่งเกิดจากการหมุนของตัวแปรสัญญาณหรือการเปลี่ยนความเร็วของเรือที่ลากเครื่องมือ ระบบที่ใช้ในการศึกษาเป็น Dual Frequency Sonar System โดยลากทางด้านท้ายเรือ เครื่องจะตั้งอยู่บนทุ่นลอยซึ่งจะด้านล่างถ่วงด้วยน้ำหนัก เพื่อทำให้ตัวเครื่องเสถียรและตัดสัญญาณรบกวนอันเนื่องมาจากการเครื่องที่ของเรือ ข้อมูลที่ได้บันทึกด้วย ISIS Sonar Software 4.5.4 ซึ่งพัฒนาขึ้นโดย Triton Elics จากนั้นประมวลผลด้วย ISIS Sonar-software 6.0.6 และ Delph Map 2.9 (Triton Elics)

3.2.3 ระบบวัดการสะท้อนของคลื่นไหวสะเทือน

การสำรวจด้วยระบบวัดการสะท้อนของคลื่นไหวสะเทือนในน้ำตื้นชนิดความละเอียดสูง (shallow water high resolution reflection seismic system) หรือ Boomer system (รูปที่ 3-13ค) จะให้ข้อมูลชั้นตะกอนด้านบน (subsurface) ของพื้นท้องทะเล โดยตัวแปลงสัญญาณ 2 ชุด จะส่งคลื่นเสียงความถี่ต่ำที่ประมาณ 300 ถึง 7,000 Hz ออกไป คลื่นเสียงความถี่ต่ำนี้จะแทรกผ่านน้ำลงไปและสามารถ

ทะลุผ่านชั้นตะกอนได้ลึกประมาณ 20 ถึง 60 เมตร ขึ้นกับลักษณะของตะกอนและพลังงานของสัญญาณเสียงที่ส่งออกไป ความเข้มสูงสุดของคลื่นเสียงที่ระบบวัดการสะท้อนของคลื่นไหวสะเทือนในน้ำสามารถส่งออกไปได้อยู่ที่ประมาณ 4,000 Hz

บริเวณรอยต่อระหว่างน้ำกับตะกอนคลื่นเสียงจะสะท้อนกลับ ขึ้นกับความต้านทานต่อการผ่านของเสียง (acoustic impedance) ที่แตกต่างกันของวัตถุที่ตกกระทบ โดยมีไฮโดรโฟนที่ลากเรียงกันเป็นแถว(hydrophone array) อยู่ด้านท้ายเรือ เป็นตัวรับสัญญาณคลื่นเสียงที่สะท้อนกลับ ข้อมูลเสียงสะท้อนจะถูกบันทึกโดย software NWC 1.4.1 (Nautic Seismic Recording System) ซึ่งพัฒนาโดย Nautik Nord GmBH

3.2.4 การสำรวจตัวแปรด้านตะกอนในคอลัมน์น้ำ

สำรวจตัวแปรด้านตะกอนในคอลัมน์น้ำ (water column) โดยใช้เครื่อง CTD ที่ติดตั้งตัวรับสัญญาณ (sensor) 3 ตัว ได้แก่ (1) OBS sensor สำหรับตรวจวัดภาระบรรทุกของตะกอนแขวนลอย (2) fluorescence sensor สำหรับตรวจวัดปริมาณสารอินทรีย์ และ (3) LISST sensor สำหรับตรวจวัดการแพร่กระจายของขนาดอนุภาคตะกอนแขวนลอยในน้ำแต่ละระดับความลึก

3.3 การเก็บตัวอย่างดินตะกอนจากพื้นทะเล

เก็บตัวอย่างดินตะกอนเพื่อนำมาวิเคราะห์และจำแนกความแตกต่างของตะกอนทะเลทางตะกอนวิทยา ธรณีเคมี และเพื่อยืนยันเสริมกับแผนที่พื้นท้องทะเลทั้ง 3 รูปแบบ และผลสำรวจตัวแปรด้านตะกอนในคอลัมน์น้ำ เครื่องมือเก็บตัวอย่างตะกอนที่ใช้ในเรือสำรวจ ประกอบด้วยเครื่องมือเก็บตัวอย่างตะกอนดินพื้นผิวท้องทะเลแบบ Van-Veen-Grab-Sampler (รูปที่ 3-13จ) และเครื่องมือเก็บตัวอย่างตะกอนดินตามความลึกแบบ RUMOHR gravity corer (รูปที่ 3-13ง)

เก็บตัวอย่าง surface sediment ด้วย Van-Veen Grab Sampler และเก็บตัวอย่าง core sediement ด้วย RUMOHR Gravity Corer ในจุดเก็บตัวอย่างที่กำหนดจากข้อมูลที่ได้จากการสำรวจทางธรณีฟิสิกส์ เมื่อได้ตัวอย่างตะกอนผิวหน้าที่ได้จากแต่ละจุดเก็บตัวอย่าง ทำการบันทึกภาพ ตรวจสอบลักษณะทั่วไปของตะกอน และแบ่งตัวอย่างออกเป็น 4 ส่วน สำหรับวิเคราะห์ทางตะกอนวิทยาและธรณีเคมีในห้องปฏิบัติการ โดยส่วนที่จะนำไปวิเคราะห์ polycyclic aromatic hydrocarbons (PAHs) เก็บรักษาโดยการแช่แข็ง

จากการเก็บตัวอย่างในรอบ 2 เรือ ได้ตัวอย่างตะกอนดินผิวหน้ารวม 112 จุด และตัวอย่างตะกอนยาวประมาณ 2 เมตร รวมทั้งสิ้น 42 จุด เก็บตัวอย่างในแนวตั้ง นำตัวอย่างกลับห้องปฏิบัติการเพื่อดูโครงสร้างของชั้นตะกอน และวิเคราะห์ทางตะกอนวิทยาและธรณีเคมี

3.4 การวิเคราะห์ในห้องปฏิบัติการ

3.4.1 การวิเคราะห์ในห้องปฏิบัติการ

แบ่งออกเป็น 2 ส่วน คือ

1) การวิเคราะห์ทางธรณีวิทยาของตะกอน

เพื่อวิเคราะห์หาโครงสร้าง (structure) และสมบัติทางกายภาพ (physical properties) ของตะกอน เพื่อตรวจหาร่องรอยของแร่ที่มีแหล่งที่มาจากแผ่นดิน (land derived tracer mineral) โดยถ่ายรูปตะกอนด้วยเทคนิค X-radiography เพื่อดูความแตกต่างของชั้นตะกอน

2) การวิเคราะห์ทางธรณีเคมีของตะกอน

เพื่อวิเคราะห์หา PAHs (polycyclic aromatic hydrocarbons) และสัดส่วนของ PAHs ในตะกอนและวิเคราะห์หาอายุตะกอนโดยใช้ไอโซโทปกัมมันตรังสีโดย ^{210}Pb

3.4.2 ผลวิเคราะห์จากห้องปฏิบัติการ

ขณะที่ตะกอนที่ตกสะสมบนฝั่ง (onshore) เนื่องจากคลื่นสึนามิไหลบ่าขึ้นฝั่ง ประกอบไปด้วยสารอินทรีย์และอนินทรีย์ที่มีแหล่งกำเนิดในทะเล (marine origin) ตะกอนที่ถูกคลื่นสึนามิไหลย้อนพาไปสะสมนอกชายฝั่ง (offshore) ก็ควรที่จะประกอบไปด้วยสารที่บ่งชี้ได้ชัดเจนว่ามีกำเนิดมาจากแผ่นดิน ซึ่งใช้เป็นสารตามรอย (tracer-material) ได้ ซึ่งจะเป็นสารประเภทใดก็ขึ้นอยู่กับลักษณะพื้นที่ (landform) และลักษณะการทับถมอันเนื่องมาจากคลื่นสึนามิ (ABRANTES et al. 2008, CHOOWONG et al. 2008, FUJIWARA & KAMATAKI 2007, HAWKES et al. 2007)

3.4.2.1 การวิเคราะห์ขนาดอนุภาคและเนื้อตะกอนดิน

การวิเคราะห์เริ่มจากการวิเคราะห์ขนาดอนุภาคและเนื้อตะกอน (grain size analysis และ particle texture) ของตัวอย่างตะกอนดินผิวหน้าพื้นทะเล เพื่อนำข้อมูลไปใช้ปรับเทียบข้อมูลภาพที่ได้จากเครื่องโซนาร์กวาดทางข้าง และจัดสร้างแผนที่กระแพร่กระจายของตะกอน

3.4.2.2 การวิเคราะห์สมบัติทางกายภาพ

วิเคราะห์สมบัติทางกายภาพ (physical properties) และสมบัติเรื่องด้านเสียง (acoustical properties) ของตะกอน ด้วยใช้เครื่อง Multi sensor core logger (MSCL) (รูปที่ 3-15) เครื่อง MSCL ตรวจวัดโดยอาศัยสมบัติของตะกอน เช่น การลดทอนรังสีแกมมา (gamma-ray attenuation), ความหนาแน่นรวม (bulk-density), ความเร็วของคลื่น P-wave (P-wave velocity) และความไวต่อคลื่นแม่เหล็ก (magnetic susceptibility) โดยตรวจวัดด้วยความละเอียดสูงที่ทุก 1 เซนติเมตร ตลอดความ

ยาวของแท่งตะกอน รูปที่ 3-16 แสดงตัวอย่างข้อมูลสมบัติทางกายภาพจาก Core 07-20 ซึ่งจะไม่ทำลายโครงสร้างของตะกอน

สมบัติทางกายภาพและเสียงที่เปลี่ยนแปลงในแต่ละชั้นของแท่งตะกอนเป็นสมบัติที่ใช้ทั่วไปในการศึกษาด้านสมุทรศาสตร์บรรพกาล (paleooceano-graphy) ภูมิอากาศบรรพกาล (paleoclimate) และการแบ่งชั้นของตะกอน (stratigraphic study) (MIENERT et al. 1988, HERBERT & MEYER 1991, SHACKLETON et al. 1995) แต่ก็สามารถนำมาประยุกต์ใช้กับการศึกษาคลื่นสึนามิได้ เพราะสามารถระบุการเปลี่ยนแปลงอย่างทันทีทันใดที่ถูกบันทึกไว้ในแท่งตะกอน

3.4.2.3 การวิเคราะห์องค์ประกอบธาตุ

การตรวจวิเคราะห์หาปริมาณสัมพัทธ์ขององค์ประกอบธาตุต่างๆ ในตะกอนโดยใช้เครื่องกวาดตรวจเอกซ์ฟลูออเรสเซน (X-ray Fluorescence scanner หรือ XRF scanner) (รูปที่3-17) เป็นการวิเคราะห์ที่ไม่ทำลายโครงสร้างของดินตะกอน และข้อมูลที่ได้สามารถใช้ระบุแหล่งของตะกอน (sediment provenance identification) (JANSEN et al. 1998, PÄLIKE et al. 2001, WELTJI & TJALLINGII 2008)

การวิเคราะห์ ทำโดยผ่าครึ่งแท่งตะกอน จากนั้นกวาดตรวจโดยตรงที่บริเวณผิวตะกอนจากด้านหนึ่งไปจนสุดความยาวแท่งตะกอนอีกด้านหนึ่ง เครื่องมือจะอ่านค่าความเข้มของธาตุ (element intensities) เป็นจำนวนนับต่อวินาที (count per second) โดยธาตุ Al, K, Si, Ti และ Fe จะสมนัย (correspond) กับองค์ประกอบที่มาจากแผ่นดิน (terrigenous content) แต่ถ้ามี Ca มากจะบ่งบอกว่าตะกอนมีแหล่งมาจาก $CaCO_3$ ซึ่งเป็นลักษณะที่พบมาในตะกอนทะเล

ในตะกอนที่มีวัสดุจากแผ่นดินมาปะปนอยู่ในปริมาณสูงค่าสัมพันธ์ระหว่างสัดส่วนของธาตุ (Fe/Ca, Ti/Ca) จะจำแนกตะกอนส่วนที่มีแหล่งกำเนิดในทะเลออกได้ (LAMMY et al. 2001, BAHR et al. 2005, OHTA & ARAI 2007) ดังนั้นจึงใช้จำแนกความแตกต่างระหว่างตะกอนที่ถูกสึนามิพามาสะสม ซึ่งในชั้นตะกอนจะมีองค์ประกอบจากแผ่นดินปะปนอยู่ อย่างไรก็ดี เปลือกหอยที่พบปะปนอยู่ในตะกอนที่เป็นตะกอนที่ถูกพามาจากแผ่นดิน จะเป็นตัวรบกวนการแปลผล เนื่องจากมันจะเปลี่ยน Ti/Ca ไปทาง Ca

3.4.2.4 การบันทึกภาพถ่ายรังสีเอกซ์

บันทึกภาพถ่ายรังสีเอกซ์ (X-radiography images) ของผิวหน้าของตะกอนในแท่งตะกอนเพื่อดูความแตกต่างของชั้นตะกอน โดยการแยกประเภทของตามลักษณะที่แตกต่างกัน โดยปกติตะกอนไหล่ทวีปจะมีลักษณะ macroscopically uniform มองไม่เห็นความแตกต่างด้วยตาเปล่า ซึ่งวิธีนี้เหมาะกับวิเคราะห์ตะกอนประเภท unconsolidated sediments ในเบื้องต้น (AXELSSON & HÄNDEL 1972, JACKSON et al. 1996) รูปที่ 3-18 เป็นตัวอย่างตัวอย่างภาพถ่ายรังสีเอกซ์จากแท่งตะกอนจากพื้นที่ศึกษา ซึ่งจะเห็นความแตกต่างของชั้นตะกอนชัดเจน

3.4.2.5 การวิเคราะห์แร่ดินเหนียว

องค์ประกอบแร่ดินเหนียว (clay mineralogy) วิเคราะห์โดยแยกตะกอนขนาด 2 ไมโครเมตร ออกจากตัวอย่างตะกอนดินหลังกำจัดสารอินทรีย์และคาร์บอเนตแล้ว วิเคราะห์ด้วยเครื่อง X-ray Diffractometer (XRD) รูปที่ 3-19 แสดงตัวอย่างของ 2θ peak ของ surface sediment ในพื้นที่ศึกษา

3.4.2.6 การหาอายุตะกอน

การหาอายุตะกอนโดยวิธี Pb-210 ดำเนินการที่ Institute of Geology, Adam Mickiewicz University in Poznan เนื่องจากค่าใช้จ่ายที่สูง การวิเคราะห์อายุตะกอนในแท่งตะกอนจึงไม่ได้ทำทุกสถานี นำตัวอย่างที่ต้องการหาอายุมาทำให้แห่ง บดละเอียด บรรจุในภาชนะพลาสติกสำหรับนำเข้าเครื่อง ปิดผนึกภาชนะ ทิ้งไว้อย่างน้อย 3 สัปดาห์ เพื่อให้ ^{222}Rn สลายตัวหมด

ตรวจวัดรังสีแกมม่า (gamma emission) ที่ปล่อยจากนิวไคลน์กัมมันตรังสี (radionuclides; ^{210}Pb, ^{214}Pb, ^{214}Bi, ^{137}Cs) ด้วย high purity coaxial wide energy Germanium detector (Canberra GX2520) (relative efficiency 25%, resolution <2.0 keV) โดยใช้ remote detector chamber option (RDC-6 inches) สำหรับลด backdround ในช่วง low energy ปลาย detector ปิดด้วย polycarbon window บางๆ ตัว detector บรรจุไว้ในแท่งตะกั่วที่มีความหนาของผนัง 10 เซนติเมตร แสดงผล spectrums โดย DSA1000 MCA ที่มี digital signal processing

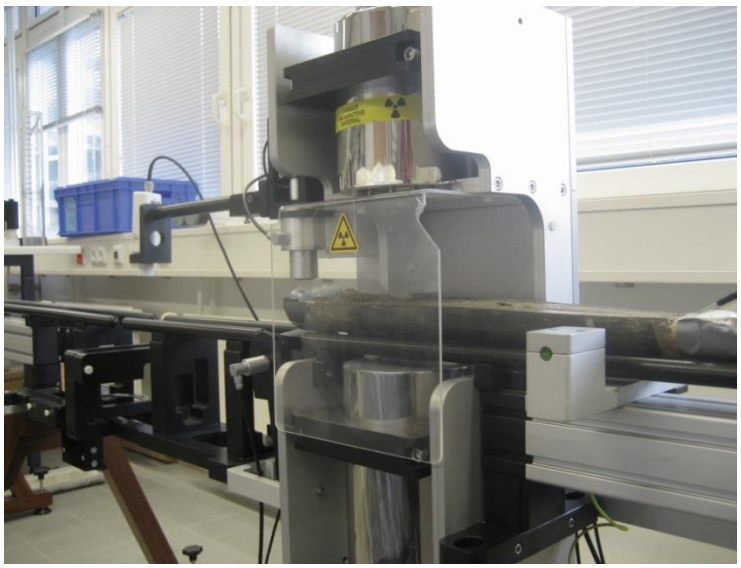
ทำการ characterize ตัว detector โดยวิธี MCNP method ซึ่งเรียกว่า ISOCS/ LabSOCS Characterization ประสิทธิภาพของ measured geometry ตรวจวัดด้วย LabSOCS code ซึ่งใช้ในการปรับแก้ค่า sample geometry, matrix และชนิดภาชนะที่ใช้บรรจุตัวอย่าง สำหรับการตรวจวัดในช่วงพลังงาน 45 – 3000 keV ผลการวัดวิเคราะห์ด้วย software GENIE 2000 ซึ่งมี gamma analysis option ความแม่นยำ (precision) และ MDA (minimum detectable activity) ของการตรวจวัด ทำตามขั้นตอนวิธีมาตรฐานของโปรแกรม (standard GENIE 2000 algorithms) ซึ่งจะรายงานความไม่แน่นอนของการวิเคราะห์ในค่า 2sigma error

เนื่องจากค่า activities ของไอโซโทป (isotopes) ที่ตรวจวัดมีค่าต่ำ แต่ละตัวอย่างใช้เวลาในการตรวจวัดเฉลี่ย 155 ชั่วโมง (6.5 วัน) ในการหาลำดับเวลาทางธรณี (geochronology) ของ ^{210}Pb ต้องตรวจวัดทั้ง supported ^{210}Pb (เกิดขึ้นอย่างต่อเนื่องในตะกอน) และ excess ^{210}Pb (มาจากแหล่งภายนอก) ค่า activity ของ supported ^{210}Pb หาได้จากการวัด ^{214}Pb, ^{226}Ra and ^{214}Bi ส่วน activity ของ excess ^{210}Pb หาได้จากการนำค่า supported ^{210}Pb (ค่าเฉลี่ยของ ^{214}Pb, ^{214}Bi activities) จากค่า ^{210}Pb ในแต่ละความลึกที่ตรวจวัด ในการศึกษาครั้งนี้ตรวจวัด ^{137}Cs และ ^{40}K ด้วย

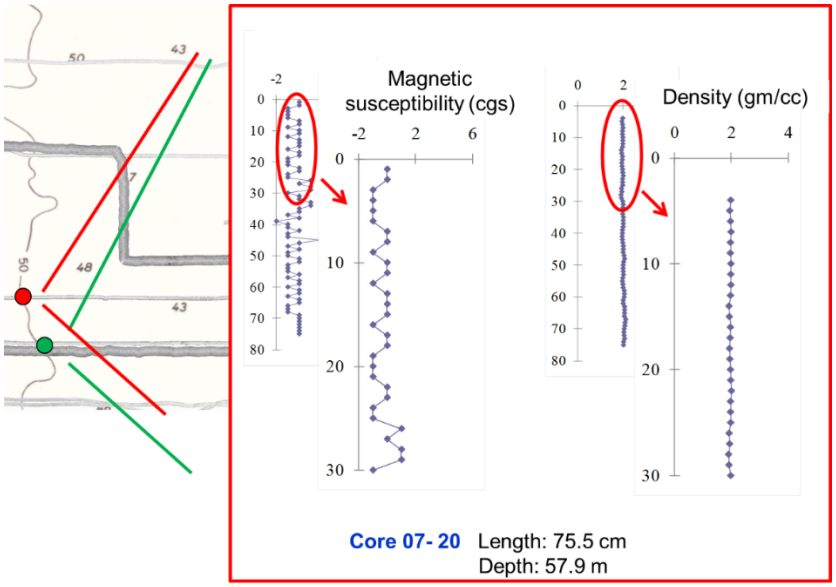
3.4.2.7 การวิเคราะห์ Polycyclic aromatic hydrocarbons (PAHs)

ดินตะกอนที่แช่แข็งนำไป freeze dried และสกัดตะกอนแห้งด้วยเทคนิค solvent extraction ด้วยชุดสกัด Soxhlet extraction ทำการ purify และ preconcentrate สารละลายที่ได้ จากนั้นลดปริมาตร เปลี่ยนตัวทำละลายเพื่อให้เหมาะสมกับการฉีดเข้าเครื่องGC/MS จากนั้นวิเคราะห์ polycyclic aromatic hydrocarbons (PAHs) โดยใช้เครื่องVarian Saturn 2200 Gas Chromatography/ Mass Spectrometric detector–Ion–Trap (GC/MS–Ion-Trap) (รูปที่ 3-20) โดยเลือก selective ion monitoring mode เพื่อจำแนกชนิดของ PAHs

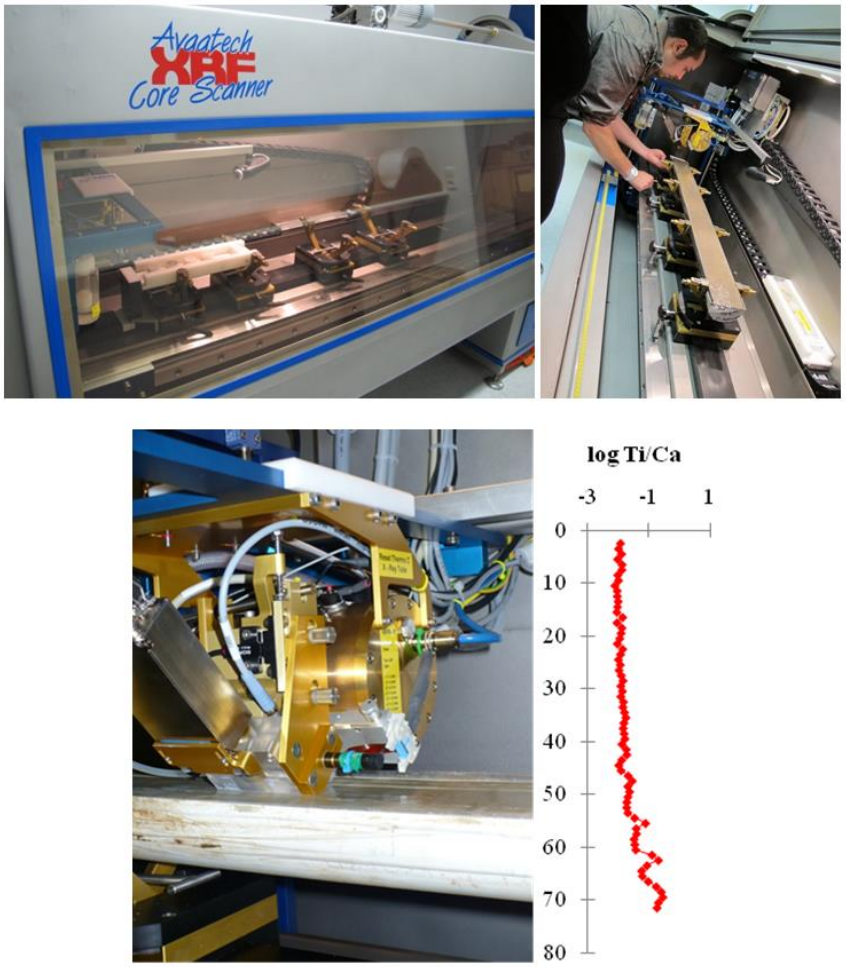
วิเคราะห์ปริมาณโดยเทียบกับสารละลายมาตรฐาน ตรวจสอบความแม่นยำของการวิเคราะห์ (quality control โดยวิเคราะห์ซ้ำ 10% ของตัวอย่าง และตรวจสอบความถูกต้อง (quality assurance) ของข้อมูลที่ได้โดยวิเคราะห์สารอ้างอิงมาตรฐาน (Standard Reference Materials; SRMs) 4 ชนิด ด้วยวิธีเดียวกัน (รูปที่ 3-21)



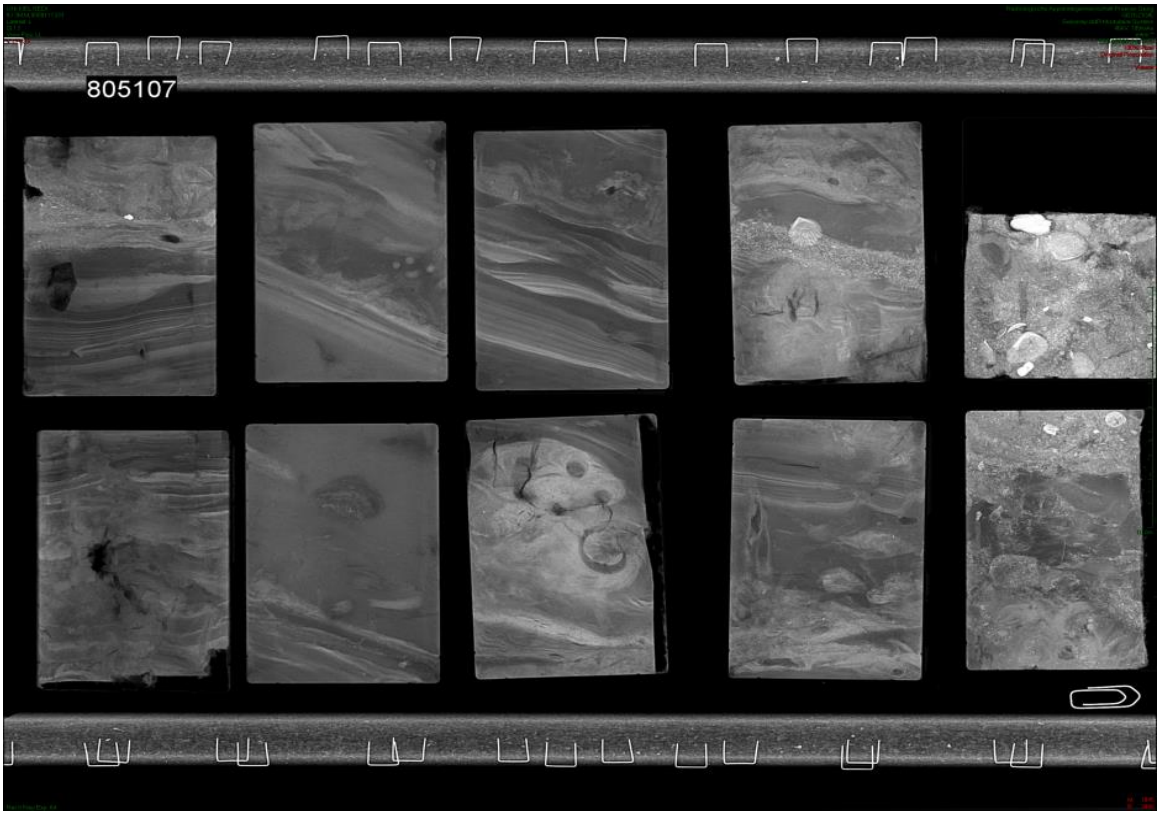
รูปที่ 3-15 เครื่อง Multi sensor core logger (MSCL) ณ Christian-Albrechts-University of Kiel ประเทศเยอรมนี



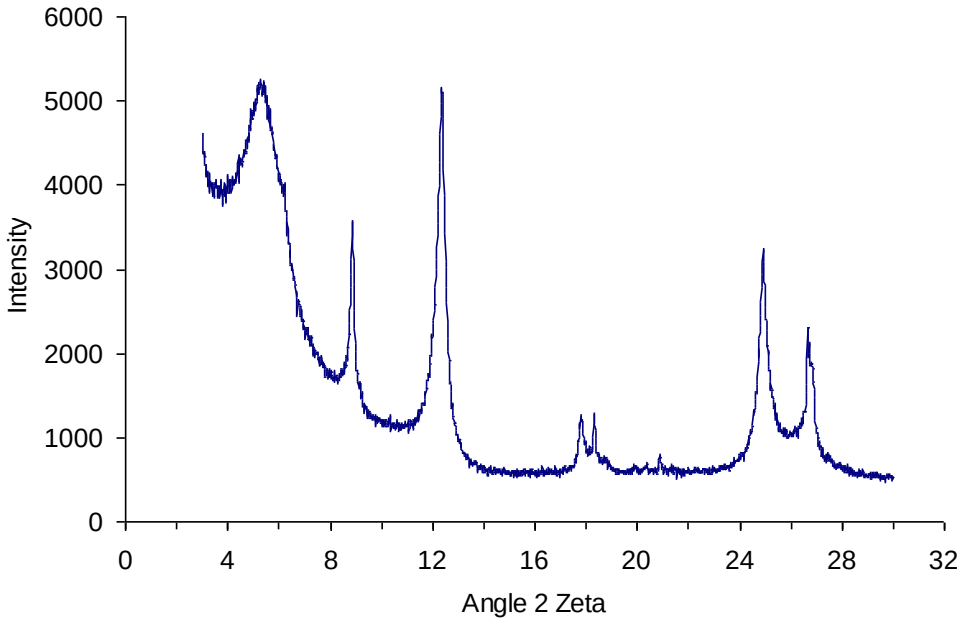
รูปที่ 3-16 การวิเคราะห์สมบัติทางกายภาพ (physical properties) แบบ (core loggers)



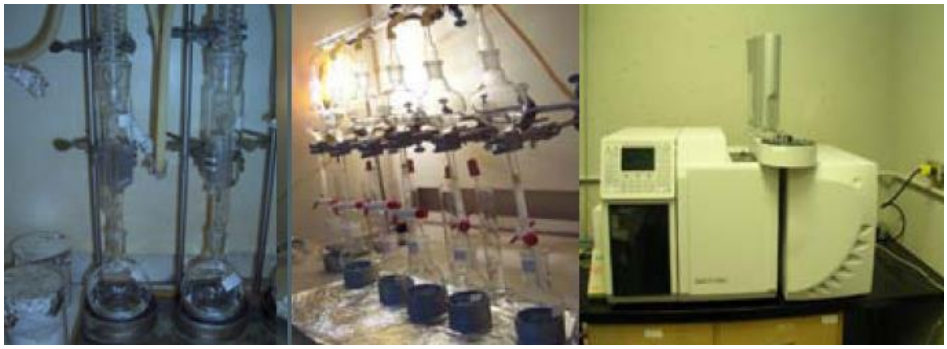
รูปที่ 3-17 เครื่องกวาดตรวจเอกซ์ฟลูออเรสเซน (X-ray Fluorescence scanner หรือ XRF scanner) ณ Christian-Albrechts-University of Kiel ประเทศเยอรมนี และการหาสัดส่วนของธาตุ (Ti/Ca)



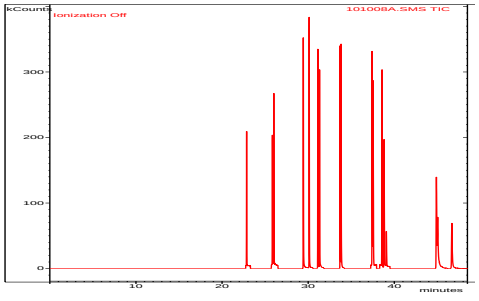
รูปที่ 3-18 ภาพถ่ายรังสีเอกซ์ (X-radiography images) ของแท่งตะกอน



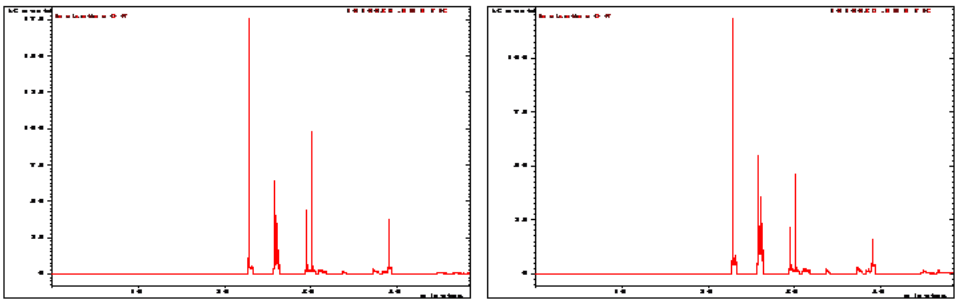
รูปที่ 3-19 ตัวอย่าง X-ray Diffraction Peak ของแร่ดินเหนียว



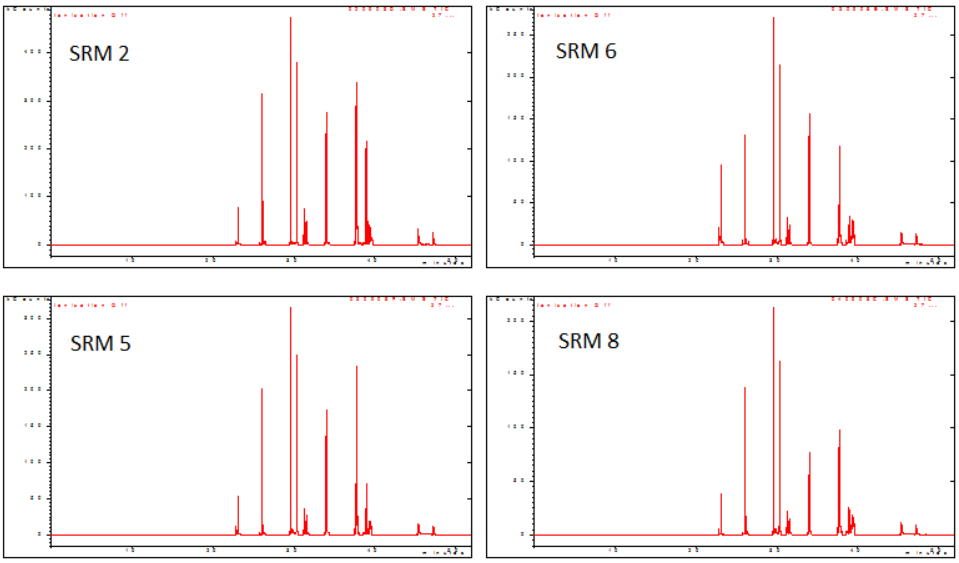
รูปที่ 3-20 ชุดสกัด Soxhlet extraction และเครื่อง Varian Saturn 2200 Gas Chromatography/Mass Spectrometric detector–Ion–Trap (GC/MS–Ion-Trap)



(ก)



(ข)



(ค)

รูปที่ 3-21 ตัวอย่าง Chromatograms ของ (ก) สารละลายมาตรฐาน, (ข) ตัวอย่างจากสถานี และ (ค) สารอ้างอิงมาตรฐาน

3.5 การวิเคราะห์ผล

เนื่องจากการศึกษาดำเนินการตั้งแต่เขตน้ำตื้นใกล้ฝั่งจนถึงเขตน้ำลึกไกลฝั่งออกไป ความจำกัดของเครื่องมือที่ใช้จึงทำให้ภาพโครงสร้างต่างๆ ที่ได้ ชัดเจนในเขตน้ำตื้น แต่จะเลือนไปบ้างในเขตน้ำลึก ระดับอ้างอิง (reference level) ที่ใช้ในการปรับ (adjust) เครื่องหยั่งความลึกด้วยเสียงชนิดหลายลำคลื่น (Multibeam) เพื่อที่จะให้ได้ข้อมูลความลึกน้ำที่เชื่อถือได้ (reliable bathymetrical data) คือ ระดับน้ำต่ำสุดในช่วงน้ำเกิด (spring tide low water) โดยข้อมูลทั้งหมดจะปรับแก้กับค่าระดับน้ำต่ำสุดในช่วงน้ำเกิดจากสถานีตรวจวัดระดับน้ำที่อ่าวเขาหลัก โดยใช้โปรแกรม Wxtide32 (www.wxtide32.com)

3.5.1 หย่อมโคลนที่ความลึกน้ำตั้งแต่ 7 เมตร ถึง 15 เมตร

ในบริเวณใกล้ฝั่งเข้ามา มีพื้นที่ที่ปกคลุมไปด้วยตะกอนละเอียดเป็นหย่อมๆ โดยพบที่ความลึกตั้งแต่ 7 เมตร ถึง 15 เมตร ซึ่งคลุมพื้นที่ไกลออกไปจากฝั่งประมาณ 6 กิโลเมตร หย่อมโคลนเหล่านี้พบเป็นหย่อมๆ ทางด้านทิศเหนือและด้านทิศใต้ของแหลมปะการัง โดยทางทิศเหนือและทิศใต้ครอบคลุมพื้นที่ประมาณ 9 และ 6 ตารางกิโลเมตร ตามลำดับ ธรณีสัณฐานของหย่อมโคลนในทิศทางที่ตั้งฉากกับแนวชายฝั่งของหย่อมโคลนทั้ง 2 ชุด แตกต่างกัน (รูปที่ 3-22)

หย่อมโคลนบางหย่อมอยู่บนแนวพื้นที่ที่ลาดเข้าหาฝั่ง บางหย่อมโดยเฉพาะอย่างยิ่งทางด้านทิศใต้ของพื้นที่ศึกษาพบหนาถึง 2 เมตร หย่อมโคลนเหล่านี้พบบริเวณด้านหน้าของยกพื้น ทั้งที่ที่เป็นแนวหินปูน (ปะการังเก่า) และแนวชั้นหินแกรนิต ซึ่งหินทั้ง 2 ประเภท พบได้ทั่วไปในพื้นที่ใกล้ฝั่งแถบนี้ หย่อมโคลนเหล่านี้มักจะมองไม่เห็นใน seismic profiles ทั้งนี้เป็นเพราะว่าความหนาของหย่อมโคลนต่ำเกินกว่าที่ตรวจจับได้ด้วยระบบวัดการสะท้อนของคลื่นไหวสะเทือน และถึงแม้ว่าจะมองเห็นใน seismic profiles ความหนาของมันมักไม่เกิน 1.5 เมตร ตัวอย่างเช่น ตะกอนละเอียดผิวหน้าดินที่พบในแท่งตะกอนหมายเลข CORE 071208-05 ที่ได้จากพื้นที่ศึกษา มีความหนาเพียง 15 เซนติเมตร ต่ำจากชั้นนี้ลงไปที่ความลึกระหว่าง 15 ถึง 21 เซนติเมตร มีชั้นที่ตะกอนเป็นทรายหยาบ แต่ไม่แยกชั้นได้ชัดเจน เพราะว่ามีส่วนของตะกอนละเอียดปะปน ลึกลงไปตามแนวแท่งตะกอนจะมีอีกช่วงที่มีความไม่ต่อเนื่อง เห็นความแตกต่างได้ชัดเจน พบทรายหยาบและเปลือกหอยปะปนอยู่ (ดูรายละเอียดในรูปที่ 3-23 และ 3-24)

ตัวอย่างตะกอนดินที่ได้จากพื้นที่มีหย่อมโคลนกระจายอยู่ ส่วนใหญ่จะประกอบไปด้วยขนาดทรายแป้ง (silt) ที่พื้นผิวหน้า โดยจะมีก้อนกรวด (clasts) ตั้งแต่ขนาดทราย (sand) ถึงขนาด (gravel) รองอยู่ด้านล่าง ในตัวอย่างตะกอนผิวหน้าหมายเลข GRAB 061208-11 (ตำแหน่งเก็บตัวอย่างแสดงไว้ในรูปที่ 3-22) พบพวกเศษดินลูกรัง (laterite) ในตะกอนจำพวกทรายคละขนาด (รูปที่ 3-25) และพื้นทะเลบริเวณโดยรอบหย่อมโคลนส่วนมากจะเป็นพวกทรายหยาบ

3.5.2 แนวร่องที่ความลึกน้ำตั้งแต่ 10 เมตร ถึง 16 เมตร

บริเวณน้ำลึก 10 ถึง 16 เมตร ภาพที่ประมวลได้จากการปะติดปะต่อข้อมูลภาพจากเครื่องโซนาร์กวาดทางข้าง (side scan sonar data) จะเห็นลักษณะพื้นทะเลที่เป็นร่องๆ (รูปที่ 3-23) ต่อเนื่องมาจากหย่อมโคลน พื้นท้องทะเลลักษณะเช่นนี้ พบที่ความลึกน้ำระหว่าง 30 ถึง 150 เมตร จากข้อมูลจาดเครื่องโซนาร์กวาดทางข้าง ตะกอนที่เติมเต็มร่องเหล่านี้เป็นตะกอนละเอียดเมื่อเทียบกับตะกอนข้างเคียง ห่างออกไปนอกฝั่งร่องอาจมีขนาดลึกถึง 2 เมตร เห็นได้ชัดในข้อมูล bathymetric data จากเครื่องหยั่งความลึกด้วยเสียงสะท้อนชนิดหลายลำคลื่น (multibeam echo-sounder) เมื่อประมวลกับข้อมูลจากการวัดการสะท้อนของคลื่นไหวสะเทือน (seismic data) พบว่าตะกอนในร่องแบ่งออกเป็น 2 ชั้น (รูปที่ 3-24) พื้นทะเลบริเวณข้างเคียงร่องก็มีลักษณะแบ่งชั้นเช่นกัน ตัวอย่างตะกอนผิวหน้าหมายเลข GRAB 021207-12 ที่เก็บจากบริเวณใกล้ร่องพบเศษพืชประเภทหญ้าที่มาจากบนฝั่ง (รูปที่ 3-26) ตัวอย่างแท่งตะกอนหมายเลข CORE 051207-32 (รูปที่ 3-27) เก็บจากบริเวณร่องที่ความลึกน้ำ 14.4 เมตร ประกอบไปด้วยชั้นโคลน (muddy layer) ซึ่งมีก้อนโคลนแข็งและเศษไม้ ชั้นดังกล่าวถูกคลุมด้วยชั้นที่เป็นทรายหยาบและเศษเปลือกหอย สัดส่วนความเข้มของ Ti/Ca และ Fe/Ca ตลอดแท่งตะกอน (รูปที่ 3-27) มีค่าต่ำในชั้นที่เป็นทราย (sand layers) และมีค่าสูงในบริเวณชั้นที่เป็นโคลน (muddy layers) ภาพถ่ายรังสีเอ็กซ์แสดงให้เห็นว่าชั้นที่เป็นโคลนมีเศษเปลือกหอยอยู่ใต้ฐานลงไป

3.5.3 สัณฐานที่เป็นสันเขา (ridges) จากความลึกน้ำ 15 เมตร ไปถึงนอกฝั่ง

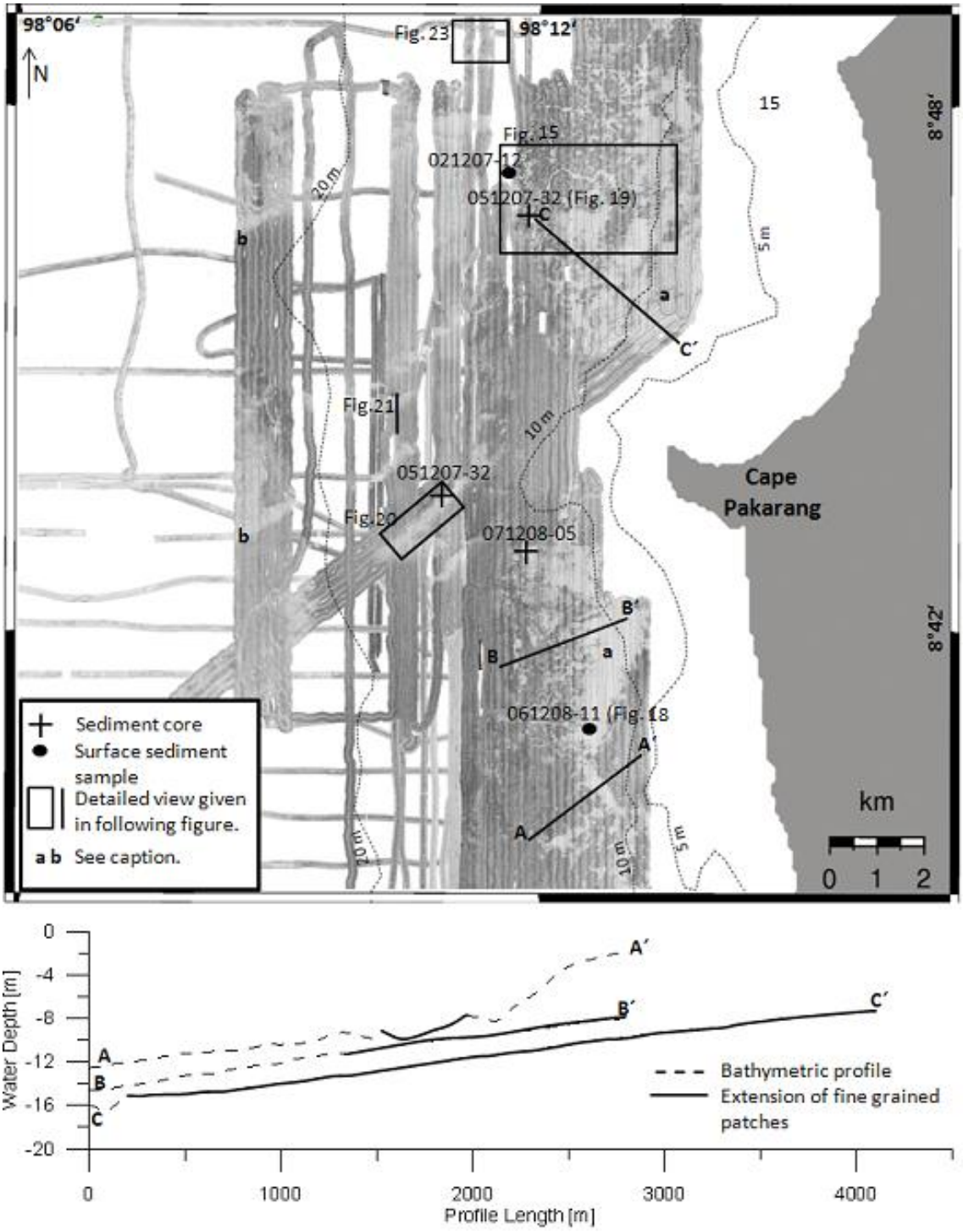
ในเขตน้ำลึกตามแนว SW-NE จากข้อมูล hydroacoustic และ bathymetric data จะเห็นเป็นสันเขา (ridges) (รูปที่ 3-22 และรายละเอียดขยายในรูปที่ 3-28) ลักษณะเช่นนี้พบได้ทั่วไปตั้งแต่นอกชายฝั่งทับละมุไปถึงแหลมปะการัง พบว่าได้เช่นกันหน้าเกาะพระทอง และทางด้านทิศเหนือของพื้นที่ศึกษา แต่ไม่พบแนวสันเขาพบพื้นทะเลบริเวณระหว่างเกาะคอเขากับเกาะพระทอง โดยทั่วไปโครงสร้างพื้นทะเลลักษณะนี้จะเริ่มพบที่ความลึกประมาณ 15 เมตร ต่อเนื่องไปจนถึงที่ความลึกประมาณ 30 เมตร เนื่องจากยังไม่มีการสำรวจไปไกลกว่านั้นจึงไม่อาจรู้ได้ว่าแนวสันเขานี้จะต่อเนื่องไปในที่ลึกกว่า 30 เมตร หรือไม่

แนวสันเขานี้มีความสูงประมาณ 2 เมตร จากพื้นทะเล ลักษณะจะหักชันในแนว NW และค่อยๆ ลาดเอียงลงในแนว SE ความยาวอาจจะถึงหลายกิโลเมตร และกว้างหลายร้อยเมตร ระยะระหว่างยอดสันเขา 2 ลูก อยู่ระหว่าง 1 ถึง 5 กิโลเมตร ข้างหน้าด้านที่ชันทาง NE จะเห็นเป็นแนวร่องที่บางครั้งบากลึกลงไปถึง 1 เมตร (รูปที่ 3-29)

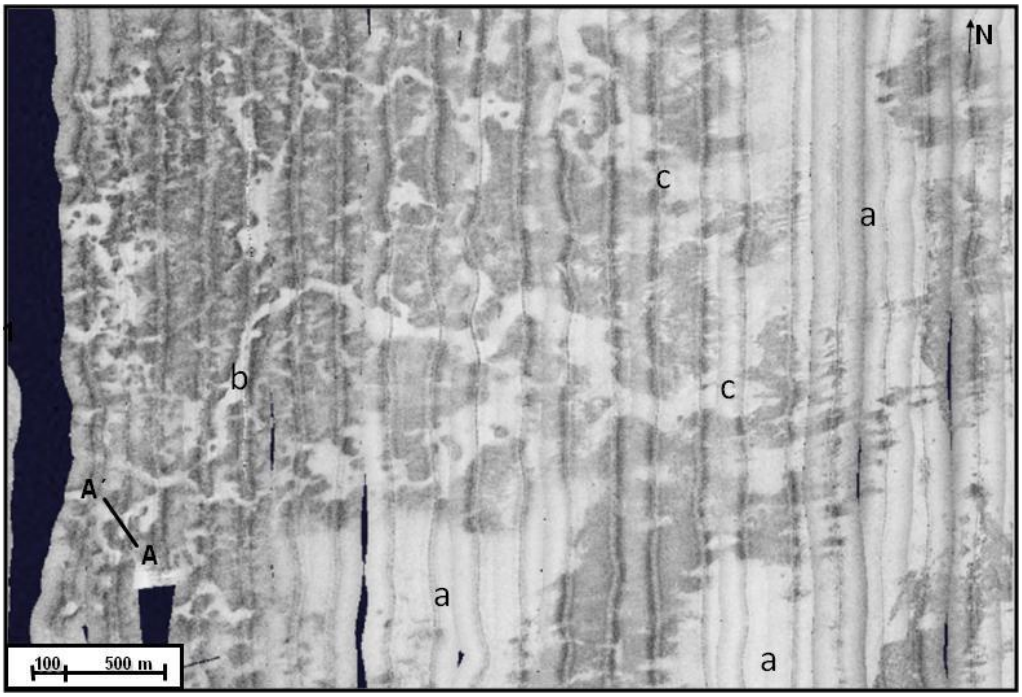
รูปที่ 3-28 แสดงภาพจากปะต่อข้อมูลภาพจากเครื่องโซนาร์กวาดทางข้าง เปรียบเทียบความสัมพันธ์ระหว่างโครงสร้างตะกอน (sedimentary structures) กับสัณฐานวิทยา (morphology) เงื่อนไขในการจัดทำภาพดังรูปที่ 20 นี้ จะต้องมีข้อมูลความลึกท้องทะเลโดยละเอียด (detailed bathymetric data) ตัวอย่างตะกอนผิวหน้าที่เก็บรอบสันเขาแสดงให้เห็นว่าสมบัติของตะกอนในพื้นที่

เล็กๆ นี้ มีความแตกต่างกันสูง แนวสว่างตามความยาวสันเขา และมีหย่อมตะกอนที่มีรูปร่างคล้ายเปลวเพลิง (flame-shaped sediment patches) อยู่ตามแนวลาดเอียง (slope) ของสันเขา ประกอบไปด้วยตะกอนทรายละเอียดถึงหยาบปานกลางที่มีการคัดขนาดดี (well sorted fine sand to medium sand) ที่ฐานของลาดเขามีลักษณะของการถล่มลงของตะกอน (slump-like sedimentary structures) เห็นได้ชัดเจนในภาพจากเครื่องโซนาร์กวาดทางข้าง จากตัวอย่างตะกอนผิวหน้าที่เก็บจากบริเวณนี้ พบว่าลึกลงไปจากตะกอนหยาบเพียง 2-3 เซนติเมตร จะประกอบไปด้วยโคลน ตัวอย่างแท่งตะกอนหมายเลข CORE 051207-37 (รูปที่ 3-30) จากบริเวณที่ลาดเอียง (slope) ของสันเขา ก็พบชั้นโคลนที่ความลึก 10 เซนติเมตร ที่ชั้นโคลนนี้พบว่าสัดส่วน Fe/Ca และ Ti/Ca มีค่าสูงกว่าส่วนอื่นๆ ในแท่งตะกอน ลึกลงไปกว่าชั้นนี้จะเป็นเปลือกหอยทั้งที่สมบูรณ์และที่เป็นเศษแตกหักสะสมอยู่ ลึกลงไปอีกจะเป็นทรายปนโคลน (muddy sand) ที่มีเปลือกหอยปะปน

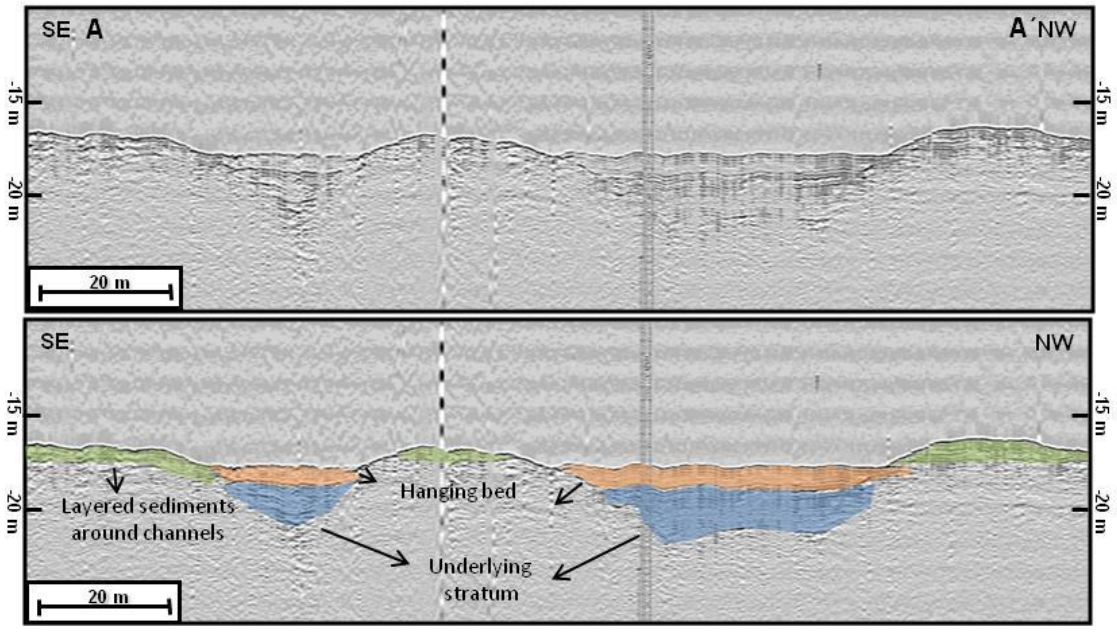
บางพื้นที่เศษหินปูนปะการัง (carbonatic reef fragments) ขนาดตั้งแต่ขนาดกรวด (gravel) ถึงขนาดก้อนกินมนใหญ่ (boulder) สะสมอยู่บริเวณฐานของสันเขาด้านที่มีความลาดชันสูง (ดูภาพจากวีดีโอใต้น้ำในรูปที่ 3-28) จากข้อมูลจากการวัดการสะท้อนของคลื่นไหวสะเทือน (seismic data) ในรูปที่ 3-29 โครงสร้างตะกอนของสันเขาไม่ต่อเนื่องกับโครงสร้างด้านล่าง และเห็นความแตกต่างของโครงสร้างตะกอนได้ชัดเจนว่าไม่มีความต่อเนื่อง (unconformity) โดยทั่วไปแล้วตะกอนรอบๆ สันเขาจะเป็นทรายหยาบ



รูปที่ 3-22 ภาพบน: ภาพที่ได้จากการปะติดปะต่อข้อมูลภาพจากเครื่องโซนาร์กวาดทางข้าง (side scan sonar) แสดงสภาพนอกชายฝั่งแหลมปะการัง (ข้อมูลจากการสำรวจปี พ.ศ. 2551) สีเข้มแสดงพื้นที่ที่มีลักษณะเป็นทราย ส่วนพื้นที่ที่มีสีอ่อนเป็นพื้นที่ที่ปกคลุมด้วยตะกอนละเอียด (พื้นที่ a ในภาพ) พาดไปตามแนว SW-NE และยังปรากฏให้เห็นแม้ว่าจะห่างฝั่งออกไปไกล (พื้นที่ b ในภาพ) และภาพล่าง: ภาพตัดขวางความลึก (bathymetric profiles) แสดงสัณฐานของหย่อมโคลน ตามแนว A – A’, B – B’ และ C – C’ ในภาพบน



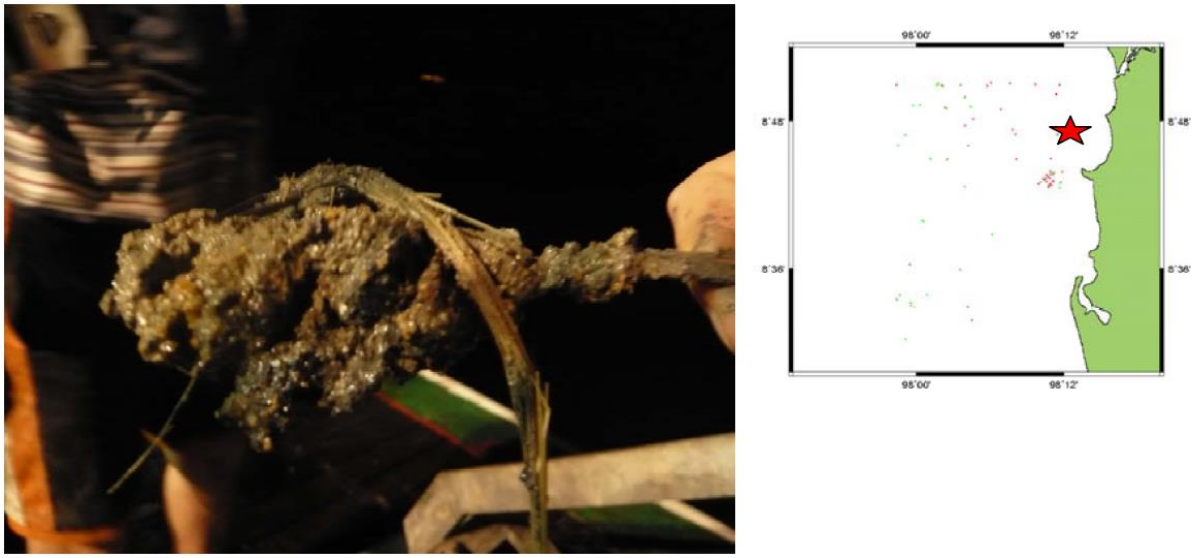
รูปที่ 3-23 ภาพแสดงหย่อมของตะกอนที่เป็นทรายแห้งและที่เป็นโคลน (a) นอกฝั่ง 3 ถึง 7 กิโลเมตร ความลึกน้ำ 7 ถึง 15 เมตร ไกลออกไปนอกฝั่งลักษณะเช่นนี้จะเห็นเป็นแนวแคบลง (b) ที่ยังคงเชื่อมต่อ (c) กับหย่อมโคลนใกล้ฝั่ง Profile A – A´ (รูปที่ 3-22 แสดงตำแหน่งการสำรวจ)



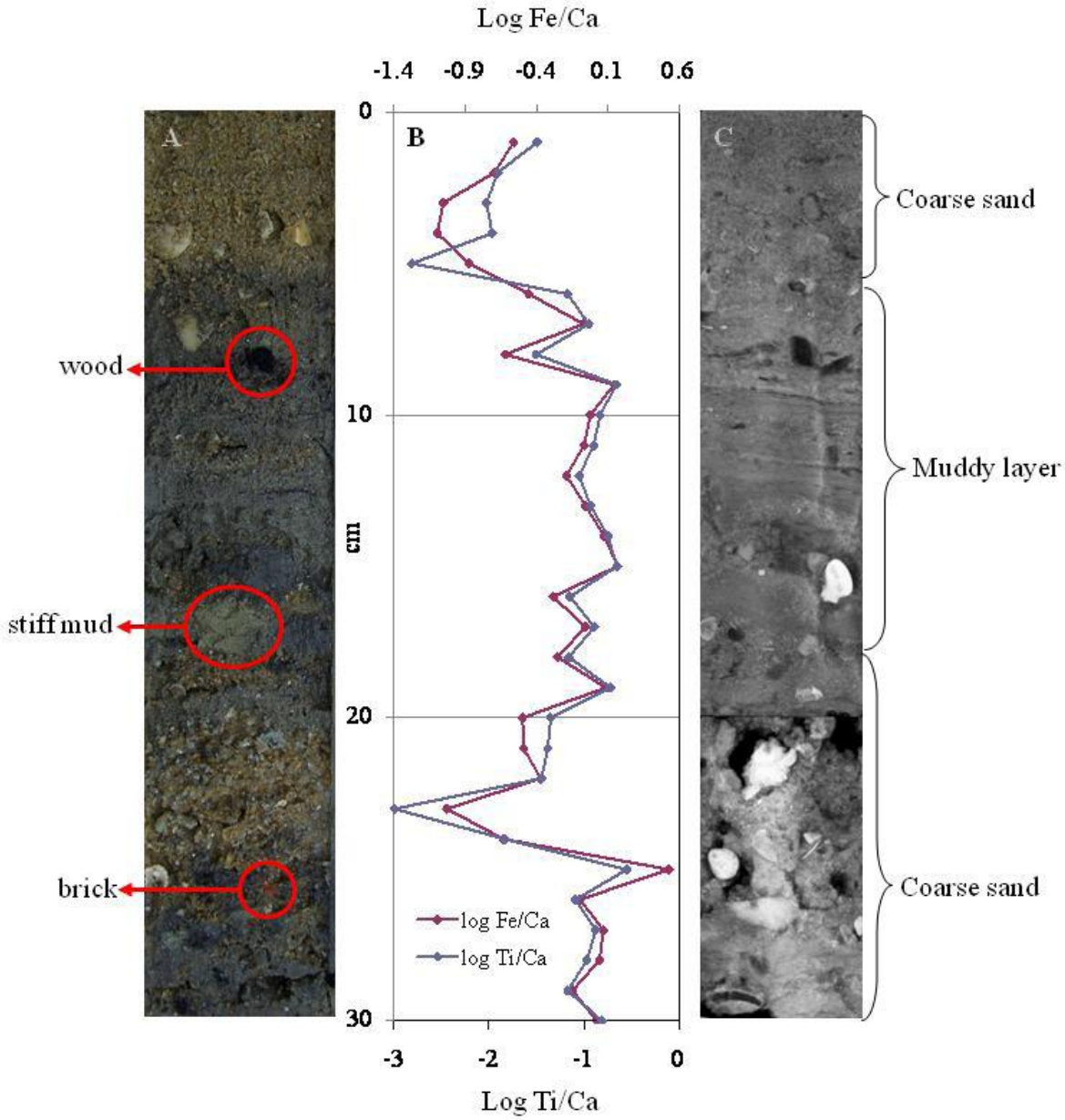
รูปที่ 3-24 Seismic profile ตัดพาดร่องโคลน (profile A-A´ ในรูปที่ 3-23) ในภาพจะเห็นร่อง 2 ร่อง ที่ถูกเติมเต็ม (ส่วนที่เป็นสีส้มและสีฟ้าในรูป) โครงสร้างของพื้นท้องทะเลโดยรอบเห็นเป็นชั้น ๆ เช่นกัน (ส่วนที่เป็นสีเขียว)



รูปที่ 3-25 ก้อนกรวด (clasts) ขนาดทรายหยาบประกอบไปด้วยเศษลูกรัง (laterite) ที่พบในตัวอย่างดินตะกอนผิวหน้าหมายเลข GRAB 061208-11 ที่เก็บที่ 3.5 กิโลเมตร นอกฝั่งแหลมปะการัง (ตำแหน่งเก็บตัวอย่างแสดงในรูปที่ 3-22)



รูปที่ 3-26 ตัวอย่างตะกอนผิวหน้าหมายเลข GRAB 021207-12 จากพื้นที่ใกล้ฝั่ง พบว่ามีซากพืชที่มีลักษณะคล้ายหญ้าบนบก ซึ่งหญ้าดังกล่าวถูกตะกอนขนาดหยาบปนละเอียดทับถมอยู่ลึกประมาณ 3 เซนติเมตร

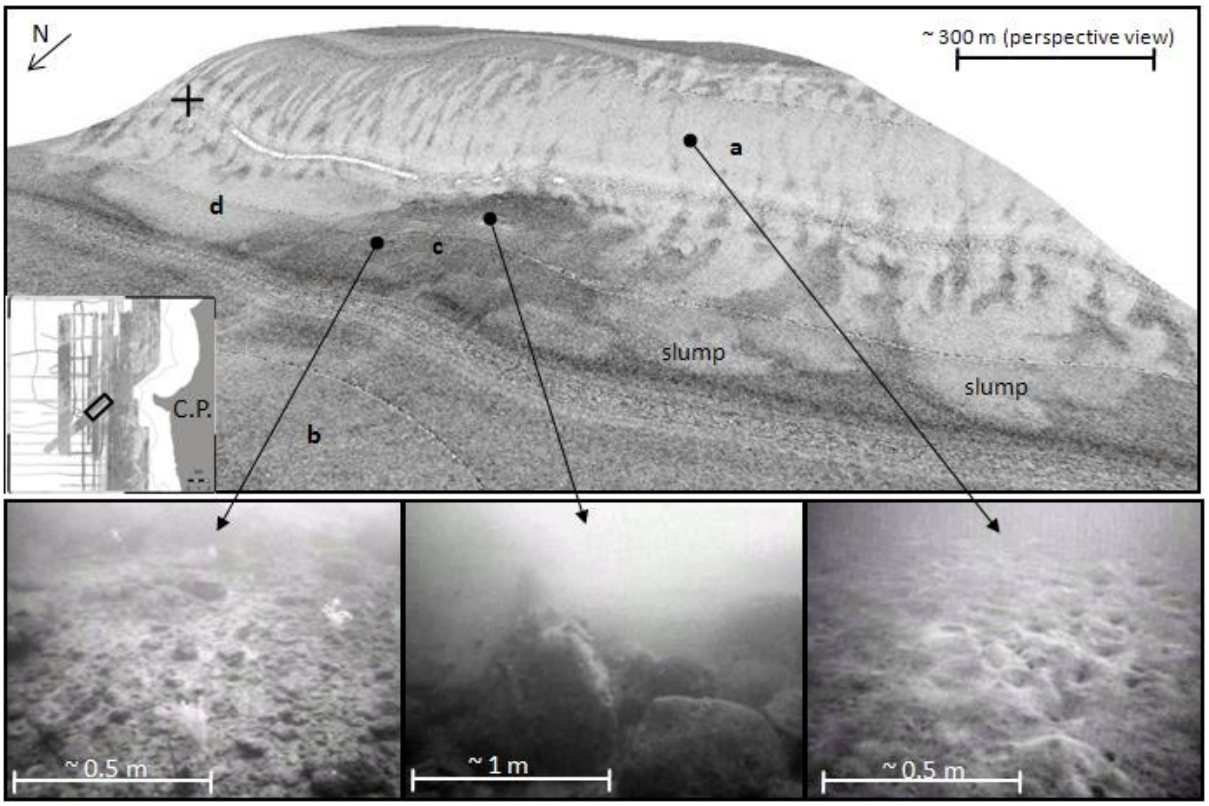


รูปที่ 3-27 แท่งตะกอนหมายเลข CORE 051207-32 ที่เก็บในพื้นที่ที่เป็นร่อง ที่ความลึกน้ำ 14.4 เมตร (ตำแหน่งเก็บตัวอย่างแสดงในรูปที่ 3-22)

ซ้าย: ภาพถ่ายแสดงลักษณะตะกอนในแท่งตะกอน

กลาง: กราฟแสดงสัดส่วน Ti/Ca และ Fe/Ca ที่ระดับความลึกต่างๆ ในแท่งตะกอน

ขวา: ภาพถ่ายรังสีเอกซ์ (X-radiography images)



รูปที่ 3-28 ภาพปะต่อจากข้อมูลที่ได้จากเครื่องโซนาร์กวาดทางข้าง (side scan sonar image) ของแนวสันเขาที่พบในชุดข้อมูลความลึก (bathymetric dataset) (รูปไม่ได้แสดงสัดส่วนจริง vertical exaggeration = 50x) (C.P. = แหลมปะการัง)

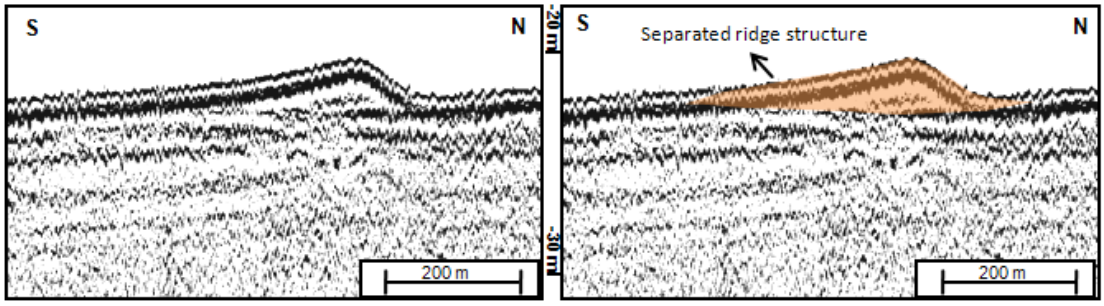
(a) รูปหย่อมตะกอนรูปร่างคล้ายเปลวเพลิง (flame-shaped sediment patches) ประกอบด้วยทรายขนาดละเอียดถึงหยาบปานกลาง (fine to medium sand)

(b) ตะกอนทรายหยาบ (coarse sand)

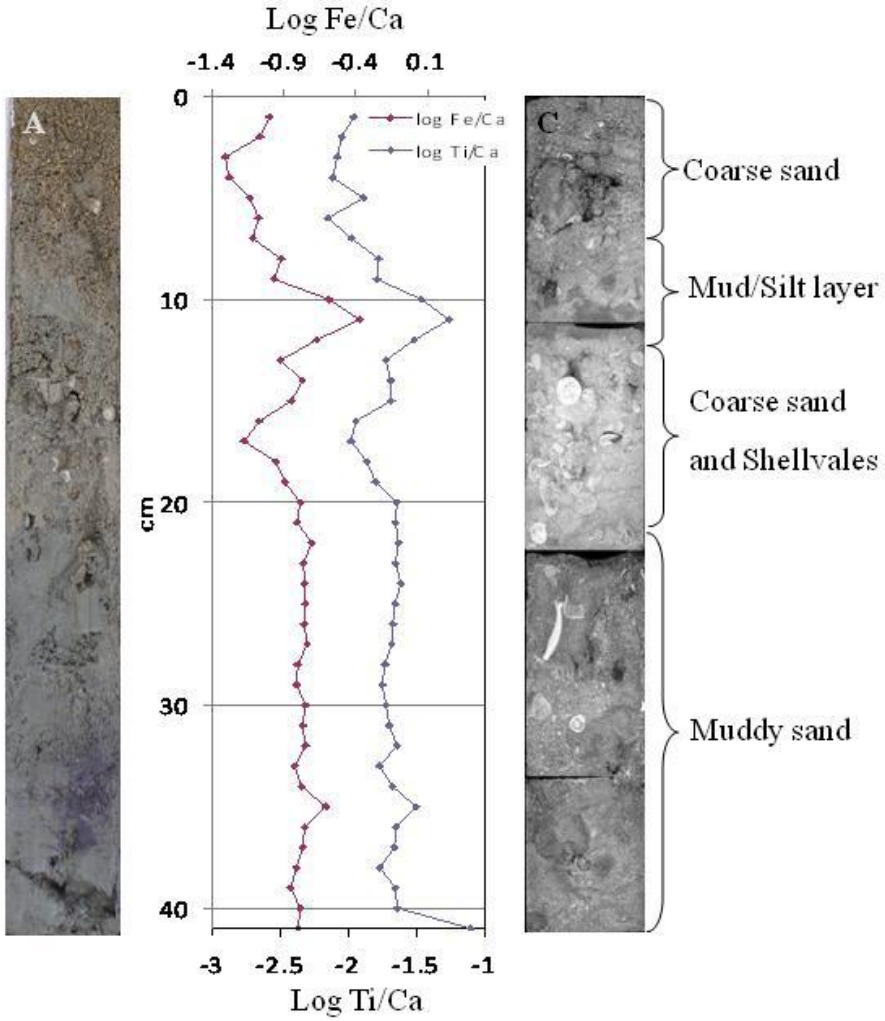
(c) กรวด (gravel) และก้อนหินมนใหญ่ (boulders) ประกอบไปด้วยเศษซากหินปูน (ภาพจากกล้องวีดีโอ)

(d) ผิวบนเป็นทราย (sand) และมีโคลนอยู่ด้านล่าง

(e) เครื่องหมาย + แสดงตำแหน่งเก็บตัวอย่างแท่งตะกอนหมายเลข CORE 051207-37 (รูปที่ 3-28) ตะกอนด้านบนเป็นทราย ชั้นตะกอนละเอียดพบลึกลงไปจากผิวราว 10 เซนติเมตร



รูปที่ 3-29 Seismic profile ตัดขวางแนวสันเขา (ตำแหน่งพื้นที่แสดงในรูปที่ 3.22) จะเห็นลักษณะที่ไม่สมมาตร (asymmetric form) ของสันเขา ซึ่งบ่งชี้ว่าการเคลื่อนย้ายตะกอนในแนวจากทิศใต้ไปทิศเหนือ ยิ่งไปกว่านั้นใต้สันเขายังเห็นแยกเป็นชั้น ๆ



รูปที่ 3-30 แท่งตะกอนหมายเลข CORE 051207-37 ที่เก็บจากบริเวณลาดเอียง (slope) ของสันเขา ด้านซ้าย: ภาพถ่ายแสดงลักษณะตะกอนในแท่งตะกอน ตรงกลาง: กราฟแสดงสัดส่วน Ti/Ca และ Fe/Ca ที่ระดับความลึกต่าง ๆ ในแท่งตะกอน และด้านขวา: ภาพถ่ายรังสีเอกซ์ (X-radiography images)

3.5.4 ผลการศึกษาด้านอื่นที่ได้จากข้อมูลธรณีฟิสิกส์และตะกอนวิทยา

3.5.4.1 เศษซากร่องรอย (remnants) จากการทำเหมืองแร่ดีบุก

ที่ความลึกน้ำ 20 ถึง 25 เมตร ทางทิศตะวันตกเฉียงเหนือของแหลมปะการัง เศษซากร่องรองการทำเหมืองแร่ดีบุกในอดีตของพื้นที่หน้าเขาหลัก โดยมีลักษณะเป็นหลุมลึก บางหลุมลึกถึง 7 เมตร หลุมเหล่านี้เห็นได้ชัดเจนจากข้อมูลภาพจากเครื่องโซนาร์กวาดทางข้าง (รูปที่ 3-31) โดยจะเป็นบริเวณที่มีสีอ่อนกว่าพื้นที่รอบๆ ซึ่งอาจจะเนื่องมาจากการที่หลุมเหล่านี้มีตะกอนละเอียดลงมาตกสะสม

3.5.4.2 ลานหินและหลุมเล็ก ๆ ที่ความลึกน้ำระหว่าง 30 ถึง 35 เมตร

ที่ความลึกน้ำระหว่าง 30 ถึง 35 เมตร พบลานหินและก้อนหินมนใหญ่ (stone and boulder fields) เป็นแนวยาว ปรากฏชัดเจนในข้อมูลภาพจากเครื่องโซนาร์กวาดทางข้าง (รูปที่ 3-32A) ไกลออกจากไปอีกจะพบลักษณะที่เป็นหลุมกลมขนาดเล็ก เส้นผ่านศูนย์กลางประมาณ 10 เมตร ปรากฏให้เห็นในข้อมูลภาพจากเครื่องโซนาร์กวาดทางข้าง พบได้ทั่วไปที่ความลึกน้ำประมาณ 35 เมตร (รูปที่ 3-32B) แต่ลักษณะพื้นทะเลเช่นนี้ไม่สามารถเห็นได้จากข้อมูลความลึกท้องทะเล (bathymetric data) จากเครื่องหยั่งความลึกด้วยเสียง เนื่องจากปัญหาทางเทคนิคในการปรับแก้ค่าการเคลื่อนที่ที่หัวรับสัญญาณ (heave correction of the motion sensor) ในบางวัน เมื่อคราวสำรวจปี 2550 จากข้อมูลภาพจากเครื่องโซนาร์กวาดทางข้าง เมื่อเปรียบเทียบลักษณะข้อมูลตะกอนในในหลุมกับพื้นที่ข้างเคียง หลุมเหล่านี้น่าจะมีตะกอนละเอียดมาสะสม แต่เนื่องจากขนาดที่เล็กของหลุ่มทำให้ไม่สามารถเก็บตัวอย่างตะกอนขึ้นมาดูได้

3.5.4.3 อายุตะกอนจากแท่งตะกอนจากระดับความลึกน้ำ 52 เมตร

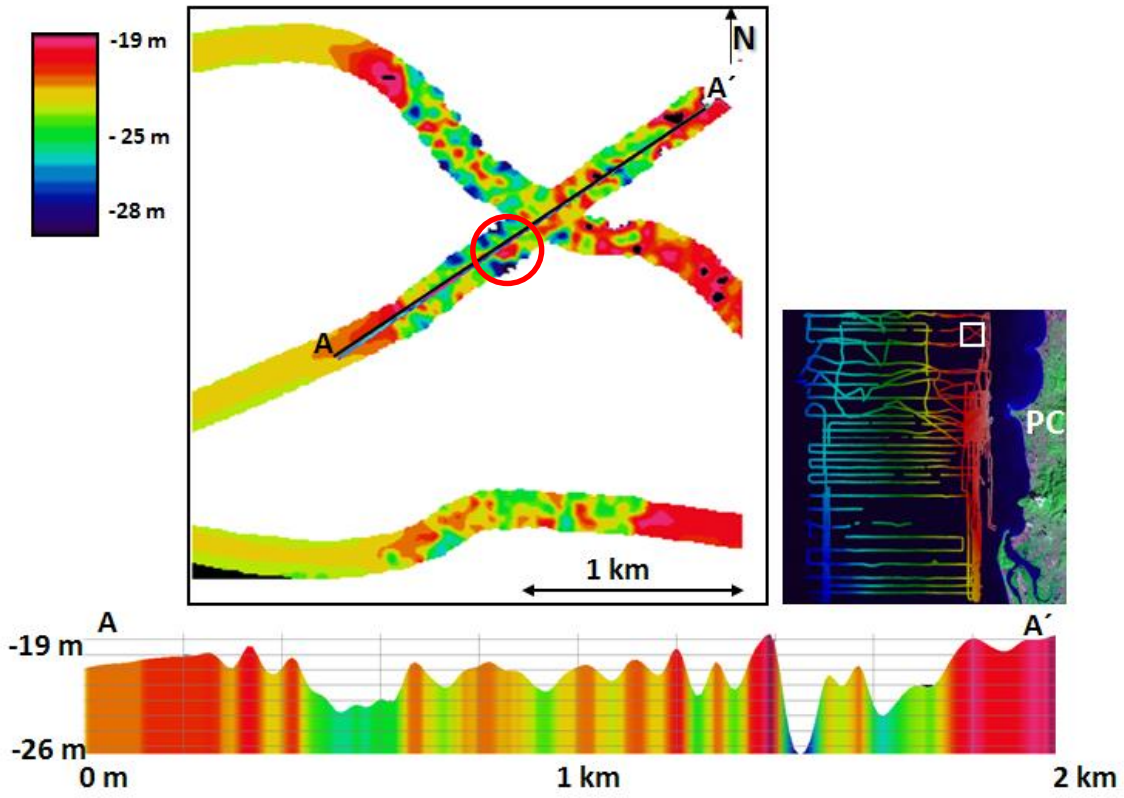
แท่งตะกอนที่ได้จากระดับความลึกน้ำ 50 ถึง 60 เมตร แสดงให้เห็นถึงโครงสร้างภายในจากตัวอย่างแท่งตะกอนหมายเลข CORE 021207-18 (รูปที่ 3-33) พบว่าเป็นโคลนปนทราย (sandy mud) ซึ่งมีเปลือกหอยปะปนตบอดแท่งตะกอน จากข้อมูลขนาดตะกอนแสดงให้เห็นการกระจายตัวของตะกอนว่ามีความหยาบเพิ่มขึ้นเล็กน้อยเป็นลำดับ (slight coarsening-upward sequence) จากฐานขึ้นมาจนถึงระดับความลึก 10 เซนติเมตร แต่จากระดับ 10 เซนติเมตร ขึ้นมาถึงผิวตะกอนพบว่ามีการกระจายขนาดของตะกอนจากละเอียดมาเป็นหยาบขึ้นเป็นลำดับอยู่ 2 ชุด อย่างไรก็ตามจากการวิเคราะห์ Pb-210 บ่งชี้ว่าชุดที่อยู่บนสุดน่าจะเกิดขึ้นในช่วงเหตุการณ์อุบัติภัยคลื่นสึนามิเมื่อปี พ.ศ. 2547 ส่วนชุดที่อยู่ล่างลงไปตะกอนมีอายุแก่กว่า

จากการวิเคราะห์เพื่อหาอายุตะกอนนั้น ต้องมีการทำ age model แสดงในกราฟเส้นสีม่วง รูปที่ 3-33 และแสดงค่า range ของอายุที่เป็นไปได้ดังเส้นสีน้ำเงินและเหลือง ตามลำดับ จากการสร้าง age model นั้นพบว่า ตะกอนหมายเลข CORE 021207-18 แบ่งออกเป็น 3 ชั้น ชั้นที่ 1 และชั้นที่ 3 มีอัตราการสะสมตัวของตะกอน มีค่า 0.3 ซม. ต่อปี แต่ชั้นที่ 2 คือช่วงกลางของแท่งตะกอนจะมีการตกตะกอนอย่างรวดเร็ว และ/หรือ มีการผสมกันในชั้นตะกอน จากความแตกต่างนี้ทำให้เห็นได้ว่าบริเวณนี้มีการสะสมตัวของ

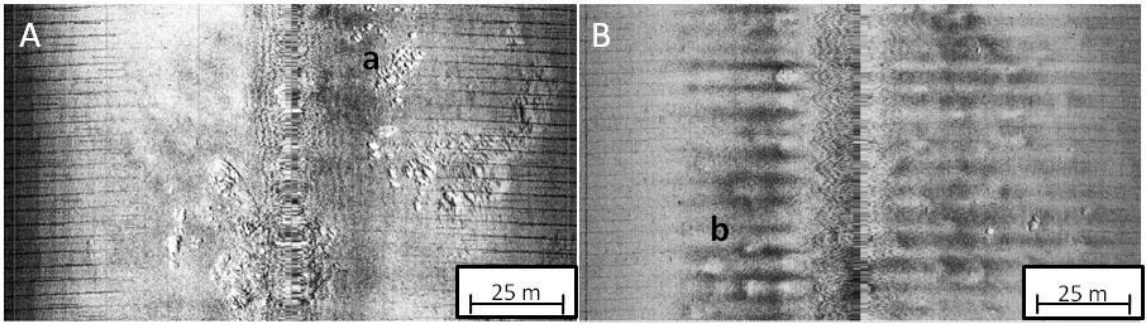
ตะกอนที่แตกต่างกัน ดังจะเห็นได้ว่าตะกอนชั้นบนและชั้นที่ 3 นั้นเป็นการสะสมตัวแบบปกติ แต่มีเหตุการณ์ที่มีผลต่อรูปแบบการสะสมตัวของตะกอนเกิดขึ้นในช่วงที่ 2 โดยเฉพาะช่วงอายุของปี 1990 พบว่า อัตราการสะสมตัวของตะกอนของตะกอนชั้นบน มีค่าประมาณ 0-5 ซม. ซึ่งสอดคล้องกับการเกิดเหตุการณ์พายุไต้ที่มีการบันทึกผลกระทบต่อทะเลอันดามัน คือ ไต้ฝุ่นเกย์ในปี พ.ศ. 2532 (ค.ศ. 1989)

3.5.4.4 ข้อมูลจากระดับความลึกน้ำ 60 ถึง 80 เมตร

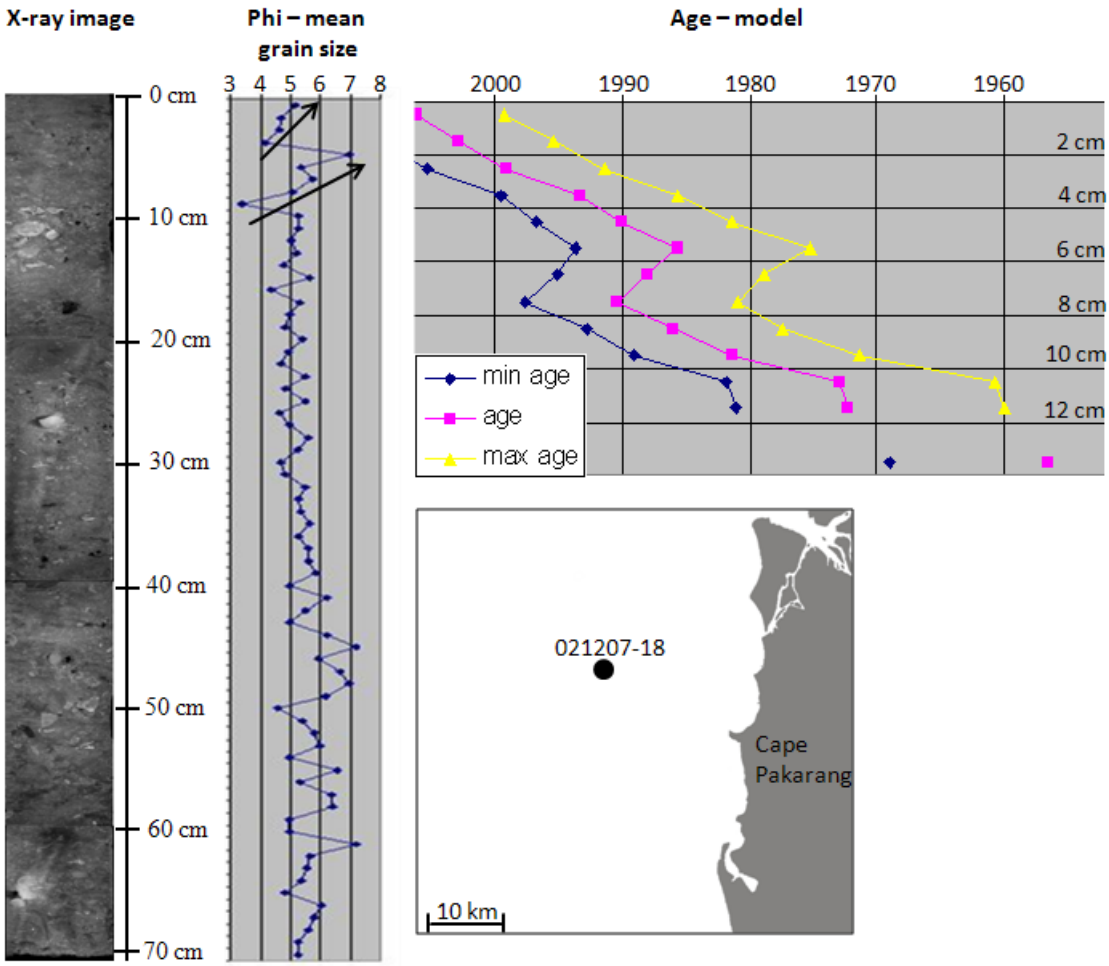
ส่วนใหญ่แล้ว พื้นที่ลาดเอียงของพื้นทะเลที่ความลึกน้ำ 30 เมตร ลงไปจนถึง 80 เมตร พบการยกตัวในแนวเหนือ-ใต้ หลายแห่ง ร่องลึกหลายเมตรพบเห็นได้ในหลาย profiles บริเวณตะวันตกเฉียงใต้ของพื้นที่ศึกษา ที่ความลึกประมาณ 80 เมตร จากข้อมูลจากระบบวัดการสะท้อนของคลื่นไหวสะเทือน (seismic data) ชุดแรกจากการสำรวจในปี 2550 พบว่าตะกอนสมุทร (marine sediments) วางตัวเป็นแผ่นบางๆ (thin sheet) บนสัณฐานบรรพกาล (paleomorphology) (รูปที่ 3-34)



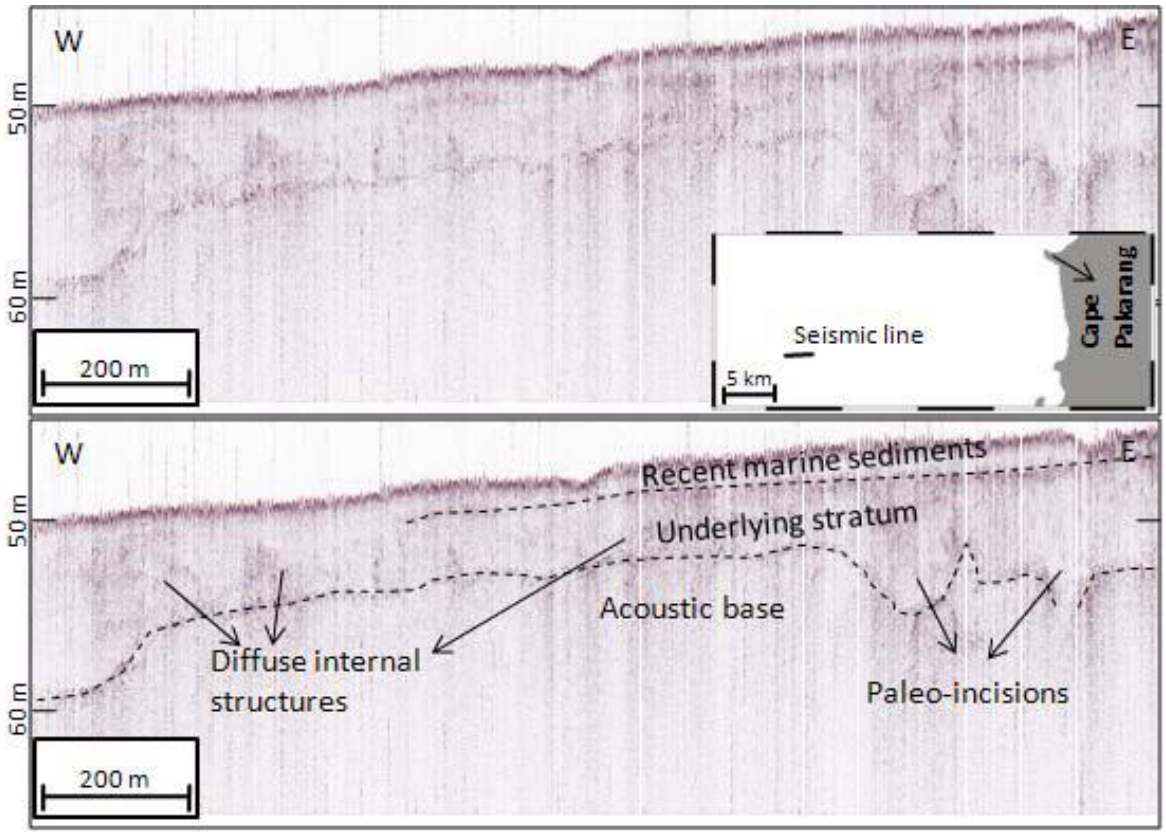
รูปที่ 3-31 ข้อมูลพื้นท้องทะเล (Bathymetric data) ทางตะวันออกเฉียงเหนือของแหลมปะการัง (PC) เมื่อครั้งการสำรวจในปี 2550 จะเห็นร่องรอยการทำเหมืองดีบุกได้ชัดเจน ในลักษณะเป็นหลุมลึกที่เกิดขึ้นเป็นหย่อมๆ ในพื้นที่ตอนเหนือของพื้นที่ทำการสำรวจ (ในรูปทางด้านขวา)



รูปที่ 3-32 รูป A: บริเวณ (a) ในรูป เป็นลานหิน (Stone fields) ที่พบที่ความลึกน้ำ 30 ถึง 35 เมตร รูป B: บริเวณ (b) ในรูป เป็นหลุมเล็กๆ (small depressions) พบทั่วไปที่ความลึกน้ำ 35 เมตร (ตำแหน่งที่พบแสดงในรูปที่ 3-31)



รูปที่ 3-33 ภาพถ่ายรังสีเอกซ์ (X-radiography images), ขนาดเฉลี่ยของตะกอน และโครงสร้างอายุ (age model) ของแท่งตะกอนหมายเลข CORE 021207-18 ซึ่งเก็บตัวอย่างจากนอกชายฝั่ง 24 กิโลเมตร ที่ระดับความลึกน้ำ 52 เมตร บริเวณที่มีการกระจายขนาดของตะกอนจากหยาบมาละเอียดขึ้นเป็นลำดับ ซึ่งมีอยู่ 2 ชุด แสดงไว้โดยลูกศร



รูปที่ 3-34 ในเขตน้ำลึก ตะกอนสมุทรยุคปัจจุบัน (recent marine sediments) ดูเหมือนจะเกิดเป็นแนวบาง ๆ อยู่ปกคลุมอยู่ด้านบนและวางตัวอยู่ใต้ชั้นฐาน (underlying stratum) ในชั้นใต้ชั้นตะกอนสมุทรจะพบโครงสร้าง diffuse internal structures ซึ่งยังไม่รู้มูลเหตุกำเนิด

3.5.5.5 ผลการศึกษารูปแบบของการสะสมตัวของตะกอนสึนามิ

การวิเคราะห์แท่งตะกอน ดังตาราง 3-1 เพื่อจำแนกร่องรอยและรูปแบบของการสะสมตัวของตะกอนสึนามิในแท่งตะกอน โดยดูลักษณะการเรียงตัวของชั้นตะกอน เช่น การสะสมตัวแบบชั้นหย่อมโคลน ชั้นทราย เหนือชั้นตะกอนสึนามิ โดยแสดงดังตารางที่ 3-1 ทั้งนี้การจำแนกดูได้จากลักษณะทางกายภาพ เช่น ชั้นที่มีเศษซากเปลือกหอย ชั้นของ clay-clasts ชั้นกรวด ชั้นเศษดินลูกรัง หรือการเรียงตัวในรูปแบบอื่นๆ โดยนำไปวิเคราะห์ด้วย ไอโซโทป Pb-210 เพื่อจำแนกเหตุการณ์ที่เกิดขึ้นในอดีต

ตาราง 3-1 ข้อมูลแท่งตะกอนจากบริเวณ offshore area (คำย่อ:TL = Tsunami Layer คือ ชั้นตะกอนสึนามิ WT = Water Depth คือ ความลึกน้ำ)

ชื่อแท่งตะกอน	วันที่เก็บ	ตำแหน่ง	ความลึกน้ำ (ม.)	ระยะทางจากฝั่ง (กม.)	ความยาวแท่งตะกอน (ม.)	ความหนาของชั้นสึนามิ (ซม.)	ความหนาของชั้นเหนือชั้นสึนามิ (ซม.)
031207-23	03.12.07	08°44.879'N 98°01.173'E	57.0	25.5	0.70	---	---
051207-31*	05.12.07	08°47.176'N 98°11.724'E	15.9	7.2	0.70	12.0	0.0
051207-32/2(c)	05.12.07	08°46.725'N 98°11.814'E	14.4 (ch)*	7.2	0.30	5.0	>25.0
030310- C2+	03.03.10	08°36.474'N 98°12.454'E	11.5	3.3	0.23	12.0	5.0
030310- C3**+	03.03.10	08°38.708'N 98°12.931'E	9.5	3.2	0.97	18.0	22.0
030310- C7+	03.30.10	08°41.053'N 98°12.763'E	11.9	2.9	0.65	39.0	3.0
050310-C2	05.03.10	08°45.438'N 98°13.186'E	9.8	1.5	0.75	9.0	31.0
050310-C3	05.03.10	08°46.352'N 98°13.182'E	11.2	3.9	0.52	13.0	5.0
050310-C4+	05.03.10	08°46.659'N 98°12.269'E	15.3	6.3	0.55	13.0	2.0
050310-C6***	05.03.10	08°38.761'N 98°12.967'E	9.6 (mp)*	3.1	0.99	18.0	22.0

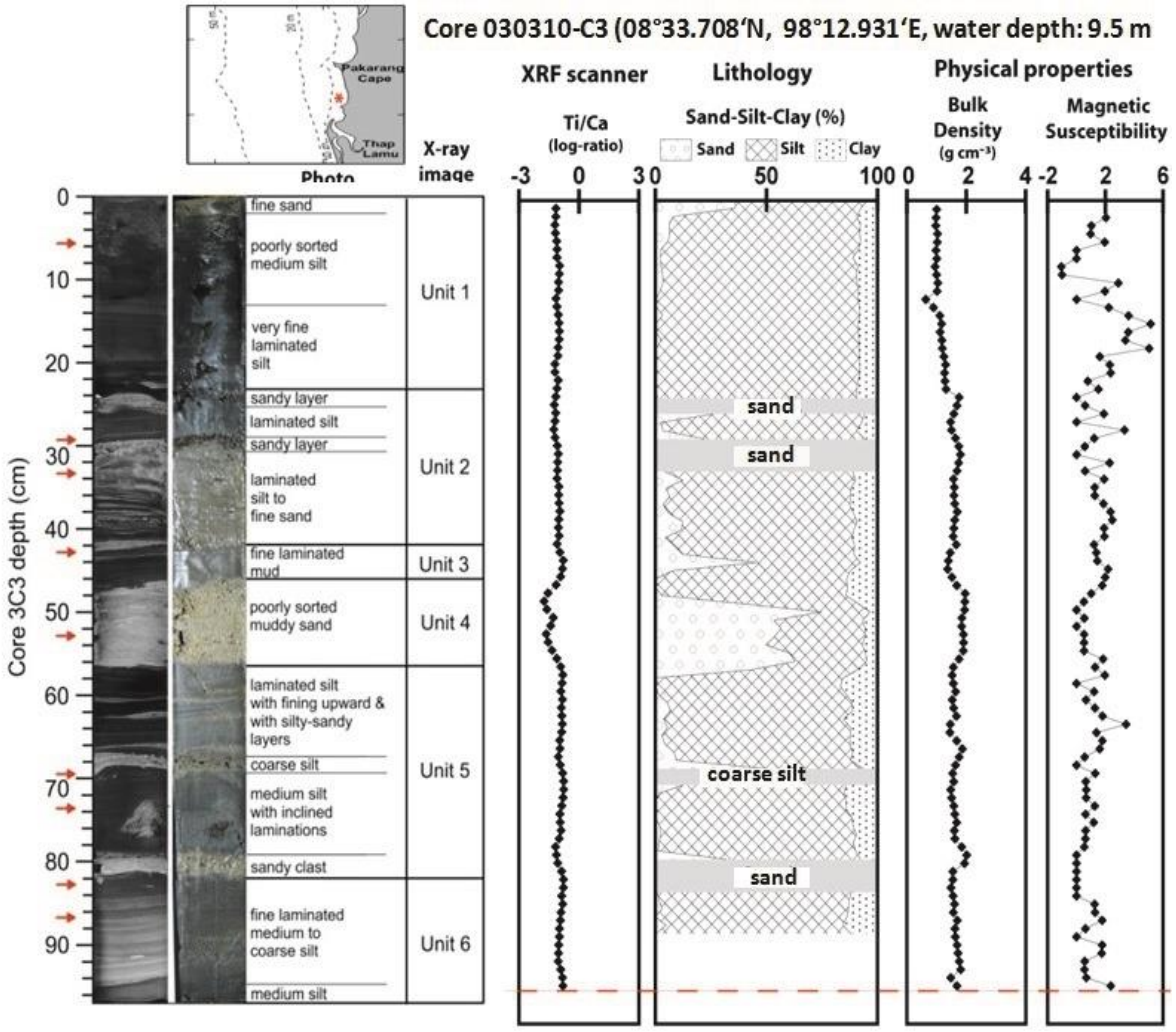
* ch = channel structure, mp = mud patch, ** รูปที่ 3-35, *** รูปที่ 3-36,

+ หมายถึงพบชั้นของ storm ใต้ชั้น tsunami

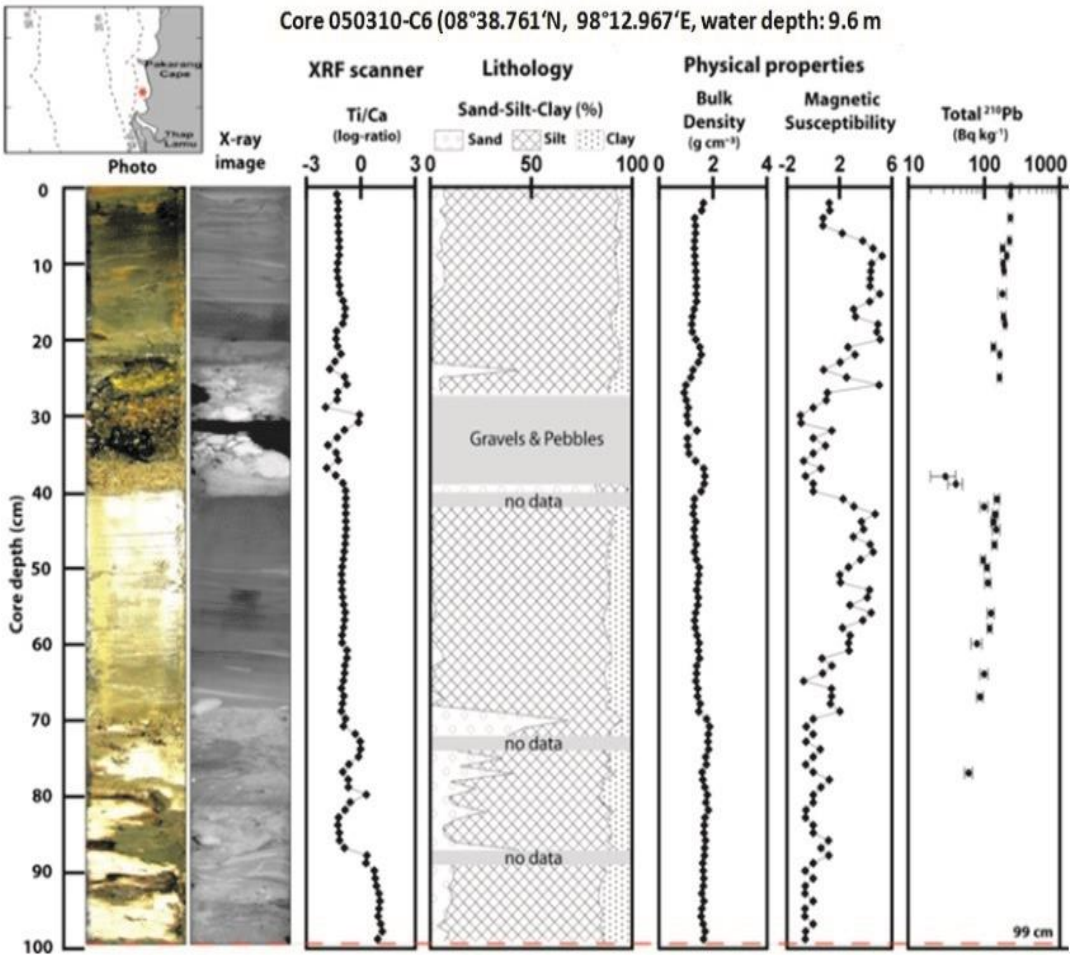
จากรูปที่ 3-35 และ รูปที่ 3-36 ทำการวิเคราะห์หา สัดส่วนความเข้มของ Ti/Ca แบบ log-ratio ตลอดแท่งตะกอน พบว่าสัดส่วนมีค่าค่อนข้างคงที่ในแท่งตะกอน 030310-C3 และ 050310-C6 และประกอบภาพถ่ายรังสีเอ็กซ์แสดงให้เห็นว่าในแท่งตะกอนนี้ไม่มีชั้นร่องรอยสึนามิอย่างชัดเจน แต่ทั้งนี้การวิเคราะห์ โดยวิธี PCA จากข้อมูล XRF ทำให้ทราบว่าแหล่งที่มาของตะกอนที่ทับถมในบริเวณนี้มีการผสมกันจากหลายแหล่ง ทำให้สามารถจำแนกชั้นตะกอนได้จากคุณลักษณะทางกายภาพ จากการวิเคราะห์องค์ประกอบอื่น ได้พบชั้น event layer ที่เป็นร่องรอยของเหตุการณ์ต่างๆที่เกิดขึ้น ในแท่งตะกอน 050310-C6 พบชั้นของ run up พบชั้นตะกอนที่เกิดจากกระแสไหลย้อนของคลื่นสึนามิขาออกที่ไหลกลับลงสู่ทะเล การวิเคราะห์ข้อมูล foraminifera หน้าดิน (benthic foraminifera) พบการกระจายตัวในแท่งตะกอน 030310-C3 และ 050310-C4 ซึ่งสามารถแยกชนิดของ foraminifera ซึ่งแสดงให้เห็น zonations ของชนิดและสายพันธ์ต่างๆ ของ foraminifera ตามความลึกจากตัวอย่างตะกอนพื้นทะเลที่ความลึกน้ำตั้งแต่ 9.5 เมตร (แท่งตะกอน 030310-C3) - 63.4 เมตร (050310-C4) โดย แท่งตะกอน 030310-C3 พบชั้นของตะกอนจากความลึก 20 เมตรซึ่งมีระยะห่างจากฝั่งประมาณ 5 กม.

นอกจากนี้การพบชั้นตะกอนสึนามิแล้วนั้น ยังสามารถระบุชั้นตะกอนที่เกิดจากพายุในอดีต โดยจะพบชั้นตะกอนทรายที่ลักษณะแตกต่างกัน เช่น ในแท่งตะกอน 030310-C3 และ 051207-03 จะพบชั้นเหตุการณ์ 3 ชั้น ในแท่งตะกอน 030310-C7 พบชั้นเหตุการณ์ 2 ชั้นและแท่งตะกอน 050310-C4 พบเพียง 1 ชั้น แสดงว่ามีการเคลื่อนที่ของตะกอนจากน้ำลึกไปยังตำแหน่งของแท่งตะกอน ที่บ่งชี้ได้ในชั้นเหตุการณ์ที่เกิดพายุ ประกอบกับการวิเคราะห์ด้วย Pb-210 ของชั้นเหนือและใต้ฐานของชั้นเหตุการณ์สามารถทราบถึงอัตราการสะสมตัวของตะกอนอยู่ระหว่าง 1.3 - 5.7 ซม.ต่อปี

รูปแบบการกระจายตัวของ PAH ในตะกอนดินจะลดลงเรื่อย ๆ จากใกล้ฝั่งไปจนนอกฝั่ง แต่จากฝั่งแหลมปะการังพบว่าการกระจายตัวจะเพิ่มขึ้น ทั้งนี้ค่า PAH จะเพิ่มขึ้นตามระยะทางที่เพิ่มขึ้นจากชายฝั่งจนถึงประมาณ 25 กม.ห่างจากฝั่ง และการติดตามแหล่งกำเนิดของ PAH นั้น ทั้งนี้จากรูปที่ 3-35 และรูปที่ 3-36 แสดงให้เห็นว่า ที่บริเวณที่มีความลึกน้ำเดียวกัน กล่าวคือ อยู่บนเส้นความถี่ของความลึกเดียวกันนั้น จะพบชั้นสินามิใกล้เคียงกัน คือ มีความหนาของชั้นสึนามี 18 ซม. และมีชั้นตะกอนเหนือชั้นสึนามิ 22 ซม. เท่ากัน



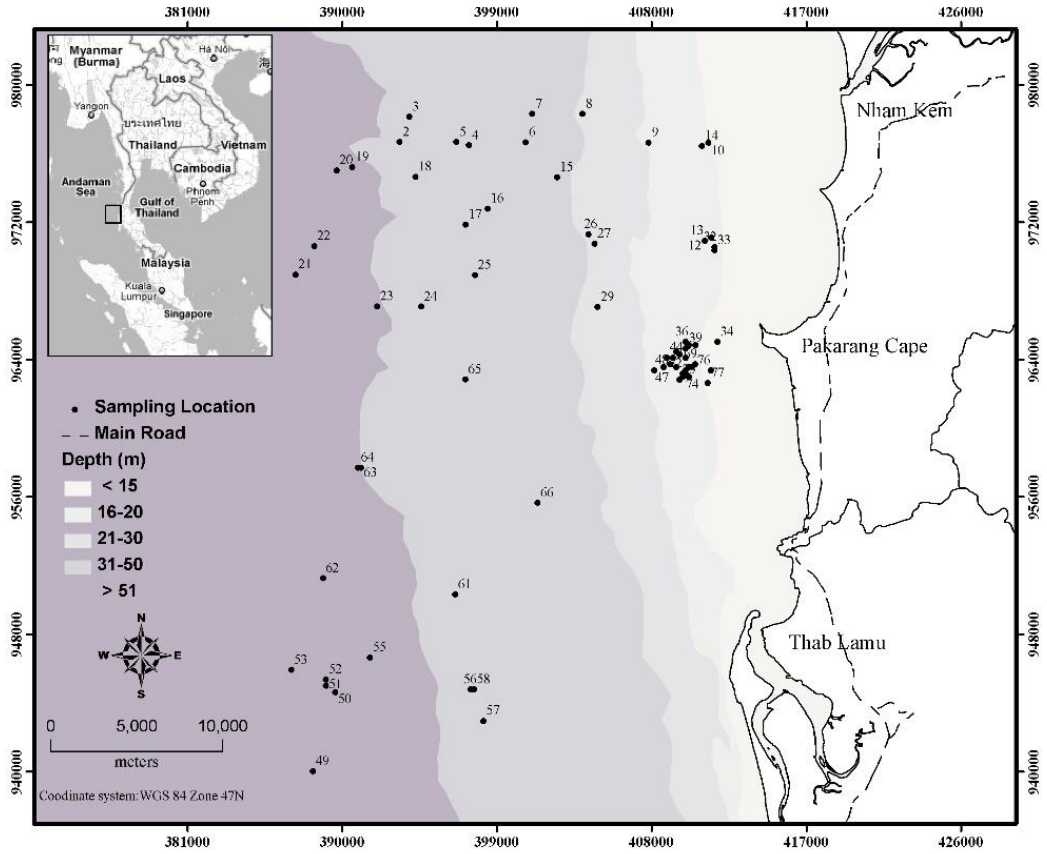
รูปที่ 3-35 ภาพถ่ายรังสีเอกซ์, รูปแท่งตะกอนและคุณลักษณะของแท่งตะกอน 030310-C3 โดยเทคนิคการวิเคราะห์ micropalaeontological, sedimentological and geochemical analyses โดยแท่งตะกอนนี้มีการแบ่งชั้นตะกอนออกเป็น 6 รูปแบบ



รูปที่ 3-36 ภาพถ่ายรังสีเอกซ์, รูปแท่งตะกอนและคุณลักษณะของแท่งตะกอน 050310-C6 โดยเทคนิคการวิเคราะห์ micropalaeontological, sedimentological and geochemical analyses โดยแท่งตะกอนนี้มีการแบ่งชั้นตะกอนออกเป็น 4 รูปแบบ

3.5.5.6 ผลการศึกษาปริมาณ Polycyclic aromatic hydrocarbons

ผลวิเคราะห์ปริมาณ Polycyclic aromatic hydrocarbons (PAHs) แต่ละชนิดในตะกอนผิวหน้า ซึ่งเก็บตัวอย่างในปีที่ 1 แสดงในตารางที่ 3-2 จุดเก็บตัวอย่างแสดงในรูปที่ 3-37



รูปที่ 3-37 ตำแหน่งเก็บตัวอย่างตะกอนผิวหน้าสำหรับการวิเคราะห์หาสาร Polycyclic aromatic hydrocarbons (PAHs) จากการสำรวจปีที่ 1 พ.ศ. 2550 จำนวน 70 ตัวอย่าง

ตารางที่ 3-2 ปริมาณ PAHs แต่ละชนิดใน surface sediment

Station	Phe	An	Fluo	Pyr	B[a]A	Chry	B[b]F	B[k]F	B[e]P	B[a]P	Ind	D[a,h]A	B[g,h,i]P	∑ PAHs
2	8.72	0.45	1.36	2.57	0.24	0.25	nd	6.53	2.62	nd	4.94	13.38	18.59	60.1
3	17.57	4.34	8.90	16.28	0.27	0.19	0.04	nd	0.08	0.05	0.09	0.16	0.34	48.5
4	16.31	2.08	21.86	22.79	3.87	5.15	1.28	0.72	1.11	0.70	1.28	12.20	1.53	100.3
5	15.41	0.84	5.53	6.95	0.79	0.80	0.13	0.19	0.12	0.06	0.19	2.07	0.58	34.7
6	12.40	1.71	3.28	10.15	0.45	0.25	1.67	2.79	4.55	3.32	2.87	28.29	7.69	79.9
7	15.97	2.16	3.22	7.69	0.42	0.28	0.05	0.08	0.05	nd	0.04	0.50	0.15	31.1
8	15.36	2.00	4.01	8.02	0.23	0.15	0.08	0.05	0.05	0.05	0.07	0.15	0.22	30.7
9	22.31	3.25	2.79	2.71	0.69	0.34	nd	0.04	0.15	nd.	0.14	0.45	0.63	34.6
10	14.56	0.83	8.26	4.15	0.39	0.29	0.12	0.08	0.18	0.07	0.19	0.48	1.05	31.5
11	7.07	1.19	1.04	1.63	0.26	0.21	nd	nd	0.09	nd	0.10	0.16	0.34	12.6
12	36.74	7.37	6.27	6.05	4.48	5.51	5.12	1.39	4.29	2.65	5.79	6.59	9.41	112.3
13	11.90	1.28	2.13	2.78	0.61	0.66	nd	nd	0.57	0.05	0.34	0.52	2.06	23.6
14	14.89	2.15	1.72	4.15	0.57	0.45	0.08	0.11	0.12	nd	0.08	0.74	0.24	26.2
15	20.58	2.47	5.03	7.74	1.23	1.53	0.04	nd	0.85	0.05	2.17	19.05	2.74	66.3
16	16.65	2.21	2.56	3.65	1.01	1.43	1.60	1.36	1.66	nd	2.23	7.78	3.78	48.6
17	20.24	2.52	6.44	7.00	0.52	0.87	nd	nd	0.60	0.05	0.53	2.95	1.06	44.7
18	27.86	2.35	6.72	9.27	1.54	1.69	0.04	2.99	1.23	nd	1.48	3.67	2.90	64.0
19	4.43	0.77	4.92	11.21	1.02	0.70	nd	nd	nd	0.05	nd	16.74	6.51	47.8
20	23.18	2.66	7.54	20.77	0.51	nd	0.04	4.54	2.89	nd	1.54	14.82	4.11	83.6
21	15.14	1.38	11.84	25.49	4.84	5.76	0.79	1.18	1.25	1.01	0.74	2.70	0.83	75.6
22	21.28	3.17	4.98	10.52	1.33	1.24	16.06	18.10	12.70	0.05	21.07	72.59	16.62	202.7
23	12.07	1.54	1.77	4.38	0.52	0.52	3.90	4.78	3.73	1.92	4.80	23.91	4.19	69.6
24	21.62	2.21	14.59	13.55	0.98	1.64	nd	7.70	11.72	8.59	20.76	21.42	20.39	158.3
25	17.39	2.28	14.24	18.06	1.13	1.36	nd	nd	18.45	11.15	16.92	41.48	21.48	170.2
26	22.09	7.92	5.82	14.90	1.59	2.12	nd	nd	1.77	0.92	1.34	2.99	2.45	67.4
27	15.36	0.52	1.78	9.92	0.31	0.12	0.04	0.04	0.65	nd.	0.45	nd.	1.11	30.8
29	4.33	0.3	1.72	5.23	0.21	0.12	nd	nd	1.3	0.05	1.04	1.39	3.61	19.8

หมายเหตุ: Phe = Phenanthrene; An = Anthracene; Fluo = Fluorene; Pyr = Pyrene; B[a]A = Benzo[a]anthracene; Chry = Chrysene; B[b]F = Benzo[b]fluoranthene; B[k]F = Benzo[k]fluoranthene; B[e]P = Benzo[e]pyrene; B[a]P = Benzo[a]pyrene; Ind = Indeno[1,2,3cd]pyrene; D[a,h]A = Dibenzo[a,h]anthracene; B[g,h,i]P = Benzo[g,h,i]perylene; ∑PAHs = ผลรวมของ PAHs 13 ชนิดข้างต้น

ตารางที่ 3-2 (ต่อ)

Station	Phe	An	Fluo	Pyr	B[a]A	Chry	B[b]F	B[k]F	B[e]P	B[a]P	Ind	D[a,h]A	B[g,h,i]P	∑ PAHs
31	10.64	1.14	11.79	12.66	0.44	0.65	5.78	4.1	11.35	4.67	15.38	11.8	14.93	110.8
32	17.13	2.15	4.27	8.94	0.54	0.93	0.04	0.04	5.08	nd	8.74	4.5	14.12	67.7
33	15.16	1.46	7.39	8.39	0.85	1.08	nd	nd	20.55	0.05	22.32	24.67	22.3	128.8
34	18.96	2.42	17.02	18.49	0.6	0.51	4.62	3.83	3.98	5.11	13.64	113.8	46.53	272.0
35	11.24	2.11	10.6	18.18	0.6	0.5	0.04	6.89	12.43	2.7	5.89	27.38	16.95	117.0
36	16.39	1.95	6.57	15.12	0.38	0.31	nd	11.99	8.11	nd	4.38	25.18	12.82	104.3
37	16.05	1.97	10.42	23.77	0.52	0.46	0.04	8.88	7.3	3.1	0.06	24.13	6.21	104.1
39	14.95	1.63	7.05	10.4	0.68	0.7	nd	1.36	1.56	0.05	0.62	3.87	1.74	46.2
40	16.05	2.59	5.63	13.63	0.37	0.41	0.04	9.25	10.65	7.72	3.92	15.74	4.96	92.1
41	22.97	1.55	2.53	5.43	0.15	0.48	nd	13.04	6.66	7.2	5.71	25.29	13.02	104.5
42	5.94	0.28	1.25	2.45	0.13	0.12	0.04	0.04	0.05	nd	3.54	3.62	3.77	21.5
43	16.79	1.33	15.87	21.86	0.28	0.27	nd	nd	0.75	0.05	nd	0.04	0.33	65.2
44	13.36	1.26	2.24	2.69	0.3	0.23	0.04	3.79	5.91	nd	2.36	8.48	9.8	50.9
45	27.58	2.77	6.14	14.48	0.43	0.19	nd	0.04	0.33	0.05	0.47	0.38	0.82	54.6
46	13.17	1.3	15.73	37.58	0.99	1.04	1.47	1.76	2.19	1.12	2.21	4.81	2.98	87.7
47	12.33	1.39	5.24	11.9	0.9	0.73	0.17	0.15	0.19	nd	0.34	1.1	1.16	36.9
48	14.45	1.58	5.51	15.85	0.49	0.22	0.21	nd	0.38	0.36	0.29	0.7	1.01	41.7
49	37.17	4.11	7.44	15.86	0.59	0.24	0.55	0.04	0.95	0.05	0.65	1.43	2.03	71.6
50	11.15	1.48	5.41	6.82	0.2	0.14	1.83	1.68	3.11	nd	4.14	9.66	10.94	57.0
51	13.91	1.59	2.83	5.17	0.42	0.49	0.04	0.34	0.25	0.25	0.83	0.74	2.85	32.8
52	19.38	1.59	14.39	32.64	0.53	0.33	nd	nd	0.55	0.05	0.5	0.49	0.98	72.6
53	27.9	2.92	8.49	15.83	0.2	0.12	0.04	0.32	0.47	nd	0.33	0.57	0.71	60.9
55	10.64	1.28	2.58	6.4	0.37	0.23	nd	0.04	3.66	0.05	5.39	5.19	13.57	50.1
56	13.53	1.52	5.67	12.66	0.26	0.14	0.04	nd	0.68	nd	0.41	0.68	0.92	37.0
58	15.60	1.67	5.85	12.43	0.32	0.21	nd	0.04	0.87	0.44	0.34	0.63	0.94	48.1
57	25.43	2.95	4.25	18.16	0.78	0.63	2.53	2.41	2.51	1.52	3.92	10.44	8.08	85.5

หมายเหตุ: Phe = Phenanthrene; An = Anthracene; Fluo = Fluorene; Pyr = Pyrene; B[a]A = Benzo[a]anthracene; Chry = Chrysene; B[b]F = Benzo[b]fluoranthene; B[k]F = Benzo[k]fluoranthene; B[e]P = Benzo[e]pyrene; B[a]P = Benzo[a]pyrene; Ind = Indeno[1,2,3cd]pyrene; D[a,h]A = Dibenzo[a,h]anthracene; B[g,h,i]P = Benzo[g,h,i]perylene; ∑PAHs = ผลรวมของ PAHs 13 ชนิดข้างต้น

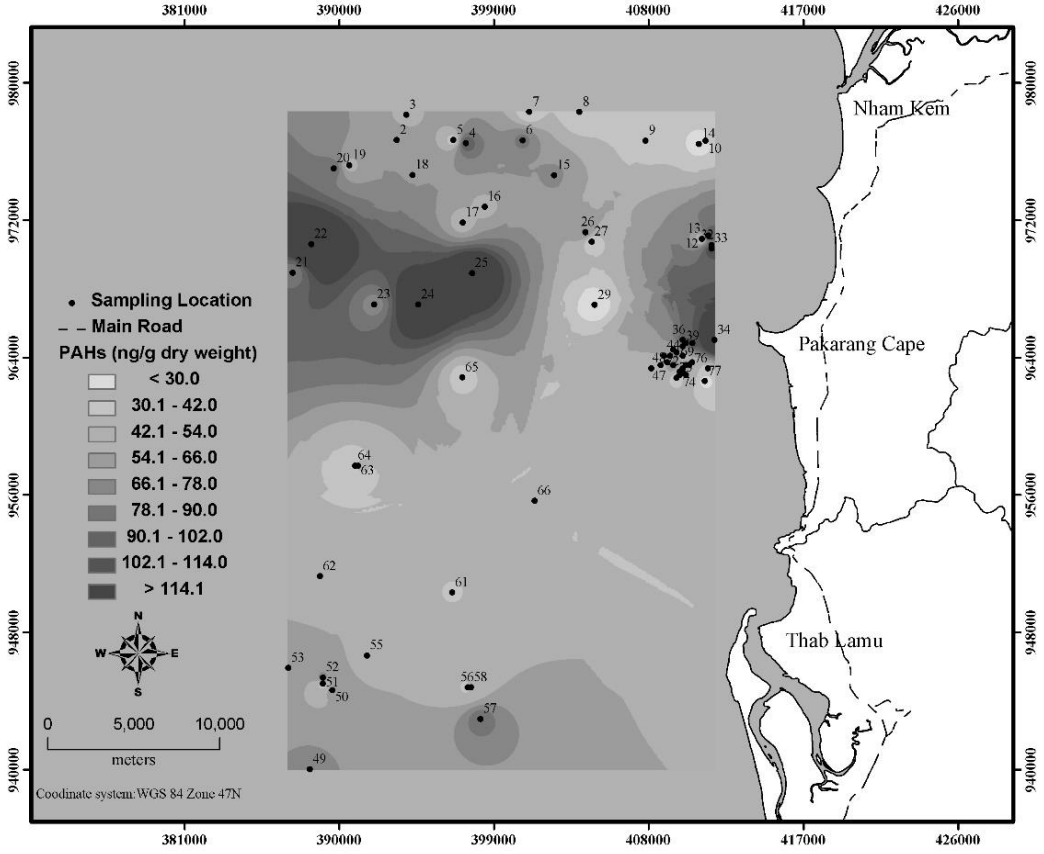
ตารางที่ 3-2 (ต่อ)

Station	Phe	An	Fluo	Pyr	B[a]A	Chry	B[b]F	B[k]F	B[e]P	B[a]P	Ind	D[a,h]A	B[g,h,i]P	∑ PAHs
61	14.33	1.86	4.66	11.18	0.43	0.31	0.80	0.44	0.50	0.31	1.15	1.74	3.05	41.6
62	13.79	2.09	4.65	11.13	0.49	0.23	0.76	0.29	0.95	0.05	1.29	3.16	6.49	46.2
63	12.10	1.60	3.09	7.53	0.43	0.38	0.04	1.06	1.70	nd	3.42	4.91	12.42	49.4
64	12.50	1.35	4.07	6.61	0.31	0.17	nd	0.60	0.68	0.05	0.28	0.25	1.50	28.9
65	15.41	1.83	5.32	10.37	0.26	0.19	0.04	nd	0.67	nd	0.45	0.47	1.15	36.4
66	10.64	1.45	7.49	21.15	0.31	nd	nd	0.19	0.38	0.10	0.46	0.10	0.83	43.6
68	12.56	1.40	4.09	15.95	0.71	0.49	1.82	1.73	1.01	0.91	1.56	5.95	3.31	53.1
69	11.00	1.19	3.80	10.53	0.29	0.22	0.04	0.78	1.05	0.05	1.40	1.94	6.92	39.4
70	16.82	2.23	9.16	23.59	0.41	0.30	nd	0.04	2.05	nd	3.05	5.04	13.40	76.4
71	12.41	1.77	5.60	13.09	0.68	0.51	0.04	nd	1.01	0.05	1.88	3.21	8.85	50.6
72	9.68	1.06	3.65	7.96	0.31	0.23	0.84	0.61	1.40	0.43	2.95	5.75	15.31	50.9
73	14.58	1.84	10.68	9.41	0.34	0.18	1.15	1.52	1.98	0.05	1.99	6.65	13.11	63.6
74	14.17	0.86	2.73	4.22	0.32	0.26	0.04	0.11	0.10	nd	0.12	0.17	0.29	23.7
75	12.69	1.08	4.04	8.06	0.24	0.18	nd	nd	0.07	0.05	0.11	0.21	0.52	27.5
76	11.11	0.98	4.04	9.08	0.22	0.18	1.07	0.04	0.85	nd	0.69	0.59	3.57	32.7
77	11.75	1.55	1.70	3.43	0.22	0.11	0.04	nd	0.43	0.05	0.45	0.63	1.63	22.3
78	9.40	1.41	1.82	3.40	0.35	0.24	nd	0.04	1.43	nd	1.76	3.50	6.38	0.3

หมายเหตุ: Phe = Phenanthrene; An = Anthracene; Fluo = Fluorene; Pyr = Pyrene; B[a]A = Benzo[a]anthracene; Chry = Chrysene; B[b]F = Benzo[b]fluoranthene; B[k]F = Benzo[k]fluoranthene; B[e]P = Benzo[e]pyrene; B[a]P = Benzo[a]pyrene; Ind = Indeno[1,2,3cd]pyrene; D[a,h]A = Dibenzo[a,h]anthracene; B[g,h,i]P = Benzo[g,h,i]perylene; ∑PAHs = ผลรวมของ PAHs 13 ชนิดข้างต้น

การแพร่กระจายของ PAHs บนพื้นทะเลในตะกอนจากข้อมูล total PAHs ในตารางที่ 3-2 นำมาสร้างภาพการแพร่กระจายโดยใช้วิธี kriging interpolation method ได้รูปแบบการกระจายความเข้มข้นของ PAHs ในตะกอนดินผิวหน้า ดังแสดงในรูปที่ 3-38

การพิสูจน์แหล่งกำเนิด (source identification) โดยการวินิจฉัย PAH isomer ratios แหล่งกำเนิด PAHs ต่างกัน จะให้ PAHs ต่างชนิดกัน ดังนั้น รูปแบบเฉพาะของ PAHs ที่สะสมในตะกอน จึงสามารถใช้บ่งชี้แหล่งกำเนิดของ PAHs ที่มาสะสมในตะกอนนั้นๆ ได้ การวินิจฉัย isomer ratios ของ PAHs สามารถที่จะใช้วิเคราะห์ว่า PAHs ที่มีอยู่ในตะกอนมีแหล่งกำเนิดจากในทะเล (มาจากธรรมชาติ) หรือมาจากแผ่นดิน (มาจากการใช้เชื้อเพลิงปิโตรเลียมของชุมชน) แหล่ง (YUNKER et al., 2002).



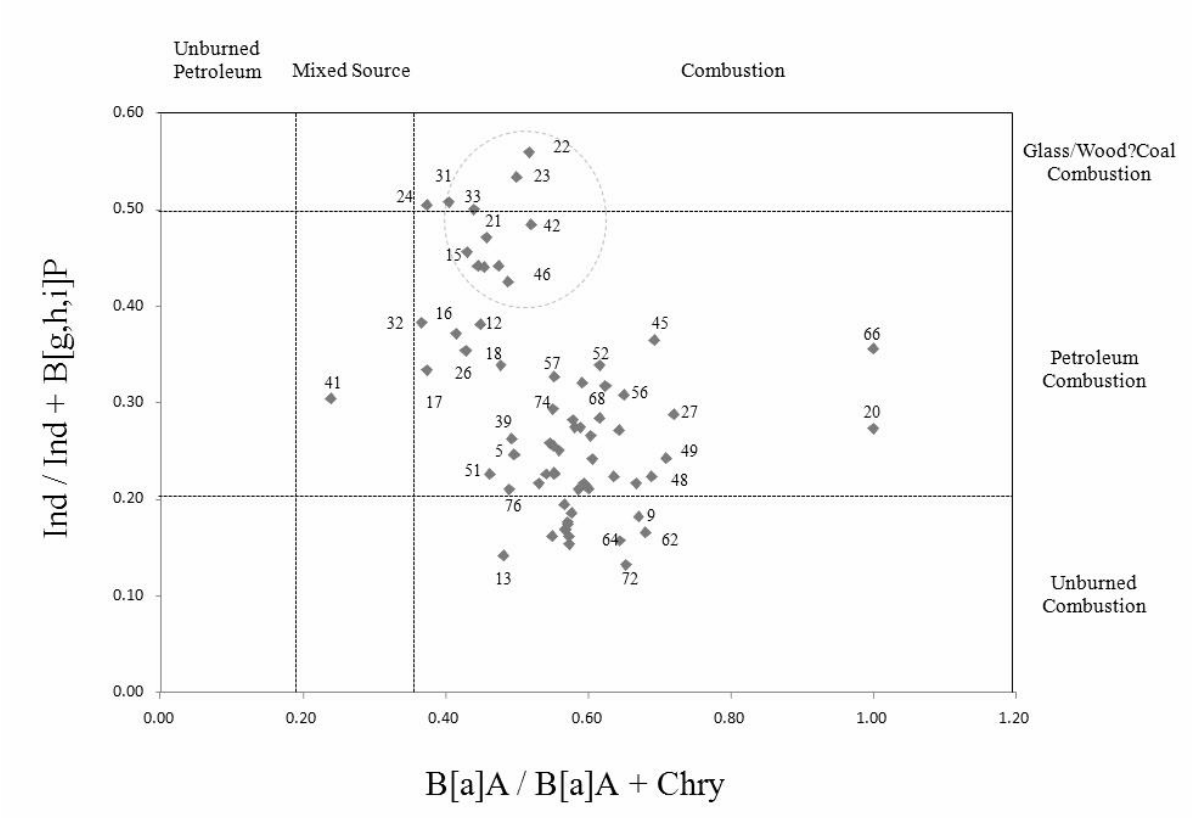
รูปที่ 3-38 รูปแบบการแพร่กระจายของ PAHs ในตะกอนผิวหน้านอกชายฝั่งเขาหลัก

การศึกษาครั้งนี้ใช้ PAH isomer pairs 4 คู่ คือ (1) An/(An+Phe) (MW 178), (2) lou/(Flou+Pyr) (MW 202), (3) B[a]A/(B[a]A+Chry) (MW 228) และ (4) Ind/(Ind+B[g,h,i]P) (MW 276) ในการวินิจฉัยเพื่อหาแหล่งกำเนิดของ PAHs ว่าเป็น PAHs ชนิดที่มีแหล่งกำเนิดเป็น pyrogenic (จากการเผาไหม้) และ petrogenic (จากปิโตรเลียม) ซึ่งทั้ง 2 ประเภท พบได้ทั่วไปในตะกอนชายฝั่ง (LaFLAMME & HITES, 1978) ค่า diagnostic ratios ของตัวอย่างทั้งหมดแสดงในตารางที่ 3-2 และจากตารางตารางที่ 3-3 B[a]A/(B[a]A+Chry) และ Ind/(Ind+B[g,h,i]P) มีค่าเท่ากับ 0.50 และ 0.52-0.54 ตามลำดับ บ่งชี้ว่าแหล่งกำเนิดอาจจะมาจากยางมะตอย (asphalt) ที่ทำพื้นถนน ตัวอย่างที่พบ diagnostic PAHs มีค่า isomer ratio ที่บ่งชี้ว่ามีแหล่งกำเนิดจากยางมะตอย คือ สถานี 22, 23, 31, 33 และ 42 (รูปที่ 3-39) เนื่องจากสถานีดังกล่าวอยู่ไกลจากฝั่ง และมีระดับ total PAHs ที่สูงกว่า สถานีที่ใกล้ฝั่งกว่า (รูปที่ 3-39) ทำให้เชื่อว่าตะกอนในสถานีดังกล่าวน่าจะถูกพากับกระแสไหลย้อนของคลื่นสึนามิ

รูปที่ 3-39 แสดง cross-plot ระหว่าง B[a]A/(B[a]A+Chry) ratio กับ Ind/(Ind+B[g,h,i]P) ratio เพื่อที่จะหา potential sources ของ PAHs ผลการวิเคราะห์บ่งชี้ว่าตะกอนส่วนมากมีกำเนิดแบบ mixed pyrogenic sources ซึ่งเป็นผลมาจากการเผาไหม้ที่ไม่สมบูรณ์ของสารอินทรีย์

ตารางที่ 3-3 Characteristic values ของ selected diagnostic ratios สำหรับ petroleum และ single-source combustion (Modified from YUNKER et al. 2002)

Source	An / (An+Phe)	Flou/ (Flou+Pyr)	B [a]A / (B[a]A + Chry)	Ind / (Ind+B[g,h,i]P)
Petroleum				
Lubicating oil	-	0.29	0.1	0.12
Asphalt	-	-	0.5	0.52-0.54
Combustion				
Gasoline (n=2)	0.11	0.44	0.33-0.38	0.09-0.22
Road dust	0.18	0.42	0.13	0.51
Used engine oil, gasoline passenger car	0.22	0.3	0.5	0.18
Used engine oil, diesel car, truck and bus	-	0.37	-	0.29



รูปที่ 3-39 Cross-plot ระหว่าง B[a]A/(B[a]A+Chry) ratio กับ Ind/(Ind+B[g,h,i]P) ratio

การพิสูจน์แหล่งกำเนิด (source identification) โดยการวิเคราะห์ทางสถิติ นำข้อมูลทั้งหมดมาวิเคราะห์ทางสถิติ โดยแปลงข้อมูลให้อยู่ในรูป logarithm เสียก่อน (y = log (x+1)) เทคนิคนี้นิยมใช้จัดการข้อมูลสิ่งแวดล้อม เนื่องจากข้อมูลสิ่งแวดล้อมมักมีการกระจายของข้อมูลแบบ non-normal distribution (FIELD et al., 1982) จากนั้นวิเคราะห์ข้อมูลด้วย Principal Component Analysis (PCA) และ Hierarchical Cluster Analysis (HCA)

1) <u>การพิสูจน์แหล่งกำเนิดโดยใช้ Hierarchical Cluster Analysis (HCA)</u>

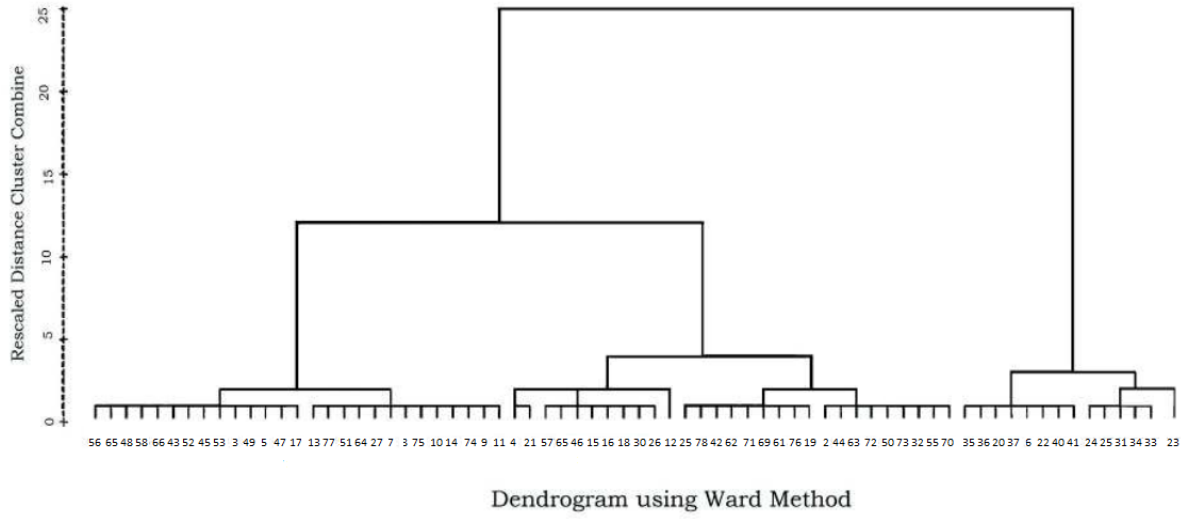
HCA ใช้ในการบ่งชี้กลุ่มตะกอนที่มีชนิด PAHs ที่คล้ายคลึงกัน รูปที่ 3-40 แสดง hierarchical dendogram ของตัวอย่างทั้ง 70 สถานี จากรูปจะเห็นว่าสามารถแบ่งออกเป็น 3 กลุ่ม

กลุ่มที่ 1 ประกอบด้วย B[a]A, Chry, B[b]F, B[k]F, B[a]P และ An ซึ่งมีแหล่งกำเนิดจาก pyrogenic source (FANG et al., 2009) ซึ่งมาจากการเผาไหม้น้ำมันเชื้อเพลิง น้ำมันเชื้อเพลิงที่รั่วไหลและฝุ่นจากถนน (DAHLE et al., 2003) จากที่เคยมีรายงานการศึกษาไว้พบว่า PAHs ที่มี 3–4 ring พบในฝุ่นจากถนนในตัวเมือง (BOONYATUMANOND et al., 2007; ZAKARIA et al., 2002)

กลุ่มที่ 2 ประกอบด้วย B[e]P, Ind, D[a,h]A และ B[g,h,i]P ซึ่งเป็นพวก high molecular weight PAHs มี 5–6 rings กลุ่มนี้มีแหล่งกำเนิดจากยางมะตอย น้ำมันดิบ และ bitumen (AHRENS & DEPREE, 2010) และฝุ่นจากถนน (LARSEN & BAKER, 2003; BOONYATUMA-NOND et al., 2007)

กลุ่มที่ 3 ประกอบด้วย Pyr, Fluo และ Phe ซึ่งเป็น anthropogenic PAHs จากผลิตภัณฑ์ปิโตรเลียม (ZHOU et al., 1999) อาจกล่าวได้ว่า PAHs จากแหล่งกำเนิดทั้ง 3 กลุ่ม ถูกพาจากแหล่งกำเนิดลงสู่ทะเลโดยกระแสไหลย้อนของคลื่นสึนามิ

จากรูปที่ 3-40 ผลการจัดกลุ่ม พบว่ามีอยู่ 2 กลุ่มหลัก กลุ่มแรกประกอบด้วยสถานี 6, 20, 22, 23, 24, 25, 31, 33, 34, 35, 36, 37, 40 และ 41 สถานีเหล่านี้มีค่า PAHs สูงโดนเด่นกว่าสถานีอื่นในพื้นที่ (รูปที่ 3-40) ดังนั้น กลุ่มนี้น่าจะเป็นกลุ่มที่ถูกพามากับกระแสไหลย้อนของคลื่นสึนามิ จากข้อมูลทำให้สามารถประมาณทิศทางของกระแสไหลย้อนของคลื่นสึนามิได้ว่าน่าจะมาจากแหลมปะการังออกสาชายฝั่งไปสะสมในตะกอนนอกชายฝั่ง ไกลถึง 25 กิโลเมตร



รูปที่ 3-40 Hierarchical Cluster Analysis (HCA) ของตัวอย่างตะกอนดิน 70 ตัวอย่าง จากนอกชายฝั่งเขาหลัก

2) <u>การพิสูจน์แหล่งกำเนิดโดยใช้ Principal Component Analysis (PCA)</u>

ในการศึกษาครั้งนี้ ใช้ PAHs 13 ชนิด เป็น active variables และตัวอย่าง 70 ตัวอย่างเป็น subjects Majority ของ variance (72.9%) ของ scaled data อธิบายโดย eigenvectors–principal components 2 ตัว Principal component ตัวที่ 1 (PC1) และตัวที่ 2 (PC2) สามารถใช้อธิบาย 61.4% และ 11.6 % ของ total variance ตามลำดับ ดังแสดงในตารางที่ 3-4

ค่า PC1 ถ่วงน้ำหนักอยู่ที่ B[b]F, B[e]P, Ind, D[a,h]A และ B[g,h,i]P ซึ่งเป็น high molecular weight PAHs (5–6 rings) กลุ่มนี้มีกำเนิดมาจากยางมะตอย น้ำมันดิบ และ bitumen (AHRENS & DEPREE, 2010) และฝุ่นจากถนน (LARSEN & BAKER, 2003; BOONYATUMA-NOND et al., 2007) LARSEN & BAKER (2003) รายงานว่าระดับ B[k]F ที่สูง เมื่อเทียบกับ PAHs ชนิดอื่น บ่งชี้ว่ามีแหล่งมาจากเครื่องยนต์ที่ใช้น้ำมันดีเซลเป็นเชื้อเพลิง ดังนั้น PC1 เป็นตัวแทนของแหล่งกำเนิด PAHs ที่มาจากฝุ่นจากถนน ส่วน PC2 ประกอบไปด้วย Fluo และ Pyr เป็นส่วนใหญ่ กลุ่มนี้มีแหล่งกำเนิดจากผลิตภัณฑ์ปิโตรเลียมและการเผาไหม้น้ำมันเชื้อเพลิง FANG et al. (2006) รายงานว่า ค่า loading ที่สูงของ Pyr, Fluo, B[g,h,i]P, Chry และ B[a]P บ่งชี้ถึงการเผาไหม้ที่ไม่สมบูรณ์ของน้ำมัน PAHs ในกลุ่มนี้จึงเป็นกลุ่มที่มีแหล่งกำเนิดจากการเผาไหม้น้ำมัน

ตารางที่ 3-4 Rotated component matrix ของ PAHs 13 ชนิด จากตัวอย่างตะกอน 70 ตัวอย่างจากนอกชายฝั่งเขาหลัก[a]

PAH composition	Principle component (PC)	
	PC1	PC2
Phe	0.02	0.58
An	0.08	0.53
Fluo	0.12	**0.88**
Pyr	0.04	**0.86**
B[a]A	0.15	0.54
Chry	0.24	0.48
B[b]F	0.47	0.22
B[k]F	**0.75**[b]	0.18
B[e]P	**0.89**	0.19
B[a]P	0.60	0.42
Ind	**0.91**	0.03
D[a,h]A	**0.93**	0.17
B[g,h.i]P	**0.92**	– 0.10
Estimatied source	**Road dust**	**Oil burning**
Variance (%)	**61.4**	**11.6**

[a] Rotation Method: Varimax with Kaiser Normalization

[b] Bold loading > 0.70

จากการวิเคราะห์ PCA บ่งชี้ว่า PAHs ในบริเวณนี้ น่าจะมีแหล่งกำเนิด 2 แหล่ง ซึ่งสนับสนุนสมมติฐานที่ว่า PAHs จากแผ่นดินถูกพาไปกับกระแสไหลย้อนของคลื่นสึนามิไปตกสะสมอยู่บนพื้นทะเลใกล้ชายฝั่ง

3) <u>การใช้ PAHs เป็น proxy ในการบ่งชี้กระแสไหลย้อนของคลื่นสึนามิ</u>

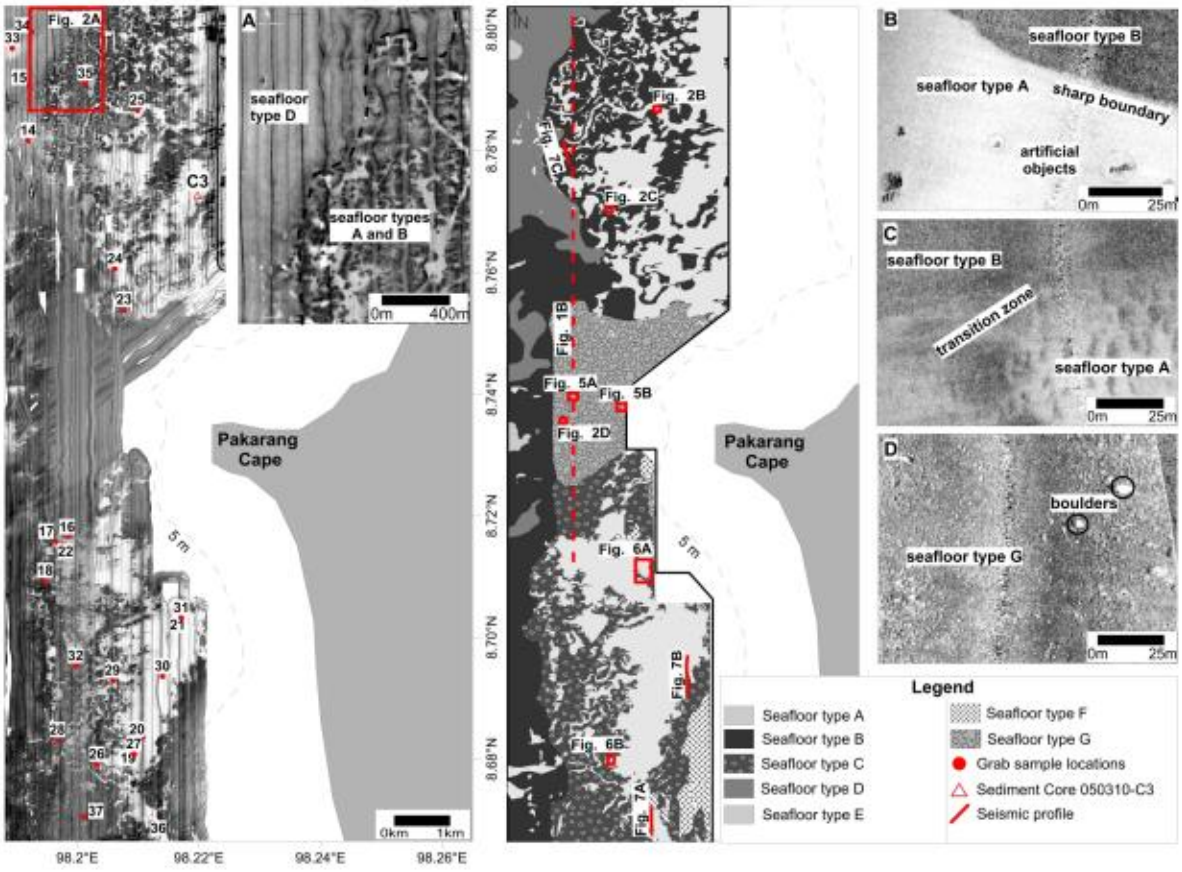
จากการวิเคราะห์องค์ประกอบของ PAHs ที่สะสมในตะกอนดิน ร่วมกับการวิเคราะห์ทางสถิติโดยใช้เทคนิค multivariate descriptive statistics บ่งบอกว่า PAHs สามารถใช้เป็นตัวบ่งชี้กระแสไหลย้อนของคลื่นสึนามิบริเวณเขาหลักได้ รูปแบบการแพร่กระจายของ PAHs บ่งชี้ได้ว่าบริเวณใดที่สารจากแผ่นดิน (land-derived materials) ถูกพาไปทับถม จากผลการศึกษาที่พบลักษณะที่เด่นชัดของการสะสม PAHs ในตะกอนบริเวณนี้ แสดงว่ากระแสไหลย้อนของคลื่นสึนามิมีบทบาทสำคัญในการพาเอา anthropogenic PAHs ไปสะสมบนพื้นทะเลห่างฝั่งออกไปราว 25 กิโลเมตร และจากผลการวินิจฉัย PAH isomer ratios ชี้ว่าแหล่งกำเนิดของ PAHs ที่ถูกพาไปกระแสไหลย้อน เป็นพวกยางมะตอยที่ถูกกัดกร่อนมวลน้ำจำนวนมหาศาลที่ไหลย้อนกลับลงสู่ทะเล

3.5.5.7 แผนที่การกระจายตัวของตะกอนสึนามินอกชายฝั่งแหลมปะการัง

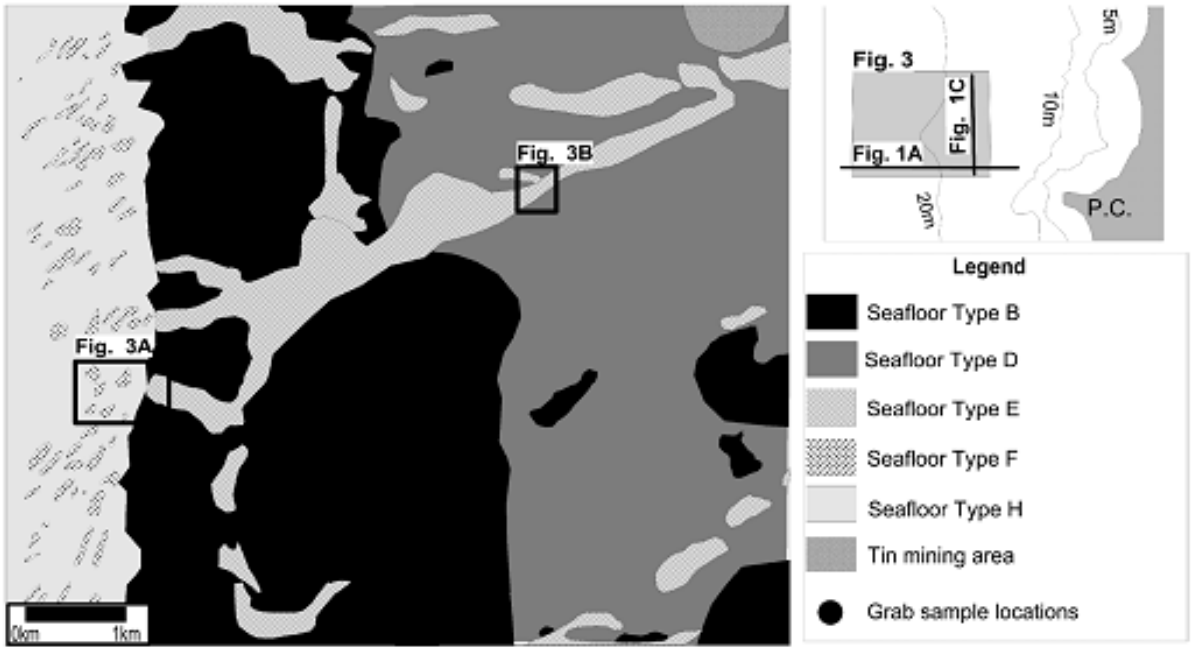
จากข้อมูลต่าง ๆ ได้จัดทำแผนที่การกระจายตัวของตะกอนสึนามิบนพื้นทะเล ซึ่งต้องใช้ข้อมูลจากแท่งดินตะกอนตามความลึก ซึ่งในการศึกษาในครั้งนี้ไม่สามารถทำการวิเคราะห์ตัวอย่างแท่งดินตะกอนตามความลึกทั้งหมดได้ เนื่องจากข้อจำกัดในงบประมาณและเวลา ดังนั้นจึงได้จัดทำแผนที่พื้นท้องทะเลเฉพาะพื้นที่ที่ได้ศึกษาทางตะกอนวิทยาของแท่งดินตะกอนอย่างละเอียดแล้ว ซึ่งพื้นที่ดังกล่าวอยู่นอกชายฝั่งแหลมปะการัง ซึ่งเป็นพื้นที่ที่โครงการนี้ทำการศึกษาเจาะลึก จากข้อจำกัดดังกล่าว จึงไม่สามารถนำเสนอภาพการกระจายตัวในแนวราบของพื้นที่ศึกษาทั้งหมด แต่ทราบเฉพาะรูปแบบการสะสมตัวเท่านั้น

รูปที่ 3-41 และ 3-42 เป็นภาพพื้นท้องทะเลและการจำแนกประเภทของพื้นท้องทะเลนอกชายฝั่งแหลมปะการังและเขาหลัก ตามลำดับ จากข้อมูลภาพจากเครื่องโซนาร์กวาดทางข้าง (side scan sonar) รูปที่ 3-42 ยังแสดงพื้นที่ที่ได้รับอิทธิพลจากเหมืองดีบุกเก่าในพื้นที่ศึกษา (ดูข้อมูลรายละเอียดใน Feldens, P., Schwarzer, K., Sakuna, D, Szczuciński, W. and Sompongchaiyakul, P. (2012) Sediment distribution on the inner continental shelf off Khao Lak (Thailand) after the 2004 Indian Ocean Tsunami. Earth, Planet and Space 64: 875-887)

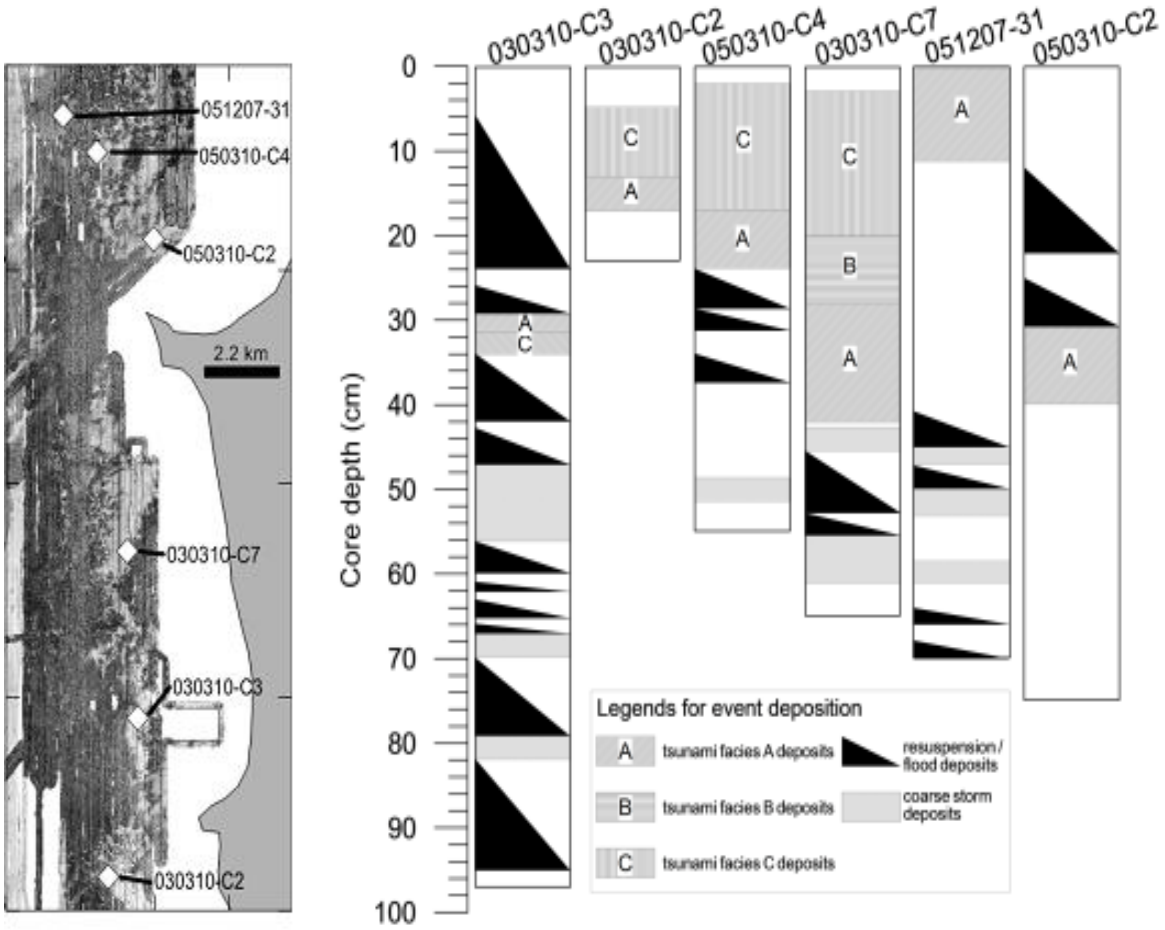
รูปที่ 3-43 แสดงการเปรียบเทียบแท่งตะกอนดิน 6 แท่ง ที่จำแนกเหตุการณ์ต่าง ๆ ที่บันทึกในชั้นตะกอนในเขตน้ำตื้น (ความลึกน้ำไม่เกิน 16 เมตร) เช่น สึนามิ น้ำท่วม และพายุ (ดูข้อมูลรายละเอียดใน Sakuna-Schwartz, D., Feldens, P., Schwarzer, K., Khokiattiwong, S., Stattegger, K. (2014). "Internal structure of event layers preserved on the Andaman Sea continental shelf, Thailand: Tsunami vs. Storm and Flash Flood deposits", Nat. Hazards Earth Syst. Sci., Discuss., 2, 7225 – 7267, doi: 10.5194/nhessd-2-7225-2014)



รูปที่ 3-41 ภาพที่ได้จากการปะติดปะต่อข้อมูลภาพจากเครื่องโซนาร์กวาดทางข้าง (side scan sonar) แสดงสภาพนอกชายฝั่งแหลมปะการัง (ข้อมูลจากการสำรวจปี พ.ศ. 2551) (ซ้าย) และภาพจากการ interpretation ของพื้นท้องทะเลที่ความลึกน้ำประมาณ 15 เมตร โดยแบ่งเป็น 7 ประเภท คือ A, B, C, D, E, F, G จากการจำแนกโดยข้อมูลโซนาร์กวาดทางข้าง (ขวา)



รูปที่ 3-42 การจำแนกผิวพื้นท้องทะเลบริเวณนอกชายฝั่ง หน้าเขาหลัก ที่ความลึกน้ำประมาณ 35 เมตร จากการจำแนกโดยข้อมูลโซนาร์กวาดทางข้างและการวิเคราะห์จากตะกอนผิวหน้าดิน แสดงชนิดของผิวพื้นท้องทะเลชนิด B D E F H และแสดงพื้นที่เหมืองเก่าด้านบนของภาพ



รูปที่ 3-43 เปรียบเทียบแท่งตะกอนดิน 6 แท่ง ในเขตน้ำตื้น (ความลึกน้ำไม่เกิน 16 เมตร) ที่บันทึกเหตุการณ์ต่าง ๆ ได้แก่ ตะกอนสึนามิแบบ A, แบบ B และแบบ C ตะกอนที่การสะสมตัวในช่วงน้ำท่วม (flood) และตะกอนที่ถูกพามาโดยพายุ

3.6 การพัฒนาบุคลากร

ตามวัตถุประสงค์ของโครงการในด้านการพัฒนาบุคลากร เพื่อเพิ่มประสบการณ์และความชำนาญในการใช้เครื่องมือและอุปกรณ์ดังที่กล่าวมาข้างต้นและรวมถึงการได้พัฒนาองค์ความรู้เพื่อประกอบการวิเคราะห์ข้อมูลเชิงธรณีฟิสิกส์และการวิเคราะห์ตะกอน ดังนั้น

ในปีที่ 1 ได้จัดส่งบุคลากร 2 คน คือ น.ส.ดรุณวรรณ สกุณาและนายดนัย ทิพย์มณี ไปฝึกอบรมเพื่อเรียนรู้เทคนิคและวิธีการตั้งแต่ระดับปฏิบัติการจนถึงระดับงานวิจัยขั้นสูง หลักสูตร “Introduction Marine Geophysics and Geology” นาน 4 สัปดาห์ โดยแบ่งการอบรมเป็น 2 เรื่อง คือ ความรู้เบื้องต้นเกี่ยวกับ Marine Geophysic ที่ Leibniz Institute of Marine Sciences (IFM-GEOMAR), Kiel และ Hydroacoustic ที่ Christian-Albrechts-University of Kiel แต่ทั้งนี้บุคลากรทั้ง 2 มีความถนัดทางด้านธรณีเคมีและเคมี จึงเน้นการฝึกอบรมในด้านธรณีเคมีและตะกอนวิทยา ดดยการปฏิบัติงานจริงกับแท่งตะกอนตามความลึกที่เก็บจากการออกเรือสำรวจ

ในปีที่ 2 ส่งบุคลากร 1 คน คือ น.ส. สุรัตตา บุญสมบูรณ์สกุลเพื่อเรียนรู้เทคนิคการวิเคราะห์ข้อมูลทางธรณีฟิสิกส์และธรณีเคมีเพิ่มเติม ที่ Christian-Albrechts-University of Kiel เนื่องจากการพัฒนาบุคลากรในปีที่ 1 นั้น เน้นด้านธรณีเคมีและตะกอนวิทยา โดยทางฝ่ายเยอรมันจะเป็นผู้วิเคราะห์ข้อมูลทางธรณีฟิสิกส์ทั้งหมด แต่ทั้งนี้เนื่องจากต้องมีการรายงานผลการวิเคราะห์ แป็นภาษาไทยด้วย ซึ่งพบว่าการแปรข้อมูลละเองนั้น ยังขาดความชำนาญและทำได้ค่อนข้างช้า จึงจำเป็นต้องส่งบุคลากรดังกล่าวไปเพื่อรับการฝึกอบรมทางด้านธรณีฟิสิกส์และร่วมการวิเคราะห์ข้อมูลกับฝ่ายเยอรมัน ระหว่างวันที่ 16-28 กุมภาพันธ์ 2552

ในปีที่ 3 บุคลากรที่ได้รับการพัฒนาในโครงการ 2 ปีแรก ได้จบการศึกษาระดับปริญญาเอกแล้ว 1 คน คือ นายดนัย ทิพย์มณี จากจุฬาลงกรณ์มหาวิทยาลัย จะจบการศึกษา 1 คน คือ น.ส.ดรุณวรรณ สกุณา ที่ Christian-Albrechts-University of Kiel และอีก 1 คน คือ น.ส.สุรัตตา บุญสมบูรณ์สกุล กำลังศึกษาระดับปริญญาเอกทางด้าน Marine Geology ซึ่งเป็นโครงการ JOINT DOCTORAL PROGRAM ภายใต้ความร่วมมือระหว่างภาควิชาวิทยาศาสตร์ทางทะเล จุฬาลงกรณ์มหาวิทยาลัย ประเทศไทย และ State Key Laboratory of Marine Geology และ School of Ocean and Earth Science, Tongji University ประเทศสาธารณรัฐประชาชนจีน โดยเป็นการพัฒนาบุคลากรทาง Marine Geology อย่างต่อเนื่องจากงานที่ดำเนินการภายใต้ความร่วมมือไทย-เยอรมัน

บทที่ 4
สรุปผลการวิจัยและข้อวิจารณ์

จากการสำรวจพื้นท้องทะเลด้วยเทคนิคที่ใช้คลื่นเสียง (marine acoustic techniques) ประกอบด้วย multibeam echo sounding, side-scan sonar mapping และ boomer system เพื่อสร้างแผนที่พื้นท้องทะเลนอกชายฝั่งแหลมปะการัง จังหวัดพังงา ระหว่างอ่าวทับละมุและเกาะพระทอง ซึ่งเป็นพื้นที่ที่ถูกคลื่นยักษ์สึนามิซัดถล่มอย่างรุนแรง โดยมีระยะทางในการสำรวจทั้งสิ้นประมาณ 1,500 ไมล์ทะเล (nautical mile) หรือประมาณ 2,780 กิโลเมตร รวมเวลาทั้งสิ้นกว่า 400 ชั่วโมง ในการจัดทำแผนที่พื้นท้องทะเลในครั้งนี้ ได้ทำการวิเคราะห์ข้อมูลเบื้องต้นทันทีบนเรือสำรวจ เพื่อทราบลักษณะทางธรณีวิทยาทางทะเล การกระจายตัวของตะกอน เพื่อเป็นข้อมูลประเมินการกำหนดจุดในการเก็บตัวอย่างตะกอนดินทั้งแบบผิวหน้าและตามความลึกของชั้นตะกอน ในบริเวณที่พบร่องรอยของคลื่นสึนามิ และทำการวิเคราะห์พื้นท้องทะเลอย่างละเอียดในห้องปฏิบัติการ

4.1 ธรณีสัณฐาน การกระจายตัว และรูปแบบการสะสมตัวของดินตะกอน

ผลการศึกษาทางธรณีฟิสิกส์ พบว่าธรณีสัณฐานทั่วไปของพื้นที่ศึกษา มีความลาดเอียงจากฝั่งออกไปและความชันของพื้นทะเลจะเพิ่มขึ้นอย่างรวดเร็วตั้งแต่ความลึกน้ำ 25 เมตรขึ้นไป ที่ระดับความลึก 10-20 เมตร นอกชายฝั่งแหลมปะการัง พบแนวร่องธรรมชาติ 3 แนว ตามแนวตะวันตกเฉียงเหนือ-ตะวันออกเฉียงใต้ (NW-SE) แต่ละร่องกว้างประมาณ 150-300 เมตร แต่มีความยาวหลายกิโลเมตร เมื่อเกิดสึนามิจึงเป็นร่องที่มีดินตะกอนมาสะสมตัวมากกว่าบริเวณอื่น ๆ การศึกษาชั้นตะกอนในบริเวณนี้จึงเป็นตัวแทนที่ดีในการศึกษาตะกอนสึนามิ

การวิเคราะห์แผนภาพข้อมูล side-scan sonar พื้นทะเลและตะกอนวิทยา พบว่าการกระจายตัวและรูปแบบการสะสมตัวของดินตะกอนนอกฝั่ง มีลักษณะ ดังนี้

- ที่ความลึก 7-15 เมตร ปกคลุมด้วยดินตะกอนละเอียดและมีหย่อมโคลนบริเวณใกล้ฝั่ง
- ที่ความลึก 10-16 เมตร เป็นแนวร่อง และการวิเคราะห์ภาพตัดขวางจะพบการสะสมตัวของชั้นตะกอนที่ต่างกัน คือ ชั้นเศษซากพืช เศษเปลือกหอย สะสมตัวเป็นชั้นสลับกับชั้นโคลน (muddy) และมีลักษณะที่ถูกเติมตะกอนใหม่ลงไปในร่อง และสามารถคำนวนอัตราการสะสมตัวของตะกอนจากการเติมเต็มได้
- ที่ความลึก ตั้งแต่ 15 เมตรไปถึงนอกชายฝั่ง พบลักษณะเป็นสันเขาสูงประมาณ 2 เมตร จากพื้นทะเล ที่ฐานของสันเขาดังกล่าว ประกอบไปด้วยตะกอนทรายละเอียด

ถึงหยาบที่มีการคัดขนาดดี (well sorted fine sand) และพบการถล่มของชั้นตะกอนที่ฐานดังกล่าว

- ลักษณะพิเศษอื่น ๆ ที่พบ คือ พื้นที่หน้าเขาหลักพบเศษซากร่องรอยจากการทำเหมืองแร่ดีบุกที่ ความลึกน้ำ 20-25 เมตร มีลานหินเล็ก ๆ ที่ความลึกน้ำ 30-35 เมตร

แม้คลื่นสึนามิขาเข้า (incoming tsunami) จะส่งผลต่อการพาตะกอนจากพื้นท้องทะเลขึ้นสู่ฝั่ง แต่ไม่ชัดเจนเท่ากับผลของกระแสไหลย้อน (backwash) ของคลื่นสึนามิขาออกที่ไหลกลับลงสู่ทะเล ซึ่งจะส่งผลต่อรูปแบบของดินตะกอนและภูมิลักษณ์ของพื้นทะเล (sea bottom topography) ของน่านน้ำใกล้ฝั่ง หน้าฝั่งทั้งด้านบนและด้านล่าง (upper and lower shoreface) และไหล่ทวีป ดังผลการศึกษาที่รายงานไว้ในหัวข้อ 3.5.5.5 บทที่ 3

ผลของคลื่นสึนามิต่อการเปลี่ยนแปลงด้านตะกอนวิทยาและโครงสร้างของดินตะกอนพื้นท้องทะเลใกล้ฝั่ง ดูรายละเอียดเพิ่มเติมใน

1. Milker, Y., Wilken, M., Schumann, J., Sakuna, D., Feldens, P., Schwarzer, K., Schmiedl, G. (2014). "Sediment transport on the inner shelf off Khao Lak Andaman Sea, Thailand) during the 2004 Indian Ocean tsunami and former storm events: evidence from foraminiferal transfer functions", Nat. Hazards Earth Syst. Sci. 13: 3113 – 3128.
2. Feldens, P., Schwarzer, K., Szczuciński, W., Stattegger, K., Sakuna, D. and Somgpongchaiyakul, P. (2009) Impact of the 2004 Indian Ocean Tsunami on Seafloor Morphology and Sediments Offshore Pakarang Cape, Thailand. Polish J. of Environ. Stud. 18(1): 63-68.
3. Tipmanee, D., Deelaman, W., Pongpiachan, S., Schwarzer, K. and Sompongchaiyakul, P. (2012). Using Polycyclic Aromatic Hydrocarbons (PAHs) as a Chemical Proxy to Indicate Tsunami 2004 Backwash in Khao Lak Coastal Area, Thailand. Natural Hazards and Earth System Sciences 12(5): 1441-1451.
4. Schwarzer, K., Feldens, P., Sakuna-Schwartz, D., Pongpiachan, S., Milker, Y., Tipmanee, D. (2015). “The Indian Ocean tsunami 2004: Identification of Tsunami Deposits in the Andaman Sea by Different

Proxis", Conference: Coastal Sediments 2015, SanDiego, DOI: 10.1142/9789814689977_0184

ผลของคลื่นสึนามิต่อการเปลี่ยนแปลงด้านตะกอนวิทยาและโครงสร้างของดินตะกอนพื้นท้องทะเลหน้าฝั่ง ดูรายละเอียดเพิ่มเติมใน

1. Feldens, P., Schwarzer, K., Sakuna, D, Szczuciński, W. and Sompongchaiyakul, P. (2012) Sediment distribution on the inner continental shelf off Khao Lak (Thailand) after the 2004 Indian Ocean Tsunami. Earth, Planet and Space 64: 875-887.
2. Sakuna-Schwartz, D., Feldens, P., Schwarzer, K., Khokiattiwong, S., Stattegger, K. (2014). "Internal structure of event layers preserved on the Andaman Sea continental shelf, Thailand: Tsunami vs. Storm and Flash Flood deposits", Nat. Hazards Earth Syst. Sci., Discuss., 2, 7225 – 7267, doi: 10.5194/nhessd-2-7225-2014.

ผลของคลื่นสึนามิต่อการเปลี่ยนแปลงด้านตะกอนวิทยาและโครงสร้างของดินตะกอนพื้นท้องทะเลไหล่ทวีป ดูรายละเอียดที่รายงานไว้ในโครงการย่อย โครงการเสถียรภาพของชั้นตะกอนและการเกิดแผ่นดินถล่มใต้ทะเลบริเวณขอบไหล่ทวีปในทะเลอันดามัน

4.2 ธรณีเคมีของดินตะกอน

จากตัวอย่างดินตะกอนผิวหน้ารวม 112 จุด และตัวอย่างแท่งดินตะกอนยาวประมาณ 2 เมตร 42 จุด ซึ่งระบุตำแหน่งเก็บจากแผนที่พื้นท้องทะเลที่ได้ข้างต้น ผลการศึกษาขนาดอนุภาคตะกอนจากตัวอย่างดินตะกอนผิวหน้า นำใช้ประกอบการแปลความหมายข้อมูลทางธรณีฟิสิกส์เพิ่มเติม เพื่อจำแนกพื้นผิวทะเลให้แม่นยำขึ้น และเมื่อการบันทึกภาพรังสีเอ๊กซ์ของแท่งดินตะกอนในบริเวณที่พบลักษณะเป็นแนวร่องพบว่าแต่ละชั้นตะกอนมีรายละเอียดความแตกต่างของชั้นตะกอนแต่ละชั้น ที่ไม่สามารถมองเห็นจากผิวหน้าแท่งตะกอนที่ผ่าครึ่งแล้ว ผลการศึกษาทางธรณีเคมี พบว่า

1) ชั้นตะกอนที่มีทรายมาก (sand layers) มีสัดส่วน Ti/Ca มีค่าต่ำ และชั้นที่เป็นโคลน (muddy layers) จะมีค่าสูง

2) ดินตะกอนในแนวร่องมีสัดส่วน Ti/Ca แตกต่างกับดินตะกอนนอกแนวร่อง แสดงถึงความแตกต่างของโครงสร้างชั้นตะกอนที่เกิดการพามาสะสมในแนวร่องนั้นโดยคลื่นสึนามิมีลักษณะต่างกับบริเวณรอบข้าง ๆ อย่างชัดเจน ทั้งลักษณะทางกายภาพ คือ มีเนื้อละเอียด และลักษณะทางธรณีเคมี

3) สัดส่วน Ti/Ca ในแต่ละชั้นของแท่งตะกอน แตกต่างกันตามความลึก แสดงถึงความแตกต่างของแหล่งที่มาของตะกอนที่มาสะสม หากสัดส่วน Ti/Ca ค่อนข้างคงที่ แสดงว่าในชั้นตะกอนนั้นเป็นตะกอนชนิดเดียวกัน ไม่มีการผสมกันของมวลตะกอน ซึ่งจากผลการศึกษา ไม่ปรากฏร่องรอยการถล่มในชั้นตะกอนจากแท่งดินตะกอนตัวแทน

4) ผลการวิเคราะห์ทางตะกอนวิทยาและธรณีเคมีตัวอย่างแท่งดินดินตะกอน หมายเลข 030310-C3 และ 050310-C6 ที่เก็บตัวอย่างจากแนวร่อง ที่ระดับความลึกน้ำเดียวกัน คือ ประมาณ 9 เมตร พบร่องรอยของดินตะกอนที่ถูกพาลงทะเลไปกับการไหลกลับของอย่างชัดเจนในแท่งดินตะกอนทั้ง 2 แท่ง อีกทั้งยังพบชั้นตะกอนสึนามิ ที่มีความหนาของชั้นดินตะกอน 18 เซนติเมตรเท่ากัน ซึ่งเป็นหลักฐานที่ดีในการศึกษาชั้นตะกอนสึนามิและอัตราการสะสมตัวของตะกอนไหลย้อน

5) จากการหาอายุของดินตะกอนแท่งดินตะกอนด้วยไอโซโทป Pb-210 พบว่าอัตราการสะสมตัวของดินตะกอนบริเวณนี้อยู่ระหว่าง 1.3 ถึง 5.7 เซนติเมตรต่อปี นอกจากนี้แท่งดินตะกอนตัวแทนยังได้บันทึกเหตุการณ์ที่เกิดขึ้นในอดีตได้ เช่น พายุ จากค่าอายุตะกอนที่ต่างกันของชั้นเหนือและใต้ฐานชั้นเหตุการณ์

6) ปกติรูปแบบการกระจายตัวของ PAHs ในดินตะกอนจะลดลงเรื่อย ๆ จากใกล้ฝั่งไปจนนอกฝั่ง เนื่องจากแหล่งที่มาหลักอยู่บนบก แต่ในพื้นที่ศึกษาพบว่า PAHs ในดินตะกอนนอกชายฝั่งแหลมปะการังมีค่าเพิ่มขึ้นตามระยะทางที่เพิ่มขึ้นจากชายฝั่งไปจนถึงระยะประมาณ 25 กิโลเมตร จากฝั่ง

7) จากค่า PAH isomer ratios บ่งชี้ว่าแหล่งกำเนิดของ PAHs ที่มาสะสมในดินตะกอนในพื้นที่ศึกษามีแหล่งที่มาต่างกัน เมื่อนำมาวิเคราะห์ด้วยสถิติขั้นสูง พบว่าดินตะกอนบริเวณนี้มีอยู่ 2 กลุ่มหลัก กลุ่มแรกมีค่า PAHs สูง ซึ่งเป็นกลุ่มที่ถูกพามากับกระแสไหลย้อนของคลื่นสึนามิ จากแหลมปะการังออกไปสะสมนอกชายฝั่ง ไกลถึง 25 กิโลเมตร กับกลุ่มที่เป็นการสะสมตัวแบบปกติ ซึ่งเป็นการบ่งชี้ได้ว่าดินตะกอนจะถูกคลื่นสึนามิที่ไหลกลับลงทะเลพาออกไปไกลจากชายฝั่งได้ไกลถึง 25 กิโลเมตรนอกชายฝั่ง

การขาดข้อมูลวิจัยที่ดีและเพียงพอในการเปรียบเทียบก่อนและหลังเกิดเหตุการณ์ ทำให้วิธีวิจัยครั้งนี้ จำเป็นต้องเป็นการวิเคราะห์ข้อมูลหลายด้านประกอบกันแบบ multi-method และ multi-proxy เพื่อการแปลผลให้แม่นยำ แม้ว่าจะมีปัญหาอุปสรรคในการสำรวจฯ ได้แก่ สภาพความพร้อมและขีดจำกัดของเรือสำรวจ ภาระกิจหลักของเรือสำรวจฯ ไม่สอดคล้องกับโครงการ และข้อจำกัดในเรื่องอุปกรณ์และบุคลากร อีกทั้งการวิเคราะห์ข้อมูลต้องอาศัยโปรแกรมและเครื่องมือที่เฉพาะ การสำรวจของโครงการฯ ก็ยังสามารถตอบวัตถุประสงค์ที่ตั้งไว้ แต่นักวิจัยคาดหวังว่าน่าจะได้ข้อมูลครอบคลุมพื้นที่กว้างกว่านี้ ซึ่งควรมีการศึกษาต่อไปในอนาคต

4.3 การพัฒนาบุคลากร

โครงการนี้ได้พัฒนาบุคลากรเพื่อต่อยอดการทำงานวิจัยร่วมกับทางนักวิจัยเยอรมนี โดยมีนักวิจัยและนักศึกษา ที่ได้รับการฝึกอบรม ร่วมวิจัย และศึกษาระดับปริญญาโทและเอก ทั้งทางฝ่ายไทยและเยอรมนี ดังนี้

4.3.1 บุคลากรฝ่ายไทย

1) รศ. ดร. ศิวัช พงษ์เพียจันทร์ ผู้ช่วยศาสตราจารย์จากคณะการจัดการสิ่งแวดล้อม มหาวิทยาลัยสงขลานครินทร์ ซึ่งเข้าร่วมวิจัยและผลิตผลงานวิจัยจากโครงการลงตีพิมพ์ในวารสารวิชาการ จนปัจจุบันเป็นรองศาสตราจารย์ ที่คณะพัฒนาสังคมและสิ่งแวดล้อม สถาบันบัณฑิตพัฒนบริหารศาสตร์ (NIDA)

2) ดร.ดนัย ทิพย์มณี ศึกษาระดับดุษฎีบัณฑิตภายใต้โครงการ ที่หลักสูตรการจัดการสิ่งแลดล้อมและของเสียอันตราย (นานาชาติ) จุฬาลงกรณ์มหาวิทยาลัย ปัจจุบันสำเร็จการศึกษาและเป็นอาจารย์ ดร.ดนัย ทิพย์มณี ที่คณะเทคโนโลยีและสิ่งแวดล้อม มหาวิทยาลัยสงขลานครินทร์ วิทยาเขตภูเก็ต

3) นางสาวสุรัตตา บุญสมบูรณ์สกุล นักวิจัยที่ศูนย์เครือข่ายงานวิเคราะห์วิจัยและฝึกอบรมการเปลี่ยนแปลงของโลก จุฬาลงกรณ์มหาวิทยาลัย ร่วมทำวิจัยกับโครงการจนปัจจุบัน และศึกษาต่อที่ภาควิชาวิทยาศาสตร์ทางทะเล คณะวิทยาศาสตร์ จุฬาลงกรณ์มหาวิทยาลัย ในระดับดุษฎีบัณฑิต แบบ Double Degree ระหว่างจุฬาลงกรณ์มหาวิทยาลัย กับ State Key Laboratory of Marine Geology, Tongji University ประเทศสาธารณรัฐประชาชนจีน

4) นางสาวดรุณวรรณ สกุณา นักวิจัย นักวิจัยที่สถาบันวิจัยและพัฒนาทรัพยากรทางทะเล ชายฝั่งทะเล และป่าชายเลน จังหวัดภูเก็ต ร่วมทำวิจัยกับโครงการจนปัจจุบัน กำลังจะจบการศึกษาระดับดุษฎีบัณฑิตจาก Institute of Geosciences, Sedimentology, Coastal and Shelf Geology, Christian-Albrechts-Universität zu Kiel ประเทศเยอรมนี

4.3.2 บุคลากรฝ่ายเยอรมัน

1) Dr. Peter Feldens ทำวิทยานิพนธ์ภายใต้โครงการ ปัจจุบันจบการศึกษาระดับดุษฎีบัณฑิตจาก Institute of Geosciences, Sedimentology, Coastal and Shelf Geology, Christian-Albrechts-Universität zu Kiel ประเทศเยอรมนี

2) นายวิษณุกร พูนชัย ทำวิทยานิพนธ์ภายใต้โครงการ ปัจจุบันจบการศึกษาระดับมหาบัณฑิตจาก Institute of Geosciences, Sedimentology, Coastal and Shelf Geology, Christian-Albrechts-Universität zu Kiel ประเทศเยอรมนี และทำงานวิจัยอยู่ที่ University of Bremen ประเทศเยอรมนี

เอกสารอ้างอิง

ABRANTES, F., ALT-EPPING, U., LEBREIRO, S., VOELKER, A., SCHNEIDER, R., 2008. Sedimentological record of tsunamis on shallow-shelf areas: The case of the 1969 AD and 1755 AD tsunamis on the Portugese Shelf off Lisbon. Marine Geology 249: 283-293.

AXELSSON, V. & HÄNDEL, S.K., 1972. X-radiography of unextruded sediment cores. Geografiska Annaler. 54: 34-37.

BAHR, A., LAMY, F., ARZ, H., KUHLMANN, H., WEFER, G., 2005. Late glacial to Holocene climate and sedimentation history in the NW Black Sea. Marine Gelology 214: 309-322.

BEST, A.I. & GUNN, D.E., 1999. Calibration of marine sediment core loggers for quantitative acoustic impedance studies. Marine Geology 160: 137-146.

BELL, R., COWAN, H., DALZIELL, E., EVANS, N., O`LEARY, M., RUSH, B., YULE, L., 2005. Survey of impacts on the Andaman Coast, Southern Thailand following the great Sumatra-Andaman earthquake and tsunami of December 26, 2004. Bull. of The New Zealand Soc. For Earthquake Eng. 38(3), 123-148.

BRYANT, E. 2001. Tsunami. The Underrated Hazard: Cambridge, 320 p.

CANTALAMESSA, G., DI CELMA, C., 2005. Sedimentary features of tsunami backwash deposits in a shallow marine Miocene setting, Mejillones Peninsula, northern Chile. Sedimentary Geology, 178, 259 – 273.

CHOOWONG, M., MURAKOSHI N., HISADA K. 2008. 2004 Indian Ocean tsunami inflow and out flow at Phuket, Thailand. Marine Geology. 248: 179-192.

COWELL, P.J., HANSLOW, D.J., MELEO, J.F., 1999. The shoreface. In: SHORT, A.D. (ed.), Handbook of beach and shoreface morphodynamics, Chichester: Wiley, 39 – 71.

DAWSON, A.G., SHI, S., DAWSON, S., TAKAHASHI, T., SHUTO, N., 1996. Coastal sedimentation associated with the june 2nd and 3rd, 1994 tsunami at Rajegwesi, Java. Quat. Science Review, 15, 901 – 912.

DAWSON, A.G., STEWART, I. (2008) Offshore tractive current deposition: The forgotten tsunami sedimentation process. In: Tsunamiites – Features and Implications. 153 – 160.

FUJIWARA, O., KAMATAKI, T., 2007. Identification of tsunami deposits considering the tsunami waveform: An example of subaqueous tsunami deposits in Holocene sjallow bay on southern Boso Peninsula, Central Japan. Sedimentary Geology, 200, 295 – 313.

GOFF, J., CHAGUÉ-GOFF, C., NICHOLS, S., 2001. Palaeotsunami deposits: a New Zealand perspective. Sediment. Geol., 143, 1 – 6.

GOTO, K. CHAVANICH, S.A., IMAMURA, F., KUNTHASAP, P., MATSUI, T., MINOURA, K., SUGAWARA, D., YANAGISAWA, H., 2007. Distribution, origin and transport process of boulders deposited by the 2004 Indian Ocean tsunami at Pakarang Cape, Thailand. Sed. Geol. 202, 821-837.

HAWKES, A.D., BIRD, M., COWIE, S., GRUNDY-WARR, C., HORTON, B.P., TAN SHAU HWAI, A., LAW, L., MACGREGOR, C., NOTT, J., ONG, J.E., RIGG, J., ROBINSON, R., TAN-MULLINS, M., TIONG SA, T., YASIN, Z., WAN AIK, L., 2007. Sediments deposited by the 2004 Indian Ocean Tsunami along the Malaysia – Thailand Peninsula. – Marine Geology, 242, 169 – 190.

HERBERT, T.D., MEYER, L.A., 1991. Long climatic time series from sediment physical property measurements. J. Sediment. Petrol., 61(7): 1089-1108.

JACKSON, P.D., BRIGGS, K.B., FLINT, R.C., 1996. Evaluation of sediment heterogeneity using microresistivity imaging and X-radiography. Geo-Marine Latters 16: 219-225.

JANKAEW, K., ATWATER, B.F., SAWAI, Y., CHOOWONG, M., CHAROENTITIRAT, T., MARTIN, M.E., PRENDERGAST, A., 2008. Medieval forewarning of the 2004 Indian Ocean tsunami in Thailand. Nature 455, 1228-1231.

JANSEN, J.H.F., VAN DER GAAST, S.J., KOSTER, B., VAARS, A.J., 1998. CORTEX, a shipboard XRF-scanner for element analyses in split sediment cores. Marine Geology 151: 143-153.

LAY, T., KANAMORI, H., AMMON, J.C., NETTLES, M., 2005. The great Sumatra-Andaman earthquake of 26 December 2004. Science, 306, 1127 – 1133.

LE ROUX, J.P.,VARGAS, G., 2005. Hydraulic behaviour of tsunami backflows: insights from their modern and ancient deposits. Environ. Geol 49, 65-75.

LIU, P.L.F., LYNETT, P., FERNANDO, P., JAFFE, H., FRITZ, B., HIGMAN, H., MORTON, B., GOFF, J., SYNOLAKIS, C. 2005. Observation by the international tsunami survey team in Sri lanka. Science 308, 1595.

MAMO, B., Strotz, L. and Dominey-Howes, D. 2009. Tsunami sediments and their foraminiferal assemblages. Earth-Science Reviews 96: 263-278.

MIENERT, J., CURRY, W.B., SARNTHEIN, M., 1988. Sonostratigraphic records from equatorial Atlantic deep-sea carbonates: paleoceanographic and climatic relatinships. Marine Geology 83: 9-20.

MINOURA, K., NAKAYA, S., 1991. Traces of Tsunami preserved in intertidal lacustrine and marsh deposits: some examples from northeast Japan. Journal of Geology, 99, 265 – 287.

MOORE, A., GELFENBAUM, G., TRIYONO, 2005. Sedimentary depositsof the 26th December 2004 tsunamion the northwest coast of Aceh, Indonesia. Earth Planets Space, 58, 253 – 258.

NANAYAMA, F., SHINEGO, K., SATAKE, K., SHIMOKAKA, K., KOITABASHI, S., MIYASAKA, S., ISHII, M., 2000. Sedimentary differences between the 1993 Hokkaido-nansei-oki tsunami and the 1959 Miyakijima typhoon at Taisei, southwestern Hokkaido, northern Japan. Sediment. Geol. 187, 139 – 158.

NODA A., KATAYAMA, H., SAGAYAMA, T., SUGA K., UCHIDA Y., SATAKE K., ABE K., OKAMURA Y., 2007. Evaluation of tsunami impacts on shallow marine sediments: An example from the tsunami caused by the 2003 Tokachioki earthquake, northern Japan. Sed. Geol. 200, 314-327.

OHTA, T., ARAI, H., 2007. Statistical empirical index of chemical weathering in igneous rocks: A new tool for evaluating the degree of weathering. Chemical Geology 240: 280-297.

PÄLIKE, H., SHACKLETON, N.J., RÖHL, U., 2001. Astronomical forcing in Late Eocene marine sediments. Earth Planet. Sci. Lett. 193: 589-602.

SCHULTTHEISS, P.J.,WEAVER, P.P.E., 1992. Multi-Sensor Core Logging for Science and Industry. In: IEEE Xplore.

SHACKLETON, N.J., CROWHURST, S., HAGELBERG, T., PISIAS, N.G., SCHNEIDER, D.A., 1995. A New Late Neogene time scale: application to Leg 138 sites. In: N.G. Pisias, L.A. Mayer et al. (Editors), Proc. ODP Sci. Results 138: 73-101.

SIRIPONG, A., 2006. Andaman Seacoast of Thailand Field Survey after the December 2004 Indian Ocean Tsunami. Earthquake Spectra 22 (S3), 187-202.

SUGAWARA, D., MINOURA, K., NEMETO, N., TSUKAWAKI, S., GOTO, K., IMAMURA, F., 2009. Foraminiferal evidence of submarine sediment transport and deposition by backwash during the 2004 Indian Ocean tsunami. Island Arc. doi: 10.1111/j.1440-1738.2009.00677.

SUWANWERAKAMTORN, R., PAIJITPRAPAPORN, A., DOWNREASNG, D., SUWANASING, P., 1990. Sediment dispersion from offshore TIN dredging along Andaman sea coast using satellite data. Proc. Asian Association on Remote Sensing.

SYNOLAKIS, C.E., KONG, L., 2006. Runup measurements of the December 2004 Indian Ocean Tsuanmi. Earthquake Spectra 22 (S3), 67-91.

THAMPANYA, U., VERMAAT, J.E., SINSAKUL, S., PANAPITUKKUL, N., 2006. Coastal erosion and mangrove progradation of Southern Thailand. Estuar., Coast. Shelf Sci. 68:75-85.

THANAWOOD, C., YONGCHALERMCHAI, C., DENSRISEREEKUL, O., 2006. Effects of the December 2004 tsunami and disaster management in southern Thailand. Science of Tsunami Hazards, 24, 206 – 217.

TSUJI, Y., NAMEGAYA, Y., MATSUMOTO, H., IWASAKI, S.I.., KANBUA, W., SRIWICHAI, M., MEESUK, V., 2006. The 2004 Indian tsunami in Thailand. Surveyed runup heights and tide gauge records. Earth Planets Space 58, 223-232.

WEISS, R., BAHLBURG, H. 2006. The Coast of Kenya Field Survey after the December 2004 Indian Ocean Tsunami. Earthquake Spectra 22 (S3), 235-240.

WELTJI, G.J., TJALLINGII, R., 2008. Calibration of XRF core scanners for quantitative geochemical logging of sediment cores: Theory and application. Earth Planet. Sci. Lett. 274: 423-438.

WIEGEL, R.L., 2006a. Tsunami information sources. Science of Tsunami Hazards, 24 (2), 58 p.

WIEGEL, R.L., 2006b. Tsunami information sources. Science of Tsunami Hazards, 25 (2), 67 p.

YUNKER, B.M., MACDONALD, W.R., VINGARZAN, R., MITCHELL, H.R, GOYETTE, D., SYLVESTRE, S. 2002. PAHs in the Fraser River basin: a critical appraisal of PAH ratios as indicators of PAH source and composition. Organic Geochemistry, 33: 489-515.

Polish J. of Environ. Stud. Vol. 18, No. 1 (2009), 63-68

Original Research

Impact of 2004 Tsunami on Seafloor Morphology and Offshore Sediments, Pakarang Cape, Thailand

P. Feldens[1]*, K. Schwarzer[1], W. Szczuciński[2], K. Stattegger[1], D. Sakuna[1], P. Somgpongchaiykul[3]

[1]Institute of Geosciences, Coastal and Shelf Research, Kiel University, Olshausenstrasse 40, 24118 Kiel, Germany
[2]Institute of Geology, Adam Mickiewicz University in Poznań, Maków Polnych 16, 61-606 Poznań, Poland
[3]Biogeochemical and Environmental Change Research Unit, Prince of Songkla University, P.O. Box 50, Kho Hong, hat Yai, Songkhla 90112, Thailand

Received: 8 October, 2008
Accepted: 25 November, 2008

Abstract

This study documents seafloor morphology and sediments based on multibeam, side-scan sonar and boomer surveys, as well as sediment samples taken on the inner to mid shelf of the Andaman Sea after the 2004 Indian Ocean tsunami. Preservation of submarine relief in former underwater mining areas points to limited impact of the tsunami, while channel structures parallel to the observed tsunami backwash indicate a possible higher impact. Therefore, the tsunami impact seems to be focused on some areas. The impact was probably most effective during the backwash, when stiff mud deposits containing grass, wood fragments and shells were transported by high density backwash flows. Moreover, several boulders, which might have been deposited during the tsunami backwash flow, were found in the channels in front of Pakarang Cape.

Keywords: 2004 Indian Ocean tsunami, seafloor mapping, tsunami backwash, inner continental shelf, Andaman Sea

Introduction

Most of the research published about erosion and deposition of recent tsunamis focus on the onshore areas. The offshore effects, although theoretically significant [1] and more common in older geological records compared to onshore deposits [2], have only been documented in a few studies [3-5]. Surprisingly, offshore impacts of the well studied 2004 Indian Ocean tsunami are also almost unknown. Few authors reported offshore deposition of muddy sediments [6-8]. Offshore was postulated through analyses of microfossils in onshore tsunami deposits [9-12].

This article presents results of a four-week research cruise, undertaken in November and December 2007, focussing on the inner continental shelf next to Pakarang Cape (Phang Nga province, Thailand). During this cruise, hydroacoustic data (side-scan sonar, multibeam echo sounder, shallow water reflection seismic) as well as sediment samples were collected to obtain further insight about the impact of the 2004 tsunami on the shallow seafloor.

*e-mail: pfeldens@gpi.uni-kiel.de

The Research Area

The Andaman Sea continental shelf adjacent to the Malay Peninsula is narrow and slightly inclined. The area is dominated by two monsoonal winds: the northeast monsoon from mid October to March and the southwest monsoon from May to September. The southwest monsoon generates the highest waves along the coast. The tide is mixed semidiurnal with a tidal range between 1.1 and 3.6 m, taking into account spring and neap tide [13]. The research area, about

1,000 km², is situated off Khao Lak (Phang Nga province), in water depths between 10 and 70 meters. For decades, tin mining activities took place in parts of the studied area [14], but ceased about 20 years ago. This study focuses on a part of the shelf next to Phang Nga province, especially around Cape Pakarang (Fig. 1). The research area was chosen because tsunami-induced change of the seafloor can be expected in this area, as the coastline was highly damaged during the tsunami [15, 16]. Furthermore, the absence of large river mouths in this area increases the visibility of tsunami-induced structures on the seafloor in hydroacoustic data. The run-up at Pakarang Cape reached a height of more than 15 m [17] due to shoaling processes and the interaction of the tsunami wave with the seabottom. During the tsunami event a layer of a few cm to about 0.5 m thickness, composed of sand and silty sand, was deposited over almost the whole inundation zone [7, 18-20]. According to eyewitnesses reports, the tsunami wave arrived from three different directions at Pakarang Cape [17]. The backwash pattern was documented by satellite images taken after the tsunami (indicated in Fig. 2). Obviously, the waves were forming a complex run-up and backwash pattern, heavily influenced by the nearshore bathymetry [7]. At the tip of Pakarang Cape, an area of about 12,500 m² was completely eroded during the tsunami [21]. Hundreds of reef rocks more than 1 m in diameter were transported landwards by the tsunami and deposited in shallow waters around Pakarang Cape [22, 23]. Tsunamigenic incisions, with a spacing between 50 and 200 m at the coastline of Khao Lak, were created during the run-up, and enlarged during the backwash of the tsunami [24]. Furthermore, it was observed that the channels are fan-shaped, and are wider at the coastline and narrower further inshore. This indicates a control of spacing and dimension of these return channels by the wave height of the tsunami. [24]. Westward of the research area, about 2 m sand from the seafloor have been eroded around a coral reef boulder in 30 m water depth, probably due to the tsunami [6].

Methods

Material for the study was collected during a research cruise on RV CHAKRATONG TONGYAI in November and December 2007. Acoustic properties of the seafloor sediment were measured using a side scan sonar (500 kHz) with digital data acquisition. A shallow water multibeam echo sounder with a working frequency of 180 kHz was welded to the portside of the research vessel to record bathymetric data. Shallow water reflection seismic data were obtained using a high resolution EG&G boomer system (about 500-15000 Hz). The covered area is shown in Fig. 1. For ground-truthing of the hydroacoustic data and for further sediment analysis, 77 grab samples were taken using a Van-Veen-type grab sampler. 40 short sediment cores of up to 125 cm in length were obtained using a gravity corer. However, for the present study only grab sample material was analyzed. To determine the grain-size parameters, sediment samples were dried and sieved. The grain-size statistics were calculated using Gradistat software [25].

Results

Bathymetry

The obtained bathymetric map of the area in front of Pakarang Cape is shown in Fig. 2. Down to 18 m, the slope is inclined with an angle of about 0.8°. Below this depth, the overall slope angle decreases (to about 0.1°), and the seafloor shows a “step like” morphology (Figs. 2 and 3). At the base of the southern slope of these steps, SW-NE striking channels, with a width of several hundred meters

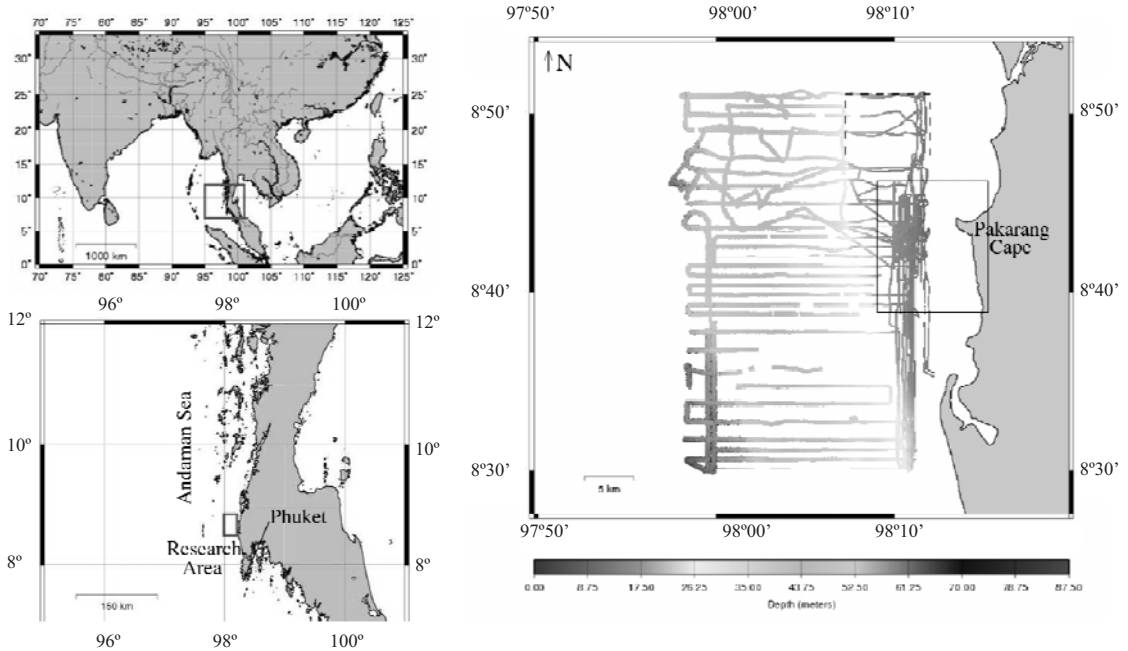


Fig. 1. The research area offshore Phang Nga province.

and a depth between 0.5 to 2 m are cut in the seafloor. Bathymetric cross sections (Fig. 3) reveal that the channels are asymmetrical, with the deepest incisions situated close to their southern slope. The dipping angles of the channels are low, reaching 1 to 1.2° at the southern slopes and about 0.2° at the northern slope. Towards the coastline, corresponding with the onset of the steeper slope angle in water depths between 14 and 18 m, the number of channels increases. The continuation of these channels both in deeper and shallower water is unknown, although first data from shallow water reflection seismics suggests a continuing propagation of the channels further offshore. The seismic data does not show any connection between the channels and subsurface structures. Remnants of these tin mining activities in this area (indicated in Fig. 1) are visible in the form of steep holes up to 7 m deep.

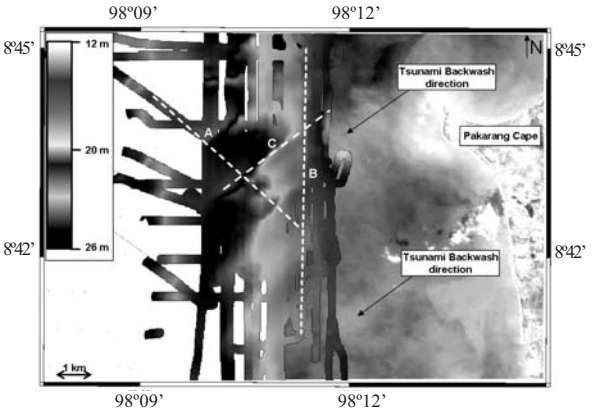


Fig. 2. Bathymetry around Pakarang Cape merged with a satellite image taken shortly after the 2004 tsunami. The dashed lines indicate the profiles shown in Fig. 3. (satellite image: Images acquired and processed by CRISP, National University of Singapore. IKONOS image © 2004. www.crisp.nus.edu.sg/tsunami/tsunami.html, modified.)

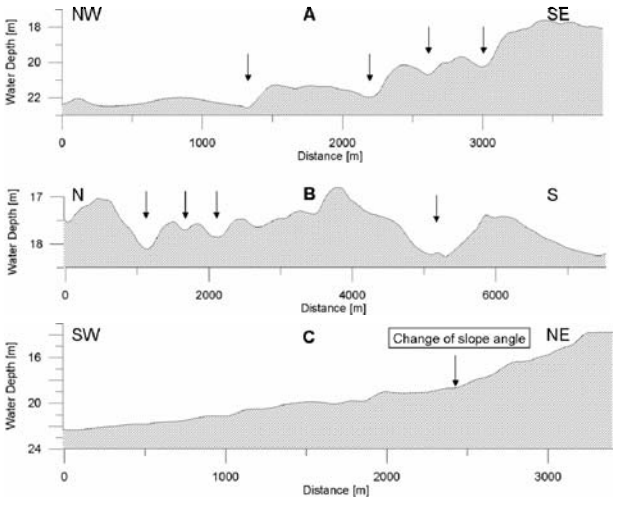


Fig. 3. Cross sections from several parts of the seafloor. Channels are marked by arrows. For the positions, refer to Fig. 2.

Seafloor Sediments

Large elongated sediment patches, appearing nearly white in the side-scan sonar images, with the same strike direction as the aforementioned channels, were documented in front of Pakarang Cape. There is a distinct transition between these areas and the surrounding seafloor (appearing darker in the side-scan sonar image shown in Fig. 4). Light-coloured areas in the side scan sonar data correspond to finer or non-consolidated sediment, while darker areas correspond to coarser or more consolidated sediment. The southern boundary of the elongated patches is very irregular and appears "flame-shaped" (Fig. 5). A combination of side-scan sonar and multibeam echo sounder data indicates that the large elongated areas of fine sediment are situated at the steeper southern slopes of the channels. In many cases, it was not possible to distinguish between the layers of fine to medium sand in the seismic data, taken simultaneously with the side scan sonar data. When it was possible to recognize these layers in the seismic data, their thickness appeared to be on the order of a few decimetres. Small patches of the same, fine sediment are visible closer to the coastline and are commonly situated in smaller channels and depressions (Fig. 6).

The results of the grain size analysis are incorporated in Fig. 4. The elongated sediment patches are composed of fine to medium sand, while the surrounding seafloor consists of coarse sand. Both types of sediment are poorly to moderately sorted. In one grab sample, taken from about 16 m water depth a stiff mud, covered by a 3 cm thick layer of coarse, well sorted sand was found. It contained terrestrial organic remnants: grass and pieces of wood, moreover, clasts of clay were found. Additionally, side-scan sonar data revealed the presence of numerous boulders with diameters around 1 m, as determined on the basis of their acoustic shadows in the side-scan sonar images. Most of these boulders appear between the aforementioned sediment patches close to the

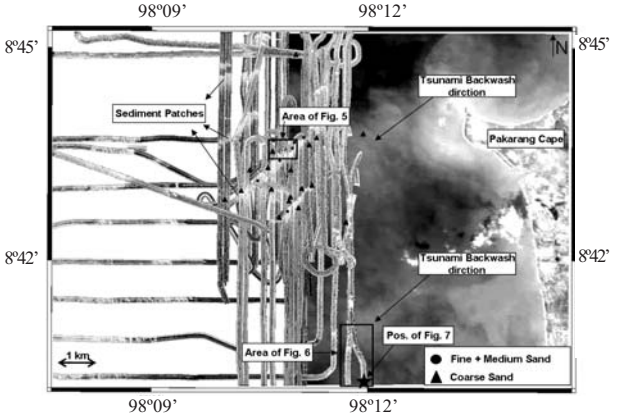


Fig. 4. Side Scan Sonar data merged with a satellite image taken shortly after the 2004 tsunami. Indicated are sediment types based on grain size analysis, as well as the locations of the following figures. (satellite image: Images acquired and processed by CRISP, National University of Singapore. IKONOS image © 2004. www.crisp.nus.edu.sg/tsunami/tsunami.html, modified.)

coastline (Fig. 7). However, some boulders, located at a distance of about 4 to 6 km from the tip of Pakarang Cape, are situated within a larger channel directly north of an elongated sediment patch (Fig. 5).

Discussion

Although the survey took place three years after the 2004 Indian Ocean tsunami, it is likely that several of the observed features may be ascribed to this impact. For instance, the channels and elongated sediment patches observed in front of Pakarang Cape have a striking resemblance to the backwash pattern observed in the satellite images taken after the tsunami event (Fig. 4). The erosion potential of a tsunami run-up and backwash is commonly mentioned in the literature [26, 27]. The impacts of the backwash depend on the amount of water flowing back into the sea, which itself depends on wave height [24], and on the formation of high density hyperpycnal flows [28]. High tsunami run-up heights at Pakarang Cape and the local presence of stiff mud with grass and wood found in offshore sediment samples suggest that both conditions enhancing the erosion potential of the backwash were met. Therefore, it is possible that the observed channels were formed mainly during the channelized tsunami backflow. Although due to a lack of pre-tsunami data it is not possible to exclude that the channels already existed prior to that event, several features suggest their origin or at least reshaping during the tsunami. A good correlation between the spacing of onshore incisions, interpreted to be created during run-up and backwash, and tsunami wave height is reported [24]. River mouths in the Nam Khem plain (north from Pakarang Cape) changed into wedge-shaped channels [29] with a width of 50-200 m, mainly due to the effect of a concentrated tsunami backwash. As the onshore return channels of the tsunami are wedge-shaped, and widening towards the coastline, it could be assumed that a connection between the onshore incisions and the wider channels, observed in shallow waters, exists. The rapid transition of these channels into the deeper, and even wider, channels in water depths of about 17 to 18 m might be caused by a change of the hydraulic behaviour of the backwash due to the changing slope angle of the seafloor (Figs. 2 and 3). The channels in deeper waters are asymmetrical in cross section. Related to this observation, it is interesting to note that regularly spaced, very shallow swales with asymmetrical profiles and filled by very fine-grained sandstones, and interpreted to be created during a paleotsunami event, have been reported [30].

Local erosion (adjacent to a large reef boulder where the formation of scour structures was possible) of up to 2 m

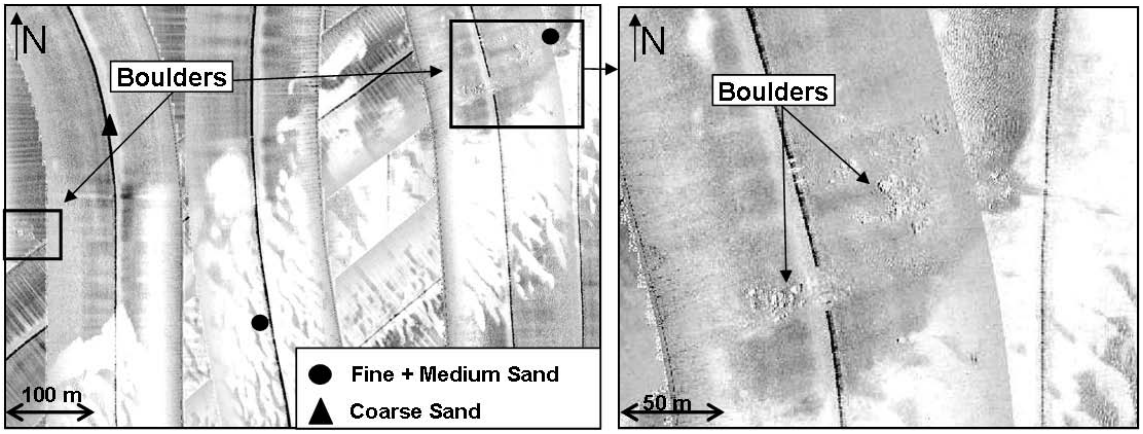


Fig. 5. Detailed view of one elongated sediment patch in front of Pakarang Cape. To the north of the patches, boulders are visible. For the location of the figure, refer to Fig. 4.

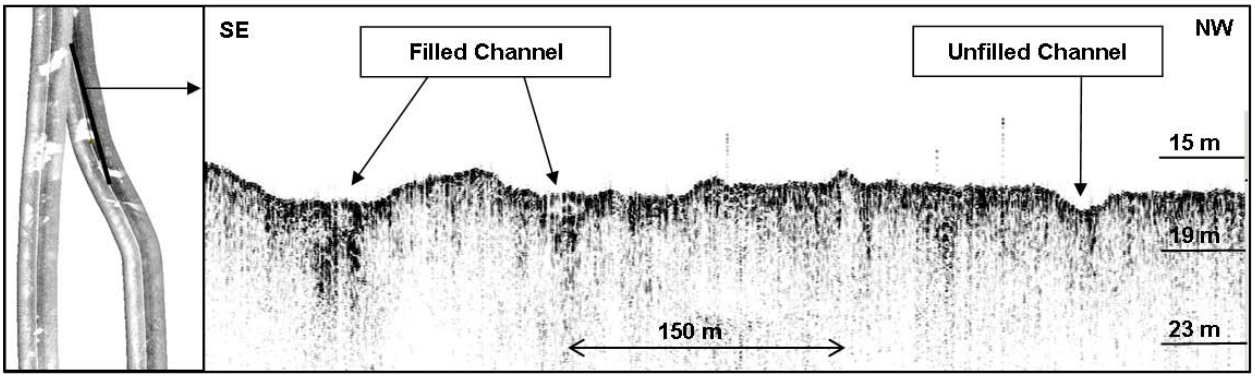


Fig. 6. Shallow seismic profiles close to the coastline with small channels. Some of these channels are filled with finer sediment, which appears white in the side scan sonar data. For the location of the figure, refer to Fig. 4.

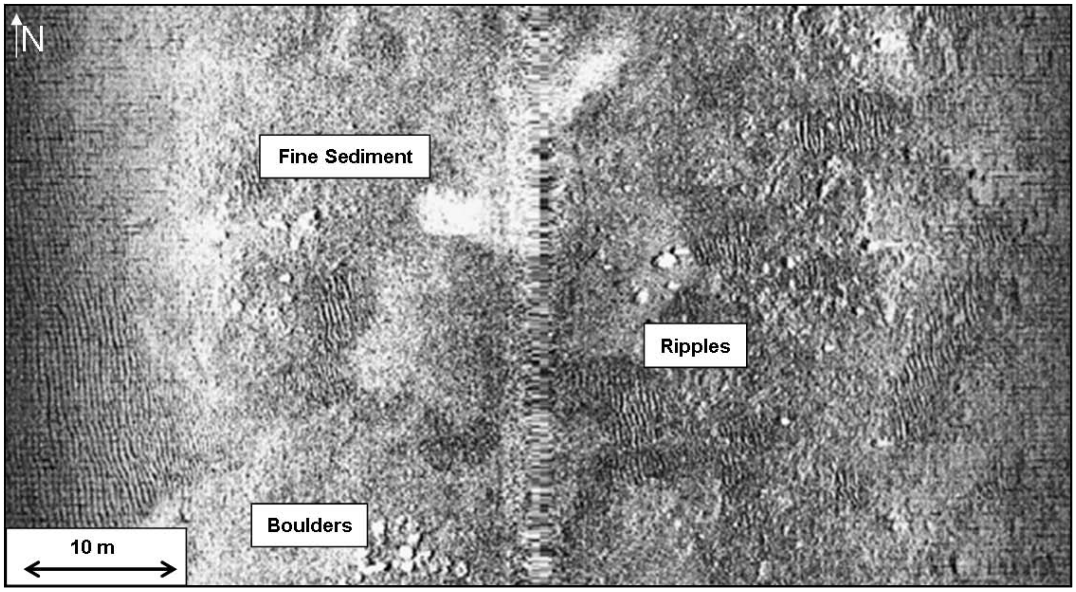


Fig. 7. Detailed view of side scan sonar data from a profile recorded close to the coastline. Different sediment types, including boulders, fine sediment and rippled sand, are deposited within a distance of a few meters. The location of this figure is indicated in Fig. 4.

during the tsunami event in a water depth of 30 m was reported [6]. Our data suggest erosion of a lower but comparable magnitude in the channels, and less erosion of the surrounding seafloor, as indicated by well preserved tin mining holes. This observation confirms previous suggestions [28] that tsunami effects are largely related to confined channelized flows during backwash and, possibly, run-up. The elongated areas and the small patches of fine and medium sand found in the channels and closer to the coastline could have been deposited during the backwash of the tsunami. If these sediments were deposited before the tsunami, one could expect that the tin mining holes would have been filled with the finer material during the past decades. However, the "flame-like" shape (indicating sediment transport) of the fine to medium sand sediment patches, as well as the presence of these sediments on the steeper southern slopes of the channels, may suggest their reworking during the post-tsunami period. In particular, their asymmetrical distribution in the channels may be a result of monsoon-related circulation and preservation of the finer sediments in relatively sheltered locations [8].

The existence of stiff muddy sediments containing pieces of grass and wood, which should be floating unless transported in a high turbidity and high density hyperpycnal flow, is strong supporting evidence of tsunami backwash and its potential erosion power. On the other hand, these deposits being covered by distinctly different coarse sand, typical for this part of the continental shelf, are already preserved in the geological record. This finding is promising for the search for paleotsunami evidence in this setting.

Interesting is the presence of boulders within the larger return channels in front of Pakarang Cape. The backwash velocity was modelled to be around 3.0 m/s at Cape Pakarang [22], slightly higher than the calculated critical velocity to move boulders. While some authors do not believe that the backwash, due to its short duration, transported boulders from the tidal flat back to the deeper waters, [22], it is very likely that boulders could easily be transported downhill from their original position on the coral reef slope during the tsunami backwash.

Conclusions

One of the first studies of offshore impacts of the 2004 tsunami indicates:

- Existence of a system of channels slightly oblique to the coastline, which are partly filled with finer sediments and could have been created during the backwash of the 2004 Indian Ocean tsunami.
- Variability in the channel system, which is changing with water depth and slope angle; probably as a result of changing hydrodynamic properties of the backwash (hyperpycnal flow).
- Validity of the assumptions on a channelized backwash, and maybe even run-up of the tsunami.
- Characteristic sediment deposition during the backwash, suggesting deposition from highly turbulent, high density flow.
- The backwash had enough power to transport boulders from the coral reef slope to deeper waters.

Acknowledgement

The study was supported by the DFG through research grant SCHW/11-1. W. Szczuciński was supported by a Foundation for Polish Science (FNP) fellowship. We are grateful to Phuket Marine Biological Center (PMBC) for providing us with RV CHAKRATONG TONGYAI. The help of cruise participants is greatly acknowledged.

References

1. WEISS R. Sediment grains moved by passing tsunami waves: Tsunami deposits in deep water. Mar. Geol. **250**, 251, **2008**.
2. DAWSON A. G., STEWART I. Tsunami deposits in the geological record. Sed. Geol. **200**, 166, **2007**.
3. VAN DEN BERGH G.D., BOER W., DE HAAS H., VAN WEERING TJ.C.E., VAN WIJHE R. Shallow marine tsunami deposits in Teluk Banten (NW Java, Indonesia), generated by the 1883 Krakatau eruption. Mar. Geol. **197**, 13, **2003**.
4. NODA A., KATAYAMA H., SAGAYAMA T., SUGA K., UCHIDA Y., SATAKE K., ABE K., OKAMURA Y. Evaluation of tsunami impacts on shallow marine sediments: An example from the tsunami caused by the 2003 Tokachi-oki earthquake, northern Japan. Sed. Geol. **200**, 314, **2007**.
5. ABRANTES F., ALT-EPPING U., LEBREIRO S., VOELKER A., SCHNEIDER R. Sedimentological record of tsunamis on shallow-shelf areas: The case of the 1969 AD and 1755 AD tsunamis on the Portuguese Shelf off Lisbon. Mar. Geol. **249**, 283, **2008**.
6. CHAVANICH S., SIRIPONG A., SOJISUPORN P., MENASVETA P. Impact of Tsunami on the seafloor and corals in Thailand. Coral Reefs **24**, 535, **2005**.
7. SZCZUCIŃSKI W., CHAIMANEE N., NIEDZIELSKI P., RACHLEWICZ G., SAISUTTICHAI D., TEPSUWAN T., LORENC S., SIEPAK J. Environmental and Geological Impacts of the 26 December 2004 Tsunami in Coastal Zone of Thailand – Overview of Short and Long-Term Effects. Polish J. Environ. Stud. **15** (5), 793, **2006**.
8. DI GERONIMO I., ROBBA E., CHARUSIRI P., CHOOWONG M., AGOSTINO I., MARTINO C., DI GERONIMO R., PHANTUWONGRAJ S. Marine modern sediments and rocky bottoms of Khao Lak coastal area, Changwat Phang Nga, Andaman Sea, SW Thailand. Color Map, 1:30.000, Catania, Bangkok, **2008**.
9. RAZZHIGAEVA N.G., GANZEI L.A., GREBENNIKOVA T.A., IVANOVA E.D., KAISTRENKO V.M. Sedimentation particularities during the tsunami of December 26, 2004, in northern Indonesia: Simelue Island and the Medan coast of Sumatra Island. Oceanology **46**, 875, **2006**.
10. HAWKES A.D., BIRD M., COWIE S., GRUNDY-WARR C., HORTON B.P., SHAU HWAI A.T., LAW L., MACGREGOR C., NOTT J., ONG J.E., RIGG J., ROBINSON R., TAN-MULLINS M., SA T.T., YASIN Z., AIK L.W. Sediments deposited by the 2004 Indian Ocean tsunami along the Malaysia-Thailand peninsula. Mar. Geol. **242**, 169, **2007**.
11. DAHANAYAKE K., KULASENA N. Recognition of diagnostic criteria for recent- and paleo-tsunami sediments from Sri Lanka. Mar. Geol. **254**, 180, **2008**.
12. KOKOCIŃSKI M., SZCZUCIŃSKI W., ZGRUNDO A., IBRAGIMOW A. Diatom assemblages in 26 December 2004 tsunami deposits from coastal zone of Thailand as sediment provenance indicators. Polish J. Environ. Stud. **18**, 93, **2009**.
13. THAMPANYA U., VERMAAT J.E., SINSAKUL S., PANAPITUKKUL N. Coastal erosion and mangrove progradation of Southern Thailand. Estuar., Coast. Shelf Sci. **68**, 75, **2006**.
14. USIRIPRISAN C. CHIEMCHINDARATANA S., SHOOSUWAN S., CHATRAPAKPONG Y. Offshore exploration for tin and heavy minerals in the Andaman Sea. Department of Mineral Resources, Thailand, pp. 224, **1987**.
15. BELL R., COW AN H., DALZI ELL E., EVANS N., O'LEARY M., RU SH B., YU LE L. Survey of impacts on the Andaman Coast, Southern Thailand following the great Sumatra-Andaman earthquake and tsunami of December 26, 2004. Bull. of The New Zealand Soc. For Earthquake Eng. **38** (3), 123, **2005**.
16. TSUJI Y.Y., NAMEGAYA H., MATSUMOTO S.I., IW ASZKI W., KANBUA M., SRIWI CHAI M., MEESUK V. The 2004 Indian tsunami in Thailand. Surveyed runup heights and tide gauge records. Earth Planets Space, **58**, 223, **2006**.
17. SIRIPONG A. Andaman Seacoast of Thailand Field Survey after the December 2004 Indian Ocean Tsunami. Earthquake Spectra **22** (S3), 187, **2006**.
18. SZCZUCIŃSKI W., NIEDZIELSKI P., RACHLEWICZ G., SOBCZYŃSKI T., ZIOŁA A., KOWALSKI A., LORENC S., SIEPAK J. Contamination of tsunami sediments in a coastal zone inundated by the 26 December 2004 tsunami in Thailand. Environ. Geol. **49**, 321, **2005**.
19. HORI K., KUZUMOTO R., HIROUCHI D., UMITSU M., JANJIRAWUTTIKUL N., PATANAKANOG B. Horizontal and vertical variation of 2004 Indian tsunami deposits: An example of two transects along the western coast of Thailand. Mar. Geol. **239**, 163, **2007**.
20. CHOOWONG M., MURAKOSHI N., HISADA K., CHARUSIRI P., DAORERK V., CHAROENTITIRAT T., CHUTAKOSITKANON V., JANKAEW K., KANJANAPAYONT P. Erosion and deposition by the 2004 Indian Ocean tsunami in Phuket and Phang-nga Provinces, Thailand. J. Coast. Res. **23**, 1270, **2007**.
21. SYNOLAKIS C.E., KONG L. Runup measurements of the December 2004 Indian Ocean Tsunami. Earthquake Spectra **22** (S3), 67, **2006**.
22. GOTO K., CHAVANICH S.A., IMAMURA F., KUNTHASAP P., MATSUI T., MINOURA K., SUGAWARA D., YANAGISAWA H. Distribution, origin and transport process of boulders deposited by the 2004 Indian Ocean tsunami at Pakarang Cape, Thailand. Sed. Geol. **202**, 821, **2007**.
23. GOTO K., IMAMURA F., KEERTHI N., KUNTHASAP P., MATSUI T., MINOURA K., RUANGRASSAMEE A., SUGAWARA D., SUPHARATID S. Distribution and significance of the 2004 Indian Ocean tsunami deposits: initial results from Thailand and Sri Lanka. In: Tsunamiites – Features and Implications. Shiki et al. (eds.) Elsevier, pp. 105-122, **2008**.
24. FAGHERAZZI S., DU X. Tsunamigenic incisions produced by the December 2004 earthquake along the coasts of Thailand, Indonesia and Sri Lanka. Geomorphology **99**, 120, **2008**.
25. BLOTT S.J., PYE K. Gradistat: a grain size distribution and statistics package for the analysis of unconsolidated sediments. Earth Surface Processes and Landforms **26**, 1237, **2001**.
26. DAWSON A. G. Geomorphological effects of tsunami run-up and backwash. Geomorphology **10**, 83, **1994**.
27. DAWSON A. G., SHI S. Tsunami deposits. Pure and Applied Geoph. **157**, 875, **2000**.
28. LE ROUX J. P., VARGAS G. Hydraulic behavior of tsunami backflow: insights from their modern and ancient deposits. Environ. Geol. **49**, 65, **2005**.
29. UMITSU M., TANAVUD C., PATANAKANOG B. Effects of landforms on tsunami flow in the plains of Banda Aceh, Indonesia, and Nam Khem, Thailand. Mar. Geol. **242**, 141, **2007**.
30. ROSETTI D.D.F., GÓES A.M., TRUCKENBRODT W., ANAISSE JR J. Tsunami-induced large scale scour-and-fill structures in Late Albian to Cenomanian deposits of the Grajaú Basin, northern Brazil. Sedimentology **47**, 309, **2000**.

Schwarzer, Schrottke & Stattegger (eds.):
From Brazil to Thailand – New Results in Coastal Research
***Coastline Reports 16 (2010)**, ISSN 0928-2734, ISBN 978-3-9811839-9-3*
S. 15-24

Shallow water sediment structures in a tsunami-affected area (Pakarang Cape, Thailand)

Peter Feldens[1], Daroonwan. Sakuna[1,2], Penjai Somgpongchaiyakul[3] & Klaus Schwarzer[1]

[1]Kiel University, Germany
[2]Phuket Marine Biological Centre, Thailand
[3]Biogeochemical and Environmental Change Research Unit, Prince of Songkla University, Thailand

Abstract

The influence of tsunami on the seafloor is poorly understood. Detailed hydroacoustic surveys and sediment sampling campaigns were carried out in 2007 and 2008 offshore Pakarang Cape (Thailand) to catalogue the geomarine effects of the 2004 Indian Ocean tsunami. A major problem in determining tsunami influence in offshore deposits is the lack of pre-tsunami mappings. Starting in 15 m water depth, a system of sand ridges composed of coarse sand exists offshore Pakarang Cape. Elongated sediment transport structures on the NW-flanks of the sand ridges, slowly fading during the annual cycle, indicate the presence of a current oblique to the coastline. This current might coincide with the 2004 Indian Ocean Tsunami. A several cm-thick event layer found at the base of a sand ridge is composed of silty sediment, which could be related to the tsunami backwash or strong floods during the monsoon. These event deposits are covered by coarse sand. They might enter the geological record.

1 Introduction

Tsunamis are among the largest catastrophic events in the world. They are recorded since historical times and numerous investigations have been done about their origin, wave distribution and energy release along coastlines. On December 26th, 2004 an M 9.3 submarine earthquake was generated off the northwest coast of the Indonesian island Sumatra due to a complex tectonic activity between the Indo-Australian plate and the Sunda-Plate. This generated a giant tsunami which had an impact over many SE Asian coastlines, reaching to the East-coast of Africa (Lay et al. 2005).

Compared to the influence of the 2004 Indian Ocean Tsunami to onshore areas, the impact to the offshore environment is not well understood. Only few studies document tsunami effects offshore (e.g. Van den Bergh et al. (2003), Noda et al. (2007), Abrantes et al. (2008), Feldens et al. (2009), Paris et al. (2009), but influence and physical properties of the sediment-loaded tsunami backwash are largely unknown. Dawson & Stewart (2007) propose that offshore tsunami deposits are more common in the geological record than onshore deposits. A secure identification of offshore tsunami deposits would therefore be of great value for the recognition of paleotsunamis. A major, but common problem is the missing data about pre-tsunami conditions when working on recent tsunamigenic structures on continental shelf areas. It has to be carefully considered, if observed structures have existed before a tsunami hit the area, were created during the tsunami event or were altered by the tsunami impact. We present observations and first results of selected sedimentological and morphological features, recorded during cruises in the framework of the TUNWAT project (Tsunami deposits in near-shore- and coastal waters of Thailand; funded by the Human Research Foundation (DFG), Grant: SCHW/11-1) offshore the tsunami impacted coastline of Khao Lak, Phang Nga Province, Thailand.

2 Investigation area

The continental shelf of the Andaman Sea adjacent to the Malay Peninsula is narrow and slightly inclined; the 50 m isobaths is reached approximately 7 km offshore Phuket and about 30 km offshore Phang Nga Province located towards north. The coastal area is dominated by rocky cliffs altering with sandy lowlands and pocket beaches. From December to February the NE-monsoon dominates while the SW-monsoon is active from May to September (Khokiattiwong et al. 1991). The influence of storms and typhoons on this part of Thailand's coastline is low (Kumar et al. 2008, Jankaew et al. 2008). The tide is mixed semidiurnal, ranging between 1.1 m and 3.6 m (Thampanya et al. 2006).

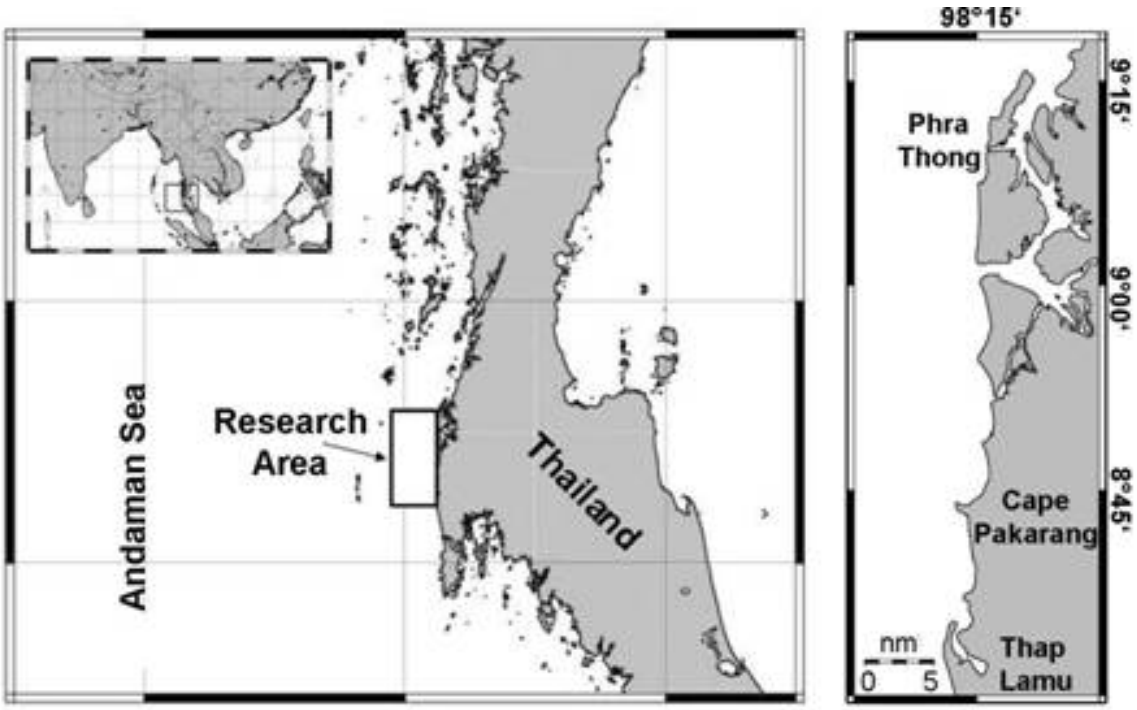


Figure 1: The research area is located in front of Khao Lak, Phang Nga province, Thailand.

The research area, between Thap Lamu and Phra Thong Island comprises of approximately 1.000 km² (figure 1). It was selected as it was hit severely by the 2004-Indian-Ocean-Tsunami (Bell et al. 2005, Tsuji et al. 2006). The wave run-up heights reached more than 15 m at Pakarang Cape (Siripong 2006) and up to 20 m at Phra Thong Island (Jankaew et al. 2008). At Pakarang Cape an area of about 12.500 m² was eroded by the tsunami (Synolakis & Kong 2006) and hundreds of reef rocks could be observed on the intertidal area after the event (Goto et al. 2007). For the investigation area the fluvial discharge is small, which increases the preservation potential of tsunamigenic features on the seafloor.

3 Methods

Two cruises have been carried out; a first one in Nov./Dec. 2007 with RV CHAKRATONG TONGYAI and a second with RV BOONLERT PASOOK in Nov./Dec. 2008. Both ships are operated by the Phuket Marine Biological Center (PMBC). Different side scan sonar systems were applied; a Klein 595 with digital data acquisition in 2007 and a Benthos 1624 digital side scan sonar system in 2008. Side scan sonar systems measure acoustical properties of the seafloor, which mainly depend on grain size distribution, seafloor roughness and the angle of the seafloor slope (Lurton 2002). Features protruding from the seafloor, e.g. boulders, but as well large ripples are easily recognized in side scan sonar images due to the acoustic shadow formed behind them. In this study, fine grained deposits

appear in lighter colours, while coarse grained material is represented by darker colours. For ground-truthing of the side-scan sonar data grab samples were taken on selected positions.

A shallow water multibeam echosounder (ELAC SeaBeam 1185) was used to acquire bathymetric data. Multibeam echo sounders provide many simultaneous depth measurements over a narrow section of the seafloor. The SeaBeam 1185 system is working with a frequency of 180 kHz, which is suitable for a high resolution mapping in shallow waters. The acoustic beam of the system has a fan width of 153°, giving a theoretical swath width of 8.3 times the water depths. Calibration for tidal fluctuations was done by using the software WX-Tide32 (www.wxtide32.com), as no direct water level measurements are available in or close to the research area.

Shallow water high resolution reflections seismics (C-Boom System), in combination with the recovery of short gravity cores, was used to obtain information about the uppermost layers of the seafloor. X-radiography images of thin slabs taken from the core surface were prepared to detect sedimentary structures that cannot be seen otherwise (Jackson et al. 1996). The database of the cruises carried out in 2007 and 2008 include about 1500 nautical miles (nm) of hydroacoustic profiles, 112 Surface sediment samples and 42 short sediment cores.

4 Results

Side scan sonar images offshore Khao Lak show several different sedimentary structures in depths from 7 to 30 m (figure 2). In water depths between 7 and 15 m, extended patches of fine grained sediments are deposited. Connected to these patches is a small scale channel system starting at 10 m water depth. Here we focus on structures appearing at 15 m water-depth. Elongated SW-NE striking morphological ridges are visible in the hydroacoustic data (Figure 2). These structures are common along the whole coastline between Thap Lamu and Pakarang Cape, and up to Phra Thong Island towards north. The continuation of the ridges into deeper waters is yet unknown. The ridges, with a steep NW- and a gently dipping SE flank reach heights of about 2 m, while their length exceeds several kilometres. The distance between two ridge crests varies from several hundred meters to several kilometres. In front of the steep north-eastern side of these ridges, small channels with incision depths of approximately 1 m are sometimes cut into the seafloor. According to seismic data, the ridges are not connected to subsurface structures, but are clearly separated from the sedimentological structures below by an unconformity (figure 5).

For one ridge, a side scan sonar mosaic was draped over the bathymetry (figure 3) to correlate sedimentology and morphology. Grab samples taken around the ridge (figure 3) reveal the presence of different sediment properties in a small area: Generally, the south-western, landward flank of the ridge and the surface of the seafloor surrounding the ridge are composed of coarse sand. Bright elongated sediment structures are deposited on the seaward flank of the ridge and are composed of well sorted fine to medium sand. The patches are separated from each other by thin bands of coarser sediment. From their appearance in the side scan sonar image, the structures resemble large-scale flaser beddings. However, as the genesis of the observed features is different to flaser beddings, which are formed due to tidal activities, the term will not be used.

The sediment patches are commonly observed on the seaward, northern flank of sand ridges along the coastline. Rarely, they are found on the flat seafloor. Boulders are sometimes exposed in close vicinity (figure 3, figure 4). At the base of the ridge flank shown in figure 3, grab samples contain muddy material just a few centimetres below the seafloor.

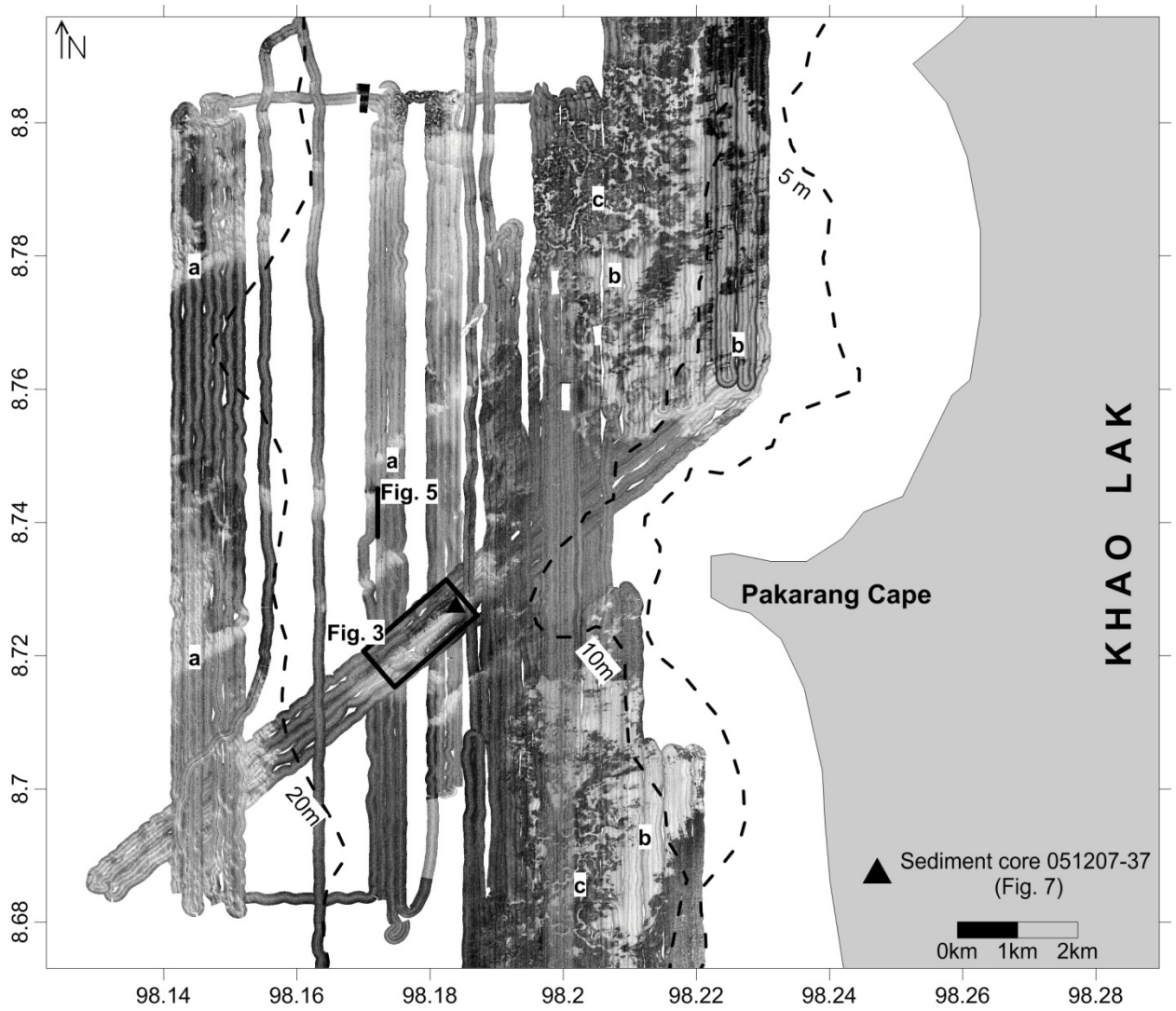


Figure 2: Side scan sonar data around Pakarang Cape. Sampling stations and the positions of fig. 3 and fig. 4 are indicated. Sediment core 051207-37 is shown in fig. 7. This article is focusing on SW-NE striking sediment structures visible as lighter-coloured bands in the side-scan sonar image (a). Closer to the coastline, extended areas of fine grained sediment (b) and a small scale channels (c) are visible.

Core 051207-37 (figure 7) is divided in four sedimentary units. Unit 1 (0-8 cm core depth) is mainly composed of brown sand, including some shell fragments. Between 8 and 11 cm, a layer composed of silt, containing no sand, is apparent (unit 2). The lower boundary of unit 2 is sharp, while its upper boundary is not well defined. Between app. 11 to 12 cm core depth, unit 3A is composed of well sorted sand. Below, unit 3B (12 to 20 cm core depth) contains higher amounts of clay and silt. Various shell fragments are abundant in unit 3B. From 20 cm to the base of the core, unit 4 is composed of sandy silt, and includes some shell fragments. Partly, layers containing higher amounts of sediments in the sand fraction are recognized in the x-ray images.

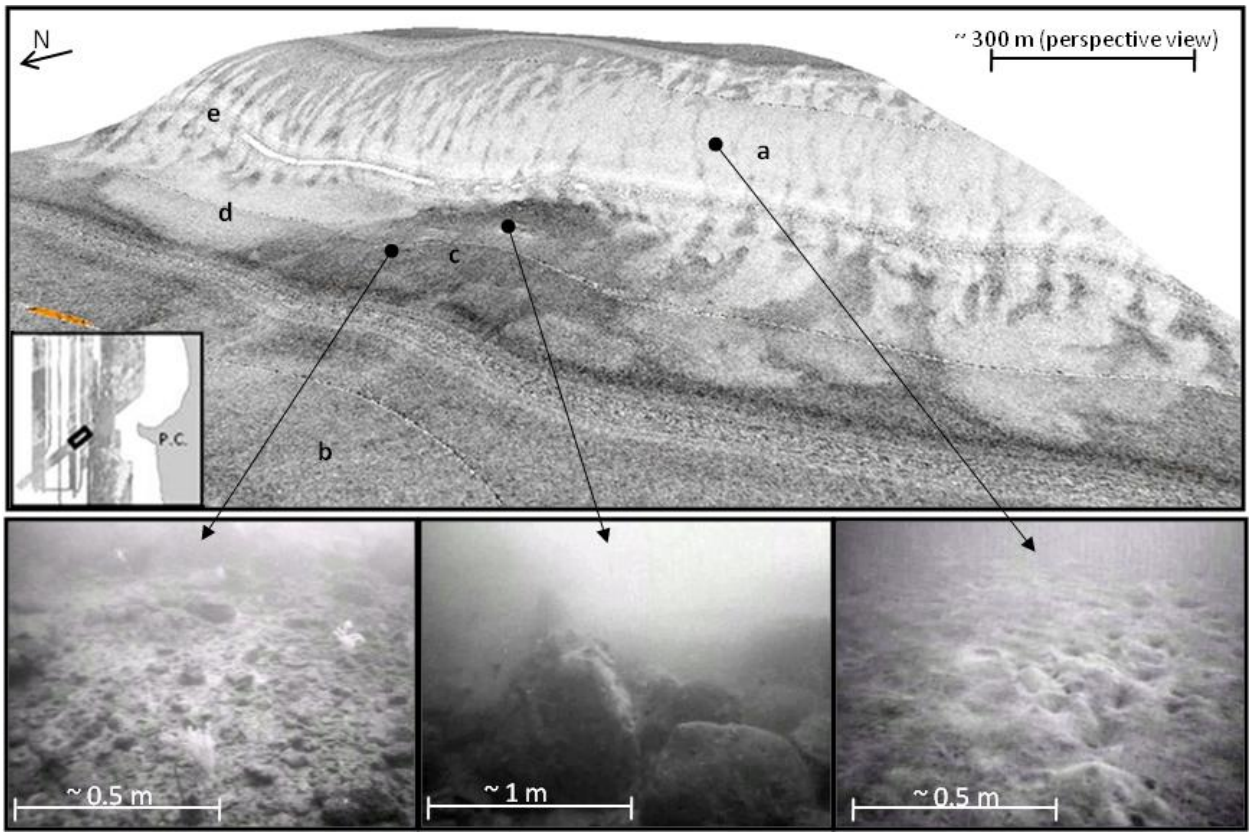


Figure 3: Side scan sonar draped over the bathymetric dataset. For position see figure 2. The length of the ridge is approx. 1500 m (perspective view). a) elongated sediment patches, consisting of fine to medium sand b) coarse sand c) carbonatic gravel and boulders (notice video image) d) sand at the surface, muddy material below e) position of short core (051207-37, fig. 7), composed of sandy material on top and a fine grained layer at 10 cm depth.

5 Discussion

Sand ridges are formed due to regular hydrodynamic processes, e.g. tidal currents in inlets, ocean currents at the shelf margin or during storms (Ernstsen et al. 2006, Flemming 1978, Holland & Elmore 2008), although moribund ridges as remnants from times with a lower sea level are known (Dyer & Huntley 1999). Goff et al. (1999) report that sand ridges on the northeast US Atlantic shelf are asymmetric, having steeper seaward flanks. Holland & Elmore (2008) report that grain sizes across sand ridges typically range from coarse to fine sand. The typical height of storm generated sand ridges is given with 3 to 12 m (van de Meene & van Rijn 2000). Commonly, sand ridges are oblique to the coastline, with the acute angle opening into the prevailing flow direction (Swift et al. 1978, Holland & Elmoore 2008). Most of these features are found in the observed ridge system. The strike direction of the ridges indicates an approximately south-north directed current which was responsible for their formation. This was not the main current direction observed during the tsunami (images of the IKONOS satellite, Goto et al. 2007). Therefore, the ridge system existed prior to the tsunami, although the definite process responsible for its formation has not yet been identified.

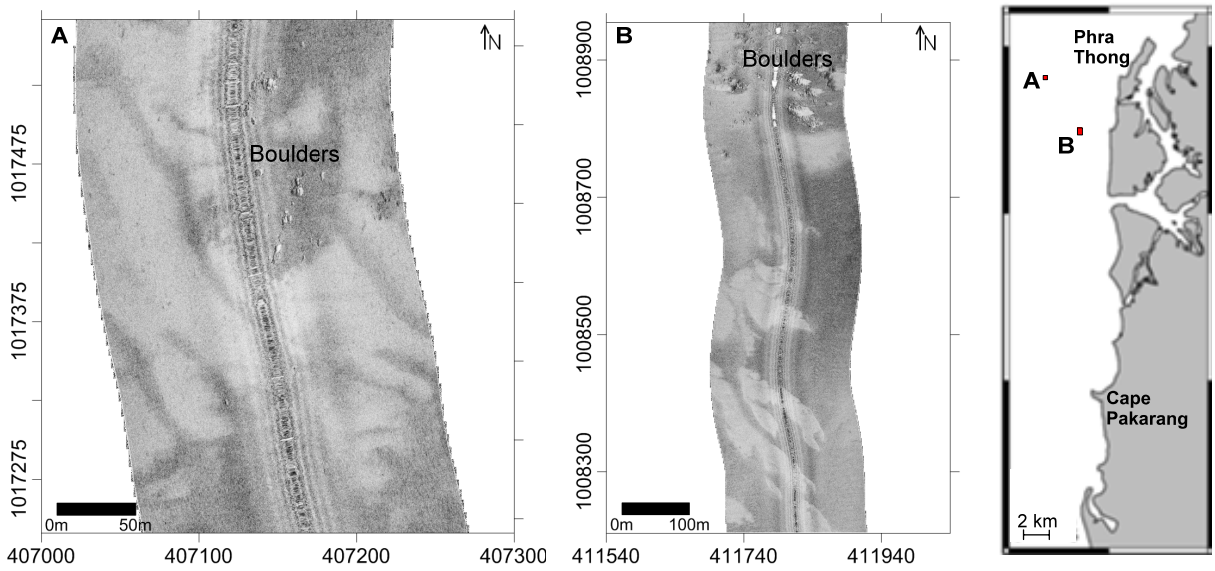


Figure 4: Elongated sedimentary structures offshore Phra Thong. Frequently, boulders are exposed in close vicinity to these structures. Water depth at A: 27 m. Water depth at B: 21 m.

Notable are elongated sediment patches commonly found on the northern flanks of the sand ridges. While finer sediment on the steeper slope of asymmetrical sand ridges is common, in front of storm dominated coasts (Holland & Elmore 2008). Here fine sediments are not visible over the entire length of the flank, but instead they are deposited in small patches separated by coarser sediment. Similar bedforms on the continental shelf offshore Brazil have been formed due to storm events (Moscon & Bastos 2010). The comparison of side scan sonar images from 2007 and 2008 (figure 6) indicates that the general shape of the patches is preserved, but smaller parts begin to fade during one annual cycle, indicating an out-of-equilibrium event based deposition and ongoing reworking of the sediment. Additionally, the existence of identical sediment structures on the flat seafloor further indicates that their formation is not connected with the formation of the sand ridges. Therefore these elongated patches of fine grained sediment have to be interpreted as bedforms created by currents along the north-east/south-west direction. The general stability of these bedforms, combined with the slow fading of delicate structures suggests that no frequently occurring event is responsible for their formation. Since strong storms are rare in the area, and none occurred between the 2004 tsunami and our measurements (based on tracks published by the Regional Specialised Meteorological Centre – Tropical Cyclones (RMSC), New Delhi), it is reasonable to assume that the observed sediment pattern was influenced by the 2004 tsunami, either during the run-up or the backwash.

It is assumed that the muddy material frequently found in grab samples at the base of the sand ridge corresponds to unit 2 in core 051207-37. Therefore, such material is present over a larger area at the base of the sand ridge, and not only locally in one core. Considering the silt separating two units of coarse sand, its deposition likely corresponds to a single event. Similar deposits in cores offshore the Eel River have been described by Crocket & Nittrouer (2004) as flood deposits, which could be generated in the research area by strong monsoon events. But also a tsunami backwash transports large amounts of fine-grained material offshore (Shi & Smith 2003). The process responsible for the formation cannot be determined with certainty. However, a deposition of this material during the monsoon is unlikely, as more regularly occurring structures would be expected. Regardless of the origin of their formation, these event deposits were preserved in the comparably sheltered environments at the base of the sand ridges. They are covered by coarse sand (unit 1), typical for this area of the shelf, indicating some sediment dynamics in the area. This agrees to the change of sedimentological boundaries observed in side scan sonar mosaics between 2007 and 2008 (figure 6). A

potential deposition of the sediments beneath unit 2 during an event, indicated for instance by the marked change in sand content of unit 3A compared to unit 3B, or the abundance of shell fragments in unit 3B, is uncertain. Further analysis is needed to identify the origin and the spatial extension of these potential tsunami deposits, especially closer towards the shoreline.

Interesting are frequent observations of boulders close to the elongated patches deposited at the seaward flank of the sand ridges. Many of these boulders show no connection to structures in the subsurface, and must have been transported to their current position. Potentially, this could have happened during the tsunami, either during the run-up from source areas in deeper waters, or during the backwash (compare Paris et al. 2009)

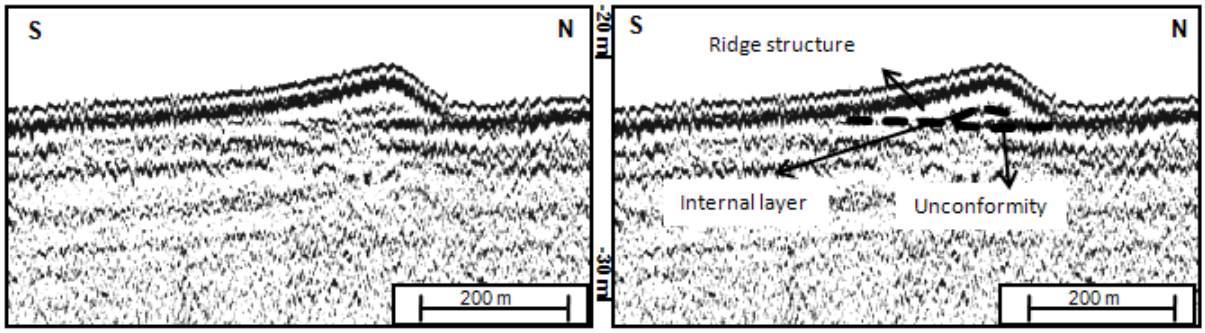


Figure 5: Seismic profile crossing a sand ridge (for position see Figure 2). Clearly visible is the asymmetric form of the ridge which is indicating a transport direction from South to North. Additionally, the ridge is separated from the older surface below by an unconformity.

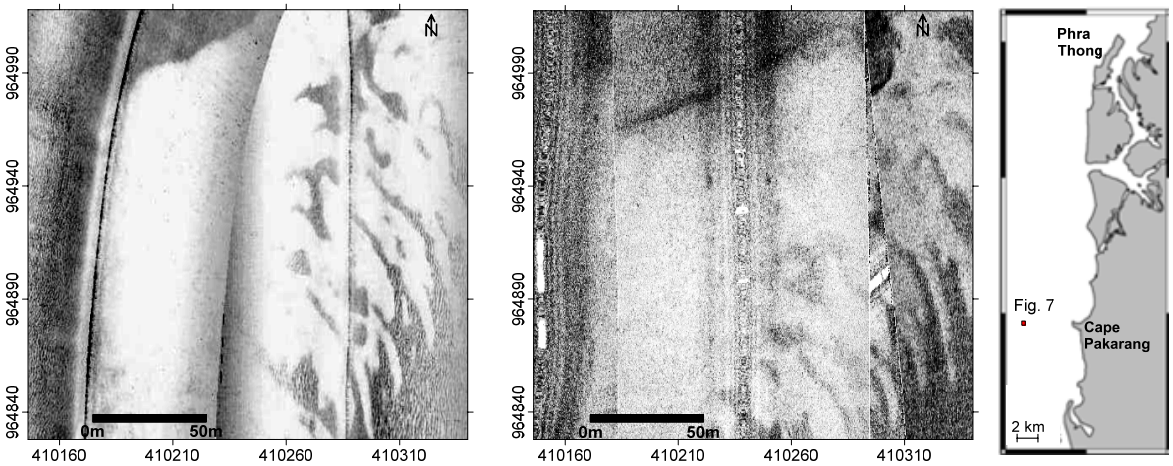


Figure 6: Two side-scan sonar images showing a comparison of a detail of the sand ridge shown in figure 3. The left image was recorded in 2007, the right image in 2008. Small differences are visible. The contours of the elongated sedimentary structures are more pronounced in 2007.

During the tsunami run-up, many boulders were transported towards the intertidal area on Pakarang Cape (Goto et al. 2007). The backwash at Pakarang Cape was modelled by Goto et al. (2007). The authors show that the current speed of the backwash was in the order of 3m/s. This is strong enough to move the observed boulders (Goto et al. 2007, Imamura et al. 2008), which have a diameter of less than 1 meter according to underwater images. Taking into account a channelized backwash (Le Roux & Vargas 2005, Fagherazzi & Du 2007), it is possible that in some areas the current speed was strong enough to transport boulders downslope from the reef platform fringing Pakarang Cape back towards

the sea. However, this cannot explain the presence of boulders found several kilometers offshore (Fig. 4).

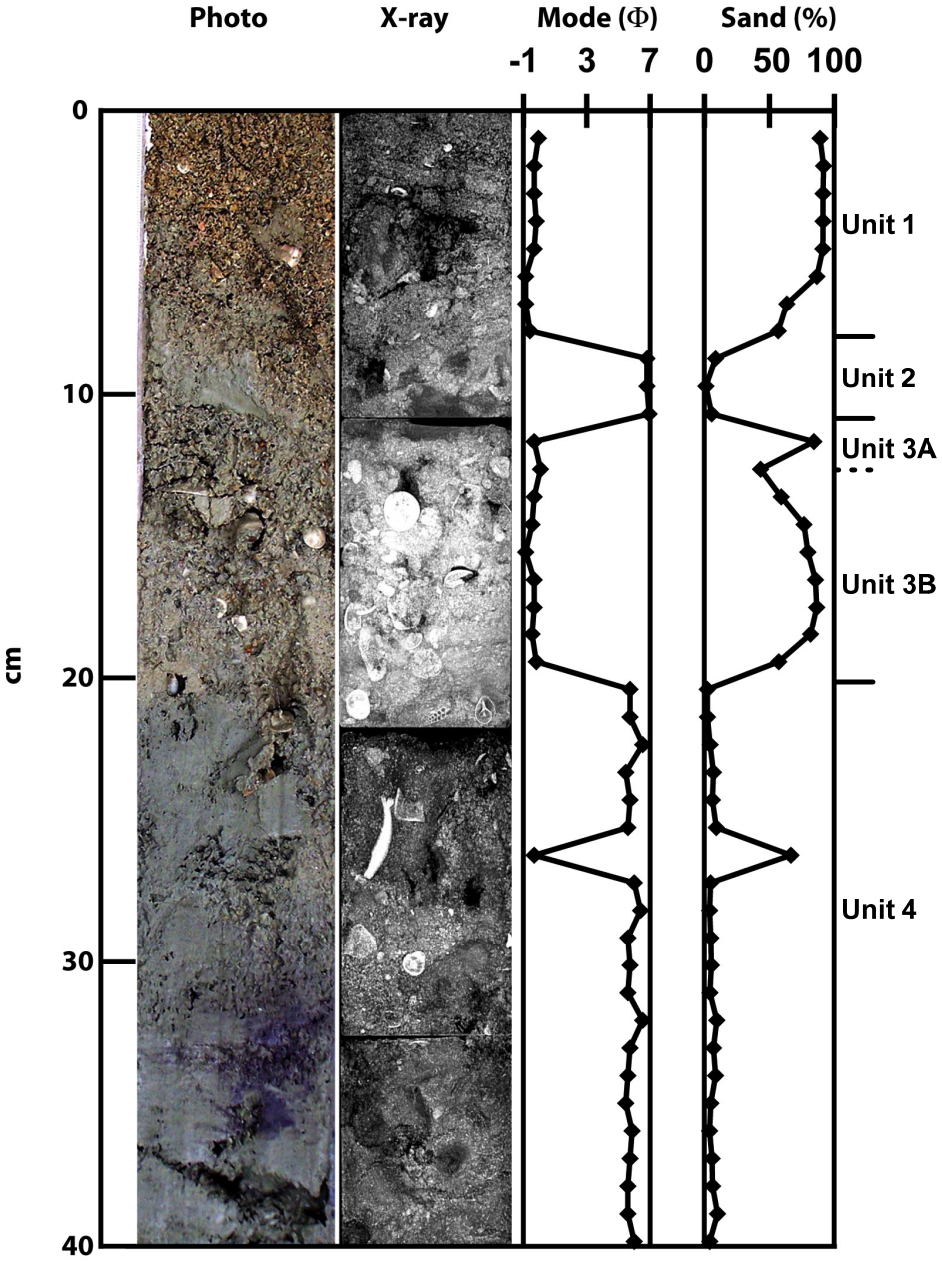


Figure 7: Properties of core 051207-37. From left to right, photo, x-ray image, first mode in phi-degrees, sand content and sedimentary units are presented. For position, refer to Fig.2.

6 Conclusion

Detailed hydroacoustic surveys have been carried out offshore Phang Nga province (Thailand) in 2007 and 2008 and sediment samples have been collected. Starting at 15 m water depth, a system of sand ridges, formed by coarse sand, was discovered. The sand ridges existed prior to the 2004 Indian Ocean Tsunami. Elongated sediment patches on the seaward flank of the sand ridges consist of fine to medium sand, and indicate a current oblique to the coastline. They fade slowly during the annual cycle, and were potentially reworked during the 2004 Indian Ocean Tsunami. An event layer found at the base of a sand ridge is composed of silty sediment, which could be related to the tsunami backwash or floods during the monsoon. These event deposits are covered by coarse sand, and might enter the geological record.

References

Abrantes, F., U. Alt-Epping, S. Lebreiro, A. Voelker & R. Schneider (2008): Sedimentological record of tsunamis on shallow-shelf areas: The case of the 1969 AD and 1755 AD tsunamis on the Portugese Shelf off Lisbon. In: Marine Geology 249: 283–293.

Bell, R., H. Cowan, E. Dalziell, N. Evans, M. O`Leary, B. Rush & L. Yule (2005): Survey of impacts on the Andaman Coast, Southern Thailand following the great Sumatra-Andaman earthquake and tsunami of December 26, 2004. In: Bull. of The New Zealand Soc. For Earthquake Eng. 38 (3), 123–148.

Crockett, J.S. & C.A. Nittrouer (2004): The sandy inner shelf as a repository for muddy sediment: an example from Northern California. In: Continental Shelf Research 24: 55–73.

Dawson, A.G. & I. Stewart (2007): Tsunami deposits in the geological record. In: Sedimentary Geology 200: 166–183.

Dyer, K.R. & D.A. Huntley (1999): The origin, classification and modelling of sand banks and ridges. In: Continental Shelf Research 19 (10), 1285–1330.

Ernstsen, V.B., R. Noormets, C. Winter, D. Hebbeln, A. Bartholomä, B.W. Flemming & J. Bartholdy (2006): Qunatification of dune dynamics during a tidle cycle in an inlet channel of the Danish Wadden Sea. In: Geo-Mar Lett 26 (3): 151–163.

Fagherazzi, S. & X. Du (2007): Tsunamigenic incisions produced by the December 2004 earthquake along the coasts of Thailand, Indonesia and Sri Lanka. In: Geomorphology 99: 120–129.

Feldens, P., K. Schwarzer, W. Sczcuciński, K. Stattegger, D. Sakuna & P. Sompongchaiykul (2009): Impact of 2004 Tsunami on seafloor morphology and offshore sediments, Pakarang Cape, Thailand. In: Polish J. of Environ. Stud. 18: 63–68.

Flemming, B.W. (1978): Underwater sand dunes along the southeast African continental margin – observations and implications. In: Mar. Geol. 26: 177–198

Geronimo, I.D., M. Choowong, S. Phantuwongraj (2009): Geomorphology and superficial bottom sediments of Khao Lak coastal area (SW Thailand). In: Polish J. of Environ. Stud. 18(1): 111–121.

Holland, K.T. & P.A. Elmore (2008): A review of heterogenous sediments in coastal environments. In: Earth-Science Reviews 89: 116–134.

Goff, J.A., D.J.P. Swift, C.S. Duncan, L.A. Mayer & J. Hughes-Clarke (1999): High-resolution swath sonar investigation of sand ridge, dune and ribbon morphology in the offshore environment of the New Jersey margin. In: Marine Geology 161: 307–337.

Goto, K. S.A. Chavanich, F. Imamura, P. Kunthasap, T. Matsui, K. Minoura, D. Sugawara & H. Yanagisawa (2007): Distribution, origin and transport process of boulders deposited by the 2004 Indian Ocean tsunami at Pakarang Cape, In: Thailand. Sed. Geol. 202: 821–837.

Imamura, F., K. Goto & S. Ohkubo (2008): A numerical model for the transport of a boulder by tsunami. In: Journal of Geophysical Research 113, C01008, doi:10.1029/2007JC004170.

Jackson, P.D., K.B. Briggs & R.C. Flint (1996): Evaluation of sediment heterogeneity using microresistivity imaging and X-radiography. In: Geo-Marine Latters 16: 219–225.

Jankaew, K., B.F. Atwater, Y. Sawai, M. Choowong, T. Charoentitirat, M.E. Martin & A. Prendergast (2008): Medieval forewarning of the 2004 Indian Ocean tsunami in Thailand. In: Nature 455: 1228–1231.

Kelletat, D., S.R. Scheffers & A. Scheffers (2007): Field signatures of the SE-Asian Mega-Tsunami along the West Coast of Thailand compared to Holocene Paleo-Tsunami from the Atlantic Region. In: Pure appl. Geophys. 164: 413–431.

Khokiattiwong, S., P. Limpsaichol, S. Petpiroon, P. Sojisuporn & B. Kjerfve (1991): Oceanographic variations in Phangnga Bay, Thailand under monsoonal effects. In: Phuket Marine Biological Center Research Bulletin, 55: 43–76.

Kumar, V.S, V. Ramesh Babu, M.T. Babu, G. Dhinakaran & G.V. Rajamanickam (2008): Assessment of Storm Surge Disaster Potential for the Andaman Islands. In: Journal of Coastal Research 24(2):171–177.

Lay, T., H. Kanamori, J.C. Ammon & M. Nettles (2005): The great Sumatra-Andaman earthquake of 26 December 2004. In: Science 306: 1127–1133.

Le Roux, J.P. & G. Vargas (2005): Hydraulic behaviour of tsunami backflows: insights from their modern and ancient deposits. In: Environ. Geol 49: 65–75.

Lurton, X. (2002): Underwater Acoustics: An introduction. Springer (Berlin) 347 S.

Moscon, D.M.C. & A.C. Bastos (2010): Occurence of storm-generated bedforms along the inner continental shelf - southeastern Brazil. In: Brazilian Journal of Oceanography 58: 45–56.

Noda A., H. Katayama, T. Sagayama, K. Suga, Y. Uchida, K. Satake, K. Abe & Y. Okamura (2007): Evaluation of tsunami impacts on shallow marine sediments: An example from the tsunami caused by the 2003 Tokachioki earthquake, northern Japan. In: Sed. Geol. 200: 314–327.

Paris, R., J. Fournier, E. Poizot, S. Etienne, J. Morin, F. Lavigne & P. Wassmer (2010): Boulder and fine sediment transport and deposition by the 2004 tsunami in Lhok Nga (western Banda Aceh, Sumatra, Indonesia): A coupled offshore-onshore model. In: Marine Geology 268 (1-4): 43–54

Pälike, H., N.J. Shackleton & U. Röhl (2001): Astronomical forcing in Late Eocene marine sediments. In: Earth Planet. Sci. Lett. 193: 589–602.

Shi, S. & D.E. Smith (2003): Coastal tsunami geomorphological impacts and sedimentation processes: Case studies of modern and prehistorical events. International Conference on Estuaries and Coasts. November 9-11, 2003, Hangzhou, China

Siripong, A. (2006): Andaman Seacoast of Thailand Field Survey after the December 2004 Indian Ocean Tsunami. In: Earthquake Spectra 22 (S3): 187–202.

Swift, D.J.P., G. Parker, N.W. Lanfredi, G. Perillo & K. Figge (1978): Shoreface-connected Sand Ridges on American and European Shelves: A Comparison. In: Estuarine and Coastal Marine Science 7: 257–271.

Synolakis, C.E. & L. Kong (2006): Runup measurements of the December 2004 Indian Ocean Tsuanmi. In: Earthquake Spectra 22 (S3): 67–91.

Thampanya, U., J.E. Vermaat, S. Sinsakul & N. Panapitukkul (2006): Coastal erosion and mangrove progradation of Southern Thailand. In: Estuar., Coast. Shelf Sci. 68: 75–85.

Tsuji, Y., Y. Namegaya, H. Matsumoto, S.I. Iwasaki, W. Kanbua, M. Sriwichai & V. Meesuk (2006): The 2004 Indian tsunami in Thailand. Surveyed runup heights and tide gauge records. In: Earth Planets Space 58: 223–232.

Van Den Bergh G.D., W. Boer, H. De Haas, TJ.C.E. Van Weering & R. Van Wijhe (2003): Shallow marine tsunami deposits in Teluk Banten (NW Java, Indonesia), generated by the 1883 Krakatau eruption. In: Marine Geology 197: 13–34.

Van de Meene, J.W.H. & L.C. van Rijn (2000): The shoreface-connected ridges along the central Dutch coast – part 1: field observations. In: Continental Shelf Research 20: 2295–2323.

Weiss, R. & H. Bahlburg (2006): The Coast of Kenya Field Survey after the December 2004 Indian Ocean Tsunami. In: Earthquake Spectra 22 (S3): 235–240.

Acknowledgement

We are grateful to NRCT (National Research Council Thailand) and PMBC (Phuket Marine Biological Center) for providing us with the research vessels CHAKRATONG TONGAI and BOONLERT SOOK. We thank masters and crew of both vessels for their outstanding support during the cruise. The German part of this study was supported by DFG through research grant SCHW/11-1. Many thanks go to Witold Sczcuciński and Karl Stattegger for good discussions.

Address

Peter Feldens
University of Kiel - Institute of Geosciences
Otto-Hahn Platz 1
24418 Kiel, Germany

pfeldens@gpi.uni-kiel.de

Nat. Hazards Earth Syst. Sci., 12, 1441–1451, 2012
www.nat-hazards-earth-syst-sci.net/12/1441/2012/
doi:10.5194/nhess-12-1441-2012
© Author(s) 2012. CC Attribution 3.0 License.



Natural Hazards and Earth System Sciences

Using Polycyclic Aromatic Hydrocarbons (PAHs) as a chemical proxy to indicate Tsunami 2004 backwash in Khao Lak coastal area, Thailand

D. Tipmanee[1,2], W. Deelaman[3], S. Pongpiachan[4], K. Schwarzer[5], and P. Sompongchaiyakul[6]

[1]International Postgraduate Program in Environmental Management, Graduate School, Chulalongkorn University, Bangkok, Thailand
[2]Center of Excellence for Environmental and Hazardous Waste Management (EHWM), Chulalongkorn University, Bangkok, Thailand
[3]Environmental Research and Training Center, Department of Environmental Quality Promotion, Ministry of Natural Resources and Environment, Pathumthani, Thailand
[4]The Graduate School of Social and Environmental Development, National Institute of Development Administration, Bangkapi, Bangkok, Thailand
[5]Institute of Geosciences, Coastal and Shelf Research, Kiel University, Otto-Hahn-Platz 1, 24118 Kiel, Germany
[6]Department of Marine Science, Faculty of Science, Chulalongkorn University, Bangkok, Thailand

Correspondence to: P. Sompongchaiyakul (penjai.s@chula.ac.th)

Received: 29 December 2011 – Accepted: 7 February 2012 – Published: 14 May 2012

Abstract. In this study, we attempted to use PAHs as a chemical proxy to trace the transport of land-derived materials caused by the tsunami backwash to better understand how it may have affected the distribution of sedimentary deposition throughout the seabed of Khao Lak coastal areas. By analyzing the compositions of sedimentary PAHs in combination with application of the multivariate descriptive statistical techniques, PAHs were proven to be a promising chemical proxy to indicate the tsunami backwash in the study area. Their spatial distribution could indicate that the tsunami backwash plays an important role in transporting anthropogenic PAHs to the nearby coastal area as far as approximately 25 km from the shoreline. In addition, the results from diagnostic PAH isomer ratios suggested that road paving asphalt, originated from heavy erosion by the tsunami wave in front of Pakarang Cape, was among the identified sources of PAHs. Principle Component Analysis (PCA) results provided 2 estimated land-derived sources of PAHs, which were the road dust and oil burning sources. These estimated signature sources clearly support our hypothesis that PAHs were transported from the potential sources on land and deposited into the near-shore seabed during tsunami backwash.

1 Introduction

On 26 December 2004, the Indian Ocean tsunami attacked the Andaman coastal zones in Thailand, especially in the Phang Nga coastal area. The powerful nature of the 2004 tsunami resulted in extensive erosion and deposition of sediment throughout near-shore portions of the seabed in the Phang Nga coastal zones. The marine and terrestrial environments along the coastal zones were destroyed and caused widespread introduction of contaminated materials to the sea (Feldens et al., 2009; Tang et al., 2006; UNEP, 2005; Zhang et al., 2009). Therefore, in the area which was heavily affected by the withdrawal of the tsunami wave should contain more terrigenous sediments and thus relatively high proportions of anthropogenic derived sediment-associated contaminants.

A number of approaches have been used to distinguish between marine and terrigenous components in marine sediments, including polycyclic aromatic hydrocarbons (PAHs), hopanes and cholestanes (Mostafa et al., 2009; Takada et al., 1991; Tolosa et al., 2004; Yunker et al., 1995, 2002). However, PAHs are amongst the most promising sediment-associated contaminants that can indicate the sedimentary deposition which was affected by tsunami backwash. This is due to the fact that they are known to enter aquatic environments through petroleum spills, coal and fossil fuels combustion, automobile exhausts, biomass burning and from non-point sources such as street runoff and atmospheric

fall-out (Ahrens and Depree, 2010; Jiang et al., 2009; Tolosa et al., 2009).

For decades, PAHs have been used as a "chemical proxy" to distinguish the anthropogenic source and biogenic source in marine sediment (Cantwell et al., 2007; Christensen et al., 1996; Fang et al., 2009; Tobiszewski and Namieśnik, 2012). They can be categorized as anthropogenic combustion sources (i.e. oil spill, automobile exhaust, and street runoff) and as natural combustion sources (i.e. forest fires, volcano eruption) by using PAHs diagnostic ratios (Yunker et al., 2002, 2011; Yunker and Macdonald, 2003). PAHs of molecular mass 178, 202 and 258 are commonly used to distinguish between pyrogenic (combustion-derived) and petrogenic (unburned petroleum-derived) sources. In addition, Phenanthrene/Anthracene (*m/z* 178), Fluorantene/Pyrene (*m/z* 202) and Benz[a]Anthracene/Chrysene (*m/z* 258) have been previously used by some works (Khairy et al., 2009; Liu et al., 2009; Wang et al., 2006). Because of their usefulness in source identification, the use of PAHs as a chemical proxy may provide better understanding of huge terrigenous sediments caused by the rare events such as the withdrawal of tsunami waves.

Like many newly developed coastal tourist places, intensive economic-related activities, including the steadily increasing number of houses, hotels, restaurants, rapid urbanization along the coast, are major contributions for the significant accumulation of anthropogenic PAHs to the marine environment in the Khao Lak coastal area. Motor vehicle emissions, leakage of used oil, vehicle tire and asphalt road surfaces are typically diffuse sources of the anthropogenic PAHs in the coastal areas (Brown and Peake 2006; Kose et al., 2008).

During the tsunami backwash, severe damages occurred, including coastal shoreline erosion and destructive infrastructures such as buildings, road networks, bridges, fishing vessels, as well as the near-shore environment. As a consequence, the anthropogenic PAHs were believed to be transported from the potential sources on land and deposited into the near-shore seabed. Moreover, their spatial distribution should provide the extinctive patterns (concentration profile from shoreline to off-shore, compositions and concentrations of transporting PAHs) different from the normal transporting mechanisms such as those associated with the annual reversals of monsoons and hydro-meteorological extreme events or high precipitation in rainy season.

In this study, we attempt to use PAHs spatial distribution to trace the transport and fate of land-derived materials caused by the tsunami backwash to better understand how it may have affected the distribution of sedimentary deposition throughout the seabed in the Khao Lak coastal areas. In addition, the composition of the sedimentary PAHs of the Khao Lak coastal areas was analyzed using PAH diagnostic ratios in combination with the multivariate descriptive statistical techniques to distinguish among different sources of PAHs.

2 Materials and methods

2.1 Study area and sampling methods

Located on the east of the Andaman Sea, the near-shore of Kho Lak coastal zone, Phang Nga Province, Thailand was chosen as a study area, because it has heavily affected by the tsunami, which inundated the coastal plain from a few hundred meters up to more than one kilometer inland. The tsunami runup height at the maximum inundation limit varied from <3 m on Kho Khao Island to almost 10 m at the Nham Kem and the Pakarang Cape (Szczuciñski, 2011). The tsunami wave height reached over 15 m at the Nham Kem (Tsuji et al., 2006) and the Pakarang Cape (Siripong, 2006). The sediment samples were collected in the study area covering approximately 750 km^2 (east-west extension: 25 km, north-south extension: 30 km).

The sampling stations were selected on the basis of the data acquired from hydroacoustic mapping using equipment, which consisted of Multibeam, Side Scan Sonar and a Boomer system to investigate the sedimentary deposition on the near-shore seabed (Feldens, et al., 2009). Surface sediment samples were collected along the Khao Lak coastal area in order to analyze the distribution of 13 individual PAHs. The sampling stations are shown in Fig. 1.

The Van Veen Grab Sampler was used to collect the 70 surface sediment samples during 1–8 December 2007. Sediment samples were wrapped in clean aluminum foil, placed in a glass bottle, and kept frozen at −20°C. They were freeze-dried prior to being grounded and sieved to homogenize the samples, and then kept in the refrigerator at −4°C until analysis.

2.2 PAHs analysis

All solvents were HPLC grade, purchased from Fisher Scientific. A mix standard solution of 15 native PAHs [Norwegian Standard (NS 9815: S-4008-100-T): phenanthrene (Abbreviation : Phe), anthracene (An), fluoranthene (Fluo), pyrene (Pyr), 11 H-benzo[a]fluorene (11H-B[a]F), 11 H-benzo[b]fluorene (11H-B[b]F), benz[a]anthracene (B[a]A), chrysene (Chry), benzo[b]fluoranthene (B[b]F), benzo[k]fluoranthene (B[k]F), benzo[a]pyrene (B[a]P), benzo[e]pyrene (B[e]P), indeno[1,2,3-cd]pyrene (Ind), dibenz[a,h]anthracene (D[a,h]A), and benzo[g,h,i]perylene (B[g,h,i]P)] and a mix of recovery internal standard (IS) PAHs [d_{12}-perylene (d_{12}-Per) and d_{10}-fluorene (d_{10}-Fl)] were purchased from Chiron AS (Stiklestadveine 1, N-7041 Trondheim, Norway). Standard stock solutions of deuterated and native PAHs were prepared in nonane. Working solutions were obtained by appropriate dilution in cyclohexane.

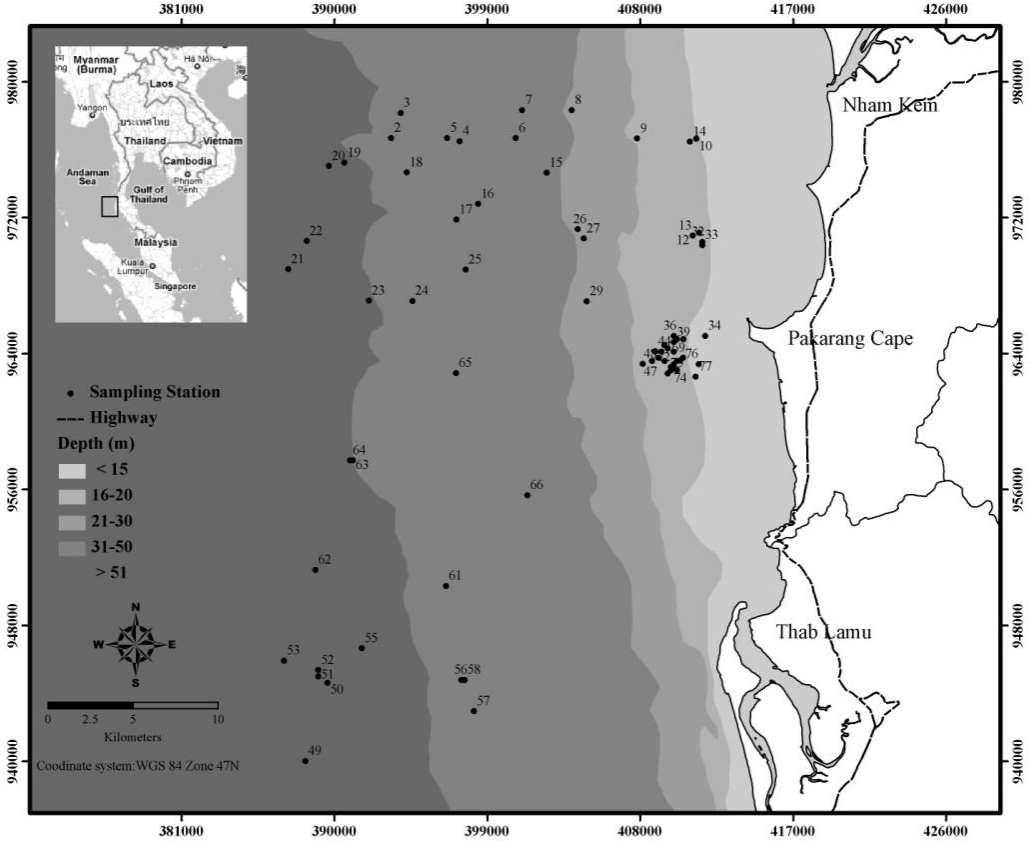


Fig. 1. Sampling site locations at Khao Lak coastal areas, Phang Nga Province, Thailand. (The study area is indicated by the black box; numbers indicate sampling stations; the color contours represent the water depth).

Approximately 5 grams of dried sediment were extracted by a Soxhlet extractor for 8 h, using dichloromethane as a solvent. Before the extraction, dried sediments were spiked with a known amount of d_{10}-Fl and d_{12}-Per as internal standards. Fractionation/clean-up process was carried out following the method of Gogou et al. (1997). The extractant was passed through a silica gel column using 4:6 (v/v) toluene:hexane as an eluant. The eluate was then purged with nitrogen to almost dryness. The solvent was then changed to cyclohexane and purged with nitrogen again until the final volume was 100 μl.

The aliquot solution was further quantified by using a Varian Saturn 2200 Gas Chromatography/Mass Spectrometric detector–Ion–Trap (GC/MS–Ion-Trap) in the selective ion monitoring mode. The targeted compounds were separated on an Agilent JW Scientific CP-5865 GC column (60 m × 0.32 mm i.d. capillary column, 1.00 μm thick film). All injections (1 μL) were performed through an injector in the splitless mode. The GC oven temperature was programmed as follows: 1 min at 40 °C, heated at 8 °C min^{-1} to 300 °C, and held constant for 45 min. Accuracy was evaluated using the standard SRM 1941b. Mean recovery (based on extraction of matrix-matched certified reference materials, ($n = 8$) was in range of 77–119 %. The precision of the procedure, calculated as relative standard deviation on the duplicate samples, was less than 15 %. All sample concentrations were calculated using standardized relative response factors run with each batch.

2.3 Statistical analysis

Before performing statistical analysis, data were subjected to the logarithmic transformation ($y = \log(x + 1)$). This technique is the most common approach for transforming environmental data, as it is robust to non-normal data distribution (Field et al., 1982). The significance level, Kaiser-Meyer-Olkin (KMO) and Bartlett's test of sphericity were performed to test the adaptability of Principal Component Analysis (PCA) (Wang et al., 2010). Data prepared for multivariate statistical analysis were arranged in the matrix, where columns correspond to PAH compositions and rows represent sampling stations. The normalized data matrix was then analyzed by PCA and Hierarchical Cluster Analysis (HCA).

PCA as a multivariate analytical tool was used to reduce the set of original observed variables (PAH compositions

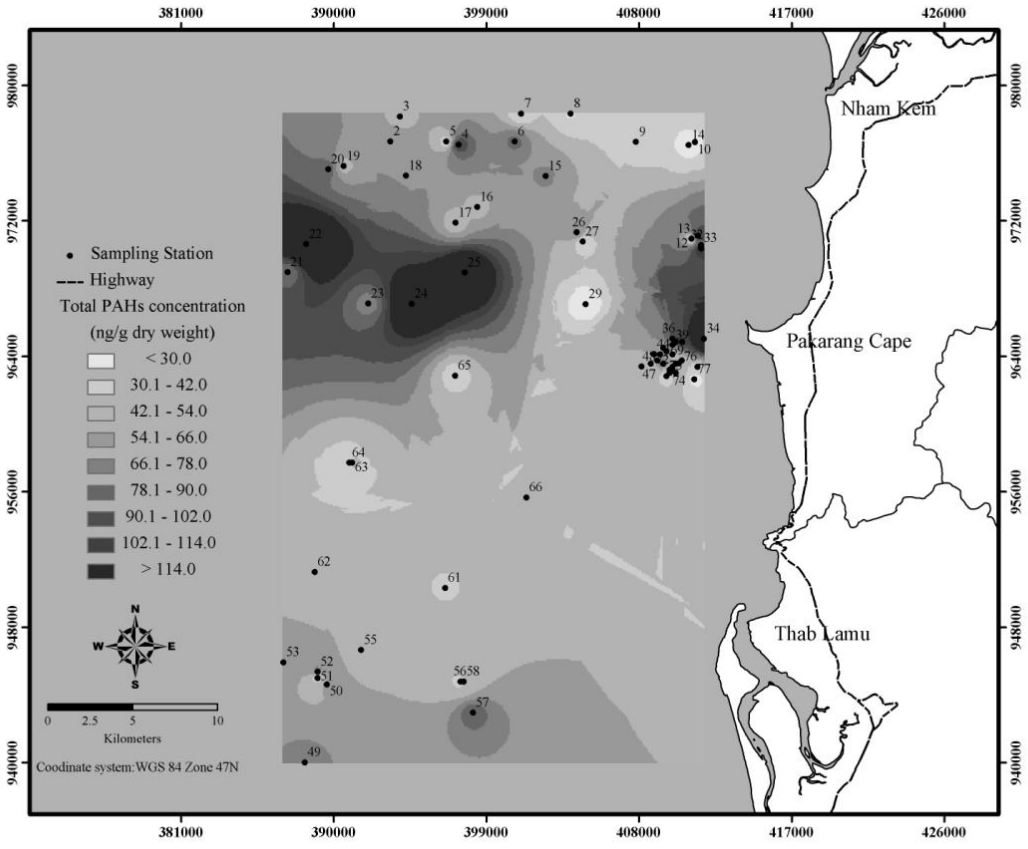


Fig. 2. The spatial distribution of sedimentary PAHs in the Khao Lak coastal area. (Numbers indicate sampling stations; the contour scale represents total PAHs concentrations as labeled in the legend).

Table 1. Comparisons of $\sum$PAHs in surface sediment collected from different coastal areas and bays (ng g^{-1} dry weight).

Location	Range	Mean	Reference
Phang Nga Coast	12.6–272.0	64.5	This study
Gulf of Thailand			Wattayakorn, 2005
Coastal areas	11–1992	506	
Offshore areas			
Upper Gulf	39–95	70	
Eastern Seaboard	11–324	79	
Lower Gulf	14–67	51	
Dalian Bay, China	32.7–3558	152.08	Liu et al., 2001
Daya Bay, China	42.5–158.2	126.2	Yan et al., 2009
Kyeonggi Bay, Korea	9.1–1400	120	Kim et al., 1999
Malaysian riverine and coast	4–924	139.5	Zakaria et al., 2002
Casco Bay, USA	16–20,748	2900	Kennicutt et al., 1999
Northwestern Black Sea	52.6–269	136	Maldonado et al., 1999
Todos Santos Bay, Mexico	7.6–813	96	Macías–Zamora et al., 2000
Gulf of Aden, Yemen	2.2–604	82.4	Mostafa et al., 2009

Table 2. Characteristic values of selected diagnostic ratios for petroleum and single-source combustion (Modified from Yunker et al., 2002).

Source	An/ (An+Phe)	Flou/ (Flou + Pyr)	B [a]A/ (B[a]A + Chry)	Ind/ (Ind + B[g,h,i]P)
Petroleum				
Lubicating oil	–	0.29	0.10	0.12
Asphalt	–	–	0.50	0.52–0.54
Combustion				
Gasoline ($n = 2$)	0.11	0.44	0.33–0.38	0.09–0.22
Road dust	0.18	0.42	0.13	0.51
Used engine oil, gasoline passenger car	0.22	0.30	0.50	0.18
Used engine oil, diesel car, truck and bus	–	0.37	–	0.29

in sediment samples) and to extract a small number of the dominant principal components to explain the relationships among the observed variables (Larsen and Baker, 2003). To obtain more clear features, the Varimax rotation method with Kaiser normalization was used. In addition, HCA was used to group the stations by relative contents of PAH compounds in sediment samples. Distances of similarity between objects were measured as squared Euclidean distances (Fang et al., 2007). Ward's method was used for amalgamation of clusters (Savinov et al., 2000).

3 Results and discussion

3.1 PAHs contamination in Khao Lak coastal area

On the basis of sediment analysis, the total concentration of PAHs ($\sum$PAHs) is defined as the sum of Phe, An, Fluo, Pyr, B[a]A, Chry, B[b]F, B[k]F, B[e]P, B[a]P, Ind, D[a,h]A, and B[g,h,i]P. $\sum$PAHs in the Khao Lak area, which was heavily destroyed by the tsunami runup, were in range of 12.6 to 272.0 ng g^{-1} dry weight, with an average of 64.5 $\pm$ 44.3 ng g^{-1} dry weight. It should be noted that the PAHs concentrations detected in the Khao Lak coastal sediments are comparable with those contaminations found previously in some coastal areas and bays (Table 1). However, they were much lower than some coastal and harbor hot spots that are highly under an influence of human activities such as Dalian Bay, Casco Bay and Kyeonggi Bay (Table 1).

Figure 2 shows the spatial distributions of sedimentary PAHs in the Khao Lak coastal area. From the figure, the prominent feature of sediments exported from the Pakarang Cape can be observed. This evidence indicates that the tsunami backwash may play an important role in transporting anthropogenic PAHs to the nearby coastal area far from the shoreline up to approximately 25 km. It is also in good agreement with the study of Siripong (2006), who found that the tsunami wave height was over 15 m high at Pakarang Cape. Such a giant wave could have a tremendous impact on transporting massive terrigenous sediments far from the shoreline, as evidenced from the distinct spatial patterns of PAHs concentrations (Fig. 2).

Generally, PAH concentrations should gradually decrease offshore further along the distance far from the point source that has original concentration (Boonyatumanond et al., 2006). But the PAH concentrations from sediments exported from the Pakarang Cape increased further along the distance up to 25 kilometers. These behaviors are triggered by a rare event such as the tsunami backwash not originating from normal transporting mechanisms such as those associated with the annual reversals of monsoon and hydro-meteorological extreme events or high precipitation in rainy season.

3.2 Source identification by diagnostic PAH isomer ratios

The characteristics of PAH patterns in the coastal sediments are subject to different emission sources. Thus, isomer ratios of PAHs have been used to identify PAH sources, ranging from urban to marine environments (Yunker et al., 2002). Pyrogenic and petrogenic are the primary sources of PAHs commonly found in coastal marine sediments (LaFlamme and Hites, 1978).

The four PAH isomer pairs used in the present study were An/(An + Phe) (*m/z* 178), Flou/(Flou + Pyr) (MW 202), B [a]A /(B[a]A + Chry) (*m/z* 228), and Ind/(Ind + B[g,h,i]P) (*m/z* 276). Table 2 shows ranges of the 4 diagnostic PAH ratios for petroleum and single-source combustion.

Cross-plots between ratios B[a]A/(B[a]A+Chry) and Ind/(Ind+B[g,h,i]P) were applied to identify the potential sources of sedimentary PAHs in study area. The results indicated that most of sediment samples originated from the mixed pyrogenic sources as results of the incomplete combustion, pyrolysis of fuel, biomass burning and oil burning.

On the basis of the results shown in Table 2, the B[a]A/(B[a]A+Chry) and Ind/(Ind+B[g,h,i]P) ratios were 0.50 and 0.52–0.54, respectively, indicating the plausible emission source from asphalt pavements. Moreover, Yang et al. (2010) reported that even minimal contamination of sediments with pavement material may lead to a significant input

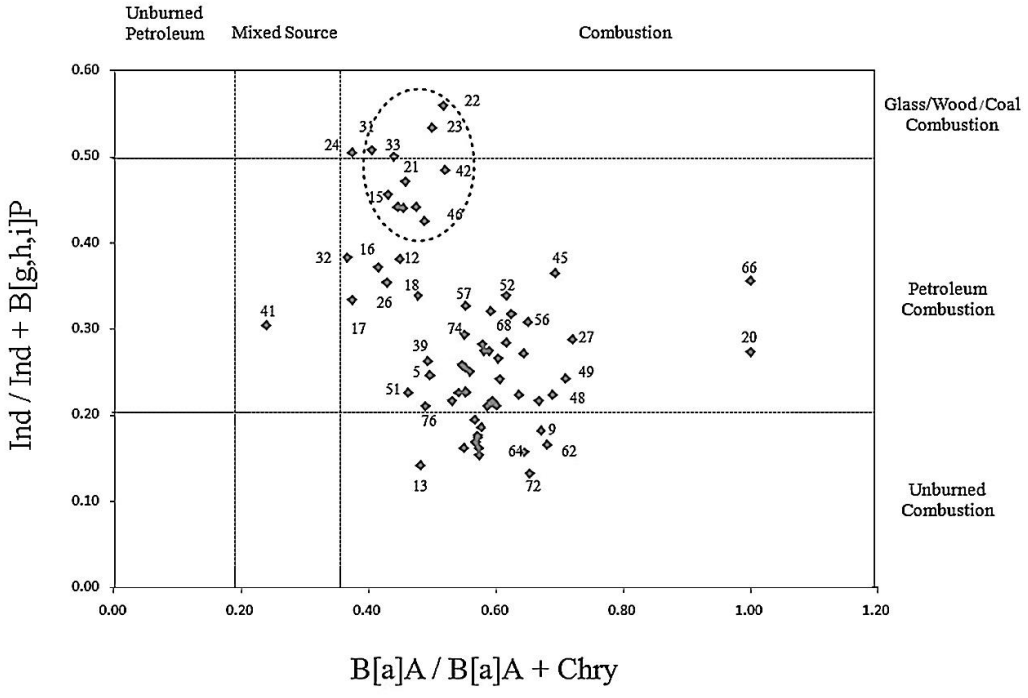


Fig. 3. Cross-plot between ratios Ind/Ind+B[g,h,i]P and B[a]A / B[a]A+Chry (numbers indicate sampling stations; the dashed circle represents the stations in which PAHs were originating from road paving asphalt).

of PAHs to the aquatic environment. This agreed with our results that hot spot stations (22, 25, 31, 33 and 42 in Fig. 2) showed the higher concentration of total PAHs. The signature diagnostic PAHs isomer ratios, which indicated to road paving asphalt were observed in the stations 22, 25, 31, 33 and 42 (The dashed circle in Fig. 3). We believe that the promising PAH sources of these stations originated from the road paving asphalt heavily eroded by the tsunami wave in front of Pakarang Cape.

Pomonis et al. (2005) reported that the damage to the road surface was observed in the areas near the Khao Lak coastline. This damage was probably due to increased pore water pressure under the flexible pavement. This evidence was visible on small areas of road surface adjacent to the beach front and especially on grasscrete surfaces (e.g. at Kamala and Pakarang Cape).

From the results derived from the diagnostic PAH isomer ratios, it meets our attempted goal to use PAHs as a chemical proxy to trace the transport of land-derived materials caused by the tsunami backwash. The diagnostic PAH isomer ratios provide clear evidence that the anthropogenic PAHs were transported from the coastal land and deposited into the nearshore seabed during the tsunami backwash.

Nevertheless, it is important to note that isomer pair ratios of the entire dataset were not restricted to the extreme values of only specific source, because there is a chance to misinterpret when the mixtures of heterogeneous PAH sources are

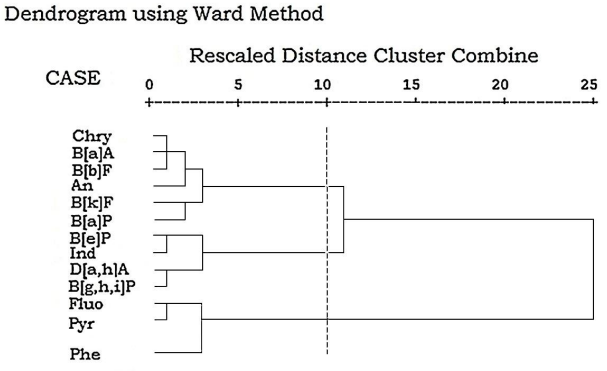


Fig. 4. Hierarchical Cluster Analysis (HCA) of 13 individual PAHs in Khao Lak sediment.

analyzed, especially in the case of the powerful and strongly turbulent tsunami wave that can transport the PAH contaminated materials to the sea floor all at once (Tang et al., 2006).

3.3 Source estimation from HCA

HCA was performed to identify the homogeneous groups of individual PAHs in the Khao Lak sediment. The hierarchical dendogram is shown in Fig. 4. What emerged from these results is that three major groups of the 13 individual PAHs were clearly distinguished. The first group contains B[a]A,

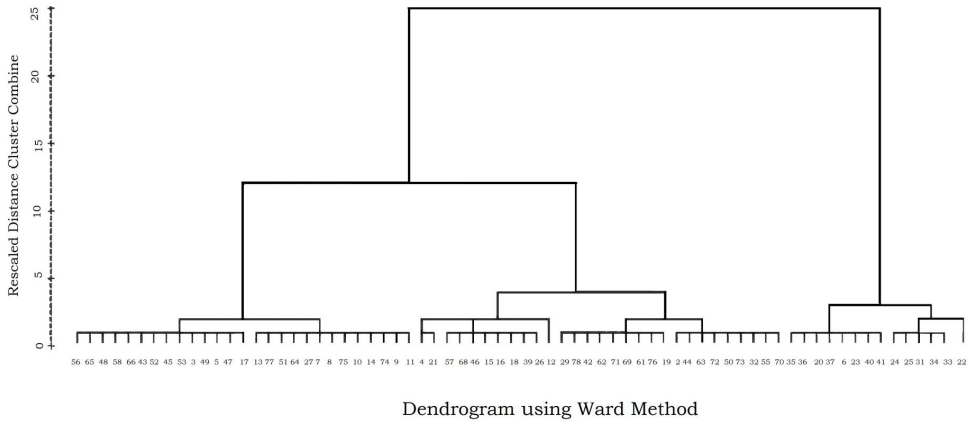


Fig. 5. Hierarchical Cluster Analysis (HCA) of 70 individual sampling stations in Khao Lak sediment.

Chry, B[b]F, B[k]F, B[a]P and An, which originated from the pyrogenic source (Fang et al., 2009; Liu et al., 2009). Motor vehicle emissions both of gasoline and diesel emission, leakage of used oil and road dust have been previously identified as original sources of this group (Dahle et al., 2003). According to the literature reports, the 3–4 ring PAHs have been found in the road dust in urban cities as well (Boonyatumanond et al., 2007; Zakaria et al., 2002).

The second group consists of B[e]P, Ind, D[a,h]A and B[g,h,i]P, which are the high molecular weight PAHs with 5–6 rings. This group usually originated from road paving asphalt, crude oil, bitumen (Ahrens and Depree, 2010) and road dust (Larsen and Baker, 2003). The last group comprises Pyr, Fluo and Phe, which are the anthropogenic PAHs from the using of petroleum products (Zhou et al., 1999).

It is reasonable to say that three of the potential sources which were identified by HCA could be transported from original sources during the tsunami backwash as we expected. Moreover, the results based on the cluster analysis by the 70 individual sampling stations revealed two major groups as shown in Fig. 5.

The first group includes stations 6, 20, 22, 23, 24, 25, 31, 33, 34, 35, 36, 37, 40 and 41. All of these stations have distinct characteristics from other areas, consistent with what is documented in Fig. 2. Thus, this group should be the representative of the tsunami backwash and so results can provide the approximate direction of the tsunami backwash that was transported from the shoreline at Pakarang Cape back to far further than 25 km into the seabed. In contrast, the second group includes the rest of sampling stations. The nearby group which has less linkage distance between homogeneous groups (more similarity), contains stations 2, 32, 44, 50, 55, 63, 70, 72 and 73, and also indicates the influence of the tsunami backwash.

Table 3. Rotated component matrix of 13 PAHs from Khao Lak coastal sediments[a].

PAH composition	Principle components (PC)	
	PC1	**PC 2**
Phe	0.02	0.58
An	0.08	0.53
Fluo	0.12	**0.88**
Pyr	0.04	**0.86**
B[a]A	0.15	0.54
Chry	0.24	0.48
B[b]F	0.47	0.22
B[k]F	**0.75**[b]	0.18
B[e]P	**0.89**	0.19
B[a]P	0.60	0.42
Ind	**0.91**	0.03
D[a,h]A	**0.93**	0.17
B[g,h,i]P	**0.92**	−0.10
Estimated source	**Road dust**	**Oil burning**
Variance (%)	**61.4**	**11.6**

[a] Rotation Method: Varimax with Kaiser normalization
[b] Bold loading >0.70

3.4 Source identification by PCA

In this study, concentrations of 13 PAHs and the 70 samples were selected as active variables and subjects, respectively. The majority of the variance (73.0 %) of the scaled data was explained by two eigenvectors–principal components. The first principal component (PC1) can explain 61.4 % of the total variance, and the second (PC2) can explain 11.6 % of the total variance, respectively, as shown in Table 3.

The PC1 is heavily weighted in B[b]F, B[e]P, Ind, D[a,h]A and B[g,h,i]P, which are the high molecular weight PAHs with 5–6 rings. This group usually originates from road

Table A4. Accuracy test withSRM 1941b.

SRM	Abbr	*n*	Reference Valve ng g^{-1} dry weight	Measuring Valve ng g^{-1} dry weight	% Accuracy
Phenanthrene	Phe	8	406 ± 44	486 ± 66	120 ± 16
Fluoranthene	Fluo	8	651 ± 50	733 ± 79	113 ± 12
Pyrene	Pyr	8	581 ± 39	551 ± 65	95 ± 11
Benzo[a]anthracene	B[a]A	8	335 ± 25	277 ± 46	83 ± 13
Chrysene	Chry	8	291 ± 31	227 ± 83	78 ± 28
Benzo[b]fluoranthene	B[b]F	8	453 ± 21	396 ± 134	87 ± 29
Benzo[k]fluoranthene	B[k]F	8	225 ± 18	197 ± 86	88 ± 38
Benzo[e]pyrene	B[e]P	8	325 ± 25	409 ± 175	126 ± 53
Indeno[1,2,3-cd]pyrene	Ind	8	341 ± 57	438 ± 92	129 ± 26
Benzo[g,h,i]perylene	B [g,h,i]P	8	307 ± 45	382 ± 84	124 ± 27

Table A5. Five of Diagnostic ratios of Khao Lak sediments.

Station	An/An + Phe	Flou/Flou + Pyr	B [a]A/B[a]A + Chry	B [a]P/B[a]P + B[e]P	Ind/Ind + B[g,h,i]P
2	0.25	0.35	0.49	–	0.21
3	0.33	0.35	0.59	0.38	0.21
4	0.09	0.49	0.43	0.39	0.46
5	0.13	0.44	0.50	0.33	0.25
6	0.34	0.24	0.64	0.42	0.27
7	0.40	0.30	0.60	–	0.21
8	0.33	0.33	0.61	0.50	0.24
9	0.54	0.51	0.67	–	0.18
10	0.09	0.67	0.57	0.28	0.15
11	0.53	0.39	0.55	–	0.23
12	0.54	0.51	0.45	0.38	0.38
13	0.38	0.43	0.48	0.08	0.14
14	0.56	0.29	0.56	–	0.25
15	0.33	0.39	0.45	0.06	0.44
16	0.46	0.41	0.41	–	0.37
17	0.28	0.48	0.37	0.08	0.33
18	0.26	0.42	0.48	–	0.34
19	0.14	0.31	0.59	1.00	–
20	0.26	0.27	1.00	–	0.27
21	0.10	0.32	0.46	0.45	0.47
22	0.39	0.32	0.52	–	0.56
23	0.47	0.29	0.50	0.34	0.53
24	0.13	0.52	0.37	0.42	0.50
25	0.14	0.44	0.45	0.38	0.44
26	0.58	0.28	0.43	0.34	0.35
27	0.23	0.15	0.72	–	0.29
29	0.15	0.25	0.64	0.04	0.22
31	0.09	0.48	0.40	0.29	0.51
32	0.33	0.32	0.37	–	0.38
33	0.16	0.47	0.44	–	0.50
34	0.12	0.48	0.54	0.56	0.23
35	0.17	0.37	0.55	0.18	0.26
36	0.23	0.30	0.55	–	0.25
37	0.16	0.30	0.53	0.30	0.01
39	0.19	0.40	0.49	0.03	0.26

Table A6. Five of Diagnostic ratios of Khao Lak sediments (continued).

Station	An/An + Phe	Flou/Flou + Pyr	B [a]A/B[a]A + Chry	B [a]P/B[a]P + B[e]P	Ind/Ind + B[g,h,i]P
40	0.32	0.29	0.47	0.42	0.44
41	0.38	0.32	0.24	0.52	0.30
42	0.18	0.34	0.52	–	0.48
43	0.08	0.42	0.51	0.06	–
44	0.36	0.45	0.57	–	0.19
45	0.31	0.30	0.69	0.13	0.36
46	0.08	0.30	0.49	0.34	0.43
47	0.21	0.31	0.55	–	0.23
48	0.22	0.26	0.69	0.49	0.22
49	0.36	0.32	0.71	0.05	0.24
50	0.21	0.44	0.59	–	0.27
51	0.36	0.35	0.46	0.50	0.23
52	0.10	0.31	0.62	0.08	0.34
53	0.26	0.35	0.63	–	0.32
55	0.33	0.29	0.62	0.01	0.28
56	0.21	0.31	0.65	–	0.31
58	0.22	0.32	0.60	0.34	0.27
57	0.41	0.19	0.55	0.38	0.33
61	0.29	0.29	0.58	0.38	0.27
62	0.31	0.29	0.68	0.05	0.17
63	0.34	0.29	0.53	–	0.22
64	0.25	0.38	0.65	0.07	0.16
65	0.26	0.34	0.58	–	0.28
66	0.16	0.26	1.00	0.21	0.36
68	0.26	0.20	0.59	0.47	0.32
69	0.24	0.27	0.57	0.05	0.17
70	0.20	0.28	0.58	–	0.19
71	0.24	0.30	0.57	0.05	0.18
72	0.23	0.31	0.57	0.23	0.16
73	0.15	0.53	0.65	0.02	0.13
74	0.24	0.39	0.55	–	0.29
75	0.21	0.33	0.57	0.42	0.17
76	0.20	0.31	0.55	–	0.16
77	0.48	0.33	0.67	0.10	0.22
78	0.44	0.35	0.59	–	0.22

paving asphalt, crude oil, bitumen and road dust. Therefore, the PC1 is a representative of the road dust sources of PAHs. In contrast, the PC2 is predominately composed of Pyr and Fluo. This group usually originates from the use of petroleum product and oil combustion. Fang et al. (2006) reported that high loadings of Pyr and Fluo indicated incomplete combustion, pyrolysis of fuel and oil burning. This factor is believed to be the oil burning source of PAHs.

Since a tsunami wave can have tremendous impacts on transporting a large amount of terrigenous sediments to the sea, the mixtures of heterogeneous PAH sources are needed to take into account source identification. Even though the PCA results are similar to those of the HCA, the estimated sources from the PCA can reduce the estimated sources from three (HCA) to two sources. Thus, the PCA makes it easier to interpret the estimated sources.

A significant correlation identified by PCA, which indicates 2 estimated sources of the PAHs signatures, clearly supports our hypothesis that PAHs were transported from the potential sources on land and deposited into the near-shore seabed during tsunami backwash.

4 Conclusions

By analyzing the compositions of sedimentary PAHs in combination with application of the multivariate descriptive statistical techniques, PAHs were proven to be a promising chemical proxy to indicate the tsunami backwash, which have affected the near-shore portions of the seabed in the Khao Lak coastal zones.

The PAHs spatial distribution could indicate the distance at which the land-derived materials were transported offshore

as a result of the tsunami backwash. The prominent feature of surface sediments exported from the Pakarang Cape could be observed. This evidence indicates that the tsunami backwash plays an important role in transporting anthropogenic PAHs to the nearby coastal area as far as approximately 25 kilometers from the shoreline. In addition, the results from diagnostic PAH isomer ratios suggested that road paving asphalt, originating from heavy erosion by the tsunami wave in front of Pakarang Cape, was among the identified sources of PAHs.

Moreover, PCA results provided 2 estimated land-derived sources of PAHs, which were the road dust and oil burning sources. These estimated signature sources clearly support our hypothesis that PAHs were transported from the potential sources on land and deposited into the near-shore seabed during tsunami backwash. However, the temporal distribution is needed to validate our innovative study in further work.

Acknowledgements. The study was financially supported by the ThaiGerman Research Cooperation (NRCT-DFG), under the project Tracing Tsunami Impacts on and offshore in the Andaman Sea Region, TRIAS, Center of Excellence for Environmental and Hazardous Waste Management (CE-EHWM) and the 90th Anniversary of Chulalongkorn University Fund (Ratchadaphiseksomphot Endowment Fund). The authors would like to thank the Phuket Marine Biological Center (PMBC) for providing us with RV CHAKRATONG TONGYAI and to Department of Marine Science, Faculty of Science, Chulalongkorn University for providing facility in this study. The authors also gratefully acknowledge the constructive comments and corrections on the manuscript by A. Limsakul. The authors gratefully acknowledge the anonymous reviewers for their valuable comments and suggestions that greatly improved this work.

Edited by: H. Sterr
Reviewed by: three anonymous referees

References

Ahrens, M. J. and Depree, C. V.: A source mixing model to apportion PAHs from coal tar and asphalt binders in street pavements and urban aquatic sediments, Chemosphere, 81, 1526–1535, 2010.

Boonyatumanond, R., Wattayakorn, G., Togo, A., and Takada, H.: Distribution and origins of polycyclic aromatic hydrocarbons (PAHs) in riverine, estuarine, and marine sediments in Thailand, Mar. Pollut. Bull., 52, 942–956, 2006.

Boonyatumanond, R., Wattayakorn, G., Amano, A., Inouchi, Y., and Takada, H.: Reconstruction of pollution history of organic contaminants in the upper Gulf of Thailand by using sediment cores: First report from Tropical Asia Core (TACO) project, Mar. Pollut. Bull., 54, 554–565, 2007.

Brown, J. N. and Peake, B. M.: Sources of heavy metals and polycyclic aromatic hydrocarbons in urban stormwater runoff, Sci. Total. Environ., 359, 145–155, 2006.

Cantwell, M. G., King, J. W., Burgess, R. M., and Appleby, P. G.: Reconstruction of contaminant trends in a salt wedge estuary with sediment cores dated using a multiple proxy approach, Mar. Environ. Res., 64, 225–246, 2007.

Christensen, E. R. and Karls, J. F.: Unmixing of lead, ^{137}Cs, and PAH records in lake sediments using curve fitting with first- and second-order corrections, Water. Res., 30, 2543–2558, 1996.

Dahle, S., Savinov, V. M., Matishov, G. G., Evenset, A., and Nas, K.: Polycyclic aromatic hydrocarbons (PAHs) in bottom sediments of the Kara Sea shelf, Gulf of Ob and Yenisei Bay, Sci. Total. Environ., 306, 57–71, 2003.

Fang, G. C., Wu, Y. S., Chen, J. C., Chang, C. N., and Ho, T. T.: Characteristic of polycyclic aromatic hydrocarbon concentrations and source identification for fine and coarse particulates at Taichung Harbor near Taiwan Strait during 2004–2005, Sci. Total. Environ., 366, 729–738, 2006.

Fang, M. D., Hsieh, P. C., Ko, F. C., Baker, J. E., and Lee, C. L.: Sources and distribution of polycyclic aromatic hydrocarbons in the sediments of Kaoping river and submarine canyon system, Taiwan, Mar. Pollut. Bull., 54, 1179–1189, 2007.

Fang, M. D., Chang, W. K., Lee, C. L., and Liu, J. T.: The use of polycyclic aromatic hydrocarbons as a particulate tracer in the water column of Gaoping (Kaoping) Submarine Canyon, J. Mar. Syst., 76, 457–467, 2009.

Feldens, P., Schwarzer, K., Szczuciñski, W., Stattegger, K., Sakuna, D., and Somgpongchaiykul, P.: Impact of the 2004 Indian Ocean Tsunami on Seafloor Morphology and Sediments Offshore Pakarang Cape, Thailand, Pol. J. Environ. Stud., 18, 63–68, 2009.

Field, J. G., Clarke, K. R., and Warwick, R. M.: A practical strategy for analysing multispecies distribution patterns, Mar. Ecol. Prog. Ser., 8, 37–52, 1982.

Gogou, A. I., Apostolaki, M., and Stephanou, G. E.: Determination of organic molecular markers in marine aerosols and sediments: one-step flash chromatography compound class fractionation and capillary gas chromatographic analysis, J. Chromatogr. A., 799, 215–231, 1997.

Jiang, J. J., Lee, C. L., Fang, M. D., and Liu, J. T.: Polycyclic aromatic hydrocarbons in coastal sediments of southwest Taiwan: An appraisal of diagnostic ratios in source recognition, Mar. Pollut. Bull., 58, 752–760, 2009.

Kim, G. B., Maruya, K. A., Lee, R. F., Lee, J. H., Koh, C. H., and Tanabe, S.: Distribution and sources of polycyclic aromatic hydrocarbons in sediments from Kyeonggi Bay, Korea, Mar. Pollut. Bull., 38, 7–15, 1999.

Kennicutt, II M. C., Wade, T. L., Presley, B. J., Requejo, A. G., Brooks, J. M., and Denoux, G. J.: Sediment contaminants in Casco Bay, Maine: inventories, sources, and potential for biological impact, Environ. Sci. Technol., 28, 1–15, 1999.

Kose, T., Yamamoto, T., Anegawa, A., Mohri, S., and Ono, Y.: Source Analysis for Polycyclic Aromatic Hydrocarbon in Road Dust and Urban Runoff Using Marker Compounds, Desalination, 226, 151–159, 2008.

Khairy, M. A., Kolb, M., Mostafa, A. R., EL-Fiky, A., and Bahadir, M.: Risk assessment of polycyclic aromatic hydrocarbons in a Mediterranean semi-enclosed basin affected by human activities (Abu Qir Bay, Egypt), J. Hazard. Mater., 170, 389–397, 2009.

LaFlamme, R. E. and Hites, R. A.: The global distribution of polycyclic aromatic Hydrocarbons in recent sediments, Geochim. Cosmochim. Ac., 42, 289–303, 1978.

Larsen, R. K. and Baker, J. E.: Source apportionment of polycyclic

aromatic hydrocarbons in the urban atmosphere: a comparison of three methods, Environ. Sci. Technol., 37, 1873–81, 2003.

Liu, X. M., Xu, X. R., Zhang, X. T., Zhou, C. G., and Li, H. A.: Preliminary study on PAHs in the surface sediment samples from Dalian Bay, Acta. Scien. Circum., 21, 507–509, 2001.

Liu, Y., Chena, L., Huang, Q. H., Li, W. Y., Tang, Y. J., and Zhao, J. F.: Source apportionment of polycyclic aromatic hydrocarbons (PAHs) in surface sediments of the Huangpu River, Shanghai, China, Sci. Total. Environ., 407, 2931–2938, 2009.

Macías-Zamora, J. V., Mendoza-Vega, E., and Villaescusa-Celaya, J. A.: PAHs composition of surface marine sediments: a comparison to potential local sources in Todos Santos Bay, BC, Mexico, Chemosphere, 46, 459–468, 2002.

Maldonado, C., Bayona, J. M., and Bodineau, L.: Sources, distribution, and water column processes of aliphatic and polycyclic aromatic hydrocarbons in the Northwestern Black Sea Water, Environ. Sci. Technol., 33, 2693–2702, 1999.

Mostafa, A. R., Wade, T. L., Sweet, S. T., Al-Alimi, A. A., and Barakat, A. O.: Distribution and characteristics of polycyclic aromatic hydrocarbons (PAHs) in sediments of Hadhramout coastal area, Gulf of Aden, Yemen, J. Marine. Syst., 78, 1–8, 2009.

Pomonis, A., Rossetto, T., Wilkinson, S. M., Del Re, D., Peiris, N., Koo, R., Manlapig, R., and Gallocher, S.: The Indian Ocean Tsunami 26th December 2004. Earthquake Field Investigation TeamReport, Institution of Structural Engineers, UK, 180 pp., 2005.

Savinov, V. M., Savinova, T. N., Carroll, J., Matishova, G. G., Dahle, S., and Naes, K.: Polycyclic Aromatic Hydrocarbons (PAHs) in Sediments of the White Sea, Russia, Mar. Pollut. Bull., 40, 807–818, 2000.

Siripong, A.: Andaman seacoast of Thailand field survey after the December 2004 Indian Ocean tsunami, Earthq. Spectra., 22, 187–202, 2006.

Szczuciñski, W.: The post-depositional changes of the onshore 2004 tsunami deposits on the Andaman Sea coast of Thailand, doi:10.1007/s11069-011-9956-8, 2011.

Takada, H., Onda, T., Harada, M., and Ogura, N.: Distribution and Sources of Polycyclic Aromatic Hydrocarbons (PAHs) in Street Dust from the Tokyo Metropolitan Area, Sci. Total. Environ., 107, 45–69, 1991.

Tang, D. L., Satyanarayana, B., Zhao, H., and Singh, R. P.: A preliminary analysis of the Sumatran tsunami influence on Indian Ocean CHL-a and SST, Adv. Geosci., 5, 15–20, 2006, http://www.adv-geosci.net/5/15/2006/.

Tobiszewski, M. and Namieśnik, J.: PAH diagnostic ratios for the identification of pollution emission sources, Environ. Pollut., 162, 110–119, 2012.

Tolosa, I., de Mora, S., Sheikholeslami, M. R., Villeneuve, J., Bartocci, J., and Cattini, C.: Aliphatic and aromatic hydrocarbons in coastal Caspian Sea sediments, Mar. Pollut. Bull., 48, 44–60, 2004.

Tolosa, I., Mesa-Albernas, M., and Alonso- Hernández, C. M.: Inputs and sources of hydrocarbons in sediments from Cienfuegos bay, Cuba, Mar. Pollut. Bull., 58, 1624–1634, 2009.

Tsuji, Y., Namegaya, Y., Matsumoto, H., Iwasaki, S. I., Kanbua, W., Sriwichai, M., and Meesuk, V.: The 2004 Indian tsunami in Thailand: Surveyed runup heights and tide gauge records, Earth Planets Space, 58, 223–232, 2006.

UNEP: After the Tsunami: Rapid Environmental Assessment. United Nations Environment Programme, Nairobi, 140 pp., 2005.

Wang, X., Sun, S., Ma, H., and Liu, Y.: Sources and distribution of aliphatic and polyaromatic hydrocarbons in sediments of Jiaozhou Bay, Qingdao, China, Mar. Pollut. Bull., 52, 129–138, 2006.

Wang, H. S., Cheng, Z., Liang, P., Shao, D. D., Kang, Y., Wu, S. C., Wong, C. K. C., and Wong, M. H.: Characterization of PAHs in surface sediments of aquaculture farms around the Pearl River Delta, Ecotox. Environ. Safe., 73, 900–906, 2010.

Wattayakorn, G.: Marine environmental status in the Thai waters, Coast. Mar. Sci., 29, 87–94, 2005.

Yan, W., Chi, J., Wang, Z., Huang, W., and Zhang, G.: Spatial and temporal distribution of polycyclic aromatic hydrocarbons (PAHs) in sediments from Daya Bay, South China, Environ. Pollut., 157, 1823–1830, 2009.

Yang, Y., Vanmetre, P. C., Mahler, B. J., Wilson, J. T., Ligouis, B., Razzaque, M. D. M., Schaeffer, D. J., and Werth, C. J.: Influence of coal-tar Sealcoat and other carbonaceous materials on polycyclic aromatic hydrocarbon Loading in an urban Watershed, Environ. Sci. Technol., 44, 1217–1223, 2010.

Yunker, M. B., Macdonald, R. W., Veltkamp, D. J., and Cretney, W. J.: Terrestrial and marine biomarkers in a seasonally ice-covered Arctic estuary – integration of multivariate and biomarker approaches, Mar. Chem., 49, l-50, 1995.

Yunker, M. B., Macdonald, R. W., Vingarzan, R., Mitchell, R. H., Goyette, D., and Sylvestre, S.: PAHs in the Fraser River basin: a critical appraisal of PAH ratios as indicators of PAH source and composition, Org. Geochem., 33, 489–515, 2002.

Yunker, M. B. and Macdonald, R. W.: Petroleum biomarker sources in suspended particulate matter and sediments from the Fraser River Basin and Strait of Georgia, Canada, Org. Geochem., 34, 1525–1541, 2003.

Yunker, M. B., Macdonald, R. W., Snowdon, L. R., and Fowler, B. R.: Alkane and PAH biomarkers as tracers of terrigenous organic carbon in Arctic Ocean sediments, Org. Geochem., 42, 1109–1146, 2011.

Zakaria, M.P., Takada, H., Ohno, K., Yamada, J., Kouno, E., and Kumata, H.: Distribution of Polycyclic Aromatic Hydrocarbons (PAHs) in Rivers and Estuaries in Malaysia: A Widespread Input of Petrogenic PAHs, Environ. Sci. Technol., 36, 1907–1918, 2002.

Zhang, X. F., Tang, D.L., Li, Z.Z., and Zhang, F. P.: The effects of wind and rainfall on suspended sediment concentration related to the 2004 Indian Ocean tsunami, Mar. Pollut. Bull., 58, 1367–1373, 2009.

Zhou, J. L., Fileman, T. W., Evans, S., Donkin, P., Readman, J. W., Mantoura, R. F. C., and Rowland, S.: The partition of fluoranthene and pyrene between suspended particles and dissolved phase in the Humber Estuary: a study of the controlling factors, Sci. Total. Environ., 244, 305–321, 1999.

Earth Planets Space, **64**, 875–887, 2012

Sediment distribution on the inner continental shelf off Khao Lak (Thailand) after the 2004 Indian Ocean tsunami

P. Feldens[1], K. Schwarzer[1], D. Sakuna[1,2], W. Szczuciński[3], and P. Sompongchaiyakul[4]

[1]*Institute of Geosciences, Kiel University, Otto-Hahn-Platz 1, 24118 Kiel, Germany*
[2]*Oceanography and Environment Unit, Phuket Marine Biological Center, P.O. Box 60, Phuket 83000, Thailand*
[3]*Institute of Geology, Adam Mickiewicz University, Maków Polnych 16, 61-606 Poznań, Poland*
[4]*Department of Marine Science, Faculty of Science, Chulalongkorn University, Bangkok 10330, Thailand*

(Received November 22, 2010; Revised August 5, 2011; Accepted September 18, 2011; Online published October 24, 2012)

The coastline of Khao Lak (Thailand) was heavily damaged by the 2004 Indian Ocean tsunami. Onshore tsunami deposits and satellite images, which show large amounts of sediment transported offshore, indicate that the seafloor was impacted by tsunami run-up and backwash. In this study, high-resolution maps of sediment distribution patterns and the geological development of the seafloor are presented. These maps are based on multibeam, side-scan sonar and seismic profiling surveys offshore Khao Lak. Paleoreefs, with associated boulder fields and sandy sediment dominate the inner continental shelf. Patches of fine-grained (silt to fine sand) sediments exist in water depths of less than 15 m. The sediment distribution pattern is stable between 2008 and 2010, apart from small shifts regarding the boundaries of the fine-grained sediment patches. In one sediment core and several grab samples an event layer was documented, situated below a cover of modern sediments which is only a few cm thick. The event-layer is traced down to 18 m water depth. It consists mostly of sand and contains compounds of terrigenous origin. It is interpreted as a 2004 Indian Ocean tsunami deposit. However, over large areas of the study-site, the impact of the tsunami is hardly identifiable by seafloor morphology or sediment distribution.

Key words: 2004 Indian Ocean tsunami, offshore tsunami deposits, continental shelf, nearshore deposits, Andaman Sea.

1. Introduction

Tsunami may cause erosion and sedimentation in various environments, including coastal lowlands, lakes, lagoons, tidal flats, beaches, and continental shelves, but also the deep sea (e.g. Shiki *et al*., 2008; Bourgeois, 2009). Among these environments, tsunami impacts in the marine realm are the least known, although, as discussed by Dawson and Stewart (2007), in theory, offshore tsunami deposits may comprise a large percentage of tsunami records in geological history.

In contrast to onshore tsunami deposits with a relatively well-established set of diagnostic features, based on many studies of recent tsunami events (e.g. Dawson and Shi, 2000; Goff *et al*., 2001; Shiki *et al*., 2008; Bourgeois, 2009; Chagué-Goff, 2010; Goto *et al*., 2010a), offshore tsunami deposits are poorly known. They have been investigated in only a few cases (e.g. van den Bergh *et al*., 2003; Noda *et al*., 2007; Abrantes *et al*., 2008; Goodman-Tchernov *et al*., 2009; Paris *et al*., 2010). The existing data are far from sufficient to establish universal key criteria for the identification of offshore tsunami deposits and to understand the controlling processes of deposition associated with tsunami passages. Even less is known about the erosion of the seafloor due to tsunami flows. Most information about seafloor erosion is derived from studies of onshore deposits containing marine microfossils like foraminifera (e.g. Nanayama and Shigeno, 2006; Uchida *et al*., 2010) or diatoms (e.g. Dawson, 2007; Sawai *et al*., 2009).

The geological impacts of the 2004 Indian Ocean tsunami are likely to lead to the most detailed investigation in the history of tsunami research. Despite that, limited literature exists regarding the resulting offshore effects, which have been found to be variable. For instance, Paris *et al*. (2010), applying side-scan sonar mapping nearby Banda Aceh (Sumatra), documented a large boulder field deposited in a water depth from 5 to 25 m, mainly by tsunami backwash flow. In the nearshore zone off India and Sri Lanka, a change in bathymetry was observed after the tsunami, caused by both erosion and deposition (Narayana *et al*., 2007; Anandan and Sasidhar, 2008; Goto *et al*., 2011). Local erosion at a water depth of approximately 30 m on the continental shelf of the Andaman Sea, adjacent to the coast of Thailand, was reported by Chavanich *et al*. (2005). Post-tsunami change in shallow water sediment distribution was documented by Kendall *et al*. (2009). Meanwhile, tsunami backwash deposits were reported from a few sites on the inner continental shelf (Feldens *et al*., 2009; Sugawara *et al*., 2009; Sakuna *et al*., 2012).

Most of the evidence of offshore effects is based on a few scattered observations or sampling sites, and does not allow an overall assessment of the tsunami impact on the

Copyright © The Society of Geomagnetism and Earth, Planetary and Space Sciences (SGEPSS); The Seismological Society of Japan; The Volcanological Society of Japan; The Geodetic Society of Japan; The Japanese Society for Planetary Sciences; TERRAPUB.

doi:10.5047/eps.2011.09.001

seafloor of the inner shelf. Topographical variations lead to changes in the tsunami run-up height and impacts onshore (e.g. Szczuciński *et al.*, 2006). Therefore, it is reasonable to expect the submarine effects of tsunami to vary spatially as a result of differing bathymetry. Moreover, satellite images show large amounts of suspended load transported offshore in plumes, due to the commonly channelized tsunami backwash flow (Umitsu *et al.*, 2007; Fagherazzi and Du, 2008; Yan and Tang, 2009). Consequently, local variations in run-up and backwash may cause variations in the characteristics and distribution of the resulting erosion and deposition caused by the tsunami. Further issues concern the potential of preservation and recognition of offshore tsunami impact. Potential offshore tsunami deposits are subjected to several processes, which may remove or alter them. These processes are, for instance, waves, currents, tides, and bioturbation. After the 2004 tsunami, the beaches along the Thai coastline, which had been heavily eroded, were rebuilt naturally. Coastal systems returned to equilibrium conditions within only a few years (e.g. Choowong *et al.*, 2009; Grzelak *et al.*, 2009). One may also expect similar transformations to occur in shallow marine areas.

The assessment of tsunami effects on the seafloor of the inner shelf, without detailed information of pre-tsunami conditions, requires repeated high-resolution seafloor mappings. This is due to the variability of tsunami impacts and the dynamics of post-tsunami processes. Seafloor mapping helps to identify modern sediment distribution patterns and annual dynamics, and, in particular, to locate sheltered environments where offshore tsunami deposits might be preserved. Offshore tsunami deposits identified in such environments may supplement the paleo-record already established from onshore deposits (e.g. Jankaew *et al.*, 2008).

The present study focuses on the inner continental shelf offshore of Khao Lak (Thailand), an area which was strongly impacted by the 2004 Indian Ocean tsunami. The major objectives are:

1. to map geological structures, to document seafloor morphology and to elaborate sediment distribution patterns;
2. to identify the interannual seabed sediment dynamics by reinvestigation of the same areas;
3. to identify sediments, deposited by the 2004 Indian Ocean tsunami, and to gain information concerning their preservation potential.

2. Investigation Area

The study area, offshore of Khao Lak (Thailand), covers about 105 km^2 ranging from a 5- to 35-m water depth. Here, the coastline consists of beaches adjacent to coastal lowlands, alternating with rocky cliffs. The tides are mixed semidiurnal and range from 1.1 to 3.6 m (Thampanya *et al.*, 2006). From December to February, the NE-monsoon dominates the weather patterns, while the SW-monsoon is active from May to September (Khokiattiwong *et al.*, 1991). Calm conditions prevail in between. Offshore wave heights during the SW-monsoon can reach up to 5 m (Choowong *et al.*, 2009). During the NE-monsoon, wave influence is negligible, yet strong typhoons can occur in this part of Thailand, although they are generally rare (Kumar *et al.*, 2008; Brand, 2009, Phantuwongraj and Choowong, 2011). No such events occurred between the 2004 Indian Ocean tsunami and the period of our measurements (data by the Regional Specialized Meteorological Centre—Tropical Cyclones, RMSC, New Delhi).

There are no large rivers discharging into the study area. Meanwhile, longshore currents and sediment transport are commonly directed from south to north (Choowong *et al.*, 2009; Di Geronimo *et al.*, 2009), leading to the formation of common coastal features such as sand spits. Offshore Khao Lak, carbonate and granitic outcrops are common on the seafloor (Di Geronimo *et al.*, 2009). In the past, extensive tin mining activities took place in Phuket-, Ranong- and Phang Nga-province on land, and offshore down to a 50-m water depth (Suwanwerakamtorn *et al.*, 1990). Mining pits, up to 100 m in diameter and 7 m in depth still exist offshore (e.g. Feldens *et al.*, 2009).

The 2004 Indian Ocean tsunami had a strong impact on the coastal areas along the Andaman Sea (Bell *et al.*, 2005; Thanawood *et al.*, 2006; Tsuji *et al.*, 2006; Szczuciński *et al.*, 2006). The maximum tsunami run-up height, in the study area, reached 15 m at Pakarang Cape (Siripong, 2006). About 12,500 m^2 of Pakarang Cape were eroded by the tsunami and a large number of boulders were transported from an offshore reef platform into the intertidal zone (Goto *et al.*, 2007). Onshore tsunami deposits contained numerous indicators of a marine origin. Microfossils suggested that seafloor erosion by the tsunami in the intertidal, nearshore and open marine (continental shelf) environments had occurred (Hawkes *et al.*, 2007; Kokociński *et al.*, 2009; Sawai *et al.*, 2009).

3. Methods

Full-coverage side-scan sonar mapping, supported by multibeam echosounding and shallow reflection seismic soundings, were performed during three cruises (Nov.–Dec. 2007, Nov.–Dec. 2008, Jan.–Feb. 2010). In 2008 and 2010, selected areas were reinvestigated to obtain information about interannual sediment dynamics. The available dataset comprises about 2000 nautical miles (nm) of hydroacoustic profiles, ranging from 5 to 90 m along the coastline off Khao Lak. Approximately 105 km^2 of full-coverage side-scan sonar images, taken offshore from Pakarang Cape in water depths ranging from 5 to 35 m, are presented in this paper.

Bathymetric data were collected using a SeaBeam 1185 multibeam system (180 kHz, ELAC Nautic GmbH). Seismic data were collected using an EG&G boomer (2007) system and a low-voltage boomer device (C-Boom, 2008 and 2010) combined with an 8-element single-channel streamer for signal recording. A high- and low-pass filter (0.3 kHz and 7 kHz) was applied to remove acoustic disturbances. A Klein 595 side-scan sonar (384 kHz) with digital data acquisition and a Benthos 1624 side-scan sonar (100 and 400 kHz) were used to obtain information about sediment distribution patterns on the seafloor. The data were mosaiced and the resulting images were improved by adjusting the white and black values in order to better display the contrast of the side-scan sonar data. In this study, low

backscatter values are displayed in a light grey, while high backscatter values appear in a darker grey.

A collection of grab samples, as ground-truth data, enables the calibration of the side-scan sonar data. Sediment cores were collected using a Rumohr type gravity corer (7-cm internal diameter). In the laboratory, the cores were cut in two halves, photographed and sampled for X-ray analysis (1-cm-thick slabs) as well as for grain-size analysis. Depending on the sediment composition, the grab samples from the sediment surface were either sieved, or analyzed using a Mastersizer 2000 laser diffraction device. Samples from the sediment core, discussed in this paper, were analyzed with the Mastersizer 2000.

For the grain-size analysis by laser diffraction, carbonate and organic material were removed by HCl and H_2O_2 prior to analyses. Moreover, $Na_4P_2O_7$ was added to avoid the aggregation of fine particles during the measuring process. Grains exceeding 1.7 mm in diameter cannot be analyzed with this method. This is an important restriction as the sediment core contained layers of coarser material. It was not possible to combine sieving and laser diffraction measurements for the analysis of core material as no representative sieving results could be obtained due to the limited amount of sediment available. Therefore, the obtained grain-size distributions do not fully represent the grain-size distributions of the sediment, when grains with a diameter >1.7 mm are present.

Grain sizes are presented in the Phi (Φ) scale with $\Phi = -\log_2 d$, where d is the grain size in mm (Krumbein, 1938). The mode of the grain-size distribution was chosen as a central statistical parameter because it is not affected by removing coarse (laser diffraction based method) or fine (sieving) parts from the grain-size distribution. Modes can also be used for bimodal sediments. Sorting values, based on unimodal samples, are given using the geometric method of moments (calculation with the software Gradistat (Blott and Pye, 2001)).

4. Results

4.1 Seafloor bathymetry

A dead fringing reef complex near Pakarang Cape (Sanfilippo *et al.*, 2010) forms a platform that extends down to a water depth of approximately 10 m (Figs. 1 and 2). Seaward from this reef platform, the seafloor gently declines by 0.1° down to a 25-m water depth, which is the depth reached about 10 km offshore of the tip of Pakarang Cape (Fig. 1(A)). North and south of Pakarang Cape, in water depths between 5 and 10 m, a system of small channels, up to 2 m deep and generally between 30 and 100 m in width, is incised into the seafloor (Figs. 1(B) and 2).

Further offshore, SW-NE striking sand ridges are present (Fig. 1(C)). Their height above the seafloor reaches up to 2 m. The distance between two sand-ridge crests varies from several hundred meters to several kilometers. The length of the ridges exceeds 5 km. These sand ridges are asymmetric, with a steeper flank exposed to the NW and with a slope of up to 1.2°. They are also marked by a gently dipping flank exposed towards the SE. In some areas, small incisions up to 1 m deep exist in front of the northwestern flanks. Most of the sand ridges can be easily recognized in the side-scan sonar images; sediment with a lower backscatter intensity is exposed on the steep northwestern flanks (seafloor type E, Fig. 3). The sand ridges are no longer found in an approximately 25-m water depth, meanwhile a slightly elevated platform is observed in the bathymetry (Fig. 1(A)). Seawards of the platform, the morphological gradient of the seafloor is greater, reaching an average descent angle of 0.5° down to a 35-m water depth.

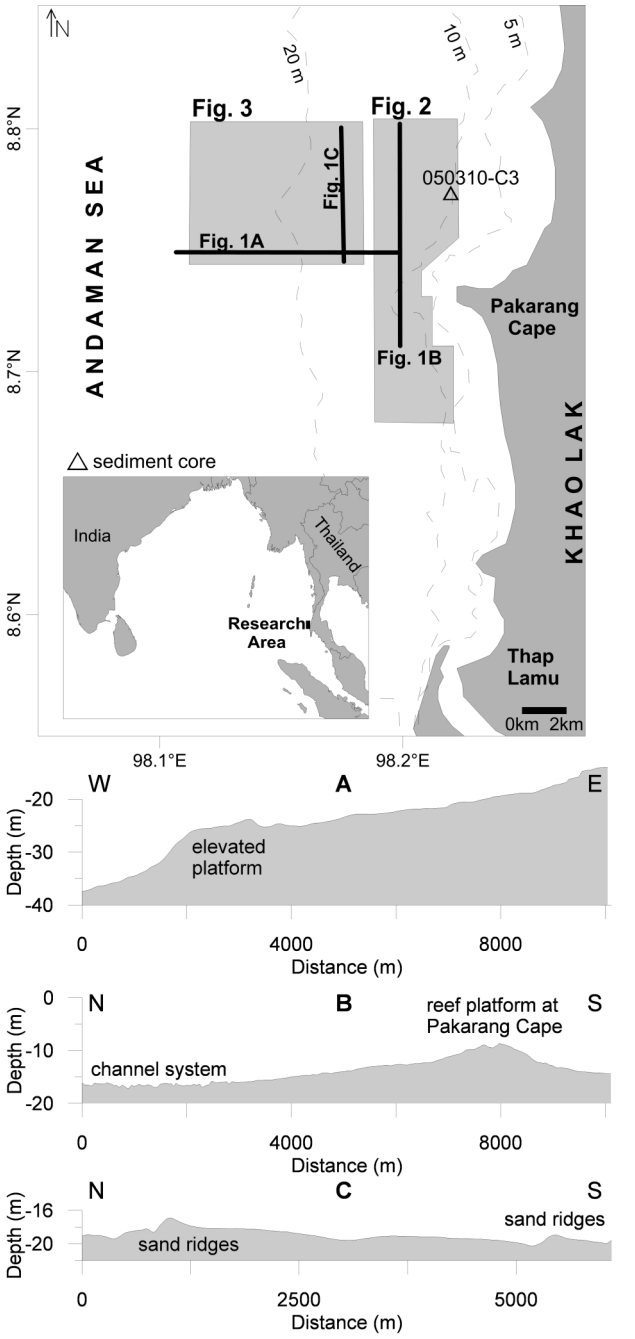


Fig. 1. Overview of the research area offshore Khao Lak and the location of bathymetric profiles (A–C, vertical exaggeration ≈ 100×). Areas shown in subsequent figures, and the position of core 050310-C3 are indicated.

4.2 Seafloor sediment distribution patterns and their interannual dynamics

Side-scan sonar mosaics based on backscatter intensities and the sedimentary composition of grab sample material

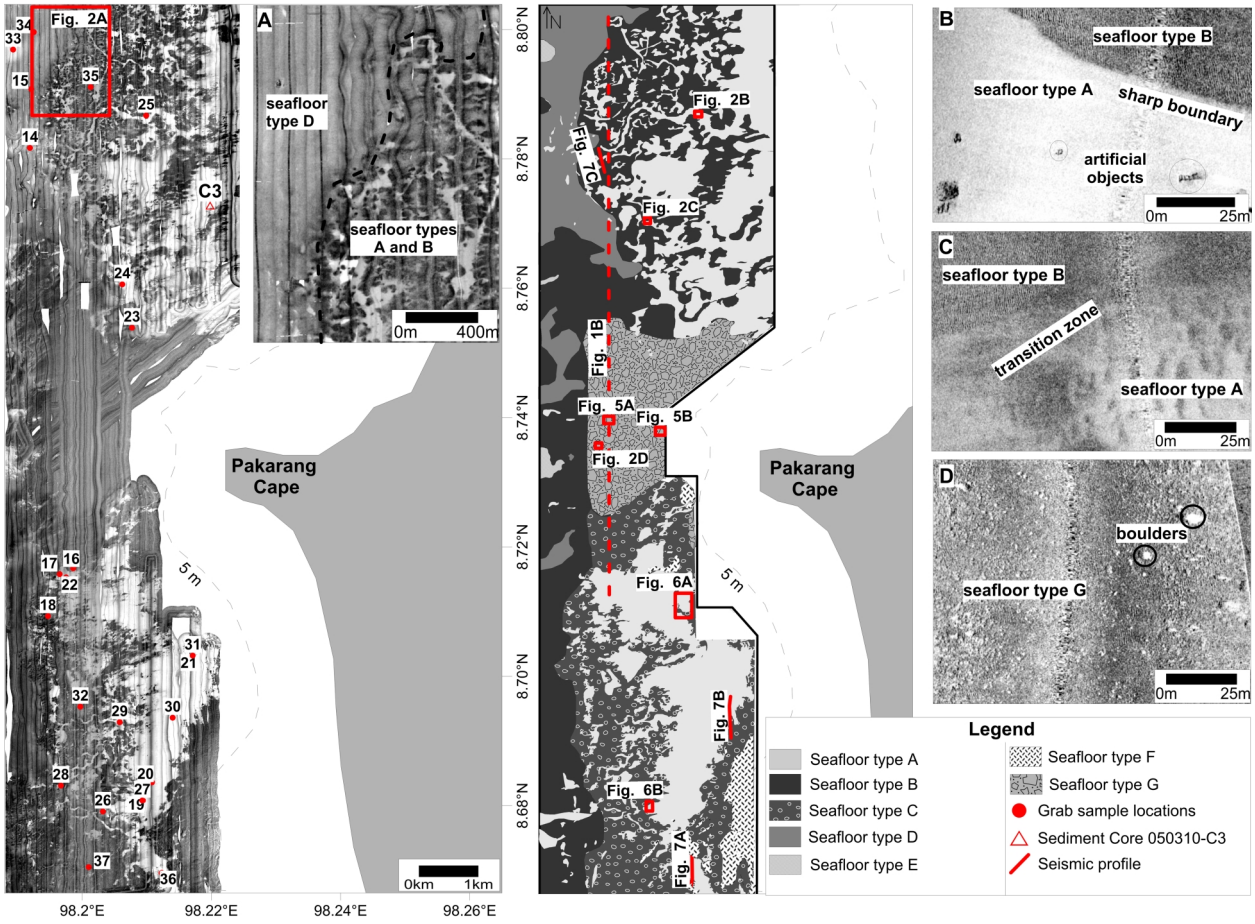


Fig. 2. Side-scan sonar image (left) and the interpretation as a map of different types of seafloor (right), down to approx. 15-m water depth. The seafloor types are determined by the classification of side-scan sonar data and are verified by surface sediment samples—Insets A, B, C and D show details discussed in the text.

identified eight major types of seafloor (named A–H; see Figs. 2 and 3): A) silt to fine sand, B) coarse sand with coral fragments, C) coarse sand, coral fragments and boulders, D) medium and coarse sands, E) medium sand, F) bedrock outcrops, G) boulders (reef platform), and H) fine and medium sands.

Sediments composed of silt to fine sand (type A), are common north and south of the reef fringing Pakarang Cape. This sediment type extends down to a 15-m water depth (Fig. 2). The landward limit of seafloor type A is above the 5-m water depth contour. It is recognized by patches of low backscatter intensity, displayed in light-grey colors in the side-scan sonar mosaics. The offshore boundaries of the patches of sediment type A are irregular, and, in some places, extend seaward filling in shallow channels. The grain size analyses revealed these sediments to be poorly, to very poorly, sorted. Samples close to the coastline are partly bimodal, with modes situated in the range of medium to coarse silt (4.6 to 5.4Φ, Fig. 4(A)), and partly in the fine-sand fraction (3.7 to 4.0Φ). The first mode generally decreases with increasing water depth (Fig. 4(A)). Notable exceptions include a coarser sample collected from a channel (sample 26 in Fig. 4(A)) and a finer sample found in a sheltered environment next to a bedrock outcrop (sample 36 in Fig. 4(A)).

Patches of seafloor type A are separated by seafloor type B (coarse sand, including coral fragments) north of Pakarang Cape and seafloor type C (coarse sand with coral fragments as well as boulders) south of the Cape. Boulders are only observed in water depths less than 15 m. Seafloor types B and C are characterized by high backscatter values, displayed in dark-grey colors. Boundaries separating seafloor types A and B, or A and C, can be either sharp (Fig. 2(B)) or transitional (Fig. 2(C)). The modes of the poorly sorted sediments representing seafloor types B and C are within the coarse-sand fraction (−0.9 to 0.4Φ). The landward limit of seafloor type B and C is situated above the 5 m depth contour. Offshore, a transitional boundary separates seafloor types B and C. A sharp boundary exists between seafloor type B and seafloor type D sediments in a water depth of 16 to 18 m (Fig. 2(A)). However, sediments classified as seafloor type B reappear further offshore and extend down to approximately a 27-m depth (Fig. 3). No correlation between the first mode and water depth is recognized in samples retrieved from seafloor types B and C (Fig. 4(B)).

Seafloor type D is composed of medium to coarse sand, which covers the seafloor between 15- and 22-m water depth. Only a few coral fragments are found within these sediments; therefore, they are recognized by intermediate backscatter values. The sediments are moderately to poorly sorted due to mixing with some coral pieces of various

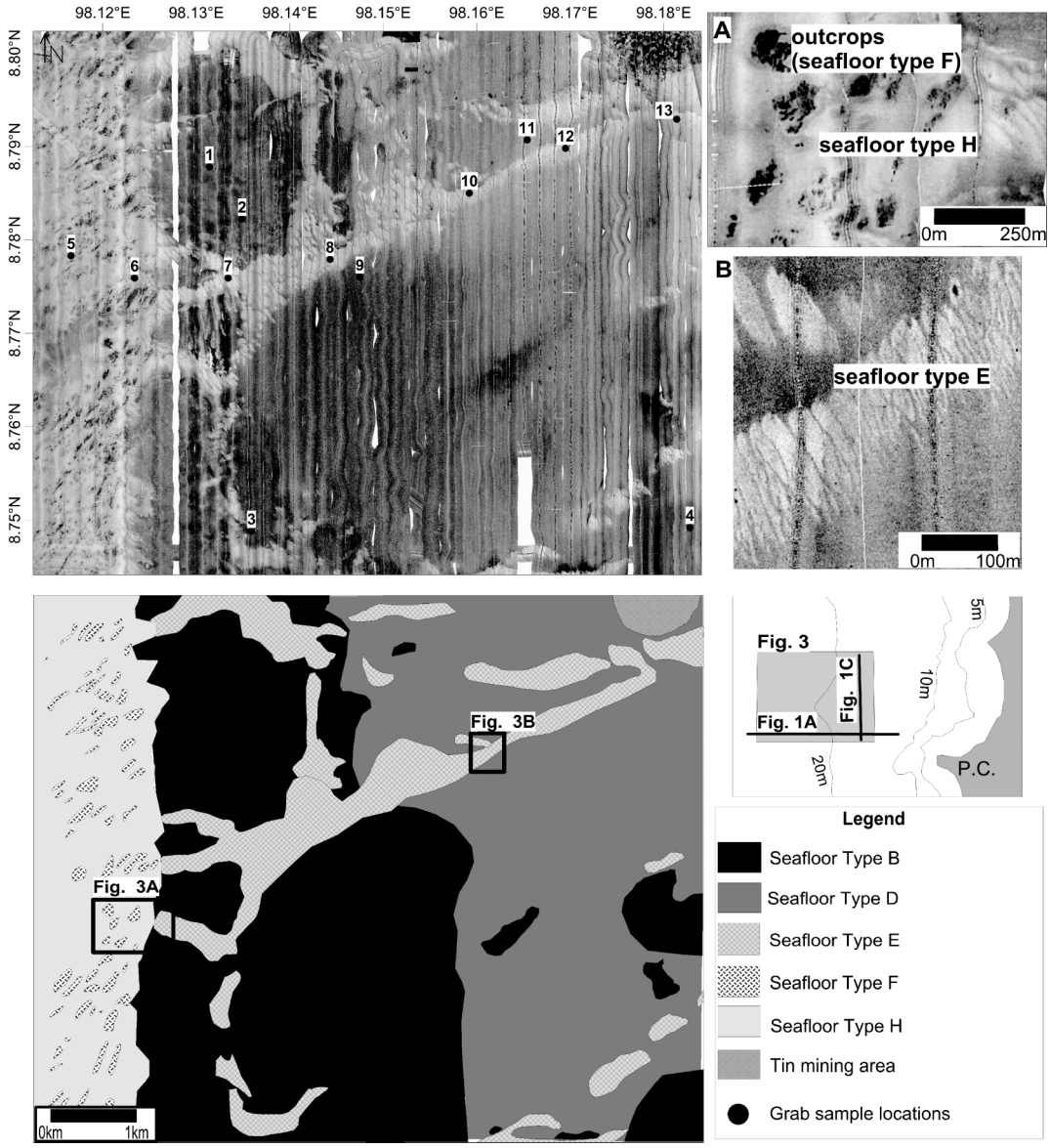


Fig. 3. Side-scan sonar image (top) and seafloor type map (bottom) offshore Khao Lak, down to approx. 35-m water depth. The seafloor type map is based primarily on the classification from side-scan sonar data and is verified by the analyses of surface sediment samples. The insets A and B show details of the borders of the seafloor types and peculiar features of the seafloor, which are discussed in detail in the text.

sizes. Their first mode varies between 1.1 to 1.4Φ. Moderately well sorted medium (first mode of 2.4Φ) sand is found in water depths from 15 to 25 m. These sediments are classified as seafloor type E (Figs. 2 and 3). They commonly occur on the northwestern flanks of the sand ridges (Fig. 3(B)). Type E sediments are easily recognized due to their elongated form, sharp boundaries with adjacent seafloor types and low backscatter intensity (Fig. 3(B)). The mode of the grain size of samples retrieved from seafloor type E is independent of the water depth.

Bedrock outcrops form parts of the seafloor. These areas are classified as seafloor type F, which occurs south of Pakarang Cape in water depths less than 10 m (Fig. 2), and further offshore in depths greater than 25 m (Fig. 3). The interface with other sediment types is very sharp (Fig. 3(A)). The appearance of the bedrock outcrops is variable in side-scan sonar mosaics, depending on the inclination angle of the outcrop surfaces in relation to the position of the side-scan sonar towfish.

The seaward boundary of the dead reef fringing Pakarang Cape is covered by a field of boulders (seafloor type G, Fig. 2(D)). This type of seafloor extends down to 10–12-m water depth. It is marked by a transitional boundary with other sediment types. The boulders are numerous and their diameter often exceeds 1 m. They are recognized as black dots with a bright acoustic shadow behind. The boulder density on the fringing reef is higher towards the offshore boundary of the reef platform (Fig. 5(A)) compared with the boulder density on its landward boundary (Fig. 5(B)).

Fine, and medium, sand below a 25-m water depth is classified as seafloor type H. This type of seafloor has a composition very similar to the sediments of type E (poorly to moderately sorted). However, type H sediment does not show specific bedforms (Fig. 3(A)). Modes of sediment comprising seafloor type H do not correlate with water depth, which is similar to samples from seafloor type E

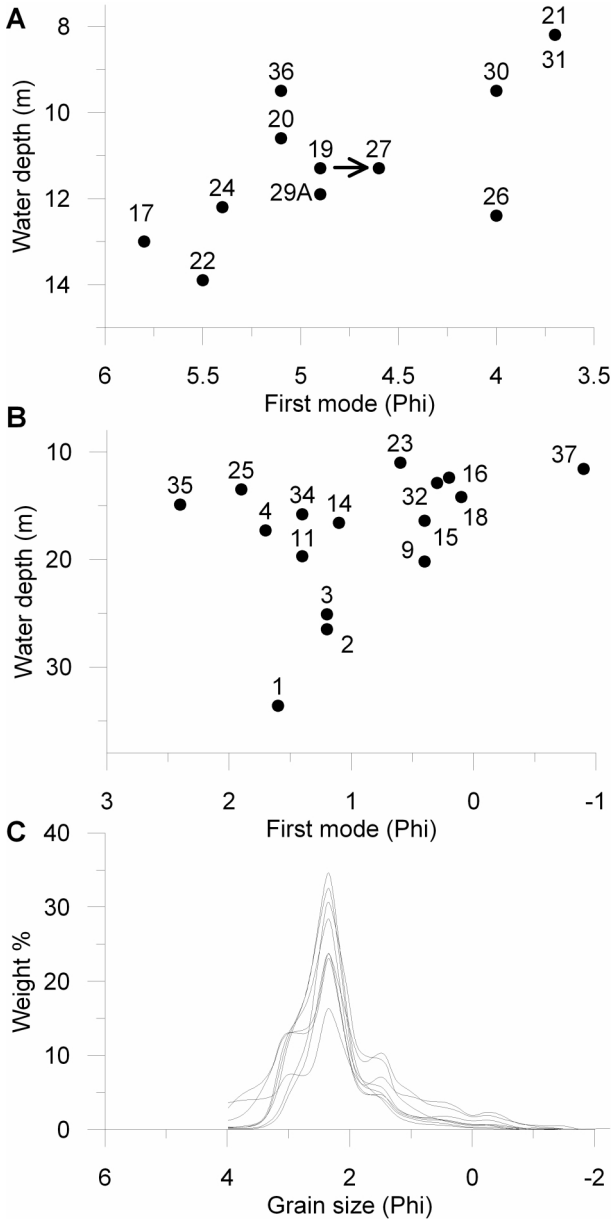


Fig. 4. Grain-size data of surface sediment samples. For sampling positions see Figs. 2 and 3. (A) The first mode of grain size versus water depth, based on samples retrieved from seafloor type A, showing a decreasing first mode with increasing water depth. Samples 19 and 27, and 21 and 31 were taken at the same positions in 2008 and 2010, respectively. (B) The first mode of grain size versus water depth based on samples from seafloor types B, C and D show no correlation. (C) The grain size distribution of samples 5, 6, 7, 10, 12, 33 obtained from seafloor type A and H. All samples have the first mode at 2.4Φ.

(Fig. 4(C)).

Repeated side-scan sonar surveys of the selected areas reveal variations in the boundaries of seafloor type A. Between 2008 and 2010, the area covered by type A sediments changes in the order of several tens of meters, either increasing or decreasing the size (Fig. 6(A)). The grain-size composition of surface sediment changes not only at sediment type boundaries, but also in the center of seafloor type A. Here, sediment changes from a sandy to a silty composition (e.g. Fig. 6(A)), or vice versa (Fig. 6(B)). Repeated grab sampling from the same position shows a slight coarsening of the first mode of the surface sediment in the center of a seafloor type A patch south of Pakarang Cape (samples 19 and 27, Fig. 4(A)), and no change in the first mode of two samples located close to Pakarang Cape (samples 21 and 31, Fig. 4(A)).

4.3 Structure of the subsurface sediments

Data concerning the subsurface sediments and the geological structure derive from three sources: reflection seismic (boomer system), grab samples and sediment cores. The seismic data provide information down to 8 m below the seafloor. Information about the development of the subbottom structure was mainly available from areas covered by seafloor type A sediments. Analysis of grab samples not only gave information about the sediments deposited directly on the seafloor, but also about sediments in 10 to 15 centimeters depth. In several cases, sediments different to those at the seafloor surfaces were found in these depths. Moreover, results of the analysis of a 55-cm-long core, taken from the area of seafloor type A, are presented.

According to the seismic records, the silty sediments comprising seafloor type A form a thin cover, usually less than 1 m thick (seismic unit 3, Figs. 7(A) and 7(B)). Within the channel system, or in areas where patches cover deeper incisions, the thickness of these deposits can reach several meters. In those cases, two sediment layers (seismic units 2 and 3), separated by an unconformity, are observed. Towards the seaward boundaries of the seafloor type A, the thickness of seismic unit 3 decreases below the resolution of the boomer system. Silty sediments still appear in the side-scan sonar images, but they can no longer be distinguished in the seismic data as a distinct layer. The surface of the cover of silty deposits is generally on the same, or at a slightly lower, morphological level as the surface of the surrounding sand (Fig. 7(B)), and at a distinctly lower level near the hard-rock outcrops (Fig. 7(A)). In part, the appearance of seismic unit 3 is homogenous; however, internal reflectors indicating layering can be observed as well. Seismic unit 2 is separated from units 1 and 3 by a distinct reflector. Moreover, internal reflectors terminating against this boundary are apparent. In some areas, the sediments forming seafloor type B can be identified in the seismic record and are situated above the acoustic basement (seismic unit 4, Fig. 7(C)). The penetration depth is generally poor, and the acoustic basement is situated close to the surface.

Sediment samples retrieved from seafloor type A occasionally contain, at depth, material different from the surface sediment. These sediments at the base of the grab sample include oval-shaped patches of dark sand (first mode at 3.7 to 4.0Φ, samples 29 and 31). They are found close to the coastline and in the channel system at the seaward boundary of seafloor type A. The subsurface sediments from grab samples, retrieved close to the coastline, also contain irregular clasts composed of coarse sand with a first mode at 0.8Φ. Gravel-sized pieces of granite (sample 21) are included as well. The latter is also frequently embedded in grab samples retrieved seawards of bedrock outcrops (e.g. sample 36). At the seaward boundary of seafloor type A, lateritic fragments are found in the lower part of grab samples (sample 22). Seaward of the boundary of seafloor

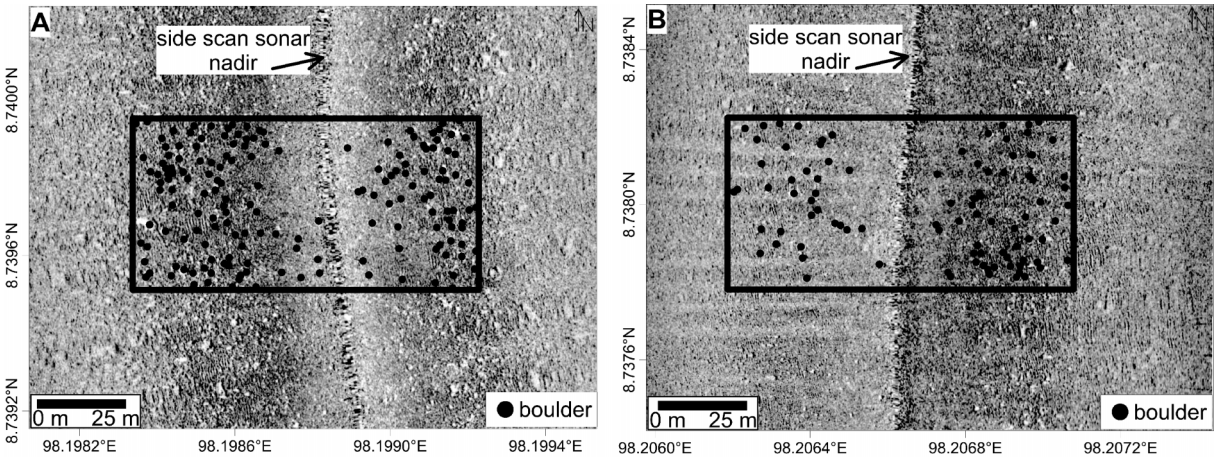


Fig. 5. The boulder density on the reef fringing Pakarang Cape (seafloor type G) is higher towards its offshore boundary (A, approx. 11-m water depth), compared with the landward boundary (B, approx. 9-m water depth). For positions, refer to Fig. 2.

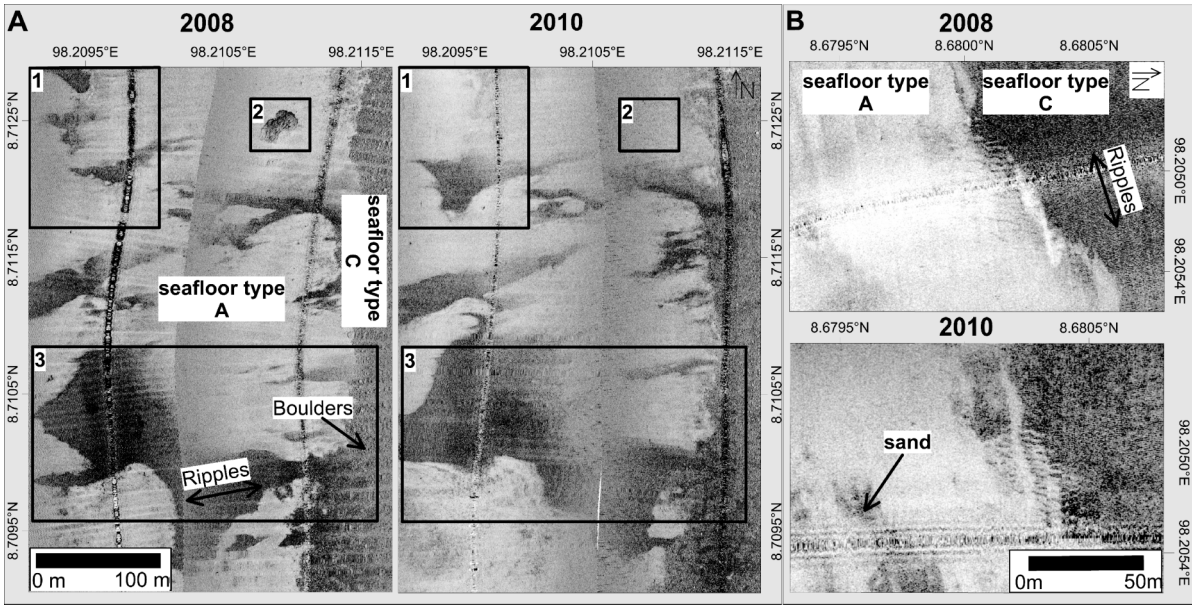


Fig. 6. Examples of repeated side-scan sonar surveys. The results focus on the sediment dynamics along a boundary of seafloor type A sediment patches (for positions, see Fig. 2. (A) Close to the coastline (water depths down to 10 m) the boundaries between the different seafloor types change in the order of tens of meters and are increasing (1), or decreasing (3), in coverage of type A sediments. Changes are observed also within the sediment patch (2). (B) Further offshore, observed changes are smaller. A change from silt to sand in the center of a type A sediment patch is marked with an arrow.

type A, plant material—embedded in mud and covered by sand—was found in grab samples retrieved from sediments of seafloor type D.

Sediment core 050310-C3 collected at a 11.2-m water depth (Fig. 8) provides an insight into the composition of seismic unit 3 (covered by seafloor type A). It is composed of variable grain sizes ranging from silt, silty sand to sandy silt, sand and intercalations of gravels. The sediments in the core are composed of six major units which can be further divided into subunits. The uppermost layer, unit 1 which is 5 cm in thickness, is mainly composed of upward fining silt (the first mode increase from 4.2 to 4.6Φ from base to top). Grain-size analysis reveals that the sediments of the upper 1 cm show a second mode in the sand fraction (0.9Φ). Therefore, it is identified as a separate subunit (1A). Unit 1 does not reveal well-preserved laminations. This is likely due to bioturbation; traces of which can be recognized in the X-ray image.

Unit 1 conformably covers a 1-cm-thick laminated layer which is composed of coarse sand containing more fine-grained material towards the surface (mode at 0.3Φ). This layer forms the uppermost part of unit 2 and is defined as subunit 2A. The lower boundary, separating units 2A and 2B, is sharp and likely to be erosional. From 5 to 18 cm, the sediment comprises poorly sorted deposits with bimodal grain-size distributions ranging from silt to gravel (unit 2B). This subunit contains reworked shells and coral debris. The sorting is slightly better towards the top of the unit. There is also an upward decrease in size and number of gravel-sized components, and an associated decrease in clay and silt content towards the top of the unit. The first and second modes in the analyzed samples range from 0.8 to 1.1Φ,

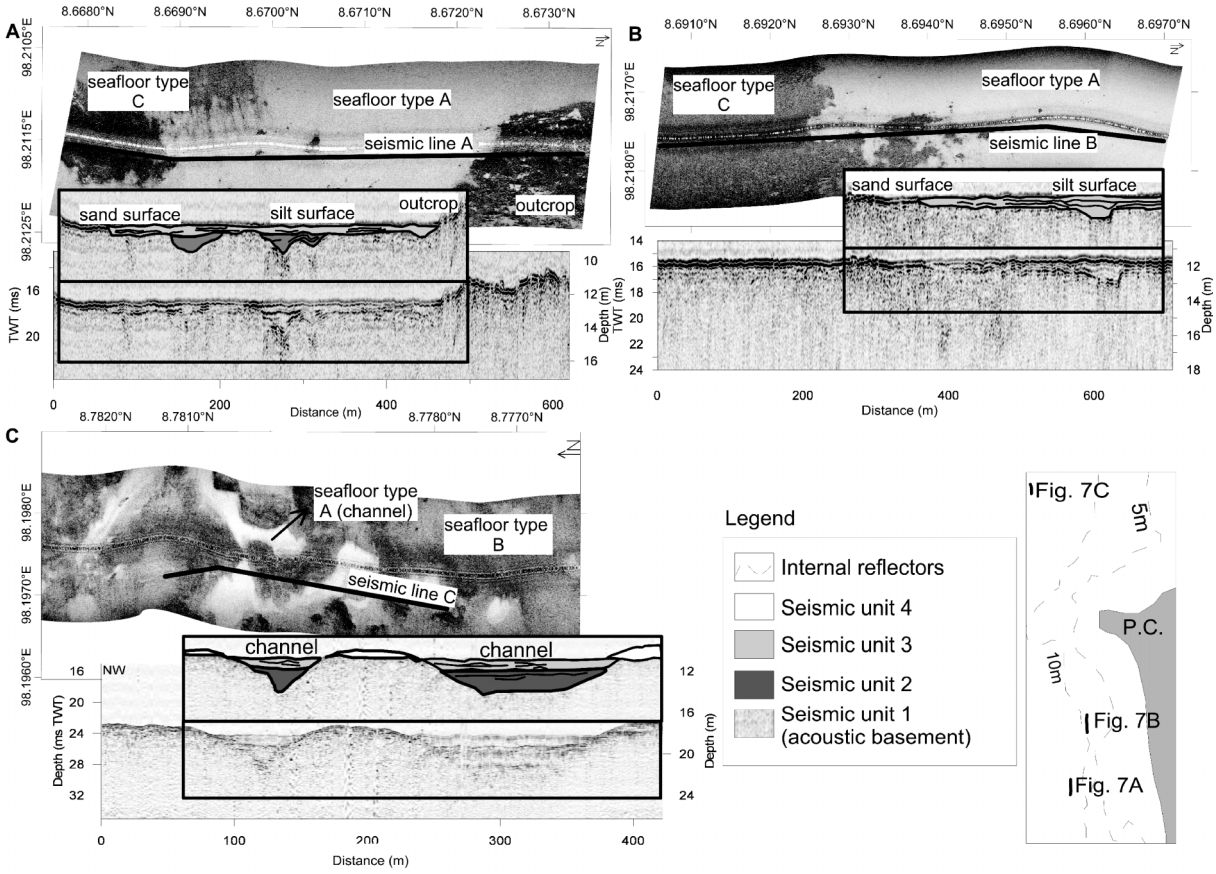


Fig. 7. Shallow-water reflection seismic profiles and side-scan sonar images in the area of seafloor types A, B and C (Fig. 2). Four seismic units are identified. The sediment of type A belongs to seismic unit 3, which forms a meter-thick cover. P.C.: Pakarang Cape.

and 4.0 to 5.1Φ, respectively. Unit 2 is separated from the underlying unit 3 by an erosional unconformity at 18-cm depth (Fig. 8). Small amounts of the older sediments are incorporated into the basal part of unit 2.

Compared with unit 2, sediments of unit 3 are characterized by a higher percentage of silt. The structure of unit 3 shows distinct horizontal, and cross-, stratifications. The first mode in the grain-size distribution ranges from 0.8 to 1.4Φ. A second mode is observed only in the upper and lower parts of the unit (subunits 3A and 3C) and ranges between 5.1 and 6.0Φ. This unit may be divided into the two silty sand subunits 3A and 3C, separated by a sand layer (3B). Subunit 3A is about 9-cm thick and is composed of almost horizontally-laminated sediments with several small-scale unconformities. At a depth of 24 cm, a pocket containing sand and gravel interdispersed with some snail shells exists. The inclined sandy layer forming subunit 3B is situated at a depth of 26 to 28 cm. It is composed of coarse sand. The layer contains numerous shell fragments and patches of finer sediments. Its lower contact is partly erosional. The 4-cm-thick subunit 3C is composed of layered silt and sand inclined in the same direction as subunit 3B. In the upper part of this subunit, a cross-lamination is preserved within an inclined silty sand layer. In general, the sediments in this subunit are coarser towards the surface. Laminae of the lower part of the unit downlap onto the upper surface of unit 4, situated at a 33-cm depth. Unit 4 is composed of similar types of sediments as the above units—bimodal silty sand with the first mode ranging from 0.8 to 1.1Φ. However, the sedimentary structure of this unit is chaotic. It reveals remnants of horizontal laminations and patches of finer sediments with shells scattered throughout. Its lower boundary is sharp. Sediment between a 42- and 52-cm depth is defined as unit 5 and consists of coarse sand with a unimodal grain-size distribution (mode between 0.8 and 1.0Φ). Shell fragments and coral debris are abundant. In some parts, it reveals a faintly visible lamination; however, in general, it has a massive structure with a chaotic distribution of sediment patches containing finer material between sand grains. The lower boundary of this unit is uneven and erosional. The lowermost part of the core consists of poorly sorted sandy silt to silty sand (unit 6), with the first mode between 3.7 and 4.7Φ. No clear sedimentary structures can be recognized in this unit.

5. Discussion

5.1 Geological features of the inner continental shelf off Khao Lak

The obtained data indicate three seabed facies offshore Khao Lak in water depths ranging from 5 to 35 m, which are differentiated by seafloor morphology and sediment composition. They are related to: (a) the fringing reef at Pakarang Cape and potential paleoreefs nearby, (b) the dominating sandy inner shelf environment, and (c) shallow water patches of fine-grained sediments.

The fringing reef offshore Pakarang Cape is covered with

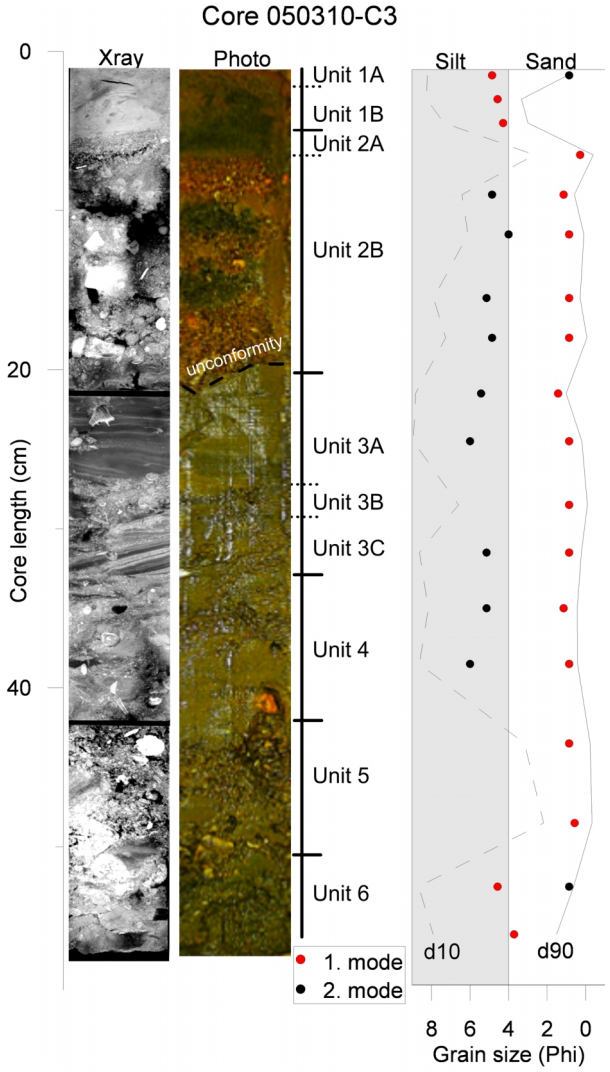


Fig. 8. Photo of sediment core 050310-C3. From left to right, X-ray image, photo, sedimentary units and the 1st and 2nd modes of grain size, and the sedimentological parameters d10 and d90 are presented.

boulders (sediment type G, Fig. 2). This reef terminates abruptly offshore (Fig. 2). Only a few coral boulders are observed seaward of the reef slope. In contrast, high amounts of coral debris, including boulders, are located north and south of the reef (seafloor types B and C, Fig. 2). Cobbles from this area, which are covered by colonies of organisms indicating a stable environment, were recently reported by Sanfilippo *et al.* (2010). Additionally, the acoustic base is situated just beneath the surface north and south of Pakarang Cape (Fig. 7), which suggests the presence of hard rock and/or very coarse material close to the seafloor. This can be seen below seismic unit 4, which is composed of coarse sand (Fig. 7(C)). It is likely that the areas directly north and south of Pakarang Cape are remnants of old reef platforms. The channel system at a depth of 15 m (Fig. 2) is incised into the surface of this old platform. The elevated morphological platform found in an approximately 25-m water depth (Fig. 1(A)) is interpreted as a paleoreef as well. This interpretation is based on its morphological appearance, which is typical for a drowned reef platform (e.g. Finkl *et al.*, 2005).

The dominant seafloor type on the shelf is composed of sandy sediments, which form a smoothly-inclined seafloor. Several kilometers-long sand ridges occur on the surface of the seafloor (Fig. 1(C)). These ridge structures are frequently observed in sandy inner continental shelf settings. They can be formed both by storm events and by regular hydrodynamic processes; for instance, tidal currents or ocean currents (Holland and Elmore, 2008). Relict ridges, so-called moribund ridges, formed during lower sea level stages also exist (Dyer and Huntley, 1999). The sand ridges in the study area have no connection to the underlying sedimentological strata, and were eventually influenced by the 2004 tsunami (Feldens *et al.*, 2010). With the applied methods, no movement of the sand ridges was observed between 2008 and 2010. However, it is not possible to explicitly conclude that these ridges represent a relict form. The presence of fine sands (seafloor type E) on the leeward side of the ridges may suggest that these structures are actively being shaped.

A remarkable feature within the research area is the fine-grained (mainly silt) sediment cover observed close to the coastline (seafloor type A, Fig. 2). This material is deposited in depressions of the inferred paleoreef platform and in the channel system north and south of Pakarang Cape (Fig. 7). The mechanisms responsible for the deposition and preservation of such fine-grained material in the inner shelf environment are still poorly understood (e.g. Hill *et al.*, 2007). However, it was found that once deposited (for example, during large floods) mud deposits can be retained even in wave-dominated, highly-energetic, inner shelf environments (Scully *et al.*, 2002; Crockett and Nittrouer, 2004). Since large rivers are absent in the study area, the source of these sediments may be associated with recent anthropogenic activities (tin mining, deforestation, earthworks), or local small river and creek flooding during the rainy season.

5.2 Mud deposits on the inner continental shelf

Accumulation of mud is observed on various continental shelves, normally due to the discharge of large rivers supplying significant amounts of fine-grained sediments (e.g. Walsh and Nittrouer, 2009). However, such a sediment source is missing in the study area. From other studies, it is known that the mud supply to the shelf has increased in historical times due to direct or indirect anthropogenic impact (Wolanski and Spagnol, 2000; Sommerfield and Wheatcroft, 2007; Szczuciński *et al.*, 2009). An increased supply of fine sediment during the last century may also be expected in the study area offshore Khao Lak, due to intensive tin mining activities, agriculture, tourism and related land-use change (e.g. deforestation).

The thickness of the fine-grained sediments offshore Pakarang Cape (sediment type A, Fig. 2, seismic unit 3, Fig. 7) decrease from a local maximum of 2 m to only a few cm, with increasing distance from the shore, and increasing water depth. Dominating sediments grade also from fine sand to silt-sized particles with increasing distance from the shore. This suggests an onshore source of these sediments. Available data indicate that most of these sediments were deposited during the last hundred years. The rate of sediment accumulation is very high, reaching more than 1

cm per year according to Pb210-dating of a sediment core taken from a mud patch at a 9.6-m water depth (Sakuna *et al.*, 2012). This is in agreement with an estimation of the sediment accumulation rate for the presented core 050310-C3 (11-m water depth, Fig. 8). Here, the uppermost 5 cm of mud (unit 1) lies above sediments interpreted as a 2004 tsunami event deposit (see Section 5.3 for the discussion). As the core was retrieved slightly more than 5 years after the tsunami occurred, the estimated accumulation rate is 0.95 cm/year.

The presented assessments of mud accumulation refer to normal conditions without influence from strong events. However, muddy sediments were also transported offshore during the tsunami, which is the most recent extraordinary event influencing the sediment distribution in this area. Observation by eyewitnesses, videos, and satellite images, show large amounts of fine-grained material transported offshore by the 2004 Indian Ocean tsunami (Umitsu *et al.*, 2007; Fagherazzi and Du, 2008; Mård Karlsson *et al.*, 2009; Yan and Tang, 2009). The suspended load extended more than 10-km offshore (IKONOS satellite images) and could be recognized for several days after the event. Therefore, a large layer of mud, transported and deposited offshore due to the tsunami, would be expected. Several post-tsunami sediment sampling surveys have been performed in the present study area or nearby, but the expected widespread layer of tsunami fine-grained deposits was never detected (Szczuciński *et al.*, 2006; Di Geronimo *et al.*, 2009; Feldens *et al.*, 2009; Sugawara *et al.*, 2009; present study). Since all of these surveys were carried out at least one year after the tsunami, it is possible that these fine-grained tsunami deposits were mostly redeposited and dispersed over a larger area by hydrodynamic activity due to the SE-monsoon. Di Geronimo *et al.* (2009) identified areas covered with mud deposits in some parts of the inner shelf off Khao Lak. They interpreted these layers as tsunami deposits due to their unusual location in shallow water. However, these muds are in the same area as the seafloor type A fine-grained sediments, which, as discussed above, seem to be the result of normal sedimentation.

Repeated side-scan sonar surveys in 2008 and 2010 allow for the assessment of the annual dynamics of seafloor type A sediments. The magnitude of change of the boundaries between seafloor type A and the surrounding sea bottom is greater closer to the coastline (Fig. 6(A)), and can reach several tens of meters. The change of the coverage of type A includes both increases and decreases in the area. The decrease may be either due to erosion, or to being covered by surrounding sediments. The available data does not allow for a determination of which situation took place. However, a change in the surface sediment type is also observed in the center of type A sediment patches (Figs. 6(A) and (B)). Therefore, it can be assumed that the sediments of type A are at least partially reworked during the annual cycle.

The evidence gathered on shallow water areas covered by fine-grained sediments (seafloor type A) imply that these regions might be affected by some kind of specific local circulation pattern, generating preferential conditions for a good preservation of the fine-grained deposits in specific, slightly lowered areas. These areas may also be preferential for the preservation of event deposits; the 2004 offshore tsunami deposits were mostly found in these regions (present study—see Section 5.3, Sakuna *et al.*, 2012).

5.3 Identification of offshore tsunami impact

The results obtained on the seafloor morphology and surface sediment distribution do not show widespread features which could be directly related to a tsunami event. It is observed that offshore tsunami deposits having the form of event deposits are restricted to specific areas. They are documented as unit 2 (Fig. 8) in sediment core 050310-C3. Large storm, and typhoon, events are generally rare in the investigation area (e.g. Phantuwongraj and Choowong, 2011) with a return period in the range of decades. Their influence is generally minor (Kumar *et al.*, 2008; Brand, 2009). No severe storm event affected the area between the time of the 2004 tsunami and the end of our sampling campaigns. Therefore, unit 2, being the most recent event layer, is interpreted as an offshore tsunami deposit. Several characteristics reported as typical for such deposits (e.g. van den Bergh *et al.*, 2003; Goodman-Tchernov *et al.*, 2009; Sakuna *et al.*, 2012) can be found in this unit. It is deposited above an erosional unconformity, contains abundant shell fragments, and is generally poorly sorted and embedded within ambient sediments. Material forming unit 2 derives partly from the nearby vicinity where similar sediments can be found both further onshore and offshore (seafloor type B, Fig. 2). The unit is composed of two subunits—2A and 2B—separated by a sharp, erosional boundary. The subunits may reflect various phases of the tsunami event, but further differentiation into run-up and/or backwash is still not possible. Macroscopic terrigenous material, which would point towards backwash influence, is not found, and the observed sedimentological structures could be formed during both tsunami phases. However, a lack of terrigenous components cannot be used to exclude a tsunami origin of unit 2. Erosion on land was observed to be limited (e.g. Szczuciński *et al.*, 2006; Umitsu *et al.*, 2007; Fagherazzi and Du, 2008), and minor in comparison with beach and nearshore zone erosion. Due to the channeled nature of the backwash (Le Roux and Vargas, 2005), it cannot be expected that land-derived material was distributed evenly throughout the inner shelf. It is also difficult to exclude explicitly the tsunami origin of unit 3; however, the laminations in its fine-grained part (units 3A and 3C) indicate recurring, more regular events (Palinkas *et al.*, 2006) in the past. Therefore, we assume that unit 3 was likely deposited before the tsunami event.

The inferred tsunami deposits of unit 2 were covered by only 5 cm of muddy material since 2004. For this reason, the tsunami deposits could also be traced by grab samples, as a penetration of up to 10 cm is possible. Indeed, several grab samples were marked by different sediments at their base than those on the surface. The subsurface sediments contain pockets of fine sand, gravel, pieces of laterites and plant materials. Such deposits are found down to a depth of 18 m, approximately 8 km offshore. The composition of these subsurface sediments varies greatly among grab samples retrieved from different locations. It is assumed that their different compositions reflect both the difference in sediments locally available for erosion and deposition,

as well as the varying spatial impact of the tsunami run-up and backwash at different locations. This is further supported by the varied internal appearance of seismic unit 3 (Fig. 7), which indicates a different composition of the first few decimeters of the seafloor beneath sediment type A. As laterites and plant material are of a terrigenous origin, parts of the material were transported offshore during the backwash.

It is interesting to note that the most inferred tsunami deposits are present below the seafloor of type A. The most likely explanation is that these sediment depocenters allow for a better preservation of tsunami deposits. It is also possible that the major tsunami influence during both run-up and backwash was focused spatially due to small-scale morphological variations both on- and offshore (Le Roux and Vargas, 2005; Umitsu *et al.*, 2007; MacInnes *et al.*, 2009).

No influence of the 2004 Indian Ocean tsunami has been found within the sediments of seafloor types B and C. This supports the findings of Sanfilippo *et al.* (2010), who reported a minor influence on corals living on cobbles in these areas. These areas seem to be mostly unaffected by the tsunami event. No direct traces of tsunami impact below an 18-m water depth were found in hydroacoustic data or sediment samples. Seafloor type E (Fig. 2), deposited on the northwestern flanks of the sand ridge system, indicates a SW-NE directed current. In incisions at the base of the sand ridges, event deposits composed of silty material covered by coarse sand were found (Feldens *et al.*, 2010). However, it is uncertain whether these features can be attributed to the 2004 Indian Ocean tsunami.

Due to the sediment dynamics in the investigation area, it is likely that existing tsunami deposits are subject to erosion and reworking processes. Tsunami deposits were not found directly at the surface, but are only covered with about 5 cm of sediment deposited after the tsunami (unit 1, Fig. 8). Therefore, we assume that deposits of the 2004 Indian Ocean tsunami are preserved only in sheltered environments offshore Khao Lak; for instance, in the channel system and in depressions seawards of granitic outcrops where post-tsunami deposition of mud or sand has taken place. This is supported by the findings of Sakuna *et al.* (2012).

The occurrence of tsunami deposits only in specific areas is in contrast to onshore tsunami deposits, which commonly form a continuous sand layer covering the inundation zone directly following flooding by the tsunami (Shiki *et al.*, 2008). Although offshore tsunami deposits were speculated to be more common than onshore deposits (Dawson and Stewart, 2007), their actual deposition and subsequent preservation depends strongly on the local geomorphological configurations of the shelf and nearshore area and onshore conditions. It is proposed that in coastal environments similar to our study area, a higher amount of tsunamigenic material is deposited and subsequently preserved onshore than offshore.

Frequently reported, and more easily preserved onshore and offshore tsunami deposits are boulders (e.g. Goto *et al.*, 2007; Scheffers, 2008; Goff *et al.*, 2010). On the seafloor off Sumatra, the movement of boulders several meters in diameter, in water depths down to 25 m, has been described and modeled by Paris *et al.* (2010). Goto *et al.* (2007) described that the offshore transport of hundreds of boulders towards the intertidal zone of Pakarang Cape is due to the 2004 Indian Ocean tsunami. They explained this transport through a numerical model showing that the majority of these boulders were transported onshore from a water depth of less than 10 m. In fact, the boulder density at the offshore boundary (10–12-m water depth) of the boulder-covered reef platform is higher than in the shallower part (indicated in Fig. 5). This supports the boulder transport model developed by Goto *et al.* (2010b), as the lower density in the shallower water depth might be due to the removal of some of the boulders towards the shoreline during the run-up phase.

6. Conclusion

The objectives of this study include the documentation of seafloor morphology and geological features, as well as the sediment distribution and its interannual changes in order to support the identification of the 2004 Indian Ocean tsunami impact to the seafloor offshore Khao Lak (Thailand). Large areas of the seafloor are dominated by coarse sediments, including sand and boulders, associated with fringing reefs. Moreover, in depressions and in a small channel system, which is incised in a palaeoreef platform, a layer of silt to fine sand is deposited down to a 15-m water depth. These sediments were found to be mobile.

An impact of the tsunami could not be identified over large areas of the study site in the seafloor morphology, the sediment distribution pattern, grain-size composition or specific morphological features. Offshore tsunami deposits could be identified only in a limited area down to an 18-m water depth. Typical features of these event deposits include layers composed of coarse sand and gravelly silty sand with a basal erosional contact. The event deposits are sandwiched by modern muddy sediments. Terrigenous compounds (laterites and plant remnants) indicate the influence of the tsunami backwash. The deposits with terrigenous constituents were already covered with a few cm of sediments. They were found in local sediment depocenters likely created by the local water circulation pattern. Although onshore tsunami deposits and satellite images indicate that the seafloor was impacted by tsunami run-up and backwash, five years after the tsunami the lasting impact offshore Khao Lak was found to be minor.

Acknowledgments. This research was funded by DFG (grant SCHW 572/11) and NRCT. We are grateful to Phuket Marine Biological Center (PMBC) for providing ship time and other facilities, and to Somkiat Khokiattiwong and Karl Stattegger for helpful advice, two anonymous reviewers for very helpful comments which improved this manuscript and John Rappaglia for helpful comments regarding the language. We wish to thank the masters and crews of RV Chakratong Tongyai, RV Boolert Pasook and MS Fahsai for their support during our research cruises.

References

Abrantes, F., U. Alt-Epping, S. Lebreiro, A. Voelker, and R. Schneider, Sedimentological record of tsunamis on shallow-shelf areas: The case of the 1969 AD and 1755 AD tsunamis on the Portuguese Shelf off Lisbon, *Mar. Geol.*, **249**, 283–293, 2008.

Anandan, C. and P. Sasidhar, Assessment of the impact of the tsunami of December 26, 2004 on the near-shore bathymetry of the Kalpakkam coast, east coast of India, *Sci. Tsunami Haz.*, **27**, 26–35, 2008.

Bell, R., H. Cowan, E. Dalziell, N. Evans, M. O'Leary, B. Rush, and L. Yule, Survey of impacts on the Andaman Coast, Southern Thailand following the great Sumatra-Andaman earthquake and tsunami of December 26, 2004, *Bull. NZ Soc. Earthq. Eng.*, **38**(3), 123–148, 2005.

Blott, S. J. and K. Pye, Gradistat: A grain size distribution and statistics package for the analysis of unconsolidated sediments, *Earth Surf. Process. Landf.*, **26**, 1237–1248, 2001.

Bourgeois, J., Geologic effects and records of tsunamis, in *The Sea, Volume 15: Tsunamis*, edited by A. R. Robinson and E. N. Bernard, Harvard University Press, 2009.

Brand, S., Typhoon havens handbook, http://www.nrlmry.navy.mil/~cannon/thh-nc/0start.htm, 2009.

Chagué-Goff, C., Chemical signatures of paleotsunamis: A forgotten proxy?, *Mar. Geol.*, **271**, 67–71, 2010.

Chavanich, S., A. Siripong, P. Sojisuporn, and P. Menasveta, Impact of Tsunami on the seafloor and corals in Thailand, *Coral Reefs*, **24**, 535, 2005.

Choowong, M., S. Phantuwongraj, T. Charoentitirat, V. Chutakositkanon, S. Yumuang, and P. Charusiri, Beach recovery after 2004 Indian ocean tsunami from Phang-nga, Thailand, *Geomorphology*, **104**, 134–142, 2009.

Crockett, J. S. and C. A. Nittrouer, The sandy inner shelf as a repository for muddy sediment: An example from Northern California, *Cont. Shelf Res.*, **24**, 55–73, 2004.

Dawson, S., Diatom biostratigraphy of tsunami deposits: Examples from the 1998 Papua New Guinea tsunami, *Sediment. Geol.*, **200**, 328–335, 2007.

Dawson, A. G. and S. Shi, Tsunami deposits, *Pure Appl. Geophys.*, **157**, 875–897, 2000.

Dawson, A. G. and I. Stewart, Tsunami deposits in the geological record, *Sediment. Geol.*, **200**, 166–183, 2007.

Di Geronimo, I., M. Choowong, and S. Phantuwongraj, Geomorphology and superficial bottom sediments of Khao Lak Coastal Area (SW Thailand), *Polish J. Environ. Stud.*, **18**(1), 111–121, 2009.

Dyer, K. R. and D. A. Huntley, The origin, classification and modeling of sand banks and ridges, *Cont. Shelf Res.*, **19**, 1285–1330, 1999.

Fagherazzi, S. and X. Du, Tsunamigenic incisions produced by the December 2004 earthquake along the coasts of Thailand, Indonesia and Sri Lanka, *Geomorphology*, **99**(1–4), 120–129, 2008.

Feldens, P., K. Schwarzer, W. Szczuciński, K. Stattegger, D. Sakuna, and P. Sompongchaiyakul, Impact of 2004 Tsunami on seafloor morphology and offshore sediments, Pakarang Cape, Thailand, *Polish J. Environ. Stud.*, **18**(1), 63–68, 2009.

Feldens, P., D. Sakuna, K. Schwarzer, and P. Somgpongchaiyakul, Shallow water sediment structures in a tsunami-affected area (Pakarang Cape, Thailand), *Coastline Rep.*, **16**, 15–25, 2010.

Finkl, C. W., L. Benedet, and J. L. Andrews, Submarine geomorphology of the continental shelf off Southeast Florida based on interpretation of airborne laser bathymetry, *J. Coast. Res.*, **21**(6), 1178–1190, 2005.

Goff, J. C., C. Chague-Goff, and S. Nichol, Paleotsunami deposits; a New Zealand Perspective, *Sediment. Geol.*, **143**, 1–6, 2001.

Goff, J., R. Weiss, and D. Dominey-Howes, Testing the hypothesis for tsunami boulder deposition from suspension, *Mar. Geol.*, **277**(1–4), 73–77, 2010.

Goodman-Tchernov, B. N., H. W. Dey, E. G. Reinhard, F. McCoy, and Y. Mart, Tsunami waves generated by the Santorini eruption reached Eastern Mediterranean shores, *Geology*, **37**, 943–946, 2009.

Goto, K., S. A. Chavanich, F. Imamura, P. Kunthasap, T. Matsui, K. Minoura, D. Sugawara, and H. Yanagisawa, Distribution, origin and transport process of boulders deposited by the 2004 Indian Ocean tsunami at Pakarang Cape, Thailand, *Sediment. Geol.*, **202**, 821–837, 2007.

Goto, K., T. Kawana, and F. Imamura, Historical and geological evidence of boulders deposited by tsunamis, southern Ryukyu Islands, Japan, *Earth-Sci. Rev.*, **102**(1–2), 77–99, 2010a.

Goto, K., K. Okada, and F. Imamura, Numerical analysis of boulder transport by the 2004 Indian Ocean tsunami at Pakarang Cape, Thailand, *Mar. Geol.*, **268**(1–4), 97–105, 2010b.

Goto, K., J. Takahashi, T. Oie, and F. Imamura, Remarkable bathymetric change in the nearshore zone by the 2004 Indian Ocean tsunami: Kirinda Harbor, Sri Lanka, *Geomorphology*, **127**, 107–116, 2011.

Grzelak, K., L. Kotwicki, and W. Szczuciński, Monitoring of Sandy Beach Meiofaunal Assemblages and Sediments after the 2004 Tsunami in Thailand, *Polish J. Environ. Stud.*, **18**(1), 43–51, 2009.

Hawkes, A. D., M. Bird, S. Cowie, C. Grundy-Warr, B. P. Horton, A. T. Shau Hwai, L. Law, C. Macgregor, J. Nott, J. E. Ong, J. Rigg, R. Robinson, M. Tan-Mullins, T. T. Sa, Z. Yasin, and L. W. Aik, Sediments deposited by the 2004 Indian Ocean tsunami along the Malaysia-Thailand peninsula, *Mar. Geol.*, **242**, 169–190, 2007.

Hill, P. S., J. M. Fox, J. S. Crockett, K. J. Curran, C. T. Friedrichs, W. R. Geyer, T. G. Milligan, A. S. Ogston, P. Puig, M. E. Scully, P. A. Traykovski, and R. A. Wheatcroft, Sediment delivery to the seabed on continental margins, in *Continental Margin Sedimentation: From Sediment Transport to Sequence Stratigraphy*, edited by C. A. Nittrouer, J. A. Austin, M. E. Field, J. H. Kravitz, J. P. M. Syvitski, and P. L. Wiberg, Blackwell Publishing, 2007.

Holland, K. T. and P. A. Elmore, A review of heterogeneous sediments in coastal environments, *Earth-Sci. Rev.*, **89**, 116–134, 2008.

Jankaew, K., B. F. Atwater, Y. Sawai, M. Choowong, T. Charoentitirat, M. E. Martin, and A. Prendergast, Medieval forewarning of the 2004 Indian Ocean tsunami in Thailand, *Nature*, **455**, 1228–1231, 2008.

Kendall, M. A., C. Aryuthaka, J. Chimonides, D. Daungnamon, J. Hills, C. Jittanoon, P. Komwachirapitak, V. Kongkaew, A. Mittermeyr, Y. Monthum, S. Nimsantijaroen, G. L. J. Paterson, R. Foster-Smith, J. Foster-Smith, and N. Thongsin, Post-tsunami recovery of shallow water biota and habitats on Thailand's Andaman Coast, *Polish J. Environ. Stud.*, **18**(1), 69–75, 2009.

Khokiattiwong, S., P. Limpsaichol, S. Petpiroon, P. Sojisuporn, and B. Kjerfve, Oceanographic variations in Phangnga Bay, Thailand under monsoonal effects, *Phuket Marine Biological Center Research Bulletin*, **55**, 43–76, 1991.

Kokociński, M., W. Szczuciński, A. Zgrundo, and A. Ibragimow, Diatom assemblages in 26 December 2004 tsunami deposits from coastal zone of Thailand as sediment provenance indicators, *Polish J. Environ. Stud.*, **18**(1), 93–101, 2009.

Krumbein, W. C., Size frequency distribution of sediments and the normal phi-curve, *J. Sediment. Petrol.*, **8**(3), 84–90, 1938.

Kumar, V. S., V. R. Babu, M. T. Babu, G. Dhinakaran, and G. V. Rajamanickam, Assessment of storm surge disaster potential for the Andaman Islands, *J. Coast. Res.*, **24**, 171–177, 2008.

Le Roux, J. P. and G. Vargas, Hydraulic behavior of tsunami backflows: insights from their modern and ancient deposits, *Environ. Geol.*, **49**, 65–75, 2005.

MacInnes, B. T., J. Bourgeois, T. K. Pinegina, and A. Kravchunovskaya, Tsunami geomorphology: Erosion and deposition from the 15 November 2006 Kuril Island tsunami, *Geology*, **37**(11), 995–998, 2009.

Mård Karlsson, J., A. Skelton, M. Sandén, M. Ioualalen, N. Kaewbanjak, N. Pophet, J. Asavanant, and A. von Matern, Reconstructions of the coastal impact of the 2004 Indian Ocean tsunami in the Khao Lak area, Thailand, *J. Geophys. Res.*, **114**, C10023, 1–14, 2009.

Nanayama, F. and K. Shigeno, Inflow and outflow facies from the 1993 tsunami in southwest Hokkaido, *Sediment. Geol.*, **187**, 139–158, 2006.

Narayana, A. C., R. Tatavarti, N. Shinu, and A. Subeer, Tsunami of December 26, 2004 on the southwest coast of India: Post-tsunami geomorphic and sediment characteristics, *Mar. Geol.*, **242**, 155–168, 2007.

Noda, A., H. Katayama, T. Sagayama, K. Suga, Y. Uchida, K. Satake, K. Abe, and Y. Okamura, Evaluation of tsunami impacts on shallow marine sediments: An example from the tsunami caused by the 2003 Tokachi-oki earthquake, northern Japan, *Sediment. Geol.*, **200**, 314–327, 2007.

Palinkas, C. M., C. A. Nittrouer, and J. P. Walsh, Inner-shelf sedimentation in the gulf of Papua, New Guinea: A mud-rich shallow shelf setting, *J. Coast. Res.*, **22**(4), 760–772, 2006.

Paris, R., J. Fournier, E. Poizot, S. Etienne, J. Morin, F. Lavigne, and P. Wassmer, Boulder and fine sediment transport and deposition by the 2004 tsunami in Lhok Nga (western Banda Aceh, Sumatra, Indonesia): A coupled offshore-onshore model, *Mar. Geol.*, **268**, 43–54, 2010.

Phantuwongraj, S. and M. Choowong, Tsunamis versus storm deposits from Thailand, *Nat. Haz.*, doi:10.1007/s11069-011-9717-8, 2011.

Sakuna, D., W. Szczuciński, P. Feldens, K. Schwarzer, and S. Khokiattiwong, Sedimentary deposits left by the 2004 Indian Ocean tsunami on the inner continental shelf offshore of Khao Lak, Andaman Sea (Thailand), *Earth Planets Space*, **64**, 931–943, 2012.

Sanfilippo, R., A. Rosso, A. Basso, D. Violanti, I. Di Geronimo, R. Di Geronimo, F. Benzoni, and E. Robba, Cobbles colonization pattern from a tsunami-affected coastal area (SW Thailand, Andaman Sea), *Facies*, doi:10.1007/s10347-010-0226-0, 2010.

Sawai, Y., K. Jankaew, M. E. Martin, A. Prendergast, M. Choowong, and T. Charoentitirat, Diatom assemblages in tsunami deposits associated with the 2004 Indian Ocean tsunami at Phra Thong Island, Thailand, *Mar. Micropaleontol.*, **73**, 70–79, 2009.

Scheffers, A., Tsunami boulder deposits, in *Tsunamiites—Features and Implications*, edited by Shiki *et al*., 299–317, 425 pp., Elsevier, 2008.

Scully, M. E., C. T. Friedrichs, and L. D. Wright, Application of an analytical model of critically stratified gravity-driven sediment transport and deposition to observations from the Eel River continental shelf, northern California, *Cont. Shelf Res*., **22**, 1951–1974, 2002.

Shiki, T., Y. Tsuji, T. Yamazaki, and T. K. Minoura, *Tsunamiites—Features and Implications*, Elsevier, 425 pp., 2008.

Siripong, A., Andaman seacoast of Thailand filed survey after the December 2004 Indian Ocean Tsunami, *Earthq. Spectr.*, **22**, 187–202, 2006.

Sommerfield, C. K. and R. A. Wheatcroft, Late Holocene sediment accumulation on the Northern California Shelf: Oceanic, fluvial and anthropogenic influences, *GSA Bull*., **119**(9–10), 1120–1134, 2007.

Sugawara, D., K. Minoura, N. Nemoto, S. Tsukawaki, K. Goto, and F. Imamura, Foraminiferal evidence of submarine transport and deposition by backwash during the 2004 Indian Ocean tsunami, *Island Arc*, **18**, 513–525, 2009.

Suwanwerakamtorn, R., A. Paijitprapaporn, D. Downresang, and P. Suwanasing, Sediment dispersion from offshore Tin dredging along Andaman Sea coast using satellite data, *Proc. Asian Association of Remote Sensing (ACRS)*, 1990.

Szczuciński, W., N. Chaimanee, P. Niedzielski, G. Rachlewicz, D. Saisuttichai, T. Tepsuwan, S. Lorenc, and J. Siepak, Environmental and geological impacts of the 26 December 2004 tsunami in coastal zone of Thailand—overview of short and long-term effects, *Polish J. Environ. Stud*., **15**(5), 793–810, 2006.

Szczuciński, W., K. Stattegger, and J. Scholten, Modern sediments and sediment accumulation rates on the narrow shelf off central Vietnam, South China Sea, *Geo.-Mar. Lett*., **29**, 47–59, 2009.

Thampanya, U., J. E. Vermaat, S. Sinsakul, and N. Panapitukkul, Coastal erosion and mangrove progradation of Southern Thailand, Estuarine, *Coast. Shelf Sci*., **68**, 75–85, 2006.

Thanawood, C., C. Yongchalermchai, and O. Densrisereekul, Effects of the december 2004 tsunami and disaster management in Southern Thailand, *Sci. Tsunami Haz*., **24**(3), 206–217, 2006.

Tsuji, Y., Y. Namegaya, H. Matsumoto, S.-I. Iwasaki, W. Kanbua, M. Sriwichai, and V. Meesuk, The 2004 Indian tsunami in Thailand: Surveyed runup heights and tide gauge records, *Earth Planets Space*, **58**, 223–232, 2006.

Uchida, J. I., O. Fujiwara, S. Hasegawa, and T. Kamataki, Sources and depositional processes of tsunami deposits: Analysis using foraminiferal tests and hydrodynamic verification, *Island Arc*, **19**(3), 427–442, 2010.

Umitsu, M., C. Tanavud, and B. Patanakanog, Effects of landforms on tsunami flow in the plains of Banda Aceh, Indonesia, and Nam Khem, Thailand, *Mar. Geol*., **242**, 141–153, 2007.

van den Bergh, G. D., W. Boer, H. de Haas, Th. C. E. van Weering, and R. van Wijhe, Shallow marine tsunami deposits in Teluk Banten (NW Java, Indonesia), generated by the 1883 Krakatau eruption, *Mar. Geol*., **197**, 13–34, 2003.

Walsh, J. P. and C. A. Nittrouer, Understanding fine-grained river-sediment dispersal on continental margins, *Mar. Geol*., **263**, 34–45, 2009.

Wolanski, E. and S. Spagnol, Environmental degradation by mud in tropical estuaries, *Reg. Environ. Change*, **1**, 152–162, 2000.

Yan, Z. and D. Tang, Changes in suspended sediments associated with 2004 Indian Ocean tsunami, *Adv. Space Res*., **43**(1), 89–95, 2009.

P. Feldens (e-mail: pfeldens@me.com), K. Schwarzer, D. Sakuna, W. Szczuciński, and P. Sompongchaiyakul

Earth Planets Space, **64**, 931–943, 2012

Sedimentary deposits left by the 2004 Indian Ocean tsunami on the inner continental shelf offshore of Khao Lak, Andaman Sea (Thailand)

D. Sakuna[1,2], W. Szczuciński[3], P. Feldens[1], K. Schwarzer[1], and S. Khokiattiwong[2]

[1]*Institute of Geosciences Sedimentology, Coastal and Continental Shelf Research, University of Kiel, Otto-Hahn-Platz 1, D-24118 Kiel, Germany*
[2]*Oceanography and Environment Unit, Phuket Marine Biological Center, P.O. Box 60, Phuket 83000, Thailand*
[3]*Institute of Geology, Adam Mickiewicz University, Maków Polnych 16, 61-606 Poznań, Poland*

(Received November 24, 2010; Revised May 3, 2011; Accepted June 15, 2011; Online published October 24, 2012)

Tsunami waves leave sedimentary signatures both onshore and offshore, although the latter are hardly known. The objective of the present study is to provide new evidence for the 2004 Indian Ocean tsunami deposits left on the inner continental shelf of the Andaman Sea (Thailand) and to identify diagnostic sedimentological and geochemical properties of these deposits. Based on extensive seafloor mapping, three sediment cores were selected for study and were analysed for their sedimentary structures, grain size composition, chemical elemental composition, physical properties and ^{210}Pb activity. Sediment cores retrieved from shallow water (9–15 m) within 7.5 km off the shore revealed distinct event layers, which were interpreted as being tsunami deposits. These 20–25 cm thick deposits were already covered with post-tsunami marine sediments. They were composed of several units, marine sand layers alternating with poorly sorted mud with terrigenous and anthropogenic components, representing different hydrodynamic conditions (probably during run-up and backwash phase). These sedimentological observations were supported by geochemical and physical data and were confirmed using ^{210}Pb dating. A sediment core taken from a depth of 57 m at a distance of 25 km offshore did not reveal clear event deposits. Comparisons with available data from offshore tsunami deposits showed that there is no single set of signatures that could be applied to identify this kind of deposits.
Key words: 2004 Indian Ocean tsunami, offshore tsunami deposits, sedimentology, Khao Lak, Thailand.

1. Introduction

Tsunamis are relatively frequent phenomena that occur worldwide (Scheffers and Kelletat, 2003). Recent examples of tsunamis include the 2004 Indian Ocean tsunami, tsunamis in Java in 2006 and Samoa in 2009, the Chilean tsunami in 2010 and the 2011 Tohoku tsunami in Japan. These events can have potentially large impacts on both the coastal zone and the continental shelf. As tsunami waves propagate into shallower water, they can erode, transport and deposit large amounts of sediments both onshore and offshore (e.g., Paris *et al*., 2010; Goto *et al*., 2011). Due to the number of processes involved (Shanmugam, 2011), tsunami deposits are very complex in terms of a number of characteristics, including grain size, sedimentary structures and sediment components (e.g., Luque *et al*., 2001; van den Bergh *et al*., 2003; Fujiwara and Kamataki, 2007; Kortekaas and Dawson, 2007; Noda *et al*., 2007; Paris *et al*., 2010; Chagué-Goff *et al*., 2011). Geological and environmental impacts of onshore tsunami deposits have been intensively studied in recent years (see Bourgeois, 2009 for a review), whereas the offshore behaviour and effects of tsunami waves during run-up and backwash are still poorly understood.

A basic problem in studying tsunamis is that our knowledge of the sedimentological features of offshore tsunami deposits is limited to a small number of case studies (e.g., van den Bergh *et al*., 2003; Noda *et al*., 2007; Paris *et al*., 2010). Tsunami impacts (erosion) on the seafloor have primarily been examined indirectly through studies of onshore deposits containing marine microfossils such as foraminifera (e.g., Hawkes *et al*., 2007; Uchida *et al*., 2010) or diatoms (e.g., Dawson, 2007; Sawai *et al*., 2009). The studies of shallow marine tsunami deposits that have been conducted to date have indicated that there is a large variability in the characteristics of these deposits. For instance, a distinct sandy layer was deposited by a tsunami generated during the Krakatau eruption in an embayment next to Java Island (van der Bergh *et al*., 2003). Around Banda Aceh, which was the most severely devastated region during the 26 December 2004 tsunami, this event left large fields of boulders on land and offshore (Paris *et al*., 2010). Displaced boulders were also previously reported by Goto *et al*. (2007) and Feldens *et al*. (2009) from the Andaman Sea coast and shelf, respectively. Sugawara *et al*. (2009) reported nearshore impacts of the 2004 tsunami in the Andaman Sea in water depths of 6 to 30 m based on the distribution of foraminifera in surface sediments. In several other studies (e.g., Abrantes *et al*., 2008; Goodman-Tchernov *et al*., 2009; Smedile *et al*., 2011), offshore tsunami deposits were interpreted from event layers composed of sediments that were coarser than the ambient marine sediments,

Copyright © The Society of Geomagnetism and Earth, Planetary and Space Sciences (SGEPSS); The Seismological Society of Japan; The Volcanological Society of Japan; The Geodetic Society of Japan; The Japanese Society for Planetary Sciences; TERRAPUB.

doi:10.5047/eps.2011.08.010

contained indicators of a terrigenous provenance and specific microfossil assemblages. However, there have been no unique criteria for identifying offshore tsunami deposits. Recently, Goto *et al.* (2011) used repeated bathymetrical surveys and modelling and found that the amount of sediments mobilised by tsunamis is much more substantial offshore than on land.

Shallow water tsunami deposits from uplifted marine sedimentary strata were investigated by Fujiwara and Kamataki (2007) in Japan, and by Cantalamessa and Celma (2005) and Le Roux and Vargas (2005) in Chile. However, these older deposits can be reinterpreted, as in the case of backwash deposits in a shallow marine Miocene setting on the Mejillones Peninsula in northern Chile (Cantalamessa and Celma, 2005), which were recently found to be debris flow deposits with no evidence permitting an interpretation as tsunami deposits of any kind (Bahlburg *et al.*, 2010).

The above examples indicate the limitations of our understanding of the processes of erosion and deposition in shallow marine settings during tsunami events and the difficulties of identifying offshore tsunami deposits. Significant progress in the search for diagnostic criteria may be accomplished only through an increased number of well-documented case studies of modern tsunami deposits. The objective of this study is to provide evidence that the impact of the 2004 Indian Ocean tsunami can be identified in shallow water deposits offshore Khao Lak by using sedimentological methods and geochemical proxies.

2. Study Area

The study area is located on the continental shelf of the Andaman Sea offshore Khao Lak (Phang Nga province, Thailand) and extends to a distance of about 25 km offshore (Fig. 1). The coast is composed of embayed areas with sandy beaches separated by rocky headlands. The shelf is relatively flat and sloping offshore, reaching water depths of 50 m at a distance of 25 km from the coastline. The sea bottom is mainly composed of sand, sandy mud, muddy sand and bedrock outcrops (Usiriprisan *et al.*, 1987; Di Geronimo *et al.*, 2009; Feldens *et al.*, 2009, 2012). In some regions, the seabed was subjected to offshore tin mining (Usiriprisan *et al.*, 1987). The climate of this region is dominated by monsoons, with the southwest monsoon remaining active from May to September and generating heavy rainfall during this period. The northeast monsoon lasts from December to February and results in a calm, dry season (Khokiattiwong *et al.*, 1991). The study area is located next to the area in Thailand which was most damaged during the 2004 Indian Ocean tsunami (Bell *et al.*, 2005; Szczuciński *et al.*, 2006). Moreover, strong storms are rare in this area, increasing the preservation potential of tsunami deposits on the seafloor (Jankaew *et al.*, 2008; Kumar *et al.*, 2008). Previous post-tsunami seafloor mapping surveys (Di Geronimo *et al.*, 2009; Feldens *et al.*, 2009) reported discontinuous muddy sediment patches and a channel-like system next to an ancient reef platform located in shallow water (5 to 15 m). Consolidated mud deposits containing grass, wood and shell fragments, likely transported by the backwash flow in the 2004 tsunami, were observed in grab samples and short cores (Feldens *et al.*, 2009). Based on these data and further hydroacoustic surveys (Feldens *et al.*, 2012), new target areas for sediment coring were selected (Figs. 1 and 2) to examine modern offshore tsunami deposits.

3. Methods

High resolution hydroacoustic mapping (Feldens *et al.*, 2009, 2012) was performed during three research cruises (Nov.–Dec. 2007, Nov.–Dec. 2008 and Feb.–Mar. 2010). Data from these surveys form the basis for the selection of sediment coring sites. Sixty sediment cores were collected using a 2 m long Ruhmor type gravity corer in water depths of 5 to 70 m. Three cores were selected for the present study (Figs. 1 and 2, Table 1), two of which were obtained in water depths of 9.6 and 14.4 m, located 3.1 and 7.2 km offshore, respectively, while the third core was collected further offshore at a water depth of 57 m, 25.5 km offshore. Moreover, three samples from sites located within various onshore environments that had been subjected to tsunami erosion (pre-tsunami soils, mangrove soils, coastal plain sands) were obtained to provide data on terrigenous geochemical end-members (Fig. 1).

The cores were first analysed using non-destructive techniques; a Multi-sensor core logger (MSCL) and an X-ray fluorescence (XRF) core scanner. The following basic physical and acoustical sediment properties were measured: bulk density, gamma-ray attenuation, magnetic susceptibility and p-wave velocity. These physical properties are commonly used to find distinct layers such as debris flows and turbidites within sediment cores (Weber *et al.*, 1997; Best and Gunn, 1999; Hofmann *et al.*, 2005). An XRF core scanner was used to semi-quantitatively assess sediment composition; this method can serve as a tool for differentiating terrigenous materials from marine sediments (Lamy *et al.*, 2001; Bahr *et al.*, 2005; Ohta and Arai, 2007). The measurements were taken every centimetre directly at the surface of a split core. The instrument was set to a count time of 30 s with a voltage of 10 kV. At this setting, the measurement range covered thirteen elements (Al, Si, P, S, Cl, K, Ca, Ti, V, Cr, Mn, Fe and Rh). Data were provided as relative element intensities in counts per second (cps). These intensities depend mainly on element concentration, matrix effects and physical properties, as well as sample geometry (Jansen *et al.*, 1998; Weltji and Tjallingii, 2008).

The relative concentrations of eight elements, Al, Si, S, K, Ca, Ti, Mn and Fe from onshore samples (101207-89, 101207-91 and 101207-93) and samples from core 050310-C6, were analysed using principal component analysis (PCA) to evaluate the sediment provenance (Marques *et al.*, 2008; Heise *et al.*, 2010). Four elements were not used, due to either very low concentrations in some samples (at detection limits: P, V, Cr, Rh) or possible changes due to sample preparation (Cl). PCA is a data reduction technique used to convert a large number of geochemical variables into a small set of new variables called principal components or factors (PC) and to group samples based on their geochemistry (Ohta and Arai, 2007; Reid and Spencer, 2009).

Digital X-radiography images were obtained from 1 cm thick slabs taken from the surface of split sediment cores.

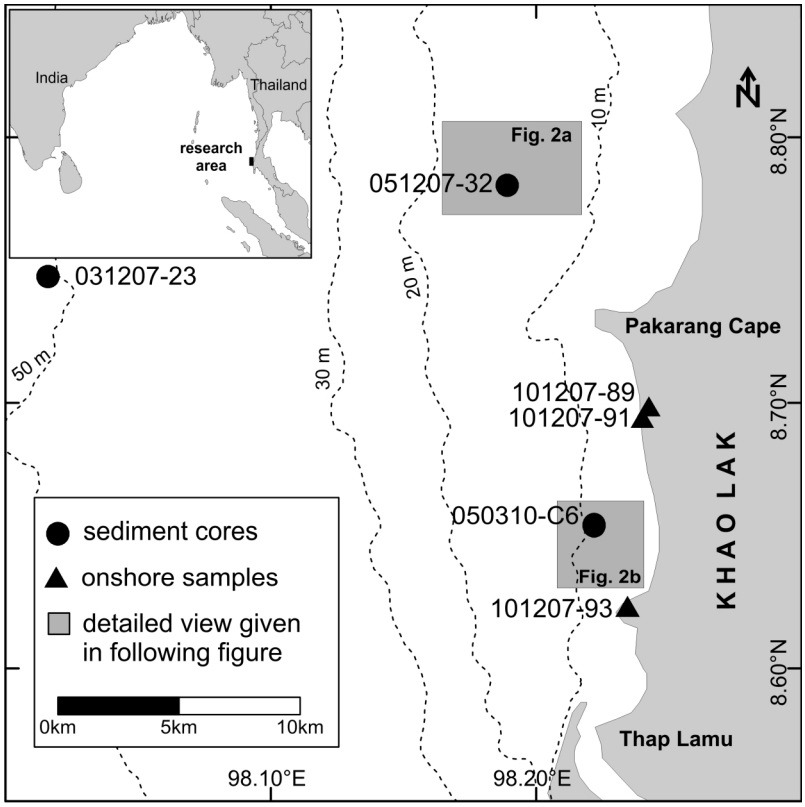


Fig. 1. Overview of the investigation area. Bathymetric data are based on nautical chart. The inset shows location of the study area within the Indian Ocean basin.

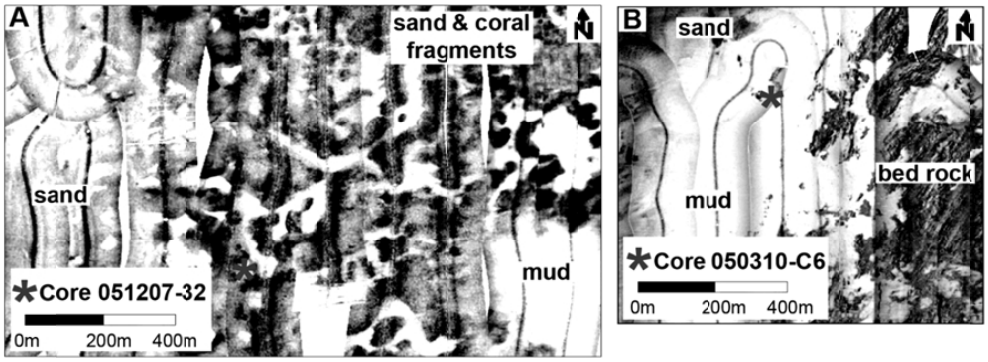


Fig. 2. Side scan sonar mosaics (refer to Fig. 1 for positions). The images show the location of sediment cores. (A) Sediment core 051207-32 was retrieved from a small mud-filled channel (displayed in light grey). The channels are separated by coarse sand, frequently containing coral fragments (displayed in dark grey). Further offshore, medium to coarse sands are deposited (displayed in intermediate grey). (B) Sediment core 050310-C6 was retrieved from a large patch covered by silty sediments (displayed in light gray) seaward of granitic bedrock outcrops. Coarse sands are deposited further offshore (displayed in dark grey).

Table 1. List of the analyzed sediment cores.

Core no.	Sampling year	Latitude (N)	Longitude (E)	Water depth (m)	Core recovery (cm)	Distance offshore (km)
050310-C6	2010	08°38.761′	98°12.967′	9.6	99	3.1
051207-32	2007	08°46.725′	98°11.814′	14.4	30	7.2
031207-23	2007	08°44.879′	98°01.173′	57.0	70	25.5

This technique is used to detect any internal sedimentary structures or unconformities not visible to the naked eye. The images (Figs. 3–5) show the relative change in sediment bulk density. High bulk density sediment, such as pebbles, shell fragments or sand, reduce X-ray penetration and are displayed in light grey, whereas low bulk density sediment, as observed for fine-grained sediments, is represented by dark grey or black (Bouma, 1964).

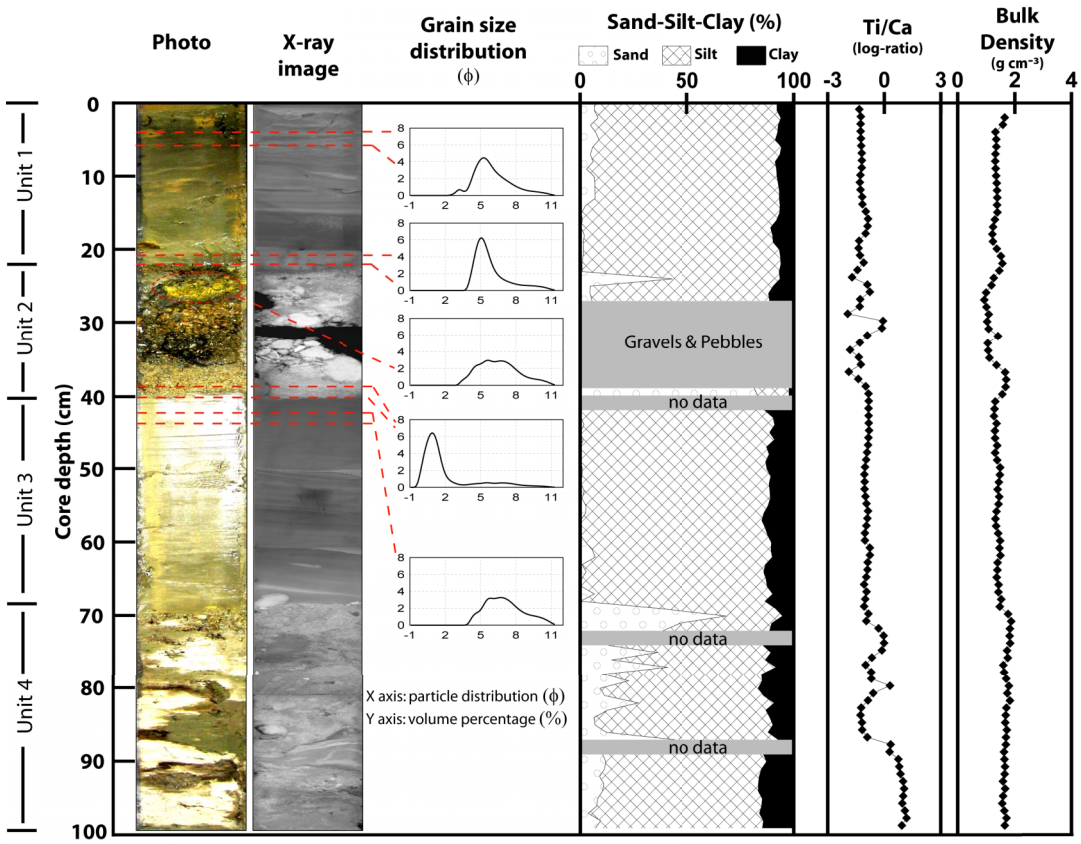


Fig. 3. Properties of sediments in core 050310-C6: division into sedimentary units, photo, X-ray image, typical grain size distributions (ϕ), amount of sand, silt and clay fraction (%), Ti/Ca log-ratio and bulk density.

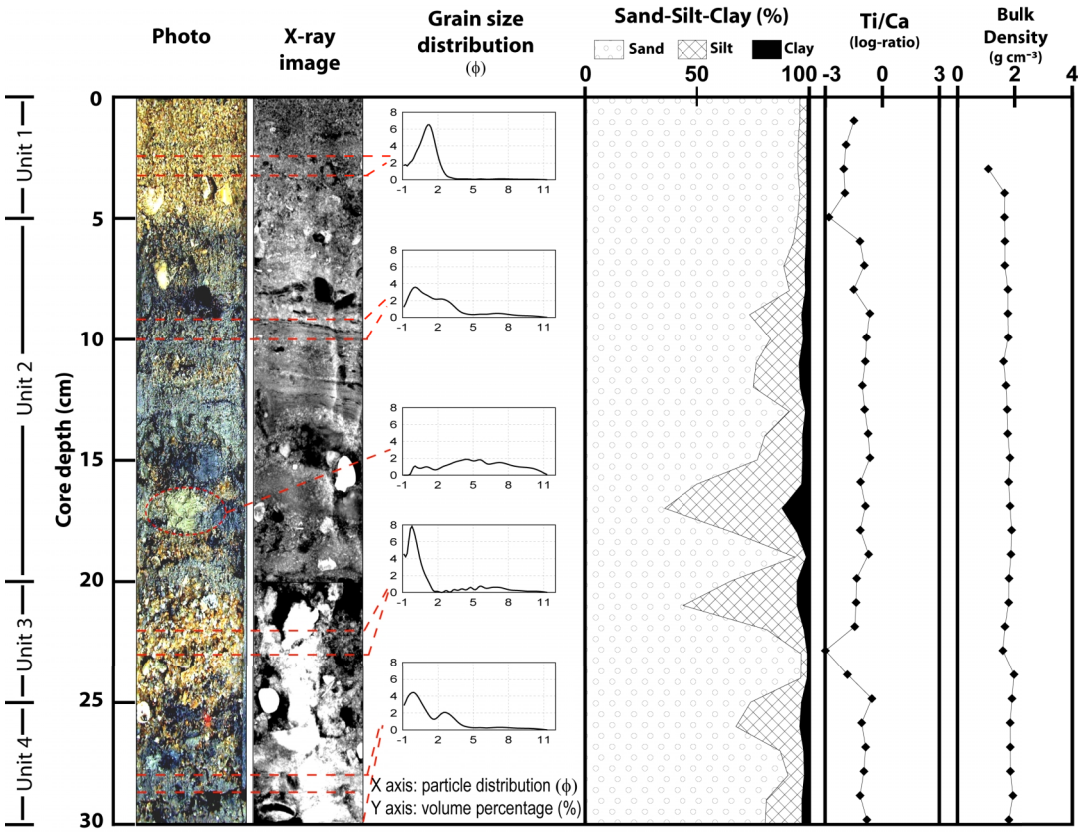


Fig. 4. Properties of sediments in core 051207-32: division into sedimentary units, photo, X-ray image, typical grain size distributions (ϕ), amount of sand, silt and clay fraction (%), Ti/Ca log-ratio and bulk density.

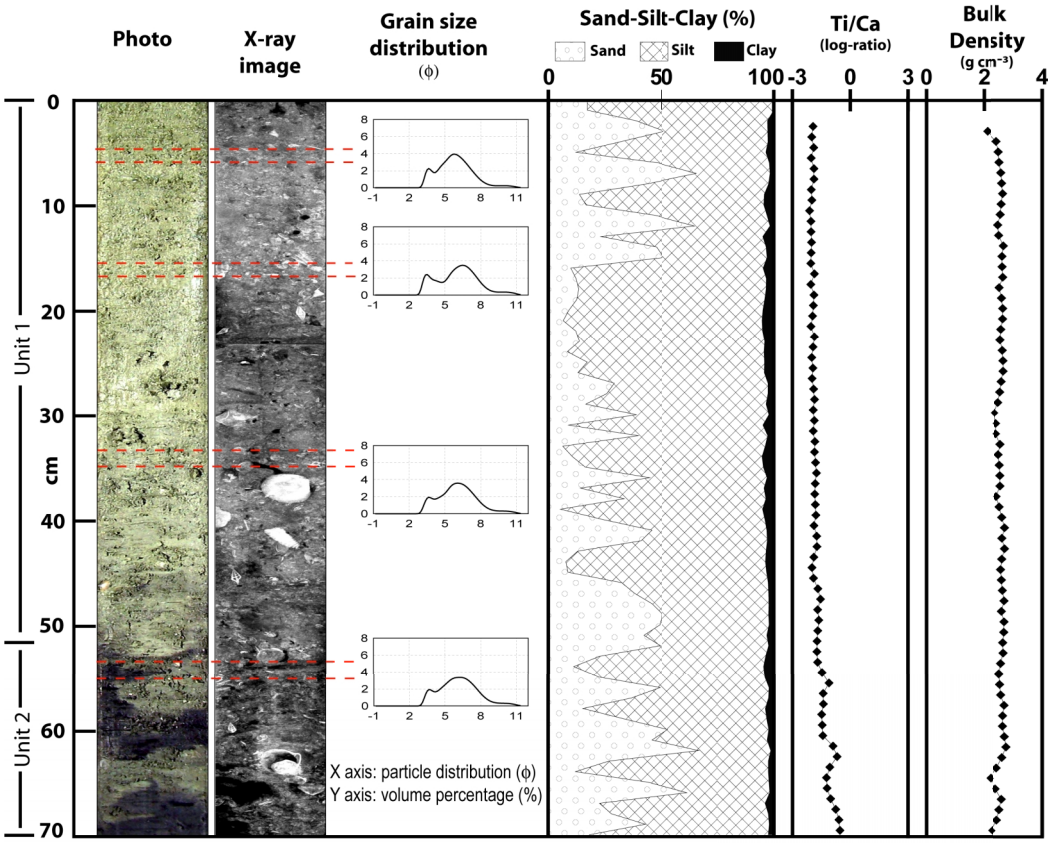


Fig. 5. Properties of sediments in core 031207-23: division into sedimentary units, photo, X-ray image, typical grain size distributions (ϕ), amount of sand, silt and clay fraction (%), Ti/Ca log-ratio and bulk density.

To determine the grain size distribution, core materials were sampled in 1 cm intervals. The materials were digested with HCl and H_2O_2 to remove carbonates and organic matter prior to analysis with a Coulter LS-13320 laser-based particle sizer device with a measuring range of 0.04 to 2000 μm. From core 050310-C6, samples composed mainly of grains in excess of sand size (27–38, 40–41, 72–73 and 87–88 cm) were not analysed. Statistical parameters of the grain size distribution (Figs. 3–5) were calculated using the logarithmic method of moments in GRADISTAT software (Blott and Pye, 2001).

^{210}Pb dating has been widely used for the assessment of sediment accumulation rates over the last 100 years. Total ^{210}Pb activity in the recent sediments comes primarily from two sources: supported (autochthonous) ^{210}Pb is produced by the radioactive decay of uranium radioactive chain isotopes in sediments and excess (allochthonous) ^{210}Pb is produced by the decay of ^{222}Rn, mostly in the atmosphere, and is then deposited with the sediments. The excess ^{210}Pb activity profile in the sediments is commonly characterised by the maximum activity at the surface and by the exponential decay, and is used for the assessment of sediment accumulation rates under several assumptions, depending on the applied model (Robbins and Edgington, 1975; Nittrouer *et al.*, 1979; Carpenter *et al.*, 1982). However, the shape of the ^{210}Pb profile may also reveal information on changes in sediment accumulation rates, the presence of major erosional events and the presence of event layers (e.g., Nittrouer *et al.*, 1979; Jaeger *et al.*, 1998; Sommerfield and Nittrouer, 1999; Crockett *et al.*, 2008; Szczuciński *et al.*, 2009). An event layer can usually be observed in the portion of the ^{210}Pb activity profile that shows no change downcore (usually due to rapid deposition during the event). However, more frequently, ^{210}Pb depletion is observed due to dilution processes in larger sediment masses and/or the admixture of sediments containing low ^{210}Pb activity due to a coarser grain size fraction.

^{210}Pb activity was measured for samples from core 050310-C6 using gamma spectrometry at the Leibniz-Laboratory for Radiometric Dating and Isotope Research (Kiel, Germany). The ^{210}Pb supported activities in the present study were assessed from minimum activities (40 Bq kg^{-1}) found in the sediment core, which are similar to the supported activities reported for similar sediments in the region (Szczuciński, 2010). However, supported activities are typically ascertained by averaging the nearly uniform, low-level ^{210}Pb activities below the region of radioactive decay or through independent measurements of ^{226}Ra (often through ^{214}Pb and ^{214}Bi; e.g., Zaborska *et al.*, 2007; Szczuciński *et al.*, 2009). Because the uniform activities in the lowermost part of the core were not reached and the ^{226}Ra was not measured, a precise estimation of ^{210}Pb supported activities could not be obtained. Supported ^{210}Pb activity values in the order of 10 to 26 Bq kg^{-1} were also reported by Kennedy *et al.* (2008) from the nearshore sediments on the Andaman Sea coast and are considered in the discussion of the calculated accumulation rates. The linear sediment accumulation rate (SAR) was determined from

the decline in the excess ^{210}Pb activities using the following equation (Robbins and Edgington, 1975; McKee *et al.*, 1983):

$$\mathrm{SAR} = \lambda \times z \times [\ln(A_0/A_z)]^{-1}$$

where λ is the decay constant ($= 0.0311$ year^{-1});

z is the depth in the core (cm)

A_0 is the specific activity of excess ^{210}Pb at a particular reference horizon (Bq kg^{-1})

A_z is the specific activity of excess ^{210}Pb at depth z below the reference horizon (Bq kg^{-1}).

Along with ^{210}Pb, ^{137}Cs activity was measured using gamma spectrometry.

4. Results

In water depths of 5 to 20 m, several regions covered with mud or revealing a channel-like morphology (Di Geronimo *et al.*, 2009; Feldens *et al.*, 2009, 2010, 2012), were found to host tsunami deposits. Representative sediment cores from these regions were selected for the present study (core 050310-C6 from a mud patch and core 051207-32 from the channel).

4.1 Sedimentary structure and grain size

Core 050310-C6, with a length of 99 cm, was retrieved from a water depth of 9.6 m (see Figs. 1 and 2 and Table 1). The core was subdivided into four major sedimentary units (Fig. 3).

- Unit 1 (0–22 cm), was composed of brown, poorly sorted laminated silt that contained up to 10.8% clay and up to 8.4% sand. Only a few bioturbation traces were preserved. This unit was divided into three subunits. The upper part (subunit 1a, 0–15 cm) was very finely laminated. It contained both horizontal and cross laminations, as well as erosional surfaces. Greyscale changes of the x-ray image suggested slight upward fining within the laminae. The second subunit (1b, 15–20 cm) was composed mostly of silt. In comparison to the units located above and below this subunit, it was slightly depleted in sand and enriched in clay. It contained very gently marked horizontal laminations. The upper contact was transitional while the lower contact was sharp. The lower subunit (1c, 20–22 cm) was composed of slightly coarser silt than the subunit above. The sediment was fining upward and conformably overlaid the sediments of unit 2.
- Unit 2 (22–40 cm) was composed of sand, gravel, clay clasts, pieces of laterites, rocks and shells. The arrangement of these particles was subhorizontal, with the largest clasts being up to 3 cm in diameter. Based on a detailed analysis, this unit was divided into two subunits. The upper subunit 2a (22–38 cm) was composed of sediments ranging from normal grading gravels to fine sand. The lower contact with subunit 2b was erosional. Subunit 2b (38–40 cm) was composed of laminated medium to coarse sand.
- Unit 3 (40–69 cm) was represented by laminated silt and clayey silt that was slightly finer than the sediment forming unit 1. Its upper contact was erosional and the basal contact was sharp. Within this unit, at least three fining-upward sequences were differentiated (3a: 40–50 cm, 3b: 50–61 cm, and 3c: 61–69 cm). These sequences began with thin sandy silt laminae and became finer with decreasing depth, eventually becoming clayey silt. Moreover, in subunit 3b, an erosional surface was preserved in the middle of the subunit. The lamination in the unit was slightly inclined, and few small vertical burrows were preserved. A 2 cm-diameter gravel was found at the bottom of this unit.
- Unit 4 (69–99 cm) was composed of laminated muddy sand, which was partly intercalated with consolidated mud that was almost white. The layering and laminations were partly disturbed. In the upper 10 cm of this unit, white consolidated mud did not extend continuously in the horizontal plane, while the lowermost 5 cm of the sediment in the core was composed entirely of this type of sediment. Some small gravel components were found at a depth of 92–94 cm.

Core 051207-32 was retrieved from a water depth of 14.4 m and was 30 cm in length (Figs. 1 and 2, Table 1). This core also revealed several different sediment types, and was therefore divided into four units (Fig. 4):

- Unit 1 (0–5 cm) was composed of a yellowish medium to coarse sand with shell fragments. This unit had a massive structure and conformably overlaid the upper surface of unit 2.
- Unit 2 (5–20 cm) had a relatively complex composition. It was composed of consolidated sandy mud, muddy sand and sand. It was variable in colour, ranging from yellow or light green to olive or black. It was partly laminated, but also contained muddy clasts, pieces of wood, laterites and red brick fragments (artefacts). Sand appeared in the form of intercalations. Moreover, gravel and small pebbles were scattered throughout the entire unit. The grain size in this unit did not show normal grading, except for the upper part. The lower contact was sharp and uneven.
- Unit 3 (20–25 cm) was a massive layer of coarse sand and gravels.
- Unit 4 (25–30 cm) was composed of muddy sand. The upper part contained admixtures of coarse sand from unit 3.

Core 031207-23 was retrieved from a water depth of 55.4 m and was 70 cm long (Figs. 1 and 5, Table 1). It was composed of poorly sorted sandy silt and silty sand, with only 5.2% of clay. Shells were abundant in this core, and it was possible to distinguish two units.

- Unit 1 (comprising the upper approx. 51 cm) was composed mostly of silty sand with intercalations of sandy silt. Laminations were poorly preserved and shells were less abundant than in the lower unit. No distinct boundary was observed between the units, and the lower boundary was selected in conjunction with changes in geochemistry. The upper part of the unit contains sandy intercalations of several cm-thick. The lowest sand content was found at a depth of 20–30 cm.
- Unit 2 (approx. 51–70 cm) was also composed of silty sand intercalated with sandy silt. The intercalations appeared in the form of poorly preserved layers. This

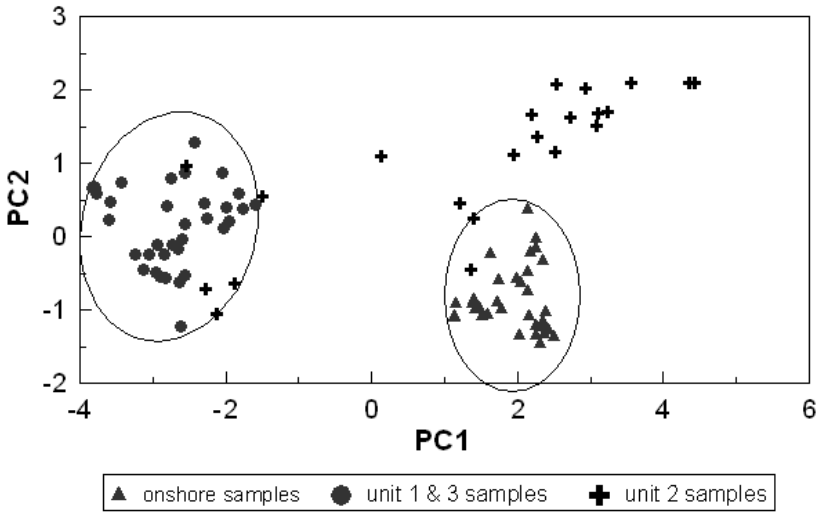


Fig. 6. PCA for chemical elemental composition data (from XRF core scanner) of onshore sediment samples which were retrieved from Khao Lak coastline (101207-89, 101207-91 and 101207-93; see position on Fig. 1) and offshore sediment samples from unit 1, 3 and 2 of core 050310-C6. Unit 1 and 3 are interpreted as post- and pre-tsunami deposits and unit 2 as tsunami deposits.

unit contained more shell fragments than unit 1.

4.2 Geochemical and physical properties

Log-ratios of Titanium (Ti) and Calcium (Ca), which represent the relative variations of terrigenous versus marine constituents, are shown in Figs. 3–5. Ti is enriched in tropical soils in the form of laterites and bauxites and is relatively inert against diagenetic processes (Calvert and Pedersen, 2007), whereas Ca reflects the occurrence of $CaCO_3$, which is mainly produced under marine conditions (Hofmann *et al.*, 2005; Weltji and Tjallingii, 2008). In all of the studied cores, changes in the Ti/Ca log-ratio roughly reflected the sedimentary units described above. In core 050310-C6 (Fig. 3), the ratio was stable in units 1 and 3, variable in unit 2 and generally elevated in unit 4. In core 051207-32 (Fig. 4), this ratio was slightly lower in the sandy, shell-rich units (units 1 and 3). This ratio was mostly uniform in core 031207-23 (Fig. 5), where only a slight downward increase was observed in unit 2.

The PCA revealed that two principal components of onshore samples and sediment samples from core 050310-C6 (PC1 and PC2) explained 80.5% of the cumulative variance. PC1 (accounting for 69.7% of the variance) had highly negative factor scores for terrestrial elements, such as Al, Si, S, K, Ti, Mn and Fe. PC2 (accounting for 10.8% of the variance) had highly positive factor scores for Ca and Si. This finding indicates that PC2 was characterised by a marine component, and Si was most likely associated with marine sands. Plotting these two main factors together (Fig. 6) indicates the grouping of sediment samples (circled on the graph). Samples from unit 2 of core 050310-C6 and onshore sediments had positive values for PC1, which indicated a stronger terrestrial influence than units 1 and 3. For PC2, most of units 1, 2 and 3 of core 050310-C6 had positive values, whereas onshore samples had negative values. This finding suggests that unit 2 of core 050310-C6 also had marine components. Therefore, sediments from unit 2 of core 050310-C6 were a mixture of terrestrial and marine components.

The bulk density of the studied cores was generally uniform, with the exception of slight variations in units 2 and 4 of core 050310-C6. The other measured physical properties did not reveal significant changes.

4.3 ^{210}Pb data and interpretation

The total ^{210}Pb activity profile of core 050310-C6 (Fig. 7) revealed a general decline of activities with depth, interrupted by one major and several minor anomalies that were interpreted as being event layers or periods of accelerated sediment accumulation. These event layers reflect a non-steady sedimentation regime.

Using data on sedimentary structures as supporting information, the total ^{210}Pb profile was divided into three major parts, referred to as sedimentary units 1, 2 and 3 (Fig. 3).

- The upper portion of unit 1 was composed of three sediment segments (approximately 0–15 cm, 15–20 cm and 20–22 cm), which were most likely deposited during events or periods of accelerated accumulation, as indicated by step-like activity profiles. The uppermost segment could also be interpreted as a surface mixed layer; however, the well-preserved laminations suggest that sediment mixing due to bioturbation was not significant. Precise calculations of sediment accumulation rates were not possible since the accumulation was not steady and the background activities were only assumed. Depending on the ^{210}Pb supported activities used and considering the analytical accuracy, the calculated sediment accumulation rates were in the range of 1.3 to 5.7 cm y^{-1}. In general, the lower the supported activities applied, the higher the accumulation rate that we obtain. Since the assumptions for this method were not fully met (the accumulation was not steady), the results should be regarded as an approximation; we can infer from these results that the accumulation rate occurring is in the order of a few cm per year. This finding suggests that the unit had to be deposited over a period of several to a dozen years. Considering that the core was sampled in 2010, it is

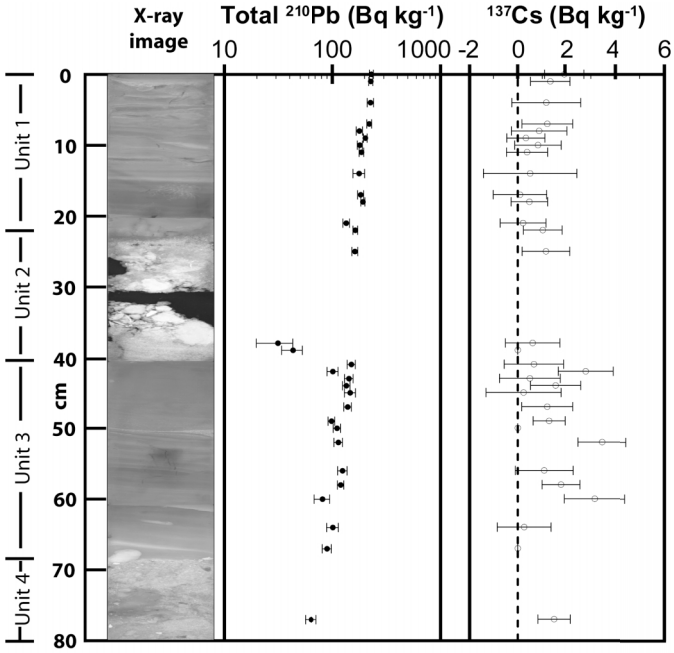


Fig. 7. Total ^{210}Pb activity (Bq kg^{-1}) profile, ^{137}Cs activity profile and X-ray image of core 050310-C6. The lowest total ^{210}Pb activity was measured in the sand layer (38–40 cm depth), and is close to assumed supported ^{210}Pb activity.

possible that the sediments in unit 1 were deposited after 2004.

- Unit 2 (around 22 to 40 cm) was partly composed of coarse sediments, which do not contain excess ^{210}Pb, as indicated by a sample taken from a depth of 38 cm which showed only the activity of supported ^{210}Pb. The activities in the upper part of the unit and below are similar. Therefore, this unit was assumed to be an event layer. Moreover, similar ^{210}Pb activities in the lowermost part of unit 1 and in the uppermost part of unit 3 also suggested that the event that created unit 2 was effectively depositional and caused little or no erosion of the older sediments.
- Unit 3 (below 40 cm) revealed a general decline of ^{210}Pb activity with depth; however, there were three segments with slightly reversed trends. Those segments were found at approximately the following depths: 40–50, 50–61 and 61–69 cm. These segments roughly corresponded to the fining-upward subunits 3a, 3b and 3c and most likely represented sedimentary events or periods of accelerated deposition. Calculations of sediment accumulation rates in this unit, under the conditions specified above, indicated rates of approximately 0.7 to 2.4 cm y^{-1}.

The ^{137}Cs values indicated very low activities, often close or below minimum detection activity levels (Fig. 7). However, the presence of ^{137}Cs throughout the core supports a ^{210}Pb-based interpretation of a high accumulation rate since ^{137}Cs has been present in the environment since the early 1950s (Robbins *et al.*, 1978). The very low activities observed were due in part to high accumulation rates and the dilution effect of the radioisotope in the large mass of sediment, and in part to generally low ^{137}Cs fallout at this latitude (see discussion in Szczuciński *et al.*, 2009).

5. Discussion

5.1 Evidence of the 2004 Indian Ocean tsunami event layer

Sediment cores were collected within three to six years after the 2004 Indian Ocean tsunami. In the period between the tsunami and the time of collection, neither big storms nor intense anthropogenic offshore activities affected the region. Several tropical cyclones were recorded during the 20th century and passed near the study area; the last major cyclone in this region was Cyclone Gay in 1989 (Kumar *et al.*, 2008; Brand, 2009). However, despite the fact that these events were recorded in middle continental shelf deposits (Szczuciński, 2010), they have not been found to cause significant sedimentological change in the eastern coastal region of the Andaman Sea due to their westward-oriented tracks (Brand, 2009). Consequently, the documented sedimentary event layers found in the inner shelf cores are considered to represent potential effects of the 2004 tsunami. For this event, maximum water velocities over the inner shelf have been modelled and show values in the order of several m s^{-1} (Suppasri *et al.*, 2011).

In core 050310-C6, the most likely result of deposition by the 2004 tsunami was sediment unit 2, which was composed of poorly sorted sand and gravel between fine-grained deposits. This event layer contains compounds of terrestrial and marine origin: clay clasts, pieces of laterites, rocks and shells. The mixed provenance of the sediments was supported by the PCA, evaluating their chemical composition. These sediments were similar to samples taken from potential onshore sources, as well as marine sands (Fig. 6). Unit 2 is also marked by similar ^{210}Pb activities above and below this unit and by anomalously low ^{210}Pb activity in some samples taken from this unit, which supports its event origin. The deposits above and below (units 1 and 3) represent rapidly accumulating sediments (>1 cm y^{-1}) with

episodes of erosion and sedimentation indicated by sedimentary structures seen in X-radiographs (Fig. 3) and reflecting the dynamic nature of shallow water environments (water depths of approximately 10 m). The ^{210}Pb-based assessment of accumulation rates confirmed, within error ranges, that unit 2 was several years old and could have been generated by the 2004 Indian Ocean tsunami.

Core 051207-32 was sampled within three years of the tsunami. The sand layer forming the uppermost portion of this core was very similar to sediments covering most of the continental shelf at water depths of 15 to 22 m (e.g., Feldens *et al.*, 2009, 2010, 2012). This layer conformably covers units 2, 3 and 4 (>25 cm in thickness), which revealed many features of event deposits, such as poorly sorted sediments ranging from mud to gravel, muddy clasts, pieces of wood, laterites and pieces of red brick. The latter suggests that the sediments had material of terrigenous origin included. The changing character of the deposits (mud/sand/mud) may reflect changing flow velocities and directions, while minor changes in the Ti/Ca log-ratio may reflect changes in sediment sources. Based on this evidence and the assumptions presented above, units 2–4 are interpreted as having been deposited during the passage of the tsunami wave train.

The potential tsunami deposits in the two cores differed from one another in terms of the number of units with event deposits, their sedimentary characteristics and the relative input of terrestrial material. These characteristics may have been related to the various water depths (9.6 and 14.4 m), the distance offshore (3.1 and 7.2 km), and variations in the hydrodynamics of tsunami waves. Video records of the 2004 tsunami, which show the situation offshore Khao Lak revealed a high variability in flow patterns, including the formation of giant gyres (e.g., Di Geronimo *et al.*, 2009).

Although there is a supporting age control for one core (in core 051207-32, it was not possible to evaluate those data due to the lack of suitable sediments above and below the event layer) and there was no evidence of recent heavy storms in the area, one may consider that the event deposits were formed by storms or cyclones. Storm deposits (tempestites) in shallow environments may reveal many various features depending on local conditions. There are no studies of storm deposits on the inner shelf in the Andaman Sea. However, in general, shallow water storm deposits may be sandy or muddy and often have basal erosional contact, normal gradation, plane lamination, wave ripples, thicknesses ranging from a few to more than 30 cm and hummocky cross stratification (e.g., Einsele *et al.*, 1991; Weidong *et al.*, 1997; Allison *et al.*, 2005). Storm deposits may contain only one or many of these features. Moreover, as indicated by modern examples (e.g., Allison *et al.*, 2005), changing flow conditions are also observed during a hurricane, and near-bottom velocities can reach more than 1 m s^{-1}. Thus, many characteristics of storms and tsunamis over the continental shelf that affect sedimentation may be similar. The major features observed in the documented event layers, which are less likely, or unlikely, in storm deposits are: the frequent presence of terrestrial components, poor sorting and a massive character of some layers. Terrestrial components may be found in storm deposits if there is a big river nearby and can also occur due to coastal erosion. However, storms primarily tend to erode the coastline (beach, dune), while tsunamis may also deliver terrestrial material further inland such as human artefacts and plants. The poor sorting and massive character of sediments may indicate a kind of sediment gravity mass flow (expected during backwash). Gravity mass flows are also known to be generated by storms, for instance in form of wave-induced fluid mud flows (e.g., Nittrouer *et al.*, 2007). However, the fluid mud flow deposits are usually better sorted, do not include oversized clasts and contain less terrestrial material when compared with tsunami deposits.

Sediments in core 031207-23 were taken from a water depth of 57 m. Distinct event layers were not recognised in this core, suggesting that the 2004 tsunami had no or very limited depositional effect in this region, which is supported by conclusion of Szczuciński (2010) based on ^{210}Pb analyses of sediment cores from the mid continental shelf offshore Khao Lak.

5.2 Processes of offshore sedimentation by the tsunami

Assuming that the interpretation of the event layers as tsunami deposits in cores 050310-C6 (unit 2) and 051207-32 (units 2–4) is correct, these deposits may serve as a source of information about tsunami sedimentation processes.

In core 050310-C6 (water depth 9.6 m, 3.1 km offshore), unit 2 (interpreted as being a tsunami deposit) began with a subunit that is approximately 2 cm thick (2b). It is composed of horizontally laminated medium to coarse sand. This subunit showed no indication of terrigenous origin (the Ti/Ca ratio was similar to that in the sediments beneath it). There are several processes able of forming laminated sandy deposits, including flows in the upper and lower flow regimes, storms and turbidity currents (Reineck and Wunderlich, 1998). In the case presented in this study, it is likely that the sand was transported from water depths of 15–22 m, where medium and coarse sands are common (Feldens *et al.*, 2012), toward the shoreline during the run-up phase. To confirm this fact, a detailed analysis of microfossils is recommended in the future. The transport of sand could occur as a unidirectional flow in lower or upper plane bed conditions. Later on, an erosional surface was created, along with the deposition of unit 2a (approximately 16 cm thick). The subunit is likely to have been deposited as a result of decelerating flow conditions because it revealed a normal gradation. Considering the largest size of pebbles found in the lower part of the unit, the water velocity had to be at least in the order of several tens of cm s^{-1}. This subunit contains many terrigenous components; moreover, its chemical composition is similar to the onshore sediments analysed (Fig. 6). Therefore, this unit probably was created during the backwash flow.

Units 2–4 in core 051207-32 (water depth 14.4 m, located 7.2 km offshore) could be interpreted as tsunami deposits. Because the retrieved sediment core does not reach below unit 4, it is unclear how the sequence of tsunami deposits begins. The lowermost unit is composed of massive consolidated mud with scattered gravel, pieces of wood, mud clasts and red brick fragments. Its chemical composition also suggests a terrigenous origin, and thus, this unit was most likely formed during backwash. This finding is sup-

Table 2. Comparison of selected signatures of offshore tsunami deposits.

Source of data	van den Bergh *et al.* (2003)	Abrantes *et al.* (2008)	Goodman-Tchernov *et al.* (2009)	Paris *et al.* (2010)	Smedile *et al.* (2011)	Present study
Region	Java, Indonesia	Portuguese shelf off Lisbon	coastal zone of Israel, Eastern Mediterranean	Sumatra, Indonesia	Augusta Bay, Eastern Sicily, Italy	Andaman Sea, Thailand
Age of tsunami (AD)	1883	1755, 1969	1630–1550 BC, 115 AD, 551 AD	2004	1169, 1693, 1908, and 8 other events	2004
Distance offshore (km)	3–14	6–15	∼4	0–5	2	3–7
Water depth (m)	2–27	88–105	10–20	10–25	72	9–15
Thickness of tsunami deposits (cm)	1–48	2–143	up to 40	boulder size up to 15 m	few to about 30	20–>25
Type of sedimentary contacts	lower-sharp, often erosional; upper sharp or blurred due to bioturbations	no visible contact, sharp contact, erosional surface	erosional lower contact	sharp	not visible, sharp	lower-sharp, erosional; upper-sharp
Grain size	sand, gravel (mainly carbonate) and mud size tephra	mud, sand and gravels	sandy mud, muddy sand, pebbles	sand, boulders of various sizes (up to 15 m)	sandy mud; often with bimodal grain size distribution	mud, sand, gravels and pebbles
Sediment sorting	poorly sorted	well sorted, poorly sorted	poorly sorted	poorly sorted	moderately to poorly sorted	poorly sorted
Terrigenous components	volcanic rock fragments	no	organic material, pumice	trees	no	wood, mud clasts, laterite
Anthropogenic artifacts	no	no	pottery	yes	no	brick pieces
Fossils	abundant broken shells; presence of autochthonous (e.g. Turritellas) and allochthonous (e.g. oysters) organisms	shell fragments	molluscs; change in foraminifera and diatom assemblages	coral boulders	significant amount of displaced epiphytic benthic foraminifera	shells
Geochemical indicators	variable Ca and Mn	variable Fe and Ca content	not studied	not studied	no	variable Ti/Ca ratio
Number of layers	1–>6	1	1–2	1	1	2–>3
Sedimentary structures	fining upward, laminated, coarsening upward at the base, shell layers	laminations, turbidite	imbrication, rip-up clasts, fining upward sequence	lobe shaped boulders arrangement; segregation of boulders with distance	not reported	laminations, massive structures, fining upward sequence, internal erosional surfaces
Presence of tephra layer	tephra and pumices	no	pumices	no	tephra is present but not related to the tsunami deposits	no
Presence of ^{210}Pb event like profile	^{210}Pb used for age control	yes	not studied	not studied	no	yes

ported by the presence of over-sized clasts "floating" in the finer sediment mass and by a relatively high sediment consolidation. This subunit was approximately 5 cm thick and was covered by coarse sand and gravel with a massive appearance. The Ti/Ca log-ratio in this thin layer was lower than that of the layer below, so these sediments may have no, or a lower, terrigenous contribution. The lack of clear lamination suggests that the deposition was rapid. The sand was covered by a complex, stiff mud with many over-sized compounds of sand and gravel (unit 2), which is very similar to the lowermost portion of unit 4. This finding is interpreted as being an effect of the backwash flow, although the

terrestrial contribution is not clear in the sediment geochemistry. However, during the backwash from the second wave, the inundated land was already mostly covered with water (e.g., Choowong *et al.*, 2008), so there was much less erosion on land than during the first wave backwash phase. The upper part of this unit was partly laminated and reflected an upward fining in grain size. It is possible that the sediment-gravity flow evolved, due to a decrease in flow density, into simple settling from suspension, or that the unit represents two (or more) events (or pulses).

5.3 Diagnostic features of offshore tsunami deposits

Onshore tsunami deposits are characterised by a complex set of diagnostic features that have been presented in many studies (e.g., Dawson and Shi, 2000; Goff *et al.*, 2001; Shiki *et al.*, 2008; Bourgeois, 2009; Mamo *et al.*, 2009; Chagué-Goff, 2010; Goto *et al.*, 2010; Chagué-Goff *et al.*, 2011). However, such criteria have not yet been summarised for offshore tsunami deposits, and the published data are limited. In the literature, offshore tsunami deposits are frequently related not only to the direct effect of deposition from tsunami-induced water flow (run-up or backwash), but also to tsunami-induced secondary processes such as turbidity currents (Dawson and Stewart, 2007; Shiki *et al.*, 2008) and formation processes of so-called "homogenites" (Cita *et al.*, 1996). The present discussion is limited to the recent shallow water deposits most likely formed due to direct deposition from tsunamis.

Table 2 summarises major features of tsunami deposits on the inner shelf or within 15 km of land that were generated by the eruption of Santorini in ca. 1630–1550 BC (Goodman-Tchernov *et al.*, 2009), the eruption of Krakatau in 1883 (van den Bergh *et al.*, 2003), earthquakes on the Portuguese margin in 1755 and 1969 (Abrantes *et al.*, 2008), several tsunamis in the Mediterranean (Smedile *et al.*, 2011) and the 2004 Indian Ocean tsunami (Paris *et al.*, 2010 and present study). Several sedimentological studies (e.g., Massari and D'Alessandro, 2000; Takashimizu and Masuda, 2000; Fujiwara and Kamataki, 2007) on potential shallow marine tsunami deposits from the geological past are not included in the discussion because they are not related to a specific tsunami event but are interpreted as being tsunami-generated based on sedimentological properties. The comparison proves how variable offshore tsunami deposits can be. The deposits may form an event layer several cm, several tens of cm or even over 1 m thick. The layers tend to have sharp lower contacts, which are often erosional. The upper contact may be blurred by bioturbations. They are composed of all grain size classes; often several classes are present in one layer resulting in poor sorting. Frequently, offshore tsunami deposits contain some typical terrigenous particles (wood, plants, etc.) and, if available, human-made pottery, brick, etc. This finding suggests the important role of tsunami backwash flows in the formation of these deposits. The fossil assemblage within the event layers may represent organisms from various environments. There was a high degree of variation in typical geochemical indicators of marine (Ca) or terrestrial origin (Fe, Mn, Ti). The tsunami deposits may appear in the form of a single layer or several layers and may present the whole range of sedimentary structures: laminations, fining or coarsening upward, a massive structure, erosional surfaces, imbrications, lag deposits, etc. Finally, the key to the interpretation of these structures is accurate dating, with analyses such as ^{210}Pb activity profiles being particularly helpful. For instance, in the case of 1969 tsunami deposits on the Portuguese shelf, there was no visible change in sediment properties apart from a slight change in the ^{210}Pb profile (Abrantes *et al.*, 2008).

The presented comparison of offshore tsunami deposit characteristics reveals that their interpretation may be even more difficult than in the case of onshore tsunami deposits. It appears that the identification will always have to be based on several characteristics and a broad knowledge of local conditions. Distinguishing offshore tsunami and storm deposits will be a considerable challenge for future studies.

6. Conclusions

The present study provided new evidence of probable 2004 Indian Ocean tsunami deposits left on the inner shelf of the Andaman Sea (Thailand) and identified the diagnostic sedimentological and geochemical properties of these deposits. The deposits were restricted to the shallow marine environment (water depths of 9–15 m) within 8 km of the shoreline. Deposition occurred during the run-up phase, causing landward redeposition of marine sand, and during backwash flow events, which also deposited terrigenous sediments. The transport and deposition of sediments were driven by several processes, including unidirectional flow in various flow regimes and high-density sediment-gravity flow.

Typical features of these event deposits included the following: a thickness in the order of 20–25 cm, a wide range of grain sizes and poor sorting, in contrast to underlying and overlying sediments, the presence of several layers, marine sand alternating with poorly sorted mud with terrigenous and anthropogenic components, representing different hydrodynamic conditions (run-up and backwash phase).

Geochemical and geophysical analyses, and particularly ^{210}Pb activity measurements, were helpful supplementary tools in the identification of event layers. However, the analysis of available data on offshore tsunami deposits showed that there is no single set of signatures that could be universally applied to identify these deposits. Future studies will need to include more proxies (microfossils and advanced geochemistry in particular) to establish an identification key for offshore tsunami deposits.

Acknowledgments. We are grateful to Phuket Marine Biological Center (PMBC) for supporting us with ship time of RV Chakratong Tongyai and RV Boonlert Pasook as well as with other facilities during field campaigns. We further thank Dr. Warner Brückmann and Dr. Dieter Garbe-Schönberg for supporting the MSCL and XRF scanner measurements. Gratitude is also expressed to Dr. Nils Anderson and Dr. Helmut Erlenkeuser for their helpful comments and ^{210}Pb determination. We thank Dr. Björn Heise and Daniel Unverricht for their tremendous help and inspiring ideas. Acknowledgements are due to Dr. P. M. De Martini and Dr. C. Chagué-Goff for their very constructive and detailed reviews. This research was funded by Deutsche Forschungsgemeinschaft (DFG) grant SCHW 572/11, National Research Council of Thailand (NRCT) and DAAD (Deutscher Akademischer Aus-

tausch Dienst) fellowship provided to Ms. Daroonwan Sakuna for a Ph.D. study at Kiel University.

References

Abrantes, F., U. Alt-Epping, S. Lebreiro, A. Voelker, and R. Schneider, Sedimentological record of tsunamis on shallow-shelf areas: The case of the 1969 AD and 1755 AD tsunamis on the Portuguese Shelf off Lisbon, *Mar. Geol.*, **249**, 283–293, 2008.

Allison, M. A., A. Sheremet, M. A. Goñi, and G. W. Stone, Storm layer deposition on the Mississippi-Atchafalaya subaqueous delta generated by Hurricane Lili in 2002, *Continental Shelf Res.*, **25**, 2213–2232, 2005.

Bahlburg, H., M. Spiske, and R. Weiss, Comment on "Sedimentary features of tsunami backwash deposits in a shallow marine Miocene setting, Mejillones Peninsula, northern Chile" by G. Cantalamessa and C. Di Celma [*Sediment. Geol.*, **178**, 259–273, 2005], *Sediment. Geol.*, **228**, 77–80, 2010.

Bahr, A., F. Lamy, H. Arz, H. Kuhlmann, and G. Wefe, Late glacial to Holocene climate and sedimentation history in the NW Black Sea, *Mar. Geol.*, **214**, 309–322, 2005.

Bell, R., H. Cowan, E. Dalziell, N. Evans, M. Ó Leary, B. Rush, and L. Yule, Survey of impacts on the Andaman Coast, Southern Thailand following the great Sumatra-Andaman earthquake and tsunami of December 26, 2004, *Bull. New Zealand Soc. Earthq. Eng.*, **38**, 123–148, 2005.

Best, A. I. and D. E. Gunn, Calibration of marine sediment core loggers for quantitative acoustic impedance studies, *Mar. Geol.*, **160**, 137–146, 1999.

Blott, S. J. and K. Pye, Gradistat: a grain-size distribution and statistics package for the analysis of unconsolidated sediments, *Earth Surf. Process. Landforms*, **26**, 1237–1248, 2001.

Bouma, A. H., Notes on X-ray interpretation of marine sediments, *Mar. Geol.*, **2**, 278–309, 1964.

Bourgeois, J., Geologic effects and records of tsunamis, in *The Sea, Volume 15: Tsunamis*, edited by Robinson, A. R. and E. N. Bernard, 53–91, Harvard University press, Amsterdam, 2009.

Brand, S., Typhoon havens handbook, in http://www.nrlmry.navy.mil/port_studies/Havens_Handbook/thh-nc/0start.htm, edited by Brand, S., 2009.

Calvert, S. E. and T. F. Pedersen, Elemental proxies for paleoclimatic and paleoceanographic variability in marine sediments: interpretation and application, in *Developments in Marine Geology*, edited by Hillaire-Marcel, C. and A. de Vernal, 567–644, 2007.

Cantalamessa, G. and C. D. Celma, Sedimentary features of tsunami backwash deposits in a shallow marine Miocene setting, Mejillones Peninsula, northern Chile, *Sediment. Geol.*, **178**, 259–273, 2005.

Carpenter, R., M. L. Peterson, and J. T. Bennett, ^{210}Pb-derived sediment accumulation and mixing rates for the Washington continental slop, *Mar. Geol.*, **48**, 135–164, 1982.

Chagué-Goff, C., Chemical signatures of paleootsunamis: A forgotten proxy?, *Mar. Geol.*, **271**, 67–71, 2010.

Chagué-Goff, C., J.-L. Schneider, J. R. Goff, D. Dominey-Howes, and L. Strotz, Expanding the proxy toolkit to help identify past events—Lessons from the 2004 Indian Ocean Tsunami and the 2009 South Pacific Tsunami, *Earth-Sci. Rev.*, doi:10.1016/j.earscirev.2011.03.007, 2011.

Choowong, M., N. Murakoshi, K. Hisada, P. Charusiri, T. Charoentitirat, V. Chutakositkanon, K. Jankaew, P. Kanjanapayont, and S. Phantuwongraj, 2004 Indian Ocean tsunami inflow and outflow at Phuket, Thailand, *Mar. Geol.*, **248**, 179–192, 2008.

Cita, M. A., A. Camerlenghi, and B. Rimoldi, Deep-sea tsunami deposits in the eastern Mediterranean: new evidence and depositional models, *Sediment. Geol.*, **104**, 155–173, 1996.

Crockett, J. S., C. A. Nittrouer, A. S. Ogston, and M. A. Goni, Variable styles of sediment accumulation impacting strata formation on a clinoform: Gulf of Papua, Papua New Guinea, in *The Fly River, Papua New Guinea: Environmental Studies in an Impacted Tropical River System*, edited by Bolton, B., 177–207, Elsevier, Amsterdam, 2008.

Dawson, A. G. and S. Shi, Tsunami deposits, *Pure Appl. Geophys.*, **157**, 875–897, 2000.

Dawson, A. G. and I. Stewart, Tsunami deposits in the geological record, *Sediment. Geol.*, **200**, 166–183, 2007.

Dawson, S., Diatom biostratigraphy of tsunami deposits: Examples from the 1998 Papua New Guinea Tsunami, *Sediment. Geol.*, **200**, 328–335, 2007.

Di Geronimo, I., M. Choowong, and S. Phantuwongraj, Geomorphology and superficial bottom sediments of Khao Lak coastal area (SW Thailand), *Polish J. Environ. Stud.*, **18**, 111–121, 2009.

Einsele, G., W. Ricken, and A. Seilchaer, in *Cycles and Events in Stratigraphy*, edited by Einsele, G., W. Ricken, and A. Seilchaer, 955 pp., Springer-Verlag, Berlin, Heidelberg, New York, 1991.

Feldens, P., K. Schwarzer, W. Szczuciński, K. Stattegger, D. Sakuna, and P. Somgpongchaiykul, Impact of 2004 tsunami on seafloor morphology and offshore sediments, Pakarang Cape, Thailand, *Polish J. Environ. Stud.*, **18**, 63–68, 2009.

Feldens, P., D. Sakuna, P. Somgpongchaiykul, and K. Schwarzer, Shallow water structures in a tsunami-affected area (Pakarang Cape, Thailand), in *From Brazil to Thailand—New Results in Coastal Research*, *Coastline Reports*, edited by Schwarzer, K., K. Schrottke, and K. Stattegger, **16**, 15–24, 2010.

Feldens, P., K. Schwarzer, D. Sakuna, W. Szczuciński, and P. Sompongchaiyakul, Sediment distribution on the inner continental shelf off Khao Lak (Thailand) after the 2004 Indian Ocean tsunami, *Earth Planets Space*, **64**, 875–887, 2012.

Fujiwara, O. and T. Kamataki, Identification of tsunami deposits considering the tsunami waveform: An example of subaqueous tsunami deposits in Holocene shallow bay on southern Bobo Penisular, Central Japan, *Sediment. Geol.*, **200**, 295–313, 2007.

Goff, J. C., C. Chagué-Goff, and S. Nichol, Paleotsunami deposits; a New Zealand Perspective, *Sediment. Geol.*, **143**, 1–6, 2001.

Goodman-Tchernov, B. N., H. W. Dey, E. G. Reinhard, F. McCoy, and Y. Mart, Tsunami waves generated by the Santorini eruption reached Eastern Mediterranean shores, *Geology*, **37**, 943–946, 2009.

Goto, K., S. A. Chavanich, F. Imamura, P. Kunthasap, T. Matsui, K. Minoura, D. Sugawara, and H. Yanagisawa, Distribution, origin and transport process of boulders deposited by the 2004 Indian Ocean tsunami at Pakarang Cape, Thailand, *Sediment. Geol.*, **202**, 821–837, 2007.

Goto, K., T. Kawana, and F. Imamura, Historical and geological evidence of boulders deposited by tsunamis, southern Ryukyu Islands, Japan, *Earth-Sci. Rev.*, **102**, 77–99, 2010.

Goto, K., J. Takahashi, T. Oie, and F. Imamura, Remarkable bathymetric change in the nearshore zone by the 2004 Indian Ocean tsunami: Kirinda Harbor, Sri Lanka, *Geomorphology*, **127**, 107–116, 2011.

Hawkes, A. D., M. Bird, S. Cowie, C. Grundy-Warr, B. P. Horton, A. Hwai, L. Law, C. Macgregor, J. Nott, J. E. Ong, J. Rigg, R. Robinson, M. Tan-Mullins, T. T. Sa, Z. Yasin, and L. W. Aik, Sediments deposited by the 2004 Indian Ocean Tsunami along the Malaysia-Thailand Penisula, *Mar. Geol.*, **242**, 169–190, 2007.

Heise, B., B. Bobertz, and J. Harff, Classification of the Perl River Estuary via Principal Component Analysis and Regionalisation, *J. Coast. Res.*, **26**, 769–779, 2010.

Hofmann, D. I., K. Fabian, F. Schneider, B. Donner, and U. Bleil, A stratigraphic network across the Subtropical Front in the central South Atlantic: Multi-parameter correlation of magnetic susceptibility, density, X-ray fluorescence and δ^{18}O records, *Earth Planet. Sci. Lett.*, **240**, 694–709, 2005.

Jaeger, J. M., C. A. Nittrouer, N. D. Scott, and J. D. Milliman, Sediment accumulation along a glacially impacted mountainous coastline: Northeast Gulf of Alaska, *Basin Res.*, **10**, 155–173, 1998.

Jankaew, K., B. F. Atwater, Y. Sawai, M. Choowong, T. Charoentitirat, M. E. Martin, and A. Prendergast, Medieval forewarning of the 2004 Indian Ocean tsunami in Thailand, *Nature*, **455**, 1228–1231, 2008.

Jansen, J. H. F., S. J. Van der Gaast, B. Koster, and A. J. Vaars, CORTEX, a shipboard XRF-scanner for element analyses in split sediment cores, *Mar. Geol.*, **151**, 143–153, 1998.

Kennedy, J., B. Barry, A. Markwitz, K. Srisuksawad, and A. Limsakul, Pixe analysis of sediments affected by the December 2004 Indian Ocean Tsunami, *Int. J. PIXE*, **18**, 227–240, 2008.

Khokiattiwong, S., P. Limpsaichol, S. Petpiroon, P. Sojisuporn, and B. Kjerfve, Oceanographic variations in Phangnga Bay, Thailand under monsoonal effects, *Phuket Mar. Biol. Cent. Res. Bull.*, **55**, 43–76, 1991.

Kortekaas, S. and A. G. Dawson, Distinguishing tsunami and storm deposits: An example from Martinhal, SW Portugal, *Sediment. Geol.*, **200**, 208–221, 2007.

Kumar, V. S., V. R. Babu, M. T. Babu, G. Dhinakaran, and G. V. Rajamanickam, Assessment of storm surge disaster potential for the Andaman Islands, *J. Coast. Res.*, **24**, 171–177, 2008.

Lamy, F., D. Hebbeln, U. Röhl, and G. Wefer, Holocene rainfall variability in southern Chile: a marine record of latitudinal shifts of the Southern Westerlies, *Earth Planet. Sci. Lett.*, **185**, 369–382, 2001.

Le Roux, J. P. and G. Vargas, Hydraulic behaviour of tsunami backflows: insights from their modern and ancient deposits, *Environ. Geol.*, **49**, 65–75, 2005.

Luque, L., J. Lario, C. Zazo, J. L. Goy, C. J. Dabrio, and P. G. Silva, Tsunami deposits as paleoseismic indicators: Examples from the Spanish coast, *Acta Geol. Hispanica*, **36**, 197–211, 2001.

Mamo, B., L. Strotz, and D. Dominey-Howes, Tsunami sediments and their foraminiferal assemblages, *Earth-Sci. Rev.*, **96**, 263–278, 2009.

Marques, W. S., A. N. Sial, E. A. Menor, V. P. Ferreira, G. S. S. Freire, E. A. M. Lima, and V. A. V. Manso, Principal component analysis (PCA) and mineral associations of litoraneous facies of continental shelf carbonates from northeastern Brazil, *Cont. Shelf Res.*, **28**, 2709–2717, 2008.

Massari, F. and A. D'Alessandro, Tsunami-related scour-and-drape undulations in Middle Pliocene restricted-bay carbonate deposits (Salento, south Italy), *Sediment. Geol.*, **135**, 265–281, 2000.

McKee, B. A., C. A. Nittrouer, and D. J. DeMaster, The concepts of sediment deposition and accumulation applied to the continental shelf near the mouth of the Yangtze River, *Geology*, **11**, 631–633, 1983.

Nittrouer, C. A., R. W. Sternberg, R. Carpenter, and J. T. Bennett, The use of Pb-210 geochronology as a sedimentological tool: Application to the Washington continental shelf, *Mar. Geol.*, **31**, 297–316, 1979.

Nittrouer, C. A., J. A. Austin, M. E. Field, J. H. Kravitz, J. P. M. Syvitski, and P. Wiberg, in *Continental Margin Sedimentation*, edited by Nittrouer, C. A., J. A. Austin, M. E. Field, J. H. Kravitz, J. P. M. Syvitski, and P. Wiberg, 560 pp., *International Association of Sedimentologists, Spec. Publ.*, **37**, 2007.

Noda, A., H. Katayama, T. Sagayama, K. Suga, Y. Uchida, K. Satake, K. Abe, and Y. Okamura, Evaluation of tsunami impacts on shallow marine sediments: An example from the tsunami caused by the 2003 Tokachi-oki earthquake, northern Japan, *Sediment. Geol.*, **200**, 314–327, 2007.

Ohta, T. and H. Arai, Statistical empirical index of chemical weathering in igneous rocks: A new tool for evaluating the degree of weathering, *Chem. Geol.*, **240**, 280–297, 2007.

Paris, R., J. Fournier, E. Poizot, S. Etienne, J. Mortin, F. Lavigne, and P. Wassmer, Boulder and fine sediment transport and deposition by the 2004 tsunami in Lhok Nga (western Banda Aceh, Sumatra, Indonesia): A coupled offshore-onshore model, *Mar. Geol.*, **268**, 43–54, 2010.

Reid, M. K. and K. L. Spencer, Use of principal components analysis (PCA) on estuarine sediment datasets: The effect of data pre-treatment, *Environ. Poll.*, **157**, 2275–2281, 2009.

Reineck, H. E. and F. Wunderlich, Lamination and laminated rhythmites in water-laid sands, *Senckenbergiana Maritima*, **28**, 227–235, 1998.

Robbins, J. A. and D. N. Edgington, Determination of recent sedimentation rates in Lake Michigan using Pb-210 and Cs-137, *Geochim. Cosmochim. Acta*, **39**, 285–304, 1975.

Robbins, J. A., D. N. Edgington, and A. L. W. Kemp, Comparative ^{210}Pb, 137Cs, and pollen geochronologies of sediments from Lakes Ontario and Erie, *Quatern. Res.*, **10**, 256–278, 1978.

Sawai, Y., K. Jankaew, M. E. Martin, A. Prendergast, M. Choowong, and T. Charoentitirat, Diatom assemblages in tsunami deposits associated with the 2004 Indian Ocean tsunami at Phra Thong Island, Thailand, *Mar. Micropaleontol.*, **73**, 70–79, 2009.

Scheffers, A. and D. Kelletat, Sedimentological and geomorphologic tsunami imprints worldwide—a review, *Earth-Sci. Rev.*, **63**, 83–92, 2003.

Shanmugam, G., Process-sedimentological challenges in distinguishing paleo-tsunami deposits, *Nat. Haz.*, doi:10.1007/s11069-011-9766-z, 2011.

Shiki, T., Y. Tsuji, T. Yamazaki, and K. Minoura, in *Tsunamiites—Features and Implications*, edited by Shiki, T., Y. Tsuji, T. Yamazaki, and K. Minoura, 425 pp., Elsevier, Amsterdam, 2008.

Smedile, A., P. M. De Martini, D. Pantosti, L. Bellucci, P. Del Carlo, L. Gasperini, C. Pirrotta, A. Polonia, and E. Boschi, Possible tsunami signatures from an integrated study in the Augusta Bay offshore (Eastern Sicily-Italy), *Mar. Geol.*, **281**, 1–13, 2011.

Sommerfield, C. K. and C. A. Nittrouer, Modern accumulation rates and sediment budget for the Eel shelf: A flood-dominated depositional environment, *Mar. Geol.*, **154**, 227–241, 1999.

Sugawara, D., K. Minoura, N. Nemoto, S. Tsukawaki, K. Goto, and F. Imamura, Foraminiferal evidence of submarine sediment transport and deposition by backwash during the 2004 Indian Ocean tsunami), *Island Arc*, **18**, 513–525, 2009.

Suppasri, A., S. Koshimura, and F. Imamura, Developing tsunami fragility curves based on satellite remote sensing and the numerical modeling of the 2004 Indian Ocean tsunami in Thailand, *Nat. Haz. Earth Syst. Sci.*, **11**, 173–189, 2011.

Szczuciński, W., Impacts of 2004 Indian Ocean tsunami on mid continental shelf of Andaman Sea, in *The 3rd International Tsunami Field Symposium*, 57–58,Program and abstracts, Sendai, Japan, 10–11 April, 2010, 2010.

Szczuciński, W., N. Chaimanee, P. Niedzielski, G. Rachlewicz, D. Saisuttichai, T. Tepsuwan, S. Lorenc, and J. Siepak, Environmental and geological impacts of the 26 December 2004 tsunami in coastal zone of Thailand—Overview of short and long-term effects, *Polish J. Environ. Stud.*, **15**, 793–810, 2006.

Szczuciński, W., K. Stattegger, and J. Scholten, Modern sediments and sediment accumulation rates on the narrow shelf off central Vietnam, South China Sea, *Geo-Mar. Lett.*, **29**, 47–59, 2009.

Takashimizu, Y. and F. Masuda, Depositional facies and sedimentary successions of earthquake-induced tsunami deposits in Upper Pleistocene incised valley fills, central Japan, *Sediment. Geol.*, **135**, 231–239, 2000.

Uchida, J. I., O. Fujiwara, S. Hasegawa, and T. Kamataki, Sources and depositional processes of tsunami deposits: Analysis using foraminiferal tests and hydrodynamic verification, *Island Arc*, **19**, 427–442, 2010.

Usiriprisan, C., S. Chiemchindaratana, S. Shoosuwan, and Y. Chatrapakpong, *Offshore Exploration for Tin and Heavy Minerals in the Andaman Sea*, 224 pp., Department of Mineral Resources, Bangkok and UNDP, New York, 1987.

van den Bergh, G. D., W. Boer, H. de Haas, Tj. C. E. van Weering, and R. van Wijhe, Shallow marine tsunami deposits in Teluk Banten (NW Java, Indonesia), generated by the 1883 Krakatau eruption, *Mar. Geol.*, **197**, 13–34, 2003.

Weber, M. E., F. Niessen, G. Kuhn, and M. Wiedicke, Calibration and application of marine sedimentary physical properties using a multisensor core logger, *Mar. Geol.*, **136**, 151–172, 1997.

Weidong, D., Y. Baoguo, and W. Xiaogen, Studies of storm deposits in China: A review, *Cont. Shelf Res.*, **17**, 1645–1658, 1997.

Weltji, G. J. and R. Tjallingii, Calibration of XRF core scanners for quantitative geochemical logging of sediment cores: Theory and application, *Earth Planet. Sci. Lett.*, **274**, 423–438, 2008.

Zaborska, A., J. Caroll, C. Papucci, and J. Pempowiak, Intercomparison of alpha and gamma spectrometry techniques used in ^{210}Pb geochronology, *J. Environ. Radioact.*, **93**, 38–50, 2007.

D. Sakuna (e-mail: daroonwan@gpi.uni-kiel.de), W. Szczuciński, P. Feldens, K. Schwarzer, and S. Khokiattiwong

Hindawi Publishing Corporation
Journal of Analytical Methods in Chemistry
Volume 2012, Article ID 659858, 12 pages
doi:10.1155/2012/659858

Research Article

Parameters Influencing Sulfur Speciation in Environmental Samples Using Sulfur K-Edge X-Ray Absorption Near-Edge Structure

Siwatt Pongpiachan,[1] Kanjana Thumanu,[2] Charnwit Kositanont,[3] Klaus Schwarzer,[4] Jörg Prietzel,[5] Phoosak Hirunyatrakul,[6] and Itthipon Kittikoon[6]

[1] *NIDA Center for Research & Development of Disaster Prevention & Management, School of Social and Environmental Development, National Institute of Development Administration (NIDA), 118 Moo 3, Sereethai Road, Klong-Chan, Bangkapi, Bangkok 10240, Thailand*
[2] *Synchrotron Light Research Institute (Public Organization), 111 University Avenue, P.O. Box 93, Nakhon Ratchasima 30000, Thailand*
[3] *Inter-Department of Environmental Science, Faculty of Graduate Studies, Chulalongkorn University, Bangkok 10330, Thailand*
[4] *Institute of Geosciences Sedimentology, Coastal and Continental Shelf Research, Otto-Hahn-Platz 1, 24118 Kiel, Germany*
[5] *Lehrstuhl für Bodenkunde, Technische Universität München, Weihenstephan 85350 Freising, Germany*
[6] *Bara Scientific Co., Ltd., 968 Rama 4 Silom Bangrak, Bangkok 10500, Thailand*

Correspondence should be addressed to Siwatt Pongpiachan, pongpiajun@gmail.com

Received 23 May 2012; Revised 9 August 2012; Accepted 19 September 2012

Academic Editor: Ki-Hyun Kim

Copyright © 2012 Siwatt Pongpiachan et al. This is an open access article distributed under the Creative Commons Attribution License, which permits unrestricted use, distribution, and reproduction in any medium, provided the original work is properly cited.

This paper aims to enhance the credibility of applying the sulfur K-edge XANES spectroscopy as an innovative "fingerprint" for characterizing environmental samples. The sensitivities of sulfur K-edge XANES spectra of ten sulfur compound standards detected by two different detectors, namely, Lytle detector (LyD) and Germanium detector (GeD), were studied and compared. Further investigation on "self-absorption" effect revealed that the maximum sensitivities of sulfur K-edge XANES spectra were achieved when diluting sulfur compound standards with boron nitride (BN) at the mixing ratio of 0.1%. The "particle-size" effect on sulfur K-edge XANES spectrum sensitivities was examined by comparing signal-to-noise ratios of total suspended particles (TSP) and particulate matter of less than 10 millionths of a meter (PM_{10}) collected at three major cities of Thailand. The analytical results have demonstrated that the signal-to-noise ratios of sulfur K-edge XANES spectra were positively correlated with sulfate content in aerosols and negatively connected with particle sizes. The combination of hierarchical cluster analysis (HCA) and principal component analysis (PCA) has proved that sulfur K-edge XANES spectrum can be used to characterize German terrestrial soils and Andaman coastal sediments. In addition, this study highlighted the capability of sulfur K-edge XANES spectra as an innovative "fingerprint" to distinguish tsunami backwash deposits (TBD) from typical marine sediments (TMS).

1. Introduction

During the past decades, considerable research has been intensively focused on the topic of sulfur speciation in the environment. It has become more evident that the plant uptake availability [1] and climate forcing capability [2, 3] of sulfur compounds depend not purely on their concentrations but, severely, on the chemical forms in which they exist in natural compartments. Furthermore, ammonium salts such as ammonium chloride (NH_4Cl), ammonium nitrate (NH_4NO_3), ammonium sulfate ($(NH_4)_2SO_4$), and bisulfate (NH_4HSO_4) are widely considered as acidic aerosols and may have been responsible for the acid rain in pristine area [4, 5]. Hence, information on the chemical state of sulfur in aerosol is important from the viewpoint of environmental science, in order to study the origins of the acid rain and the causes of climate change.

Continuing developments in various atomic spectrochemical techniques enable researchers to extract some useful information related to the physicochemical properties of sulfur contents in atmospheric aerosols. For instance, the chemical speciation of sulfate aerosols collected weekly for a

one-year period in Matsue, Shimane prefecture, Japan, was investigated by X-ray powder diffraction (XRD) [6]. It is also important to note that X-ray photoelectron spectroscopy (XPS) has been widely employed to determine the surface composition and structure of sulfur in aerosols collected at Salt Lake city [7], Jinan city of China [8], and four towns in southern Poland [9]. Although XPS provides insight into the elemental composition, empirical formula, chemical state, and electronic state of sulfur on surface aerosol, this quantitative spectroscopic technique requires not only ultra high vacuum (UHV) condition but also a considerable amount of aerosol loading on the filter. Furthermore, it is not practical to use XRD to measure the chemical state of sulfur in amorphous or poorly crystalline particle such as atmospheric aerosol.

Recent research has found that X-ray absorption near-edge structure (XANES) can be used to determine the oxidation state of sulfur compounds even in the case of aerosol samples, which usually exist in trace levels. This innovative approach presents the potential for elucidating the very complicated chemical forms of sulfur in the natural environment. It is well known that fluorescent mode XANES (FL-XANES) is the most suitable method applied to dilute samples where "self-absorption effect" (i.e., the fluorescence X-ray signals are attenuated by reabsorption of absorber atoms in the sample) is often considered of major importance. Unlike transmission mode XANES (TM-XANES), which requires sample having X-ray absorbing atoms at high density (>5% wt), only small amount of sample is sufficient to be detected in FL-XANES. Therefore, it seems logical to conduct sulfur speciation measurement of environmental sample in FL-XANES. However, some critical facts have been identified and need to be investigated with great caution.

Since the fluorescence excitation spectra detected by FL-XANES are more susceptible to various extraneous factors in the beam path, it is therefore crucial to estimate the signal-to-noise (S/N) ratio of target sulfur compound measured in different types of fluorescence detectors such as Germanium detector (GeD) and Lytle detector (LyD). Although the relationship between the S/N ratio of sulfur K-edge XANES spectra and the grain size was previously investigated [10], little is known about the impact of "grain size effect" on spectra absorption in aerosol sample. In addition, the availability of using sulfur speciation as a new proxy to discriminate "typical marine sediment" and "tsunami backwash deposit" will be carefully investigated. The overall aims of this study are the following.

(1) To investigate the impact of GeD and LyD on S/N ratio of sulfur K-edge XANES spectra of ammonium sulfate ($(NH_4)_2SO_4$), calcium sulfate ($CaSO_4$), aluminium sulfate ($Al_2(SO_4)_3$), manganese sulfate ($MnSO_4$), zinc sulfate ($ZnSO_4 \cdot 7H_2O$), potassium thiosulfate ($K_2S_2O_3$), chromic sulfate ($Cr_2(SO_4)_3 \cdot 15H_2O$), cobalt sulfate ($CoSO_4 \cdot 7H_2O$), nickel sulfate ($NiSO_4 \cdot 6H_2O$), and copper sulfate ($CuSO_4 \cdot 5H_2O$) including the self-absorption effects in FL-XANES.

(2) To conduct the statistical investigation of "grain size effect" on sulfur K-edge XANES spectra sensitivity in total suspended particle (TSP) and particle with diameter less than or equal to 10 microns (PM10) collected at the urban sampling sites of Bangkok, Chiang-Mai, and Hat-Yai, Thailand.

(3) To evaluate the variation of sulfur speciation in both "typical marine sediments (TMS)" and "tsunami backwash deposits (TBD)" collected at the 2004 tsunami-affected coastal areas of Andaman Sea, Thailand.

2. Materials and Methods

2.1. Sample Collection and Sampling Site Descriptions. Ambient air samples were collected over periods of 6 h (09:00–15:00) using a Graseby-Andersen high volume air sampler with TSP and PM_{10} TE-6001, operating at the flow rate of 1.4 $m^3\,min^{-1}$. TSP and PM_{10} were collected on 47 mm Whatman quartz microfiber filters (QM/A). The filters were preheated at 800°C for 12 h prior to sampling. The exposed filters were stored in a refrigerator at about 4°C until sulfur speciation analysis to prevent the evaporation of volatile compounds. All the field sampling and filters weighing were performed in compliance with the US EPA's guideline of standard operating procedure for sampling and handling of $PM_{2.5}$ filters. It is important to note that all filters were weighed by Mettler Toledo AB204-S Analytical Balance before sending to Synchrotron Light Research Institute (Public Organization), Thailand. All the three sampling sites are located in the city center of Bangkok, Chiang-Mai, and Hat-Yai, representing the capital, the largest cities in northern and southern regions of Thailand, respectively (Table 1). Air samples were collected above the ground level at Bai-Yok Suit Hotel Observatory Site in February 18–21, 2008, at Centara Duangtawan Hotel Observatory Site in February 25–28, 2008 and at Novotel Centara Hat-Yai Hotel Observatory Site in December 17–20, 2007 as monitoring sites for Bangkok, Chiang-Mai, and Hat-Yai in that order. It is well known that traffic emissions are considered as main sources of air pollutants in Bangkok atmosphere, whilst agricultural burnings are major air pollution problems in Chiang-Mai. Furthermore, Hat-Yai is located only 30 km at the west of the Gulf of Thailand. Thus, one can safely assume that aerosol samples used in this study may consist of traffic aerosols with the mixture of industrial exhausts, biomass burning, and sea salt aerosols in the case of Bangkok, Chiang-Mai, and Hat-Yai, respectively.

Sediment sample collection was carried out offshore along the west coast of Phang Nga province, Thailand, which was heavily affected by the 2004 tsunami [11]. The research area covers approximately 1,000 km^2 between Thap Lamu and Pakarang Cape, up to a water depth of 70 meters. During the research cruises in November-December 2007 with RV Chakratong Tongyai, approximately 1,500 nautical miles of hydroacoustic profiles (side scan sonar, multibeam echo sounder and shallow reflection seismics with a boomer system) were recorded at the front of

Table 1: Location and general description of sampling sites.

Sampling location	Sample number	Sample type	Sample descriptions	Latitude	Longitude
Bangkok, Thailand		PM_{10} and TSP	Traffic and industrial aerosols	13° 44′ 496″ N	100° 59′ 819″ E
Chiang-Mai, Thailand		PM_{10} and TSP	Traffic and biomass burning aerosols	18° 47′ 015″ N	98° 59′ 519″ E
Hat-Yai, Thailand		PM_{10} and TSP	Traffic and maritime aerosols	07° 00′ 087″ N	100° 27′ 262″ E
PSU, Thailand		PM_{10} and TSP	Urban background aerosols	07° 21′ 280″ N	100° 29′ 533″ E
Andaman Sea, Thailand	20	Marine sediment	Coarse silt, moderately sorted (water depth 57.80 m)	08° 49′ 296″ N	97° 59′ 819″ E
Andaman Sea, Thailand	34	Tsunami deposit	Coarse sand, well sorted (water depth 16.70 m)	08° 43′ 835″ N	98° 11′ 916″ E
Andaman Sea, Thailand	36	Tsunami deposit	Very coarse sand, well sorted (water depth 17.30 m)	08° 43′ 875″ N	98° 10′ 945″ E
Andaman Sea, Thailand	48	Tsunami deposit	Coarse sand, well sorted (water depth 17.80 m)	08° 42′ 901″ N	98° 09′ 988″ E
Andaman Sea, Thailand	49	Marine sediment	Muddy fine sand, poorly sorted (water depth 62.00 m)	08° 30′ 222″ N	97° 59′ 124″ E
Andaman Sea, Thailand	53	Marine sediment	Medium sand, moderately sorted (water depth 59.80 m)	08° 33′ 421″ N	97° 58′ 422″ E
Andaman Sea, Thailand	55	Marine sediment	Muddy medium sand, poorly sorted (water depth 57.10 m)	08° 33′ 810″ N	98° 00′ 908″ E
Andaman Sea, Thailand	61	Marine sediment	Muddy medium sand, poorly sorted (water depth 45.60 m)	08° 35′ 863″ N	98° 03′ 630″ E
Andaman Sea, Thailand	71	Tsunami deposit	Coarse sand, moderately sorted (water depth 15.80 m)	08° 42′ 928″ N	98° 10′ 906″ E
Andaman Sea, Thailand	77	Tsunami deposit	Silty coarse sand, poorly sorted (water depth 13.90 m)	08° 42′ 569″ N	98° 11′ 680″ E
Schlöppnerbunnen, Germany	A-Of oxisch	Terrestrial soil	Endostagnic, Leptic Cambisol (alumic)	50° 08′ 140″ N	11° 53′ 070″ E
Schlöppnerbunnen, Germany	A-Oh oxisch	Terrestrial soil	Endostagnic, Leptic Cambisol (alumic)	50° 08′ 140″ N	11° 53′ 070″ E
Schlöppnerbunnen, Germany	A-Aeh oxisch	Terrestrial soil	Endostagnic, Leptic Cambisol (alumic)	50° 08′ 140″ N	11° 53′ 070″ E
Schlöppnerbunnen, Germany	A-Bv oxisch	Terrestrial soil	Endostagnic, Leptic Cambisol (alumic)	50° 08′ 140″ N	11° 53′ 070″ E
Schlöppnerbunnen, Germany	B-H1 oxisch	Terrestrial soil	Histic Stagnosol (albic, alumic)	50° 08′ 140″ N	11° 53′ 070″ E
Schlöppnerbunnen, Germany	B-H2 oxisch	Terrestrial soil	Histic Stagnosol (albic, alumic)	50° 08′ 140″ N	11° 53′ 070″ E
Schlöppnerbunnen, Germany	B-Aeh oxisch	Terrestrial soil	Histic Stagnosol (albic, alumic)	50° 08′ 140″ N	11° 53′ 070″ E
Schlöppnerbunnen, Germany	B-Srw oxisch	Terrestrial soil	Histic Stagnosol (albic, alumic)	50° 08′ 140″ N	11° 53′ 070″ E
Schlöppnerbunnen, Germany	C-H1 oxisch	Terrestrial soil	Leptic Rheic Hemic Histosol (dystric)	50° 08′ 140″ N	11° 53′ 070″ E
Schlöppnerbunnen, Germany	C-H2 oxisch	Terrestrial soil	Leptic Rheic Hemic Histosol (dystric)	50° 08′ 140″ N	11° 53′ 070″ E
Schlöppnerbunnen, Germany	C-Aa oxisch	Terrestrial soil	Leptic Rheic Hemic Histosol (dystric)	50° 08′ 140″ N	11° 53′ 070″ E
Schlöppnerbunnen, Germany	C-Gr oxisch	Terrestrial soil	Leptic Rheic Hemic Histosol (dystric)	50° 08′ 140″ N	11° 53′070″ E
Schlöppnerbunnen, Germany	D-H2 oxisch	Terrestrial soil	Leptic Rheic Hemic Histosol (dystric)	50° 08′ 380″ N	11° 51′ 410″ E
Schlöppnerbunnen, Germany	D-H3 oxisch	Terrestrial soil	Leptic Rheic Hemic Histosol (dystric)	50° 08′ 380″ N	11° 51′ 410″ E
Schlöppnerbunnen, Germany	D-H4 oxisch	Terrestrial soil	Leptic Rheic Hemic Histosol (dystric)	50° 08′ 380″ N	11° 51′ 410″ E
Schlöppnerbunnen, Germany	D-Go oxisch	Terrestrial soil	Leptic Rheic Hemic Histosol (dystric)	50° 08′ 380″ N	11° 51′ 410″ E

Pakarang Cape. In this study, two types of coastal sediments, namely, "tsunami deposit" and "typical marine sediment" were carefully identified based on previous geophysical information [10]. The sediment samples were taken with a Van-Veen-type grab sampler. Soil samples were collected from four locations at two different sites in the Lehstenbach watershed (Fichtelgebirge, Germany). In this study, three different types of terrestrial soils, namely, Endostagnic Leptic Cambisol (alumic), Histic Stagnosol (albic, alumic), and Leptic Rheic Hemic Histosol (dystric) were used for the analysis of sulfur K-edge XANES spectra for comparison purpose. Since the soil types and sampling sites have been described in detail in previous publication [12], therefore only a short summary is provided here.

2.2. Sulfur K-Edge XANES Experiment. XANES of the samples and standards were measured at the beamline No.8 at the Siam Photon Laboratory [13]. Photon energy of an X-ray beam transported through the beamline was scanned by InSb(111) double crystals equipped in the monochromator. The beam size illuminating the sample was 10 mm (w) × 1 mm (h). A 10 cm long ion chamber filled with a gas mixture of N_2 (30 mbar) and He (983 mbar) was employed to measure intensity of the X-ray beam. The ion chamber absorbed only 10% of the beam intensity for ionization of the filling gas and produced small electrical current signal proportional to the beam intensity.

Fluorescence X-rays were emitted from the sample and collected by either a 13-channel Germanium detector (GeD) or a Lytle detector (LyD). The GeD has advantage over the LyD in discrimination of X-ray fluorescence energy. With the use of a digital window, only K_α photons from sulfur were counted. The final photon counts were averaged over all the channels. Similar to the ion chamber, the LyD produces small electrical current signal corresponding not only to fluorescence X-rays from sulfur but other elements present in the sample and the scattered photons from the primary beam. The sample chamber was flowed in with He gas to reduce X-ray absorption and scattering by air. A thin polypropylene window was required to protect the GeD from He gas, which can diffuse through thin detector seal of beryllium spoiling cryostat vacuum of the detector. A minimum air gap of 5 mm was introduced for detector clearance. The distances from the sample to detector were 7 mm and 9 mm for GeD and LyD, respectively. XANES spectra were recorded from 2450 eV to 2520 eV with the energy step of 0.2 eV and energy-calibrated using the maximum absorption of iron sulfate at 2481.4 eV [14]. In addition the resolving power (E/DE) is 10,000. Absorbance was calculated by the ratio of photon counts from the fluorescent detector to the ion chamber.

For sensitivity test $(NH_4)_2SO_4$, $CaSO_4$, $Al_2(SO_4)_3$, $MnSO_4$, $ZnSO_4 \cdot 7H_2O$, $K_2S_2O_3$, $Cr_2(SO_4)_3 \cdot 15H_2O$, $CoSO_4 \cdot 7H_2O$, $NiSO_4 \cdot 6H_2O$, and $CuSO_4 \cdot 5H_2O$ were diluted by physically mixing with boron nitride (BN) with the mixing ratios (standard: BN in percentage) of 0.1%, 1.0%, 10.0%, and 100%. The dilute standards were applied on adhesive side of the polyimide tape and placed at 45°C to the beam path in the sample chamber. Without dilution, similar approach was used for the preparation of environmental samples. The data processing and quantitative XANES analyses were conducted by ATHENA program in the IFEFFIT computer package [15]. In this study, SNR (signal-to-noise ratio) was employed to characterize the sensitivity of S-K-edge XANES spectra. "Noise" was calculated by using the standard deviation of peak intensities of preedge region (i.e., 2,450–2,475 eV), whilst the definition of "signal" was termed as the difference between main peak at 2,482 eV and the average peak intensity of preedge region (i.e., baseline).

2.3. Determination of Water Soluble Ionic Species (WSIS) in Aerosol Samples. All filter samples were stored in a refrigerator at about 4°C as soon as possible after sampling was completed. This was necessary to prevent any negative artifacts caused by losses of semivolatile compounds. Also field blank filters were collected to subtract the positive artifacts due to adsorption of gas phase organic compounds onto the filter during and/or after sampling. The analysis of water soluble ionic species (WSIS) including cation (Na^+, NH_4^+, K^+, Ca^{2+}) and anion (Cl^-, NO_3^-, SO_4^{2-}) was performed by using Metrohm Ion Chromatography (IC) analyzer with the combination of IC 818 pump, IC 819 detector, IC 830 advance interface, and IC 833 Advanced IC Liquid Handling Pump Unit—two-channel peristaltic pump for use with the Metrohm Suppressor Module (MSM).

Metrosep A Supp 16–250 and Metrosep C 4–250 columns were employed for the analysis of anion and cation species, respectively. Filters were cut, placed in a polyethylene vial (50 mL), and extracted with 10 mL of Milli-Q water for 30 min. The extract was filtered through 0.2 μm pore size Millipore Teflon filters for cleanup. In addition, standard solutions were purchased from Fuka (Multielement Ion chromatography: number 89886.0050 and No.89316.0050 and Ammonium ion standard solution: number 09685.0250).

3. Results and Discussion

Ten sulfur compound standards, six aerosols, ten marine sediments, and five urban soils were analyzed by XANES in fluorescence mode detected with two different detectors. Generally, XANES can be measured in three different ways, namely, transmission, fluorescence, and electron yield modes. These three modes are widely adopted depending upon purposes. For instances, the scanning transmission X-ray microscope can be applied for imaging various biological as well as polymer samples at 55 nm Rayleigh resolution, whilst the fluorescent mode can be used for measuring X-ray absorption spectra of crystalline (*c*)-Si–C–N thin film [16, 17].

In the case of conventional transmission mode, the intensity of the monochromatic X-ray incident is detected before (I_0) and after processing through the target sample (I_n) employing ion chamber gas detectors. As a consequence, the XANES spectrum will then demonstrate the oscillation of log (I_0/I_n) versus energy (eV). Whilst it is widely accepted that the transmission mode is suitable for those

"high density thin layer" type sample, the electron yield mode coupled with total external reflection fluorescence is generally considered as the most appropriate detector for analyzing those "high density high layer" type sample. It is also important to stress that the fluorescence detector has the greatest advantage to apply with those dilute, relatively low K-edge energies, and small samples [16]. Furthermore, a recent study reveals that the combination of high-purity Germanium (HPGe) detector and fluorescence mode can combat various analytical difficulties such as the complex signal processing electronics and limitation of sample size and amount [17]. Thus, it seems logical to apply fluorescence mode for overcoming the problems of limited sample loading with typical high-matrix containing such as environmental samples.

3.1. Comparison of Sensitivity Test between GeD and LyD. The sulfur K-edge XANES spectra for $(NH_4)_2SO_4$, $CaSO_4$, $Al_2(SO_4)_3$, $MnSO_4$, $ZnSO_4{\cdot}7H_2O$, $K_2S_2O_3$, $Cr_2(SO_4)_3{\cdot}15H_2O$, $CoSO_4{\cdot}7H_2O$, $NiSO_4{\cdot}6H_2O$, and $CuSO_4{\cdot}5H_2O$ exhibited the main peak at 2,482 eV for both detectors. The degree of reproducibility of main peak was relatively stable within ±0.3 eV for various sulfate compounds and also consistent with other previous studies of sulfur speciation [18, 19]. For this reason it appears difficult to utilize the energy level to characterize each sulfate compounds. However, there were some differences among sulfur K-edge XANES spectra observed in the postedge region between 2,482 and 2,500 eV as displayed in Figure 1. It is likely that the change in subsequent structure must be ascribed to electron transitions with a d-type shape resonance, which is dependent on cation type associated with sulfate ions [20, 21]. The obvious difference in the sulfur K-edge XANES spectrum between $K_2S_2O_3$ and other sulfate compounds might reflect the level of oxidation state dissimilarity.

A crucial caution for fluorescence measurements is the selection of detector types to use in the ion chamber. In general, it is desirable to adopt LyD for measuring samples with relatively high ion count rate due to its much larger solid angle of acceptance in comparison with those of GeD. On the contrary, it is preferable to use GeD for detecting more dilute elements in samples as a consequence of recent improvement in crystallographic properties, enhancement in purity concentrations with larger axial uniformity, and enlargement in detector size [22, 23]. Additionally, the electron yield mode is often used for bulk and surface-sensitive analysis [24]. In practice, however, there are many factors that may undermine the sensitivity of XANES spectrum measured by GeD. Several authors have raised concerns on significant damping of XANES spectra of standard samples caused by self-absorption effects [25, 26]. In order to minimize this effect, it is often necessary to blend sample with an inert matrix such as BN to increase the S/N ratio. Generally, XANES spectra of ten sulfur compounds indicated that better sensitivity could be achieved in both detectors with mixing ratios of standard to BN at 0.1% (Table 2). Whilst the two detectors generated similar sensitivity for XANES spectra of $(NH_4)_2SO_4$, $CaSO_4$, $Al_2(SO_4)_3$, $MnSO_4$, $ZnSO_4{\cdot}7H_2O$, $Cr_2(SO_4)_3{\cdot}15H_2O$, $CoSO_4{\cdot}7H_2O$, $NiSO_4{\cdot}6H_2O$, and $CuSO_4{\cdot}5H_2O$, the $K_2S_2O_3$ was significantly lower than others with all mixing ratios of standard to BN ($P < 0.05$).

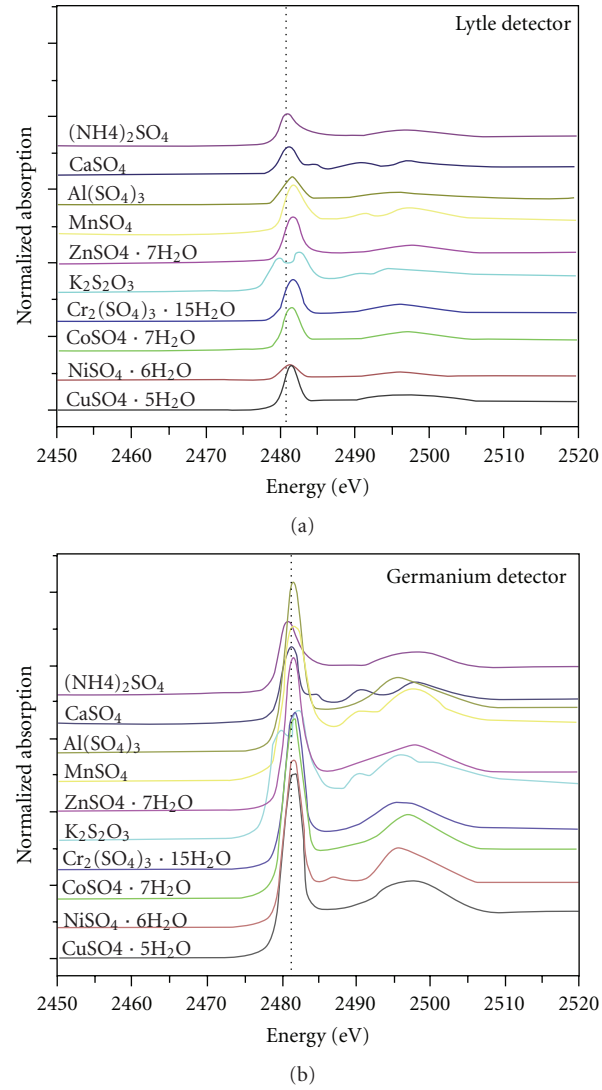


Figure 1: Normalized XANES spectra at sulfur K-edge spectra for $(NH_4)_2SO_4$, $CaSO_4$, $Al(SO_4)_3$, $MnSO_4$, $ZnSO_4{*}7H_2O$, $K_2S_2O_3$, $Cr_2(SO_4)_3{*}15H_2O$, $CoSO_4{*}7H_2O$, $NiSO_4{*}6H_2O$, and $CuSO_4{*}5H_2O$ measured by Germanium and Lytle detectors.

3.2. Particle Size Effect on Sulfur K-Edge XANES Spectra Sensitivity in Urban Aerosol. Recent studies have shown that the analysis of chemical speciation in aerosol can be conducted by using XANES technique [27–30]. However, only four studies have been examining sulfur K-edge XANES spectra in aerosol [31–33]. As shown in Figure 2, sulfur K-edge XANES spectra are obtained for both TSP and PM_{10} samples collected at Bangkok, Chiang-Mai, and Hat-Yai. All XANES spectra exhibited very strong symmetric peaks around 2,482 eV and shoulders nearby 2,485 eV. Generally, the aerosols examined produced less signals in the TSP mode compared with the PM_{10} mode. This can be explained

Table 2: Signal-to-noise ratios (S/N) of $(NH_4)_2SO_4$, $CaSO_4$, $Al(SO_4)_3$, $MnSO_4$, $ZnSO_4 * 7H_2O$, $K_2S_2O_3$, $Cr_2(SO_4)_3 * 15H_2O$, $CoSO_4 * 7H_2O$, $NiSO_4 * 6H_2O$, and $CuSO_4 * 5H_2O$ detected by GeD and LyD.

Mixing ratio % (sample : BN)	Germanium 0.1	Germanium 1.0	Germanium 10.0	Germanium 100.0	Lytle 0.1	Lytle 1.0	Lytle 10.0	Lytle 100.0
$Al_2(SO_4)_3$	4.296	3.837	3.241	2.642	4.529	3.935	3.440	3.020
$CaSO_4$	3.719	3.801	3.213	2.984	3.969	3.731	3.424	2.951
$ZnSO_4$	3.650	3.598	2.893	2.714	3.532	3.640	3.056	2.894
$NiSO_4$	4.308	3.965	3.334	3.136	4.196	4.145	3.503	3.385
NH_4SO_4	4.711	2.745	2.509	1.581	4.553	2.560	2.643	1.923
$K_2S_2O_3$	2.431	2.345	1.868	1.593	3.582	2.399	2.264	1.892
$FeSO_4$	3.936	3.551	3.216	3.021	3.778	3.749	3.409	3.132
$CuSO_4$	4.301	4.022	3.483	3.100	4.027	4.229	3.660	3.407
$CrSO_4$	4.120	4.021	3.539	2.915	3.865	4.033	3.633	3.074
$CoSO_4$	4.212	3.810	3.348	3.144	4.333	4.032	3.241	3.203
Average	3.968	3.569	3.064	2.683	4.036	3.645	3.227	2.888
Stdev %	15.7	16.0	16.9	22.4	9.0	17.6	14.0	18.8

by the signal damping caused by self-absorption effect of large particle as mentioned previously in Section 3.1. This effect seems to have become less pronounced with decreasing particle size and thus enhancing the signal of PM_{10} in comparison with those of TSP. It is also worth to note that differences in sensitivity between the two aerosol modes became more distinct after normalizing the signal intensity with particle weight (see Figure 2). However, there was one exception to this finding. While PM_{10} mode yielded excellent sensitivity for Bangkok and Chiang-Mai aerosols, TSP mode provided a better signal intensity than PM_{10} mode for Hat-Yai samples. Although the reason for the "sensitivity conversion" is not readily apparent, there are several possibilities behind the issue.

Analytical results showed that the highest ionic concentrations in Bangkok aerosols were $SO_4^{2-} > NO_3^- > K^+ > Ca^{2+}$ and $SO_4^{2-} > Ca^{2+} > NO_3^- > K^+$ for PM_{10} and TSP, respectively, whereas those of Chiang-Mai particles were following the decreasing order of $SO_4^{2-} > NO_3^- > NH_4^+ > K^+$ and $Ca^{2+} > SO_4^{2-} > NO_3^- > K^+$ for PM_{10} and TSP in that order. Previous studies found that the coarse fraction of SO_4^{2-} is generally in the form of gypsum ($CaSO_4$) reflecting the relatively high contribution of terrestrial dusts observed in Chiang-Mai TSP [34, 35]. More interestingly, sulfate was discovered as the most dominant ionic species in both types of aerosols. Since Bai-Yok Suite Hotel (i.e., Bangkok sampling site) is located in the heart of business area in Bangkok and therefore encompassed by main arteries for traffic into and out of the city center on a daily basis, it seems logical to ascribe the comparatively great input of sulfate and nitrate to vehicle exhaust emissions. Similarly, the reasonably pronounced influence of sulfate and nitrate in PM_{10} measured at Chiang-Mai was observed and thus emphasized the possibility that traffic emissions were plausibly main sources of airborne pollutants in fine particles of this city.

On the contrary, the highest contributions of Hat-Yai ionic species in TSP came from $Cl^- > SO_4^{2-} > Na^+ > Ca^{2+}$, while those in PM_{10} were following the decreasing sequence of $SO_4^{2-} > Cl^- > Na^+ > NO_3^-$. Since Hat-Yai city is located only 30 km in the west side of coastline, it appears reasonable to presuppose the moderately high loads of Na^+ and Cl^- observed in Hat-Yai aerosols as a result of sea salt aerosol production occurring above the Gulf of Thailand. The finding is comparable with prior evidence that SO_4^{2-} steadily appears to account for 36% (PM_{10}) and 24% (TSP) by mass of the total WSIS [36]. Over the past three decades, several studies suggest that SO_4^{2-} maritime aerosols in the nucleation mode can be principally generated by *gas-to-particle conversion* (GPC), which are triggered by photooxidation of sulfur containing precursor gaseous species such as SO_2, H_2S, CS_2, COS, CH_3SCH_3, and CH_3SSCH_3 [37, 38]. The highest mass percentage of particulate SO_4^{2-} was detected in Hat-Yai TSP with the value of 22.8%, which exceeded those of Bangkok (10.6%) and Chiang-Mai (5.0%) for 2.2 and 4.6 times, respectively. Similarly, the highest mass percentage of SO_4^{2-} in fine aerosol was observed in Hat-Yai PM_{10} with the value of 18.4%, which surpassed those of Bangkok (7.2%) and Chiang-Mai (2.8%) for 2.6 and 6.6 times correspondingly.

These results were in good agreement with the maximum absorption of Hat-Yai samples in sulfur K-edge XANES spectra detected at 2,482 eV for both TSP and PM_{10}, highlighting the positive correlation between percentage contribution of particulate SO_4^{2-} and XANES absorption. However, it is important to stress that the ratios of SO_4^{2-}-PM_{10}/ SO_4^{2-}-TSP showed the reverse sequence against those of SO_4^{2-} mass percentages. Interestingly, the ratios of SO_4^{2-}-PM_{10}/SO_4^{2-}-TSP were following the decreasing order of Chiang-Mai > Bangkok > Hat-Yai, suggesting that Hat-Yai aerosols were overwhelmed with contribution of SO_4^{2-} in TSP mode rather than PM_{10} mode. Hence, it seems reasonable to ascribe the "sensitivity conversion" in sulfur K-edge XANES spectra as a consequence of sulfate enrichment found in Hat-Yai TSP.

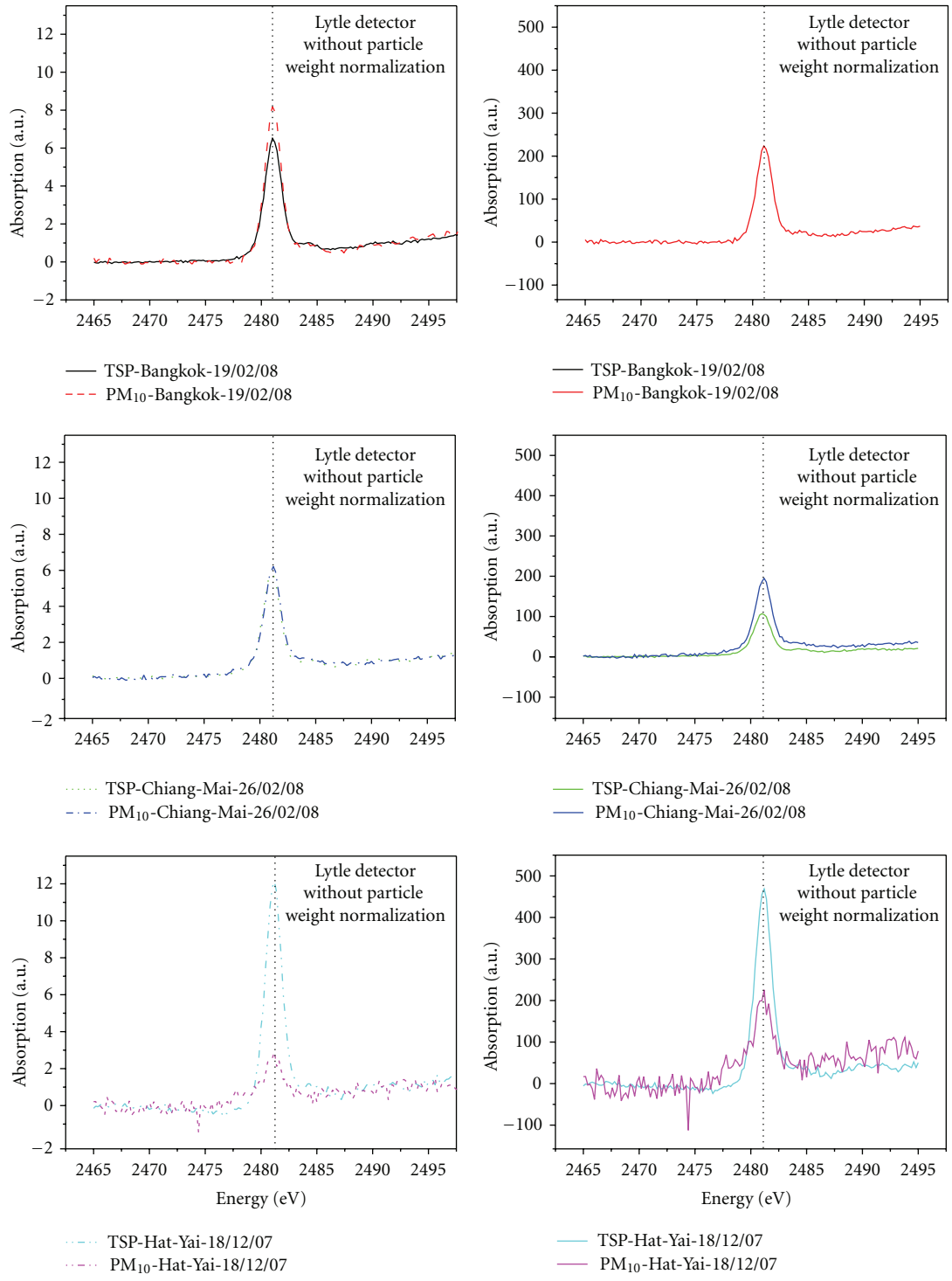


Figure 2: Comparison of sulfur K-edge XANES spectrum of urban aerosol collected at Bangkok, Chiang-Mai, and Hat-Yai measured by Lytle detector with and without particle weight normalization.

3.3. Variations of Sulfur K-Edge XANES Spectra in Different Soil and Sediment Types. The great Indian Ocean tsunami of December 26, 2004 was responsible for an estimated 250,000 of deaths and destroyed the coastal regions of the Indian Ocean nations. The December 26 tsunami is widely considered as the worst natural disaster to ever strike Thailand and thus has already provided traumatic impacts not only to the victims, but also to the scientists, policy makers, government officers, and several national and international organizations. Despite equitably large number of publications associated with several impacts of 2004 Indian Ocean tsunami on shore, little is known about the

geochemical information of tsunami backwash deposits off shore [39–42]. Since the chemical composition records of tsunami deposits are greatly significant for the studies of both modern and past tsunami episodes, it should be of great interest to discriminate between the "typical marine sediment (TMS)" and "tsunami backwash deposit (TBD)."

It was reported that the sulfur K-edge XANES spectra can be used as a "fingerprint" to characterize different types of soils [43, 44]. Thus it seems reasonable to assume that the sulfur K-edge XANES spectra can be used as a proxy to distinguish TBD from TMS. To test this hypothesis, five TMS and five TBD coupled with 16 German terrestrial soils were analyzed by the sulfur K-edge XANES in fluorescence mode as illustrated in Figure 5. The sulfur K-edge XANES spectra recorded from TMS and TBD in the present study generally showed the presence of several strong white lines at the energy level of 2,482 eV, indicating the existence of electronic oxidation state of +6, which included inorganic and ester sulfates in marine sediments. The comparatively high involvement of sulfate species in sediment is in good agreement with those reported by previous studies in Jellyfish Lake, Palau, and Oman Margin sediments [45, 46]. Interestingly, the 16 German terrestrial soils studied fluctuated noticeably in the relative proportions of the two major absorption bands in the energy ranges of 2,467–2,472 eV (i.e., the energy range of reduced oxidation state) and 2,479–2,483 eV (i.e., the energy range of oxidation state), signifying the occurrence of several oxidation states of S in the target terrestrial soils (Figure 3). Since oxidation state plays a major role in determining the electronic and physicochemical properties of sulfur species, as it exists in combination with a group of one or more other elements, the complicated S oxidation states emphasize the variety of sulfur speciation in terrestrial soil samples.

With the purpose of applying the sulfur K-edge XANES spectra as an innovative "fingerprint" to discriminate TBD from TMS, hierarchical cluster analysis (HCA) was performed by using average linkage clustering. The results demonstrated in the dendrogram (Figure 4) distinguished the 26 individual sulfur K-edge XANES spectra of marine sediments and terrestrial soil samples into two major clusters. The first major cluster (i.e., Cluster I) comprised of samples No. 53, No. 55, No. 71, No. 61, No. 49, No. 20, No. 34, No. 77, No. 48, and No. 36, which can be considered as an indicative of mixing of "TBD" and "TMS." Two major sediment types could be categorized from data similarities in line found in Cluster I. The first sediment group was characterized by samples No. 53, No. 55, No. 71, No. 61, No. 49, and No. 20 that can be considered as typical marine sediments except for sample No.71. The second one contained samples No. 34, No. 77, No. 48, and No. 36, which may be produced by the backwash of tsunami terrestrial deposits.

In order to get further insights into the sample categorization of the remaining clusters, individual dendrogram distribution of German terrestrial soils was further plotted and illustrated in Figure 4. The second major cluster (i.e., Cluster II) can be subdivided into two subclusters. The first subcluster consisted of A-Bv, B-H1, B-H2, B-Aeh, A-Of, A-Oh, A-Aeh, which were all collected at sampling site of Schlöppnerbunnen in Germany. Therefore, this subcluster represented the typical marks of Endostagnic, Leptic Cambisol (alumic), and Histic Stagnosol (albic, alumic). The second subcluster contained DH3, DH4, C-H2, C-Aa, which were found predominantly in Leptic Rheic Hemic Histosol (dystric). It was found that Cluster III was occupied by C-Gr, D-H2, D-Go, B-Srw, and C-H1, indicating the mixture of Histic Stagnosol (albic, alumic) and Leptic Rheic Hemic Histosol (dystric). Overall, HCA successfully discriminated the sulfur K-edge XANES spectra of marine sediments from those of terrestrial soils as displayed in Figure 4.

Obviously, this dendrogram is quite useful and provides valuable information to identify the differences between marine sediments and terrestrial soils. However, this dendrogram, as well as sulfur K-edge XANES spectra, should be analyzed with great caution as oxidation process coupled with microbiological activity can alter oxidation state of S during their transport from the sampling site to the analytical laboratory. With the intention of minimizing the above-mentioned uncertainties, principal component analysis (PCA) as the multivariate analytical tool was employed to reduce a set of original variables (i.e., measured sulfur K-edge XANES spectra in sediment and soil samples) and to extract a small number of latent factors (principal components (PCs)) for analyzing relationships among the observed variables. Data submitted for the analysis were arranged in a matrix, where each column corresponds to the number of sample and each row represents the absorption intensity of sulfur K-edge XANES spectra. Data matrixes were evaluated through PCA allowing the summarized data to be further analyzed and plotted.

With the aim of providing further interpretation of sulfur K-edge XANES spectra as sample fingerprints, a PCA model with three significant PCs, each representing 75.9%, 16.3%, and 4.52% of the variance, thus accounting for 96.7% of the total variation in the data, was calculated. After plotting factor scores of PC1, PC2, and PC3 in three dimensions, some distinctive features of data clustering were appeared. Firstly, 3D plots of Endostagnic, Leptic Cambisol (alumic), Histic Stagnosol (albic, alumic), and Leptic Rheic Hemic Histosol (dystric) are highly deviated from the Andaman coastal sediments in both TMS and TBD as illustrated in Figure 5(a). Secondly, a grouping of 3D plots of Andaman marine sediments can be further separated into two groups, which are (1) samples No. 20, No. 34, No. 36, No. 48, No. 49 (i.e., TMS) and (2) samples No. 53, No. 55, No. 61, No. 71, No. 77 (i.e., TBD) as displayed in Figure 5(b). As a consequence, it appears rationale to conclude that the combination of HCA and PCA could successfully distinguish German terrestrial soils from Andaman marine sediments, and thus enhancing the reliability of employing the sulfur K-edge XANES spectra as a new "fingerprint" to characterize environmental samples.

4. Conclusions

Generally, XANES spectra of $(NH_4)_2SO_4$, $CaSO_4$, $Al_2(SO_4)_3$, $MnSO_4$, $ZnSO_4 \cdot 7H_2O$, $K_2S_2O_3$, $Cr_2(SO_4)_3 \cdot 15H_2O$,

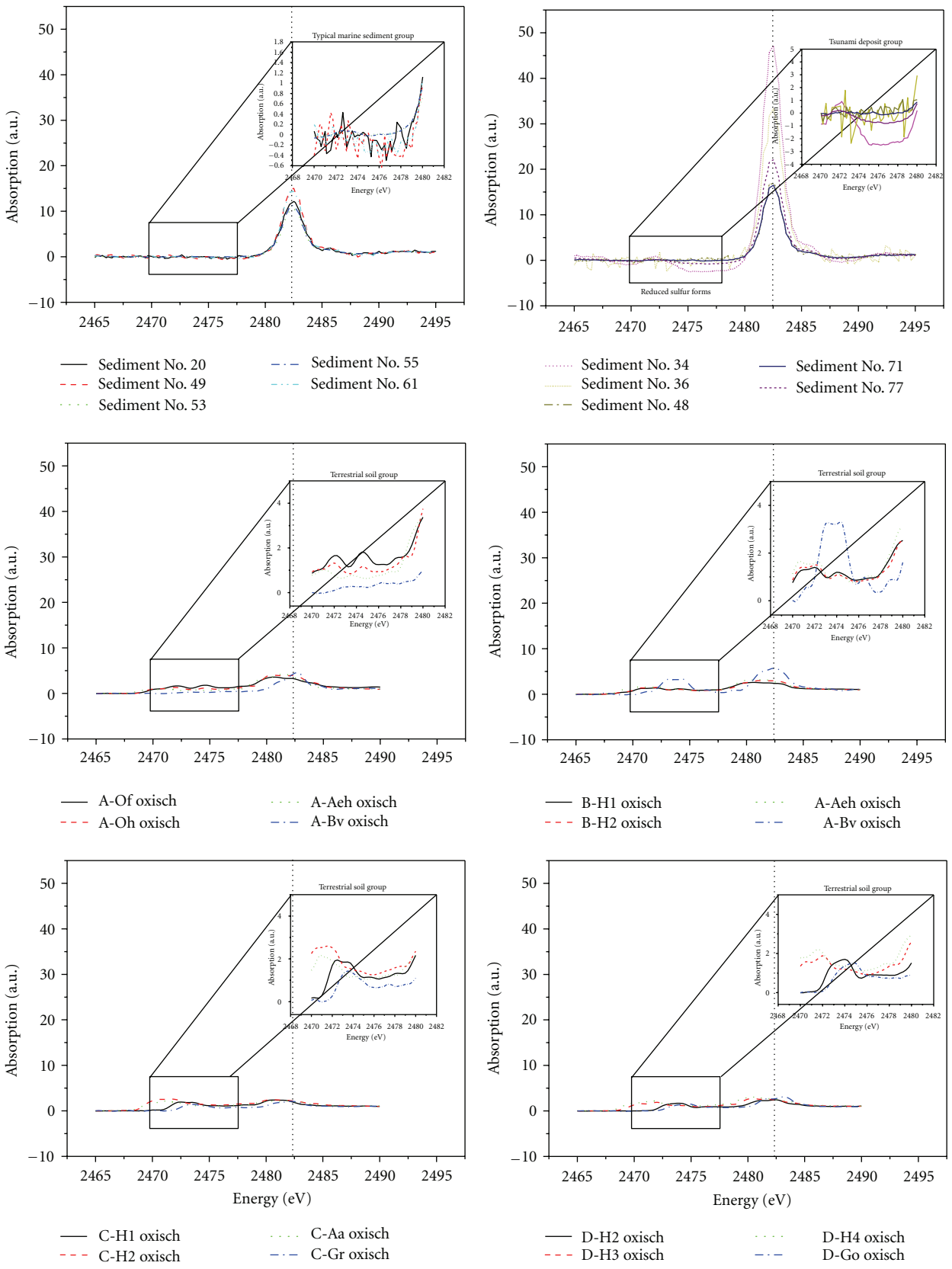


Figure 3: Sulfur K-edge XANES spectrum of typical marine sediment (TMS), tsunami backwash deposit (TBD), and German terrestrial soil (GS).

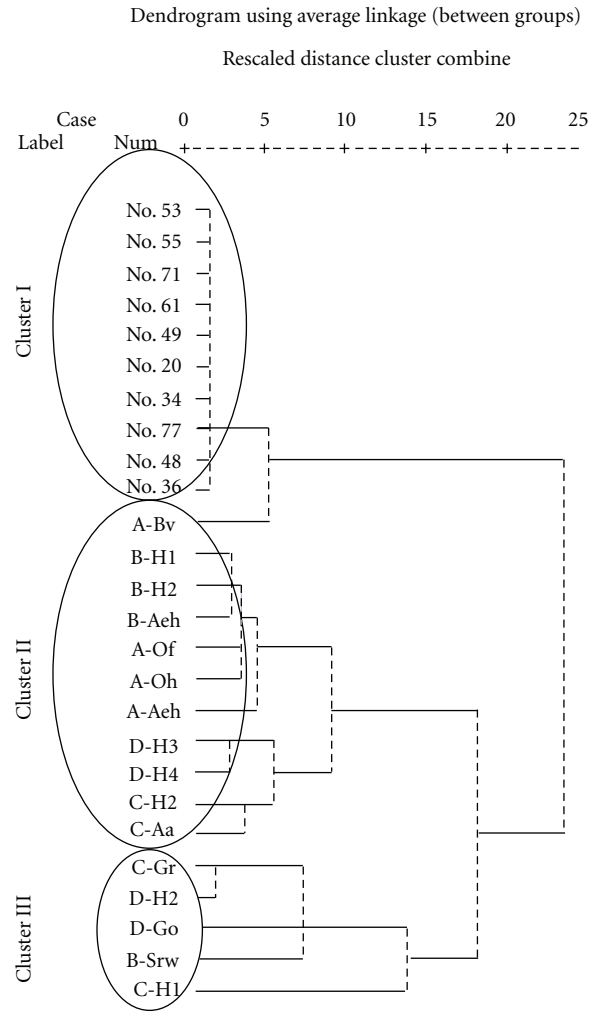


Figure 4: Dendrogram using average linkage (between groups) of Sulfur K-edge XANES spectrum of typical marine sediments (TMS), tsunami backwash deposits (TBD), and German terrestrial soils (GS).

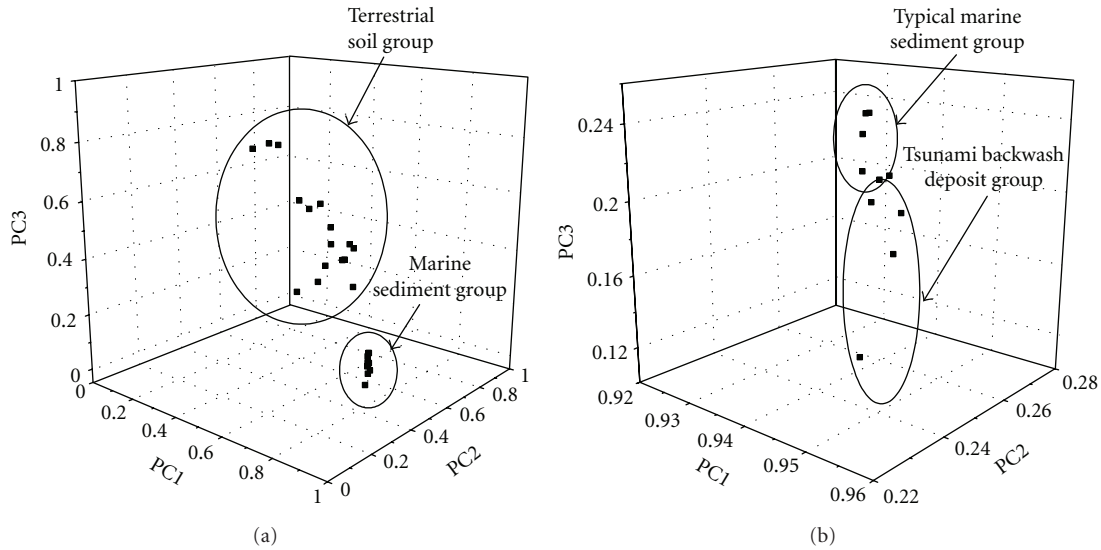


Figure 5: Three dimensional plots of principal component 1 (PC1), principal component 2 (PC2), and principal component 3 (PC3) of sulfur K-edge XANES spectrum of typical marine sediments (TMS), tsunami backwash deposits (TBD), and German terrestrial soils (GS).

$CoSO_4 \cdot 7H_2O$, $NiSO_4 \cdot 6H_2O$, and $CuSO_4 \cdot 5H_2O$ standards indicated that better sensitivity could be achieved in both detectors with mixing ratios of standard to BN at 0.1%. There were no significant differences in term of instrumental sensitivity detected by both Lytle and Germanium detectors. Further investigation was conducted to assess the sensitivities of sulfur K-edge XANES spectra as functions of atmospheric particle sizes. For urban aerosols, the S/N ratios of sulfur K-edge XANES spectra are anticorrelated with atmospheric particle sizes. However, this concept cannot be applied to sulfate-rich coarse particle-like maritime TSP. This study has proved that the sensitivities of sulfur K-edge XANES spectra were positively correlated with sulfate content in particles and negatively associated with atmospheric particle sizes. In addition, the combination of advanced statistical methods such as HCA and PCA evidently separated German terrestrial soils from Andaman marine sediment, and moderately distinguished typical marine sediments from tsunami backwash deposits.

Acknowledgments

This work has been performed with the approval of Synchrotron Light Research Institute (Public Organization). This study was bilaterally supported by the National Research Council of Thailand (NRCT) and the German Research Foundation (DFG) under the project entitled "Tsunami deposits in near-shore and coastal waters of Thailand (TUNWAT), Grant code: SCHW 572/11-1." A support from Institute of Earth Environment, Chinese Academy of Sciences (IEECAS), National Institute of Development Administration (NIDA), and National Center of Excellence for Environmental and Hazardous Waste Management, Chulalongkorn University is also acknowledged.

References

[1] X. Q. Shan, B. Chen, T. H. Zhang, F. L. Li, B. Wen, and J. Qian, "Relationship between sulfur speciation in soils and plant availability," *Science of the Total Environment*, vol. 199, no. 3, pp. 237–246, 1997.

[2] J. T. Kiehl and B. P. Briegleb, "The relative roles of sulfate aerosols and greenhouse gases in climate forcing," *Science*, vol. 260, no. 5106, pp. 311–314, 1993.

[3] R. J. Chalrson and S. E. Schwartz, "Climate forcing by anthropogenic aerosols," *Science*, vol. 255, no. 5043, pp. 423–430, 1992.

[4] W. P. Robarge, J. T. Walker, R. B. McCulloch, and G. Murray, "Atmospheric concentrations of ammonia and ammonium at an agricultural site in the southeast United States," *Atmospheric Environment*, vol. 36, no. 10, pp. 1661–1674, 2002.

[5] S. Beike, "Acid deposition: an updated review on atmospheric physico-chemical aspects of the acid deposition problem in Europe," CEC Publ. AP/53/85, 27, 1985.

[6] G. Zhou and K. Tazaki, "Seasonal variation of gypsum in aerosol and its effect on the acidity of wet precipitation on the Japan Sea side of Japan," *Atmospheric Environment*, vol. 30, no. 19, pp. 3301–3308, 1996.

[7] Y. J. Zhu, N. Olson, and T. P. Beebe, "Surface chemical characterization of 2.5-μm particulates ($PM_{2.5}$) from air pollution in salt lake city using TOF-SIMS, XPS, and FTIR," *Environmental Science & Technology*, vol. 35, no. 15, pp. 3113–3121, 2001.

[8] T. C. Xiao, W. X. Liu, H. T. Liu, and S. R. Wang, "Analysis on the Character of Atmospheric Particulates from Different Pollution Sources in Jinan City," *Environmental Chemistry*, vol. 17, p. 582, 1998.

[9] J. S. Pastuszka, A. Wawroś, E. Talik, and K. T. Paw, "Optical and chemical characteristics of the atmospheric aerosol in four towns in southern Poland," *Science of the Total Environment*, vol. 309, no. 1–3, pp. 237–251, 2003.

[10] I. J. Pickering, G. N. George, E. Y. Yu et al., "Analysis of sulfur biochemistry of sulfur bacteria using X-ray absorption spectroscopy," *Biochemistry*, vol. 40, no. 27, pp. 8138–8145, 2001.

[11] P. Feldens, K. Schwarzer, W. Szczuciński, K. Stattegger, D. Sakuna, and P. Somgpongchaiykul, "Impact of 2004 tsunami on seafloor morphology and offshore sediments, Pakarang Cape, Thailand," *Polish Journal of Environmental Studies*, vol. 18, no. 1, pp. 63–68, 2009.

[12] J. Prietzel, N. Tyufekchieva, K. Eusterhues et al., "Anoxic versus oxic sample pretreatment: effects on the speciation of sulfur and iron in well-aerated and wetland soils as assessed by X-ray absorption near-edge spectroscopy (XANES)," *Geoderma*, vol. 153, no. 3-4, pp. 318–330, 2009.

[13] W. Klysubun, P. Sombunchoo, N. Wongprachanukul et al., "Commissioning and performance of X-ray absorption spectroscopy beamline at the Siam Photon Laboratory," *Nuclear Instruments and Methods in Physics Research A*, vol. 582, no. 1, pp. 87–89, 2007.

[14] R. Chauvistré, J. Hormes, E. Hartmann, N. Etzenbach, R. Hosch, and J. Hahn, "Sulfur K-shell photoabsorption spectroscopy of the sulfanes R-Sn-R, n = 2-4," *Chemical Physics*, vol. 223, no. 2-3, pp. 293–302, 1997.

[15] M. Newville, "IFEFFIT: interactive XAFS analysis and FEFF fitting," *Journal of Synchrotron Radiation*, vol. 8, no. 2, pp. 322–324, 2001.

[16] E. H. Shaban, D. P. Siddons, and A. Kuczewski, "Gas electron multiplier (GEM) enhanced ionization chamber for fluorescence detector," *Nuclear Instruments and Methods in Physics Research A*, vol. 582, no. 1, pp. 185–186, 2007.

[17] P. Sangsingk, K. D. Berry, E. J. Dumas, T. W. Raudorf, and T. A. Underwood, "Advances in germanium detector technology," *Nuclear Instruments and Methods in Physics Research A*, vol. 505, no. 1-2, pp. 183–186, 2003.

[18] Y. Takahashi, Y. Kanai, H. Kamioka et al., "Speciation of sulfate in size-fractionated aerosol particles using sulfur K-edge x-ray absorption near-edge structure," *Environmental Science and Technology*, vol. 40, no. 16, pp. 5052–5057, 2006.

[19] F. E. Huggins, G. P. Huffman, and J. D. Robertson, "Speciation of elements in NIST particulate matter SRMs 1648 and 1650," *Journal of Hazardous Materials*, vol. 74, no. 1-2, pp. 1–23, 2000.

[20] H. Sekiyama, N. Kosugi, H. Kuroda, and T. Ota, "Sulfur K-edge absorption spectra of Na_2SO_4, Na_2SO_3, $Na_2S_2O_3$, and $Na_2S_2O_x$ (x=5–8)," *Bulletin of the Chemical Society of Japan*, vol. 59, no. 2, pp. 575–579, 1986.

[21] S. C. M. Myneni, "Soft X-ray spectroscopy and spectromicroscopy studies of organic molecules in the environment," *Reviews in Mineralogy and Geochemistry*, vol. 49, no. 1, pp. 485–579, 2002.

[22] X. Zhang, H. Ade, C. Jacobsen et al., "Micro-XANES: chemical contrast in the scanning transmission X-ray microscope," *Nuclear Instruments and Methods in Physics Research A*, vol. 347, no. 1–3, pp. 431–435, 1994.

[23] W. F. Pong, Y. K. Chang, H. H. Hsieh et al., "Electronic and atomic structures of Si-C-N thin film by X-ray-absorption spectroscopy," *Journal of Electron Spectroscopy and Related Phenomena*, vol. 92, no. 1–3, pp. 115–118, 1998.

[24] Y. Takahashi, T. Miyoshi, S. Yabuki, Y. Inada, and H. Shimizu, "Observation of transformation of calcite to gypsum in mineral aerosols by Ca K-edge X-ray absorption near-edge structure (XANES)," *Atmospheric Environment*, vol. 42, no. 26, pp. 6535–6541, 2008.

[25] G. Falkenberg, G. Pepponi, C. Streli, and P. Wobrauschek, "Comparison of conventional and total reflection excitation geometry for fluorescence X-ray absorption spectroscopy on droplet samples," *Spectrochimica Acta B*, vol. 58, no. 12, pp. 2239–2244, 2003.

[26] F. Meirer, G. Pepponi, C. Streli et al., "Application of synchrotron-radiation-induced TXRF-XANES for arsenic speciation in cucumber (Cucumis sativus L.) xylem sap," *X-Ray Spectrometry*, vol. 36, no. 6, pp. 408–412, 2007.

[27] Y. Takahashi, T. Miyoshi, S. Yabuki, Y. Inada, and H. Shimizu, "Observation of transformation of calcite to gypsum in mineral aerosols by Ca K-edge X-ray absorption near-edge structure (XANES)," *Atmospheric Environment*, vol. 42, no. 26, pp. 6535–6541, 2008.

[28] J. Osán, F. Meirer, V. Groma et al., "Speciation of copper and zinc in size-fractionated atmospheric particulate matter using total reflection mode X-ray absorption near-edge structure spectrometry," *Spectrochimica Acta B*, vol. 65, no. 12, pp. 1008–1013, 2010.

[29] U. E. A. Fittschen, F. Meirer, C. Streli et al., "Characterization of atmospheric aerosols using Synchroton radiation total reflection X-ray fluorescence and Fe K-edge total reflection X-ray fluorescence-X-ray absorption near-edge structure," *Spectrochimica Acta B*, vol. 63, no. 12, pp. 1489–1495, 2008.

[30] C. Streli, G. Pepponi, P. Wobrauschek et al., "Recent results of synchrotron radiation induced total reflection X-ray fluorescence analysis at HASYLAB, beamline L," *Spectrochimica Acta B*, vol. 61, no. 10-11, pp. 1129–1134, 2006.

[31] S. Frisia, A. Borsato, I. J. Fairchild, and J. Susini, "Variations in atmospheric sulphate recorded in stalagmites by synchrotron micro-XRF and XANES analyses," *Earth and Planetary Science Letters*, vol. 235, no. 3-4, pp. 729–740, 2005.

[32] F. Cozzi, I. Pellegrini, G. Adami, E. Reisenhofer, M. Bovenzi, and P. Barbieri, "Sulphur speciation of PM10 samples by XANES spectroscopy," *Central European Journal of Chemistry*, vol. 7, no. 3, pp. 395–401, 2009.

[33] M. Higashi and Y. Takahashi, "Detection of S(IV) species in aerosol particles using XANES spectroscopy," *Environmental Science & Technology*, vol. 43, no. 19, pp. 7357–7363, 2009.

[34] S. Henning, E. Weingartner, M. Schwikowski et al., "Seasonal variation of water-soluble ions of the aerosol at the high-alpine site Jungfraujoch (3580 m asl)," *Journal of Geophysical Research D*, vol. 108, no. 4030, 10 pages, 2003.

[35] G. Zhou and K. Tazaki, "Seasonal variation of gypsum in aerosol and its effect on the acidity of wet precipitation on the Japan Sea side of Japan," *Atmospheric Environment*, vol. 30, no. 19, pp. 3301–3308, 1996.

[36] J. A. Moralesa, D. Pirelab, M. G. Navaa, B. S. Borregoa, H. Velásqueza, and J. Durána, "Inorganic water soluble ions in atmospheric particles over Maracaibo Lake Basin in the western region of Venezuela," *Atmospheric Research*, vol. 46, no. 3-4, pp. 307–320, 1998.

[37] M. O. Andrea, "The emissions of sulfur to the remote atmosphere: background paper," in *The Biogeochemical Cycling of Sulfur and Nitrogen in the Remote Atmosphere*, J. N. Galloway, R. I. Charlson, M. O. Andreae, and H. Rodhe, Eds., p. 5, Reidel, Dordrecht, The Netherlands, 1985.

[38] J. W. Fitzgerald, "Marine aerosols: a review," *Atmospheric Environment A*, vol. 25, no. 3-4, pp. 533–545, 1991.

[39] M. Choowong, N. Murakoshi, K. I. Hisada et al., "2004 Indian Ocean tsunami inflow and outflow at Phuket, Thailand," *Marine Geology*, vol. 248, no. 3-4, pp. 179–192, 2008.

[40] W. Szczuciński, P. Niedzielski, G. Rachlewicz et al., "Contamination of tsunami sediments in a coastal zone inundated by the 26 December 2004 tsunami in Thailand," *Environmental Geology*, vol. 49, no. 2, pp. 321–331, 2005.

[41] W. Szczuciński, N. Chaimanee, P. Niedzielski et al., "Environmental and geological impacts of the 26 December 2004 tsunami in coastal zone of Thailand—overview of short and long-term effects," *Polish Journal of Environmental Studies*, vol. 15, no. 5, pp. 793–810, 2006.

[42] A. Siripong, "Andaman seacoast of Thailand field survey after the december 2004 Indian ocean tsunami," *Earthquake Spectra*, vol. 22, supplement 3, pp. 187–202, 2006.

[43] J. Prietzel, J. Thieme, N. Tyufekchieva, D. Paterson, I. McNulty, and I. K. Knabner, "Sulfur speciation in well-aerated and wetland soils in a forested catchment assessed by sulfur k-edge x-ray absorption near-edge spectroscopy (xanes)," *Journal of Plant Nutrition and Soil Science*, vol. 172, no. 3, pp. 393–403, 2009.

[44] J. Prietzel, J. Thieme, M. Salomé, and H. Knicker, "Sulfur K-edge XANES spectroscopy reveals differences in sulfur speciation of bulk soils, humic acid, fulvic acid, and particle size separates," *Soil Biology and Biochemistry*, vol. 39, no. 4, pp. 877–890, 2007.

[45] A. L. Bates, E. C. Spikera, W. H. Orema, and W. C. Burnettb, "Speciation and isotopic composition of sulfur in sediments from Jellyfish Lake, Palau," *Chemical Geology*, vol. 106, no. 1-2, pp. 63–76, 1993.

[46] E. Lallier-Vergès, P. Bertrand, and A. Desprairies, "Organic matter composition and sulfate reduction intensity in Oman Margin sediments," *Marine Geology*, vol. 112, no. 1–4, pp. 57–69, 1993.

ISSN 8755-6839

SCIENCE OF TSUNAMI HAZARDS

Journal of Tsunami Society International

Volume 32 Number 1 2013

USING FOURIER TRANSFORM INFRARED (FTIR) TO CHARACTERIZE TSUNAMI DEPOSITS IN NEAR-SHORE AND COASTAL WATERS OF THAILAND

S. Pongpiachan[1*], K. Thumanu[2], W. Na Phatthalung[2], D. Tipmanee[3, 4], P. Kanchai[1], P. Feldens[5] and K. Schwarzer[6]

[1]NIDA Center for Research & Development of Disaster Prevention & Management, School of Social and Environmental Development, National Institute of Development Administration (NIDA), Bangkok, THAILAND

[*]Corresponding author: pongpiajun@gmail.com

[2]Synchrotron Light Research Institute (Public Organization), Ministry of Science and Technology, THAILAND

[3]International Postgraduate Program in Environmental Management, Graduate School, Chulalongkorn University, Bangkok, THAILAND

[4]Center of Excellence for Environmental and Hazardous Waste Management (EHWM), Chulalongkorn University, Bangkok, THAILAND

[5]GEOMAR Helmholtz Centre for Ocean Research Kiel, GERMANY

[6]Institute of Geosciences Sedimentology, Coastal and Continental Shelf Research, Christian Albrechts University of Kiel, Kiel, GERMANY

ABSTRACT

Understanding the tsunami cycle requires a simple method for identification of tsunami backwash deposits. This study investigates Fourier transform infrared (FTIR) spectroscopy followed by careful analysis of variance (ANOVA), Gaussian distribution, hierarchical cluster analysis (HCA) and principal component analysis (PCA) for the discrimination of typical marine sediments and tsunami backwash deposits. In order to test the suitability of FTIR spectra as innovative methods for classifications of tsunami deposits, typical marine sediments and terrestrial soils were classified into three zones, namely zone-1 (i.e. typical marine sediments), zone-2 (i.e. including tsunami backwash deposits) and zone-3 (i.e. coastal terrestrial soils). HCA was performed to group the spectra according to their spectral similarity in a dendrogram and successfully separate FTIR spectra of all three sampling zones into two main clusters with five sub-clusters. The *simplicifolious* (i.e. single-leafed) type of dendrogram was observed with the strong dissimilarity of terrestrial components in subcluster-5. Graphical displays of PC1 *vs* PC2 highlight the prominent features of zone-1, which is explicitly

different from those of zone-2 and zone-3. The acceptable discrimination of typical marine sediments and tsunami backwash deposits, even six years after the tsunami on Boxing Day 2004, dramatically demonstrates the potential of the method for the identification of paleotsunami.

***Keywords**: Tsunami Deposits, Fourier Transform Infrared Spectroscopy (FTIR), Analysis of Variance, Hierarchical Cluster Analysis, Principal Component Analysis, Andaman Sea*

1. INTRODUCTION

The 2004 Indian Ocean earthquake is widely acknowledged by the scientific community as one of the world's greatest natural disasters in modern times. The earthquake-generated tsunami caused more than 225,000 of deaths, and damaged the coastal areas of the Indian Ocean countries. The tsunami studies on modern and ancient onshore sedimentary deposits related to the alteration of geological and sedimentological features received massive attention after the Chile tsunami in 1960. For instance, several tsunami-related studies were conducted in North America (Atwater, 1987; Benson et al., 1997; Clague and Bobrowsky, 1994), Thailand (Choowong et al., 2007, 2008a, 2008b, 2009; Szczuciński et al., 2005, 2006, 2007), Papua New Guinea (Gelfenbaum and Jaffe, 2003), Kamchatka (Pinegina and Bourgeois, 2001), Scotland (Dawson et al., 1988; Dawson et al., 1991) and Norway (Bondevik et al., 1997). In addition, the frequency of hurricane/Indian Ocean monsoon (IOM) contributes to the continental input significantly to the offshore regions (Narayana et al., 2008; Scheffers et al., 2009). Despite of a fairly large number of papers dealing with several impacts of the extreme event onshore, little is known about the geomorphological, sedimentological and geological alterations offshore. Since the offshore physical data is substantially crucial for the study of both the modern and past extreme event, it is therefore important to distinguish the difference between terrestrial deposit and background submarine sediment.

In principle, there are several physical evidences to prove the existence of extreme event--originated terrestrial deposits. For example, it is well known that the enrichment of plant debris in sediment can be considered as signatures of terrestrial records (Cantalamessa and Di Celma, 2005; Narayana et al., 2008; Scheffers et al., 2009). However, there are also several problems associated with the employment of these conventional proxies due to its low preservation potential in the submarine environment. Firstly as the plant fragments settle through the water column, several biogeochemical transformations such as remineralization, chemical decomposition and microbial degradation take place. Secondly, the power of wind-generated waves, hurricane/monsoon waves, daily tides, and even anthropogenic activities such as the clean-up of the contaminated sediments coupled with natural bioturbation can dramatically alter both the topographical and sedimentological features of tsunami deposit. Thirdly, there is no single feature to categorize tsunami, hurricane, monsoon and other types of extreme event deposits except through the careful comprehensive investigation of variability in sediment grain-size, shape, roundness, packing, sorting with the precise assessment of the lateral geometry of the entire sedimentary body (Cantalamessa and Di Celma, 2005; Dawson et al., 1988; Dawson and Shi, 2000). In the light of these difficulties, more alternative well-preserved terrestrial indicators are essentially required to enhance the reliability of data interpretation.

In this study, the authors hypothesize that the employment of Fourier Transform Infrared Spectroscopy (FTIR) coupled with various analogies of statistical analysis assist in a better understanding of offshore terrestrial deposit distribution pattern, which can be subject to erosion by tsunami/monsoon waves and surface runoff by heavy rain in the tsunami-affected coastal areas of Andaman Sea, Thailand. Note that it is the purpose of this paper to illustrate the general principle of using organic functional group analyzed by FTIR for the first time as an innovative proxy to separate the terrestrial deposit from the background sediment in tsunami-affected coastal areas. Neither the source apportionment, nor the analysis of spatial variation of organic functional group in sediments is the main focus of this study. In addition, the risks and possibilities of applying FTIR spectral feature as an alternative extreme event proxy will be reviewed and discussed.

2. MATERIALS AND METHODS

2.1 Study area and sampling methods

The Phang Nga coastal zone was chosen as the study area, where is located in the Andaman Sea, eastern part of the Indian Ocean (see Fig. 1). The study area is approximately 1000 km² (east-west extension: 25 km, north-south extension: 40 km) where some part was heavily destroyed by the Tsunami 2004. Soil samples were also collected along the coastline from Thub Lamu to Ban Nam Khem in Phang Nga province. The surface sediment samples were collected along the Phang Nga coastal area during December 2007 and March 2010. The criteria for selecting the sampling station was based on the evidence of sedimentary deposit in the study area which Feldens and co-worker (2009) surveyed by using the combination of Multi-beam, Side Scan Sonar and Boomer system. One hundred and seven surface sediment samples were collected by using Van-veen Grab Sampler. Sediment samples were kept in clean aluminum foil, placed in a glass bottle, and stored at - 20ºC. After removing stones and shell residuals, they were freeze-dried and sieved to <0.076 mm (200 mesh), and then kept at -20^{o}C until analysis. Soil sampling stations (27 stations) were collected during 18-22 July 2009. The areas, which were affected by the 2004 tsunami (Szczucinski, et al., 2005), were taken into consideration for choosing the sampling station. About a half kilogram of composite sample from 2-m^2 area of each station was collected by using the shovel and then pre-treated as follows as surface sediment samples. All samples were investigated using FTIR to discriminate between the terrestrial sediment and background marine sediment.

2.2 FTIR and statistical analysis

Infrared spectroscopy technique has been widely used for determinations of chemical compositions in sediments (Kovač et al., 2006; Moros et al., 2009; Ramasamy et al., 2009). Recently, in the past few years, FTIR has received much attention as an alternative analytical instrument for determination of organic functional groups in both terrestrial soils and marine sediments because of its relatively fast processing speed, simple operating system and reasonable costs (Moros et al., 2010; Parikh et al., 2008). In this study, the sediment samples were mixed with KBr at various ratios. The optimum

condition for KBr mixing was chosen at 1:15 ratio (sample: KBr) as it gives the highest signal to noise ratio. The mixture was then pressed into a transparent disc in an evacuable pellet die at sufficiently high pressure. The infrared spectra were collected using FTIR Spectroscopy with transmission sampling module and coupled with the highly sensitive mercury cadmium telluride (MCT) detector cooled with liquid nitrogen over the measurement range from 4000 to 600 cm^{-1}. The measurements were performed with a spectral resolution of 4 cm^{-1} with 64 scans co-added. (Bruker Optics Ltd, Ettlingen, Germany). The relative integral areas of each peak were then performed using OPUS 6.5 software (Bruker optic, German). In addition, statistical analysis of T-Test, ANOVA, Hierarchical Cluster Analysis (HCA) and Principal Component Analysis (PCA) were performed by using SPSS Version 13.0.

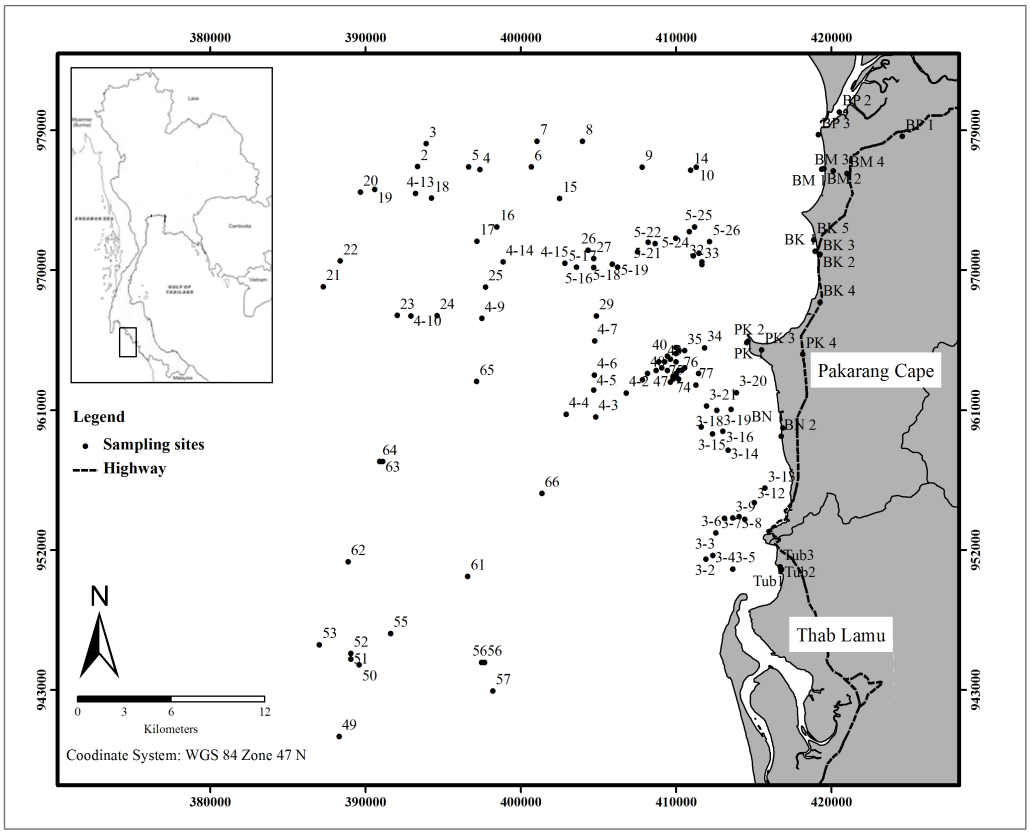


Fig. 1. Sampling site locations at Khao Lak coastal areas, Phang Nga Province, Thailand. (The study area is indicated by the black box; numbers indicate sampling stations).

3. RESULTS AND DISCUSSION

3.1.Characteristics of FTIR spectra

In order to test the availability of FTIR spectra as fingerprints for characterization of tsunami deposits, all marine sediments and terrestrial soils were classified into three zones, namely zone-1 (typical marine sediments), zone-2 (tsunami backwash deposits) and zone-3 (coastal terrestrial soils).

All sampling codes and zone descriptions are clearly illustrated in Table 2.

Table 1. Sampling code, date and description of marine sediments and terrestrial soil samples.

Sampling code	Sampling date	Sampling description
		Terrestrial Soil
Tub1	July-18-2009	Canal bank
Tub2	July-18-2009	Tsunami deposit layer
Tub3	July-18-2009	Rubber Plantation
PK 1	July-19-2009	Beach
PK 2	July-19-2009	Tsunami deposit layer
PK 3	July-19-2009	Shrimp pond
PK 4	July-19-2009	Road side
BK 1	July-19-2009	Tsunami deposit layer
BK 2	July-19-2009	Rubber Plantation
BK 3	July-19-2009	Rubber Plantation
BK 4	July-19-2009	Rubber Plantation
BK 5	July-19-2009	Tsunami deposit layer
BN 1	July-20-2009	Canal bank
BN 2	July-20-2009	Canal bank
BM 1	July-20-2009	Tsunami deposit layer
BM 2	July-20-2009	Pond
BM 3	July-20-2009	Rubber Plantation
BM 4	July-20-2009	Palm Plantation
BP 1	July-20-2009	Pond
BP 2	July-20-2009	Mangrove
BP 3	July-20-2009	Nam Khen port
		Sediment
2,3,4,5,6,7,8,9,10	December-1-2007	Pakarang cape sediment
11,12,13,14,15,16,17,18,19,20	December-2-2007	Pakarang cape sediment
21,22,23,24,25,26,27,29	December-3-2007	Tsunami affected sediment
31,32,33,34,35,36,37,39,40,41,42,43,44,45,46,47,48	December-5-2007	Tsunami affected sediment
49,50,51,52,53,55,56,57,58,61,62,63,64,65,66	December-7-2007	Thup Lamu Sediment
68,69,70,71,72,73,74,75,76,77,78	December-8-2007	Tsunami affected sediment
3-1,3-2,3-3,3-4,3-5,3-6,3-7,3-8,3-9,3-10,3-11,3-12,3-13-3-14,3-15,3-16,3-17,3-18,3-19,3-20,3-21,3-23	March-3-2010	Khao lak near shore sediment
4-1,4-2,4-3,4-4,4-5,4-6,4-7,4-9,4-10,4-13,4-14,4-15	March-4-2010	Pakarang cape sediment
5-16,5-17,5-18,5-19,5-20,5-21,5-22,5-23,5-24,5-25,5-26	March-5-2010	Pakarang cape sediment

Table 2. Sample members of each zone

Zone	Sample members	Zone description
Zone-1	25, 04-09, 04-10, 6, 7, 4-13, 16, 17, 18, 19, 20, 22, 50, 52, 53, 55, 56, 49, 57, 61, 62, 63, 64, 66, 23	Zone-1 sediment samples seem not to be affected by tsunami backwash and can be considered as typical marine sediments. All sampling positions were located within the range of 12 to 24 km offshore.
Zone-2	2, 3, 4, 5, 8, 9, 10, 11, 12, 14, 15, 26, 27, 29, 30, 31, 32, 34, 35, 36, 37, 39, 40, 42, 43, 44, 45, 46, 47, 48, 54, 69, 70, 71, 72, 73, 76, 77, 3-02, 3-03, 3-04, 3-05, 3-06, 3-07, 3-08, 3-10, 3-13, 3-14, 3-15, 3-16, 3-17, 3-18, 3-19, 3-20, 3-21, 4-01, 4-02, 4-03, 4-04, 4-05, 4-06, 4-07, 4-08, 4-14, 4-15, 5-12, 5-16, 5-17, 5-18, 5-19, 5-20, 5-21, 5-22, 5-23, 5-24, 5-25, 5-26	According to the acoustic profile data, Zone-2 is most likely to be influenced by the tsunami backwash deposits. All sampling positions were situated within 12 km from the shoreline.
Zone-3	Tub1, Tub2, Tub3, PK1, PK2, PK3, PK4, BK1, BK2, BK3, BK4, BK5, BN1, BN2, BM1, BM2, BM3, BM4, BP1, BP2, BP3	Zone-3 is characterized as natural samples of onshore terrestrial soils.

The FTIR spectra for all sampling zones are compared in Fig. 2. Overall, the spectra of all samples are generally quite similar to each other, which can be characterized by *i*) broad and strong absorption band in the 3750-3000 cm^{-1} intervals (OH vibration of hydroxyl groups in alumino-silicates and OH vibration of water and OH groups organic fraction of sediments) followed by moderate C-H stretching bands in the interval from 2960 to 2800 cm^{-1}; *ii*) moderately strong CO_3^{2-} absorption peaks in the frequency range of 2660-2450 cm^{-1}; *iii*) the overlap of several possible absorption peaks, namely free water, C-C stretching of aromatics and alkene double bonds, C=O stretch of secondary amides corresponding NH, COO asymmetric stretching of metal carboxylates and carbonate minerals (calcite) in the interval from 1756 to 1268 cm^{-1} and iv) strong Si-O (silicate mineral) absorption peaks in the frequency range of 1270-895 cm^{-1}.

Although FTIR spectra of all sampling zones display relatively similar distribution pattern in the frequency range from 3750 to 750 cm^{-1}, some subtle differences were observed in the vibrational modes of organic components indicating the dissimilarities of chemical compositions in each sampling zones. For instance, the prominent feature of three small sharp peaks on the first broad main peak was detected in the interval of 3750-3500 cm^{-1} of zone-3, highlighting the differences in contribution of hydrogen bond lengths and orientations that mostly corresponding to the OH and NH groups (Wolkers et al., 2004). This can possibly be explained by the relatively high contribution of kaolinite in terrestrial soils, which had previously been mentioned in several studies (Martinez et al., 2010; Rong et al., 2008; Yusiharni and Gilkes, 2012). Interestingly, the characteristic peaks of humic acids (HA) and fulvic acids (FA), which can be explained by two intense bands at 1700 cm^{-1} and 1640 cm^{-1} were always observed for all sampling zones. The first absorption band is characterized as C=O stretching vibration of carboxylic acid groups (Mac Carthy and Rice, 1985, Davis et al., 1999 and Richard et al., 2007), whilst the second band is interpreted as the mixture of the stretching vibrations of C=C aromatic bonds, conjugated carbonyl groups (quinone), carboxylic salt groups and amide groups (Vergnoux et al., 2011). Another crucial feature is characteristic peak of lignin spectrum,

which can be assigned to an aromatic νC=C stretching vibration in the interval of 1517–1509 cm^{-1} (Duarte et al., 2007; Tinoco et al., 2006). Apart from the characteristic peaks of kaolinite, HA, FA and lignin observed in zone-2 and zone-3, the sharp peak appears in the interval range of 947-895 cm^{-1} detected in zone-1 emphasizing the influence of relatively high contribution of silicate mineral in typical marine deposits.

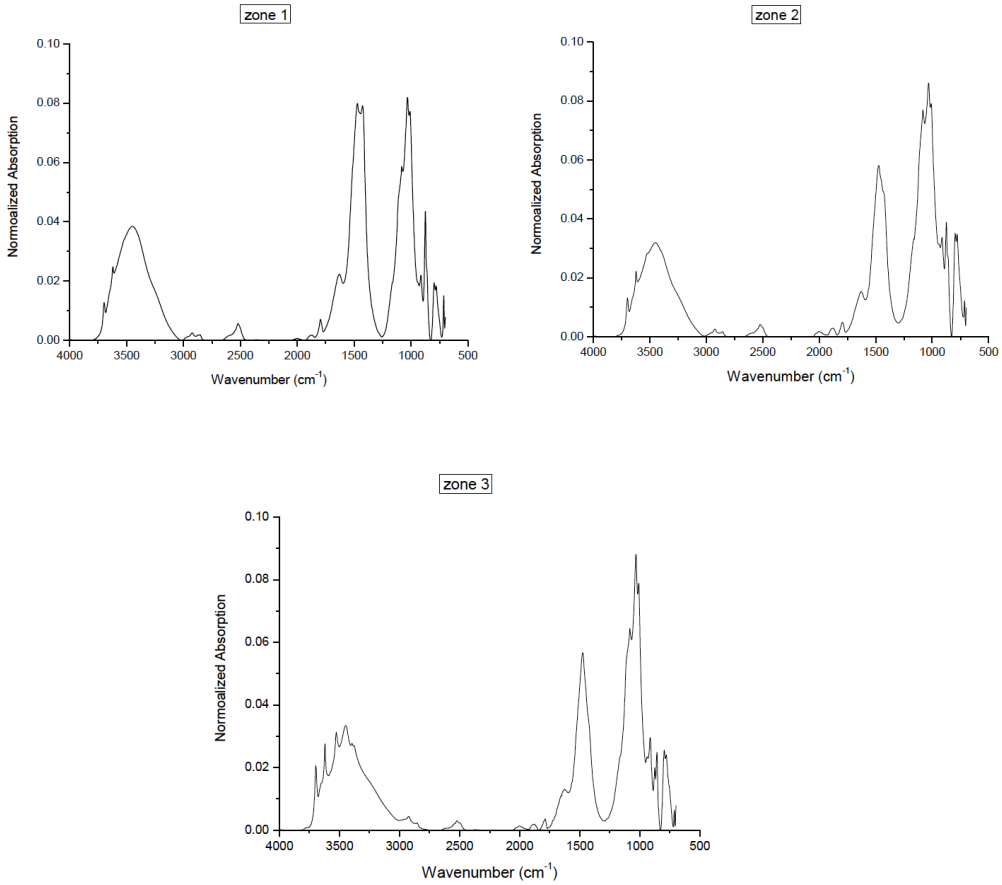


Fig. 2. FTIR spectral of Zone-1, Zone-2 and Zone-3 in 4000-500 cm^{-1} frequency range.

3.2. Comparison of integrated peak area of FTIR

Averages and standard deviations of integrated peak area of FTIR spectra at 12 different absorption bands (i.e. 3715-3608 cm^{-1}, 3608-3048 cm^{-1}, 3020-2800 cm^{-1}, 2660-2450 cm^{-1}, 2066-1930 cm^{-1}, 1930-1846 cm^{-1}, 1832-1760 cm^{-1}, 1756-1600 cm^{-1}, 1600-1268 cm^{-1}, 1270-895 cm^{-1}, 895-831 cm^{-1}, 831-708 cm^{-1}) of all sampling zones were carefully investigated and compared as shown in Fig. 3. A visual comparison reveals fundamental differences between sampling zones observed in the frequency range of 3608-3048 cm^{-1}, 1756-1600 cm^{-1}, 1600-1268 cm^{-1} and 831-708 cm^{-1}. Significant differences were observed for these four absorption bands based on the analysis of variance (ANOVA). For instance,

zone-1 shows significantly higher integrated peak area observed in the frequency range of 3608-3048 cm^{-1} and 1600-1268 cm^{-1}, which can be explained by relatively larger contribution of OH group organic fractions and calcites as typical chemical components often found in marine sediments (Kovač et al., 2005, 2006). No significant differences of alumino-silicates and carbonate minerals were observed in the interval of 3020-1760 cm^{-1}, highlighting the homogeneity of these chemical substances in sampling sites. Interestingly, zone-3 displays significantly higher contributions of aromatic compounds and alkene double bond in the absorption bands of 1756-1600 cm^{-1}that might represent the existence of HA, FA and lignin in terrestrial soils.

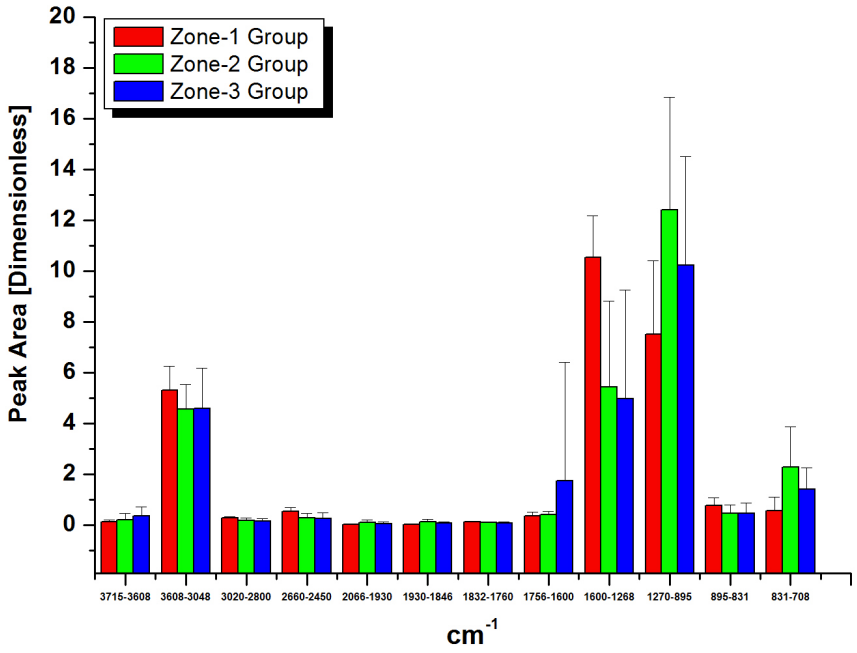


Fig. 3. Integrated peak area of FTIR spectra at 12 different absorption bands for Zone-1, Zone-2 and Zone-3 group.

In order to achieve more comprehensive analysis of FTIR spectra characteristics of each sampling zone, percentage area graphs of 12 absorption bands were plotted and illustrated in Figure 4. Symmetrical triangle shapes of percentage area graphs of all sampling zones appear in the absorption bands from 3715 to 2800 cm^{-1}. However, the dissimilarity between percentage area graphs becomes apparent at the frequency range of 1756-831 cm^{-1}. This discrepancy arises essentially from the fact that zone-2 was more influenced by terrestrial materials of zone-3 in comparison with zone-1. Since the FTIR absorption bands from 1756 to 831 cm^{-1} contain relatively complicated mixture of several organic compounds, mainly HA, FA and lignin, it appears reasonable to interpret the strong similarity of percentage area graphs observed in zone-2 and zone-3 as a consequence of tsunami backwash that

dragged large amounts of terrestrial materials from coastal area into near shore zone.

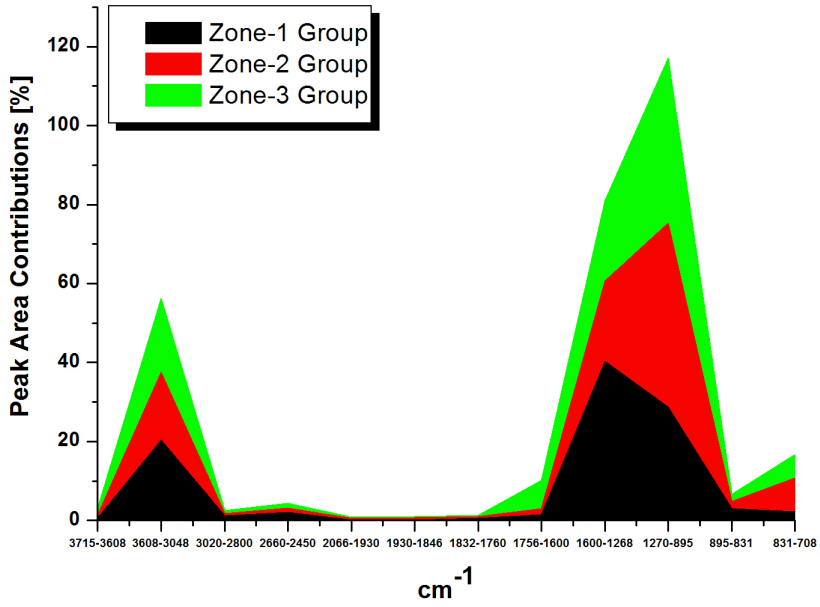


Fig. 4. Percentage contributions of integrated peak areas of FTIR spectra at 12 different absorption bands for Zone-1, Zone-2 and Zone-3 group.

3.3 Probability distribution function (PDF)

The probability distribution function (PDF) was applied to all FTIR spectra at 12 different absorption bands as previously mentioned in section 3.2. PDF is a function that explains the comparative probability for this random variable to take on a given value. The probability for the random variable to fall within a particular region is given by the Gaussian distribution, which can be described as follows:

$$y = \frac{1}{\sigma\sqrt{2\pi}} \exp\left(\frac{-(x-\mu)^2}{2\sigma^2}\right) \qquad (1)$$

where y, σ, σ^2, μ and x represent for probability distribution function, standard deviation, variance, average and peak area of spectrum of each zone respectively. As clearly illustrated in Fig. 5, some characteristic features can be extracted directed from the original images. Firstly, a sharp symmetrical bell-shape curve was observed in zone-1 samples for most absorption bands. Since the measured values of the variable are more concentrated in the middle than in the tails, it appears reasonable to assume this fact is a circumstance of moderately homogeneous spatial distribution of organic functional groups in background marine sediments that were much less affected by the tsunami.

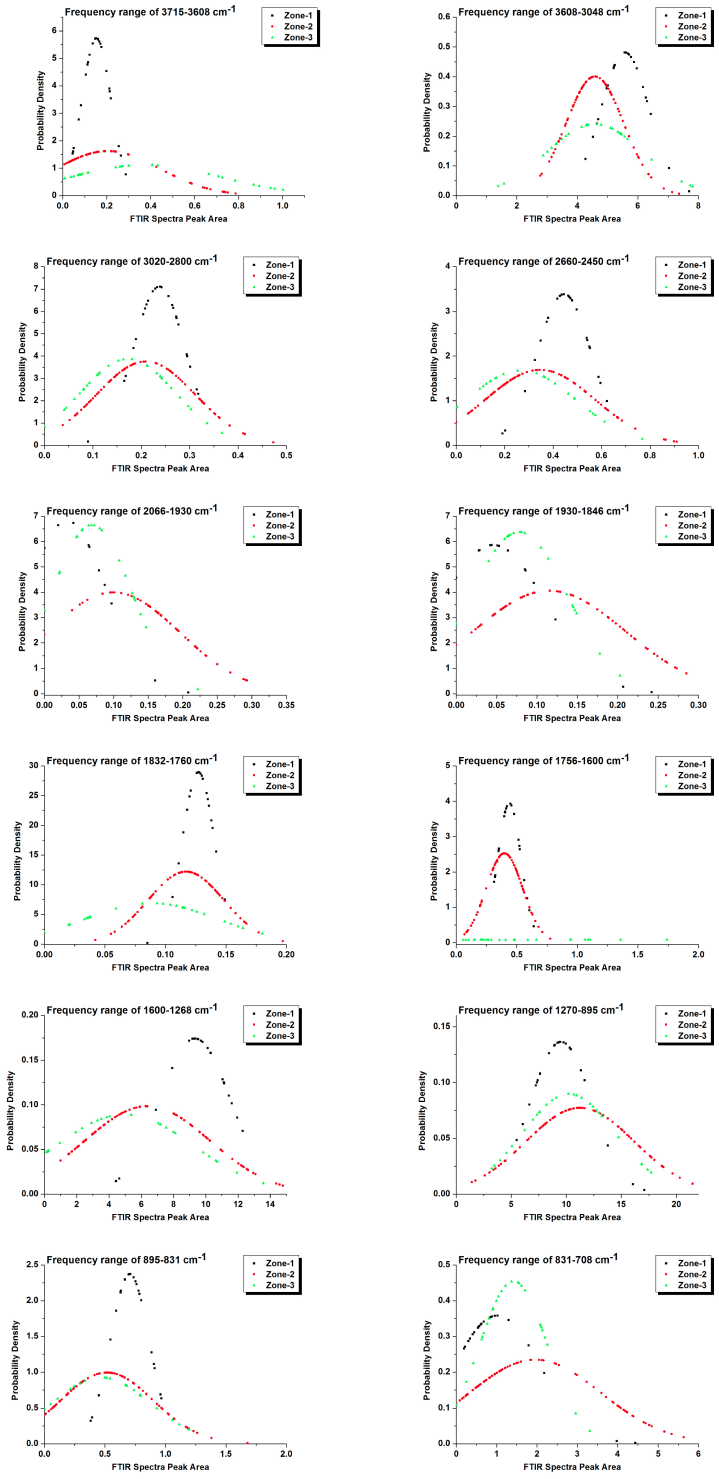


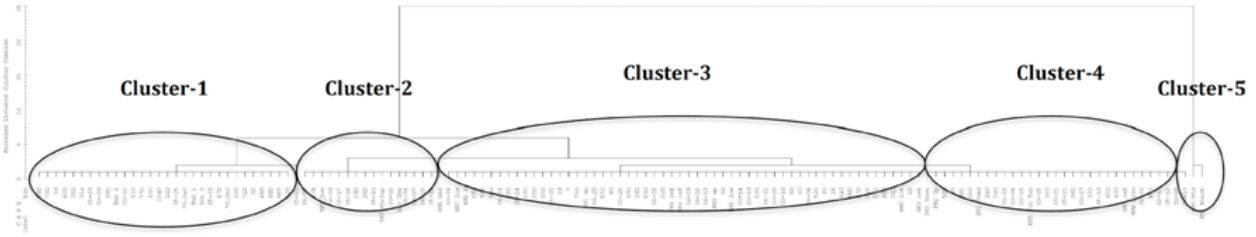
Fig. 5. Probability distribution function graphs of FTIR spectra at 12 different absorption bands of sediment and soil samples collected at zone-1, zone-2 and zone-3.

backwash. For instance, the subtle differences between zone-1 and other zones were detected at the frequency range of 3715-3608 cm^{-1}, 3020-2800 cm^{-1}, 2660-2450 cm^{-1}, 1832-1760 cm^{-1} and 895-831 cm^{-1}. This can be inferred as a result of fairly harmonized spatial distribution of kaolinites, CH-stretching mode compounds, carbonates and silicates observed in marine sediments. Secondly, zone-3 shows extremely broad peaks with flat tops at the interval range of 3715-3608 cm^{-1}, 1832-1760 cm^{-1} and 1756-1600 cm^{-1}, emphasizing the high degree of chemical diversity of kaolinite mineral silicates, carbonate minerals, aromatics and alkene double bond components in terrestrial soils. Thirdly, zone-2 demonstrates positive skews in the frequency range of 3715-3608 cm^{-1}, 2660-2450 cm^{-1}, 2066-1930 cm^{-1} and 1930-1846 cm^{-1}, 895-831 cm^{-1} and 831-708 cm^{-1}, indicating that the bulk of spectra peak areas lie to the left of the mean. These asymmetrical distribution curves also reveal the fact that the mean is generally higher than the median and thus underlining the importance of tsunami backwash that dragged large amount of terrestrial materials out to zone-2.

3.4 Hierarchical cluster analysis (HCA)

Hierarchical clustering allows users to select a definition of distance, then select a linking method of forming clusters, then determine how many clusters best suit the data. *Hierarchical clustering* methods do not require present knowledge of the number of groups. There are three general approaches to clustering FTIR spectra, namely "*Hierarchical Cluster Analysis*", "*K-means Cluster Analysis*" and "*Two-Step Cluster Analysis*". In both *K-means clustering* and *two-step clustering*, researchers have to specify the number of clusters in advance, and then calculate how to assign cases to the *K* clusters. Furthermore, these two clustering techniques require a very large scale of data set (e.g. $n > 1{,}000$). On the contrary, *Hierarchical Cluster Analysis* (HCA) is appropriate for smaller samples (e.g. $n < 200$) and can be carried out without any data pre-treatment (Dach *et al*., 1999). Therefore, classification of FTIR spectra according to spectral similarity was conducted with the assistance of hierarchical cluster analysis (Fig. 6).

To test the hypothesis that zone-2 contains more tsunami backwash deposits in comparison with those of zone-1, HCA had been conducted on the 12 variables (i.e. 12 different absorption bands as previously mentioned in section 3.2). The HCA revealed the presence of two main clusters with five different sub-clusters. The first major cluster consists of all zone samples with the average percentage contribution of 24%, 56% and 20% for zone-1, zone-2 and zone-3 respectively. This cluster can be divided into four subgroups; the first consists of zone-1 (0%), zone-2 (87%), zone-3 (13%), and the second is composed of zone-1 (47%), zone-2 (29%), zone-3 (24%), the third contains zone-1 (41%), zone-2 (43%), zone-3 (16%) and the fourth constructs zone-1 (10%), zone-2 (64%), zone-3 (26%). According to dendrogram, the members present in the first subgroup can be considered to be a mixture of "tsunami-backwash deposits" and "terrestrial components" with the percentage contribution of 22% ($n = 30$) to all samples ($n = 136$). Cluster-5 is another key-feature in dendrogram, which illustrates the strong presence of terrestrial components namely PK1 and BM2. Since these two samples represent the terrestrial components, it appears reasonable to assume the disagreement of cluster-5 in comparison with other sub-clusters is a consequence of relatively high contribution of HA, FA and lignin.



Cluster-1 (n = 30; Percentage contribution 22%)										
9	73	16	40	35	31	5-26	3-09	46	Tub 2	3-10
11	77	10	13	14	5-25	78	Tub 1	Tub 3	5-23	17
68	44	72	32	48	69	BP2	42			
Cluster-2 (n = 17; Percentage contribution 13%)										
5-21	4-05	47	BK1 low	4-06	5-17	29	26	05-16	PK3	3-02
BK5 Tsu	4-04	4-07	4-15	5-22	BM1 mid					
Cluster-3 (n = 56; Percentage contribution 41%)										
3-04	BN2 low	BM2 up	5	70	64	4-14	45	5-24	43	25
20	5-20	19	7	71	BM1 up	58	57	8	3-20	49
39	53	4-02	22	PK4	BK4	4-09	4-10	4-13	BN2 up	2
BM1 low	3-14	3-19	55	4-01	3-06	3-16	6	42	4-08	52
3	18	54	66	27	30	23	61	41	BM2 low	5
BK3										
Cluster-4 (n = 31; Percentage contribution 23%)										
PK2 down	PK2up	50	4	BN1	33	BP1	15	76	3-03	3-08
3-15	BK5 pre Tsu	3-05	34	3-21	5-21	36	3-17	37	5-19	62
63	BM3	BM4	4-03	BP3	3-07	5-12	3-18	3-13		
Cluster-5 (n = 2; Percentage contribution 1%)										
BM2 mid	PK1									

Fig. 6. Hierarchical cluster analysis of FTIR spectra of terrestrial soils and coastal sediments in the 2004 tsunami-affected Khao Lak area.

3.5 Principal component analysis (PCA)

Factor analysis offers the advantages of not requiring prior knowledge of the chemical composition and size distribution of emissions from specific sources (source profiles) but has the drawback of being mathematically indeterminate, allowing a wide range of possible solutions even when it is applied to relatively simple simulated data sets. In natural soils and sediments, which are composed by many potential and diverse sources, principal component analysis (PCA) has been chosen by many researchers for source apportionment of chemical contaminants such as polycyclic aromatic hydrocarbons (Liu et al., 2009; Yunker et al., 2011; Zhang et al., 2012). This technique has also been widely applied to FTIR spectra as main purposes for classifications of biological and chemical materials (Bombalska et al., 2011; Cotrim et al., 1999). In this study, Varimax rotation was selected to maximize the sum of the variances of the squared loadings and thus enable us to seek the similarity of chemical components in sediment and soil samples. FTIR spectra of the samples listed in Table 1 were analyzed by PCA. The principal component patterns for Varimax rotated components of 136 samples composed of three PC, which account for 91.75 %, 6.69 % and 1.47 % for the total of variances of PC1, PC2 and PC3 respectively. The contribution of PC1 and PC2 explains 98.44 % of total variance, and moreover PC1 is 13.7 and 62.4 times higher than PC2 and PC3 respectively.

A plot of the scores of the first two PCs is presented in Fig. 7. It can be easily seen that the full black squares (zone-1) constitute a very broad group along the positive values of PC2 (*y*-axis) adjacent to 1.0 and then gently decrease exponentially to positive side of PC1 (*x*-axis). On the contrary, the full black triangle (zone-2) and full black circle (zone-3) resemble each other with a quarter circle curve from north to east, indicating that these samples might share similar organic functional groups. Three possibilities can be considered to be responsible for this phenomenon; *i*) the tsunami inundation might uplift bottom marine sediments to onshore area, *ii*) the tsunami backwash conveyed terrestrial components to marine environment and *iii*) both tsunami inundation and backwash account for the similarity of two-dimensional plots of PCA appearing in Fig. 7. Another key feature is horizontally deviated samples namely 31, 3-9, 5-21, 5-25, 5-26, 10, 14, 42, BK3, BM3, BP2, Tub3 and PK2, which are located parallel to *x*-axis. Since these samples are representative of onshore soils and coastal sediments adjacent to shoreline, it appears reasonable to conclude that the application of PCA on FTIR spectra can successfully discriminate typical marine sediments from terrestrial components and tsunami backwash deposits in near shore and coastal waters of Thailand.

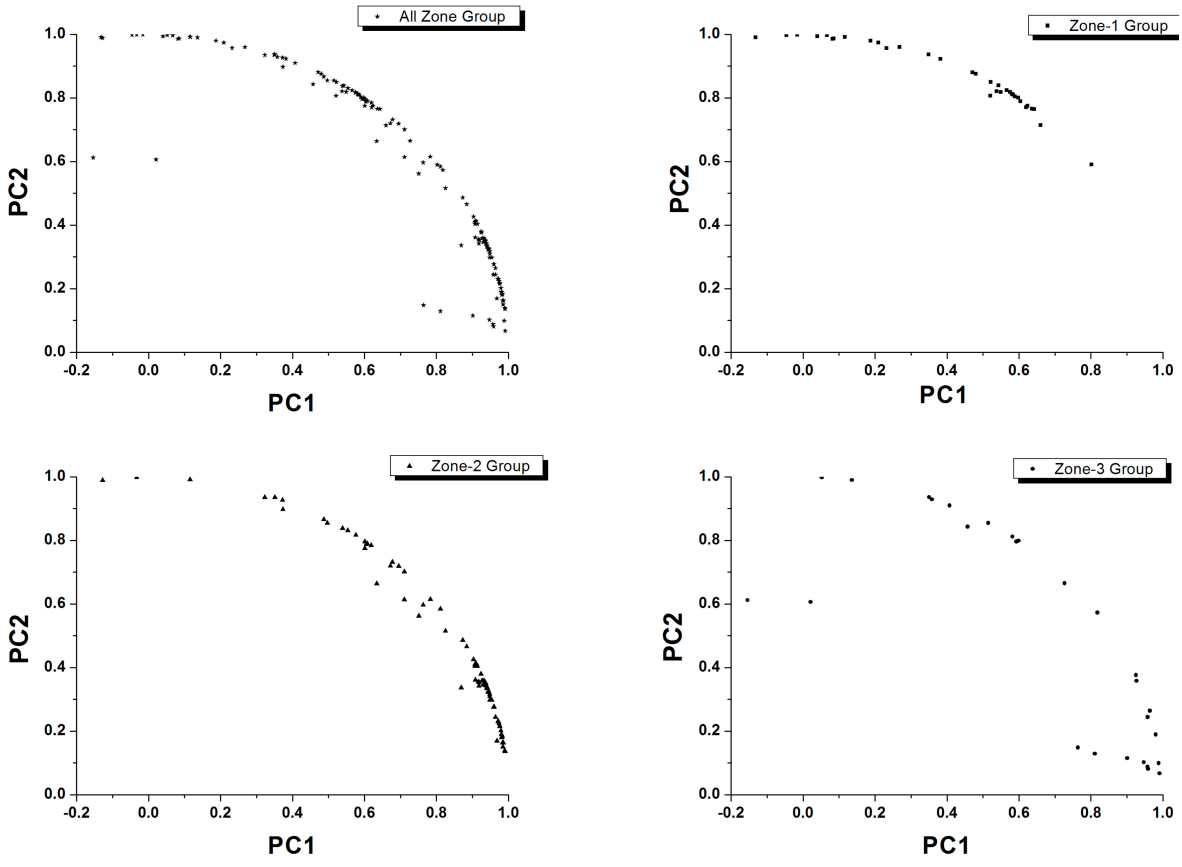


Fig. 7. Two-dimensional plots of PC1 and PC2 using FTIR spectra of terrestrial soils and coastal sediments in the 2004 tsunami-affected Khao Lak area.

3.6 Implications for the identification of tsunami deposits

HCA, PDF and PCA analysis of FITR spectra are able to discriminate terrestrial material in the marine environment. Offshore Khao Lak, tsunami deposits are preserved within fine-grained sediments that were found to be transported towards offshore during normal conditions during the monsoon without the influence of strong events (Feldens et al., 2012). The proxies discussed in this study are thus not able to differentiate between different processes transporting material from on- towards offshore. Nevertheless, they show great potential for the recognition of (paleo) tsunami events: Depending on the local setting, the identification monsoon-generated deposits is possible (e.g., Kempf et al., 2003, Hanebuth and Stattegger, 2004, Schettler et al., 2006) thus allowing to differentiate tsunami and from sediment deposited under normal conditions. In contrast, one of the most discussed concerns in tsunami research is the differentiation between storm and tsunami deposits (e.g., Phantuwongraj and Choowong, 2011, Chagué-Goff et al., 2011, Switzer et al., 2009, Kortekaas and Dawson, 2007, Nott, 2003), especially offshore. No reliable criteria have been developed so far, with rip-up clasts and antidunes being the most characteristic sedimentological differentiation between tsunami and storm deposits in Thailand (Phantuwongraj and Choowong, 2011). However, in general, storms tend to erode the beach and the coastline, and thus transport less material from onshore towards offshore compared to tsunami waves that inundate the hinterland. Thus, when event-layers of uncertain origin are encountered, frequently partly reworked due to erosion or bioturbation, the determination of the terrestrial input within the layer can be a decisive factor for their interpretation. This is especially true for paleotsunamis for which no historical information is available, as the organic functional groups are expected to be preserved within the sediment for at least 12,500 years (Silliman et al., 1996).

Table 3. IR absorptions for representative functional groups

Functional Group & Molecular Motion	Wave number (cm^{-1})*,**
OH vibration of hydroxyl groups in alumino-silicates (Kaolinite mineral silicates)	3715-3608
OH vibration of water and OH groups organic fraction of sediments	3608-3048
CH stretching mode	3020-2800
Carbonate (CO_3^{2-}) sediment	2660-2450
	2066-1930
Carbonate (CO_3^{2-}) minerals	1930-1846
	1832-1760
Free water, C-C Stretching of aromatics and alkene double bonds, C=O Stretch of secondary amides corresponding NH, COO asymmetric stretching of metal carboxylates	1756-1600
Carbonate minerals (calcite)	1600-1268
Silicate mineral (Si-O)	1270-951
	947-895
Other carbonates (Li+, K+, Na+)/Other silicate (Overlapping bands)	895-831
	831-708

*Ramasamy et al., 2009
**Kotoky et al., 2006

4. CONCLUSIONS

The current study showed the high potential of FTIR spectroscopy coupled with hierarchical cluster analysis (HCA) and principal component analysis (PCA) for the discrimination of tsunami backwash deposits and typical marine sediments. According to our best knowledge, this has been the first time that the appropriateness of FTIR spectroscopy for classification of tsunami backwash deposits has been demonstrated. The dissimilarities between the FTIR spectra of all sampling zones were particularly noticeable in the OH vibration of water and OH group organic fraction associated absorption bands from 3608 to 3048 cm^{-1}, C-C stretching of aromatics and alkene double bonds related frequency range of 1756-1600 cm^{-1}, calcite linked interval of 1600-1268 cm^{-1} and other carbonates (Li+, K+, Na+) and silicates at the absorption bands from 831 to 708 cm^{-1}. Some considerable discrimination of terrestrial components and tsunami backwash deposits was possible with the assistance of HCA, although the separation in some sub-clusters still remain ambiguous and thus reveals a high degree of similarity in FTIR spectra and chemical composition of natural samples in tsunami-affected area. Two-dimensional plots of PCA highlight the similarities of a quarter circle curve from north to east detected in zone-2 and zone-3, which can be explained by the relatively strong influence of terrestrial components dragged by tsunami backwash within 12 km from the shoreline.

ACKNOWLEDGEMENTS

This work was performed with the approval of Deutsche Forschungsgemeinschaft (DFG) and National Research Council of Thailand (NRCT). The authors acknowledges all research staff at Phuket Marine Biological Center (PMBC) for their support with ship time of RV Chakratong Tongyai and RV Boonlert Pasook as well as other contributions on other facilities during field measurements. The authors would also like to express special gratitude to Synchrotron Light Research Institute (Public Organization), Ministry of Science and Technology, Thailand for their contribution of FTIR measurements.

REFERENCES

Atwater, B.F.: Evidence for great Holocene earthquakes along the outer coast of Washington State, Science., 236, 942-944, 1987.

Benson, B. E., Grimm, K. A., and Clague, J. J.: Tsunami deposits beneath tidal marshes on northwestern Vancouver Island British Columbia, Quaternary. Res., 48, 192-204, 1997.

Bombalska, A., Oliwa, M. M., Kwaśny, M., Włodarski, M., Kaliszewski, M., Kopczyński, K., Szpakowska, M., and Trafny, A. E.: Classification of the biological material with use of FTIR spectroscopy and statistical analysis. Spectrochim. Acta. A., 78 (4), 1221-1226, 2011.

Bondevik, S., Sevendsen, J. I., and Mangerud, J.: Tsunami sedimentary facies deposited by the Storegga tsunami in shallow marine basins and coastal lakes, western Norway, Sedimentology., 44, 1115-1131, 1997.

Cantalamessa, G., and Di Celma, C.: Sedimentary features of tsunami backwash deposits in a shallow marine Miocene setting, Merillones Peninsula, Northern Chile. Sed. Geol., 178 (3-4), 259-273, 2005.

Clague, J.J., and Bobrowsky, P.T.: Tsunami deposits beneath tidal marshes on Vancouver Island, British Columbia, Geol. Soc. Am. Bull., 106, 1293-1303, 1994.

Chagué-Goff, C., Schneider, J.L., Goff, J.R., Dominey-Howes, D., and Strotz, L.: Expanding the proxy toolkit to help identify past events—Lessons from the 2004 Indian Ocean Tsunami and the 2009 South Pacific Tsunami, Earth. Sci. Rev., 107, 107–122, 2011.

Choowong, M., Murakoshi, N., Hisada, K., Charusiri, P., Daorerk, V., Charoentitirat, T., and Chutakositkanon, V., Jankaew, K., and Kanjanapayont, P.: Erosion and deposition by the 2004 Indian Ocean tsunami in Phuket and Phang-nga Provinces, Thailand, J. Coastal. Res., 23(5), 1270–1276, 2007.

Choowong, M., Murakoshi, N., Hisada, K., Charusiri, P., Charoentitirat, T., Chutakositkanon, V., Jankaew, K., Kanjanapayont, P., and Phantuwongraj, S.: 2004 Indian Ocean tsunami inflow and outflow at Phuket, Thailand, Mar. Geol., 248(3–4), 179–192, 2008a.

Choowong, M., Murakoshi, N., Hisada, K., Charoentitirat, T., Charusiri, P., Phantuwongraj, S., Wongkok, P., Choowong, A., Subsayjun,R., Chutakositkanon, V., Jankaew, K., and Kanjanapayont, P.: Flow conditions of the 2004 Indian Ocean tsunami in Thailand inferred from capping bedforms and sedimentary structures, Terra. Nova., 20, 141–149, 2008b.

Choowong, M., Phantuwongraj, S., Charoentitirat, T., Chutakositkanon, V., Yumuang, S., and Charusiri, P.: Beach recovery after 2004 Indian Ocean tsunami from Phang-nga, Thailand, Geomorphology., 104, 134–142, 2009.

Cotrim, R. A., Ferraz, A., Gonçalves, R. A., Silva, T. F., and Bruns, E. R.: Identifying the origin of lignins and monitoring their structural changes by means of FTIR-PCA and –SIMCA. Bioresource. Technol., 68 (1), 29-34, 1999.

Dachs, J., Bayona, J. M., Fillaux, J., Saliot, A., and Albaiges, J.: Evaluation of anthropogenic and biogenic inputs into the western Mediterranean using molecular markers. Mar. Chem., 65(3-4), 195-210, 1999.

Davis, W.M., Erickson, C. L., Johnston, C. T., Delfino, J. J., and Porter, J. E.: Quantitative Fourier transform infrared spectroscopic investigation on humic substance functional group composition, Chemosphere., 38, 2913–2928, 1999.

Dawson, A.G., Long, D., and Smith, D.E.: The Storegga slides: Evidence from eastern Scotland for a possible tsunami. Mar. Geol., 82, 271-276, 1988.

Dawson, A.G., Foster, I. D. L., Shi, S., Smith, D.E., and Long, D.: The identification of tsunami deposits in coastal sediment sequences, Sci. Tsunami. Hazards., 9, 73-82, 1991.

Dawson, A.G., and Shi, S.: Tsunami deposits, Pur Appl. Geophys., 157, 875-897, 2000.

Duarte, R. M. B. O., Santos, E. B. H., Pio, C. A., and Duarte, A. C.: Comparison of structural features of water-soluble organic matter from atmospheric aerosols with those of aquatic humic substances, Atmos. Environ., 41, 8100–8113, 2007.

Feldens, P., Schwarzer, K., Szczuciński, W., Stattegger, K., Sakuna, D., and Somgpongchaiykul, P.: Impact of the 2004 Indian Ocean Tsunami on Seafloor Morphology and Sediments Offshore Pakarang Cape, Thailand, Pol. J. Environ. Stud., 18, 63-68, 2009.

Feldens, P., Schwarzer, K., Sakuna, D., Szczuciński, W., and Sompongchaiyakul, P.: Sediment distribution on the inner continental shelf off Khao Lak (Thailand) after the 2004 Indian Ocean tsunami. Earth Planets Space., 64, 875–887, 2012.

Gelfenbaum, G., and Jaffe, B.: Erosion and sedimentation from the July 17, 1998 Papua New Guinea tsunami, Pure. Appl. Geophys., 160, 1969-1999, 2003.

Kortekaas, S., and Dawson, A.G.: Distinguishing tsunami and storm deposits: An example from Martinhal, SW Portugal, Sediment. Geol., 200, 208–221, 2007.

Kotoky, P., Bezbaruah, D., Baruah, J., Borah, C. G., and Sarma, N. J.: Characterization of clay minerals in the Brahmaputra river sediments, Assam, India, Curr. Sci., 91 (9), 1247-1250, 2006.

Kovač, N., Faganeli, J., Bajt, O., Orel, B., and Vuk, Š. A.: Investigation of sediment samples from the Gulf of Trieste (northern Adriatic) by FTIR spectroscopy, Mater. Geoenvi., 52(1), 81-85, 2005.

Kovač, N., Faganeli, J., Bajt, O., Šket, B., Vuk, Š. A., Orel, B., and Mozetič, P.: Degradation and Preservation of Organic Matter in Marine Macroaggregates, Acta. Chim. Slov., 53, 81-87, 2006.

Liu, Y., Chen, L., Huang, H. Q., Li, Y. W., Tang, J. T., and Zhao, F. J.: Source apportionment of polycyclic aromatic hydrocarbons (PAHs) in surface sediments of the Huangpu River, Shanghai, China. Sci. Total. Environ., 407(8), 2931-2938, 2009.

Mac Carthy, P., and Rice, J.A.: Spectroscopic methods (other than NMR) for determining functionality in humic substances. In: Aiken, G. R., McKnight, D. M., Wershaw, R. L., MacCarthy, P. (Eds.), Humic Substances in Soil, Sediment and Water.. John Wiley and Sons, NewYork, pp.527–559, 1985.

Martinez, E. R., Sharma, P., and Kappler, A.: Surface binding site analysis of Ca^{2+}-homoionized clay–humic acid complexes. J. Colloid. Interf. Sci., 352(2), 526-534, 2010.

Moros, J., Vallejuelo, F. S., Gredilla, A., Diego, D. A., Madariaga, M. J., Garrigues, S., and Guardia, M.: Use of Reflectance Infrared Spectroscopy for Monitoring the Metal Content of the Estuarine Sediments of the Nerbioi-Ibaizabal River (Metropolitan Bilbao, Bay of Biscay, Basque Country), Environ. Sci. Technol., 43, 9314-9320, 2009.

Moros, J., Cassella, J. R., Alonso, B. C. M., Piñeiro, M. A., Hermelo, H. P., Barrera, B. P., Garrigues, S., and Guardia, M.: Estuarine sediment quality assessment by Fourier-transform infrared spectroscopy. Vib. Spectrosc., 53 (2), 204-213, 2010.

Narayana, A. C., Jago, C. F., Manojkumar, P. and Tatavarti, R., Nearshore sediment characteristics and formation of mudbanks along the Kerala coast, southwest India.: Estuarine. Coastal. Shelf. Sci., 78, 341–352, 2008.

Nott, J.: Tsunami or Storm Waves? - Determining the Origin of a Spectacular Field of Wave Emplaced Boulders Using Numerical Storm Surge and Wave Models and Hydrodynamic Transport Equations, J. Coastal. Res., 19, 348–356, 2003.

Parikh, J. S., Lafferty, J. B., and Sparks, L. D.: An ATR-FTIR spectroscopic approach for measuring rapid kinetics at the mineral/water interface, J. Colloid. Interface. Sci., 320 (1), 177-185, 2008.

Phantuwongraj, S., and Choowong, M.: Tsunamis versus storm deposits from Thailand, Nat. Hazards., 63, 31–50, 2011.

Pinegina, T.K., and Bourgeois, J.: Historical and paleo-tsunami deposits on Kamchatka, Russia: long-term chronologies and long-distance correlations, Nat. Hazard. Earth. Sys. Sci., 1, 177-185, 2001.

Ramasamy, V., Rajkumar, P., and Ponnusamy, V.: Depth wise analysis of recently excavated Vellar river sediments through FTIR and XRD studies, Indian. J. Phys., 83 (9), 1295-1308, 2009.

Richard, C., Guyot, G., Rivaton, A., Trubetskaya, O., Trubetskoj, O., Cavani, L., and Ciavatta, C.: Spectroscopic approach for elucidation of structural peculiarities of Andisol soil humic acid fractionated by SEC-PAGE setup, Geoderma., 142, 210–216, 2007.

Rong, X., Huang, Q., He, X., Chen, H., Cai, P., and Liang, W.: Interaction of Pseudomonas putida with kaolinite and montmorillonite: A combination study by equilibrium adsorption, ITC, SEM and FTIR. Colloids. Surf. B., 64(1), 49-55, 2008.

Scheffers, S.R.; Haviser, J.; Browne, T.; Scheffers, A. Tsunamis, hurricanes, the demise of coral reefs and shifts in prehistoric human populations in the Caribbean. Quatern. Int., 195, 69-87, 2009.

Silliman, E. J., Meyers, A. P., and Bourbonniere, A. R.: Record of postglacial organic matter delivery and burial in sediments of Lake Ontario, Org, Geochem., 24 (4), 463-472, 1996.

Switzer, A.D., Pucillo, K., Haredy, R.A., Jones, B.G., and Bryant, E.A.: Sea level, storm, or tsunami: enigmatic sand sheet deposits in a sheltered coastal embayment from southeastern New South Wales, Australia, J. Coastal. Res., 21, 655–663, 2009.

Szczuciński, W., Niedzielski, P., Rachlewicz, G., Sobczyński, T., Zioła, A., Kowalski, A., Lorenc, S., and Siepak, J.: Contamination of tsunami sediments in a coastal zone inundated by the 26 December 2004 tsunami in Thailand, Environ. Geol., 49 (2), 321-331, 2005.

Szczuciński, W., Chaimanee, N., Niedzielski, P., Rachlewicz, G., Saisuttichai, D., Tepsuwan, T., Lorenc, S., and Siepak, J.: Environmental and geological impacts of the 26 December 2004 tsunami in coastal zone of Thailand—overview of short and long-term effects, Pol. J. Environ. Stud., 15 (5), 793–810, 2006.

Szczuciński, W., Niedzielski, P., Kozak, L., Frankowski, M., Zioła, A., and Lorenc, S.: Effects of rainy season on mobilization of contaminants from tsunami deposits left in a coastal zone of Thailand by the 26 December 2004 tsunami, Environ. Geol., 53 (2), 253-264, 2007.

Tinoco, P., Almendros, G., Sanz, J., Gonzalez-Vasquez, R., and Gonzalez-Vila, F.J.: Molecular descriptors of the effect of fire on soils under pine forest in two continental Mediterranean soils, Org. Geochem., 37, 1995–2018, 2006.

Vergnoux, A., Guiliano, M., Di Rocco, R., Domeizel, M., Théraulaz, F., and Doumenq, P.: Quantitative and mid-infrared changes of humic substances from burned soils. Environ. Res., 111(2), 205-214, 2011.

Wolkers, W.F., Oliver, A.E., Tablin, F., and Crowe, J. H.: A Fourier-transform infrared spectroscopy study of sugar glasses, Carbohydr. Res., 339(6),1077–1085, 2004.

Yunker, B. M., Macdonald, W. R., Snowdon, R. L., and Fowler, R. B.: Alkane and PAH biomarkers as tracers of terrigenous organic carbon in Arctic Ocean sediments. Org. Geochem., 42 (9), 1109-1146, 2011.

Yusiharni, E., and Gilkes, R.: Rehydration of heated gibbsite, kaolinite and goethite: An assessment of properties and environmental significance, Appl. Clay. Sci., 64, 61-74, 2012.

Zhang, Y., Guo, S. C., Xu, J., Tian, Z. Y., Shi, L. G., and Feng, C. Y.: Potential source contributions and risk assessment of PAHs in sediments from Taihu Lake, China: Comparison of three receptor models. Water. Res., 46(9), 3065-3073, 2012.

ISSN 8755-6839

SCIENCE OF **TSUNAMI HAZARDS**

Journal of Tsunami Society International

Volume 32 **Number 2** **2013**

SEDIMENTARY FEATURES OF TSUNAMI BACKWASH DEPOSITS AS ASSESSED BY MICRO-BEAM SYNCHROTRON X-RAY FLUORESCENCE (μ-SXRF) AT THE SIAM PHOTON LABORATORY

Siwatt Pongpiachan[1], Kanjana Thumanu[2], Waraporn Tanthanuch[2], Danai Tipmanee[3,4], Panatda Kanchai[1], Klaus Schwarzer[5] and Somchai Tancharakorn[2*]

[1]NIDA Center for Research & Development of Disaster Prevention & Management, School of Social and Environmental Development, National Institute of Development Administration (NIDA), 118 Moo-3, Sereethai Road, Klong-Chan, Bangkapi, Bangkok 10240 THAILAND
[2]Synchrotron Light Research Institute (Public Organization), Ministry of Science and Technology, THAILAND
[3]International Postgraduate Program in Environmental Management, Graduate School, Chulalongkorn University, Bangkok, THAILAND
[4]Center of Excellence for Environmental and Hazardous Waste Management (EHWM), Chulalongkorn University, Bangkok, THAILAND
[5]Institute of Geosciences Sedimentology, Coastal and Continental Shelf Research, Christian Albrechts University Kiel, Otto Hahn Platz 1, D - 24118 Kiel, GERMANY

ABSTRACT

Over the past few years, several attempts have been performed to find alternative "*chemical proxies*" in order to discriminate "tsunami backwash deposits" from "typical marine sediments". A wide range of statistical tools has been selected in order to investigate the sediments and/or terrestrial soils transportation mechanism during the tsunami inundation period by using several types of chemical tracers. To relate the physical and chemical characteristics of Typical Marine Sediments (TMS),

[*]Corresponding author landline phone: (66) 44-217040 ext 1477; mobile phone: (66) 860319900; fax: (66) 044-217047; e-mail: somchai@slri.or.th

Tsunami Backwash Deposits (TBD), Onshore Tsunami Deposits (OTD) and Coastal Zone Soils (CZS) with their synchrotron radiation based micro-X-ray Fluorescence (μ-SXRF) spectra, the μ-SXRF spectra were built in the appropriate selected spectra range from 3,000 eV to 8,000 eV. Further challenges were considered by using the first-order derivative μ-SXRF spectra coupled with Probability Distribution Function (PDF), Hierarchical Cluster Analysis (HCA) and Principal Component Analysis (PCA) in order to investigate the elemental distribution characteristics in various types of terrestrial soils and marine sediments. Dendrographic classifications and multi-dimensional plots of principal components (i.e. bi-polar and three dimensional plots) could indicate the impacts of terrestrial soils and/or marine sediments transport on onshore and/or offshore during the tsunami inundation period. Obviously, these advanced statistical analyses are quite useful and provide valuable information and thus shed new light on the study of paleotsunami.

Keywords: *Andaman Sea; Tsunami Backwash Deposits; Micro-beam Synchrotron X-ray Fluorescence (μ-SXRF); First Order Derivative; Hierarchical Cluster Analysis; Principal Component Analysis.*

1. INTRODUCTION

The 2004 Sumatra-Andaman earthquake and tsunami was commonly considered as the worst natural disaster to ever attack Southeast Asian countries, triggering death and injury as well as major destruction to the transportation system, property, and environmental and economic sustainability (Griffin *et al*., 2013; Matsumaru *et al*., 2012). The severe impact on the beach zone between the Pakarang Cape and the Khao Lak, Phang-nga province of Thailand in turn had serious consequences on the scoured features existed in both on the beach side and in the embayment of tidal channels (Choowong *et al*., 2007, 2009; Fagherazzi and Du, 2007). In spite of various papers focusing on geomorphological, sedimentological and geological alterations in tsunami-affected areas (Choowong *et al*., 2007, 2008a, 2008b, 2009;Szczuciński *et al*., 2005, 2006, 2007), the knowledge of chemical distribution is strictly limited.

As a consequence, several challenges have been made to conduct both qualitative and quantitative analyses of various chemical species in both onshore and offshore of tsunami-affected regions (Goff *et al*., 2012; Jagodziński *et al*., 2012; Pongpiachan *et al*., 2012; Pongpiachan *et al*., 2013; Sakuna *et al*., 2012; Tipmanee *et al*., 2012). In order to understand the destructive behaviour of tsunami affecting both onshore and offshore areas, numerous studies have attempted to draw the scientific community's attention on the feasibility of chemical tracers to characterize tsunami backwash deposits from those of typical marine sediments (Pongpiachan *et al*., 2012; Pongpiachan et al., 2013; Tipmanee *et al*., 2012). Since the identification of tsunami backwash deposit is the first step to gain information on tsunami impacts, it is therefore essentially crucial to find an alternative method to discriminate tsunami backwash deposits from those of natural background submarine sediments.

In the past few years, X-ray fluorescence (XRF) have been widely used for the determination of

elements in sedimentological record of tsunamis on the Portuguese Shelf off Lisbon (Abrantes *et al*., 2008), geoarchaeological evidence of multiple tsunamigenic imprint on the Bay of Palairos-Pogonia, Greece (Vött *et al*., 2011)) and most recently sedimentary deposits left by the 2004 Indian Ocean tsunami on the inner continental shelf offshore of Khao Lak, Andaman Sea, Thailand (Sakuna *et al*., 2011). XRF has gained more popularity on studies of environmental sciences because of its relatively low cost solution compared to other analytical instruments, non-destructive testing solution, fast processing time, typical detection limit of around 0.01% for most elements and quantitative analysis. Recently, the shared use of synchrotron radiation based micro-X-ray Fluorescence (μ-SXRF) permits analysis of objects at the micron-scale owing to its high intensity and energy tenability in comparison with those of conventional light sources such as sealed-tube or rotating-anode generators (Tancharakorn *et al*., 2012). Because of micrometer sized X-ray beam, one can use μ-SXRF not only to quantify the elemental compositions in target samples but also its distribution at the micrometer scale (Kanngießer & Haschke, 2006).

In this research, the author postulates that the use of μ-SXRF in cooperation with the first derivative, probability distribution functions (PDF), hierarchical cluster analysis (HCA) and principal component analysis (PCA) provides a better insight of sedimentary features of tsunami backwash deposits in comparison with those of typical marine sediments and terrestrial components. Note that this is the first time to employ μ-SXRF with assistance of synchrotron radiation in order to assess the elemental distribution of tsunami backwash deposits in micro-scale. It is also worth mentioning that neither the source apportionment, nor the analysis of spatial variation of chemical components in sediments is the principal objective of this paper.

2. MATERIALS & METHODS

2.1 Sampling sites & sampling procedure

2.1.1 Surface marine sediment

The research area is governed by two seasonal monsoons: the northeast monsoon from mid October until March and the southwest monsoon from May to September. This study was carried out offshore along the west coast of Phang Nga province, in the southwest region of Thailand, which was heavily affected by the 2004 tsunami. The research area covers approximately 1,000 km^2 between Thap Lamu and Pakarang Cape, up to a water depth of 70 meters. Our research was carried out on research cruises taken from one year apart, from November-December 2007 with RV CHAKRATONG TONGYAI and November-December 2008 with RV BOONLERT PASOOK, covering approximately 1500 nautical miles of hydroacoustic profiles (side scan sonar, multibeam echo sounder and shallow reflection seismic with a boomer system) were recorded at Pakarang Cape. Twenty of sediment samples were collected during 18-20 July 2009 (Fig. 1)). The sampling stations were selected on the basis of the basic data acquired from hydroacoustic mapping using equipment, which consisted of Multi-beam, Side Scan Sonar and Boomer system to investigate the sedimentary deposition on near-

shore seabed (Feldens *et al*., 2009; Feldens *et al*., 2012). These supporting data provided the geophysical structure of seabed, which was promising evidence of terrestrial deposits in the study area. Van-veen Grab Sampler was used to collect the 20 surface sediment samples. Sediment samples were wrapped in clean aluminum foil, placed in a glass bottle, and kept frozen at – 20 ºC.

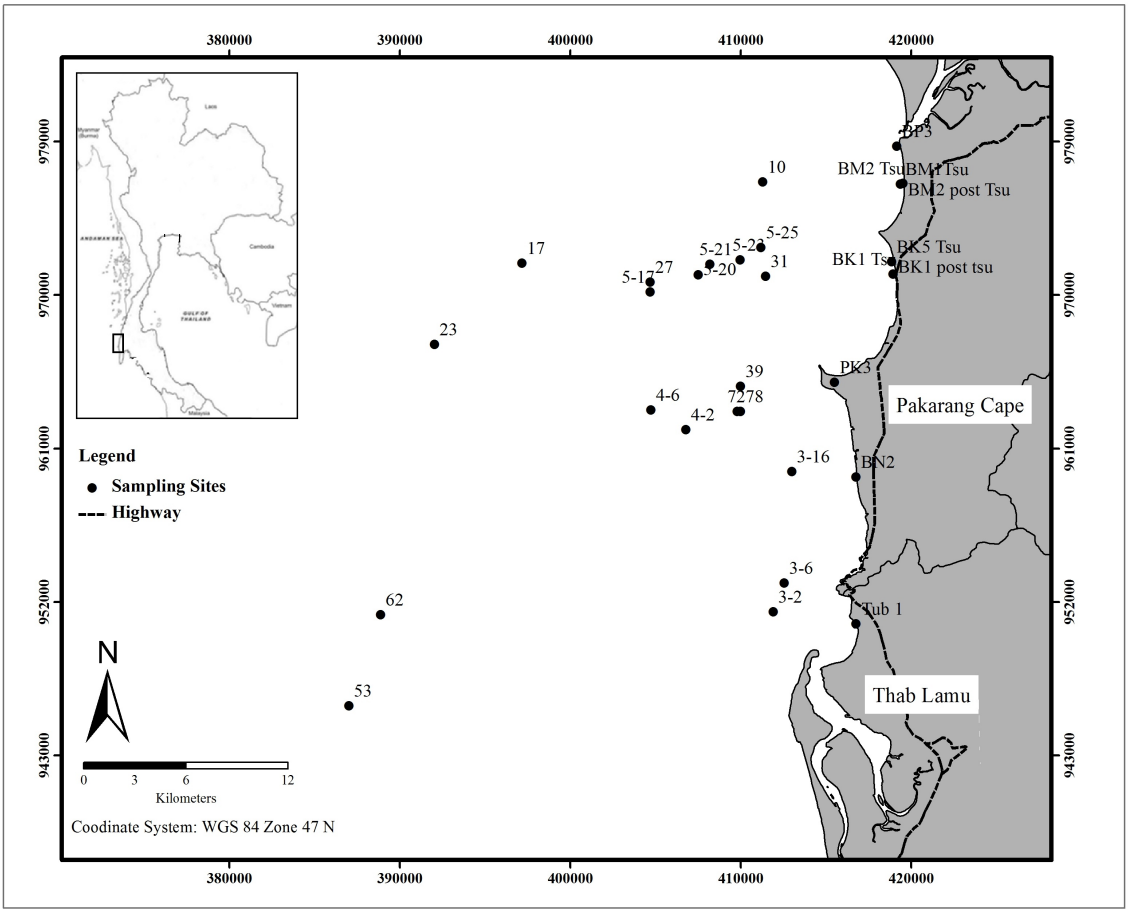
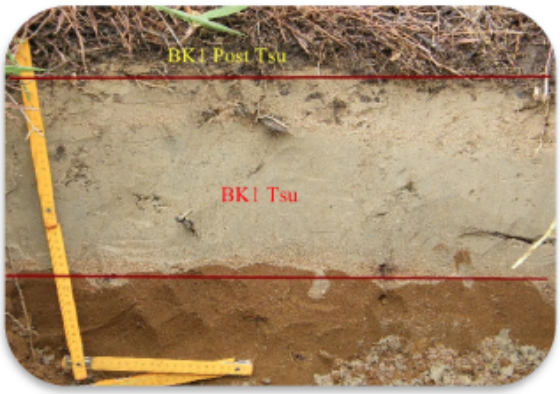


Fig. 1: Sampling site description at tsunami affected area at Khao Lak, Phang-nga province of Thailand.

2.1.2 Terrestrial soils

Ten of terrestrial soil samples were collected during 18-20 July 2009. Soil sampling stations were selected by considering the areas, which were affected by the 2004 Tsunami (Szczucinski *et al*., 2005). In addition, the locations of soil sampling stations were also in the transect line of the surface sediment sampling stations (Fig.1-2). They were collected during 18-20 July 2009. The surface layer was collected by using a clean shovel. About half kilogram of composite samples from 2 m^2 area of each station was taken (Badin *et al*., 2008). They were wrapped in clean aluminum foil, placed in a glass bottle, and kept frozen at - 20ºC



Tsunami deposition layer at station BK 1. (BK1 Post Tsu and BK1Tsu layer)



Tsunami deposition layer at station BK 5. (BK5 Tsu layer)



Tsunami deposition layer at station BM 1. (BM1 Tsu layer)



Tsunami deposition layer at station BM 2 (BM2 Post Tsu and BM2Tsu layer)

Fig. 2: Tsunami and Post-tsunami deposition layer at Khao Lak, Phang-nga province of Thailand.

2.2 Sample preparation for μ-SXRF

Due to the heterogeneity of sediment, all samples for XRF measurement were prepared in homogenous and flat discs using grinding and pelletizing processes. In the grinding process, 100 g of powder was weighted and put into a 10 ml ZrO_2 grinding bowl with two ZrO_2 balls (Ø 10 mm) and seven SiO_2 balls (Ø 5 mm) and shaken at 1,800 oscillations/min for 30 minutes (Fig. 3). Then, in the pelletizing process, 50 g of homogenous powder was put into a steel mould and pressurized at 4 tons for 1 minute to form a 13 mm in diameter disc.



Fig. 3: sediment powder with grinding balls in a ZrO2 bowl before (a) and after (b) grinding process, and after (c) pelletizing process.

2.3 μ-SXRF Experiment

Synchrotron X-ray fluorescence experiments were carried out at the μ-SXRF end-station (Tancharakorn *et al*., 2012) attached to beamline 2.2 of the Siam Photon Laboratory to utilize monochromatic X-ray beam. In this beamline, X-rays can be generated by the 1.2 GeV storage ring travelling 21 m through an evacuated pipe to the sample. The beamline consists of a double multilayer monochromator (DMM) (at 8.8 m downstream) to select desired energy between 6 keV to 9 keV, focusing mirror (FM) (at 11.0 m downstream) to increase photon flux and beryllium window of 200 μm thickness (at 21 m downstream) to separate high vacuum region and atmospheric pressure. Details of the beam line 2.2 can be found in previous literature (Soontaranon *et al*., 2012). In the experiment, samples were mounted on a motorized sample stage in air. An energy-dispersive Si-PIN detector from AMPTEK, USA, with energy resolution of 160 eV at the Mn K_{α} emission line was used to collect XRF signals. Six spots were randomly chosen to be exposed with 9 keV X-rays for 100 seconds for each spot. XRF signals were collected in the detector and then sent to MCA8000A multichannel analyzer (AMPTEK, USA) where each signal is stored in each channel corresponding to the certain energy. Therefore, the detector must be first calibrated to find a relationship between channel and photon energy. Here commercial XRF metal standards (titanium, vanadium and iron foils) were used. The energy-dispersive data were finally created in a single-column file, which can be analyzed using the *pyMCA*. In this code, a Guassian function is used to characterized position, width and height or area of each peak. The position of each peak is used to identify element, while its area is directly related to its concentration. The code also deals with the background signal. The algorithm of the pyMCA can be found in (Sole *et.al*., 2007).

2.4 Statistical analysis

The derivative spectrophotometric method is based on transformation of zero-order spectra of sediment and soil samples into the first-order derivative (ΔPhoton Energy (eV)/ΔIntensity (counts)). In this study, the value of first derivative was performed by using the Software OPUS Version 7.0. In addition, first derivatives of the spectral data from each sampling location were treated through hierarchical cluster analysis (HCA) and principal component analysis (PCA) with the orthogonal Varimax solution using Statistical Package for the Social Sciences (SPSS) Version 13.0.

3. RESULTS & DISCUSSION

3.1.Characteristics of the first-order derivative μ-SXRF spectra

Although several attempts have been made by several researchers to quantify chemical contents in sediments in order to elucidate tsunami backwash mechanism (Pongpiachan *et al*., 2012; Pongpiachan *et al*., 2013; Sakuna *et al*., 2012; Tipmanee *et al*., 2012;), some alternative proxies are always required to enhance the reliability of data interpretation. In this study, the assessment of μ-SXRF spectra as an alternative "fingerprint" to discriminate tsunami backwash deposit from typical marine sediments was performed by using the concept of first derivative. All samples were classified into four groups namely "Typical Marine Sediments (TMS)", "Tsunami Backwash Deposits (TBD)", "Onshore Tsunami Deposits (OTD)" and "Coastal Zone Terrestrial Soils (CTS)" as clearly described in Table 1.

Table 1. Sample information of marine sediments and terrestrial soils.

Sampling code	Sampling date	Sampling description
Coastal Zone Soils (CZS)		
Tub1	July-18-2009	Canal bank
PK 3	July-19-2009	Shrimp pond
BN 2	July-20-2009	Canal bank
BP 3	July-20-2009	Mangrove
Onshore Tsunami Deposits (OTD)		
BK 1 Post Tsu, BK1 Tsu	July-19-2009	Tsunami deposit layer
BK 5 Tsu	July-19-2009	Tsunami deposit layer
BM 1 Tsu	July-20-2009	Tsunami deposit layer
BM 2 Post Tsu, BM2 Tsu	July-20-2009	Pond

Typical Marine Sediments (TMS)		
10, 17	December-1-2007	Pakarang cape sediment
3-2 ,3-6, 3-16, 4-2, 4-6, 5-20, 5-25	March-4-5- 2010	Pakarang cape sediment
53, 62	December-7-2007	Thup Lamu Sediment
Tsunami Backwash Deposits (TBD)		
23, 27, 31, 39, 72, 78	December-3-2007	Tsunami affected sediment
5-17, 5-21, 5-23	March-5- 2010	Tsunami affected sediment

The average μ-SXRF spectra of four sample groups are compared and carefully investigated (See Fig. 4). Generally, all sample groups display similar spectral characteristics. There are four prominent features, which are common to all μ-SXRF spectra: *a*) main element which can be found in all samples is calcium (K_α at 3.69 keV, K_β at 4.01 keV); *b*) all samples have a relatively small amount of titanium (K_α at 4.51 keV, K_β at 4.93 keV) and manganese (K_α at 5.90 keV, K_β at 6.49 keV); *c*) another main element contained in all samples is iron(K_α at 6.40 keV, K_β at 7.06 keV); and *d*) low concentration of three elements which are potassium ((K_α at 3.31 keV, K_β at 3.59 keV), titanium and manganese were detected in OTD samples. Based on these results, one can deduce that all elemental species in samples share comparable distribution patterns.

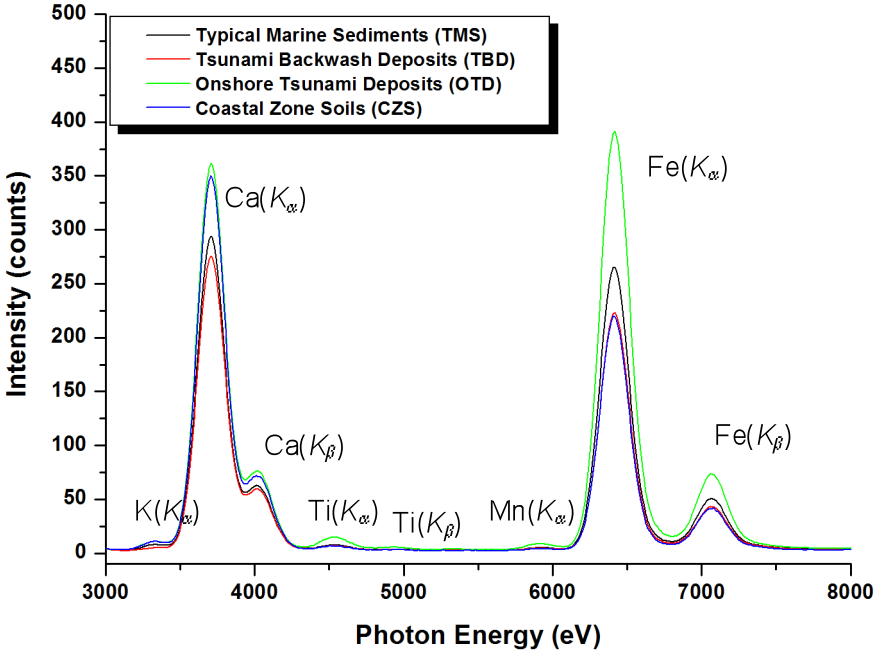


Fig. 4: μ-SXRF spectra of typical marine sediments (TMS), tsunami backwash deposits (TBD), on-shore tsunami deposits (OTD) and coastal zone soils (CZS).

Although all sample groups show comparatively similar μ-SXRF spectra features in the photon energy range from 3000 to 8000 eV, some subtle relative changes can be enhanced by computing the first-order derivative of raw spectra (Balsam and Deaton, 1991). The computation of the first-order derivative generates curves that have peaks where the rate of change of the raw μ-SXRF spectral curves is at maximum and are flat where spectral curves display no change in slope. TMS is characterized by its four positive major peaks in the first derivative situated at 5104 eV, 5165 eV, 5735 eV and 7754 eV, followed by three negative main peaks located at 3110 eV, 5091 eV and 5661 eV respectively. On the contrary, the disappearances of two main peaks at 3110 eV and 7754 eV were detected at TBD, OTD and CZS samples, highlighting the absence of some typical marine elements in non-marine samples. It is well known that marl and calcareous clay, glauconite, kalolinite, organic matter, phosphorite, hematite and goethite show relatively high contribution in marine sediments as previously mentioned in several publications (Balsam and Beeson, 2003). Recent studies also reveal the significance of Ca, Fe, K, Sr, and Ti in selected sediment sections from a continental margin sediment core by using Micro-XRF analyzer (Micro-XRF) with a 100-μm resolution and an XRF whole-core scanner (XRF-S) with a 5-mm resolution (Böning *et al*., 2007). Hence, the discrepancy of μ-SXRF spectra features between marine and non-marine samples can be ascribed to the differences in elemental compositions.

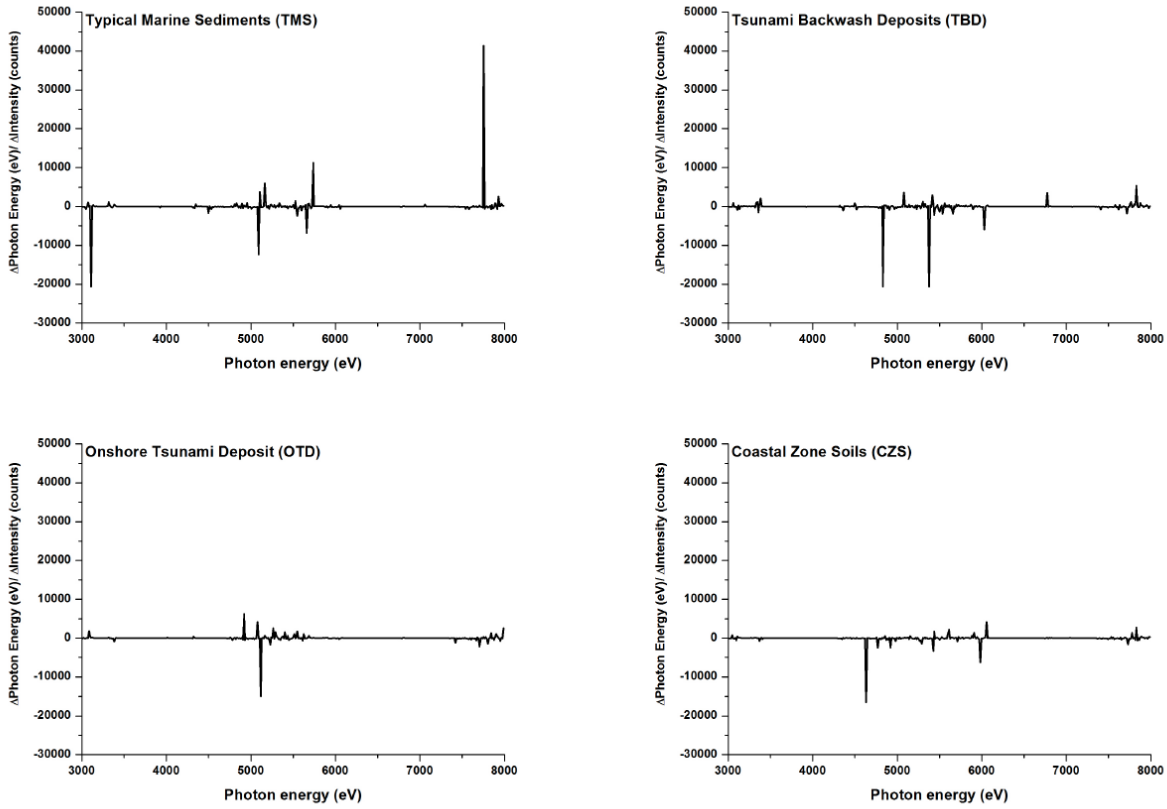


Fig. 5: First derivative plot of typical marine sediments (TMS), tsunami backwash deposits (TBD), on-shore tsunami deposits (OTD) and coastal zone soils (CZS).

3.2 Probability distribution function (PDF)

In probability theory, a probability density function (PDF) is a function that defines the comparative possibility for this random variable to take on a certain value. The probability for the random variable to fall within a particular region is given by the integral of this variable's density over the region. The probability density function is nonnegative everywhere, and its integral over the entire space is equal to one. PDF was employed to all μ-SXRF spectra in the intensity range from 0 to 400 counts as clearly displayed in Fig. 6. Generally, the probability density of standard normal distribution can be described as follows:

$$f(x) = \frac{1}{\sqrt{2\pi}} e^{\frac{-x^2}{2}} \tag{1}$$

where e, x and π represent for exponential constant (i.e. 2.718), intensity (counts) and pi value (i.e. 3.142) respectively. If a random variable X is provided and its distribution possesses a probability density function f, then the estimated value of X can be computed as

$$E[X] = \int_{-\infty}^{\infty} x f(x) dx \tag{2}$$

A distribution has a density function if and only if its cumulative distribution function $F(x)$ is absolutely continuous. In this case: F is almost everywhere differentiable, and its derivative can be used as probability density:

$$\frac{d}{dx} F(x) = f(x) \tag{3}$$

PDF is a function that describes the relative likelihood for this random variable to take on a given value. The probability for the random variable to fall within a particular region is given by the Gaussian distribution, which can be described as follows:

$$y = \frac{1}{\sigma\sqrt{2\pi}} \exp\left(\frac{-(x-\mu)^2}{2\sigma^2} \right) \tag{4}$$

where y, σ, σ^2, μ and x represent for probability distribution function (PDF), standard deviation of μ-SXRF spectra intensity, variance of μ-SXRF spectra intensity, average of μ-SXRF spectra intensity and μ-SXRF spectra intensity of all samples respectively.

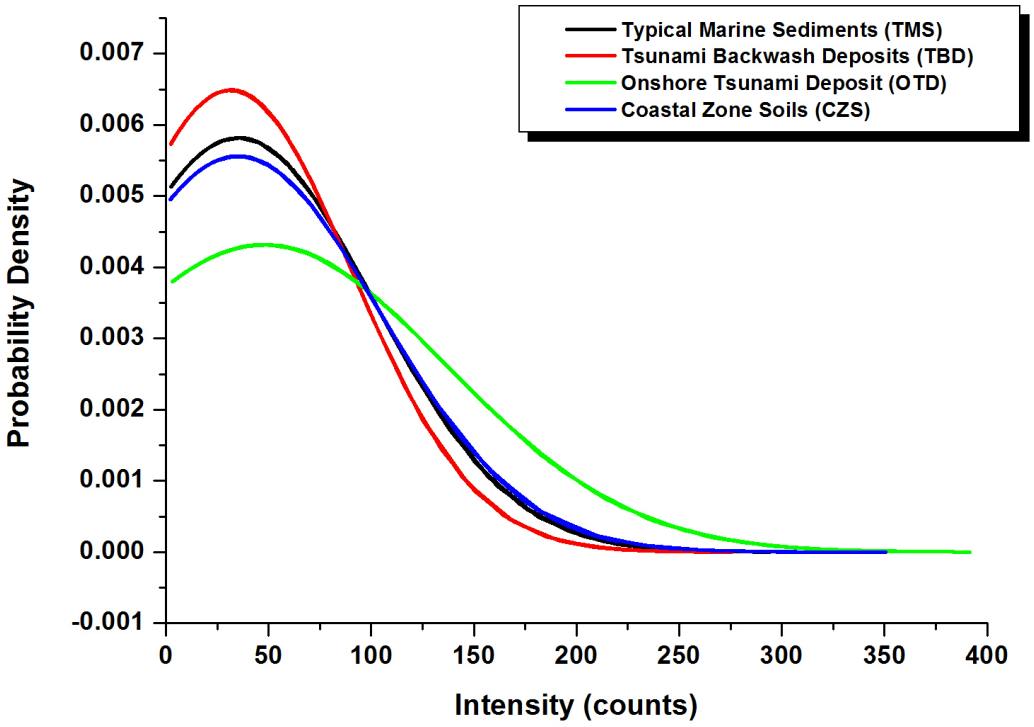


Fig. 6: Probability distribution of μ-SXRF of typical marine sediments (TMS), tsunami backwash deposits (TBD), on-shore tsunami deposits (OTD) and coastal zone soils (CZS).

As noticeably displayed in Fig. 6, some prominent curve features can be obtained directly from these unique plots. It is worth mentioning that "*skewness*" is a degree of the asymmetry of the curve plots between μ-SXRF spectra intensity and PDF of a real-valued random variable (i.e. μ-SXRF spectra intensity). Basically, there are three types of "*skewness*" values, which can be termed as positive skew, negative skew and undefined. A positive skew designates that the tail on the right side is longer than the left side, whilst a negative skew implies that the tail on the left side is longer than the right side. It is also important to stress that the bulk of the PDF values (including the median) of positive skew and negative skew situate at the left and right of the mean respectively. Qualitatively, a zero value implies that the PDF values are comparatively consistently dispersed on both sides of the mean, characteristically indicating a symmetric distribution.

Firstly, the relatively symmetrical bell-shape curves were detected in the curve plots between averaged μ-SXRF spectra intensity and PDF of TMS, TBD and CZS with moderately longer tails in the right side with most of the data still concentrated on the left indicating the "*positive skewness*" type of normal distribution. Since the majority of the PDF curve peaks are more focused in the intensity range of 50 ± 5 counts, it seems rational to assume that this phenomenon is a consequence of comparatively homogeneous spatial elemental distribution in typical marine sediments, tsunami

backwash deposits and coastal zone soils. Interestingly, both TMS and CZS have considerably similar curve plots in spite of its different sampling backgrounds. This can be explained by the invariability of elemental compositions (i.e. Cl, K, Ca, Ti, Cr, Mn, Fe, V) observed in both marine sediments and terrestrial soils. Secondly, the irrelevant curve feature of OTD was detected with "*positive skewness*" type of bell shape distribution with exceedingly broad peaks coupled with flat tops at the interval range of 50 to 300 counts in comparison with those of TMS, TBD and CZS. This reflects highly deviated elemental distributions involved in onshore tsunami deposits as a result of more complex chemical mixtures derived from both terrestrial components and marine deposits.

3.3 Hierarchical cluster analysis (HCA)

Cluster analysis (CA), also called segmentation analysis or taxonomy analysis, seeks to identify homogeneous subgroups of cases in a population. That is, cluster analysis seeks to identify a set of groups, which both minimize within-group variation and maximize between-group variation. In this study, CA was conducted using SPSS 13.0 for Windows. CA techniques may be *hierarchical* (i.e. the resultant classification has an increasing number of nested classes) or *non-hierarchical* (i.e. *k*-means clustering). *Hierarchical clustering* allows users to select a definition of distance, then select a linking method of forming clusters, then determine how many clusters best suit the data. *Hierarchical clustering* methods do not require pre-set knowledge of the number of groups.

Two general methods of *hierarchical clustering* methods are available: divisive and agglomerative. The divisive technique starts by assuming a single group, partitioning that group into subgroups, partitioning these subgroups further into subgroups and so on until each object forms its own subgroup. The agglomerative techniques start with each object describing a subgroup, and then combine like subgroups into more inclusive subgroups until only one group remains. In either case, the results of the application of the clustering technique are best described using a dendrogram or binary tree. The objects are represented as nodes in the dendrogram and the branches illustrate when the cluster method joins subgroups containing that object. The length of the branch indicates the distance between the subgroups when they are joined.

In this study, Hierarchical Cluster Analysis (HCA) was applied to test the hypothesis that μ-SXRF spectra can be used as an alternative "*fingerprint*" in order to distinguish "tsunami backwash deposits" from those of "typical marine sediments". Two types of datasets, namely raw and first derivative μ-SXRF spectra of all samples, were employed to HCA as clearly illustrated in Fig. 7-8. The HCA of raw μ-SXRF spectra showed the existence of two major clusters with four different sub-clusters. The first main cluster constitutes[consists of?] of all sample types with the average percentage contribution of 37 %, 21 %, 26 % and 16% for TMS, TBD, OTD and CZS respectively. This cluster can be divided into two sub-clusters; the first sub-cluster constitutes of TMS (30 %), TBD (20 %), OTD (40 %), CZS (10 %) and the second sub-cluster is composed of TMS (44 %), TBD (22 %), OTD (11 %), CZS (22 %). According to dendrogram, the second major cluster [is constructed of?]constructs of all groups with the average percentage contribution of 35 %, 48 %, 8 % and 8% for TMS, TBD, OTD and CZS respectively. The second major cluster can be separated into two sub-

clusters; the third sub-cluster [is comprised of?]comprises of TMS (20 %), TBD (80 %), OTD (0 %), CZS (0 %) and the fourth sub-cluster is composed of TMS (35 %), TBD (48 %), OTD (8 %), CZS (8 %). The second major cluster can be considered as a mixture of "typical marine sediments" and "tsunami backwash deposits", which has been highly characterized in the third sub-cluster (See Fig. 7).

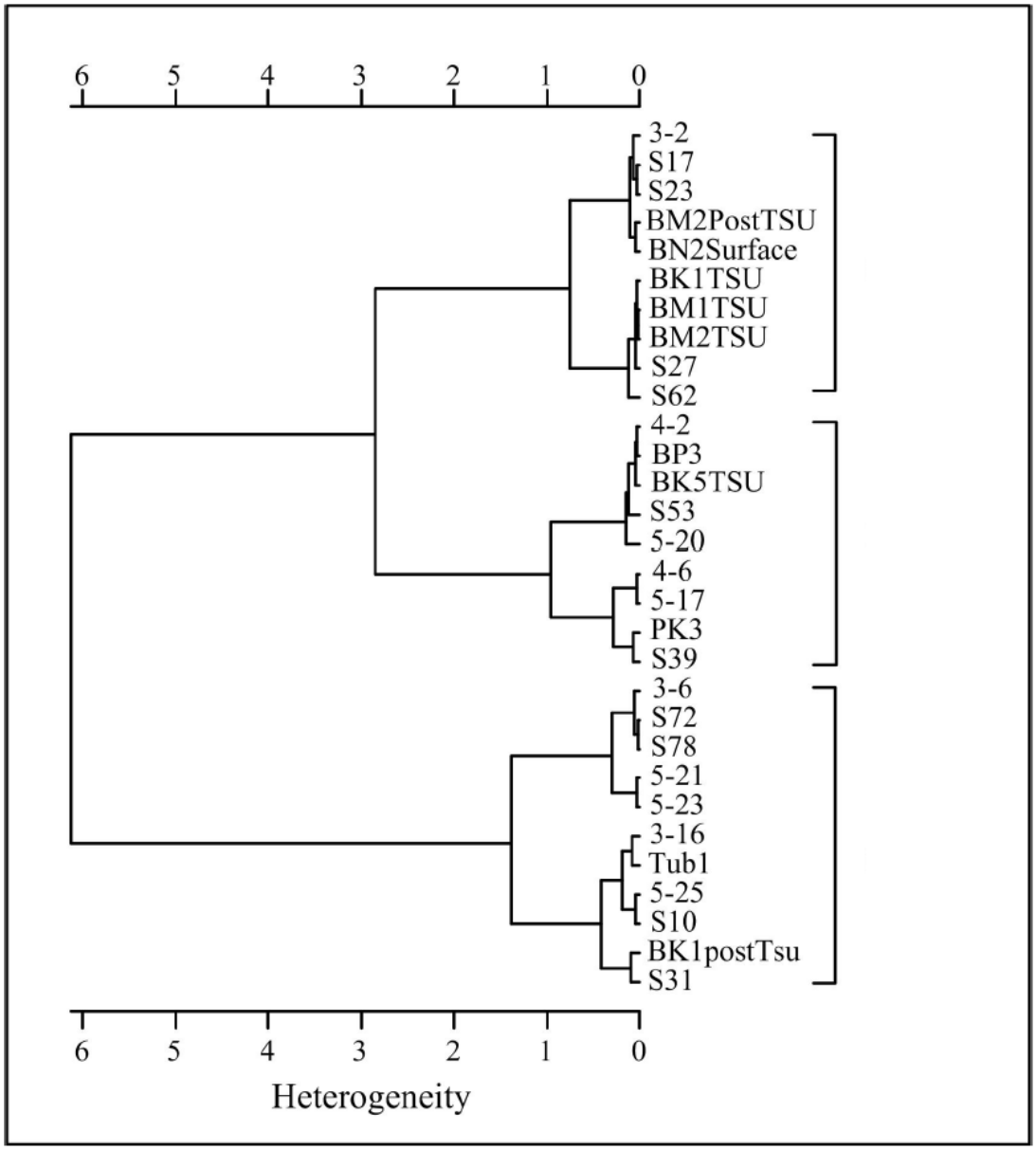


Fig. 7: Dendrographic classification with raw data of typical marine sediments (TMS), tsunami backwash deposits (TBD), on-shore tsunami deposits (OTD) and coastal zone soils (CZS). The Euclidean distance after vector normalization spectra and the Ward linkage method were employed. For details about cluster group composition see data in Table 1.

Further efforts to underline the importance of μ-SXRF spectra as an alternative "*fingerprint*" have been conducted by using the first derivative data. It can be seen in Fig. 8 that the OTD samples are highly deviated from CZS samples, which emphasizes the strong discrepancy in elemental distribution between onshore tsunami deposits and coastal zone soils. Interestingly, TMS samples have a high degree of similarity with those of OTD samples. This particular phenomenon can be ascribed as heavily influenced by advancement of large-scale tsunami inundation, which is responsible for extensive sediment transport from the offshore and subsequently deposited over the coastal areas. Similarly, TBD samples share a high level of affinity with those of CZS samples. This unique occurrence can be attributed to rapid tsunami backwash, which carried terrestrial debris from the onshore to the offshore.

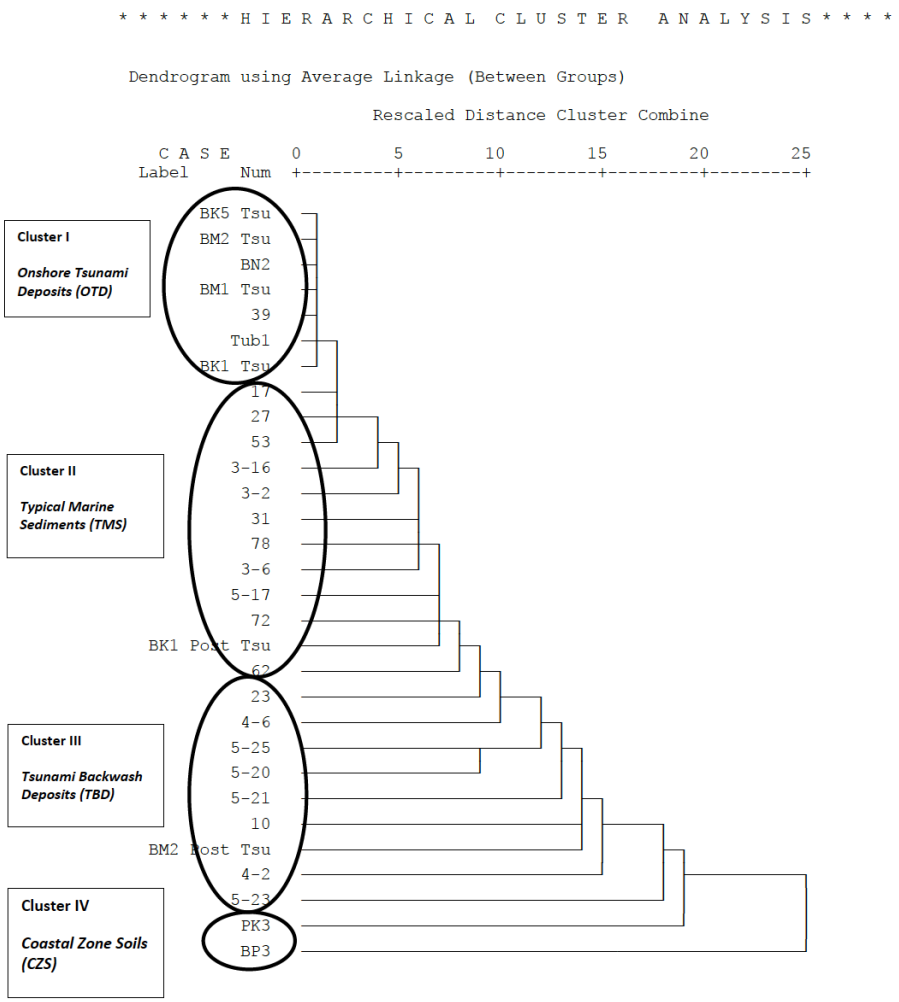


Fig. 8: Dendrographic classification with the first-order derivative data of typical marine sediments (TMS), tsunami backwash deposits (TBD), on-shore tsunami deposits (OTD) and coastal zone soils (CZS). The Euclidean distance after vector normalization spectra and the Ward linkage method were employed. For details about cluster group composition see data in Table 1.

3.4 Principal component analysis (PCA)

In PCA, all variables are expressed in standardized form with a mean of 0 and a standard deviation of 1. The total variance therefore equals the total number of variables, and the variance of each factor expressed as a fraction of the total variance is referred to as the eigenvalue. If a factor has a low eigenvalue, then it is contributing little to the explanation of variances in the variables and may be ignored. PCA is generally used when the research purpose is data reduction (i.e. to reduce the information in many measured variables into a smaller set of components). PCA seeks a linear combination of variables such that the maximum variance is extracted from the variables. It then removes this variance and seeks a second linear combination that explains the maximum proportion of the remaining variance, and so on. This is called the principal axis method and results in orthogonal (uncorrelated) factors. Thus, the largest combination, accounting for most of the variance, becomes principal component 1 (PC1), the second largest accounts for the next largest amount of variances and becomes principal component 2 (PC2), and so on. In general, the first component (P_1) for observed variables X_1, X_2, ……, X_p can be expressed as:

$$P_1 = a_{(1)1}X_1 + a_{(1)2}X_2 + ... + a_{(1)p}X_p \tag{5}$$

where the $a_{(1)1}, a_{(1)2}, ..., a_{(1)p}$ are the weights chosen to maximise the ratio of the variance of P_1 to the total variation, subject to the constraint that

$$\sum_{i=1}^{p} a_{(1)i}^2 = a_{(1)}^t a_{(1)} = 1 \tag{6}$$

The second principal component (P_2) is the combination of the observed variables, which is uncorrelated with the first linear combination and which accounts for the maximum amount of the remaining total variance not already accounted for by P_1. Assume that the data set has n samples for p variables. The basic ($n \times p$) data matrix can be written as:

$$\underset{(n\times p)}{X} = \begin{bmatrix} X_{11} & X_{12} & ... & ... & X_{1p} \\ X_{21} & X_{22} & ... & ... & X_{2p} \\ ... & ... & ... & ... & ... \\ ... & ... & ... & ... & ... \\ X_{n1} & X_{n2} & ... & ... & X_{np} \end{bmatrix} \tag{7}$$

where X_{ij} is the value of variable j obtained for sample i. When the matrix X is used, P can be rewritten as:

$$P = (X - M)A \tag{8}$$

where M is the mean matrix given by:

$$\underset{(n\times p)}{M} = \begin{bmatrix} \overline{X_1} & \overline{X_2} & \ldots & \ldots & \overline{X_p} \\ \overline{X_1} & \overline{X_2} & \ldots & \ldots & \overline{X_p} \\ \ldots & \ldots & \ldots & \ldots & \ldots \\ \ldots & \ldots & \ldots & \ldots & \ldots \\ \overline{X_1} & \overline{X_2} & \ldots & \ldots & \overline{X_p} \end{bmatrix} \tag{9}$$

where Equation 9 is the mean for variable j.

$$\overline{X_j} = \left(\frac{1}{n}\right)\sum_{i=1}^{n} X_{ij} \tag{10}$$

The matrix of *standardised loadings*, A, is a ($^{p\times p}$) matrix such that $A^T A = I$. The *scores matrix*, P, is a ($^{n\times p}$) matrix such that $P^T P$ is a diagonal matrix. Equation 7 becomes

$$X = M + PA^T \tag{11}$$

In this study, Varimax rotation was selected to maximize the sum of the variances of the squared loadings and thus enable us to seek the similarity of chemical components in sediment and soil samples. μ-SXRF spectra of the samples listed in Table 1 were analysed by PCA. The principal component patterns for Varimax rotated components of 30 samples composed of two PC, which account for 82.9 % and 17.0 % for the total of variances of PC1 and PC2 respectively. The contribution of PC1 and PC2 explains 99.9 % of total variance, and moreover PC1 is 4.87 times higher than PC2.

Multi dimensional (MD) plots of PC1, PC2 and PC3 have been frequently employed as diagnostic tools of chemical sources in environmental samples (Marcosa *et al*., 2010; Pongpiachan, 2006; Pongpiachan *et al*., 2012; Pongpiachan *et al*., 2013; Tipmanee *et al*., 2012). MD distribution patterns of PCs can be used as a characteristic diagnostic parameter to identify their elemental distribution characteristics in soil and sediment samples. However, these MD plots, as well as HCA and PDF, should be used with great caution as physiochemical processes can alter elemental distribution pattern during their transport from the emission source to the receptor site. Apart from using only raw data of μ-SXRF spectra, a second approach was also pioneered by using the first-order derivative dataset for three-dimensional (3D) plots of PCs in order to minimize the above-mentioned uncertainties.

In bi-polar plots of PC1 versus PC2 (see Figure 9), the vast majority of data points were clustered along the positive values of PC2 (y-axis) adjacent to 1.0 and subsequently decrease exponentially to positive side of PC1 (x-axis). The clearest features in MD plots (see Fig. 9-10) are: (*i*) 2D plots of samples No.23, No.31, No.39, No.72, No.78, No.5-21 and No.5-23, which were clustered close to

each other. It seems rational to interpret this cluster as evidence of tsunami backwash deposit samples. (*ii*) 2D plots of CZS samples (i.e. No.Tub1, No.PK3, No.BN2, No.BP3) with the mixture of TMS samples (i.e. No.17, No.53, No.62) and OTD samples (i.e. No. BM1-Tsu, No.BM2-Tsu, No.BP3, No.BK5-Tsu, No.BM2-Post-Tsu). It appears reasonable to ascribe this cluster as a mixture of terrestrial components and marine deposits. This can be deduced as a consequence of inferior mixing process between tsunami backwash deposits and typical marine sediments after tsunami inundation; (*iii*) OTD samples are highly deviated from TMS and TBD samples but possess similar distribution pattern with those of CZS samples as noticeably illustrated in 3D plots of first-order derivative PCs (see Fig. 10). This can be explained by the high degree of similarity in elemental distribution between onshore tsunami deposits and coastal zone soils.

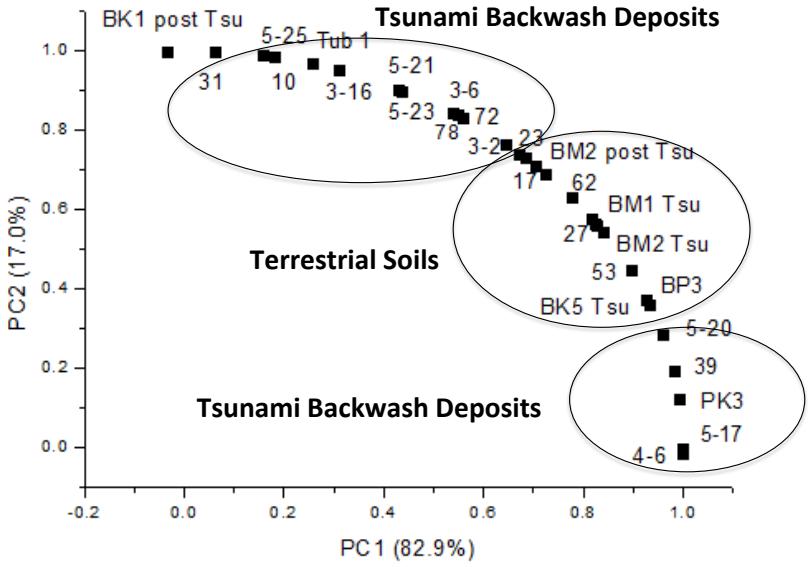


Fig. 9: Three-dimensional plots of principal components (PC) with raw data of typical marine sediments (TMS), tsunami backwash deposits (TBD), on-shore tsunami deposits (OTD) and coastal zone soils (CZS).

4. SYNTHESIS AND CONCLUSIONS

The above statistical analysis of collected data reveals that μ-SXRF spectra can yield authentic and valuable insight upon the terrestrial soils and/or marine sediments transportation processes affecting elemental distribution in the tsunami affected area. Subsequently, the authors support interpreting μ-SXRF spectra on the basis of various types of advanced statistical analyses rather than the simple use of raw spectra, which seems to be difficult for drawing any conclusions.

The major conclusions that occur from this data interpretation are described as follows:

(a) The prominent μ-SXRF spectra features of Typical Marine Sediments (TMS), Tsunami Backwash Deposits (TBD), Onshore Tsunami Deposits (OTD) and Cluster Zone Soils (CZS) can be achieved only through the employment of first order derivative data.

(b) The analysis of Probability Distribution Function (PDF) for different sample categories shows a clear influence of terrestrial soils and/or marine sediments transportation on elemental distribution.

(c) The Hierarchical Cluster Analysis (HCA) analysis of both raw and first order derivative data successfully discriminate terrestrial components from typical marine sediments with the assistance of dendrographic classification.

(d) The multi-dimensional plots of principal components (PCs) by using both raw and first order derivative data highlights the characteristic features of onshore tsunami deposits and coastal zone soils as clearly demonstrated in Fig.9-10.

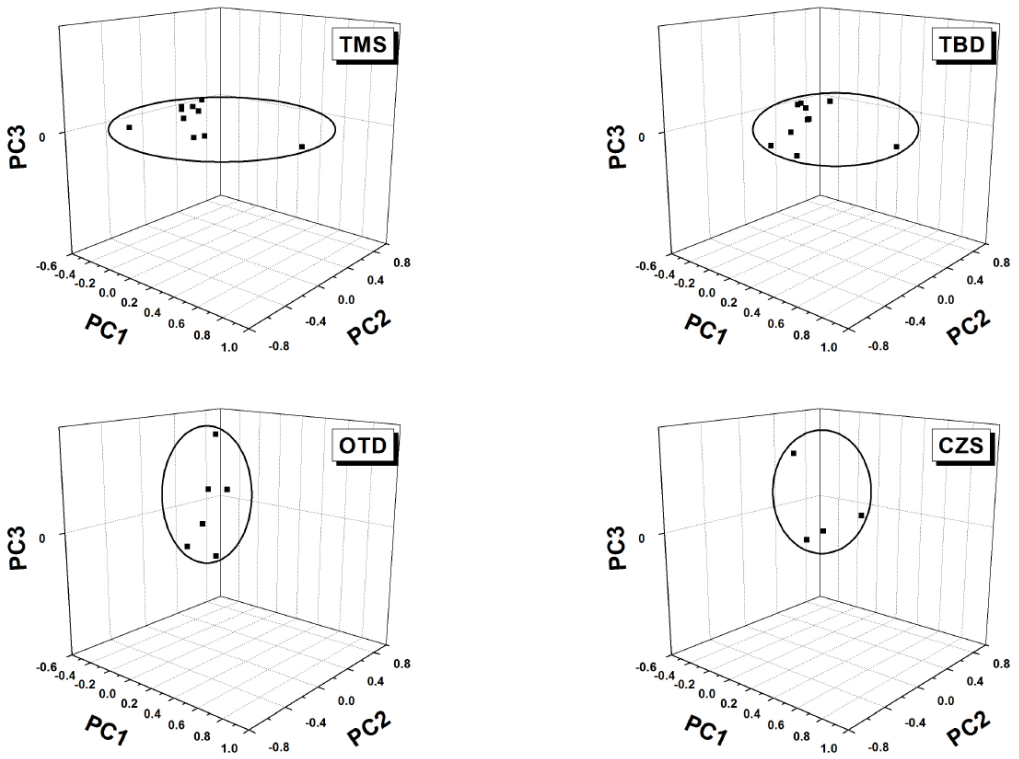


Fig. 10: Three-dimensional plots of principal components (PC) with the first-order derivative data of typical marine sediments (TMS), tsunami backwash deposits (TBD), on-shore tsunami deposits (OTD) and coastal zone soils (CZS).

5. ACKNOWLEDGEMENTS

This work was performed with the approval of Deutsche Forschungsgemeinschaft (DFG, Grant SCHW/ 11-1) and National Research Council of Thailand (NRCT). The authors acknowledge Phuket Marine Biological Center (PMBC) for their support with ship time of RV Chakratong Tongyai and RV Boonlert Pasook, as well as other contributions and facilities during field measurements. We are greatful to Mrs. D. Sakuna for support during all cruises. The authors would also like to express special gratitude to Synchrotron Light Research Institute (Public Organization), Ministry of Science and Technology, Thailand for their contribution of μ-SXRF measurements.

REFERENCES

ABRANTES, F., ALT-EPPING, U., LEBREIRO, S., VOELKER, A. & SCHNEIDER, R. (2008). *Mar. Geol*. **249 (3–4)**, 283-293.

BADIN, A. L., FAURE, P., BEDELL, J. P. & DELOLME, C. (2008). *Sci. Total. Environ*. **403**, 178-187.

BALSAM, W. L. & DEATON, B. C. (1991). *Rev. Aquat. Sci*. **4**, 411-447.

BALSAM, W. L. & BEESON, J. P. (2003). *Deep. Sea. Res. Pat. I*. 50, 1421-1444.

BÖNING, P., BARD, E. & ROSE, J. (2007). *Geochem. Geophy. Geosy*. **8 (5)**, DOI: 10.1029/2006GC001480.

CHOOWONG, M., MURAKOSHI, N., HISADA, K., CHARUSIRI, P., DAORERK, V., CHAROENTITIRAT, T., CHUTAKOSITKANON, V., JANKAEW, K. & KANJANAPAYONT, P. (2007). *J. Coastal. Res*. **23(5)**, 1270–1276.

CHOOWONG, M., MURAKOSHI, N., HISADA, K., CHARUSIRI, P., CHAROENTITIRAT, T., CHUTAKOSITKANON, V., JANKAEW, K., KANJANAPAYONT, P. & PHANTUWONGRAJ, S. (2008a) *Mar. Geol*. **248 (3–4)**, 179–192.

CHOOWONG, M., MURAKOSHI, N., HISADA, K., CHAROENTITIRAT, T., CHARUSIRI, P., PHANTUWONGRAJ, S., WONGKOK, P., CHOOWONG, A., SUBSAYJUN,R., CHUTAKOSITKANON, V., JANKAEW, K. & KANJANAPAYONT, P. (2008b). *Terra. Nova*. **20**, 141–149.

CHOOWONG, M., PHANTUWONGRAJ, S., CHAROENTITIRAT, T., CHUTAKOSITKANON, V., YUMUANG, S. & CHARUSIRI, P. (2009). *Geomorphology*. **104**, 134–142.

FAGHERAZZI, S. & DU, X. (2007). *Geomorphology*. **99**, 120-129.

FELDENS, P., SCHWARZER, K., SZCZUCIŃSKI, W., STATTEGGER, K., SAKUNA, D. & SOMGPONGCHAIYKUL, P. (2009). *Polish. J. Enivron*. **18**, 63-68.

FELDENS, P., SCHWARZER, K., SAKUNA, D., SZCZUCIŃSKI, W. & SOMPONGCHAIYAKUL, P. (2013). *Earth. Planets. Space.* **64(10)**, 875-887.

GOFF, C. C., ANDREW, A., SZCZUCIŃSKI, W., GOFF, J. & NISHIMURA, Y. (2012). *Sediment. Geol.* 282, 65-77.

GRIFFIN, C., ELLIS, D., BEAVIS, S. & NANTES, Z.D. (2013). *Ocean. Coast. Manage*. **71**, 176-186.

JAGODZIŃSKI, R., STERNAL, B., SZCZUCIŃSKI, W., GOFF, C. C. & SUGAWARA, D. (2012). *Sediment. Geol*. **282**, 57-64.

KANNGIEβER, B. & HASCHKE, M. (2006). *Handbook of Practical X-ray Fluorescence Analysis*, edited by B. Beckhoff, B. Kanngieber, N. Langhoff, R. Wedell and H. Wolff, pp. 442-462. Berlin, Spinger-Verlag.

MARCOSA, M. M., HARRISON, M. R., SCHUHMACHER, M., DOMINGO, L. J. & PONGPIACHAN, S. (2010). *Sci. Total. Environ*. **408**, 2387-2393.
MATSUMARU, R., NAGAMI, K. & TAKEYA, K. (2012). *IATSS. Res*. **36 (1)**, 11-19.
PONGPIAJUN, S. (2006). Atmospheric Chemistry of Semi-Volatile Organic Compounds in Urban and Rural Air, University of Birmingham.
PONGPIACHAN, S., THUMANU, K., KOSITANONT, C., SCHWARZER, K., PRIETZEL, J., HIRUNYATRAKUL, P. & KITTIKOON, I. (2012). *J. Anal. Methods. Chem*. Article ID 659858, doi: 10.1155/2012/659858.
PONGPIACHAN, S., THUMANU, K., NA PHATTHALUNG, W., TIPMANEE, D., KANCHAI, P., FELDENS, P & SCHWARZER, K. (2013). *Sci. Tsu. Haz.* (ISSN 8775-6839), **32 (1)**, 39-57.
SAKUNA, D., SZCZUCIŃSKI, W., FELDENS, P., SCHWARZER, K. & KHOKIATTIWONG, S. (2012). *Earth. Planets. Space*. **64**, 931-943.
SOLE, V. A., PAPILLON, E., COTTE, M., WALTER, PH., & SUSINI, J. (2007). *Spectrochim. Acta B*, **62**, 63-68.
SOONTARANON, S. & RUGMAI, S. (2012). Small angle X-ray scattering at Siam photon laboratory, *Chinese. J. Phys*. **50 (2)**, 204–210, 2012.
SZCZUCIŃSKI, W., NIEDZIELSKI, P., RACHLEWICZ, G., SOBCZYŃSKI, T., ZIOŁA, A., KOWALSKI, A., LORENC, S. & SIEPAK, J. (2005). *Environ. Geol*. **49 (2)**, 321-331.
SZCZUCIŃSKI, W., CHAIMANEE, N., NIEDZIELSKI, P., RACHLEWICZ, G., SAISUTTICHAI, D., TEPSUWAN, T., LORENC, S. & SIEPAK, J. (2006). *Pol. J. Environ. Stud*. **15 (5)**, 793–810.
SZCZUCIŃSKI, W., NIEDZIELSKI, P., KOZAK, L., FRANKOWSKI, M., ZIOŁA, A. & LORENC, S. (2007). *Environ. Geol*. **53 (2)**, 253-264.
SZCZUCIŃSKI, W. (2012). *Nat. Hazards Earth Syst*. *Sci*. **60**,115–133.
TANCHARAKORN, S., TANTHANUCH, W., KAMONSUTTHIPAIJIT, N., WONGPRACHANUKUL, N., SOPHON, M., CHAICHUAY, S., UTHAISAR, C. & YIMNIRUN, R. (2012). *J. Synchrotron. Rad*. **19**, 536-540.
TIPMANEE, D., DEELAMAN, W., PONGPIACHAN, S., SCHWARZER, K. & SOMPONGCHAIYAKUL, P. (2012). *Nat. Hazards Earth Syst. Sci*. **12**, 1441–1451.
VÖTT, A., LANG, F., BRÜCKNER, H., PAPANASTASSIOU, G. K., MAROUKIAN, H., PAPANASTASSIOU, D., GIANNIKOS, A., HADLER, H., HANDL, M., NTAGERETZIS, K., WILLERSHÄUSER, T. & ZANDER, A. (2011). *Quatern. Int*. **242(1)**, 213-239.

ISSN 8755-6839

SCIENCE OF TSUNAMI HAZARDS

Journal of Tsunami Society International

Volume 32 Number 4 2013

A CRITICAL REVIEW AND EVALUATION OF APPLYING SEMI-VOLATILE ORGANIC COMPOUNDS (SVOCS) AS A GEOCHEMICAL TRACER TO INDICATE TSUNAMI BACKWASH: The Bilateral, Deutsche Forschungsgemeinschaft (DFG) and National Research Council of Thailand (NRCT) Funded Project "Tsunami Deposits in Near-Shore- and Coastal Waters of Thailand (TUNWAT)"

Siwatt Pongpiachan[1] & Klaus Schwarzer[2]

*[1]NIDA Center for Research & Development of Disaster Prevention & Management, School of Social and Environmental Development, National Institute of Development Administration (NIDA), 118 Moo-3, Sereethai Road, Klong-Chan, Bangkapi, Bangkok 10240 Thailand**

Corresponding author phone: (66) 2727-3090; mobile phone: (66) 819751456; fax: (66) 27273747; e-mail: pongpiajun@gmail.com

[2]Institute of Geosciences Sedimentology, Coastal and Continental Shelf Research, Christian Albrechts University Kiel, Otto Hahn Platz 1, D - 24118 Kiel, Germany

ABSTRACT

Tsunamis symbolize one of the most harmful natural disasters for low-lying coastal zones and their residents, due to both its destructive power and irregularity. The 2004 Boxing Day tsunami, which attack the Andaman Sea coast of Thailand, resulted 5,395 of deaths and inestimable casualties, interrupted economies and social well-being in numerous coastal villages and caused in extreme alterations of both onshore and offshore coastal morphology. The Great Indian Ocean tsunami also highlighted that there are many missing jigsaw puzzle pieces in scientific knowledge, starting from the generating of tsunamis offshore to the countless influences to the marine ecosystems on the continental shelf, coastal areas and on land and to the economic and social systems consequences. As with all deposits that do not have a direct physical link to their causative sources, marine tsunami deposits must be distinguished from other deposits through regional correlation, dating and criteria for recognition within the deposits themselves. This study aims to provide comprehensive reviews on using Polycyclic Aromatic Hydrocarbons (PAHs) as a chemical proxy to discriminate tsunami related

deposits from typical marine sediments. The advantages and disadvantages of this chemical tracer will be critically reviewed and further discussed.

Keywords: *Tsunami Deposits, Marine Sediments, Polycyclic Aromatic Hydrocarbons (PAHs), Andaman Sea*

1. INTRODUCTION

Tsunamis has been a cause of concern all over the world for their tremendous destructive power. This destruction was particularly great in Asia where tsunamis have occurred often throughout history. The 2004 Indian Ocean earthquake is generally recognized as one of the world's largest and deadliest natural disasters in modern times, responsible for estimated US$ 10 billions of damages including the number of deaths approximately 230,000 people. Since tsunamis dominate natural catastrophe statistics in term of causing casualties and damaging constructions, a large number of studies have been performed over the last three decades to assess the alteration of geological and sedimentological features related to tsunami impact around the world (Atwater, 1987; Benson et al., 1997; Bondevik et al., 1997; Choowong et al., 2007, 2008a, 2008b, 2009; Clague and Bobrowsky, 1994; Dawson et al., 1988, 1991; Gelfenbaum and Jaffe, 2003; Pinegina and Bourgeois, 2001; Szczuciński et al., 2005, 2006, 2007). Tsunamis are recorded since historical times and numerous investigations have been done about their origin, wave distribution and energy release along coastlines, potential for coastal changes as well as on sediment deposition further inland (Bryant, 2001). Tsunamis have been compared to storms even if they are two genetically unrelated phenomena. Both are remarkably similar in their physical power and in their ability to transport sediment across the shelf and to deposit it in deeper water environments, but there is some difference between large storms with long wave periods and the effects of tsunamis in terms of hydrodynamics on the shelf (Bryant, 2001). The differences exist in (*i*) the capacity of eroding sediments from the sea-floor and the beach-face and to carry and to deposit this material onshore if there are suitable topographic conditions existing and (*ii*) in the tremendous backflow of tsunami water masses from the inundated areas carrying land-borne material offshore. While it is accepted that storm surges result in the deposition of discrete sedimentary units, tsunami waves generally result in deposition of sediment sheets over relatively wide areas and considerable distances inland (Dawson, 1999). According to a recent review by Gusiakov (2005), 688 tsunamis occurred in the tsunamigenic regions of the Indo-Pacific including Indonesia during 1901 – 2000 and at least 100 megatsunamis have occurred during the past 2000 years worldwide (Scheffers and Kelletat 2003). In historical times 5 Tsunamis hit the coast of Sumatra (1797, 1833, 1843, 1861 and 1883) and might have affected the coast of Thailand as well (Department of Mineral Resources, 2005).

Most of the knowledge about offshore, shallow marine tsunami deposits results from onshore outcrops of ancient lithified strata (Cantalamessa and Di Celma, 2005). Indicators of backrush flow in Miocene sediments are described by le Roux and Vargas (2005). They consider sandstone injections and dikes associated with intraclasts, penetrating underlying strata, as well as debris flow including "wave-smoothed" beach material, as the most reliable evidence. Poor knowledge exists about the

deposition on the upper and lower shore face induced by tsunami across-shelf backwash, which might produce sediment aprons, sand bars or large sediment waves. Only very few investigations have been made on submerged unconsolidated Holocene marine deposits (Le Roux and Vargas, 2005, Vargas et al. 2005). The successive run-up and backwash of tsunami waves can produce strong seaward currents causing additional erosion and sediment re-deposition, depending on the nature of the coastal topography and bathymetry (Bondevik et al., 1997; Shi et al., 1998; Dawson and Shaozhong, 2000). Also, large objects (boulders, coral blocks and human artifacts) may be dragged or deposited on the seafloor producing a debris field and other evidence on the seafloor. Einsele (1988), who proposed diagnostic criteria for tsunami deposits, noted that the backflow of tsunamis is commonly focused by the coastal geomorphology into channelized flows. Due to this channeling, the velocity of the backwash flow is more erosive and powerful than the run-up flow. Le Roux and Vargas (2005) show that the backrush of the 1960 tsunami, which hit the coastline of Chile with up to 14 m high waves, developed as kind of rip currents. In short cores obtained from water depth between 75 – 100 m Vargas et al (2005) observed features and sediment material in two layers originating from areas shallower than 50 m. They relate these deposits to the tsunami backwash. By dating with radioisotopes and lateral correlation they inferred ages as between A.D.1409 – 1449 and A.D.1754 – 1789.

As tsunami backflows advance offshore from the coastline, they will undergo several changes known as flow transformation (Fisher 1983). Flow channelization seems to play an important role in lateral flow transformations leading to unusual deposits. Hyper concentrated flow conditions may therefore develop within the morphologically deepest channel zones, accompanied by intraclasts ripped up from the substrate. Very dense sediment-water mixtures, which the backrush might be, may initially behave as Bingham Fluids dominated by frictional grain interactions and shearing, so that shear carpets may develop at their base. According to Nittrouer and Wright (1994) the midshelf region is in many cases the dead end for many of the particles transported across continental shelves due to storm events. Besides the investigations of Le Roux and Vargas (2005) to our knowledge nothing is known about the fate and the area where most of the tsunami related material is deposited offshore. However, Shanmugam (2005) assumes that tsunami-related deposits should be volumetrically important in coastal, shallow-water and deep-water environments.

For a long time it was neglected that on wave dominated coastal and shelf areas the impact of tsunami waves on shore-face deposits can be preserved in modern sediments. However recent investigations based on modern high resolution remote sensing mapping techniques for marine areas revealed that even in highly dynamic areas and even if the perturbed shore face is in a disequilibrium state, a preservation potential of sediment distribution patterns and shore face geomorphology exist for decades (Schwarzer et al., 2003; Murray & Thieler, 2004; Ferrini & Flood, 2005; Diesing et al. 2006). Conceivably, on the deeper parts of the lower shore face and inner shelf the elevated water level may induce deposition (similar to the classic "Bruun Rule" response) if there is sufficient accommodation space. Thus, the initial morphological response of the shore face to the tsunami is hypothesized to have a pattern of sediment deposition on the lower shore face and inner shelf, erosion on the upper shore face and beach face, and deposition landward of the beach.

1.1 General background of Tsunami Deposits in Near-Shore- and Coastal Waters of Thailand (TUNWAT) Project

In the months following the tsunami disaster, consultations between the National Research Council of Thailand (NRCT) and the German Research Foundation (DFG) resulted in a general agreement for a bilateral cooperation, which was focused on tsunami-related research. Backed by discussions during a joint NRCT-DFG workshop in Bangkok in July 2006, German and Thai scientists agreed to propose research projects, which specifically address scientific issues dealing with tsunami triggering, tsunami wave development and interaction with the sea-bottom and the impacts, alterations and risks to gain a better understanding of tsunamis, their origin, propagation, physical-, social- and economic impacts, resulting destructions and long-term effects and, thus, to improve risk management in the Andaman Sea Region (see Fig.1-3).

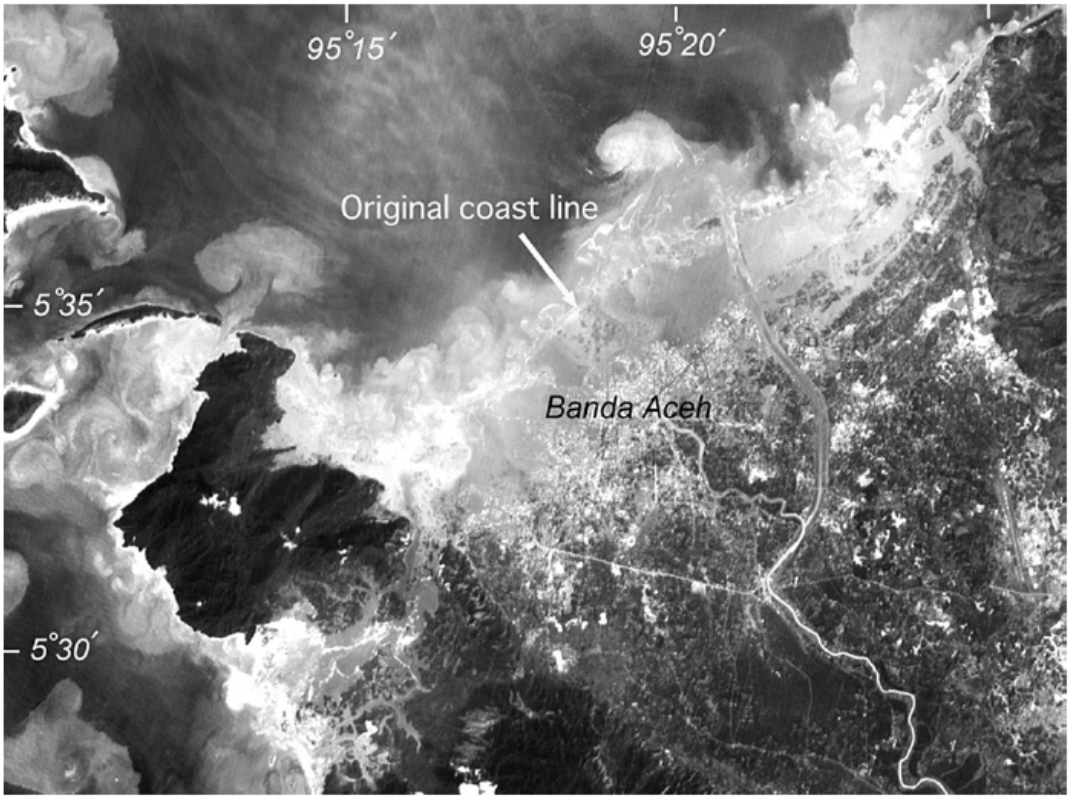


Figure 1. Inundation and tsunami flow of the Banda Ache Plain shown in the SPOT2 image. The image was taken about 4 h after the earthquake. (Includes material from CNES2005, Distribution Spot Image S.A., France, all rights reserved). Taken from Umitsu, M. et al., 2006. Own comment: Rip current eddies can be observed along the whole coastline.

Within the framework of this theme, several topics have been brought forth. As there is a common focus on tsunamis and impacts, the research issues of the individual projects are interlinked by the fact

that they are aiming at providing complementary answers to key questions about tsunamis in the study region and their potential impacts. These major questions can be described as follows; (*i*) Where and how can tsunamis be triggered in the Andaman Sea? (*ii*) How often have tsunamis struck this coast in the recent past? (*iii*) How does a tsunami wave propagate from offshore (deep water) via the shelf and near-shore zone onto the adjacent low-lying land areas? (*iv*) What are the impacts of tsunami waves to the seafloor topography, to the sediment cover and to the marine & littoral ecosystems while progressing onshore? (*v*) How does the land-sea loaded backflow influence the marine abiotic and biotic system? (*vi*) How is tsunami wave energy attenuated in the near shore zone, beachfront and hinterland and how is this attenuation influenced by the presence of natural barriers such as coastal forests? (*vii*) What factors determine the tsunami-related vulnerability of low-lying coastal areas, their population, communities and economies? (*viii*) Which kind of socio-economic, institutional and/or other factors make coastal societies or communities resilient against tsunami impacts? (*ix*) How can risk management, including early warning, be improved to prevent or mitigate future tsunami disasters along this coast?

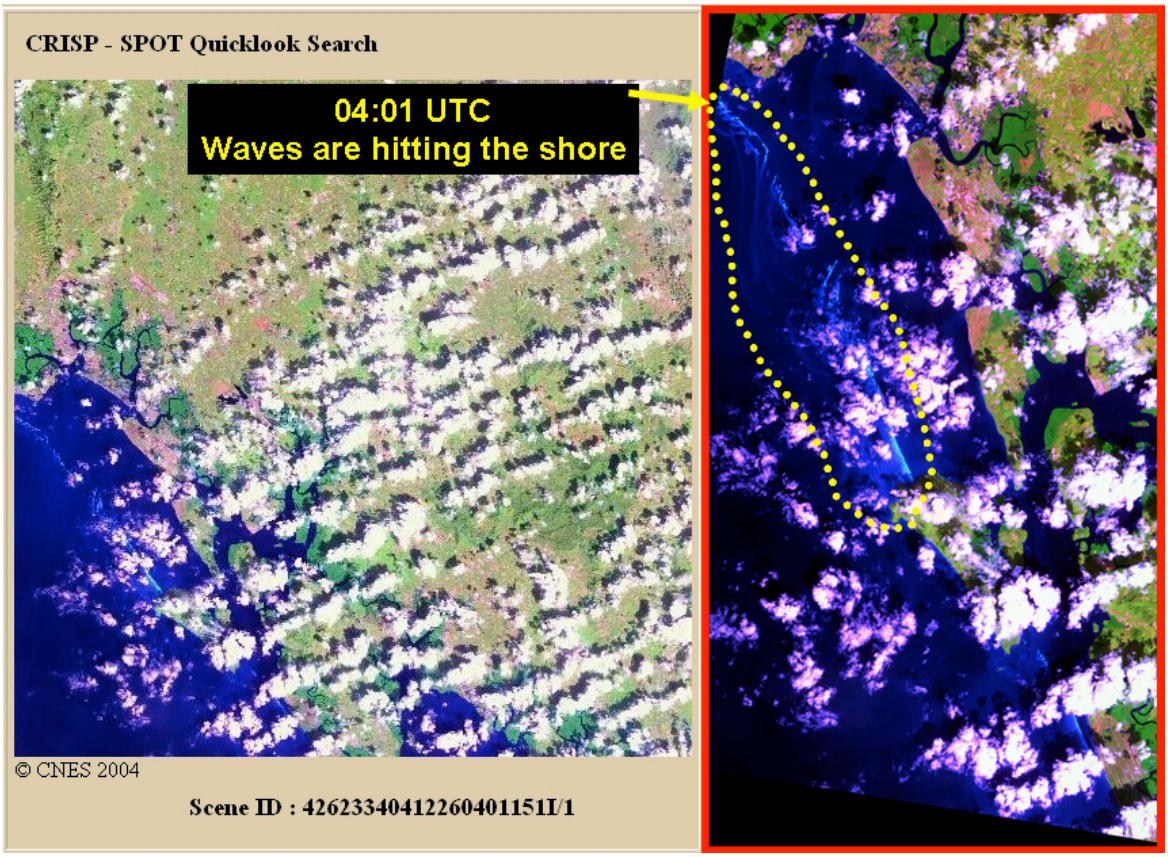


Figure 2. The coastal area of Thailand when the Tsunami waves hit the shore. Far offshore the influence of the sea bottom to the tsunami waves becomes obvious when due to bottom friction by wave transformation and wave-breaking occurs (Source: http://www.crisp.nus.edu.sg/tsunami/tsunami.html).

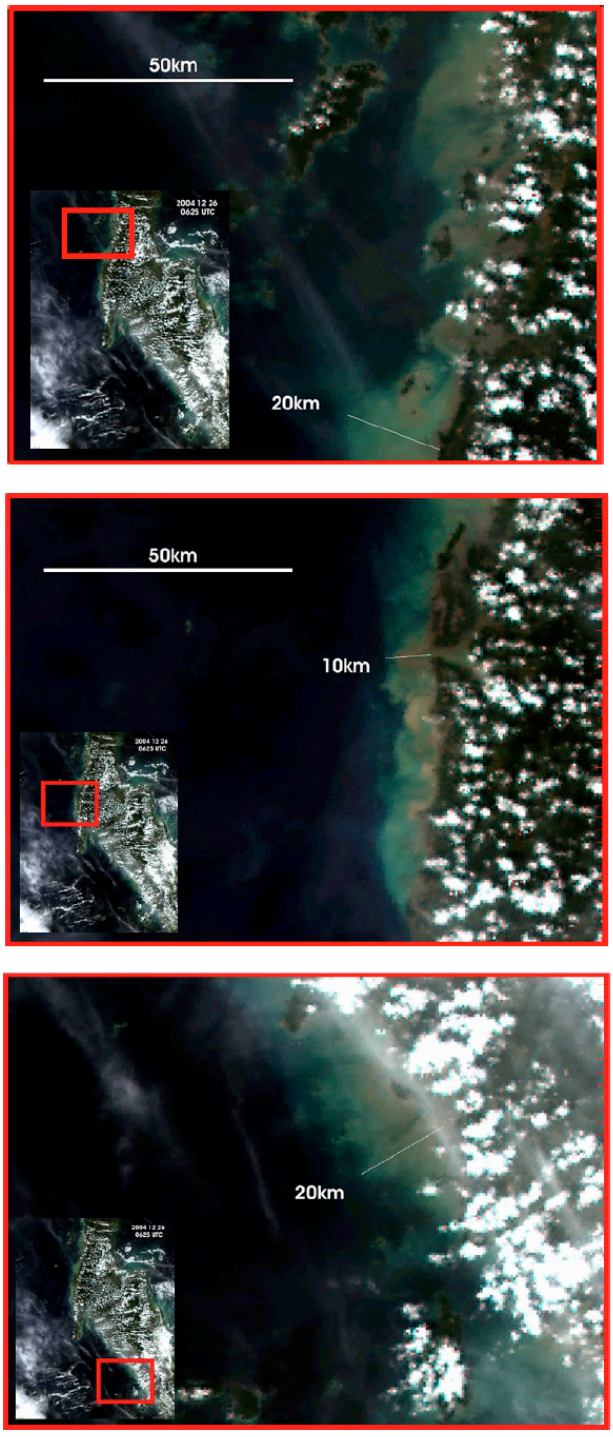


Figure 3. The coast of Thailand 2 hours after the tsunami hit the coast on December 26th, 2004 at 06:25 UTC. The suspension load plume of the backrush extends approximately 20 km offshore. (Source: http://www.crisp.nus.edu.sg/tsunami/tsunami.html).

The questions above provide a feasible basis for addressing key issues of regional tsunami research. They also outline some spatial structure, as the planned projects may be seen as lining up along an offshore – onshore transect from the deep Andaman ocean across the shelf, near shore and beach zone into the coastal hinterland as far as a mega-tsunami can reach. While in the offshore domain natural processes dominate, towards onshore and especially on land anthropogenic influences increase and trigger the vulnerability. Consequently, the intention of the group is to establish a German – Thai tsunami research network in which project data ought to be exchanged and results ought to be generated/synthesized as to contribute to the enhancement of the region's ability to cope with tsunami risks.

Based on this concept of interlinked and spatially adherent projects the German-Thai research group attempts to focus on the following issues:

- Analyze the possibility of tsunami-triggering by slides / slumps at the continental margin of the Andaman Sea;
- Detecting changes in seafloor topography and sediment pathways by use of remote sensing methods (satellite image investigation, mapping by multi-beam and side scan sonar techniques), sediment coring, sampling and dating by radio isotopes;
- Detection and reconstruction of previous tsunami events in order to determine the long-term history of tsunamis along this coast;
- Numerical modeling of wave propagation and run-up during the Dec. 26, 2004 tsunami. Validation of different models by comparing measured tsunami run-up characteristics with results from numerical model simulations;
- Determining the influence of coastal ecosystems, in particular coastal forests and mangroves, on the physical impacts of tsunami waves along the whole western coast of Thailand;
- Generating a scientific knowledge base and developing/validating prediction models for the tsunami attenuation performance of coastal forests;
- Assessment and evaluation of tsunami risks in flood-prone coastal areas and communities. Assisted by remote sensing techniques and field surveys, quantitative indicators are to be derived for ecologic, economic and social vulnerability as well as for local resilience;
- Comparing local and global interactions in disaster prevention and recovery in two regions strongly hit by the 2004 tsunami: Khao Lak, Thailand and Aceh, Indonesia;
-

The main objective of the proposed sub-projects is to complement individual research issues in such a way that a clear picture can be drawn about the destructive forces and processes of the recent tsunami and past tsunamis and to elaborate and to suggest measures how to avoid or mitigate future tsunami impacts and destructions in Thailand. Most of the deposits that are known to occur or may occur in marine environments require improvements in the criteria for recognition. Developments of such criteria are best done when there are deposits of unquestioned origin. The recognition of deposits of this tsunami gives the opportunity to extend the relatively short or non-existent historical record of tsunamis in this area. Presently most of the literature regarding marine tsunami deposits comes from ancient geologic record and cannot be tested. The December 2004 Sumatra-India earthquake and following tsunami represents an opportunity to catalogue geomarine effects from a very well recorded series of events, many of which are unknown or poorly known at present. A modern deposit of

unquestioned origin is invaluable for defining the palaeo record. This event represents the best-recorded mega-tsunami in human history and offers a unique opportunity to collect data, which have been never recorded yet. Even if offshore records offer the potential of good preservation, good spatial coverage and long-term span, data should be collected as soon as possible after this event as much of the information may be altered or destroyed over time.

Numerous field surveys have been carried out to measure the inundation, run up and deposition of marine derived sediment onshore caused by tsunamis, but no systematically detailed study exist up to now to measure geomorphological, sedimentological and geological alterations offshore beyond the upper shore face. This project aims to assess the impact of tsunami waves on changes and/or offsets of large-scale bed forms, on changes and/or offsets of shelf sediment distribution patterns and on estimating the spatial extension of erosion as well as on deposition by the backwash. The following offshore impacts are expected:

- Erosion by the onshore moving tsunami wave;
- Erosion by the channelized backwash currents;
- Transport of huge sediment plumes offshore and deposition from the shore face to the mid- or outer shelf.

Therefore the scientific questions in detail are:

- How do incoming tsunami waves influence sediments and sea bottom topography on the shelf and in near shore waters?
- How does the offshore flowing backrush influence sediments and sea bottom topography on the shelf and in near shore waters?
- Are there distinguished conduits for the sediment backflow?
- At which water-depth and at which offshore distance can a tsunami triggered alteration of the seafloor be observed?
- How will offshore tsunami deposits look like?
- How does an archive record of tsunami affected shelf deposits look like?
- How far offshore sediments are transported by the tsunami backwash?
- Was more sediment transported and deposited onshore or offshore?

To achieve the objectives of this project a multidisciplinary approach is required combining remote sensing methods, geophysical and sedimentological methods and geochemical methods.

1.2. Concept of using Semi-Volatile Organic Compounds (SVOCs) as geochemical tracers to characterize tsunami backwash deposits

Geochemical tracers have been extensively used as environmental tools to investigate the behavior and fate of target compounds in the environment (Pongpiachan et al., 2012a,b). While onshore tsunami deposits are supposed to contain organic and inorganic material of marine origin, offshore transported material should contain tracer-material originating from land, depending on landforms and

deposits, which are exposed in the areas, which were hit by the tsunami waves. For decades, both PAHs and aliphatics have been used as a "proxy" to distinguish the anthropogenic source and biogenic source. In this study we make the assumption that (*i*) terrestrial soils contain many anthropogenic PAHs coupling with aliphatics from terrestrial plants and (*ii*) marine sediments contain many of phytoplankton derived biomarkers. By analyzing these organic tracers from different points coupling with careful statistical treatments, it should be possible to investigate the impact of the tsunami to the distribution of terrestrial sediments in the recent deposits of the Andaman Sea.

Understanding the mechanisms and spatial variations of tsunami backwash sediment distribution patterns and burial within the offshore area of the Andaman Sea requires an ability to discriminate between terrigenous and marine components of organic compounds. Furthermore, the role of the shelf as a source area must be distinguished from those of basins, as sink areas and the coupling between the two should also be understood as well. A number of approaches have been used to distinguish between marine and terrigenous components in marine sediments including SVOCs such as PAHs, hopanes and cholestanes (Westerhom et al., 1992; Yunker et al., 2002, 2003; Kalaitzoglou et al., 2004). SVOCs have the advantage that they are all released into the atmosphere by imperfect combustion of organic matters and thus can be used as indicators to identify anthropogenic combustion sources (i.e. traffic emissions, industrial activities, incinerators etc) from natural combustion sources (i.e. forest fires, volcano activities, re-evaporization, etc.) by using specific binary ratios (Pongpiachan, 2013a,b,c; Pongpiachan et al., 2013c,d; Tipmanee et al., 2012; Yunker et al., 2002). Those areas which were most affected by the backrush of tsunami waters should contain more terrigenous sediments and thus as well relatively higher proportions of anthropogenic source derived organic compounds. Specific organic biomarkers such as 17 α(H) -22,29,30-Tris (Tm), 17 β(H), 21 β (H) -hopane, 17 β (H), 21 α (H) -30-northpane (Isoadiatane), 17 β (H), 21 α (H) -hopane (Moretane), 17 α (H), 21 β (H) –hopane, 18 α (H), 22,29,30-Trisnorneohopane (Ts), on the other hand, often yield clear evidence of sources (terrigenous and marine) even though they represent only a small proportion of the total organic material found in the sediments (Belicka et al., 2004). Furthermore, the value of CPI1 (Carbon Preference Index 1), CPI2 (Carbon Preference Index 2), CPI3 (Carbon Preference Index 3), ACL (Average Carbon Length), C_{max} (Carbon Maximum Number), Pristane and Phytane can be used as biomarkers to distinguish between terrigenous and marine derived sources of sediments (Yunker et al., 2002, 2003). By calculating SVOC concentrations against background values the spatial extension of the sediment load of the tsunami backrush can be estimated. In addition, there are other alternative analytical tools such as Attenuated Total Reflectance Fourier Transform Infrared Spectroscopy (ATR-FTIR) and micro-beam synchrotron X-Ray Fluorescence (μ-SXRF) that can be used to characterize the tsunami backwash deposits (Pongpiachan et al., 2013a,b).

1.3. Physicochemical properties, fates and environmental risks of PAHs

PAHs are a class of very stable organic molecules made up of only carbon and hydrogen and contain two to eight fused aromatic rings. PAHs are formed during incomplete combustion of organic materials such as fossil fuels, coke and wood. By definition as organic compounds with vapor pressure ranging from 10^{-3} – 10^{-7} Pa (see Table 1), PAHs, alkanes, cholestanes, hopanes and anthropogenic sourced chemicals like organochlorine pesticides, polychlorinated biphenyls (PCBs),

dioxins can be termed as SVOCs (Paasivirta *et al*., 1999). These molecules were oriented horizontal to the surface, with each carbon having three neighboring atoms much like graphite (see Table 2-5). The structures of a variety of representative PAHs can be seen in Table 2. In order to reduce the atmospheric concentration of SVOCs, the UK's Expert Panel on Air Quality Standard (EPAQS) has selected benzo[*a*]pyrene (B[*a*]P) as a marker for levels of ambient PAHs in recognition of its carcinogenicity and mutagenicity. An annual mean of 0.25 ng m^{-3} has been set. However, this value exceeded the annual mean concentration of B[*a*]P measured in a number of UK cities since 1997. The long term monitoring of SVOCs in urban air, therefore, is a significant approach to investigate the annual trends and seasonal variations of targeted compounds. However, the environmental persistence and a wide range of vapor pressure of SVOCs have made this group of organic compounds globally ubiquitous and thus subject to unique atmospheric fate/behavior. The complexity of its existence in the atmospheric environment together with varieties of emission sources attributed the uncertainties in source apportionment of these specific compounds. Since SVOCs can be measured in the most remote areas like Antarctica, the worldwide concerns are also focused on the long-range atmospheric transportation (LRAT).

Epidemiological evidence suggests that human exposures to PAHs, especially B[*a*]P are high risk factors for carcinogenic and mutagenic effects. There are hundreds of PAH compounds in the environment, but only 16 of them are included in the priority pollutants list of US EPA (EPA, 2003). Many PAHs have also been identified as cancer-inducing chemicals for animals and/or humans (IARC, 1983). In 1775, the British surgeon, Percival Pott, was the first to consider PAHs as toxic chemicals with the high incidence of scrotal cancer in chimney sweep apprentices (IARC, 1985). Occupational exposure of workers by inhalation of PAH-both volatile and bound to respirable particulate matter- and by dermal contact with PAH-containing materials, occurs at high levels during coke production, coal gasification, and iron and steel founding. Coke oven workers have a 3- to 7-fold risk increase for developing lung cancer (IARC, 1984 and IARC, 1987). For this reason, the monitoring of PAHs in environmental media is a reasonable approach to assess the risk for adverse health effects. Since the fate of PAHs in the natural environment is mainly governed by its physiochemical properties, the study of general properties of the compounds is of great concern. In spite of a large number of publications related to the environmental fates of PAHs around the world, there are only few studies conducted in Thailand (Boonyatumanond et al, 2007; Chetwittayachan et al, 2002; Pongpiachan et al., 2009; Pongpiachan, 2013b,c; Pongpiachan et al., 2013c,d, e; Ruchirawat et al, 2002, 2005, 2007; Tipmanee et al., 2012).

In this study, the authors hypothesize that the employment of PAHs coupled with various analogies of statistical analysis assist in a better understanding of offshore terrestrial deposit distribution pattern, which can be subject to erosion by tsunami/monsoon waves and surface runoff by heavy rain in the tsunami-affected coastal areas of Andaman Sea, Thailand. Note that it is the purpose of this paper to critically review both the advantages and disadvantages of using SVOCs as an innovative proxy to separate the terrestrial deposit from the background sediment in tsunami-affected coastal areas. Neither the source apportionment, nor the analysis of spatial variation of SVOCs in sediments is the main focus of this study. In addition, the risks and possibilities of applying other geochemical tracers as an alternative extreme event proxy will be reviewed and discussed.

2. Source characterization of SVOCs

2.1 Source characterization of PAHs

The binary ratio method for PAH source identification, involves comparing ratios between pairs of frequently found PAH compound characteristics of different sources. Stationary source combustion emissions from the use of coal, oil and wood are low in coronene (Cor) relative to B[*a*]P, while mobile source combustion emissions from diesel and petroleum use are high in B[*g,h,i*]P and Cor relative to B[*a*]P (Stenberg et al., 1979). The ratio of these PAHs can be used to distinguish between traffic dominated PAH profiles and other sources (Brasser, 1980; Mainwaring and Stirling, 1981). Lim et al., (1999) used two methods in evaluation of PAH traffic contribution. Both of methods were adapted from Nielsen (Nielsen, 1996). Equation 1 based on the assumption that all Cor is traffic-generated, the concentration of B[*e*]P which is traffic generated is given by

$$B[e]P_{traffic} = \frac{Cor_{concentration}}{\frac{\delta Cor}{\delta B[e]P}}$$

Equation1

Crucial to this method is the assumption that all Cor is traffic generated. Although this is likely to be an oversimplification, many studies have shown a high correlation between Cor and vehicular emissions. In addition, the ratios of B[*g,h,i*]P/B[*e*]P and Cor/B[*e*]P can also be used as traffic indicators, since both B[*g,h,i*]P and Cor have been reported to correlate closely with traffic emissions . Other PAHs such as retene (Ret) is also considered as a common biomarker of coniferous wood combustion, and resin acids such as abietic acid commonly found in smoke samples.

Since PAHs contents in atmosphere are sensitive to both anthropogenic and natural emissions, a more effective marker of traffic emissions is substantially required. Another potential index to distinguish the traffic emission is the use of inorganic tracers. It is widely known that particles from road dust appear to contain Pb, Fe, Mn, Ca and sometimes Zn, (Harrison et al., 1996). This can be explained by the attrition of road surfaces, resuspension of street dirt and soil dust (i.e. source of Ca and Mn; Pierson and Brachaczek, 1993), particles from tyre wear (i.e. source of Zn; Ondov et al., 1992), brake-drum abrasion, and debris from wear and rusting. In order to investigate the contributions of traffic related pollutants, several attempts were made for source apportionment of PAHs in Birmingham air by using inorganic source markers such as Cu, Fe, Pb, Zn and Mn. Lim et al (1999) reported high loading on higher MW PAHs (B[*a*]A to Cor) and moderate loading on BNT and Ph and the gasoline powered vehicle marker, Pb.

Based on size distribution of various elements at a road site location in Birmingham (BROS), Fe, Cu, Mg, Sr, Mo, Ce and Ba were found to be the major components in the traffic related coarse particle (i.e. 2 – 10 μm aerodynamic diameter, Harrison et al., 2003). Whilst strong correlations of Cu (r^2 > 0.74), Mo (r^2 > 0.54), Ba (r^2 > 0.73), Pb (r^2 > 0.68), Mn (r^2 > 0.54) and Zn (r^2 > 0.61) with NO_x indicated that these elements probably originate in road site particles. Until 1997, Pb and Br had been

widely employed as indicators of road traffic emissions (Harrison et al., 1997). Lead (Pb) is added to petrol in the form of an organic tetramethyl lead, an anti-knock agent, and is emitted by the exhaust stream in inorganic particulate forms, predominantly as PbClBr and $2PbClBr*NH_4Cl$. Thus, the combination of Pb with Br can be used as classical marker elements for traffic emissions. However, the worldwide decline of Pb concentrations in the atmosphere has been observed due to the introduction of unleaded gasoline into the market in 1989 (Salma, et al., 2000). As a consequence, the Br/Pb ratio for determining the automotive contribution to the atmospheric lead burden may not be possible. In this study, *n*-alkanes and petroleum biomarkers such as hopanes and cholestanes had been introduced into the receptor models instead of inorganic marker elements like Pb. Alternatively, hopanes and cholestanes can be used as petroleum biomarkers, because: (*i*) these organic compounds are found mainly in exhausted gas from petroleum combustion and thus overlap PAHs combustion profiles, (*ii*) these organic compounds are not formed by atmospheric chemical reactions, (*iii*) these organic compounds are continuously released to the atmosphere by automotive emissions, and (*iv*) these organic compounds are prone to degradation in the environment. Because of these unique characteristics, hopanes and cholestanes have been widely used to define both the fossil origin and geological source of petroleum residues, (Rogge et al., 1993; Simoneit, 1984).

2.1.1 PAHs in aerosols from different countries

2.1.1.1 UK

PAH monitoring campaign was performed at two sites in London by Kendall et al (2001). The first sampling site was located at Bounds Green (BG) in North London. The second sampling site was positioned at St Paul's Cathedral (SP) in Central London. The annual means of the majority of the individual PAH compounds and ΣPAHs was higher at SP (7.24 ng m^{-3}) than at BG (4.27 ng m^{-3}). Both sites showed the same seasonal pattern of the lowest concentration during the summer and the highest average concentration during the autumn. B[*g,h,i*]P was the most abundant PAH at both London sites, followed by B[*a*]A and Chry, and these three PAHs dominated during all four seasons. The highest concentrations of these compounds were measured during the sampling week containing Bonfire Night at BG and during January at SP. Concentrations of these three compounds contributed over 50% of the ΣPAHs In London, the winter ΣPAHs concentrations were only approximately twice the summer concentrations, possibly reflecting the small number of PAHs sources in London, with vehicles dominating PAHs production.

2.1.1.2 Indonesia

The burning of biomass as a method to clear and fertilise land is practiced in Indonesia every year by farmers and forestry companies. In 1997, Indonesia had been extremely dry due to El Nino, and what is now known as the Indonesia forest fire started to get out of control in the middle part of June. Emissions from biomass burning can vary widely because the material and the burning conditions can differ greatly. In a forest fire of this duration and magnitude, the burning material and conditions can vary from time to time as well as location to location. The ΣPAHs concentration ranged from 7 ng m^{-3} to 46 ng m^{-3} (Fang et al., 1999). The highest value of B[*a*]P was measured in Pudu on 27-09-97 at 3 ng m^{-3} while the lowest was at the same site on 04-09-97 at 0.1 ng m^{-3}. These values are comparable to those measured in Hong Kong, and the highest value matches some of the street-level monitoring

results (Fang et al., 1996). The concentration increase in ΣPAHs from the early to late September samples was the lowest. Retene, a common biomarker of coniferous wood combustion, and resin acids such as abietic acid commonly found in smoke samples in controlled studies, were not found in any of the samples in this study. This may be due to the transformation occurring in the long distance transportation of the aerosols, although retene was found to be relatively stable in sediments and did not vary in the same way as other PAHs (Ramdahl, 1983).

2.1.1.3 Greece

The field campaign took place in a conifer forest of central, continental Greece. Measurements were taken as part of the European Commission project, "Aerosols formation from biogenic organic carbon" (AEROBIC), during the period of 20 July-12 August, 1997. PAHs and oxy-PAHs detected in the Greek aerosols present an increase of concentrations with the number of benzene rings, with a dominance of PAHs with more than 5 rings. ΣPAHs concentrations (0.1 ng m^{-3} -18.5 ng m^{-3}) were, in general, higher compared to that reported for a Portuguese forest, 0.1 ng m^{-3} - 0.9 ng m^{-3} (Kavouras et al., 1999), and other rural area of Greece, 0.2 ng m^{-3} - 2.0 ng m^{-3} (Gogou et al., 1996). However, these levels are lower than those presented for urban aerosols of a Greek island, 21.4 ng m^{-3} - 59.0 ng m^{-3} (Gogou et al., 1996).

2.1.1.4 Hong Kong

Hong Kong, with an area of 1092 km^2 and over 6.5 million in population, is surrounded by the South China Sea to the south and east, Pearl River Estuary on the west, and the landmass with complicated terrain on the north. It is also under the influence of the Asian Monsoon System. The summer monsoon brings in clean oceanic aerosols while a polluted air mass from the mainland comes with the northeasterly wind in the winter season. Thus the characteristics of Hong Kong's aerosols are represented by outside sources superimposed on very strong local emissions. ΣPAHs concentration was in the range of 0.7 ng m^{-3} - 12.2 ng m^{-3} (Zheng et al., 2000). In general, higher PAHs concentrations were found in the winter $PM_{2.5}$ samples. Other studies show that the changes in emission patterns (stationary and vehicular) and meteorological conditions (including less daylight hours, reduced ambient temperatures, and lower volatilization and photochemical activity) contribute to the higher PAHs levels during winter (Ramdahl et al., 1982, 1983; Freeman and Cattell, 1990, Baek et al., 1991a,b). The association of B[*g,h,i*]P with vehicle exhaust has long been established (Baek et al., 1991a,b), and a good correlation with total PAHs was obtained in this study. This suggests that vehicular emission was the dominant source of PAHs in the $PM_{2.5}$ cut of the aerosols in Hong Kong. The low molecular weight (LMW) PAHs such as Phe, Fluo and Pyr were enriched in the fall and winter samples. Comparing the spring and summer samples, the winter and fall samples contained more LMW PAHs. The LMW PAHs tend to be more concentrated in the vapour phase while the higher molecular weight ones are often associated with particulates. In addition, more details of PAHs in aerosols around the world are displayed in Table 6.

2.2 Source characterization of aliphatics

The enormous range of organic compounds detected in urban particles may be divided into two major source groups; primary condensates and oxidized hydrocarbons. Primary condensates (alkanes (C_{17}-

C_{36}), alkenes) originate directly from the incomplete combustion of fossil fuels and are sorbed onto the surface of particulate matter. Oxidized hydrocarbons (carboxylic acids, aldehydes, ketones, quinines, esters and phenols) may either be attached to the particulate as a primary condensate or may be produced during atmospheric oxidation reactions (Cautreels, 1978). Bray and Evans (1961) developed the carbon preference index (CPI) as an indicator of the extent of odd or even carbon number homologues within a sample. The CPI is expressed as a summation of the odd number homologues within a specified range of carbon numbers divided by a summation of the even number homologues within the same range. This inter-sample comparison is useful in identifying sources and establishing dominant sources of aerosol organic matter, as certain biologically produced *n*-alkanes show a pronounced predominance of odd carbon numbers (Bray and Evans, 1961). For example, organic matter of recent biogenic origin shows a preference for odd carbon numbered *n*-alkanes with CPI_{odd} values of 6-9 and more. Hydrocarbons of abiological origin (e.g. fossil fuels) typically show no carbon number preference or tend towards low CPI values (i.e. CPI < 1). To reconcile sources of organic species, CPI was calculated as follows (Tarek et al., 1996):

$$CPI_1 = \frac{\sum (C_{15} - C_{31})}{\sum (C_{14} - C_{32})}$$

Equation 2

CPI_1 represents whole range for *n*-alkanes

$$CPI_2 = \frac{\sum (C_{15} - C_{25})}{\sum (C_{14} - C_{24})}$$

Equation 3

CPI_2 represents petrogenic *n*-alkanes

$$CPI_3 = \frac{\sum (C_{25} - C_{31})}{\sum (C_{26} - C_{32})}$$

Equation 4

CPI_3 represents biogenic *n*-alkanes

The biogenic "wax" concentration of *n*-alkanes was calculated as follows:

$$Wax - n - Alkane = [C_n] - \left[\frac{(C_{n+1} - C_{n-1})}{2}\right]$$

Equation 5

Note that wax* has traditionally referred to a substance that is secreted by bees (i.e. beeswax) and used them in constructing their honeycombs. Additionally waxes may be natural or artificial. In this context, wax is natural oily substance. Chemically, a wax may be a combination of other fatty alcohols with fatty acids.

Scalan and Smith (1970) proposed the *odd-to-even* predominance *n*-C_{29} OEP ratios by using the following equation;

$$n - C_{29}OEP = \frac{(C_{27} + 6C_{29} + C_{31})}{(4C_{28} + 4C_{30})}$$

Equation 6

OEP values were plotted against carbon chain length to construct the OEP curves. The pattern of the OEP curve is determined by the source of *n*-alkanes, which indicates the potential fingerprint for source apportionment. U:R is a good indicator of petroleum residue contribution. Under the resolved peaks in a typical *n*-alkane gas chromatogram, there is an unresolved complex mixture (UCM) in the form of an envelope, which contains branched and cyclic hydrocarbons. The UCM is also termed as the "hump" and is believed to be the contribution from fossil fuel residue. U:R is the ratio of the areas of the unresolved to resolved components (peaks) and is an indicator of the contamination by anthropogenic sources (Mei, 2000).

Hopanes are widespread in both recent and ancient sediments. The origin of most hopane is the bacterial C_{35} tetroltetrahydroxybacteriohopane. Hopane hydrocarbons present in sediments range from C_{35} and down to C_{27}, usually with the C_{30} isomers as the predominant. Hopanoid are produced by most living organism with $\beta\beta$-configuration (17β(H),21β(H)). Increasing maturity leads to the more thermodynamically stable $\alpha\beta$-hopanes and $\beta\alpha$-hopanes, with the former being the predominant isomer. Molecular calculations have shown that the $\alpha\alpha$-isomers are less stable than the $\alpha\beta$-hopanes and $\beta\alpha$-hopanes, but more stable than $\beta\beta$-isomer (Philip et al., 1984). Most hopanoids are bio-synthesized with the 17β(H),21β(H) stereochemistry. C_{29} and higher homologues of hopane are isomerized to 17α(H),21β(H) at any early stage of diagenesis. The degree of maturation can be calculated as follows:

$$\frac{17\alpha(H),21\beta(H)}{17\beta(H),21\beta(H) + 17\alpha(H),21\beta(H)} = \frac{\alpha\beta}{\beta\beta + \alpha\beta}$$

Equation 7

The ratio of equation 1.7 usually reach one simultaneously with the disappearance of 17β(H),21β(H). Furthermore, maturation enhances the content of 17α(H),21β(H) relative to 17β(H),21α(H). C_{27}-Hopanes have no side-chain and the conversion of 17β(H) to17α(H) (T_m) reaches completion at maturity between the disappearance of 17β(H),21β(H) hopanes and 17α(H),21β(H) hopanes, that is prior to the onset of intense hydrocarbon generation. As illustrated in Figure 1.2, 18α(H)-Trisnorhopane (T_s) is not affected by maturity changes, and the ratio: T_m/T_s can thus be used as a maturity indicator (Yunker et al., 2003). Recent studies have highlighted on the heterogeneous nature of hopane and sterane biomarkers in several river-dominated margins (Yunker et al., 2003 and Mudge, 2002). In the last two decades these petroleum biomarker parameters have been developed by organic geochemists to differentiate between oils, and determine their source in the aquatic environment and to trace their point sources (Zakaria et al., 2001).

For decades, pristine and phytane have been considered as biodegradable and thus these ratios might be valuable in the early stages of biodegradation (Prince et al., 1994). In particular, Burns and Teal (1979) stated that the branched alkanes extracted from marsh sediments at the West Falmouth site were completely degraded within the first seven years after the oil spill. These findings were based first on measurements of the pristine/phytane ratios. It was found that this ratio was 1.5 in the original Florida oil and that it decreased over a period of six years to 0.2. This is in contrast to another recent finding that have shown that *n*-alkane band in the fuel oil range (n-C_{10}-n-C_{24}) was no longer present, whereas all other compound classes such as nor-pristine, pristine and phytane are evident within the residual oil at the same sampling site (i.e. the West Falmouth site, Reddy et al., 2002). These latest results suggest that these compounds will be very useful petroleum biomarkers in understanding the distribution pattern of traffic-emitted aerosol components. In addition, steroid skeletons have been widely used as an indicator of diagenesis and the biological origin (biomarker) of organic matter (Jasper, 1993; Huang and Meinschein, 1976; Simoneit, 1984; Venkatesan et al., 2003). Steroids are also source tracers for biogenic material in complex mixtures of dissolved and particulate matter in the geosphere, especially in the marine environment (Brault and Simoneit, 1988 and Wang et al., 2004).

2.3 Cluster analysis & receptor models

2.3.1 Cluster analysis (CA)

Cluster analysis (CA), also called segmentation analysis or taxonomy analysis, seeks to identify homogeneous subgroups of cases in a population. That is, cluster analysis seeks to identify a set of groups which both minimise within-group variation and maximise between-group variation. In this study, CA was conducted using SPSS 13.0 for Windows. CA techniques may be *hierarchical* (i.e. the resultant classification has an increasing number of nested classes) or *non-hierarchical* (i.e. *k*-means clustering). *Hierarchical clustering* allows users to select a definition of distance, then select a linking method of forming clusters, then determine how many clusters best suit the data. *Hierarchical clustering* methods do not require pre-set knowledge of the number of groups. Two general methods of *hierarchical clustering* methods are available: divisive and agglomerative. The divisive technique start by assuming a single group, partitioning that group into subgroups, partitioning these subgroups further into subgroups and so on until each object forms its own subgroup. The agglomerative techniques start with each object describing a subgroup, and then combine like subgroups into more inclusive subgroups until only one group remains. In either case, the results of the application of the clustering technique are best described using a dendogram or binary tree. The objects are represented as nodes in the dendogram and the branches illustrate when the cluster method joins subgroups containing that object. The length of the branch indicates the distance between the subgroups when they are joined.

After selecting the *hierarchical clustering* method, it is important to select the clustering algorithm (i.e. the rules which govern between which point distances are measured to determine cluster membership). There are many methods available, the criteria used differ and hence different classifications may be obtained for the same data. Five algorithms, available within SPSS, are (*i*) average linkage clustering, (*ii*) complete linkage clustering, (*iii*) single linkage clustering, (*iv*) within

groups clustering and (*v*) Ward's method. Average linkage clustering is defined as the dissimilarity between clusters and calculated using cluster average values. The most common method to calculate an average is UPGMA (Un-weighted Pair-Groups Method Average). Complete linkage clustering (Maximum or Furthest-Neighbour Method) can be described as the dissimilarity between two groups is equal to the greatest dissimilarity between a member of cluster *i* and a member of cluster *j*. This method tends to produce very tight clusters of similar cases. On the other hand, single linkage clustering can be simply explained, as the dissimilarity between two clusters is the minimum dissimilarity between members of two clusters. This method has been widely employed in numerical taxonomy. Besides, it is crucial to note that within groups clustering is similar to UPGMA except clusters are fused so that within clusters variances is minimized. This tends to produce tighter clusters than the UPGMA method. Finally, Ward's Method is assessed by calculating the total sum of squared deviations from the mean of a cluster. The criterion for fusion is that it should produce the smallest possible increase in the error sum of squares.

2.3.2 Receptor models

Receptor models can be categorized into two types, namely, Chemical Mass Balance (CMB) and multivariate models. The most widely used multivariate models are principal component analysis (PCA), positive matrix factorization (PMF), and UNMIX model. CMB predicts the contribution of different sources to measured target compound concentrations in atmosphere by means of an inverse variance weighted least-square linear regression, (Watson *et al*., 2001). The concept of CMB model, based on the principle of mass conservation, assumes that the total concentration of chemical species, C_i, at the receptor site, is the sum of the contributions from all sources *j* which emit species *i*.

$$C_i = \sum_{j=1}^{p} \alpha_{ij} \times f_{ij} \times S_j$$

Equation 8

where S_j is the fractional mass contribution of source *j* to the pollutant of target compound in the atmosphere, f_{ij} is the fraction of chemical species *i* in the emission from source *j*, for *p* sources. α_{ij} is the coefficient of fractionation used to correct uncertainties in f_{ij} between the source and the atmosphere, (Watson *et al*., 1990 and Engelbrecht *et al*., 2002).

Unlike other receptor models, which extract source compositions from the data, CMB model assumptions are based on: (*i*) compositions of source emissions are constant over the period of ambient and source sampling, (*ii*) chemical species do not react with each other, (*iii*) all sources with a potential for contributing to the receptor have been identified and have had their emissions characterized, (*iv*) the number of sources or source categories is less than or equal to the number of species, (*v*) the source profiles are linearly independent of each other, and (*vi*) the uncertainties are random, uncorrelated, and normally distributed, (CMB8 Applications and Validation Protocol for $PM_{2.5}$ and VOCs announced by Desert Research Institute US). CMB have been widely used to assess sources of air pollutants because it: (*i*) theoretically yields the most likely solutions based on chemical source profiles, (*ii*) uses all available chemical measurements, (*iii*) estimates the uncertainty of the source contributions based on resolution of both the ambient concentrations and source profiles, (*iv*) provides greater influence to chemical species with higher resolution in both the source and receptor

measurements than to species with lower resolution. However, the major weaknesses of the CMB are its difficulty to account for non-stable compounds and incapability to identify those sources that have similar contributions. Moreover, CMB requires chemical source profiles as fingerprints for source apportionment of environmental pollutant.

The fundamental principles of various chemical methods for receptor modeling, including chemical mass balance (CMB) and multivariate method, have been review in detail (Gordon, 1988; Watson, 1994). Factor analysis offers the advantages of not requiring prior knowledge of the chemical composition and size distribution of emissions from specific sources (source profiles) but has the drawback of being mathematically indeterminate, allowing a wide range of possible solutions even when it is applied to relatively simple simulated data sets. In urban atmosphere, which is composed by many potential and diverse sources, PCA has been chosen by many workers for source apportionment. This technique has been widely applied to source apportionment of particulate pollutants, especially trace metals, and more recently, PAHs. In order to identify sources, multivariate receptor modeling can be applied to the observed target compound data. Multivariate approaches are based on the idea that the time dependence of a chemical species at the receptor site will be the same for species from the same source. Chemical species are measured in a large number of samples gathered at a single receptor site over time. Species of similar variability are grouped together in a minimum number of factors that explain the variability of data set. It is assumed that each factor is associated with a source or source type. However, the method has some limitations in that it can recognize at most only about eight individual source categories in any study, and poor discrimination of closely related source categories is commonly found. A further disadvantage of multivariate factor analysis is that large numbers of ambient air samples must be collected and analyzed (usually at least 50) and the statistically independent source tracers are required for each major source type.

In contrast to CMB model, multivariate techniques such as PCA are preferable since they require no qualitative insight of the sources of certain chemical species, and thus overcome the limitations of CMB, (Rachdawong et al., 1998 and Park et al., 2005). The aim of PCA is to identify the major sources of air pollutant emissions and to select statistically independent source tracers, (Bruno et al., 2001; Miller et al., 2002 and Gou et al., 2003). All variables are expressed in standardized form with a mean of 0 and a standard deviation of 1. The total variance therefore equals the total number of variables, and the variance of each factor expressed as a fraction of the total variance is referred to as the eigenvalue. If a factor has a low eigenvalue, then it is contributing little to the explanation of variances in the variables and may be ignored. PCA is generally used when the research purpose is data reduction (i.e. to reduce the information in many measured variables into a smaller set of components). PCA seeks a linear combination of variables such that the maximum variance is extracted from the variables. It then removes this variance and seeks a second linear combination that explains the maximum proportion of the remaining variance, and so on. This is called the principal axis method and results in orthogonal (uncorrelated) factors. Thus, the largest combination, accounting for most of the variance, becomes principal component 1 (PC1), the second largest accounts for the next largest amount of variances and becomes principal component 2 (PC2), and so on.

Over a period of about 10 years the combination of interest driven by regulations with advances in instrumental analytical analysis and the wide availability of computers resulted in the innovative field of source apportionment/receptor modeling. The first applications of a receptor model using factor analysis were done by Hopke *et al*. (1977) and Garrenstrom *et al*. (1977). The first Ph.D. thesis on multivariate air quality receptor modeling was that of Henry (1977). This work made explicit the connection between the statistical and physical models underlying multivariate receptor models for the first time. Finally, the initial development of UNMIX was fulfilled by Henry and Hidy (1979), who discovered physically significant air quality patterns in the first multivariate analysis of an air quality data set that combined pollutant gas concentrations, particulate composition, and meteorological variables.

UNMIX is a multivariate receptor modeling package that inputs observations of particulate composition and seeks to find the number, composition, and contributions of the contributing sources or source types. This model also produces estimates of the uncertainties in the source compositions. UNMIX uses a generalization of the self-modeling curve resolution method developed by Henry *et al* (1997). Using only ambient data, UNMIX outputs the following information: (*i*) number of sources, (*ii*) composition of each source, (*iii*) source contributions to each sample, (*iv*) uncertainties in the source compositions, and (*v*) apportionment of the average total mass, if total mass is included in the model. The major advantages of the UNMIX are described as follows: (*i*) no assumptions about the number or compositions of sources are needed, (*ii*) no assumptions or knowledge of errors in the data are needed, and (*iii*) UNMIX automatically correct source compositions for effects of chemical reactions. A major difference between UNMIX and PMF is that UNMIX does not make explicit use of errors or uncertainties in the ambient concentrations. This is not to imply that the UNMIX approach regards data uncertainty as unimportant, but rather that the UNMIX model results implicitly incorporate error in the ambient data. Assume that *N* air quality samples are analyzed for n species, which come from m sources. If these species are conservative, then mass balance on each species requires that

$$C_{i,j} = \sum_{k=1}^{m} a_{jk} S_{ik} + errors$$

Equation 9

Where C_{ij} is the concentration of the j^{th} (j=1,…..,n) species in the i^{th} sample (i=1,…..,N), a_{jk} is the mass fraction of species j in source k (k=1,…..,m), and S_{ik} is the total mass of material from source k in the i^{th} sample. In the parlance of receptor modeling, the a_{jk} are the source compositions, and the S_{ik} are the source contributions. The equation above includes errors, which may be the results of analytical uncertainty and variations in the sources' composition. The existence of errors profoundly complicates solution of the mixture problem, which is an ill-posed problem in that there are an insufficient number of constraints to define a unique solution. Several attempts to define a unique solution had been made by adding the obvious constraints of non-negativity of the source contribution and narrowing down the range of possible solutions based on physical knowledge of the sources (Henry *et al*., 1994, 2003 and 2005). However, the question remains under what conditions can a unique solution be found using only the data without a priori knowledge. To answer this question, the

graphical approach had been introduced for solving the mixture problem. The main idea is to reduce the dimension of the problem by projection generalizes to any number of species and sources. Fig. 4 illustrates the single source case in which all the data points lie, except for errors, on a ray coming from origin. The direction of the ray is determined by the composition of the source. If $[p_1, p_2, p_3]$ is any point on the line, and $[a_1, a_2, a_3]$ is the source composition then $[p_1, p_2, p_3] = k[a_1, a_2, a_3]$. Since the ratio of each element relative to all others in the source composition, the mixture problem can be solved for the single source case, except that the source composition is only determined up to a multiplicative constant. In the case of two sources, as demonstrated in Fig. 5, the data are distributed in a plane through the origin. The problem is to find the vectors (or points) that represent the source composition. There are two possible choices for the source vectors namely (*i*) the source composition vectors of the two sources must lie in the same plane as the data and (*ii*) the source vectors must also be non-negative (Henry *et al*., 2002). This further limits the data points to lie on the plane between the two rays defined by the two source compositions. If one source is missing from some of the data points then these data points will lie along a ray defined by the composition of the single, remaining source. These data points will be distributed so that an edge is apparent (see Fig. 5) and a line drawn along that edge will give the relative source composition, just as in the single source case.



Figure 4. Plot for the one source, three species case showing the data points lying along the ray defined by the source composition (Henry *et al*., 1997).

However, if there are three or more sources, then the points with one source missing have two or more sources present, and it is not so simple to determine the source compositions. As illustrated in Fig. 6, all the data points are composed of three sources of three species. In this case the points with one source missing are located on the planes defined by the rays through the remaining two sources. While this can be difficult to visualize those remaining two sources in a three-dimensional plot, a projection from the origin into a plane as demonstrated in Fig. 5 enables the location of the source vectors much easier to see. In most cases of environmental data, however, data points are composed of more than three sources and many more than three species. In this case the generalization to more than three dimensions requires the concepts of a hyperplane and simplex. A hyper-plane is the

generalization of a plane. For instance, a plane in 3-space is two dimensional, so a hyper-plane in *n*-space has dimension *n*-1. Thus, the process of reducing dimensions of the data points in UNMIX is to find the edges in the data (i.e. finding hyper-planes that define a simplex). Finally, UNMIX uses these edges to find the source points in data set.

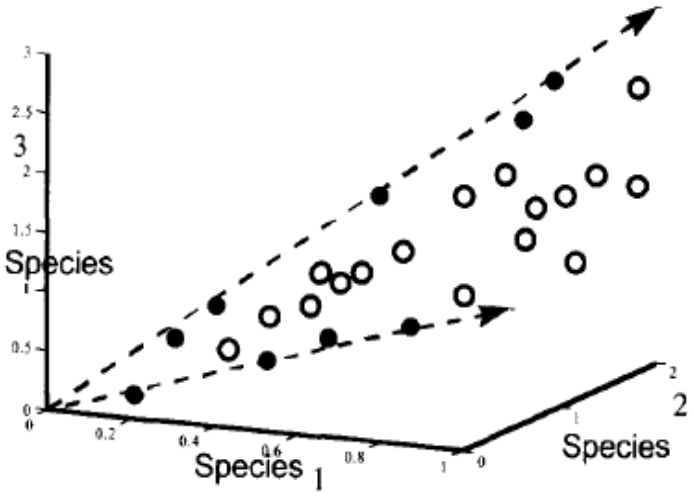


Figure 5. Plot for the two sources, three species case showing the data points lying in the plane defined by the two source composition rays. The solid circles are edge points, which have one source missing or low. The edges defined by these points give the relative source composition for the two sources (Henry *et al*., 1997).

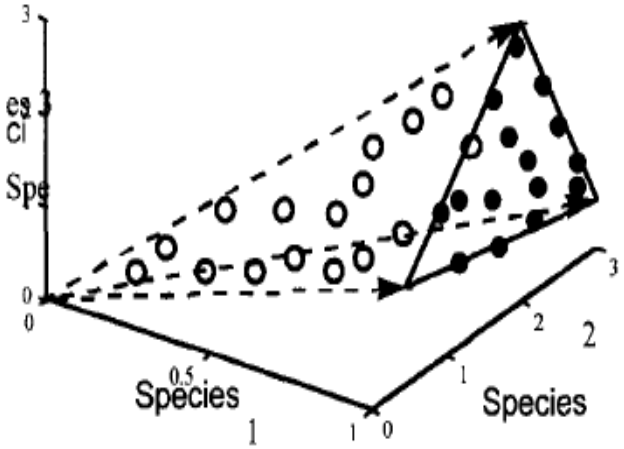


Figure 6. Plot for the three sources, three species case showing the data points (open circles) and the projection of the data points from the origin to the plane Species I = 1 (solid circles). Among the projected points, the edge points are easy to identify (Henry *et al*., 1997).

3. DISCUSSION & CONCLUSION

Despite of considerably large number of studies focusing on tsunami impact onshore, little is known about their geomorphologic imprints offshore. In order to gain more insights on return periods of both earthquake and tsunami hazard, it is therefore crucial to study past tsunami events by carefully investigate offshore tsunami deposits. There remain substantial difficulties, however, in discriminating between deposits triggered by tsunamis and those caused by extreme events such as hurricane/Indian Ocean monsoon (IOM) and/or other sedimentary processes. Hence, it is important to emphasize that the term of "tsunami deposit" is that it defines deposits that have created by numerous distinctive geological processes that are not necessarily specific to marine deposits formed during the tsunami 'backwash' phase (Shanmugam, 2006; Shiki and Yamazaki, 2008). Tipmanee et al (2012) attempted to use PAHs as a chemical proxy to trace the transport of land-derived materials caused by the tsunami backwash to better understand how it may have affected the distribution of sedimentary deposition throughout the seabed of Khao Lak coastal areas. The article provides interesting application of diagnostic binary ratios of PAHs from coastal sediments and marine deposits in tsunami 2004 affected coastal area of Thailand. The application of PAHs as a chemical proxy to identify tsunami backwash patterns is interesting and very challenging, however, there are several concerns and questions that need clarification as well as some of the following points for a thorough reconsideration of the proposed concept.

- As the tsunami wave approaches the shoreline its wavelength become shorter and horizontal water velocity increases. It carries large amount of marine sediments to inundated land. After reaching its maximum run-up, the backwash phenomenon is occurred and responsible for channelized and erosions in specific places. The mixture of marine sediments, beach sediments, minor part of eroded terrestrial soils and eroded older sediments from backwash channels are transported back to the sea as high density flows, part is transferred as suspension load as well as simultaneously mobilization of marine sediments. Hence, it is most likely that offshore tsunami deposits contain both terrestrial signatures and re-deposited marine sediments. In normal conditions terrestrial component may be delivered to the sea bottom as well. However, this phenomenon will take longer time than the "tsunami backwash", which the debris flow is very fast and sediments are buried rapidly then the "terrestrial set of PAH signatures" might be hypothetically preserved.

- It is also important to emphasize that not only "tsunami wave" but also "monsoon wave" can transfer terrigenous components from land to deposit in sea bottom. Therefore, it is crucial to consider the difference in nature of "tsunami wave" and "monsoon wave". While monsoon prolongs for several hours with relatively lower magnitude of power, the tsunami wave occurred in a greater magnitude of power but shorter in backwash time (i.e. several minutes). The tsunami deposit tends to contain "suspended particle", whereas the monsoon-derived sediments typically are produced through "bed-load transport". In these particular cases, two types of hypothesis can be considered;

Hypothesis I (Difference in transportation pattern)
It is well known that different types of PAHs exist in different sizes of particles (Kukkonen and Landrum, 1996; Wang et al., 2001). Since tsunami waves are capable of transport all particle sizes of terrestrial sediments via suspended load transport, it is most likely that tsunami deposit will have a different "distribution pattern of PAHs" from those of monsoon derived sediments.

Hypothesis II (Difference in erosion time)
Tsunami backwash occurred in relatively short time scale of minutes whereas the inundation of monsoon prolonged for several hours. Differences in "time dimension" cause the fractionization of PAHs due to its differences in term of "water solubility". For instance, Phe tends to have a higher water solubility than B[a]P (Lu et al., 2008). The longer the erosion, the higher amount of Phe will dissolve into backwash water in comparison with B[a]P. As a result, the monsoon derived deposit will contain Phe more than B[a]P. However, this fractionization effect will not happen in the case of tsunami deposit. Firstly, the tsunami involved only three large waves. Once the waves had passed and receded the event was over. Therefore, both Phe and B[a]P will be washed back by tsunami wave simultaneously without providing any time for the fractionization effect. For these reasons, the fingerprint of terrestrial PAHs may hypothetically be well preserved and possibly be a better proxy than conventional terrigenous biomarker "lignin" (Tareq et al., 2004), which is highly sensitive to microdegradation procedure due to its weak chemical structure in comparison with PAHs.

- Fingerprinting reflects the chemical characteristics of various source emissions of the sediment samples collected at any receptor. Because a simple ratio of two or three PAHs is sensitive to both photolysis and chemical/biological degradation and may be insufficient to identify PAH emission sources at fixed monitoring sites, the best strategy to investigate the impact of backwash tsunami is the use of the entire PAH profiles. Hence, the establishment of PAHs profile of individual “end member” is therefore essentially crucial.

- It is well known that Ret can be used as indicators of “wood combustion” (Gonçalves et al., 2011). During the bonfire night episode, the highest contributions of individual PAH came from Fl, Ac, Ret, B[*b+j+k*]F, Ind, B[*g,h,i*]P, while alkane concentrations was following the decrease order of $C_{29} > C_{24} > C_{27} > C_{22}$. The *chain-saw-distribution* of alkanes was evident at the range of C_{23} to C_{31} during the bonfire night episode, suggesting a strong signal of biomass burnings (Pongpiachan, 2013a). The contribution of diesel engine to atmospheric PAHs concentrations, especially those of Fl and Phe, has been widely investigated for many years (Williams *et al*., 1986). It is well known that diesel fuel is relatively rich in PAHs and most of them are alkylated PAHs compared to that of the parent PAHs. Several factors like diesel-engine type and engine operating conditions reflect the ratio of MePhe/Phe in urban air. For example, the relatively high MePhe/Phe ratio was found when the combustion and exhaust temperatures were low (Barbella et al., 1989). Takada et al (1991) and Westerholm et al (1992) reported the values of MePhe/Phe ratios exhausted from diesel engine vehicle, bus and petrol engine vehicle as 5.5, 4.8 and 0.7 respectively. It is worth mentioning that the

- MePhe/Phe ratio of 5.5 was the average of five types of diesel engine ranging from 1500 cc to 14000 cc running without engine load and at a constant speed of 3000 rpm. In order to enhance the reliability of using PAHs as proxy of tsunami backwash deposits, one should consider the analysis of Ret, MePhe and Phe as well as the employment of *chain-saw-distribution* of alkanes and CPI index. In addition, it is also important to use cholestanes and hopanes as alternative biomarkers to distinguish "typical marine sediments" from "tsunami backwash deposits".

- The representative of the "tsunami backwash" group as discussed by Tipmanee et al (2012) is not as far as approximately 25 km from the shoreline. Special signal found in this group could just be a particular dominant source, not necessary to be tsunami backwash signal. The results generated from binary ratios of PAHs, HCA coupled with PCA results obtained from Tipmanee et al (2012) were only surface sediments and there is no direct and strong evidence that the source of PAHs resulted from the tsunami in 2004. It could increase the strength if there are dated core sediment samples and showed the temporal distribution in this area. Furthermore, there are uncertainties in the estimation of source contribution by using PCA and UNMIX. Further source apportionment techniques such as a positive matrix factorisation (PMF) and a chemical mass balance (CMB) model should be conducted to increase the reliability of source contributions.

-

ACKNOWLEDGEMENTS

This work was performed with the approval of Deutsche Forschungsgemeinschaft (DFG) and National Research Council of Thailand (NRCT). The authors acknowledge the Research Center of National Institute of Development Administration (NIDA), Thailand for financial support.

REFERENCES

Allard, B., Rager, M.N., and Templier, J., 2002: Occurrence of high molecular weight lipids (C80+) in the trilaminar outer cell walls of some freshwater microalgae. A reappraisal of algaenan structure. Org. Geochem., 33, 789-801, 2002.

Atwater, B.F., 1987: Evidence for great Holocene earthquakes along the outer coast of Washington State. Science., 236, 942-4, 1987.

Baek, S.O., Goldstone, M.E., and Kirk, P.W., 1991: Phase distribution and particle size dependency of polycyclic aromatic hydrocarbons in the urban atmosphere. Chemosphere., 22, 503-20, 1991a.

Baek, S.O., Field, R.A., Goldstone, M.E., Kirk, P.W., Lester, J.N., and Perry, R., 1991b: A review of atmospheric polycyclic aromatic hydrocarbons: sources, fate and behavior. Water, Air, and Soil Pollution., 60, 279-300, 1991b.

Barbella, R., Ciajolo, A., Anna, D.A., and Bertoli, C., 1989: Effect of fuel aromaticity on diesel emissions. Combust. Flame., 77(3-4), 267-77, 1989.

Belicka, L.L., Macdonald, W.R., Yunker, B.M., and Harvey, R.H., 2004: The role of depositional regime on carbon transport and preservation in Arctic Ocean sediments. Mar. Chem., 86, 65-88, 2004.

Benson, B. E., Grimm, K. A., and Clague, J. J.: Tsunami deposits beneath tidal marshes on northwestern Vancouver Island British Columbia. Quaternary. Res., 48, 192-204, 1997.

Blokker P., van Bergen P. F., Pancost R. D., Collinson M. E., Sinninghe Damst J. S., and de Leeuw J. W.: The chemical structure of Gloeocapsamorpha prisca microfossils: implication for their origin. Geochim. Cosmochim. Acta., 65, 885-900, 2001.

Bondevik, S., Sevendsen, J. I., and Mangerud, J.: Tsunami sedimentary facies deposited by the Storegga tsunami in shallow marine basins and coastal lakes, western Norway. Sedimentology., 44, 1115-31, 1997.

Boonyatumanond, R., Murakami, M., Wattayakorn, G., Togo, A., and Takada, H.: Sources of polycyclic aromatic hydrocarbons (PAHs) in street dust in a tropical Asian mega-city, Bangkok, Thailand. Sci. Tot. Environ., 384 (1–3), 420-32, 2007.

Brasser, L. J.: Polycyclic aromatic hydrocarbon concentrations in the Netherelands. VDI-Berichete Nr., 348, 171-80, 1980.

Brault, M., and Simoneit, T.R.B.: Steroid and triterpenoid distributions in bransfield strait sediments: Hydrothermally-enhanced diagenetic transformations. Org. Geochem., 13(4-6), 697-705, 1988.

Bray, E.E., and Evans, E.D.: Distribution of n-paraffins as a clue to recognition of source beds. Geochim. Cosmochim. Acta., 22, 2-15, 1961.

Bruno, P., Caselli, M., Curri, L.M., Genga, A., Striccoli, R., and Traini, A.: Chemical characterisation of ancient pottery from south of Italy by Inductively Coupled Plasma Atomic Emission Spectroscopy (ICP-AES): Statistical multivariate analysis of data. Anal. Chim. Acta., 410(1-2), 193-202, 2000.

Bryant, E.: Tsunami. The Underrated Hazard: Cambridge, 320, 2001.

Burns, K.A., and Teal, J.M.: The West Falmouth oil spill: hydrocarbons in the salt marsh ecosystem. Est. Coast. Mar. Sci., 8, 349-60, 1979.

Cantalamessa, G., and Di Celma, C.: Sedimentary features of tsunami backwash deposits in a shallow marine Miocene setting, Mejillones Peninsula, northern Chile. Sediment. Geol., 178, 259 – 73, 2005.

Cautreels, W., and Van Cauwenburghe, K.: Experiments on the distribution of organic pollutants between airborne particulate matter and the corresponding gas phase. Atmos. Environ., 12, 1133-41, 1978.

Chetwittayachan, T., Shimazaki, D., and Yamamoto, K.: A comparison of temporal variation of particle-bound polycyclic aromatic hydrocarbons (pPAHs) concentration in different urban environments: Tokyo, Japan, and Bangkok, Thailand. Atmos. Environ., 36 (12), 2027-37, 2002.

Choowong, M., Murakoshi, N., Hisada, K., Charusiri, P., Daorerk, V., Charoentitirat, T., Chutakositkanon, V., Jankaew, K., and Kanjanapayont, P.: Erosion and deposition by the 2004 Indian Ocean tsunami in Phuket and Phang-nga Provinces, Thailand. J. Coastal. Res., 23(5), 1270–76, 2007.

Choowong, M., Murakoshi, N., Hisada, K., Charusiri, P., Charoentitirat, T., Chutakositkanon, V., Jankaew, K., Kanjanapayont, P., and Phantuwongraj, S.: 2004 Indian Ocean tsunami inflow and outflow at Phuket, Thailand. Mar. Geol., 248(3–4), 179–92, 2008a.

Choowong, M., Murakoshi, N., Hisada, K., Charoentitirat, T., Charusiri, P., Phantuwongraj, S., Wongkok, P., Choowong, A., Subsayjun, R., Chutakositkanon, V., Jankaew, K., and Kanjanapayont, P.: Flow conditions of the 2004 Indian Ocean tsunami in Thailand inferred from capping bedforms and sedimentary structures. Terra. Nova., 20, 141–9, 2008b.

Choowong, M., Phantuwongraj, S., Charoentitirat, T., Chutakositkanon, V., Yumuang, S., and Charusiri, P.: Beach recovery after 2004 Indian Ocean tsunami from Phang-nga, Thailand. Geomorphology., 104, 134–42, 2009.

Chagué-Goff, C., Schneider, J.L., Goff, J.R., Dominey-Howes, D., and Strotz, L.: Expanding the proxy toolkit to help identify past events—Lessons from the 2004 Indian Ocean Tsunami and the 2009 South Pacific Tsunami. Earth. Sci. Rev., 107, 107–22, 2011.

Dawson, A.G., Long, D., and Smith, D.E.: The Storegga slides: Evidence from eastern Scotland for a possible tsunami. Mar. Geol., 82, 271-6, 1988.

Dawson, A.G., Foster, I. D. L., Shi, S., Smith, D.E., and Long, D.: The identification of tsunami deposits in coastal sediment sequences. Sci. Tsunami. Hazards., 9, 73-82, 1991.

Dawson, A.G.: Linking tsunami deposits, submarine slides and offshore earthquakes. Quarternary Intern., 60, 119 – 26, 1999.

Dawson, A.G., and Shaozong, S.: Tsunami Deposits. Pure. Appl. Geophys., 157, 875 – 97, 2000.

Department of Mineral Resources, 2005. Goehazard Mitigation: How to survive a tsunami, 34 p.

Diesing, M., Kubicki, A., Winter, C., and Schwarzer, K.: Decadel scale stability of sorted bedforms, German Bight, Southeastern North Sea. Cont. Shelf. Res., 26, 902 – 16, 2006.

Duan, J., Bi, X., Tan, J., Sheng, G., and Fu, J.: The differences of the size distribution of polycyclic aromatic hydrocarbons (PAHs) between urban and rural sites of Guangzhou, China. Atmos. Environ., 78, 190-203, 2005.

Einsele, G.: Event stratigraphy: recognition and interpretation of sedimentary event horizons. In: Doyle, P. and Bennett, M.R. (eds.). Unlocking the stratigraphic record: advances in modern stratigraphy, 145 – 193, 1998.

Engelbrecht, P.J., Swanepoel, L., Chow, C.J., Watson, G.J., and Egami, T.R.: The comparison of source contributions from residential coal and low-smoke fuels, using CMB modelling, in South Africa. Environ. Sci. Pol., 5(2), 157-67, 2002.

EPA Appendix A to 40 CFR, Part 423–126 Priority Pollutants Available from: http:// www.epa.gov/region01/npdes/permits/generic/prioritypollutants.pdf, (2003).

Fang, M., Wan, T., and Kwan, J.: Characterization of the organic compounds in the aerosols of Hong Kong-identification, abundance, origin and toxicity. Research Center Publication., 21-96, 1996.

Fang, M., Zheng, M., Wang, F., To, K.L., Jaafar, A.B., and Tong, S.L.: The solvent extractable organic compounds in Indonesia biomass burning aerosols – Characterisation studies. Atmos. Environ., 33, 783-95, 1999.

Fang, G.C., Chang. C.N., Wu, Y.S., Fu, P.P.C., Yang, I.L., and Chen, M.H.: Characterization, identification of ambient air and Road dust polycyclic aromatic hydrocarbons in central Taiwan, Taichung. Sci. Tot. Environ., 366(2-3), 729-38, 2006.

Ferrini, V.L., and Flood, R.D.: A comparison of Rippled Scour Depressions identified with multibeam sonar: Evidence of sediment transport in inner shelf environments. Cont. Shelf. Res., 25, 1979–95, 2005.

Fisher, R.V.: Flow transformation in sediment gravity flows. Geology., 11, 273 – 4, 1983.

Freeman, D.J., and Cattell, F.C.R.: Wood-burning as a source of atmospheric polycyclic aromatic hydrocarbons. Environ. Sci. Technol., 24, 1581-5, 1990.

Garrenstrom, D.P., Perone, P.S., and Moyers, L.J.: Application of pattern recognition and factor analysis for characterization of atmospheric particulate composition in southwest desert atmosphere. Environ. Sci. Technol., 10, 795-800, 1977.

Gelfenbaum, G., and Jaffe, B.: Erosion and sedimentation from the July 17, 1998 Papua New Guinea tsunami. Pure. Appl. Geophys., 160, 1969-99, 2003.

Gogou, A., Stratigakis, N., Kanakidou, M., and Stephanou, E.: Organic aerosol in Eastern Maditerranean: component source reconciliation by using molecular markers and atmospheric back trajectories. Org. Geochem., 25, 79-96, 1996.

Gogou, I. A., Bouloubassi, I., and Stephanou, G.E.: Marine organic geochemistry of the Eastern Mediterranean: 1. Apliphatic and polyaromatic hydrocarbons in Cretan Sea surficial sediments. Mar. Chem., 68(4), 265-82, 2000.

Gordon, G.E.: Receptor models. Environ. Sci. Technol., 22, 1132–42, 1988.

Gonçalves, C., Alves, C., Fernandes, A. P., Monteiro, C., Tarelho, L., Evtyugina, M., and Pio, C.: Organic compounds in $PM_{2.5}$ emitted from fireplace and woodstove combustion of typical Portuguese wood species. Atmos. Environ., 45 (27), 4533-45, 2011.

Gou, H., Lee, C.S., Ho, F.K, Wang, X.M., and Zou, C.S.: Particle-associated polycyclic aromatic hydrocarbons in urban air of Hong Kong. Atmos. Environ., 37, 5307–17, 2003.

Grantham, P. J., and Douglas, A. G.: The nature and origin of sesquiterpenoids in some Tertiary fossil resins. Geochim. Cosmochim. Acta., 44, 1801-10, 1980.

Gusiakov, V.K.: Tsunami generation potential of different tsunamigenic regions in the Pacific. Mar. Geol., 215, 3 – 9, 2005.

Harrison, R. M., Smith, D. J. T., and Luhana, L.: Source Apportionment of Atmospheric Polycyclic Aromatic Hydrocarbons Collected from an Urban Location in Birmingham, U.K. Environ. Sci. Technol, 30(3), 825-32, 1996.

Harrison, R.M., Smith, D.J.T., Pio, C.A., and Castro, L.M.: Comparative receptor modeling study of airborne particulate pollutants in Birmingham (United Kingdom), Coimbra (Portugal) and Lahore (Pakistan). Atmos. Environ., 31, 3309-21 1997.

Harrison, M.R., Tilling, R., Callèn Romero, S.M., Harrad, S., and Jarvis, K.: A study of trace metals and polycyclic aromatic hydrocarbons in the roadside environment. Atmos. Environ., 37, 2391-402, 2003.

Hedberg, H. D.: Significance of high-wax oils with respect to genesis of petroleum. Am. Assoc. Petrol. Geol. Bull., 52(5), 736-50, 1968.

Henry, C.R., and Hidy, M.G.: Multivariate analysis of particulate sulfate and other air quality variables by principal components-Part I: Annual data from Los Angeles and New York. Atmos. Environ., 3, 1581-96, 1979.

Henry, C.R., Lewis, C., and Collins, J.: Vehicle-related hydrocarbon source compositions from ambient data: The GRACE/SAFER method. Environ. Sci. Technol., 28, 823-32, 1994.

Henry, C.R.: Multivariate receptor modeling by *N*-dimensional edge detection. Chemom. Intell. Lab. Syst., 65, 179-89, 2002.

Henry, C.R.: Multivariate receptor modelling by N-dimensional edge detection, Chemom. Intell. Lab. Syst., 65(2), 179-89, 2003.

Henry, C.R.: Duality in multivariate receptor models, Chemom. Intell. Lab. Syst., 77(1-2), 59-63, 2005.

Holba, A. G., Dzou, L. I. P., Masterson, W. D., Hughes, W. B., Huizinga, B. J., Singletary, M. S., Moldowan, J. M., Mello, M. R., and Tegelaar, E.: Application of 24-norcholestanes for constraining source age of petroleum. Org. Geochem., 29(5-7), pp.1269-83, 1998a.

Holba, A. G., Tegelaar, E. W., Huizinga, B. J., Moldowan, J. M., Singletary, M. S., McCaffrey, M. A., and Dzou, L. I. P.: 24-norcholestanes as age-sensitive molecular fossils. Geology., 26(9), 783-6, 1998b.

Hopke, K.P., Gladney, S.E., Gordon, E.G., Zoller, H.W., and Jones, G.A.: The use of multivariate analysis to identify sources of selected elements in the Boston urban aerosol. Atmos. Environ., 10, 1015-25, 1977.

Huang, Y.W., and Meinschein, G.W.: Sterols as source indicators of organic materials in sediments. Geochimica et Cosmochimica Acta., 40(3), 323-30, 1976.

International Agency for Research on Cancer (1983) IARC Monographs on the evaluation of the carcinogenic risk of chemicals to man, Vol.32: Polycyclic aromatic hydrocarbons, Part 1: Chemical, environmental and experimental data. IARC, Lyon, France.

International Agency for Research on Cancer (1984) IARC Monographs on the evaluation of the carcinogenic risk of chemicals to man, Vol.34: Polycyclic aromatic hydrocarbons, Part 3: Industrial exposures in aluminium production, coal gasification, coke production, and iron and steel founding. IARC, Lyon, France.

International Agency for Research on Cancer (1985) IARC Monographs on the evaluation of the carcinogenic risk of chemicals to man, Bitumens, coal-tars and derived products, shale-oils and soots. Monnograph No 35, IARC, Lyon, France.

International Agency for Research on Cancer (1987) IARC Monographs on the evaluation of the carcinogenic risk of chemicals to man, Supplement, IARC, Lyon, France.

Jasper, P.J., and Gagosian, B.R.: The relationship between sedimentary organic carbon isotopic composition and organic biomarker compound concentration. Geochim. Cosmochim. Acta., 57 (1), 167-86, 1993.

Kalaitzoglou, M., Terzi, E., and Samara, C.: Patterns and sources of particle-phase aliphatic and polycyclic aromatic hydrocarbons in urban and rural sites of western Greece. Atmos. Environ., 38, 2545-60, 2004.

Kavouras, G.I., Lawrence, J., Koutrakis, P., Stephanou, G.E., and Oyola, P.: Measurement of particulate apliphatic and polynuclear aromatic hydrocarbons in Santiago de Chile: Source reconciliation and evaluation of sampling artifacts. Atmos. Environ., 33(30), 4977-86, 1999.

Kendall, M., Hamilton, S. R., Watt, J., and Williams, D. I.: Characterisation of selected speciated organic compounds associated with particulate matter in London. Atmos. Environ., 35, 2483-95, 2001.

Killops, S. D., Carlson, R. M. K., and Peters, K. E.: High-temperature GC evidence for the early formation of C40+ n-alkanes in coals. Org. Geochem, 31, 589-97, 2000.

Kukkonen, J., and Landrum, P. F.: Distribution of organic carbon and organic xenobiotics among different particle-size fractions in sediments. Chemosphere., 32 (6), 1063-76, 1996.

Le Roux, J.P., and Vargas, G.: Hydraulic behaviour of tsunami backflows: Insights from their modern and ancient deposits. Environ. Geol., 49, 65 – 75, 2005.

Li, C., Fu, J., Sheng, G., Bi, X., Hao, Y., Wang, X., and Mai, B.: Vertical distribution of PAHs in the indoor and outdoor $PM_{2.5}$ in Guangzhou, China. Build. Environ., 40, 327–39, 2005.

Lim, H. L., Harrison, M. R., and Harrad, S.: The contribution of traffic to atmospheric concentrations of polycyclic aromatic hydrocarbons. Environ. Sci. Technol, 33, 3538-42, 1999.

Lu, G. N., Dang, Z., Tao, X. Q., Yang, C., and Yi, X. Y.: Estimation of water solubility of polycyclic aromatic hydrocarbons using quantum chemical descriptors and partial least squares. Mol. Inform., 27(5), 618-26, 2008.

Mainwaring, S. J., and Stirling, D. M.: A study of the size distribution and concentrations of polynuclear hydrocarbons in Melbourne air. In "Proceedings of the 7th International Clean Air", 1981.

Mei, Z., Ming, F., and Fuwang, K.L.: Characterization of the solvent extractable organic compounds in PM2.5 aerosols in Hong Kong. Atmos. Environ., 34(17), 2691-702, 2000.

Miller, L.S., Anderson, J.M., Daly, P.E., and Milford, B.J.: Source apportionment of exposures to volatile organic compounds. I. Evaluation of receptor models using simulated exposure data. Atmos. Environ., 36(22), 3629-41, 2002.

Moldowan, J. M., Fago, F. J., Lee, C. Y., Jacobson, S. R., Watt, D. S., Slougui, N.E., Jeganathan, A., and Young, D. C.: Sedimentary 24-n-propylcholestanes, molecular fossils diagnostic of marine algae. Science., 247, 309-12, 1990.

Motelay, A., Harner, T.M., Shoeib, M., Diamond, M., Stern, G., and Rosenberg, B.: Using passive air samplers to assess urban-rural trends for persistent organic pollutants and polycyclic aromatic hydrocarbons. 2. Seasonal trends for PAHs, PCBs and Organochlorine Pesticides. Environ. Sci. Technol., 39, 5763-73, 2005.

Mudge, S.M.: Reassessment of the hydrocarbons in Prince William Sound and the Gulf of Alaska: Identifying the source using Partial Least-Squares. Environ. Sci. Technol., 36, 2354-60, 2002.

Murray, A.B., and Thieler, E.R.: A new hypothesis on exploratory model for the formation of large-scale inner shelf sediment sorting and "rippeled scour depressions". Cont. Shelf. Res., 24, 295 – 315, 2004.

Nielsen, T.: Traffic contribution of polycyclic aromatic hydrocarbons in the center of a large city. Atmos. Environ., 30(20), 3481-90, 1996.

Nittrouer, C.A., and Wright, L.D.: Transport of particles across continental shelves. Rev. Geophys., 32, 85–113, 1994.

Ohura, T., Amagai, T., Sugiyama, T., Fusaya, M., and Matsushita, H.: Characteristics of particle matter and associated polycyclic aromatic hydrocarbons in indoor and outdoor air in two cities in Shizuoka, Japan. Atmos. Environ., 38, 2045–54, 2004.

Ondov, M.J., Kelly, R.W., Holland, Z.J., Lin, C.Z., and Wight, A.S.: Tracing fly ash emitted from a coal-fired power plant with enriched rare-earth isotopes: An urban scale test. Atmos. Environ. Part B., 26(4), 453-62, 1992.

Ourisson, G., and Albrecht, P.: Hopanoids 1. Geohopanoids: the most abundant natural products on Earth? Acc. Chem. Res., 25, 398-402, 1992.

Paasivirta, J., Sinkkonen, S., Mikkelson, P., Rantio, T., and Wania, F.: Estimation of vapor pressures, solubilities and Henry's law constants of selected persistent organic pollutants as functions of temperature. Chemosphere, 39(5), 811-32, 1999.

Park, S.S., and Kim, J.Y.: Source contributions to fine particulate matter in an urban atmosphere. Chemosphere., 59(2), 217-26, 2005.

Pierson, R.W., and Brachaczek, W.W.: Particulate matter associated with vehicles on the road II. Aerosol. Sci. Technol., 2, 1-40, 1993.

Pinegina, T.K., and Bourgeois, J.: Historical and paleo-tsunami deposits on Kamchatka, Russia: long-term chronologies and long-distance correlations. Nat. Hazard. Earth. Sys. Sci., 1, 177-85, 2001.

Pongpiachan, S., Thamanu, K., Ho, K.F., Lee, S.C., and Sompongchaiyakul, P.: Predictions of gas-particle partitioning coefficients (Kp) of polycyclic aromatic hydrocarbons at various occupational environments of Songkhla province, Thailand. Southeast Asian J. Trop. Med., 40 (6), 1377-94, 2009.

Pongpiachan, S., Thumanu, K., Na Pattalung, W., Hirunyatrakul, P., Kittikoon, I., Ho, F. K., and Cao, J. J.: Diurnal variation and spatial distribution effects of Sulfur Speciation in Aerosol Samples as Assessed by X-ray Absorption Near-edge Structure (XANES). J. Anal. Methods. Chem., Article ID 696080, 10 pages, doi:10.1155/2012/696080, 2012a.

Pongpiachan, S., Thumanu, K., Kositanont, C., Schwarzer, K., Prietzel, J., Hirunyatrakul, P., and Kittikoon, I.: Parameters Influencing Sulfur Speciation in Environmental Samples Using Sulfur K-Edge X-Ray Absorption Near-Edge Structure (XANES). J. Anal. Methods. Chem., Article ID 659858, 12 pages, doi: 10.1155/2012/659858, 2012b.

Pongpiachan, S.: Fingerprint of Carcinogenic Semi-Volatile Organic Compounds (SVOCs) during Bonfire Night. Asian. Pac. J. Cancer. Prev., 14(5), 3243-54, 2013a.

Pongpiachan, S.: Vertical distribution and potential risk of particulate polycyclic aromatic hydrocarbons in high buildings of Bangkok, Thailand. Asian. Pac. J. Cancer. Prev., 14(3), 1865-77, 2013b.

Pongpiachan, S.: Diurnal Variation, Vertical Distribution and Source Apportionment of Carcinogenic Polycyclic Aromatic Hydrocarbons (PAHs) in Chiang-Mai, Thailand. Asian. Pac. J. Cancer. Prev., 14(3), 1851-63, 2013c.

Pongpiachan, S., Thumanu, K., Na Phatthalung, W., Tipmanee, D., Kanchai, P., Feldens, P., and Schwarzer, K.: Using Fourier Transform Infrared (FTIR) to Characterize Tsunami Deposits in Near-Shore and Coastal Waters of Thailand. Sci. Tsu. Haz., 32 (1), 39-57, 2013a.

Pongpiachan, S., Thumanu, K., Tanthanuch, W., Tipmanee, D., Kanchai, P., Schwarzer, K., and Tancharakorn, S.: Sedimentary features of tsunami backwash deposits as assessed by micro-beam synchrotron X-Ray Fluorescence (μ-SXRF) at the Siam Photon Laboratory. Sci. Tsu. Haz., 32 (2), 96-115, 2013b.

Pongpiachan, S., Choochuay, C., Hattayanone, M., and Kositanont, C.: Temporal and spatial distribution of particulate carcinogens and mutagens in Bangkok, Thailand. Asian. Pac. J. Cancer. Prev., 14(3), 1879-87, 2013c.

Pongpiachan, S., Ho, K. F., and Cao, J.: Estimation of Gas-Particle Partitioning Coefficients (Kp) of Carcinogenic Polycyclic Aromatic Hydrocarbons by Carbonaceous Aerosols Collected at Chiang-Mai, Bangkok and Hat-Yai, Thailand. Asian. Pac. J. Cancer. Prev., 14(4), 3369-84, 2013d.

Pongpiachan, S., Tipmanee, D., Deelaman, W., Muprasit, J., Feldens, P., and Schwarzer, K.: Risk assessment of the presence of polycyclic aromatic hydrocarbons (PAHs) in coastal areas of Thailand affected by the 2004 tsunami. Mar. Pollut. Bulletin., In Press, 2013e.

Prince, R.C., Elmendoft, D.L., Lute, R.J., and Hsu, C.E.: 17α(H),21β(H)-hopanes as a conserved internal marker for estimating the biodegradation of crude oil. Environ. Sci. Technol., 28, 142-5, 1994.

Rachdawong, P., Christensen, R.E., and Chi, S.: Source identification of PCBs in sediments from the Milwaukee Harbor Estuary, USA. Water. Sci. Technol., 37(6-7), 199-206, 1988.

Ramdahl, T.: Retene- a molecular marker of wood combustion in ambient air. Nature., 306, 580-2, 1983.

Ramdahl, T., and Becher, G.: Characterization of polynuclear aromatic hydrocarbon derivatives in emissions from wood and cereal straw combustion. Analytica. Chimica. Acta., 144(1), 83-91, 1982.

Ramdahl, T., and Møller, M.: Chemical and biological characterization of emissions from a cereal straw burning furnace. Chemosphere., 12(1), 23-4, 1983.

Reddy, M.C., Eglinton, I.T., Hounshell, A., Xu, K.W., Gaines, B.R., and Frysinger, S.G.: The West Falmouth oil spill after thirty years: The persistence of petroleum hydrocarbons in marsh sediments. Environ. Sci. Technol., 36 (22), 4754-60, 2002.

Rogge, W. F., Mazurek, M. A., Hildemann, L. M., and Cass, G. R., and Simoneit, B.R.T.: Quantification of urban organic aerosols at a molecular level: identification, abundance and seasonal variation. Environ. Sci. Technol., 27A, 1309-30, 1993.

Rohmer, M., Bouvier-Nav, P., and Ourisson, G.: Distribution of hopanoid triterpenes in prokaryotes. J. Gen. Microbiol., 130, 1137-50, 1984.

Ruchirawat, M., Mahidol, C., Tangjarukij, C., Pui-ock, S., Jensen, O., Kampeerawipakorn, O., Tuntaviroon, J., Aramphongphan, A., and Autrup, H.: Exposure to genotoxins present in ambient air in Bangkok, Thailand — particle associated polycyclic aromatic hydrocarbons and biomarkers. Sci. Tot. Environ., 287 (1–2), 121-32, 2002.

Ruchirawat, M., Navasumrit, P., Settachan, D., Tuntaviroon, J., Buthbumrung, N., and Sharma, S.: Measurement of genotoxic air pollutant exposures in street vendors and school children in and near Bangkok. Toxicol. Appl. Pharm., 206 (2), 207-14, 2005.

Ruchirawat, M., Settachan, D., Navasumrit, P., Tuntawiroon, J., and Autrup, H.: 2007. Assessment of potential cancer risk in children exposed to urban air pollution in Bangkok, Thailand. Toxicol. Lett., 168 (3), 200-9, 2007.

Salma, I., Maenhaut, W., Dubtsov, S., Zemplén-Papp, E., and Záray, G.: Impact of phase out of leaded gasoline on the air quality in Budapest. Microchemical Journal., 67(1-3), 127-33, 2000.

Sanderson, G.E., Raqbi, A., Vyskocil, A., and Farant, P.J.: Comparison of particulate polycyclic aromatic hydrocarbon profiles in different regions of Canada. Atmos. Environ., 38, 3417-29, 2004.

Scheffers, A., and Kelletat, D.: Sedimentologic and geomorphologic tsunami imprints worldwide – a review. Earth. Sci. Rev., 63, 83 – 92, 2003.

Schwarzer, K., Diesing, M., Larson, M., Niedermeyer, R.O., Schumacher, W., and Furmanczyk, K.: Coastline evolution at different time scales. - Examples from the southern Baltic Sea (Pomeranian Bight) – Mar. Geol., 194, 79 – 101, 2003.

Shanmugam, G.: The Tsunamite problem. J. Sediment. Res., 76, 718–30, 2006.

Shi, S., Dawson, A.G., and Smith, D.E.: Coastal tsunami sedimentation processes. In: CEA/DASE (eds.). Proceedings of the International Conference on Tsunamis, Paris, France, May 26 – 28, 43 – 55, 1998.

Shiki, T., and Yamazaki, T.: The term 'Tsunamiite'. In Shiki T. Tsunamiites: features and implications. Developments in Sedimentology. Elsevier. p. 5. ISBN 978-0-444-51552-0. 2008.

Simoneit, B.R.T.: Organic matter of the troposphere—III. Characterization and sources of petroleum and pyrogenic residues in aerosols over the western United States. Atmos. Environ., 18, 51–67, 1984.

Stenberg, U., and Alsberg, T.: Capillary GC-MS analysis of PAH emissions from combustion of peat and wood in hot water boiler. Chemosphere., 8, 487-96, 1979.

Summons, R. E., Jahnke, L. L., and Roksandic, Z.: Carbon isotope fractionation in lipids from methanothrophic bacteria: relevance for interpretation of the geological record of biomarkers. Geochim. Cosmochim. Acta., 58, 2853-63, 1994a.

Szczuciński, W., Niedzielski, P., Rachlewicz, G., Sobczyński, T., Zioła, A., Kowalski, A., Lorenc, S., and Siepak, J.: Contamination of tsunami sediments in a coastal zone inundated by the 26 December 2004 tsunami in Thailand. Environ. Geol., 49 (2), 321-31, 2005.

Szczuciński, W., Chaimanee, N., Niedzielski, P., Rachlewicz, G., Saisuttichai, D., Tepsuwan, T., Lorenc, S., and Siepak, J.: Environmental and geological impacts of the 26 December 2004 tsunami in coastal zone of Thailand—overview of short and long-term effects. Pol. J. Environ. Stud., 15 (5), 793–810, 2006.

Szczuciński, W., Niedzielski, P., Kozak, L., Frankowski, M., Zioła, A., and Lorenc, S.: Effects of rainy season on mobilization of contaminants from tsunami deposits left in a coastal zone of Thailand by the 26 December 2004 tsunami. Environ. Geol., 53 (2), 253-64, 2007.

Takada, H., Onda, T., Harada, M., and Ogura, N.: Distribution and sources of polycyclic aromatic hydrocarbons (PAHs) in street dust from the Tokyo Metropolitan area. Sci. Total. Environ., 107, 45-69, 1991.

Tarek, A.T.A., and Bernd, R.T.S.: Lipid geochemistry of surficial sediments from the coastal environment of Egypt I. Aliphatic hydrocarbons — characterization and sources. Mar. Chem., 54(1-2), 135-58, 1996.

Tareq, S. M., Tanaka, N., and Ohta, K.: Biomarker signature in tropical wetland: lignin phenol vegetation index (LPVI) and its implications for reconstructing the paleoenvironment. Sci.Tot. Environ., 324 (1–3), 91-103, 2004.

Tipmanee, D., Deelaman, W., Pongpiachan, S., Schwarzer, K and., Sompongchaiyakul, P. Using Polycyclic Aromatic Hydrocarbons (PAHs) as a chemical proxy to indicate Tsunami 2004 backwash in Khao Lak coastal area, Thailand. Nat. Hazards Earth Syst. Sci., 12, 1441–51, 2012.

Tsapakis, M., and Stephanou, G.E.: Polycyclic aromatic hydrocarbons in the atmosphere of the Eastern Mediterranean. Environ. Sci. Technol., 39, 6854-90, 2005.

Vargas, G., Ortlieb, L., Chapron, E., Valdes, J., and Marquardt, C.: Paleoseismic inferences from a high-resolution marine sedimentary record in northern Chile (23° S). Tectonophysics, 399, 381 – 98, 2005.

Venkatesan, I.M., Ruth, E., Rao, S.P., Nath, N.B., and Rao, R.B.: Hydrothermal petroleum in the sediments of the Andaman Backarc Basin, Indian Ocean. Applied Geochemistry., 18(6), 845-61, 2003.

Volkman, J.K.: Sterols in microorganisms. Appl. Microbiol. Biotechnol., 60, 496-506, 2003.

Wang, L.R., Brassell, C.S., Scarpitta, C.S., Zheng, P.M., Zhang, C.S., Hayde, R.P., and Muench, M.L.: Steroids in sediments from Zabuye Salt Lake, western Tibet: diagenetic, ecological or climatic signals? Org. Geochem., 35(2), 157-68, 2004.

Wang, X. C., Zhang, Y. X., and Chen, R. F.: Distribution and Partitioning of Polycyclic Aromatic Hydrocarbons (PAHs) in Different Size Fractions in Sediments from Boston Harbor, United States. Mar. Pollut. Bullet., 42 (11), 1139-49, 2001.

Watson, G.J., Robinson, F.N., Chow, C.J., Henry, C.R., Kim, M.B., Pace, G.T., Meyer, L.E., and Nguyen, Q.: The USEPA/DRI chemical mass balance receptor model, CMB 7.0. Environ. Soft., 5(1), 38-49, 1990.

Watson, J.G., Chow, J.C., Lu, Z., Fujita, E.M., Lowenthal, D.H., and Lawson, D.R.: Chemical mass balance source apportionment of PM_{10} during the Southern California air quality study. Aerosol. Sci. Technol., 21, 1-36, 1994.

Watson, G.J., Chow, C.J., and Fujita, M.E.: Review of volatile organic compound source apportionment by chemical mass balance. Atmos. Environ., 35(9), 1567-84, 2001.

Westerholm, R., Almen, J., Li, H., Rannug, U., and Rosen, A.: Exhaust emissions from gasoline-fuelled light duty vehicles operated in different driving conditions: a chemical and biological characterization. Atmos. Environ., 26B, 79-90, 1992.

Williams, T.P., Bartle, D.K., and Andrews, E.G.: The relationship between polycyclic aromatic compounds in diesel fuels and exhaust particulates. *Fuel*., 65(8), 1150-8, 1986.

Yunker, B.M., Macdonald, W.R., Vingarzan, R., Mitchell, H.R, Goyette, D., and Sylvestre, S.: PAHs in the Fraser River basin: a critical appraisal of PAH ratios as indicators of PAH source and composition. Org. Geochem., 33, 489-515, 2002.

Yunker, B.M., and Macdonald, W.R.: Petroleum biomarker sources in suspended particulate matter and sediments from the Fraser River Basin and Strait of Georgia, Canada. Org. Geochem., 34, 1525-41, 2003.

Zakaria, P.M., Okuda, T., and Takada, H.: Polycyclic aromatic hydrocarbon (PAHs) and Hopanes in Stranded Tar-balls on the coasts of Peninsular Malaysia: Applications of biomarkers for identifying sources of oil pollution. Mar. Pollut. Bulletin., 42(12), pp.1357-1366, 2001.

Zheng, M., Fang, M., Wang, F., and To, K.L.: Characterization of the solvent extractable organic compounds in $PM_{2.5}$ aerosols in Hong Kong. Atmos. Environ., 34, 2691-702, 2000.

Zundel, M., and Rohmer, M.: Hopanoids of the methylotrophic bacteria *Methylococcus capsulatus and Methylomonas* sp. As possible precursors of C_{29} and C_{30} hopanoid chemical fossils. FEMS. Microbiol. Lett., 28(1), 61-4, 1985a.

Zundel, M., and Rohmer, M.: Prokaryotic triterpenoids 1.3-methylhopanoids from Acetobacter sp. and Methylococcus capsulatus. Eur. J. Biochem., 150, 23-7, 1985b.

Zundel, M., and Rohmer, M.: Prokaryotic triterpenoids 3. The biosynthesis of 2b-methylhopanoids and 3b-methylhopanoids of Methylobacterium organophilum and Acetobacter pasteurianus sppl pasteurianus. Eur. J. Biochem., 150, 35-9, 1985c.

APPENDIX. TABLES

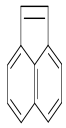
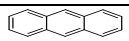
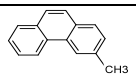
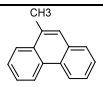
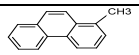
Table 1. Physiochemical properties of PAHs

Congeners	MW (g/mol)	MP (^{o}C)	BP (^{o}C)	P_S	P_L	Log K_{ow}	H	Log K_{OA}
Ace	154.2	96	277.5	0.3	1.52	3.92	12.17	6.23
Ac	150.2	92	265-275	0.9	4.14	4.00	8.40	6.47
Fl	166.2	116	295	0.09	0.72; 0.79[a]	4.18	7.87	6.68
Phe	178.2	101	339	0.02	0.11; 0.06	4.57	3.24	7.45
1-MePh	192.3	123	359			5.14		
An	178.2	216	340	1.00E-03	7.78E-02	4.54	3.96	7.34
Pyr	202.3	156	360	6.00E-04	1.19E-02; 8E-03	5.18	0.92	8.61
Flu	202.3	111	375	1.23E-03	8.72E-03	5.22	1.04	8.60
B[*a*]F	216.3	187	407			5.40		
B[*b*]F	216.3	209	402			5.75		
Chry	228.3	255	448	5.70E-07	1.07E-04	5.86	6.50E-02	10.44
Tri	228.3	199	438	2.30E-06	1.21E-04	5.49	1.20E-02	10.80
p-terp	230.1	213		4.86E-06		6.03		
B[*a*]A	228.3	160	435	2.80E-05	6.06E-04	5.91	0.58	9.54
B[*a*]P	252.3	175	495	7.00E-07	2.13E-05	6.04	4.60E-02	10.77
B[*e*]P	252.3	178		7.40E-07	2.41E-05		0.02	
Per	252.3	277	495	1.40E-08		6.25	3.00E-03	12.17
B[*b*]F	252.3	168	481			5.80		
B[*j*]F	252.3	166	480					
B[*k*]F	252.3	217	481	5.20E-08	4.12E-06	6.00	1.60E-02	11.19
B[*g,h,i*]P	268.4	277			2.25E-05	6.50	7.50E-02	11.02
D[*a,h*]A	278.4	267	524	3.70E-10	9.16E-08	6.75		
Cor	300.4	>350	525	2.00E-10		6.75		

Source: http://www.es.lancs.ac.uk/ecerg/kcjgroup/5.html

MP (^{o}C) Melting Point
BP (^{o}C) Boiling Point
P_S Vapour pressure of solid substance
P_L Vapour pressure of subcooled liquid
K_{ow} Octanol-water partition coeffic
H Henry 's Law Constant
K_{oa} Octanol-air partition coefficient

Table 2. Chemical structures of PAHs

Congener	Abbreviation	M.W. [g]	Chemical Structure
Acenaphthylene	Ac	152	
Acenaphthene	Ace	154	
Fluorene	Fl	166	
Phenanthrene	Phe	178	
Anthracene	An	178	
3-Methyl Phenanthrene	3-MePhe	192	
9-Methyl Phenanthrene	9-MePhe	192	
1-Methyl Phenanthrene	1-MePhe	192	

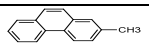
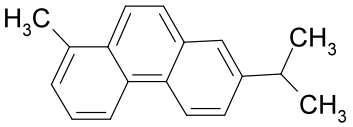
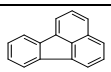
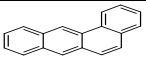
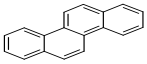
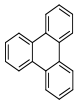
2-Methyl Phenanthrene	2-MePhe	192	
1-methyl-7-isopropyl phenanthrene (Retene)	Ret	234	
Fluoranthene	Fluo	202	
Pyrene	Py	202	
Benz[*a*]anthracene	B[*a*]A	228	
Chrysene	Chry	228	
Triphenylene	Tri	228	

Table 3. Chemical structures of alkanes.

Congener	Abbreviation	M.W. [g]	Chemical Structure
Tetradecane	C_{14}	198	
Pentadecane	C_{15}	212	
Hexadecane	C_{16}	226	
Heptadecane	C_{17}	268	
Octadecane	C_{18}	254	
Nonadecane	C_{19}	268	
Eicosane	C_{20}	282	
Heniacosane	C_{21}	296	
Docosane	C_{22}	310	
Tricosane	C_{23}	324	
Tetracosane	C_{24}	338	
Pentacosane	C_{25}	352	
Hexacosane	C_{26}	366	
Heptacosane	C_{27}	380	
Octacosane	C_{28}	394	
Nonacosane	C_{29}	408	
Triacontane	C_{30}	422	
Hentriacontane	C_{31}	436	
Dotriacontane	C_{32}	450	
Pristane	PC_{19}	268	
Phytane	PC_{20}	282	

Table 4. Chemical structures of hopanes.

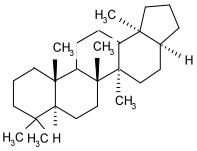
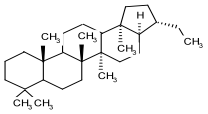
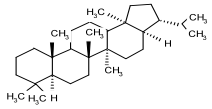
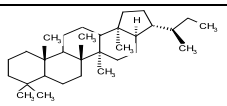
Congener	Abbreviation	M.W. [g]	Chemical Structure
17α(H)-22,29,30-Trisnorhopane	22,29,30-trisnorhopane (th)	370	
17α(H),21β(H)-30-Norhopane	17,21,ab-30-norhopane (nh)	398	
17α(H),21β(H)-Hopane	17,21,ab-hopane (hop)	412	
17α(H),21β(H)-22R-Homohopane	22R-17,21ab-30-homohopane (homo)	426	

Table 5. Chemical structures of cholestanes.

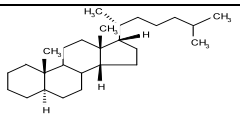
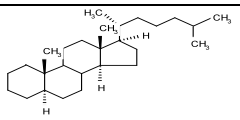
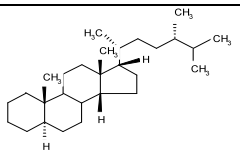
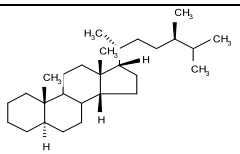
Congener	Abbreviation	M.W. [g]	Chemical Structure
αββ 20R-Cholestane	20R-abb-cholestane (abbC)	372	
ααα 20R-Cholestane	20R-aaa-cholestane (aaaC)	372	
αββ 20R 24S-Methylcholestane	20R-abb-methylcholestane (MC)	386	
αββ 20R 24R-Ethylcholestane	20R-abb-ethylcholestane (EC)	400	

Table 6. ΣPAH concentrations in different regions

Location	**Sample Type**	**ΣPAHs [ng m^{-3}]**	**Reference**
UK (London,Bounds Green)	TSP	4.27 (0.23-27.87)	Kendall et al., 2001
UK (London, St Paul)	TSP	7.24 (1.04-32.04)	Kendall et al., 2001
Indonesia (Pudu)	PM_{10}	26.5 (7-46)	Fang et al., 1999
Greece (Rural Area)	TSP	1.1 (0.2-2.0)	Gogou et al., 1996
Greece (Heraklion)	TSP	17.4 (3.2-44.9)	Gogou et al., 2000
Portugal (Forest)	TSP	0.5 (0.1-0.9)	Kavouras et al., 1999
China (Hong Kong)	$PM_{2.5}$	9.6 (0.7-12.2)	Zheng et al., 2000
China (Guangzhou)	TSP	73.7 (32.5-153.7)	Duan et al., 2005
Canada (Urban)	TSP	2.35 (1.86-2.83)	Sanderson et al., 2004
Eastern Mediterranean	TSP	0.7 (0.3-1.6)	Tsapakis and Stephanou, 2005
Canada (Toronto)	P+V	36.5 (11.5-61.4)	Motelay et al., 2005
Traffic, Hong Kong	$PM_{2.5}$	33.96	Gou et al., 2003
Industrial, Hong Kong	$PM_{2.5}$	16.72	Gou et al., 2003
Industrial (indoor), Shizuoka, Japan	$PM_{2.5}$	1.6–23.7	Ohura et al., 2004
Industrial (outdoor), Shizuoka, Japan	$PM_{2.5}$	1.1–29.5	Ohura et al., 2004
Pastureland (open) Taichung, Taiwan	$PM_{2.5}$	74.47	Fang et al., 2006
Temple (semi-open) Taichung, Taiwan	$PM_{2.5}$	284.91	Fang et al., 2006
Traffic Guangzhou, China	$PM_{2.5}$	57.89	Li et al., 2005
Residential Guangzhou, China	$PM_{2.5}$	27.06	Li et al., 2005

Table 7. Biological and/or environmental interpretation of *n*-alkanes

Biomarker	**Biological and/or environmental interpretation**	**References**
Outstanding concentrations of n15, n17 and n19 in early Paleozoic rocks	Marine phytoplankton of uncertain affinity, probably an alga, identified in Cambrian Devonian sediments but most prominent in Ordovician. Estonian kukersite is a typical source	Blokker *et al*., 2001
n-C_{27} with OEP[1]	Waxes derived from higher plants, terrestrial input, post-Silurian age	Hedberg, 1968
n-C_{40}	Predominantly degradation products of aliphatic macromolecules such as algaenan (marine, lacustrine), cutan and suberan (terrestrial, plant derived)	Allard *et al*., 2002 Killops *et al*., 2000

Table 8. Biological and /or environmental interpretation of hopanes

Biomarker	**Biological and/or environmental interpretation**	**References**
C_{30}-hopanes	Diverse bacterial lineages, few eukaryotic species (e.g. some cryptogams, ferns, mosses, lichens, filamentous fungi, protests)	Rohmer *et al*., 1984
Extended C_{31} to C_{35} hopanes (homohopanes)	Diagnostic for bacterial, biosynthesis appears to be restricted to lineages that are not strictly anaerobic	Ourisson and Albrecht, 1992, Rohmer *et al*., 1984
Extended C_{32} to C_{36} 3b-methylhopanes	Diagnostic for some microaerophillic proteobacteria (certain methylotrophs, methanotrophs, acetic acid bacteria)	Zundel and Rohmer., 1985a, 1985b, 1985c.
28,30-dinorhopane, 25,28,30-trinorhopane	Often prominent in sediments from euxinic environment	Grantham *et al*., 1980

Table 9. Biological and /or environmental interpretation of cholestanes

Biomarker	**Biological and/or environmental interpretation**	**References**
24-norcholestane (C_{26})	Possible diatom origin, high concentrations relative to 27-norcholestane indicate Cretaceous or younger crude oil	Holba *et al*., 1998a and 1998b
Cholestane	In aquatic sources probably almost exclusively derived from diverse eukaryotes	Volkman, 2003
24-*n*-propylcholestane	Pelagophyte algae, a biomarker for marine conditions with few exceptions	Moldowan *et al*., 1990
4-Methylcholestane and 4,4-dimethylcholestane	Diverse eukaryotic sources, high concentrations likely indicate a dinoflagellates origin	Summons *et al*., 1994

Author's personal copy

Marine Pollution Bulletin 76 (2013) 370–378

Contents lists available at ScienceDirect

Marine Pollution Bulletin

journal homepage: www.elsevier.com/locate/marpolbul

Baseline

Risk assessment of the presence of polycyclic aromatic hydrocarbons (PAHs) in coastal areas of Thailand affected by the 2004 tsunami

S. Pongpiachan [a,*], D. Tipmanee [b], W. Deelaman [c], J. Muprasit [c], P. Feldens [d], K. Schwarzer [d]

[a] NIDA Centre for Research & Development of Disaster Prevention & Management, School of Social and Environmental Development, National Institute of Development Administration (NIDA), 118 Moo3, Sereethai Road, Klong-Chan, Bangkapi, Bangkok 10240, Thailand
[b] International Postgraduate Program in Environmental Management, Graduate School, Chulalongkorn University, Bangkok, Thailand
[c] Faculty of Environmental Management, Prince of Songkla University, Hat-Yai, Songkla 90112, Thailand
[d] Institute of Geosciences Sedimentology, Coastal and Continental Shelf Research, Christian Albrechts University Kiel, Otto Hahn Platz 1, D-24118 Kiel, Germany

ARTICLE INFO

Keywords:
Tsunami
Polycyclic aromatic hydrocarbons (PAHs)
Risk assessment
Total toxic benzo[a]pyrene equivalent
Soil cleanup target level (SCTL)

ABSTRACT

The total concentrations of twelve, likely carcinogenic, polycyclic aromatic hydrocarbons (PAHs) (i.e., phenanthrene (Phe), anthracene (An), fluoranthene (Fluo), pyrene (Pyr), benz[a]anthracene (B[a]A), chrysene (Chry), benzo[b]fluoranthene (B[b]F), benzo[k]fluoranthene (B[k]F), benzo[a]pyrene (B[a]P), indeno[1,2,3-cd]pyrene (Ind), dibenz[a,h]anthracene (D[a,h]A), and benzo[g,h,i]perylene (B[g,h]P) in backwash deposits of the 2004 Khao Lak tsunami were carefully investigated and compared with the concentrations of world marine sediments (WMS). In general, $\sum_{12}$PAHs in this study (i.e., 69.43 ± 70.67 ng g^{-1}) were considerably lower than those values observed in marine sediments from Boston (54,253 ng g^{-1}), coastal sediments from Barcelona Harbour (15,069 ng g^{-1}), and riverine sediment from Guangzhou Channel (12,525 ng g^{-1}), but were greater than values from coastal sediments in Rosas Bay (12 ng g^{-1}), Santa Ponsa Bay (26 ng g^{-1}) and Le Planier (34 ng g^{-1}). The total toxic benzo[a]pyrene equivalent (TEQ^{Carc}) values calculated for Khao Lak coastal sediments (KCS), Khao Lak terrestrial soils (KTS), and Songkhla Lake sediments (SLS) were 10.3 ± 12.2 ng g^{-1}, 16.0 ± 47.7 ng g^{-1}, and 5.67 ± 5.39 ng g^{-1}, respectively. Concentrations of PAHs at all study sites resulted in risk levels that fell into the "acceptable" range of the US EPA model and were much lower than those of other WMS. The cancer risk levels of PAH content in KCS ranged from 7.44×10^{-8} to 2.90×10^{-7}, with an average of $1.64 \times 10^{-7} \pm 8.01 \times 10^{-8}$; this value is 119 times lower than that of WMS. In addition, soil cleanup target levels (SCTLs) for both non-carcinogens (i.e., Phe, An, Fluo and Pyr) and carcinogens (i.e., B[a]A, Chry, B[b]F, B[k]F, B[a]P, Ind, D[a,h]A and B[g,h,i]P) in the KTS samples were estimated for all target groups, with an average value of 115,902 ± 197,229 ng g^{-1}.

Crown Copyright © 2013 Published by Elsevier Ltd. All rights reserved.

The massive tsunami generated by an earthquake on December 26th, 2004 was responsible for a wide range of negative effects, such as post-traumatic stress symptoms among Norwegian tsunami survivors, malaria outbreaks in Andaman & Nicobar Islands, damage to coastal ecosystems and other adverse geological impacts. Further difficulties in establishing post-disaster recovery policies, reconstruction of transportation systems and other environmental management problems were also exacerbated (Cochard et al., 2008; Danielsen et al., 2005; Ghobarah et al., 2006; Goff et al., 2006; Heir et al., 2010; Kumari et al., 2009; Matsumaru et al., 2012; Rigg et al., 2005; Thanawood et al., 2006). Apart from these adverse effects, the deposition of a layer of sediment rich in salts and other pollutants on the inundated coastal land areas raised serious concerns for geoscientists (Chaudhary et al., 2006; Szczuciński et al., 2005, 2006; UNEP, 2005). Recent investigations examined standing brackish or saline water in numerous paddy fields on the Sendai plain caused by saltwater inundation triggered by the 2011 Tohoku-oki tsunami (Chagué-Goff, Niedzielski et al., 2011; Chagué-Goff, Andrew et al., 2011). By using geochemical marine markers (S and Cl) 2 months after the 2011 Tohoku-oki tsunami, the extent of tsunami inundation was identified as being 4.85 km from the shore (Chagué-Goff et al., 2012).

Thailand was one of the countries that was most affected by the catastrophic tsunami of December 26th, 2004, particularly in terms of coastal contamination from tsunami deposits. Pongpiachan et al. (2013a) applied Fourier Transform Infrared (FTIR) Spectroscopy followed by analysis of variance (ANOVA), Gaussian distribution, hierarchical cluster analysis (HCA) and principal component analysis (PCA) to discriminate typical marine sediments from tsunami backwash deposits. The same research group also used other environmental proxies, such as sulphur K-edge X-ray Absorption Near Edge Structure (XANES) spectroscopy and micro-beam

* Corresponding author. Tel.: +66 2727 3090, mobile: +66 819751456; fax: +66 2727 3747.
E-mail address: pongpiajun@gmail.com (S. Pongpiachan).

0025-326X/$ - see front matter Crown Copyright © 2013 Published by Elsevier Ltd. All rights reserved.
http://dx.doi.org/10.1016/j.marpolbul.2013.07.052

Author's personal copy

synchrotron X-ray fluorescence (μ-SXRF), to identify tsunami backwash deposits in Khao Lak coastal areas (Pongpiachan et al., 2012, 2013b). Despite the various adverse effects and coastal contamination reported to date, there has been no environmental risk assessment on the presence of carcinogenic substances, such as polycyclic aromatic hydrocarbons (PAHs), in the areas of Thailand affected by the tsunami.

Polycyclic aromatic hydrocarbons (PAHs) have several characteristics that make them more long-term pollutants than water soluble ionic species and/or acid-leached heavy metals: (*i*) they contain benzene rings, whose structure is especially stable and difficult to break down, so they persist over the long-term (Beck et al., 1995; Wild et al., 1991; Wild and Jones, 1995); (*ii*) they are widely distributed in aerosols, terrestrial soils and marine sediments (Mostafa et al., 2009; Neff, 2002; Pongpiachan et al., 2013c; Pongpiachan, 2013d,e; Perra et al., 2011; Tipmanee et al., 2012; Wild et al., 1991; Wild and Jones, 1995); (*iii*) they are hydrophobic compounds so rain may not effectively dilute or remove these chemical substances (Meador, 2008) and (*iv*) they have to potential to bioaccumulate and to be carcinogenic (Luch and Baird, 2010; Rosenfeld and Feng, 2011). The main sources of PAHs are traffic exhaust, emissions from the iron, steel and coke industries, accidental oil spills and biomass burning (Rajput et al., 2011; Rosenfeld and Feng, 2011; Slezakova et al., 2012; Yim et al., 2002). Without abating these root causes, PAHs are likely to remain present in depositional sedimentary environments, including the tsunami inundation zone (see Figs. 1 and 2).

Overall, the objectives of this study were (*i*) to analyse PAH content in the marine sediments and terrestrial soils affected by the 2004 tsunami, and (*ii*) to employ various analogous risk assessment models to gain a better understanding of the potential carcinogenic risk in the tsunami-affected area. This is the first study to produce such a risk assessment for this area. The purpose of this paper to illustrate the general principle of using PAHs as proxies for cancer risk assessment in tsunami inundation zones rather than to determine the source apportionment or to produce an analysis of spatial variation in PAHs. In addition, soil cleanup target levels (SCTLs) for carcinogens and non-carcinogens in affected soils were estimated and discussed.

This study was carried out offshore along the west coast of Phang Nga province, in the southwest region of Thailand, which was heavily affected by the 2004 tsunami. Climate in this area is governed by two seasonal monsoons: the northeast monsoon from mid October until March and the southwest monsoon from May to September. The research area covered approximately 1000 km^2 between Thap Lamu and Pakarang Cape, up to a water depth of 70 m. Our research was carried out on cruises taken 1 year apart, from November–December 2007 with RV CHAKRATONG TONGYAI and from November–December 2008 with RV BOONLERT PASOOK. Hydroacoustic profiles (side scan sonar, multibeam echo sounder and shallow reflection seismic scan with a boomer system) covering approximately 1500 nautical miles were recorded near Pakarang Cape.

A side scan sonar system (conventionally used for sea floor acoustic backscatter measurements) was used in conjunction with characteristics of sediment samples to create sediment distribution maps for the area. Finer sediments appeared in lighter colours, while coarser sediments were displayed in darker colours. Multibeam echo sounders were employed to create detailed bathymetric maps, and the boomer, a high-resolution shallow water seismic system, provided some information related to the sediment structures in the subsurface. The sediment samples discussed in this study were taken with a Van-Veen-type grab sampler. The grab sampling stations were located on a transect line corresponding to surface sediment sampling stations. Twenty-two soil sampling stations were selected to represent the areas affected by the 2004 tsunami (Szczuciński et al., 2005). Samples were collected from 18 to 22 July 2009 from the surface layer (approximately the first 10 cm) using a clean shovel. Approximately half a kilogram of composite sample was taken from a 2 m^2 area at each station and pre-treated as surface sediment samples.

All solvents used were HPLC grade, purchased from Fisher Scientific. A cocktail of 12 PAH Norwegian Standards (NS 9815: S-4008-100-T) (phenanthrene (Phe), anthracene (An), fluoranthene (Fluo), pyrene (Pyr), benz[a]anthracene (B[a]A), chrysene (Chry), benzo[b]fluoranthene (B[b]F), benzo[k]fluoranthene (B[k]F), benzo[a]pyrene (B[a]P), indeno[1,2,3-cd]pyrene (Ind), dibenz[a,h]anthracene (D[a,h]A), and benzo[g,h,i]perylene (B[g,h]P); each 100 μg mL^{-1} in toluene; unit 1 × 1 mL) and a mix of recovery Internal Standard PAHs (d_{10}-fluorene; d_{10}-Fl, d_{12}-perylene; d_{12}-Per); each 100 μg mL^{-1} in xylene; unit 1 × 1 mL) were supplied by Chiron AS (Stiklestadveine 1, N-7041 Trondheim, Norway). Standard stock solutions of 4 μg mL^{-1} deuterated PAHs (used as internal standards) and 100 μg mL^{-1} native PAHs were prepared in nonane. Working solutions were obtained by appropriate dilution in *n*-cyclohexane. All solutions were stored in amber coloured vials at −20 °C.

After the freeze-drying process was completed, samples were weighed and placed in pre-cleaned Whatman cellulose extraction thimbles. The extraction of PAHs was conducted using 250 mL of Soxhlet extractor, spiked with a known amount of internal standard (d_{10}-Fl: Phe, An, Fluo, Pyr, B[a]A, and Chry; d_{12}-Per: B[b]F, B[k]F, B[a]P, Ind, D[a,h]A, and B[g,h,i]P) and extracted with DCM containing 1 g of copper powder for 8 h. The fractionation/cleanup process followed the conventional method using the difference in solvent polarity (Gogou et al., 1996, 1998). After the extraction, the DCM solvent was concentrated to incipient dryness by a combination of rotary evaporation and blowing under a gentle nitrogen stream. The concentrated extract was then diluted in 10 mL of *n*-hexane before being applied to the top of a column of disposable silica gel. The extract was then fractionated into individual compound classes by flash chromatography by applying the concentrate to the top of a 30 × 0.7 cm diameter column containing 1.5 g of silica gel (activated at 150 °C for 3 h).

Nitrogen pressure was used to obtain a flow of 1.4 mL min^{-1} at the bottom of the column. The following solvents were used to elute the different compound classes: (*i*) 15 mL *n*-hexane (fraction 1, light molecular weight PAHs); and (*ii*) 15 mL toluene-*n*-hexane (5.6:9.4) (fraction 2, heavy molecular weight PAHs). In consideration of the toxicity of the solvent and the solubility of PAHs, toluene was selected for the study. After fractionation, the eluates were concentrated using a rotary evaporator followed by evaporation under a gentle nitrogen stream (flow rate set at 1.0 mbar). Because of the low dissipation capability of toluene, a percentage (5–25%) of acetone was added to increase the volatility. The sample was further reduced to incipient dryness prior and then brought to volume with cyclohexane (exactly 100 μL in a GC/MS vial insert) prior to GC/MS analysis. The recovery of the internal standards d_{10}-Fl and d_{12}-Per were 57% and 53%, respectively.

GC/MS analyses were performed using a Varian GC/MS–MS system comprised of a CP-3900 gas chromatograph (Walnut Creek, CA, USA) with a 1077 universal injector and a three-dimensional quadrupole ion-trap selected ion storage mass spectrometer (Varian Saturn 2200). The target compounds were separated on a 60 m length × 0.25 mm i.d. capillary column coated with a 0.25 μm thick film (phase composition: cross-linked/surface bonded 5% phenyl, 95% methylpolysiloxane, as specified by EPA methods 207, 508, 515, 515.2, 524.2, 525, 548.1, 680, 1625, 1653, 8081, 8141, 8270 and 8280) stationary phase (Agilent JW Scientific DB-5 GC columns). Helium (99.999%) was employed as carrier gas at a constant column flow of 1.0 mL min^{-1} and a pressure pulse of 25 psi with a duration of 0.50 min. All injections (1 μL) were performed through

Author's personal copy

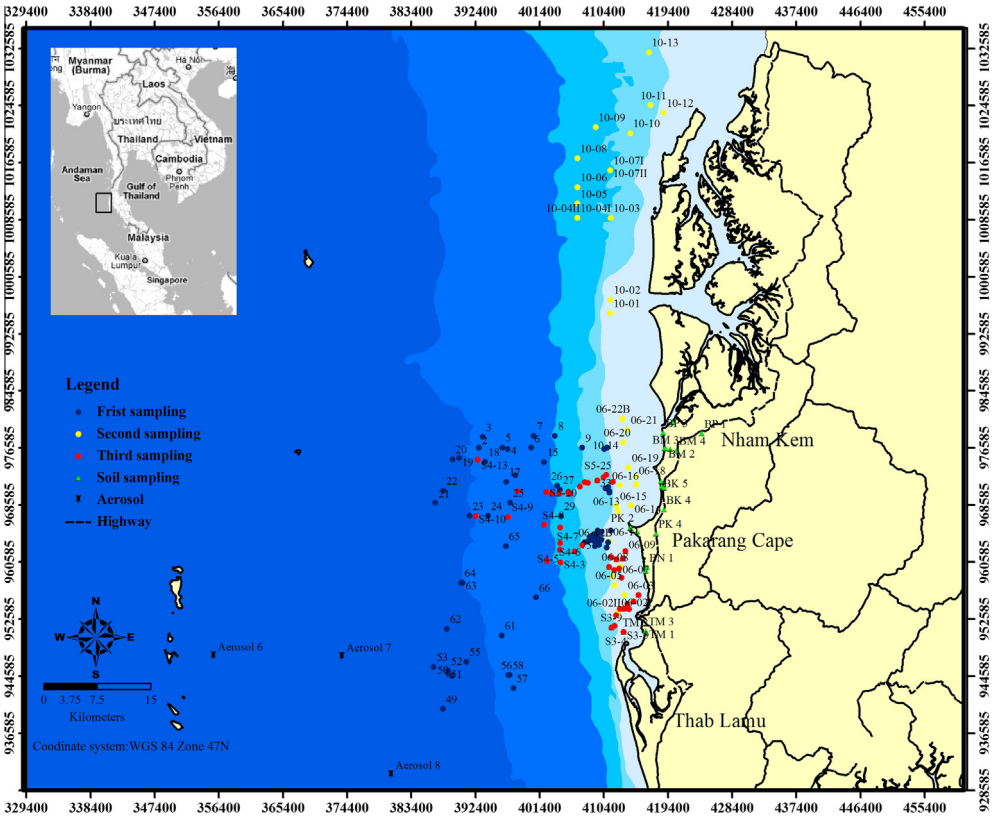


Fig. 1. Sampling sites for coastal sediments and terrestrial soils adjacent to the Khao Lak area affected by the 2004 tsunami.

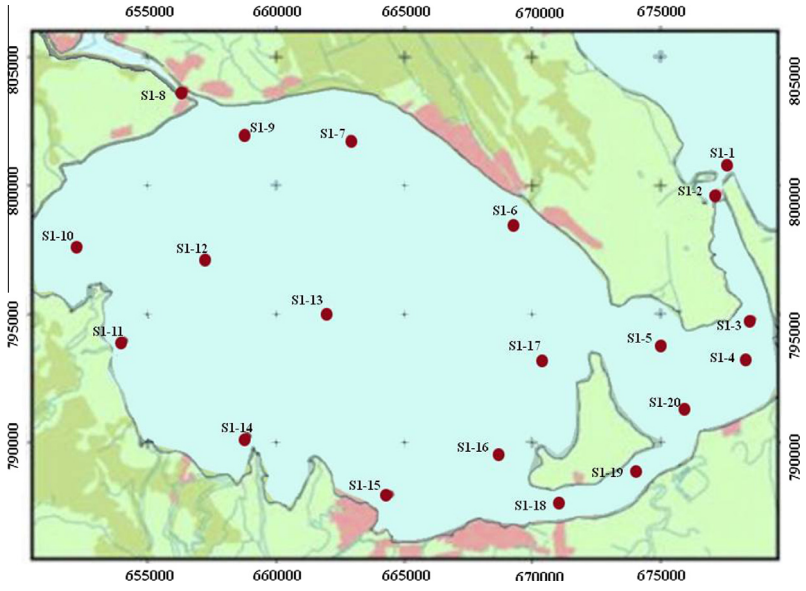


Fig. 2. Sampling sites for the Songkhla Lake sediments.

a universal injector (Varian 1077) in the splitless mode, and the standards were introduced using a 10 μL Hamilton syringe. The GC oven temperature was programmed as follows: 1 min at 40 °C increased by 8 °C min^{-1} to 300 °C and held for 45 min. By employing these chromatographic conditions it was possible to qualitatively distinguish between Ph/An and B[a]A/Chry, two pairs of isomers that are commonly co-eluted by gas chromatographic systems. All details of the GC/MS–MS ion trap operational parameters for the analytical method are given in Table 1.

The molecular markers were identified by first comparing retention times with authentic standards (within a range of ±0.2 min) and secondly by quantification of ions of each individual congener (Pongpiachan et al., 2009). The relative response factor (*RRF*), used to quantify the target congeners, was calculated as follows:

$$RRF = \frac{A_{nat}}{A_{is}} \times \frac{C_{is}}{C_{nat}} \quad (1)$$

Author's personal copy

where A_{nat} = the peak area of the native compound in the standard; C_{nat} = the concentration of the native compound in the standard; A_{is} = the peak area of the internal standard; and C_{is} = the concentration of the internal standard. The RRF_{STD} used for quantifying samples was the mean of the *RRF* values calculated for the two quantification standards run on the same day. Concentration (*C*) of analytes in sample extracts was calculated using the following formula:

$$C = \frac{A_{nat}}{A_{is}} \times \frac{1}{RRF_{STD}} \times \frac{W_s}{W_{is}} \quad (2)$$

where W_{is} = weight of internal standard (*IS*) added to the sample, and W_s = the weight or volume of the sample analysed. A recovery determination standard (*RDS*) was used for the calculation of *IS* and the sampling efficiency standard (*SES*) of recoveries during sample preparation and extraction/purification. A known amount of *RDS* was added at the final stage prior to GC/MS analysis and was assumed to suffer zero loss. The percent recovery was calculated as follows:

$$\%\text{Recovery} = \left[\left(\frac{A_{is}}{A_{RDS}}\right)_S \times \left(\frac{A_{RDS}}{A_{is}}\right)_{STD}\right] \times \left[\left(\frac{C_{is}}{C_{RDS}}\right)_{STD} \times \left(\frac{C_{RDS}}{C_{is}}\right)_S\right] \times 100\% \quad (3)$$

where A_{RDS} = the peak area of the recovery determination standard; and C_{RDS} = the concentration of the recovery determination standard. Recoveries of *IS* were used as an indication of the analytical losses during the extraction, pre-concentration, cleanup/fractionation and blow down stages. Standard reference materials (SRM-NIST1941b-Marine Sediment) were used to perform both quality control and quality assurance of analytical results. Mean recovery (based on extraction of matrix-matched certified reference materials SRM-NIST1941b-Marine Sediment, $n = 8$) ranged from 78% to 107%. The precision of the procedure, calculated as the relative standard deviation of duplicate samples, was less than 15%. Sample concentrations were calculated using *RRFs* run in between each batch.

Table 1
GC–EI–MS–MS ion trap operational parameters for PAHs analyses.

I. Ion preparation parameters	
CID waveform	Resonant and non-resonant
Mass isolation window	1
Isolation time	5 ms
Excitation time	5 ms
Ejection amplitude	20 V
Broadband amplitude	30 V
Modulation rate	30 μs step^{-1}
II. Ionisation parameters	
Ion trap temperature	200 °C
Transfer temperature	280 °C
Manifold temperature	120 °C
Axial modulating voltage	4.0 V
Emission current	90 μA
Electron multiplier voltage	1550 V
Scan rate	0.58 s scan^{-1}
Pre-scan ionisation time	1500 μs
Target TIC	20,000
Maximum ionisation time	25,000
RF pump value	650 m z^{-1}
Background mass	45 m z^{-1}
Count threshold	1 count
Isolation window	3.0 m z^{-1}
III. Injection port parameters	
Injection volume	1 μL
Injection mode	Splitless
Injector type	Glass liner
Carrier gas type	Helium
Septum purge flow rate	1 mL min^{-1}

Instrumental detection limit (*IDL*) and limit of quantification (*LOQ*) values ranged from 0.77 to 61.25 μg mL^{-1} and 2.57 to 204.17 μg mL^{-1}, respectively (Table 2). The range of the concentrations was comparable to previous studies (Helaleh et al., 2005; Ströher et al., 2007).

Table 3 lists the average, minimum, maximum and standard deviation of PAH concentrations in the marine sediments of Khao Lak coastal sediments (KCS), Khao Lak terrestrial soils (KTS), Songkhla Lake sediments (SLS) and world marine sediments (WMS). The total concentrations of twelve potentially carcinogenic PAHs in KCS ranged from 12.58 ng g^{-1} to 278.10 ng g^{-1}, with an arithmetic mean of 69.43 ± 70.67 ng g^{-1}. $\sum_{12}$PAHs refers to the sum of analysed Phe, An, Fluo, Pyr, B[a]A, Chry, B[b]F, B[k]F, B[a]P, Ind, D[a,h]A and B[g,h,i]P. The observed $\sum_{12}$PAHs were much lower than those values reported in harbour sediments from Boston (54,253 ng g^{-1}), coastal sediments from Barcelona Harbour (15,069 ng g^{-1}), riverine sediments from Guangzhou Channel (12,525 ng g^{-1}), mangrove sediments from Hong Kong (3714 ng g^{-1}), coastal sediments from Cotonou (1189 ng g^{-1}) and coastal sediments from Carteau (210 ng g^{-1}), but were higher than values from coastal sediments in Rosas Bay (12 ng g^{-1}), Santa Ponsa Bay (26 ng g^{-1}) and Le Planier (34 ng g^{-1}) (Baumard et al., 1998; Bixian et al., 2001; Deshmukh et al., 2001; Mielke et al., 2001; Soclo et al., 2000; Tam et al., 2001; Wang et al., 2001).

It is generally accepted that B[a]P can be considered a representative member of PAHs due to its relatively high carcinogenic potency factor in comparison with other potentially carcinogenic PAHs (Peters et al., 1999). Despite a relatively high diversity in molecular structure, only B[a]A, B[a]P, B[b]F, B[k]F, Chry, D[a,h]A and Ind have been classified as potentially carcinogenic in humans PAH compounds (CPAHs) by the US EPA. Percentage contribution of CPAHs to $\sum_{12}$PAHs varied from 10.19% to 64.78%, with an average of 51.54 ± 66.05%; from 2.82% to 39.40%, with an average of 38.03 ± 39.85%; and from 35.21% to 44.79%, with an average of 39.86 ± 46.81% for KCS, KTS and SLS, respectively.

Because the toxicity of PAHs is extremely structurally dependent, it was therefore crucial to adopt the concept of toxic equivalency factors ($TEFs^{Carc}$) for the evaluation of total effects caused by all probable human carcinogenic PAHs. In this study, the default $TEFs^{Carc}$ values for B[a]A, B[a]P, B[b]F, B[k]F, Chry, D[a,h]A and Ind were 0.1, 1, 0.1, 0.01, 0.001, 1 and 0.1, respectively, as defined by the US EPA. Further attempts to convert the above-mentioned seven PAHs into one toxic concentration for each observatory site were conducted using the corresponding $TEFs^{Carc}$. The evaluation of total toxic B[a]P equivalent (TEQ^{Carc}) for all seven PAHs was calculated as described below:

$$TEQ^{Carc} = \Sigma_i C_i \times TEF_i^{Carc} \quad (4)$$

Total TEQ^{Carc} values computed for samples collected at WMS, KCS, KTS and SLS varied from 1.68 to 9099 ng g^{-1} dry weight, with an average of 763 ± 2018 ng g^{-1}; from 0.0345 to 55.7 ng g^{-1} dry weight, with an average of 10.3 ± 12.2 ng g^{-1}; from 0.012 to 222 ng g^{-1} dry weight, with an average of 16.0 ± 47.7 ng g^{-1}; and from 0.869 to 18.5 ng g^{-1} dry weight, with an average of 5.67 ± 5.39 ng g^{-1}, respectively.

Notably, the average total TEQ^{Carc} values for KCS, KTS and SLS were 74, 48 and 135 times lower than for WMS, indicating a relatively low CPAH content at the study sites. Interestingly, the average CPAH content of KCS was approximately two times higher than that from SLS, possibly reflecting the influence of CPAH-contaminated terrestrial input triggered by tsunami backwash in 2004. Contribution to the total TEQ^{Carc} of KCS of the different PAH congeners was as follows, in decreasing order: D[a,h]A (68.83%) > B[a]P (20.05%) > Ind (6.27%) > B[b]F (2.63%) > B[a]A (1.94%) > B[k]F (0.26%) > Chry (0.02%). A similar der was observed in SLS, with

Author's personal copy

Table 2
Retention time (RT), instrumental detection limit (IDL), limit of quantification (LOQ), peak resolution (R), theoretical plate number (N) and height equivalent of theoretical plate (HETP) for each PAH.

PAH	RT (min)	IDL (pg μl^{-1})	LOQ (pg μl^{-1})	R	N	HETP (mm)	Low mass (m z^{-1})	High mass (m z^{-1})	Quantification ion (m z^{-1})	Excitation amplitude (V)
Phe	26.53	2.63	8.77	1.44	931693	0.064	177	179	178	0.50
An	26.63	2.80	9.33	1.44	936934	0.067	177	179	178	0.50
Fluo	30.13	1.47	4.90	7.62	2136956	0.029	201	203	202	0.40
Pyr	30.83	1.35	4.50	7.62	1624902	0.037	201	203	202	0.40
B[a]A	34.45	0.86	2.87	0.94	2418061	0.026	227	229	228	0.40
Chry	34.58	0.84	2.80	0.94	1962729	0.032	227	229	228	0.40
B[b]F	38.45	48.66	162.20	1.35	2102556	0.034	251	253	252	0.40
B[k]F	38.65	43.42	144.73	1.35	2112533	0.038	251	253	252	0.40
B[a]P	40.05	61.25	204.17	2.40	2176625	0.036	251	253	252	0.40
Ind	46.89	61.25	204.17	2.45	3913510	0.017	275	277	276	0.40
D[a,h]A	47.11	45.39	151.30	2.45	2244480	0.489	277	279	278	0.40
B[g,h,i]P	48.93	2.21	7.37	–	403043	3.930	275	277	276	0.40

Table 3
Summary statistics for PAH concentrations (ng g^{-1}) in Khao Lak coastal sediments (KCS), Khao Lak terrestrial soils (KTS), Songkhla Lake sediments (SLS) and world marine sediments (WMS).

	KCS				KTS				SLS				WMS			
	Aver[a]	Stdev[b]	Min[c]	Max[d]	Aver	Stdev	Min	Max	Aver	Stdev	Min	Max	Aver	Stdev	Min	Max
Phe	6.81	3.40	1.28	20.0	16.4	39.1	3.72	194	10.0	9.22	1.12	36.5	673	1621	1.09	7770
An	2.95	1.66	0.44	8.94	2.60	5.77	0.06	28.4	1.21	1.28	0.18	5.03	181	447	0.16	2230
Fluo	3.76	2.22	0.74	11.7	31.4	113	2.27	545	2.65	2.54	0.75	10.8	802	2285	1.53	11,610
Pyr	4.78	2.67	0.94	16.9	25.8	71.4	3.74	350	3.05	1.79	0.89	6.66	776	2095	1.30	10,548
B[a]A	2.00	1.89	ND[e]	9.91	7.97	30.8	ND	149	0.98	1.32	0.14	4.68	483	1092	0.75	4924
Chry	1.82	2.59	ND	15.3	6.95	21.5	0.28	105	1.05	1.61	0.09	6.11	407	840	1.11	3915
B[b]F	2.71	2.69	0.14	10.7	12.4	44.0	ND	213	3.05	3.76	0.42	15.1	663	1911	1.85	8130
B[k]F	2.67	3.00	0.07	18.7	3.93	12.8	ND	62.0	1.64	2.68	0.23	10.7	391	623	11.0	1910
B[a]P	2.06	2.17	ND	11.7	8.80	33.1	ND	160	1.89	1.51	0.16	3.52	376	794	1.00	3714
Ind	6.45	7.39	0.20	38.4	5.76	13.9	0.11	67.8	2.87	2.88	0.41	11.6	427	841	0.95	3112
D[a,h]A	7.09	8.83	ND	37.9	4.53	5.58	ND	18.5	3.08	3.06	0.61	11.7	225	832	0.21	3745
B[g,h,i]P	5.02	4.75	0.15	20.0	5.77	15.0	ND	73.1	5.02	4.28	0.85	19.3	347	730	0.86	2650

Note that [a]Average, [b]Standard Deviation, [c]Minimum, [d]Maximum and [e]Not Determined for WMS are averages for PAHs from marine sediments from Bayou St. John, New Orleans, USA (Mielke et al., 2001), harbour sediments form San Diego Harbour, California, USA (Deshmukh et al., 2001), marine sediments from the Northern Irish Sea, Northern Ireland, UK (Guinan et al., 2001), harbour sediments from Mystic River, Boston, USA (Wang et al., 2001), harbour sediments from Island End River, Boston, USA (Wang et al., 2001), marine sediments from Mangrove, Sai Keng, Hong Kong (Tam et al., 2001), marine sediments from Mangrove, Tolo, Hong Kong (Tam et al., 2001), Marine Sediments of Mangrove, Ho Chung, Hong Kong (Tam et al., 2001), Marine Sediments, Mangrove, Mai Po, Hong Kong (Tam et al., 2001), River Sediments of Pearl River, Guangzhou Channel, China (Bixian et al., 2001), river sediments from Pear River, Shiziyang Channel, China (Bixian et al., 2001), river sediments from Pearl River, Lingding Bay, China (Bixian et al., 2001), marine sediments from the northern Adriatic Sea, Italy (Notar et al., 2001), coastal sediments from Cotonou (Benin), Africa (Soclo et al., 2000), coastal sediments from Aquitaine, France (Soclo et al., 2000), coastal sediments from the Mediterranean, France (Baumard et al., 1998), coastal sediments from the Mediterranean, Spain (Baumard et al., 1998), coastal sediments from Brazil (Medeiros and Bícego, 2004), and coastal sediments from Guba Pechenga, Russia (Savinov et al., 2003).

D[a,h]A (54.28%) > B[a]P (33.24%) > B[b]F (5.38%) > Ind (5.07%) > B[a]A (1.73%) > B[k]F (0.29%) > Chry (0.02%). This result highlights the importance of D[a,h]A in both coastal and lake sediments in the southern part of Thailand. The contribution of PAHs to the total TEQ^{Carc} of WMS was B[a]P (49.26%) > D[a,h]A (29.55%) > B[b]F (8.69%) > B[a]A (6.33%) > Ind (5.60%) > B[k]F (0.51%) > Chry (0.05%), which highlights the major contribution of B[a]P to the total TEQ^{Carc} of worldmarine sediments.

Environmental cancer risk analyses have been widely performed on marine deposits, lake sediments and terrestrial soils around the world (Bejarano and Michel, 2010; Cachada et al., 2012; Li et al., 2012; Mebarka et al., 2012; Mirsadeghi et al., 2011; Zhang et al., 2012). In this study, an assessment of both environmental cancer and non-cancer risks was conducted following the framework proposed by The Agency for Toxic Substances and Disease Registry (ATSDR), a federal public health agency of the US Department of Health and Human Services. In addition, an evaluation of environmental cancer risks was performed to assess occurrence of adverse health effects (carcinogenic and non-carcinogenic) resulting from ingestion or dermal contact with PAH-contaminated sediments. Cancer risk was calculated as follows:

$$Cancer\ Risk = SF \times \left(\frac{CS \times IR \times EF \times ED \times CF}{BW \times AT_C} + \frac{CS \times SA \times AF \times EF \times ED \times DAF \times CF}{BW \times AT_C}\right) \quad (5)$$

where SF = slope factor (1.5 mg kg^{-1} body weight day^{-1})$^{-1}$; CS = chemical concentration (ng g^{-1}); CF = a conversion factor of 10^{-6} kg mg^{-1}; EF = an exposure frequency, set to 40 days year^{-1}; ED = exposure duration, set to 10 years; IR = ingestion rate, set to 50 mg sediment day^{-1}; BW = body weight, set to 53 kg; AT_c = averaging time for cancer risk, set to 25,550 days; AF = skin adherence factor, set to 0.3 mg sediment cm^{-1}; DAF = dermal absorption factor, set to 0.03 (unitless); and SA = skin surface area (available for contact), set to 4700 cm^2.

The evaluation of non-cancer risk was performed by calculating a Hazard Index (HI) using Eq. (6). The Hazard Index (HI) represents the non-cancer risk computed by dividing the sum of the average daily dose ingestion (ADD_i = mg kg^{-1} body weight day^{-1}) and the average daily dose dermal (ADD_d = mg kg^{-1} body weight day^{-1}) by the oral reference dose (RfD) (ATSDR, 2005) as follows:

$$HI = \frac{\frac{CS \times IR \times EF \times ED \times CF}{BW \times AT_{NC}} + \frac{CS \times SA \times AF \times EF \times ED \times DAF \times CF}{BW \times AT_{NC}}}{RfD} \quad (6)$$

Author's personal copy

Table 4
Levels of cancer risk from PAHs in Khao Lak coastal sediments (KCS), Khao Lak terrestrial soils (KTS), Songkhla Lake sediments (SLS) and world marine sediments (WMS) (ATSDR, 2005).

	KCS		KTS		SLS		WMS	
	Aver[a]	Stdev[b]	Aver	Stdev	Aver	Stdev	Aver	Stdev
Phe	2.785E−07	1.389E−07	6.720E−07	1.598E−06	4.100E−07	3.769E−07	2.751E−05	6.630E−05
An	1.208E−07	6.796E−08	1.065E−07	2.361E−07	4.963E−08	5.234E−08	7.367E−06	1.830E−05
Fluo	1.536E−07	9.062E−08	1.283E−06	4.606E−06	1.082E−07	1.038E−07	3.279E−05	9.345E−05
Pyr	1.953E−07	1.092E−07	1.054E−06	2.919E−06	1.248E−07	7.302E−08	3.175E−05	8.567E−05
B[a]A	8.159E−08	7.746E−08	3.258E−07	1.259E−06	4.022E−08	5.392E−08	1.973E−05	4.465E−05
Chry	7.439E−08	1.061E−07	2.844E−07	8.778E−07	4.274E−08	6.572E−08	1.665E−05	3.435E−05
B[b]F	1.109E−07	1.101E−07	5.057E−07	1.799E−06	1.247E−07	1.536E−07	2.711E−05	7.817E−05
B[k]F	1.090E−07	1.229E−07	1.605E−07	5.216E−07	6.695E−08	1.096E−07	1.598E−05	2.550E−05
B[a]P	8.442E−08	8.871E−08	3.599E−07	1.354E−06	7.709E−08	6.191E−08	1.536E−05	3.248E−05
Ind	2.640E−07	3.024E−07	2.355E−07	5.682E−07	1.175E−07	1.178E−07	1.748E−05	3.440E−05
D[a,h]A	2.899E−07	3.611E−07	1.853E−07	2.283E−07	1.259E−07	1.250E−07	9.215E−06	3.404E−05
B[g,h,i]P	2.052E−07	1.941E−07	2.360E−07	6.148E−07	2.053E−07	1.750E−07	1.417E−05	2.986E−05

[a] Average.
[b] Standard deviation.

where the abbreviations of incidental ingestion formula (Eq. (6)) can be described as follows:

HI: Hazard Index.
RfD: reference dose (3.0×10^{-4} mg kg^{-1} body weight day^{-1})
AT_{NC}: averaging time for non-cancer effects = 3650 days.

Cancer risk levels from PAHs in KCS ranged from 7.44×10^{-8} to 2.90×10^{-7}, with an average of $1.64 \times 10^{-7} \pm 8.01 \times 10^{-8}$, which is 119 times lower than that of WMS (Table 4). All cancer risk levels for KCS, KTS and SLS were significantly lower ($p < 0.001$) than those for WMS. Interestingly, the average cancer risk level for KCS was 2.75 times lower than for KTS but only slightly (1.32 times) higher than for SLS. No statistically significant differences were observed between KCS and KTS or between KCS and SLS, implying that the distribution of PAHs in tsunami affected areas was relatively homogeneous (see Table 5).

According to the "Role of the Baseline Risk Assessment in Superfund Remedy Selection Decisions" memorandum provided by US EPA (1991), the non-carcinogenic Hazard Index (*HI*) can be used as a parameter to assess the cumulative, non-carcinogenic, site risk to an individual based on reasonable maximum exposure. If *HI* is less than one, action is not warranted unless there are adverse environmental impacts for both current and future land use. The Superfund Program uses a cancer risk level of 10^{-6} to indicate the point at which risk management decisions should be considered. Using the same standard, the possibility of adverse cancer-causing effects in tsunami-affected areas was considerably lower in comparison to world marine sediments. In this study, the *HI* for non-cancer risk from PAHs in KCS ranged from 1.16×10^{-3} to 4.51×10^{-3}, with an average of $2.55 \times 10^{-3} \pm 1.25 \times 10^{-3}$; this risk level is 392 times lower than that of US EPA (1991) baseline. Inaddition, the average *HI* of non-cancer risk from PAHs in WMS was 3.28 times lower than the US EPA baseline, further indicating that the *HI* falls into the "acceptable level" range.

In this study, the acceptable soil cleanup target levels (SCTLs) for both carcinogens and non-carcinogens for aggregate residents were calculated using the following equations developed by FDEP (2005):

$$\mathrm{SCTL} = \frac{TR \times BW \times AT \times RBA}{EF \times ED \times FC \times \left[\left(CSF_0 \times IR_0 \times 10^{-6}\,\frac{kg}{mg}\right) + \left(CSF_d \times SA \times AF \times DA \times 10^{-6}\,\frac{kg}{mg}\right) + \left(CSF_i \times IR_i \times \left(\frac{1}{\frac{1}{3600} \times \frac{1}{0.036 \times (1-V) \times \left(\frac{U_m}{U_t}\right)^3 \times F(x)}} + \frac{1}{\frac{1}{Q} \times CF \times \frac{(3.14 \times D_A \times T)^{1/2}}{2 \times \rho_b \times D_A}}\right)\right)\right]} \quad (7)$$

where the abbreviations can be described as follows:

SCTL: soil cleanup target level.
TR: target cancer risk (unitless; 0.000001).
BW: body weight (Asian people *BW* 57.7 kg; Walpole et al., 2012).
AT: averaging time (25,500 days).
EF: exposure frequency (350 days yr^{-1}).
ED: exposure duration (30 yr).
RBA: relative bioavailability factor (unitless).
FC: fraction from contaminated source (1.0 unitless).
CSF_o: cancer slope factor for oral exposure (mg kg^{-1} day^{-1}; chemical specific from WIDNR, 1997).
IR_o: ingestion rate, oral (120 mg day^{-1}).
CSF_d: cancer slope factor for dermal exposure (mg kg^{-1} day^{-1}; chemical specific from WIDNR, 1997).
SA: surface area of skin exposed (4810 cm^2 day^{-1}).
AF: adherence factor (0.1 mg cm^{-2}).
DA: dermal absorption (0.01 unitless).
CSF_i: cancer slope factor for inhalation (mg kg^{-1} day^{-1}; chemical specific from WIDNR, 1997).
IR_i: inhalation rate (12.2 m^3 day^{-1}).
PEF: particulate emission factor, calculated as $(Q \times 3600)/(C \times 0.036 \times (1 - V) \times (U_m/U_t)^3 \times F(x))$ (2.23794×10^8 m^3 kg^{-1}; FDEP, 2005).
Q/*C*: inverse of mean concentration at centre of a 0.5 acre^2 source (g m^{-2}-s per kg m^{-3}; 85.61; US EPA, 1996b).
V: fraction of vegetative cover (dimensionless; 0.5; FDEP, 2005).
U_t: equivalent threshold value of wind speed at altitude of 30 m (m s^{-1}; 6.0; DEDP,2001).
U_m: mean annual wind speed (m s^{-1}; 4.4; DEDP, 2001).
$F(x)$: function dependent on U_m/U_t (unitless; 0.194; US EPA, 1985).
VF: volatilisation factor (m^3 kg^{-1}; chemical specific from ATSDR, 1995).
CF: conversion factor (10^{-4} m^2 cm^{-2}).
D_A: apparent diffusivity (cm^2 s^{-1}; chemical specific).
T: exposure interval (*ED* (exposure duration) × 3.1536×10^7 s).
ρ_b: dry soil bulk density (1.5 g cm^{-3}; FDEP, 2005).

The values for U_m and U_t for the areas affected by the 2004 tsunami were adopted from the Department of Energy Development and Promotion, Ministry of Energy, Thailand. The calculated value of *PEF* was 2.23794×10^8, which was one order lower than of the values of FDEP (i.e., 1.24101×10^9). It is also worth mentioning that other calculations of SCTL were performed using values of

Author's personal copy

Table 5
Levels of non-cancer risk from PAHs in Khao Lak coastal sediments (KCS), Khao Lak terrestrial soils (KTS), Songkhla Lake sediments (SLS) and world marine sediments (WMS) (ATSDR, 2005).

	KCS		KTS		SLS		WMS	
	Aver[a]	Stdev[b]	Aver	Stdev	Aver	Stdev	Aver	Stdev
Phe	4.332E−03	2.161E−03	1.045E−02	2.486E−02	6.378E−03	5.863E−03	4.280E−01	1.031E+00
An	1.879E−03	1.057E−03	1.657E−03	3.673E−03	7.720E−04	8.142E−04	1.146E−01	2.846E−01
Fluo	2.389E−03	1.410E−03	1.996E−02	7.165E−02	1.684E−03	1.615E−03	5.100E−01	1.454E+00
Pyr	3.039E−03	1.699E−03	1.640E−02	4.541E−02	1.942E−03	1.136E−03	4.939E−01	1.333E+00
B[a]A	1.269E−03	1.205E−03	5.068E−03	1.959E−02	6.257E−04	8.387E−04	3.070E−01	6.946E−01
Chry	1.157E−03	1.650E−03	4.424E−03	1.365E−02	6.648E−04	1.022E−03	2.589E−01	5.344E−01
B[b]F	1.726E−03	1.712E−03	7.867E−03	2.799E−02	1.940E−03	2.389E−03	4.216E−01	1.216E+00
B[k]F	1.696E−03	1.911E−03	2.497E−03	8.113E−03	1.041E−03	1.705E−03	2.485E−01	3.966E−01
B[a]P	1.313E−03	1.380E−03	5.599E−03	2.106E−02	1.199E−03	9.631E−04	2.390E−01	5.053E−01
Ind	4.106E−03	4.704E−03	3.664E−03	8.838E−03	1.828E−03	1.832E−03	2.719E−01	5.351E−01
D[a,h]A	4.509E−03	5.618E−03	2.882E−03	3.551E−03	1.958E−03	1.944E−03	1.433E−01	5.296E−01
B[g,h,i]P	3.193E−03	3.019E−03	3.671E−03	9.563E−03	3.193E−03	2.722E−03	2.204E−01	4.645E−01

[a] Average.
[b] Standard deviation.

Table 6
Soil clean up target level (SCTL; mg kg^{-1}) for carcinogens and non-carcinogens in Khao Lak terrestrial soils (KTS) (FDEP, 2005).

PAH congener	SCTL carcinogens			SCTL non-carcinogens		
	Worker	Child	Aggregate resident	Worker	Child	Aggregate resident
Phe	NA[a]	NA	NA	66,655	2628	35,031
An	NA	NA	NA	666,508	26,277	350,312
Fluo	NA	NA	NA	88,877	3,504	46,709
Pyr	NA	NA	NA	66,659	2628	35,032
B[a]A	1.40	0.109	2.04	NA	NA	NA
Chry	138	10.7	194	NA	NA	NA
B[b]F	1.39	0.108	2.00	NA	NA	NA
B[k]F	14.1	1.09	20.7	NA	NA	NA
B[a]P	0.140	0.0109	0.210	NA	NA	NA
Ind	1.41	0.109	2.07	NA	NA	NA
D[a,h]A	0.140	0.0109	0.210	NA	NA	NA
B[g,h,i]P	14.1	1.09	20.8	NA	NA	NA

[a] Not Available.

BW, *AF*, *AT*, *EF*, *ED*, IR_o, IR_i and *SA* of 16.8 kg, 0.2 mg cm^{-2}, 2190 days, 350 days yr^{-1}, 6 yrs, 200 mg day^{-1}, 8.1 m^3 day^{-1}, and 2960 cm^2 - day^{-1}, respectively, for children and 76.1 kg, 0.2 mg cm^{-2}, 9125 days, 250 days yr^{-1}, 25 yrs, 50 mg day^{-1}, 20 m^3 day^{-1}, 3500 cm^2 day^{-1}, respectively, for workers (FDEP, 2005).

A similar model was developed for calculating acceptable soil cleanup target levels for non-carcinogens as follows (FDEP, 2005):

$$\mathrm{SCTL} = \frac{THI \times BW \times AT \times RBA}{EF \times ED \times FC \times \left[\left(\frac{1}{RfD_o} \times IR_o \times 10^{-6}\,\frac{kg}{mg} \right) + \left(\frac{1}{RfD_o} \times SA \times AF \times DA \times 10^{-6}\,\frac{kg}{mg} \right) + \left(\frac{1}{RfD_i} \times IR_i \times \left(\frac{1}{\frac{H'}{\rho_b K_d + \theta_w + \theta_a H'} \times \frac{\left[\left(\theta_a^{10/3} D_i H' + \theta_w^{10/3} D_w \right) \right]}{n^2}} + \frac{1}{\frac{Q}{C} \times CF \times \frac{(3.14 \times D_A \times T) \times D}{T \times \rho_b \times 10^6}} \right) \right) \right]} \quad (8)$$

where *THI*, RfD_o, RfD_d and RfD_i are the target *HI* (unitless), reference dose for oral exposure (mg kg^{-1} day^{-1}; chemical specific), reference dose for dermal exposure (mg kg^{-1} day^{-1}; chemical specific) and reference dose for inhalation (mg kg^{-1} day^{-1}; chemical specific), respectively.

In addition, D_A can be calculated as follows:

$$D_A = \frac{\left[\frac{\left(\theta_a^{10/3} D_i H' + \theta_w^{10/3} D_W \right)}{n^2} \right]}{\rho_b K_d + \theta_w + \theta_a H'} \quad (9)$$

where θ_a, θ_w, D_i, D_w, H' and K_d are the air-filled soil porosity (g cm^{-3}), water-filled soil porosity (g cm^{-3}), diffusivity in air (cm^2 - s^{-1}), diffusivity in water (cm^2 s^{-1}), Henry's law constant (unitless) and soil–water partitioning coefficient (L kg^{-1}), respectively (FDEP, 2005).

Results obtained from the estimations of soil cleanup target levels (SCTLs) for carcinogens and non-carcinogens are shown in Table 6. These results were based on the concentrations recorded in KTS samples, which showed a maximum SCTL for the carcinogenic PAH Chry of 194 ng g^{-1}, 10.7 ng g^{-1} and 138 ng g^{-1} for aggregate residents, children and workers, respectively. B[a]P and D[a,h]A are two PAH congeners that require the minimum SCTL for all target groups. In addition, SCTL for the non-carcinogens Phe, An, Fluo and Pyr were estimated for KTS samples using Eq. (8). SCTL ranged from 2628 to 666,508 ng g^{-1} for all target groups, with an average value of 115,902 ± 197,229 ng g^{-1}.

The assessment of sediment toxicity based on the total toxic benzo[a]pyrene equivalent (TEQ_{carc}), evaluations of cancer and non-cancer risks, coupled with the estimation of soil cleanup target levels (SCTLs) from the PAHs data set produced by this study of the Khao Lak area affected by the 2004 tsunami, underscore two principal challenges. Firstly, the lack of knowledge related to the distribution of PAHs in tsunami-affected areas limits the ability to interpret data in comparison with other tsunami inundation zones. Secondly, the majority of default values used in the risk evaluation for both carcinogens and non-carcinogens, including calculations of SCTL, were developed for US citizens, and thus no effective Soil/Sediment Quality Guidelines (SQGs) are available for the southern part of Thailand or even the Andaman Sea. In spite of these research constraints, the approach adopted in this study emphasised that (*i*) the average concentrations of PAHs in all study sites were much lower than the average for world marine sediments, (*ii*) no adverse environmental and human health effects

Author's personal copy

have been connected with exposure to PAHs in Khao Lak coastal sediments (KCS), Khao Lak terrestrial soils (KTS) and Songkhla Lake sediments (SLS) and (iii) more comprehensive investigation based on site specific studies is necessary.

Polycyclic aromatic hydrocarbons are ubiquitous in Khao Lak coastal sediments (KCS), Khao Lak terrestrial soils (KTS) and Songkhla Lake sediments (SLS). The total concentrations of twelve potentially carcinogenic PAHs in all samples varied by three orders of magnitude, ranging from 3.97 ng g^{-1} to 1965.47 ng g^{-1}, with an arithmetic mean of 72.29 ± 161.55 ng g^{-1}. The percentage contribution of CPAHs to $\sum_{12}$PAHs in all samples varied from 2.82% to 64.78%, with an average value of 41.59 ± 50.90%. Remarkably, the average total TEQ^{Carc} values for KCS, KTS and SLS were 74, 48 and 135 times lower than those of WMS, respectively, signifying a comparatively low CPAH concentration at the study sites. It is also worth mentioning that the average *HI* for non-cancer risk from PAHs at KCS was 392 times lower than that of the US EPA (1991) baseline, emphasising the fact that the degree of *HI* falls into the "acceptable level" range. In addition, SCTL for the non-carcinogens Phe, An, Fluo and Pyr in KTS samples ranged from 2628 to 666,508 ng g^{-1} for workers, children and aggregate residents, with an average value of 115,902 ± 197,229 ng g^{-1}.

Acknowledgements

This work was performed with the approval of the National Institute of Development Administration (NIDA) and financial support from the National Research Council of Thailand (NRCT). The author acknowledges Assist. Prof. Dr. Charnwit Kositanont, Ms. Teeta Intasaen and Assist. Prof. Dr. Penjai Sompongchaiyakul from Chulalongkorn University for their contributions to field sampling and laboratory work.

References

ATSDR, 1995. Toxicological Profile for Polycyclic Aromatic Hydrocarbons (PAHs) (Update). US Department of Health & Human Services, Agency for Toxic Substances and Disease Registry, Atlanta, GA, August 1995. 458p.

ATSDR, 2005. Health consultation. Review of Sediment Data of Sylvester's (A/K/A) Gilson Road Site. Nashua, Hillsborough County, New Hampshire. EPA Facility ID: NHD099363541, August 19, 2005.

Baumard, P., Budzinski, H., Garrigues, P., Sorbe, J.C., Burgeot, T., Bellocq, J., 1998. Concentrations of PAHs (polycyclic aromatic hydrocarbons) in various marine organisms in relation to those in sediment and to trophic level. Mar. Pollut. Bull. 36, 951–960.

Beck, J.A., Alcock, E.R., Wilson, C.S., Wang, J.M., Wild, R.S., Sewart, P.A., Jones, C.K., 1995. Long-term persistence of organic chemicals in sewage sludge-amended agricultural land. Adv. Agron. 55, 345–391.

Bejarano, C.A., Michel, J., 2010. Large-scale risk assessment of polycyclic aromatic hydrocarbons in shoreline sediments from Saudi Arabia: environmental legacy after twelve years of the Gulf war oil spill. Environ. Pollut. 158 (5), 1561–1569.

Bixian, M., Jiamo, F., Gan, Z., Zheng, L., Yushun, M., Guoying, S., Xingmin, W., 2001. Polycyclic aromatic hydrocarbons in sediments from the Pearl river and estuary, China: spatial and temporal distribution and sources. Appl. Geochem. 16, 1429–1445.

Cachada, A., Pato, P., Rocha-Santos, T., Ferreira da Silva, E., Duarte, C.A., 2012. Levels, sources and potential human health risks of organic pollutants in urban soils. Sci. Total. Environ. 430, 184–192.

Chagué-Goff, C., Niedzielski, P., Wong, Y.K.H., Szczuciński, W., Sugawara, D., Goff, J., 2011. Environmental impact assessment of the 2011 Tohoku-oki tsunami on the Sendai Plain. Sediment. Geol. 282, 175–187.

Chagué-Goff, C., Andrew, A., Szczuciński, W., Goff, J., Nishimura, Y., 2012. Geochemical signatures up to the maximum inundation of the 2011 Tohoku-oki tsunami – implications for the 869 AD Jogan and other palaeotsunamis. Sediment. Geol. 282, 65–77.

Chaudhary, D.R., Gosh, A., Patolia, J.S., 2006. Characterization of soils in the tsunami-affected coastal areas of Tamil Nadu for agronomic rehabilitation. Curr. Sci. 91 (1), 99–104.

Cochard, R., Ranamukhaarachchi, L.S., Shivakoti, P.G., Shipin, V.O., Edwards, J.P., Seeland, T.K., 2008. The 2004 tsunami in Aceh and Southern Thailand: a review on coastal ecosystems, wave hazards and vulnerability. Perspect. Plant. Ecol. 10 (1), 3–40.

Danielsen, F., Sørensen, M.K., Olwig, M.F., Selvam, V., Parish, F., Burgess, N.D., Hiraishi, T., Karunagaran, V.M., Rasmussen, M.S., Hansen, L.B., Quarto, A., Suryadiptura, . The Asian Tsunami: a protective role for coastal vegetation. Science 310, 643.

Department of Energy Development and Promotion (DEDP), 2001. Wind Resource Assessment of Thailand.

Deshmukh, P.A., Chefetz, B., Hatcher, G.P., 2001. Characterization of organic matter in pristine and contaminated coastal marine sediments using solid-state ^{13}C NMR, pyrolytic and thermochemolytic methods: a case study in the San Diego harbor area. Chemosphere 45 (6–7), 1007–1022.

FDEP (Florida Department of Environmental Protection), 2005. Final Technical Report: Development of Cleanup Target Levels (CTLs) For Chapter 62–777, F.A.C.

Ghobarah, A., Saatcioglu, M., Nistor, I., 2006. The impact of the 26 December 2004 earthquake and tsunami on structures and infrastructure. Eng. Struct. 28, 312–326.

Goff, J., Liu, P.L.F., Higman, B., Morton, R., Jaffe, B.E., Fernando, H., Lynett, P., Eeri, M., Fritz, H., Synolakis, C., Fernando, S., 2006. Sri Lanka field survey after the December 2004 Indian Ocean tsunami. Earthq. Spectra 22 (3), 155–172.

Gogou, A., Stratigakis, N., Kanakidou, M., Stephanou, E., 1996. Organic aerosol in Eastern Maditerranean: component source reconciliation by using molecular markers and atmospheric back trajectories. Org. Geochem. 25, 79–96.

Gogou, I.A., Apostolaki, M., Stephanou, G.E., 1998. Determination of organic molecular markers in marine aerosols and sediments: one-step flash chromatography compound class fractionation and capillary gas chromatographic analysis. J. Chromatogr. A 799 (1–2), 215–231.

Guinan, J., Charlesworth, M., Service, M., Oliver, T., 2001. Sources and geochemical constraints of polycyclic aromatic hydrocarbons (PAHs) in sediments and mussels of two Northern Irish sea-loughs. Mar. Pollut. Bull. 42 (11), 1073–1081.

Heir, T., Piatigorsky, A., Weisæth, L., 2010. Posttraumatic stress symptom clusters associations with psychopathology and functional impairment. J. Anx. Disord. 24 (8), 936–940.

Helaleh, M.I.H., Al-Omair, A., Nisar, A., Gevao, B., 2005. Validation of various extraction techniques for the quantitative analysis of polycyclic aromatic hydrocarbons in sewage sludges using gas chromatography-ion trap mass spectrometry. J. Chromatogr. A 1083, 153–160.

Kumari, R., Joshi, L.P., Lal, S., Shah, W., 2009. Management of malaria threat following tsunami in Andaman & Nicobar Islands, India and impact of altered environment created by tsunami on malaria situation of the islands. Acta Trop. 112 (2), 204–211.

Li, H.W., Tian, Z.Y., Shi, L.G., Guo, S.C., Li, X., Feng, C.Y., 2012. Concentrations and sources of PAHs in surface sediments of the Fenhe reservoir and watershed, China. Ecotoxcol. Environ. Saf. 75, 198–206.

Luch, A., Baird, M.W., 2010. Carcinogenic polycyclic aromatic hydrocarbons. Compr. Toxicol. 14, 85–123 (second ed.).

Matsumaru, R., Nagami, K., Takeya, K., 2012. Reconstruction of the Aceh Region following the 2004 Indian Ocean tsunami disaster: a transportation perspective. IATSS Res. 36 (1), 11–19.

Meador, P.J., 2008. Polycyclic aromatic hydrocarbons. Encyclopedia Ecol., 2881–2891.

Mebarka, H.D., Taleb, S., Benghalem, A., Tundo, P., Ahmed, T.M., Arabi, M., 2012. Residue analysis of some PAHs in some Algerian soil: a preliminary environmental impact assessment. Energy Proc. 18, 1125–1134.

Medeiros, M.P., Bícego, C.M., 2004. Investigation of natural and anthropogenic hydrocarbon inputs in sediments using geochemical markers. I. Santos, SP–– Brazil. Mar. Pollut. Bull. 49 (9–10), 761–769.

Mielke, W.H., Wang, G., Gonzales, R.C., Le, B., Quach, N.V., Mielke, W.P., 2001. PAH and metal mixtures in New Orleans soils and sediments. Sci. Total. Environ. 281 (1–3), 217–227.

Mirsadeghi, A.S., Zakaria, P.M., Yap, K.C., Shahbazi, A., 2011. Risk assessment for the daily intake of polycyclic aromatic hydrocarbons from the ingestion of cockle (*Anadara granosa*) and exposure to contaminated water and sediments along the west coast of Peninsular Malaysia. J. Environ. Sci. – China 23 (2), 336–345.

Mostafa, R.A., Wade, L.T., Sweet, T.S., Al-Alimi, A.K.A., Barakat, O.A., 2009. Distribution and characteristics of polycyclic aromatic hydrocarbons (PAHs) in sediments of Hadhramout coastal area, Gulf of Aden, Yemen. J. Mar. Syst. 78 (1), 1–8.

Neff, M.J., 2002. Polycyclic Aromatic Hydrocarbons in the Ocean Bioaccumulation in Marine Organisms, pp. 241–318 (Chapter 15).

Notar, M., Leskovšek, H., Faganeli, J., 2001. Composition, distribution and sources of polycyclic aromatic hydrocarbons in sediments of the Gulf of Trieste, Northern Adriatic Sea. Mar. Pollut. Bull. 42 (1), 36–44.

Perra, G., Pozo, K., Guerranti, C., Lazzeri, D., Volpi, V., Corsolini, S., Focardi, S., 2011. Levels and spatial distribution of polycyclic aromatic hydrocarbons (PAHs) in superficial sediment from 15 Italian marine protected areas (MPA). Mar. Pollut. Bull. 62 (4), 874–877.

Peters, C.A., Knightes, C.D., Brown, D.G., 1999. Long-term composition dynamics of PAH-containing NAPLs and implications for risk assessment. Environ. Sci. Technol. 33, 4499–4507.

Pongpiachan, S., 2013d. Vertical distribution and potential risk of particulate polycyclic aromatic hydrocarbons in high buildings of Bangkok, Thailand. Asian Pac. J. Cancer Prev. 14 (3), 1865–1877.

Pongpiachan, S., 2013e. Diurnal variation, vertical distribution and source apportionment of carcinogenic polycyclic aromatic hydrocarbons (PAHs) in Chiang-Mai, Thailand. Asian Pac. J. Cancer Prev. 14 (3), 1851–1863.

Pongpiachan, S., Bualert, S., Sompongchaiyakul, P., Kositanont, C., 2009. Factors affecting sensitivity and stability of polycyclic aromatic hydrocarbons. Anal. Lett. 42 (13), 2106–2130.

Pongpiachan, S., Thumanu, K., Kositanont, C., Schwarzer, K., Prietzel, J., Hirunyatrakul, P., Kittikoon, I., 2012. Parameters influencing sulfur speciation

Author's personal copy

in environmental samples using sulfur K-edge X-ray absorption near-edge structure (XANES). J. Anal. Methods Chem. Article ID 659858, 12p, http://dx.doi.org/10.1155/2012/659858.
Pongpiachan, S., Thumanu, K., Na Phatthalung, W., Tipmanee, D., Kanchai, P., Feldens, P., Schwarzer, K., 2013a. Using Fourier transform infrared (FTIR) to characterize tsunami deposits in near-shore and coastal waters of Thailand. Sci. Tsu. Hazards 32 (1), 39–57.
Pongpiachan, S., Thumanu, K., Tanthanuch, W., Tipmanee, D., Kanchai, P., Schwarzer, K., Tancharakorn, S., 2013b. Sedimentary features of tsunami backwash deposits as assessed by micro-beam synchrotron X-Ray fluorescence (-SXRF) at the Siam Photon Laboratory. Sci. Tsu. Hazards 32 (2), 96–115.
Pongpiachan, S., Choochuay, C., Hattayanone, M., Kositanont, C., 2013c. Temporal and spatial distribution of particulate carcinogens and mutagens in Bangkok, Thailand. Asian Pac. J. Cancer Prev. 14 (3), 1879–1887.
Rajput, P., Sarin, M.M., Rengarajan, R., Singh, D., 2011. Atmospheric polycyclic aromatic hydrocarbons (PAHs) from post-harvest biomass burning emissions in the Indo-Gangetic Plain: isomer ratios and temporal trends. Atmos. Environ. 45 (37), 6732–6740.
Rigg, J., Law, L., Tan-Mullins, M., Grundy-Warr, C., 2005. The Indian Ocean tsunami: socio-economic impacts in Thailand. Geogr. J. 171 (4), 374–379.
Rosenfeld, E.P., Feng, H.G.L., 2011b. Bioaccumulation of dioxins, PCBs, and PAHs. Risks Hazard. Wastes, 201–213.
Rosenfeld, E.P., Feng, H.G.L., 2011a. 7 – Iron, steel, and coke. Risks Hazard. Wastes, 83–94.
Savinov, M.V., Savinova, N.T., Matishov, G.G., Dahle, S., Næs, K., 2003. Polycyclic aromatic hydrocarbons (PAHs) and organochlorines (OCs) in bottom sediments of the Guba Pechenga, Barents Sea, Russia. Sci. Total. Environ. 306 (1–3), 39–56.
Slezakova, K., Castro, D., Delerue-Matos, C., Alvim-Ferraz, C.M., Morais, S., Pereira, C.M., 2012. Impact of vehicular traffic emissions on particulate-bound PAHs: levels and associated health risks. Atmos. Res. 127, 141–147.
Soclo, H.H., Garrigues, P., Ewald, M., 2000. Origin of polycyclic aromatic hydrocarbons (PAHs) in coastal marine sediments: case studies in Cotonou (Benin) and Aquitaine (France) areas. Mar. Pollut. Bull. 40 (5), 387–396.
Ströher, G.L., Poppi, N.R., Raposo, J.L., Gomes de Souza, J.B., 2007. Determination of polycyclic aromatic hydrocarbons by gas chromatography–ion trap tandem mass spectrometry and source identifications by methods of diagnostic ratio in the ambient air of Campo Grande, Brazil. Microchem. J. 86, 112–118.
Szczuciński, W., Niedzielski, P., Rachlewicz, G., Sobczyński, T., Zioła, A., Kowalski, A., Lorenc, S., Siepak, J., 2005a. Contamination of tsunami sediments in a coastal zone inundated by the 26 December 2004 tsunami in Thailand. Environ. Geol. 49 (2), 321–331.
Szczuciński, W., Niedzielski, P., Rachlewicz, G., Sobczyński, T., Zioła, A., Kowalski, A., Lorenc, S., Siepak, J., 2005b. Contamination of tsunami sediments in a coastal zone inundated by the 26 December 2004 tsunami in Thailand. Environ. Geol. 49, 321–331.
Szczuciński, W., Chaimanee, N., Niedzielski, P., Rachlewicz, G., Saisuttichai, D., Tepsuwan, T., Lorenc, S., Siepak, J., 2006. Environmental and geological impacts of the 26 December 2004 tsunami in coastal zone of Thailand—overview of short and long-term effects. Polish J. Environ. Stud. 15 (5), 793–810.
Tam, N.F.Y., Ke, L., Wang, X.H., Wong, Y.S., 2001. Contamination of polycyclic aromatic hydrocarbons in surface sediments of mangrove swamps. Environ. Pollut. 114, 255–263.
Thanawood, C., Yongchalermchai, C., Densrisereekul, O., 2006. Effects of the December 2004 tsunami and disaster management in southern Thailand. Sci. Tsu. Hazards 24, 206–217.
Tipmanee, D., Deelaman, W., Pongpiachan, S., Schwarzer, K., Sompongchaiyakul, P., 2012. Using polycyclic aromatic hydrocarbons (pahs) as a chemical proxy to indicate tsunami 2004 backwash in Khao Lak coastal area, Thailand. Nat. Hazards Earth Syst. Sci. 12, 1441–1451.
UNEP, 2005. After the tsunami. Rapid Environmental Assessment, p. 140.
US EPA, 1985. US Environmental Protection Agency. Health and Environmental Effects Profile for Methyl Methacrylate. Prepared for Office of Solid Waste and Emergency Response. Environmental Criteria and Assessment Office, US EPA, Cincinnati, OH, ECAO-CIN-P144.
US EPA, 1991. Role of the Baseline Risk Assessment in Superfund Remedy Selection Decisions. Washington, DC, 20460.
US EPA (United States Environmental Protection Agency), 1996. Assessment of Sediment in the Indiana Harbor Area of Concern. EPA 905-R96-009, Great Lakes National Program Office, Region V, Chicago, IL.
Walpole, C.S., Merino, P.D., Edwards, P., Cleland, J., Stevens, G., Roberts, I., 2012. The weight of nations: an estimation of adult human biomass. BMC Public Health 12, 439.
Wang, C.X., Zhang, X.Y., Chen, F.R., 2001. Distribution and partitioning of polycyclic aromatic hydrocarbons (PAHs) in different size fractions in sediments from Boston Harbor, United States. Mar. Pollut. Bull. 42 (11), 1139–1149.
Wisconsin Department of Natural Resources (WIDNR), 1997. Bureau for Remediation and Redevelopment, Soil Cleanup Levels for Polycyclic Aromatic Hydrocarbons (PAHs) Interim Guidance. Publication PR-519-97, April 1997.
Wild, R.S., Jones, C.K., 1995. Polynuclear aromatic hydrocarbons in the United Kingdom environment: a preliminary source inventory and budget. Environ. Pollut. 88 (1), 91–108.
Wild, R.S., Obbard, P.J., Munn, I.C., Berrow, L.M., Jones, C.K., 1991. The long-term persistence of polynuclear aromatic hydrocarbons (PAHs) in an agricultural soil amended with metal-contaminated sewage sludges. Sci. Tot. Environ. 101 (3), 235–253.
Yim, H.U., Oh, R.J., Hong, H.S., Lee, H.S., Shim, J.W., Shim, H.J., 2002. Identification of PAHs sources in bivalves and sediments 5 years after the Sea Prince oil spill in Korea. Environ. Forensic. 3 (3–4), 357–366.
Zhang, Y., Guo, S.C., Xu, J., Tian, Z.Y., Shi, L.G., Feng, C.Y., 2012. Potential source contributions and risk assessment of PAHs in sediments from Taihu Lake, China: comparison of three receptor models. Water Res. 46 (9), 3065–3073.

Nat. Hazards Earth Syst. Sci. Discuss., 2, 7225–7267, 2014
www.nat-hazards-earth-syst-sci-discuss.net/2/7225/2014/
doi:10.5194/nhessd-2-7225-2014
© Author(s) 2014. CC Attribution 3.0 License.

Natural Hazards and Earth System Sciences
Open Access
Discussions

This discussion paper is/has been under review for the journal Natural Hazards and Earth System Sciences (NHESS). Please refer to the corresponding final paper in NHESS if available.

Internal structure of event layers preserved on the Andaman Sea continental shelf, Thailand: tsunami vs. storm and flash flood deposits

D. Sakuna-Schwartz[1,*], P. Feldens[1], K. Schwarzer[1], S. Khokiattiwong[2], and K. Stattegger[1]

[1]Institute of Geosciences, Kiel University, Otto-Hahn-Platz 1, 24118 Kiel, Germany
[2]Oceanography Unit, Phuket Marine Biological Center, P.O. Box 60, 83000 Phuket, Thailand
[*]now at: Oceanography Unit, Phuket Marine Biological Center, P.O. Box 60, 83000 Phuket, Thailand

Received: 10 September 2014 – Accepted: 29 October 2014 – Published: 1 December 2014

Correspondence to: D. Sakuna-Schwartz (daroonwans@gmail.com)

Published by Copernicus Publications on behalf of the European Geosciences Union.



Abstract

Tsunami, storm and flash event layers, which have been deposited over the last century on the shelf offshore from Khao Lak (Thailand, Andaman Sea), are identified in sediment cores based on sedimentary structures, grain size compositions, Ti / Ca ratios and ^{210}Pb activity. Individual offshore tsunami deposits are 12 to 30 cm in thickness and originate from the 2004 Indian Ocean tsunami. They are characterized by (1) the appearance of sand layers enriched in shells and shell debris, (2) cross lamination and (3) the appearance of rip-up clasts. Storm deposits found in core depths between 5 and 82 cm could be attributed to individual storm events by using ^{210}Pb dating in conjunction with historical data of typhoons and tropical storms and could thus be securely differentiated from tsunami deposits. Massive sand layers enriched in shells and shell debris characterize the storm deposits. The last classified type of event layer represents flash floods, which is characterized by a fining-upward sequence of muddy sediment. The most distinct difference between the storm and tsunami deposits is the lack of rip-up clasts, mud, and terrigenous material within the storm deposits. Terrigenous material transported offshore during the tsunami backwash is therefore an important indicator to distinguish between offshore storm and tsunami deposits.

1 Introduction

Tsunami waves propagating into shallow waters as well as related backwash flows can erode, transport and deposit significant amounts of sediments in the inner shelf environment (e.g. Paris et al., 2010; Goto et al., 2011), here defined as 0 to 30 m water depth. The behaviour of tsunami waves is controlled by the source earthquake or landslide and the ocean basin's morphology on a larger scale, as well as by the inner-shelf and coastal bathymetry and probably the hydrological conditions on a local scale (Cheng and Weiss, 2013; Spiske et al., 2013; Goto et al., 2014). Coastal and inner shelf bathymetry is the most important factor controlling backwash flow (Le Roux and

NHESSD
2, 7225–7267, 2014



Vargas, 2005; Paris et al., 2010; Feldens et al., 2012; Spiske et al., 2014). The structure and texture of tsunami deposits in offshore areas mainly depends on the local sediment sources, the geomorphology of the seafloor, the tsunami wave height and the number of waves if more than one wave hits the shoreline during the run-up and backwash (Sakuna et al., 2012). Both the bathymetry and available sediments are highly variable in shallow marine environments (e.g. Dartnell and Gardner, 2004). A complex composition of offshore tsunami deposits is therefore expected, with potentially quick changes both in space and time (Shanmugam, 2012). A tsunami's impact in deeper waters may be preserved within sediments below the storm wave base (e.g. Weiss and Bahlburg, 2006; Weiss, 2008). However, while the tsunami's impact increases with decreasing water depth towards the coastline, only very few offshore tsunami deposits have been reported until now.

Research on offshore tsunami deposits has to consider the low preservation potential of tsunami deposits in shallow waters due to reworking and transport by waves (Weiss and Bahlburg, 2006), tides and bioturbation (Wheatcroft and Drake, 2003). Reworking is intensified in areas with low accumulation rates, where tsunami deposits cannot quickly escape the surface mixing layer. Therefore, it is not surprising that the described offshore deposits of historical tsunami – not considering inferred tsunami palaeorecords on geological timescales (Cantalamessa and Celma, 2005; Le Roux and Vargas, 2005; Fujiwara and Kamataki, 2007; Spiske et al., 2014) – are highly variable in thickness, texture and structure (e.g. van den Bergh et al., 2003; Abrantes et al., 2008; Goodman-Tchenov et al., 2009; Paris et al., 2010; Smedile et al., 2011; Sakuna et al., 2012; Milkert et al., 2013). Offshore tsunami deposits range from centimetres to 1 m in thickness while spanning grain sizes from mud to boulders, including terrigenous and marine sediments over one or several layers, different fossil assemblages and different sedimentary structures (Sakuna et al., 2012). A further problem is the differentiation between storm and tsunami deposits, which has been widely discussed for deposits left on land (e.g. Nott, 2003; Goff et al., 2004; Kortekaas and Dawson, 2007; Morton et al., 2007; Switzer and Jones, 2008; Lario et al., 2010; Phantuwongraj and

NHESSD
2, 7225–7267, 2014



Choowong, 2011; Lorang, 2011; Richmond et al., 2011; Ramírez-Herrera et al., 2012; Brill et al., 2014b), but no reliable sedimentological criteria have yet been developed to distinguish offshore storm deposits from tsunami deposits. Generally, shallow-water, proximal tempestites are characterized by basal erosional contacts and a sequence from normal gradation to cross stratification to plane lamination, with frequently preserved ripples at the top (Einsele et al., 1991; Allison et al., 2005). However, not all tempestites comprise all these features. Furthermore, in monsoon-dominated areas, flash flood deposits occur frequently (Kale, 2003; Malmon et al., 2004) and have to be considered while identifying offshore backflow tsunami deposits. Flash floods can comprise a large percentage of a river's yearly discharge and can form hyperpycnal flows due to high suspended sand and mud concentrations (Mulder et al., 2003; Bourrin et al., 2008), which have been established for tsunami backwash flows (Le Roux and Vargas, 2005). Directly in front of river mouths or ephemeral streams, flash flood deposits are typically coarse grained (Postma, 2001) or comprise alternating sand and mud layers (Martin, 2000). However, they also comprise stratified deposits of silty clays at more remote locations (Cutter and Diaz, 2000). The Andaman Sea (Thailand) is an area where all these types of event deposits can be studied. It has been subjected to a few strong storms over the last decades, regularly impacted by the northeast and southwest monsoons, with the latter accompanied by flash floods, and hit by the 2004 Indian Ocean tsunami. Based on a collection of six sediment cores from the Andaman Sea, the objectives of this study are to (a) identify, describe and discuss the tsunami, storm and flash flood deposits in sediment cores and to (b) identify proxies that can be used to distinguish tsunami, storm and flash flood deposits from each other.

2 Regional setting

The investigation area near Pakarang Cape is located on the western side of the southern Thai-Malay peninsula offshore from Phang Nga province (Fig. 1). The Ayeyarwady–Salween river system is the main source supplying fine-grained sediment

NHESSD
2, 7225–7267, 2014



into the Andaman Sea (Rodolfo, 1969; Colin et al., 1999), which is highly seasonal, with more than 80 % of the annual discharge during the SW monsoon (Ramaswamy et al., 2004). The majority of the Andaman Basin is classified as sediment starved (Rodolfo, 1969; Panchang et al., 2008; Schwab et al., 2012). The coastline north and south of Pakarang Cape represents an embayed coast with sandy beaches commonly separated by rocky headlands. In general, the shelf gently dips offshore, reaching 60 m water depths within a distance of 30 km from the coastline. Pakarang Cape itself is surrounded by a 3 km long reef platform (Goto et al., 2007; Choowong et al., 2009; Di Geronimo et al., 2009). The tides in this area are mixed semidiurnal, with most days having two high tides and two low tides. The mean tidal range extends from 1.1 m during neap tide to 3.6 m during spring tide (Thampanya et al., 2006). Based on geomorphological evidence from sandy hooks and spits, northward-directed current-induced longshore sediment transport occurs in the study area (Choowong et al., 2009; Brill et al., 2014a). Maps of the nearshore bathymetry and sediment distribution have been created following the 2004 Indian Ocean tsunami (e.g. Di Geronimo et al., 2009; Feldens et al., 2009, 2012), but the maps cover only a small percentage of the Andaman Sea shelf. According to these studies, mud patches are widespread in water depths between 5 and 15 m north and south of Pakarang Cape. Several granite outcrops are scattered along the inner shelf at water depths of 5–10 m and on the mid-shelf at a water depth of approximately 30 m. Extensive cassiterite mining both on- and offshore has affected the area over the last century (Hylleberg et al., 1985; Usiriprisan et al., 1987). Offshore, visible remnants of the mining activities include up to 7 m deep holes at water depths of 20–25 m NW of Pakarang Cape (Feldens et al., 2009).

The climate of this region is influenced by the tropical monsoon, with the northeast monsoon lasting from December to February, causing dry weather conditions, and the southwest monsoon lasting from May to September, bringing strong westerly winds and heavy rainfall (Khokiattiwong et al., 1991). While no studies on flash floods have been published for the Andaman Coast, they are expected to occur regularly during the southwest monsoon and have been reported by the local population. Strong storm

NHESSD
2, 7225–7267, 2014



events are rare in this area (Jankaew et al., 2008; Brill et al., 2011), and only nine strong storm events were recorded within a 180-nautical-mile radius of Phuket between 1945 and 1996 (Table 1).

The coastal area of the Andaman Sea was seriously affected by the 2004 Indian Ocean tsunami (Chavanich et al., 2005; Siripong, 2006; Szczuciński et al., 2006; Choowong et al., 2007; Goto et al., 2007; Umitsu et al., 2007). Since then, several studies (Di Geronimo et al., 2009; Sugawara et al., 2009; Feldens et al., 2009, 2012) have focussed on the tsunami's impact on the shelf area offshore from Khao Lak. Only minor influence and a few deposits related to the 2004 tsunami could be found 3 to 5 years later offshore between 5 and 70 m water depths (Di Geronimo et al., 2009; Sugawara et al., 2009; Feldens et al., 2012; Sakuna et al., 2012; Milker et al., 2013). Due to the reworking of shelf sediments (Sakuna et al., 2012) and the re-establishment of the coastline (Choowong et al., 2009; Grzelak et al., 2009) following the tsunami, the remaining offshore tsunami deposits have been chiefly found in locally sheltered positions adjacent to granitic outcrops, within an incised channel system and in areas of locally higher sediment accumulation rates (Feldens et al., 2012; Sakuna et al., 2012; Milker et al., 2013).

3 Methods

During three research cruises in December 2007, December 2008 and February/March 2010, side-scan sonar data were obtained using a Klein 595 side-scan sonar (384 kHz) and a Benthos 1624 side-scan sonar (100 and 400 kHz). The side-scan sonars were towed behind the vessel with approximately 10 to 50 m offset from the GPS antenna. This offset was accounted for by a constant value for each profile when calculating the position of the tow fish. Side-scan sonar data were recorded in digital format employing the Isis software package (Triton Elics Int.). These data were processed and geo-referenced using the same software to create side-scan sonar mosaics of the study area. In this study, areas of higher backscatter are displayed with

NHESSD
2, 7225–7267, 2014



darker colours. A total of 60 gravity cores using a Ruhmor-type gravity corer (8 cm diameter) were collected (see Fig. 1) based on the on-site interpretation of the side-scan sonar and previous shallow seismic mapping (Feldens et al., 2009, 2012). Gravity cores could only be retrieved from fine-grained (silt and finer) seafloor sediments, as the corer could not penetrate into seafloor composed of sand. In all the cores, the sediment–water interface was preserved. Out of the 60 cores that have been taken, 6 are presented in this study (Fig. 1, Table 2). The sediment slabs were radiographed to detect internal sedimentary structures and unconformities. The grain size composition was determined every 1 cm with a laser-based particle sizer device with a measuring range of 0.04 to 2000 µm. Therefore, grains larger than 2000 µm were separated prior to the measurements. The statistical parameters of the grain size distributions were calculated in phi (Φ) units with $\Phi = -\log_2 d$ (d being the grain size in mm) (Krumbein, 1938) using the logarithmic method of moments available with the GRADISTAT software (Blott and Pye, 2001). Measurements of ^{210}Pb activity were done for two sediment cores (030310-C3 and 050310-C4) to assess the sediment accumulation rates. The sediment samples were dried, ground and analysed using gamma spectrometry at the Leibniz-Laboratory for Radiometric Dating and Isotope Research, Kiel, Germany. As the ^{137}Cs activity was mostly below the detection limits, these data were not used for further analysis. The sediment accumulation rates presented in this study serve only as an approximation and were assessed from the decline in the excess ^{210}Pb activity following the equations used by Robins and Edington (1975) and McKee et al. (1983).

$$\mathrm{SAR} = \lambda \times z \times [\ln(A_0/A_z)]^{-1}, \quad (1)$$

where λ is the decay constant (= 0.0311 year^{-1}), z is the depth in the core (cm), A_0 is the specific activity of excess ^{210}Pb at a particular reference horizon (Bq kg^{-1}) and A_z is the specific activity of excess ^{210}Pb at depth z below the reference horizon (Bq kg^{-1}).

NHESSD
2, 7225–7267, 2014



4 Results

4.1 Subsurface sediment sequence

The description of the sediment sequence in the sediment cores is based on X-radiographic images. If not mentioned otherwise, the depth values in the following section refer to core depths. The core positions are indicated in Fig. 1. An overview of all the available core details is given in Fig. 2, while the side-scan sonar data showing the sediment distribution from the areas where the cores have been taken are shown in Fig. 3. The sedimentary features and the interpretation of all the studied cores are summarized in Table 3 and Fig. 5. In general, four different facies are recognized within the presented cores. Most frequently occurring are layers composed of mainly clayey silt with a few sand layers, which are commonly laminated and generally fining upward with transitional boundaries (individual laminae could not be sampled). Bioturbation is rarely observed in this facies. Furthermore, sand layers that are partly massive and show slight lamination occur. Shells are scattered throughout the sand layers. At the top, rippled shapes draped with mud are partly preserved. In several cores, several-centimetres-thick layers comprised of shells and shell debris with variable fraction of coarse sand and gravel exist. Finally, poorly sorted sediment units comprising mud to sand and including mud clasts are found.

4.1.1 Core 030310-C3 (Fig. 2)

Core 030310-C3 (97 cm in length) was collected 3.2 km offshore at a water depth of 9.5 m, approximately 100 m west of a granitic outcrop (see Fig. 3a). In the vicinity of the coring position, the backscatter in the side-scan sonar is low, representing silt and fine sand proven by grab samples and grain size analyses.

The lowermost 2 cm of the core is composed of massive fine-grained sediment. At 95 cm, an erosional contact with laminated sediments exists. These laminated sediments extend up to 82 cm (Table 3a-V). The laminations are slightly inclined and the

NHESSD
2, 7225–7267, 2014



sediment is fining upward. Traces of bioturbation are not observed. Above a wavy and erosional contact at 82 cm, a massive sand layer including few shells extends up to 79 cm (Table 3a-IV). The upper boundary of the sand layer is sharp. Above, fining-upward laminated mud extends from 79 to 69 cm. No traces of bioturbation are observed here either. Notably, a large sand clast can be observed from 77 to 73 cm in this core section. Laminations bend around the base of this clast and onlap at both sides. At 70 cm, a sharp contact separates the laminated mud from a massive sand layer that extends up to 67 cm (Table 3a-III). While half of its upper boundary appears transitional, this is likely related to disturbance (smearing) during the sampling procedure. Above 67 cm, laminated sediment prevails up to 56 cm. Interbedded sand layers at 66 cm, from 63 to 62 cm and from 61 to 60 cm show preserved ripple structures, each forming a sharp upper contact. At 56 cm, an erosive unconformity separates the laminated material from a 9 cm thick sand layer. While the lower 4 cm of this sand layer appears massive, clear cross lamination is observed within its upper 5 cm up to 47 cm (Table 3a-II). No shells or bioturbation traces can be observed in the sand layer. At 47 cm, an irregular and erosional contact exists. Above, laminated sediment is present from 47 to 36 cm. In this interval, a massive sand layer, 1 cm in thickness with sharp upper and lower contacts, interbeds at 42 cm. The erosional boundary of the laminated sediment is observed at 36 cm. Mud clasts have been found between 34 and 31 cm (Table 3a-I), with the diameter increasing in the upper layer. Above a transitional boundary, a sand layer rich in shell debris is present between 31 and 29 cm (Table 3a-I). No bioturbation traces are observed within this layer. Above a sharp contact at 29 cm, laminated mud is deposited up to 26 cm. Here, a sand layer 2 cm in thickness is observed above an erosional contact. Its upper, sharp contact at 24 cm is ripple-shaped. Above the contact at 24 cm, laminated material extends up to approximately 6 cm. Single bioturbation traces are observed between 17 and 16 cm core depth. In this interval, no lamination is recognized. Apparently, the deformed features in the upper 13 cm of the core are related to disturbances during coring. A highly irregular boundary from approximately 8 to 6 cm separates the laminated material from more homogeneous sediment that includes a

NHESSD
2, 7225–7267, 2014



few coarser sand grains. Above a sharp boundary at 1 cm, homogeneous fine-grained material is observed.

4.1.2 Core 030310-C2 (Fig. 2)

Core 030310-C2, with a length of 23 cm, was retrieved from silty seafloor at 11.5 m water depth, 3.3 km offshore from the navigational entrance to Thap Lamu harbour (Fig. 1). Due to strong fishing activities with fixed nets, no side-scan sonar surveys could be carried out here.

At the base of this core, between 23 and 17 cm, bioturbated fine sand is observed. Few shells are scattered throughout the layer. A layer composed of coarse sand and gravel, including shells, laterite fragments and coral debris, is separated from the fine sand layer below. A layer composed of muddy fine sand is deposited above, separated by erosional boundaries at 17 cm at the base and at 13 cm at its top (Table 3b-II). Above 13 cm, an 8.5 cm thick layer of muddy fine sand including a few shell fragments is observed. A sharp boundary with an irregular shape – interpreted as a load clast – appears at 4.5 cm (Table 3b-I). At the top of the core, homogeneous silt to fine sand with frequent traces of bioturbation is present.

4.1.3 Core 050310-C4 (Fig. 2)

Core 050310-C4, with a length of 55 cm, was retrieved 6.3 km offshore at a water depth of 15.3 m. The position is located within a patch of silt to fine sand that is surrounded by patches of medium to coarse sand (see Fig. 3c).

Bioturbation traces are recognized in the lowermost 3.5 cm of the core from 55 to 51.5 cm within a silty to sandy material. At 51.5 cm, a layer of coarse sand, 3 cm in thickness, is separated from the sediment above and beneath by sharp erosional contacts. The layer appears massive and small shells are observed (Table 3c-IV). A finer, presumably silty layer is deposited above 48.5 cm. This layer is characterized by the occurrence of a few shells and frequent bioturbation traces. It is separated by a sharp

NHESSD
2, 7225–7267, 2014



contact at 37.5 cm from a 1 cm thick coarse sand layer. Above, a fining-upward sequence of laminated fine-grained sediment is observed from 37.5 to 28.5 cm, but the laminae could not be sampled individually as their thicknesses were too small (from 1 to 5 mm in thickness, Table 3c-III). At 28.5 cm, a sharp but irregular contact – interpreted as load clast – exists. At 24 cm, an erosional contact separates a 7 cm thick layer mainly composed of shells (Table 3c-II). Laminated sediment is found again from 17 to 15 cm. Following a sharp boundary, coarse sediment including shells is deposited above 15 cm (Table 3c-I). Due to disturbances during the sampling procedure in the field, the upper boundary of the layer cannot be clearly recognized. However, based on the abundance of shells, it is likely situated at approximately 2 cm. The upper 2 cm of the core comprises fine-grained sediment with a few bioturbation traces.

4.1.4 Core 030310-C7 (Fig. 2)

Core 030310-C7, with a length of 65 cm, was retrieved from a water depth of 11.9 m, 2.9 km offshore (approximately 4.9 km south of Pakarang Cape) in an area where the seafloor is composed of silty to fine sediment. The boundary between silt- and fine-sand-covered seafloor to coarse sand, gravel and boulders is situated approximately 70 m to the southeast. Granitic outcrops rise approximately 500 m to the east (see Fig. 3d).

At the base of the core, laminated material is fining upward between 65 and 61 cm. At 61 cm, a sharp contact with a 6 cm thick layer composed of coarse sand and occasional gravel exists (Table 3d-VII). However, the layer is not massive and no clear fining-upward or downward trend can be recognized. The layer is draped by a centimetre of muddy material on top. Cross laminations of coarser sediment are identified from light scattering in X-ray images at 54 and 53 cm (Table 3d-VI). A sharp contact has been found at 53 cm that separates a 6 cm thick fining-upward sequence of laminated fine-grained material, which shows no sign of bioturbation traces (Table 3d-V). At 47 cm, an irregular sharp contact separates the laminated sediment from a layer of sand, in which faint indications of cross laminations are observed (Table 3d-IV). At

NHESSD
2, 7225–7267, 2014



the top of the sand layer at 42.5 cm, ripple structures draped by a 0.5 cm thick layer of mud are preserved. Between 42 and 39 cm, a mixture of sand and mud clasts prevails. Above a sharp contact at 39 cm, a 4 cm thick layer comprising coarse sand and pebbles exists. A transitional contact at 35 cm separates a 1 cm thick sand layer from slightly laminated silty fine sediment. A fining-upward sequence of coarse sand, partly pebble-size corals and pebbles exists from 34 to 28 cm (Table 3d-III). Above 28 cm, an 8 cm thick sequence of cross-laminated bedforms is observed with several corals and shells scattered throughout (Table 3d-II). Up to 18 cm, the layer is covered by sand. Above 18 cm, a layer of mixed clasts composed of sand and mud exists, with few shells scattered throughout. Few bioturbation traces are observed at the top of the layer (Table 3d-I).

4.1.5 Core 050310-C2

Core 051207-31, with a length of 70 cm, was retrieved 7.2 km offshore at a water depth of 15.9 m at a boundary of patches that are composed of silt to fine sand and partly coarse sand (Fig. 3e). From sub bottom profiler data, it is known that this position is located in a partly filled incised channel system (Feldens et al., 2012).

At the core-base, laminated fine-grained material exists between 70 and 68 cm (Table 3e-VI). A transitional boundary separates a 2 cm thick layer of massive coarse grains extending from 68 to 66 cm. With transitional lower and upper boundaries, the sediment, mainly composed of muddy sand with a few shells, is fining upwards between 66 and 64 cm. Sediment changes transitionally into a 2.5 cm thick layer of massive coarse sand at approximately 61 cm (Table 3e-V). Above 58.5 cm, the sediment is gradually fining upward. At 53 cm, an erosive contact separates the fining-upward sequence from a 3 cm thick layer comprising pebbles, coarse sand and shell fragments (Table 3e-IV). Laminated material is present above up to 47 cm. A few shells are located within this layer. Following a sharp contact at 47 cm, a coarse, fining-upward sequence is present, capped by a sharp boundary at 45 cm (Table 3e-III). Fining-upward sequences with a sharp boundary composed of pebbles, coarse sand and shell frag-

NHESSD
2, 7225–7267, 2014



ments exist between 41 and 38, 38 and 34.5, 34.5 and 32, 32 and 25, 25 and 20, 20 and 15.5, and 15.5 and 11.5 cm. At 11.5 cm, an erosional contact separates a fining-upward sequence from a layer of shells that forms the upper 10 cm of this core (Table 3e-I).

4.1.6 Core 051207-31

Core 050310-C2, with a length of 75 cm, was collected at a water depth of 9.8 m, located 1.5 km northeast of Pakarang Cape. The seafloor at the sampling position is composed of silt to fine sand (Fig. 3b).

The lower part of the core from 75 to 40 cm comprises a silty matrix with a few corals and abundant shells scattered throughout. Clasts that are a few centimetres in diameter and composed of sand-sized sediment are observed at 72 and 53 cm. A bioturbation trace is found from 63 to 60 cm. Above an erosional contact at 40 cm, a 9 cm thick layer, mainly composed of large shells in a sandy matrix, is observed (Table 3f-III). Above an erosional boundary at 31 cm, laminated mud is observed (Table 3f-II). Between a sharp upper and lower contact, a sand layer in which shells are present extends from 25 to 24 cm. The sand layer is draped by a 1 cm thick layer of fine-grained, laminated sediment. A similar sequence is observed above: a 1 cm thick layer of sand (23 to 22 cm) with a sharp upper and lower boundary is draped by laminated muddy material that reaches up to 14 cm. From 20 to 14 cm, several centimetre-thick clasts composed of sandy material disrupt the laminations (Table 3f-I). Above a sharp contact at 14 cm, a 2 cm thick sequence of likely silty to fine sand material including shell fragments exists. At 12 cm, a 0.5 cm thick homogenous mud layer is draped on the layer beneath. However, it is difficult to determine whether this layer extends along the whole core width, as the left part of the core was disturbed during sampling. Above, a coarser sand layer with a sharp upper contact is deposited from 11.5 to 7.5 cm, which includes pieces of corals and shell fragments. The top of the core (above 7.5 cm core depth) was partly disturbed during sampling, but apparently consists of bioturbated but otherwise homogeneous fine-grained material, with the exception of few sandy clasts with a diameter of 1–5 mm.

NHESSD
2, 7225–7267, 2014



4.2 ^{210}Pb activity and Ti / Ca ratios

The Ti / Ca log ratios in all six cores are stable, with the exception of coarse sediment layers, where Ti / Ca log ratios vary between −2.8 and −0.1 (Fig. 2).

The excess ^{210}Pb activity profile measured in core 030310-C3 (Fig. 4) reveals a general decline of activity with core depth. The activity profile includes intervals of anomalously low activity (e.g. 50 and 68 cm core depth) that correspond to coarser-grained sediments. The average sediment accumulation rate for this core is 1.94 cm yr^{-1}. However, the maximum sediment accumulation rate for the top 20 cm could be as much as 7.5 cm yr^{-1}.

The activity profile of core 050310-C4 (Fig. 4) shows an exponential decrease in the excess ^{210}Pb activity in the sediment above the shell deposit layer in the 19–24 cm core depth range (see Fig. 2 and Table 3c-II). Below 24 cm, the profile approaches the general decline in excess ^{210}Pb activity. The average sediment accumulation rate for the whole core is 0.53 cm yr^{-1}. Using data only from the upper 10 cm, the sedimentation rate is up to 1.73 cm yr^{-1}.

5 Discussion

5.1 Identification of event deposits

The analysed core data allow us to differentiate between three types of event deposits found on the inner shelf offshore from Khao Lak. They are related to (1) flash floods, (2) storms and typhoons, and (3) the 2004 Indian Ocean tsunami.

The majority of the fine-grained, laminated sediments (Figs. 2 and 5 and Table 3) are interpreted as flash flood deposits, which have previously not been described on the Andaman Sea. In general, the most important source from which fine sediment is supplied to accumulate on continental shelves is river discharge (Kuehl et al., 1985; Wright and Nittrouer, 1995; Geyer et al., 2004; Crokett and Nittrouer, 2004; Palinkas et al.,

NHESSD
2, 7225–7267, 2014



2006). River discharge is minor in the investigation area (Jankaew et al., 2008; Feldens et al., 2009; Brill et al., 2011). However, increasing anthropogenic activities during the last century, such as tin mining, construction of tourist resorts, deforestation, agriculture and urbanization, all cause river discharge due to increased exposure weathering and the erosion of fine sediment (Wolanski and Spagnol, 2000). In the course of flash floods during the southwest monsoon (rainy season), these fine sediments will be subsequently transported through ephemeral channels towards the ocean (e.g. Curran et al., 2002; Mulder et al., 2003; Malmon et al., 2004; Owen, 2005). Enhanced sedimentation due to anthropogenic impacts was observed in different settings such as tropical estuaries in Papua New Guinea, Vietnam, Australia and Indonesia (Wolanski and Spagnol, 2000); the Pearl River in Hong Kong (Owen and Lee, 2004; Owen, 2005); and the Waiapu River in New Zealand (Wadman and McNinch, 2008). Offshore from Khao Lak, Feldens et al. (2012) found fine-grained sediments deposited above 15 m water depth that were composed of silt and fine sand and orientated parallel to the shoreline. These fine sediments offshore from Khao Lak, which show little cohesiveness due to a high percentage of coarse silt and fine sand, have been deposited during a multitude of small-scale events (Table 3a-V, 3c-III, 3d-V, 3e-VI and Fig. 5). In the X-ray images, these deposits are recognized as laminated sections of mud, silt and fine sand. Regular reworking and re-deposition from suspension is indicated by the frequent occurrence of fining-upward sequences, showing a lack of bioturbation that may be explained by high accumulation rates, which are expected during flash floods (Wheatcroft et al., 2008). Notable is the frequent occurrence of thin sand layers less than 1 cm in thickness with sharp upper and lower boundaries that are within the laminated core sections in core 051207-31. Based on side-scan sonar images, this core is situated close to a boundary of fine and coarse sediment (Fig. 3). The transport of sand into areas covered by finer sediment in the range of annual cycles without exceptional storm events was demonstrated by repeated side-scan sonar mapping offshore from Khao Lak (Feldens et al., 2012).

NHESSD
2, 7225–7267, 2014



Layers showing parts of the characteristics of proximal tempestites are frequent in the X-ray images (Figs. 2 and 5), including sharp and partly erosional lower contacts, preserved cross laminations, ripples and graded-bedded sand without mud content, which therefore follow the characteristics of proximal tempestites (Einsele, 1991). Storms influence the sedimentary record due to oscillatory water movements caused by waves, with the shear stress imposed on seafloor sediments decreasing with increasing water depth (Weidong et al., 1997; Allison et al., 2005). The Andaman Shelf is seldom affected by severe storms and typhoons (see Table 1), which commonly form in the South China Sea during the northeast monsoon (data compiled by TMD, 2014). Storms lose their energy while crossing the Thai-Malay continent. In contrast, cyclone tracks originating within the Bay of Bengal are predominantly directed towards the coast of India, Bangladesh and Myanmar (Singh et al., 2000). Based on ^{210}Pb activity, several proposed event deposits in the cores 030310-C3 and 050310-C4 have ages of less than 50 years but are older than the 2004 Indian Ocean tsunami. During the time interval from 1945 to 1996, only nine historical tropical storms passed the investigation area (Table 1). Using the estimated accumulation (based on ^{210}Pb dating) rates of 0.54 to 1.9 cm yr^{-1} for the inner continental shelf, the event layers within 47–62 cm depth have ages of 20 to 30 years. Therefore, they are likely related to Typhoon Gay, which hit this area in 1989. Similarly, core depths from 68 to 70 cm depth correspond to Tropical Storm Sally (1972) or Tropical Depression Sarah (1973). Tropical depressions from the 1960s (Harriet, Lucy and Gloria) may correspond to the event layers from 78 to 82 cm. In core 030310-C7, one event layer extends between 42.5 and 45.5 cm, which is separated from the most recent event layer above by a mud drape. While no age control exists, this layer likely resulted from Tropical Storm Forrest (1992) or tropical depression Manny (1993) or Ernie (1996). Several event layers in the upper part of the cores (layers A, B and C, Table 4 and Fig. 5) are different from the event layers beneath, which are attributed to storm events. They show a larger variability, ranging from 10 cm thick shell deposits to muddy deposits including coarse sand grains, laterites and shell debris to mud deposits including clasts of various compositions. Based on

NHESSD
2, 7225–7267, 2014



the sediment accumulation rates in cores 030310-C3 and 050310-C4, the layers are located between sediments that have been deposited within the last few years (Fig. 4). Due to the absence of large storm events, they have been most likely deposited by the 2004 Indian Ocean tsunami. It is assumed that the event layers at similar core depths within the other cores have been deposited during the 2004 Indian Ocean tsunami as well.

5.2 Identification and features of the tsunami facies

Event deposits attributed to the 2004 Indian Ocean tsunami based on ^{210}Pb dating are grouped into three facies (Table 4 and Fig. 5) representing the variable characteristics of offshore tsunami deposits. They are characterized by sand enriched with shells or shell debris (A), cross lamination (B) and massive layers (C).

Except in core 030310-C3, the observed tsunami deposit sequences show sand enriched with shells or shell debris (facies A) at their base. Seafloor dominated by shells, coral rubble and sand is frequent between 15 and 20 m water depth offshore from Khao Lak (Feldens et al., 2012). Therefore, this layer is likely to be eroded during the propagation of tsunami waves from the open ocean to shallow waters. A marine origin of these deposits is also supported by generally lower Ti / Ca ratios in the massive sand layer compared to the surrounding muddy layers (Fig. 2). Foraminifera transfer functions that developed for the suspected tsunami deposits support a transport of facies A material from these water depths (Milker et al., 2013). A depth of approximately 20 m is substantially lower compared to the depths found during previous studies of tsunami impacts based on wave theory and the analysis of microfossils (e.g. Nanayama and Shigeno, 2006; Weiss and Bahlburg, 2006; Weiss, 2008; Uchida et al., 2010). It is unknown whether the local shelf morphology offshore from Khao Lak prohibited the substantial erosion of material from deeper waters or whether the sediments transported onshore from deeper waters were not preserved. As no storm event occurred between the 2004 tsunami and the time of sampling, the latter appears unlikely, sug-

NHESSD
2, 7225–7267, 2014



gesting that the tsunami deposits offshore from Khao Lak are in fact limited to shallow water depths.

Sediments from facies type A are mostly covered by massive deposits commonly including mud or sand clasts (tsunami deposit facies type C); however, an inverted sequence is found in core 030310-C3. Sediments from facies type C are assumed to be created out of a hyperpycnal tsunami backwash flow (Goff et al., 2004; Morton et al., 2007; Goodman-Tchernov et al., 2009; Sakuna et al., 2012). Accordingly, facies type C is frequently found in the uppermost part of the tsunami sequence and includes material transported during the backwash, as shown by foraminifera indications (Milker et al., 2013) and the presence of laterites and grass (Feldens et al., 2012; Sakuna et al., 2012). The Ti / Ca ratios are not noticeably different from the inferred flash floods deposits, which have to originate from onshore. Tsunami facies type C is not observed within all the cores. The absence of backwash deposits in cores 051207-31 and 050310-C2 may be related to subsequent erosion, with flash flood deposits observed directly on top of the tsunami deposits in core 050310-C2 and the tsunami deposits exposed at the seafloor in core 051207-31. Within core C3, an inverted sequence is observed, which may be explained by several waves approaching the coastline.

Intensive cross bedding, only observed within core 030310-C7, characterizes tsunami facies type B, which is located between facies type A and type C. It may be assumed that the cross bedding is related to multiple flow reversals between the run-up and backwash of the three wave trains approaching the coastline during the 2004 tsunami event (e.g. Siripong, 2006). Cross bedding is a common feature for onshore tsunami deposits, where it was widely used to indicate the hydrodynamic regime during the deposition (Dawson et al., 1996; Nanayama et al., 2000; Goff et al., 2001; Bahlburg and Weiss, 2007; Engel and Brückner, 2011).

NHESSD
2, 7225–7267, 2014



5.3 Comparison of tsunami, storm and flash flood facies

On the Andaman Sea shelf, the presence of deposits related to tsunami, tropical storms and annual flash floods during the summer monsoon season allows us to compare the sedimentary signatures of these events at the same offshore location. The distinction of tsunami deposits from those deposited by other high-energy events, such as storms or hurricanes, are still problematic, even for deposits on land (Nanayama et al., 2000; Kortekaas and Dawson, 2007; Morton et al., 2007; Switzer and Jones, 2008; Phantuwongraj and Choowong, 2011). Previous studies proved that a series of proxies must be applied, e.g. the geomorphological setting, sedimentary structures, microfossil assemblages and geochemical components (Goff et al., 2004, 2010; Kortekaas and Dawson, 2007; Morton et al., 2007; RamÍrez-Herrera et al., 2012; Chagué-Goff et al., 2011; Richmond et al., 2011; Sakuna et al., 2012). The different signatures of the identified event deposits have been summarized in Table 5. In particular, the differentiation between tsunami facies type A and storm deposits appears to be problematic. Storms raise water levels due to their low atmospheric pressure and cause coastal flooding (Ogston et al., 2000; Harris and Heap, 2009). Sediment is kept in suspension and deposited with waning energy levels. This results in deposits of graded sand, frequently showing cross bedding. Wave ripple marks draped with mud are frequently only preserved at the top of the storm deposit sequence (Weidong et al., 1997). While a tsunami event may comprise several waves, thus allowing the deposition of several mud drapes, it is expected that later waves erode the previously deposited mud drapes. Distinct lamina of shells and their fragments are common in storm deposits, most likely because of high-frequency waves (Morton et al., 2007), and have also been observed in tsunami deposits offshore from Khao Lak (this study). Therefore, taken by themselves, neither the observed cross-laminated sections nor the presence of sand rich in shells or shell debris is suitable as a proxy to distinguish tsunami and storm deposits. In contrast, rip-up clasts (both mud and sand clasts, facies type C) were previously used to discriminate storm and tsunami deposits (e.g. Morton et al., 2007; Phantuwongraj and

NHESSD
2, 7225–7267, 2014



Choowong, 2011), as were terrestrial components and anthropogenic artefacts. The backwash transports a variety of material from the hinterland towards offshore, and the high-density backwash flows support the formation of clasts (Dawson and Stewart, 2007; Morton et al., 2007; Shanmugam, 2011; RamÍrez-Herrera et al., 2012). In contrast, erosion during storms is focused on the shoreface and the beach (Snedden et al., 1988; Allison et al., 2005); thus, clasts and terrestrial material are expected to appear less frequently within storm deposits. This highlights the importance of material deposited during the tsunami backwash for the identification of past tsunami events. Further proxies using the increased occurrence of terrestrial material for the discrimination of offshore tsunami and storm deposits could be plants, anthropogenic material (for recent events), or geochemical proxies, such as polycyclic aromatic hydrocarbon (PAH) (Tipmanee et al., 2012) or microfossils (Milker at al., 2013). Tsunami backwash deposits have to be differentiated from flash floods, which can also deposit terrigenous material out of hyperpycnal density flows (Mulder et al., 2003; Bourrin et al., 2008). In fact, little difference exists in the Ti / Ca ratios between flash flood and tsunami deposits offshore from Pakarang Cape. However, flash floods differ from the identified tsunami deposits sedimentologically: they are generally better sorted than tsunami deposits and include less sand, likely relating to the higher energy of the tsunami backwash flow. The higher energy of the backwash flow is further reflected by the generally sharp and erosional boundaries of the backwash deposits, while flash flood deposits show transitional boundaries. Additionally, mud clasts are absent in the observed flash flood deposits. However, no major river outlets exist close to the investigation area, with flash floods flowing into the ocean through a number of ephemeral channels. It is suggested that channelized flash flood deposits are more difficult to distinguish from tsunami deposits.

NHESSD
2, 7225–7267, 2014



6 Conclusions

On the Andaman Sea continental shelf, tsunami, storm and flash flood deposits have been preserved in close vicinity to each other, allowing us to compare their sedimentological characteristics. Flash flood deposits comprise laminated, fining-upward mud with occasional shell fragments. Large storm or typhoon deposits show typically sharp and partly erosional lower contacts and are composed of rippled, cross-laminated and graded sand without mud. The 2004 Indian Ocean tsunami left three different sedimentary facies, including (1) sand enriched in shell and shell debris, (2) cross-bedded sand, and (3) layers including mud and sand clasts. From this study, the most prominent difference between the storm and tsunami deposits offshore from Khao Lak area is the presence of terrestrial components, anthropogenic artefacts and mud in the latter.

Acknowledgements. The authors wish to thank the Phuket Marine Biological Center (PMBC) for supporting us with ship time of RV *Chakratong Tongyai* and RV *Boonlert Pasook* as well as with other facilities during field campaigns. This study was funded through Deutsche Forschungsgemeinschaft (DFG) grant SCHW 572/11, the National Research Council of Thailand (NRCT) and the DAAD (Deutscher Akademischer Austausch Dienst) fellowship provided to Daroonwan Sakuna-Schwartz for a PhD study at Kiel University.

References

Abrantes, F., Alt-Epping, U., Lebreiro, S., Voelker, A., and Schneider, R.: Sedimentological record of tsunamis on shallow-shelf areas, The case of the 1969 AD and 1755 AD tsunamis on the Portuguese Shelf off Lisbon, Mar. Geol., 249, 283–293, 2008.

Allison, M. A., Sheremet, A., Goñi, M. A., and Stone, G. W.: Storm layer deposition on the Mississippi-Atchafalaya subaqueous delta generated by Hurricane Lili in 2002, Cont. Shelf Res., 25, 2213–2232, 2005.

Bahlburg, H. and Weiss, R.: Sedimentology of the December 26, 2004, Sumatra tsunami deposits in eastern India (Tamil Nadu) and Kenya, Int. J. Earth Sci., 96, 1195–1209, 2007.

Bahr, A., Lamy, F., Arz, H., Kuhlmann, H., and Wefe, G.: Late glacial to Holocene climate and sedimentation history in the NW Black Sea, Mar. Geol., 214, 309–322, 2005.

NHESSD

2, 7225–7267, 2014



Best, A. I. and Gunn, D. E.: Calibration of marine sediment core loggers for quantitative acoustic impedance studies, Mar. Geol., 160, 137–146, 1999.
Blott, S. J. and Pye, K.: Gradistat, a grain-size distribution and statistics package for the analysis of unconsolidated sediments, Earth Surf. Proc. Land., 26, 1237–1248, 2001.
Bourrin, F., Friend, P. L., Amos, C. L., Manca, E., Ulses, C., Palanques, A., Durrieu de Madron, X., and Thompson, C. E. L.: Sediment dispersal from a typical Mediterranean flood, the Têt River, Gulf of Lions, Cont. Shelf Res., 28, 1895–1910, 2008.
Brill, D., Brückner, H., Jankaew, K., Kelletat, D., Scheffers, A., and Scheffers, S.: Potential predecessors of the 2004 Indian Ocean Tsunami – sedimentary evidence of extreme wave events at Ban Bang Sak, SW Thailand, Sediment. Geol., 239, 146–161, 2011.
Brill, D., Pint, A., Jankaew, K., Frenzel, P., Schwarzer, K., Vött, A., and Brückner, H.: Sediment transport and hydrodynamic parameters of tsunami waves recorded in offshore Geoarchives – a case study from Thailand, J. Coastal Res., 30, 922–941, doi:10.2112/JCOASTRES-D-13-00206.1, 2014a.
Brill, D., Jankaew, K., Neubauer, N. P., Kelletat, D., Scheffers, A., Vött, A., and Brückner, H.: Holocene coastal evolution of southwest Thailand – implications for the site-specific preservation of palaeotsunami deposits, Z. Geomorphol., 58, 273–303, doi:10.1127/0372-8854/2014/0132, 2014b.
Cantalamessa, G. and Celma, C. D.: Sedimentary features of tsunami backwash deposits in a shallow marine Miocene setting, Mejillones Peninsula, northern Chile, Sediment. Geol., 178, 259–273, 2005.
Chagué-Goff, C., Schneider, J. L., Goff, J. R., Dominey-Howes, D., and Strotz, L.: Expanding the proxy toolkit to help identify past events – lessons from the 2004 Indian Ocean Tsunami and the 2009 South Pacific Tsunami, Earth-Sci. Rev., 107, 107–122, doi:10.1016/j.earscirev.2011.03.007, 2011.
Chavanich, S., Siripong, A., Sojisuporn, P., and Menasaveta, P.: Impact of tsunami on the seafloor and corals in Thailand, Coral Reefs, 24, 535p., 2005.
Cheng, W. and Weiss, R.: On sediment extent and runup of tsunami waves, Earth Planet. Sc. Lett., 362, 305–309, 2013.
Choowong, M., Murakoshi, N., Hisada, K., Charusiri, P., Daorerk, V., Charoentitirat, T., Chutakositkanon, V., Jankaew, K., and Kanjanapayont, P.: Erosion and deposition by the 2004 Indian Ocean Tsunami in Phuket and Pang-nga Provinces, Thailand, J. Coastal Res., 23, 1270–1276, 2007.

NHESSD
2, 7225–7267, 2014



Choowong, M., Phantuwongraj, S., Charoentitirat, T., Chutakositkanon, V., Yumuang, S., and Charusiri, P.: Beach recovery after 2004 Indian Ocean Tsunami from Phang-nga, Thailand, Geomorphology, 104, 134–142, 2009.

Colin, C., Turpin, L., Bertaux, J., Desprairies, A., and Kissel, C.: Erosional history of the Himalayan and Burman ranges during the last two glacial–interglacial cycles, Earth Planet. Sc. Lett., 171, 647–660, 1999.

Crokett, J. S. and Nittrouer, C. A.: The sandy inner shelf as a repository for muddy sediment, an example from Northern California, Cont. Shelf Res., 24, 55–73, 2004.

Curran, K. J., Hill, P. S., and Milligan, T. G.: Fine-grained suspended sediment dynamics in the Eel River flood plume, Cont. Shelf Res., 22, 2537–2550, 2002.

Cutter Jr, G. R. and Diaz, R. J.: Biological alteration of physically structured flood deposits on the Eel margin, northern California, Cont. Shelf Res., 20, 235–253, 2000.

Dartnell, P. and Gardner, J. V.: Predicting seafloor facies from multibeam bathymetry and backscatter data, Photogramm. Eng. Rem. S., 70, 1081–1091, 2004.

Dawson, A. G. and Stewart, I.: Tsunami deposits in the geological record, Sediment. Geol., 200, 166–183, 2007.

Dawson, A. G., Shi, S., Dawson, S., Takahashis, T., and Shutos, N.: Coastal sedimentation associated with the June 2nd and 3rd, 1994, tsunami in Rajegwesi, Java, Quaternary Sci. Rev., 15, 901–912, 1996.

Di Geronimo, I., Choowong, M., and Phantuwongraj, S.: Geomorphology and superficial bottom sediments of KhaoLak coastal area (SW Thailand), Pol. J. Environ. Stud., 18, 111–121, 2009.

Einsele, G., Ricken, W., and Seilacher, A. (Eds.): Cycles and Events in Stratigraphy, Springer-Verlag, Berlin, Heidelberg, New York, 955 pp., 1991.

Engel, M. and Brückner, H.: The identification of palaeo-tsunami deposits – a major challenge in coastal sedimentary research, Coastline Rep., 17, 65–80, 2011.

Feldens, P., Schwarzer, K., Szczuciński, W., Stattegger, K., Sakuna, D., and Somgpongchaiykul, P.: Impact of 2004 Tsunami on seafloor morphology and offshore sediments, Pakarang Cape, Thailand, Pol. J. Environ. Stud., 18, 63–68, 2009.

Feldens, P., Schwarzer, K., Sakuna, D., Szczuciński, W., and Somgpongchaiykul, P.: Identification of offshore tsunami deposits on the shelf off KhaoLak (Thailand), Earth Planets Space, 64, 875–887, 2012.

NHESSD
2, 7225–7267, 2014



Fujiwara, O. and Kamataki, T.: Identification of tsunami deposits considering the tsunami waveform, an example of subaqueous tsunami deposits in Holocene shallow bay on southern Bobo Penisular, Central Japan, Sediment. Geol., 200, 295–313, 2007.
Geyer, W. R., Hill, P. S., and Kineke, G. C.: The transport, transformation and dispersal of sediment by buoyant coastal flows, Cont. Shelf Res., 24, 927–949, 2004.
Goff, J., Chagué-Goff, C., and Nichol, S.: Paleotsunami deposits, a New Zealand perspective, Sediment. Geol., 143, 1–6, 2001.
Goff, J., McFadgen, B. G., and Chagué-Goff, C.: Sedimentary differences between the 2002 Easter storm and the 15th-century Okoropunga tsunami, southeastern North Island, New Zealand, Mar. Geol., 204, 235–250, 2004.
Goodman-Tchernov, B. N., Dey, H. W., Reinhard, E. G., McCoy, F., and Mart, Y.: Tsunami waves generated by the Santorini eruption reached Eastern Mediterranean shores, Geology, 37, 943–946, 2009.
Goto, K., Chavanich, S. A., Imamura, F., Kunthasap, P., Matsui, T., Minoura, K., Sugawara, D., and Yanagisawa, H.: Distribution, origin and transport process of boulders deposited by the 2004 Indian Ocean Tsunami at Pakarang Cape, Thailand, Sediment. Geol., 202, 821–837, 2007.
Goto, K., Takahashi, J., Oie, T., and Imamura, F.: Remarkable bathymetric change in the nearshore zone by the 2004 Indian Ocean Tsunami, Kirinda Harbor, Sri Lanka, Geomorphology, 127, 107–116, 2011.
Goto, K., Hashimoto, K., Sugawara, D., Yanagisawa, H., and Abe, T.: Spatial thickness variability of the 2011 Tohoku-oki tsunami deposits along the coastline of Sendai Bay, Mar. Geol., doi:10.1016/j.margeo.2013.12.015, in press, 2014.
Grzelak, K., Kotwicki, L., and Szczuciński, W.: Monitoring of sandy beach meiofaunal assemblages and sediments after the 2004 Tsunami in Thailand, Pol. J. Environ. Stud., 18, 43–51, 2009.
Harris, P. T. and Heap, A. D.: Cyclone-induced net sediment transport pathway on the continental shelf of tropical Australia inferred from reef talus deposits, Cont. Shelf Res., 29, 2011–2019, 2009.
Hill, P. S., Milligan, T. G., and Geyer, W. R.: Controls on effective settling velocity of suspended sediment in the Eel River flood plume, Cont. Shelf Res., 20, 2095–2111, 2000.
Hofmann, D. I., Fabian, K., Schneider, F., Donner, B., and Bleil, U.: A stratigraphic network across the Subtropical Front in the central South Atlantic, Multi-parameter correlation of mag-

NHESSD
2, 7225–7267, 2014



netic susceptibility, density, X-ray fluorescence and $\delta^{18}O$ records, Earth Planet. Sc. Lett., 240, 694–709, 2005.
Hylleberg, J., Nateewathana, A., and Chatananthawej, B.: Temporal changes in the macrobenthos on the west coast of Phuket Island, with emphasis on the effects of offshore tin mining, Phuket Mar. Biol. Cent. Res. Bull., 37, 1–16, 1985.
ICES: Sediment dynamics in relation to sediment trend monitoring, ICES Cooperative Research Report No. 308, International Council for the Exploration of the Sea, Copenhagen, Denmark, 34 pp., 2011.
Jankaew, K., Atwater, B. F., Sawai, Y., Choowong, M., Charoentitirat, T., Martin, M. E., and Prendergast, A.: Medieval forewarning of the 2004 Indian Ocean Tsunami in Thailand, Nature, 455, 1228–1231, 2008.
Kale, V. S.: Geomorphic effects of monsoon floods on Indian rivers, Nat. Hazards, 28, 65–84, 2003.
Khokiattiwong, S., Limpsaichol, P., Petpiroon, S., Sojisuporn, P., and Kjerfve, B.: Oceanographic variations in Phangnga Bay, Thailand under monsoonal effects, Phuket Mar. Biol. Cent. Res. Bull., 55, 43–76, 1991.
Kortekaas, S. and Dawson, A. G.: Distinguishing tsunami and storm deposits, an example from Martinhal, SW Portugal, Sediment. Geol., 200, 208–221, 2007.
Krumbein, W. C.: Size frequency distribution of sediments and the normal phi curve, J. Sediment. Petrol., 8, 84–90, 1938.
Kuehl, S. A., Nittrouer, C. A., Allison, M. A., Ercilio, L., Faria, C., Dukat, D. A., Jaeger, J. M., Pacioni, T. D., Figueiredo, A. G., and Underkoffler, E. C.: Sediment deposition, accumulation, and seabed dynamics in an energetic, fine-grained, coastal environment, Cont. Shelf Res., 16, 787–815, 1985.
Lamy, F., Hebbeln, D., Röhl, U., and Wefer, G.: Holocene rainfall variability in southern Chile, a marine record of latitudinal shifts of the Southern Westerlies, Earth Planet. Sc. Lett., 185, 369–382, 2001.
Lario, J., Luque, L., Zazo, C., Goy, J. L., Spencer, C., Cabero, A., Bardají, T., Borja, F., Dabrio, C. J., Civis, J., González-Delgado, J. A., Borja, C., and Alonso-Azcárate, J.: Tsunami vs. storm surge deposits, a review of the sedimentological and geomorphological records of extreme wave events (EWE) during the Holocene in the Gulf of Cadiz, Spain, Z. Geomorphol., 54, 301–316, 2010.

NHESSD
2, 7225–7267, 2014



Le Roux, J. P. and Vargas, G.: Hydraulic behavior of tsunami backflows, insights from their modern and ancient deposits, Environ. Geol., 49, 65–75, 2005.
Lorang, M. S.: A wave-competence approach to distinguish between boulder and megaclast deposits due to storm waves versus tsunamis, Mar. Geol., 283, 90–97, 2011.
Malmon, D. V., Reneau, S. L., and Dunne, T.: Sediment sorting and transport by flash floods, J. Geophys. Res.-Earth, 109, 1–13, 2004.
Martin, A. J.: Flaser and wavy bedding in ephemeral streams, a modern and an ancient example, Sediment. Geol., 136, 1–5, 2000.
McKee, B. A., Nittrouer, C. A., and DeMaster, D. J.: The concepts of sediment deposition and accumulation applied to the continental shelf near the mouth of the Yangtze River, Geology, 11, 631–633, 1983.
Milker, Y., Wilken, M., Schumann, J., Sakuna, D., Feldens, P., Schwarzer, K., and Schmiedl, G.: Sediment transport on the inner shelf off Khao Lak (Andaman Sea, Thailand) during the 2004 Indian Ocean Tsunami and former storm events: evidence from foraminiferal transfer functions, Nat. Hazards Earth Syst. Sci., 13, 3113–3128, doi:10.5194/nhess-13-3113-2013, 2013.
Milkert, D.: Auswirkungen von Stürmen auf die Schlicksedimente der westlichen Ostsee, Ber.-Rep., Geol.-Paläont. Inst., Univ. Kiel, Kiel, 66, 153 pp., 1995.
Morton, R. A., Gelfenbaum, G., and Jaffe, B. E.: Physical criteria for distinguishing sandy tsunami and storm deposits using modern examples, Sediment. Geol., 200, 184–207, 2007.
Mulder, T., Syvitski, J. P. M., Migeon, S., Faugères, J. C., and Savoye, B.: Marine hyperpycnal flows: initiation, behavior and related deposits: a review, Mar. Petrol. Geol., 20, 861–882, 2003.
Nanayama, F. and Shigeno, K.: Inflow and outflow facies from the 1993 tsunami in southwest Hokkaido, Sediment. Geol., 187, 139–158, 2006.
Nanayama, F., Shigeno, K., Satake, K., Shimokaka, K., Koitabashi, S., Miyasaka, S., and Ishii, M.: Sedimentary differences between the 1993 Hokkaido-nansei-oki tsunami and the 1959 Miyakojima typhoon at Taisei, southwestern Hokkaido, northern Japan, Sediment. Geol., 13, 255–264, 2000.
Nott, J. F.: Waves, boulders and the importance of the pre-transport setting, Earth Planet. Sc. Lett., 210, 269–276, 2003.

NHESSD
2, 7225–7267, 2014



Ogston, A. S., Cacchione, D. A., Sternberg, R. W., and Kineke, G. C.: Observations of storm and river flood-driven sediment transport on the northern California continental shelf, Cont. Shelf Res., 20, 2141–2162, 2000.
Ohta, T. and Arai, H.: Statistical empirical index of chemical weathering in igneous rocks, a new tool for evaluating the degree of weathering, Chem. Geol., 240, 280–297, 2007.
Owen, R. B. and Lee, R.: Human impacts on organic matter sedimentation in a proximal shelf setting, Hong Kong, Cont. Shelf Res., 24, 583–602, 2004.
Palinkas, C. M., Nittrouer, C. A., and Walsh, J. P.: Inner shelf sedimentation in the Gulf of Papua, New Guinea, a mud-rich shallow shelf setting, J. Coastal Res., 22, 760–772, 2006.
Paris, R., Fournier, J., Poizot, E., Etienne, S., Mortin, J., Lavigne, F., and Wassmer, P.: Boulder and fine sediment transport and deposition by the 2004 tsunami in LhokNga (western Banda Aceh, Sumatra, Indonesia), a coupled offshore-onshore model, Mar. Geol., 268, 43–54, 2010.
Phantuwongraj, S. and Choowong, M.: Tsunamis versus storm deposits from Thailand, Nat. Hazards, 63, 31–50, 2012.
Postma, G.: Physical climate signatures in shallow- and deep-water deltas, Global Planet. Change, 28, 93–106, 2001.
Ramaswamy, V., Rao, P. S., Rao, K. K., Swe Thwin, Rao, N. S., and Raiker, V.: Tidal influence on suspended sedimen distribution and dispersal in the northern Andaman Sea and Gulf Martaban, Mar. Geol., 208, 33–42, 2004.
Ramírez-Herrera, M.-T., Lagos, M., Hutchinson, I., Kostoglodov, V., Machain, M. L., Caballero, M., Goguitchaichvili, A., Aguilar, B., Chagué-Goff, C., Goff, J., Ruiz-Fernández, A.-C., Ortiz, M., Nava, H., Bautista, F., Lopez, G. I., and Quintana, P.: Extreme wave deposits on the Pacific coast of Mexico, tsunamis or storms? – a multi-proxy approach, Geomorphology, 139–140, 360–371, 2012.
Richmond, B. M., Watt, S., Buckley, M., Jaffe, B. E., Gelfenbaum, G., and Morton, R. A.: Recentstorm and tsunami coarse-clast deposit characteristics, southeast Hawaii, Mar. Geol., 283, 79–89, 2011.
Robbins, J. A. and Edgington, D. N.: Determination of recent sedimentation rates in Lake Michigan using Pb-210 and Cs-137, Geochim. Cosmochim. Acta, 39, 285–304, 19775.
Rodolfo, K. S.: Bathymetry and marine geology of the Andaman Basin, and tectonic implications for Southeast Asia, Geol. Soc. Am. Bull., 80, 1203–1230, 1969.

NHESSD
2, 7225–7267, 2014



Rose, L. E. and Kuehl, S. A.: Recent sedimentation patterns and facies distribution on the Poverty Shelf, New Zealand, Mar. Geol., 270, 160–174, 2010.
Sakuna, D., Szczuciński, W., Feldens, P., Schwarzer, K., and Khokiattiwong, S.: Sedimentary deposits left by the 2004 Indian Ocean Tsunami on the inner continental shelf offshore of KhaoLak, Andaman Sea (Thailand), Earth Planets Space, 64, 931–943, 2012.
Schwab, J. M., Krastel, S., Grün, M., Gross, F., Pananont, P., Jintasaeranee, P., Bunsomboonsakul, S., Weinrebe, W., and Winkelmann, D.: Submarine mass wasting and associated tsunami risk offshore western Thailand, Andaman Sea, Indian Ocean, Nat. Hazards Earth Syst. Sci., 12, 2609–2630, doi:10.5194/nhess-12-2609-2012, 2012.
Shanmugam, G.: Process-sedimentological challenges in distinguishing paleo-tsunami deposits, Nat. Hazards, 63, 5–30, doi:10.1007/s11069-011-9766-z, 2011.
Singh, O. P., Ali Khan, T. M., and Rahman, M. S.: Changes in the frequency of tropical cyclones over the North Indian Ocean, Meteorol. Atmos. Phys., 75, 11–20, 2000.
Siripong, A.: Andaman Sea coast of Thailand field survey after the December 2004 Indian Ocean Tsunami, Earthq. Spectra, 22, 187–202, 2006.
Smedile, A., De Martini, P. M., Pantosti, D., Bellucci, L., Del Carlo, P., Gasperini, L., Pirrotta, C., Polonia, A., and Boschi, E.: Possible tsunami signatures from an integrated study in the Augusta Bay offshore (Eastern Sicily-Italy), Mar. Geol., 281, 1–13, 2011.
Sommerfield, C. K. and Nittrouer, C. A.: Modern accumulation rates and sediment budget for the Eel shelf, a flood-dominated depositional environment, Mar. Geol., 154, 227–241, 1999.
Sommerfield, C. K., Drake, D. E., and Wheatcroft, R. A.: Shelf record of climatic changes in flood magnitude and frequency, north-coastal California, Geology, 30, 395–398, 2002.
Spiske, M., Piepenbreier, J., Benavente, C., and Bahlburg, H.: Preservation potential of tsunami deposits on arid siliciclastic coasts, Earth-Sci. Rev., 126, 58–73, 2013.
Spiske, M., Bahlburg, H., and Weiss, R.: Pliocene mass failure deposits mistaken as submarine tsunami backwash sediments – an example from Hornitos, Northern Chile, Sediment. Geol., 305, 69–82, doi:10.1016/j.sedgeo.2014.03.003, 2014.
Sugawara, D., Minoura, K., Nemoto, N., Tsukawaki, S., Goto, K., and Imamura, F.: Foraminiferal evidence of submarine sediment transport and deposition by backwash during the 2004 Indian Ocean Tsunami), Isl. Arc, 18, 513–525, 2009.
Switzer, A. D. and Jones, B. G.: Large-scale washover sedimentation in a freshwater lagoon from the southeast Australian coast, sea-level change, tsunami or exceptionally large storm?, Holocene, 18, 787–803, 2008.

NHESSD
2, 7225–7267, 2014



Szczuciński, W., Chaimanee, N., Niedzielski, P., Rachlewicz, G., Saisuttichai, D., Tepsuwan, T., Lorenc, S., and Siepak, J.: Environmental and geological impacts of the 26 December 2004 Tsunami in coastal zone of Thailand – overview of short and long-term effects, Pol. J. Environ. Stud., 15, 793–810, 2006.

Thai Meteorological Department (TMD): Tropical cyclones moving through Thailand during 63 years (1951–2013), available at: www.tmd.go.th/programs%5Cuploads%5Ccyclones%5CTC_track_63y_n.pdf (last access: 30 November 2014), 2014.

Thampanya, U., Vermaat, J. E., Sinsakul, S., and Panapitukkul, N.: Coastal erosion and mangrove progradation of Southern Thailand, Estuar. Coast. Shelf S., 68, 75–85, 2006.

Tipmanee, D., Deelaman, W., Pongpiachan, S., Schwarzer, K., and Sompongchaiyakul, P.: Using Polycyclic Aromatic Hydrocarbons (PAHs) as a chemical proxy to indicate Tsunami 2004 backwash in Khao Lak coastal area, Thailand, Nat. Hazards Earth Syst. Sci., 12, 1441–1451, doi:10.5194/nhess-12-1441-2012, 2012.

Tjallingii, R., Stattegger, K., Wetzel, A., and Phach, P. V.: Infilling and flooding of the Mekong River incised valley during deglacial sea-level rise, Quaternary Sci. Rev., 29, 1432–1444, 2010.

Typhoon Havens Handbook: Tropical cyclones affecting Phuket, available at: http://www.nrlmry.navy.mil/port_studies/thh-nc/thailand/phuket/text/frame.htm, last access: 22 November 2014.

Uchida, J. I., Fujiwara, O., Hasegawa, S., and Kamataki, T.: Sources and depositional processes of tsunami deposits, analysis using foraminiferal tests and hydrodynamic verification, Isl. Arc, 19, 427–442, 2010.

Umitsu, M., Tanavud, C., and Patanakanog, B.: Effects of landforms on tsunami flow in the plains of Banda Aceh, Indonesia, and Nam Khem, Thailand, Mar. Geol., 242, 141–153, 2007.

Usiriprisan, C., Chiemchindaratana, S., Shoosuwan, S., and Chatrapakpong, Y.: Offshore exploration for tin and heavy minerals in the Andaman Sea, Department of Mineral Resources, Bangkok, UNDP, New York, 224 pp., 1987.

van den Bergh, G. D., Boer, W., de Haas, H., van Weering, T. C. E., and van Wijhe, R.: Shallow marine tsunami deposits in Teluk Banten (NW Java, Indonesia), generated by the 1883 Krakatau eruption, Mar. Geol., 197, 13–34, 2003.

NHESSD
2, 7225–7267, 2014



Weber, M. E., Niessen, F., Kuhn, G., and Wiedicke, M.: Calibration and application of marine sedimentary physical properties using a multi-sensor core logger, Mar. Geol., 136, 151–172, 1997.

Weidong, D., Baoguo, Y., and Xiaogen, W.: Studies of storm deposits in China, a review, Cont. Shelf Res., 17, 1645–1658, 1997.

Weiss, R.: Sediment grains moved by passing tsunami waves, tsunami deposits in deep water, Mar. Geol., 250, 251–257, 2008.

Weiss, R. and Bahlburg, B.: A note on the preservation of offshore tsunami deposits, J. Sediment. Res., 76, 1267–1273, 2006.

Wheatcroft, R. A. and Drake, D. E.: Post-depositional alteration and preservation of sedimentary event layers on continental margins, I. The role of episodic sedimentation, Mar. Geol., 199, 123–137, 2003.

Wolanski, E. and Spagnol, S.: Environmental degradation by mud in tropical estuaries, Reg. Environ. Change, 1, 152–162, 2000.

Wright, L. D. and Nittrouer, C. A.: Dispersal of river sediments in coastal seas, six contrasting cases, Estuaries, 18, 494–508, 1995.

NHESSD

2, 7225–7267, 2014



Table 1. History of nine tropical storms and typhoons that approached within a 180-nautical-mile radius of Phuket during the 52-year period (1945–1996). Modified from the Typhoon Havens Handbook (2014).

Storm	Date	Maximum wind speed at storm centre (knots)
Harriet	26 Oct 1962	30
Lucy	1 Dec 1962	20
Gloria	21 Dec 1965	30
Sally	5 Dec 1972	40
Sarah	12 Nov 1973	25
Gay	4 Nov 1989	100
Forrest	15 Nov 1992	55
Manny	16 Dec 1993	20
Ernie	18 Nov 1996	22

NHESSD
2, 7225–7267, 2014



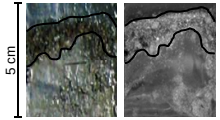
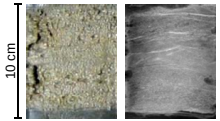
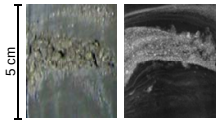
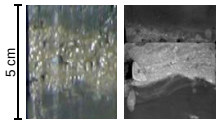
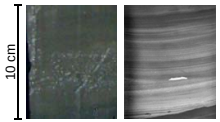
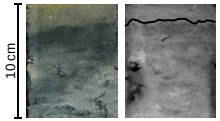
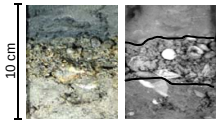
Table 2. List of the analysed sediment cores.

Core no.	Sampling year	Latitude (N)	Longitude (E)	Water depth (m)	Core recovery (cm)	Distance offshore (km)
051207-31	2007	08°47.176′	98°11.724′	15.9	70	7.2
030310-C2	2010	08°36.474′	98°12.454′	11.5	23	3.3
030310-C3	2010	08°38.708′	98°12.931′	9.5	97	3.2
030310-C7	2010	08°41.053′	98°12.763′	11.9	65	2.9
050310-C2	2010	08°45.438′	98°13.186′	9.8	75	4.1
050310-C4	2010	08°46.659′	98°12.269′	15.3	55	6.3

NHESSD
2, 7225–7267, 2014



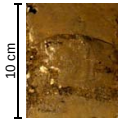
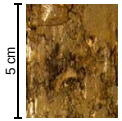
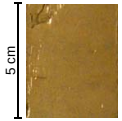
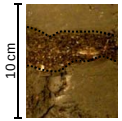
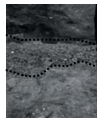
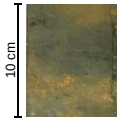
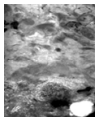
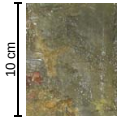
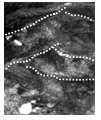
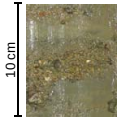
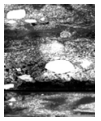
Table 3. Characteristics of the sedimentary deposit in shallow water and their event interpretation.

Core no.	Photo	X-ray image	Section depth (cm)	Type of sedimentary contact	Sediment description	Identified event
030310-C3 (a-I)	 5 cm		29–34	upper: sharp lower: erosional	Top: a 2 cm thick layer of shell debris sand Bottom: laminated mud with mud clasts	Tsunami (2004) Top: facies A Bottom: facies B
(a-II)	 10 cm		47–57	upper: erosional lower: erosional	Massive sand layer with clear cross lamination that is observed in the upper 5 cm	Typhoon Gay (1989)
(a-III)	 5 cm		66–71	upper: transitional (due to smearing) lower: sharp	Massive sand layer	Tropical storm (1972–1973)
(a-IV)	 5 cm		78–83	upper: sharp lower: erosional	Massive sand layer including few shells	Tropical storm (1962–1965)
(a-V)	 10 cm		85–95	upper: erosional lower: erosional	Fining-upward sequence laminated mud with no bioturbation	Flash flood (monsoon)
030310-C2 (b-I)	 10 cm		3–13	upper: sharp lower: erosional	Homogenous fine sand	Tsunami facies C (2004)
(b-II)	 10 cm		10–20	upper: erosional lower: erosional	A 4 cm thick layer of shell fragments with admixture of gravels, laterites, corals and sand	Tsunami facies A (2004)

NHESSD
2, 7225–7267, 2014



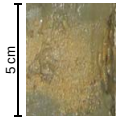
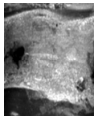
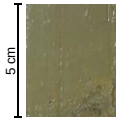
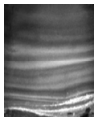
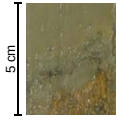
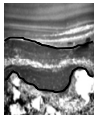
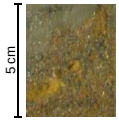
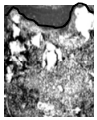
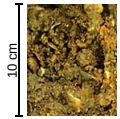
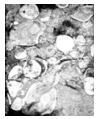
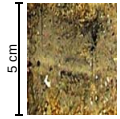
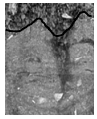
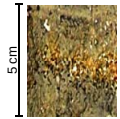
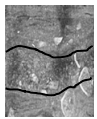
Table 3. Continued.

Core no.	Photo	X-ray image	Section depth (cm)	Type of sedimentary contact	Sediment description	Identified event
050310-C4 (c-I)			6–16	upper: sharp lower: erosional	Massive sandy mud with shell fragments scatter through the layer and laminated mud	Tsunami facies C (2004)
(c-II)			19–24	upper: erosional lower: erosional	Shell deposit in admixture of gravels, laterites and mud	Tsunami facies A (2004)
(c-III)			33–38	upper: sharp lower: sharp	Laminated fine-grained sediment	Flash flood (monsoon)
(c-IV)			47–52	upper: erosional lower: sharp	Massive coarse sand layer	Typhoon Gay (1989)
030310-C7 (d-I)			9–19	upper: transitional (due to bioturbation) lower: transional	Massive sediment that contains sandy and mud clasts scatter throughout the layer	Tsunami facies C (2004)
(d-II)			20–30	upper: transitional lower: transitional	Mud, sand and gravel partly cross laminated with generally fining upward grain size	Tsunami facies B (2004)
(d-III)			32–42	upper: transitional lower: sharp	A layer comprising coarse sand shell fragments, partly pebble-sized corals and pebbles	Tsunami facies A (2004)

NHESSD
2, 7225–7267, 2014



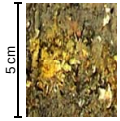
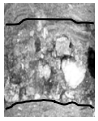
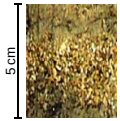
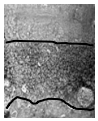
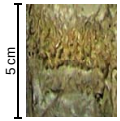
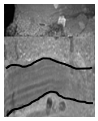
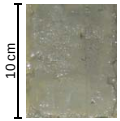
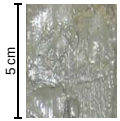
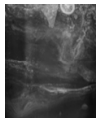
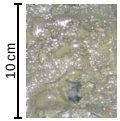
Table 3. Continued.

Core no.	Photo	X-ray image	Section depth (cm)	Type of sedimentary contact	Sediment description	Identified event
030310-C7 (cont.) (d-IV)			42–47	upper: sharp lower: sharp	Massive sand	Tropical storm (1992–1996)
(d-V)			48–53	upper: sharp lower: sharp	Laminated mud, fining-upward sequences and no bioturbation	Flash flood (monsoon)
(d-VI)			51–56	upper: sharp lower: sharp	Layers of draped mud	Resuspension
(d-VII)			54–59	upper: sharp lower: sharp	Coarse sand and occasional pebbles	Typhoon Gay (1989)
051207-31 (e-I)			1–11	lower: erosional	Layer of shell deposits	Tsunami facies A (2004)
(e-II)			41–46	upper: sharp lower: sharp	Coarse-grained sediment with fining-upward sequence	Resuspension
(e-III)			44–49	upper: sharp lower: sharp	Mixture of coarse sand and shell fragments	Tropical storm

NHESSD
2, 7225–7267, 2014



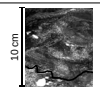
Table 3. Continued.

Core no.	Photo	X-ray image	Section depth (cm)	Type of sedimentary contact	Sediment description	Identified event
051207-31 (cont.) (e-IV)			49–54	upper: sharp lower: erosional	Coarse sand with shell fragments	Tropical storm
(e-V)			57–62	upper: sharp lower: erosional	Massive coarse sand	Tropical storm
(e-VI)			65–70	upper: transitional	Laminated fine-grained material	Flash flood
050310-C2 (f-I)			12–22	upper: sharp lower: sharp	Laminate mud. No bioturbation traces exists	Resuspension
(f-II)			25–30	upper: sharp lower: erosional	Laminate mud. No bioturbation traces exists	Resuspension
(f-III)			30–40	upper: erosional lower: erosional	Shell deposit in sandy matrix	Tsunami facies A (2004)

NHESSD
2, 7225–7267, 2014



Table 4. Tsunami facies types.

Tsunami deposits facies types	X-ray images	Core no.	Section depth (cm)	Sediment description
A: sand enriched with shells or shell debris		051207-31	−10	A 10 cm thick of shell deposit at the top of core with a lower erosional contact
		030310-C2	10–20	A 4 cm thick layer of shell fragments with admixture of gravels, laterites, corals and sand
		030310-C3	29–34	A 2 cm thick layer of shell debris sand with sharp boundary at the top and bottom layer
		050310-C2	30–40	Shell deposit in sandy maxtrix with a sharp upper and lower boundary
		050310-C4	18.5–24	Shell deposit in admixture of gravels, laterites and mud
B: cross lamination		030310-C7	20–30	Mud, sand and gravel partly cross laminated with generally fining upward grain size
C: massive layers common with mud or sand clasts		030310-C2	3–13	Homogenous fine sand with an irregular sharp contact
		030310-C3	29–34	Laminated mud with mud clasts
		030310-C7	2–12	Homogenous mud with several mud clasts
		050310-C4	6–16	Massive mud with shell fragments scatter through the layer and mud clast

NHESSD
2, 7225–7267, 2014



Table 5. Differences between the sedimentary features of flash flood, tsunami and storm deposits on the Andaman Sea shelf.

Deposition characteristics	Flash flood (monsoon effect)	Tsunami	Tropical storm
Age of events (AD)	–	2004	1962–1965, 1972–1973, 1989
Occurrence (max. water depth)	16 m	16 m	45 m
Deposit thickness	1–12 cm	12–30 cm	2–9 cm
Sedimentary contact	transitional	sharp, erosional	sharp, erosional
Grain size range	mud	mud to gravels	silt to coarse sand
Sediment sorting	poorly sorted but better than tsunami deposits	poorly sorted	poorly sorted but better than tsunami deposits
Sedimentary structure	laminated, fining-upward sequences	laminated, massive structures, fining-upward sequence, internal erosional surfaces	rippled, cross-laminated, graded sand
Presence of rip-up clast	no	yes	no
Terrigenous component	no	wood and laterites	no
Anthropogenic artefact	no	pieces of brick	no
Presence of carbonate material	occasionally shell fragments	pieces of broken shells and corals	complete shells and their fragments (typical for beach sand)
Presence of mud	yes	yes	no
Presence of sand	no	yes	yes

NHESSD
2, 7225–7267, 2014



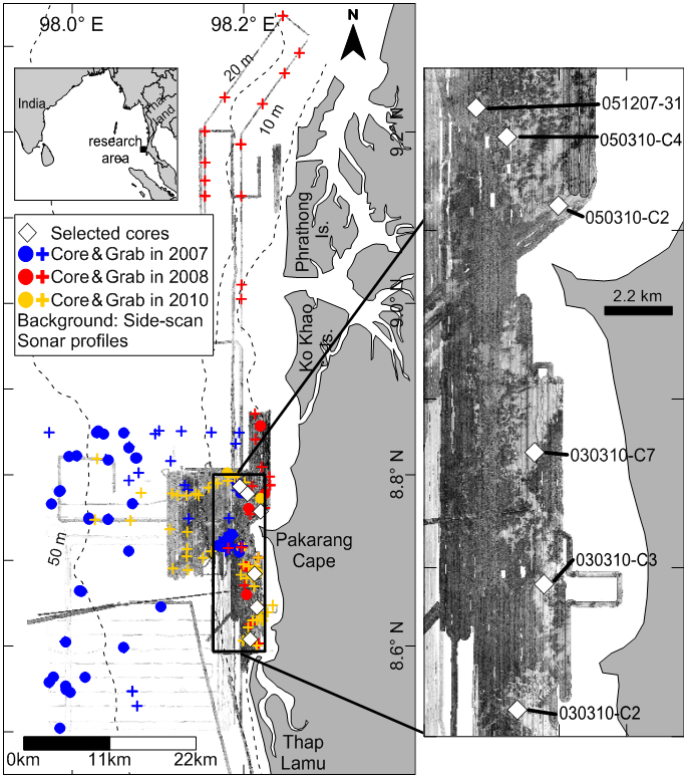


Figure 1. Overview map of the investigation area including sampling stations. The bathymetric data are based on nautical charts. The sediment samples taken during the 3-year research period are ordered due to the three different cruises in difference colours.

NHESSD
2, 7225–7267, 2014



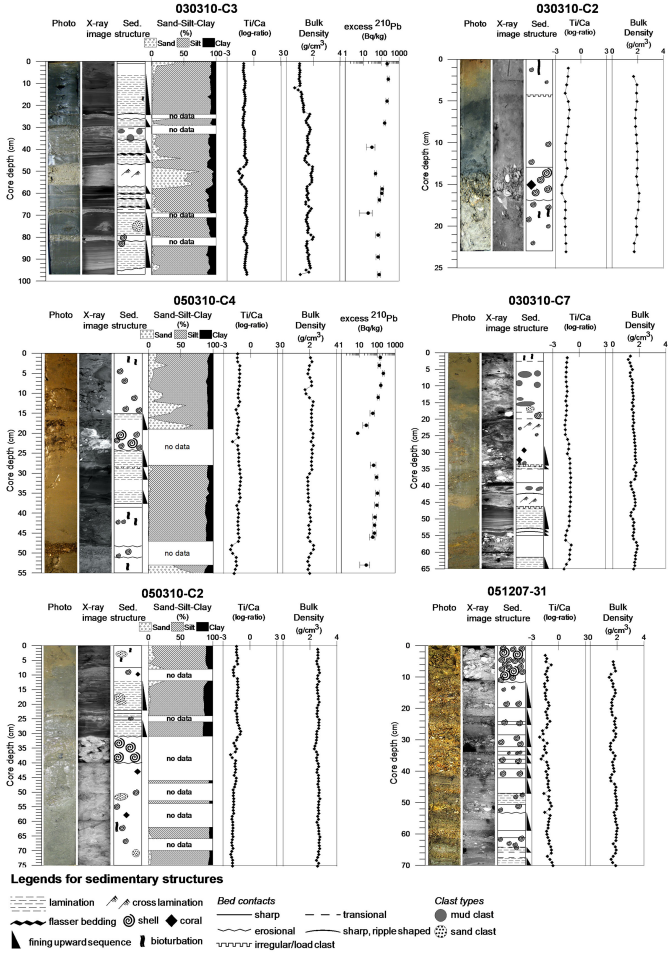


Figure 2. Interpretation of the sediment cores.

NHESSD
2, 7225–7267, 2014

Internal structure of event layers preserved on the Andaman Sea

D. Sakuna-Schwartz et al.

CC BY

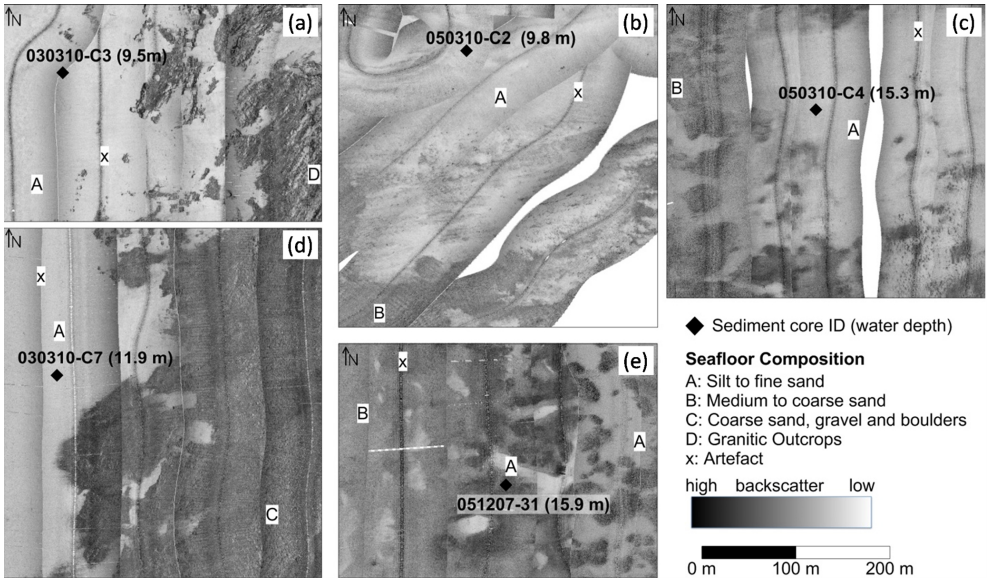


Figure 3. Cut-outs of the side-scan sonar mosaic showing the sediment distribution at the coring positions. No data are available for core 030310-C2. The composition of the seafloor was established based on the ground truthing of the backscatter data with grab samples and underwater video images (Feldens et al., 2012).

NHESSD
2, 7225–7267, 2014



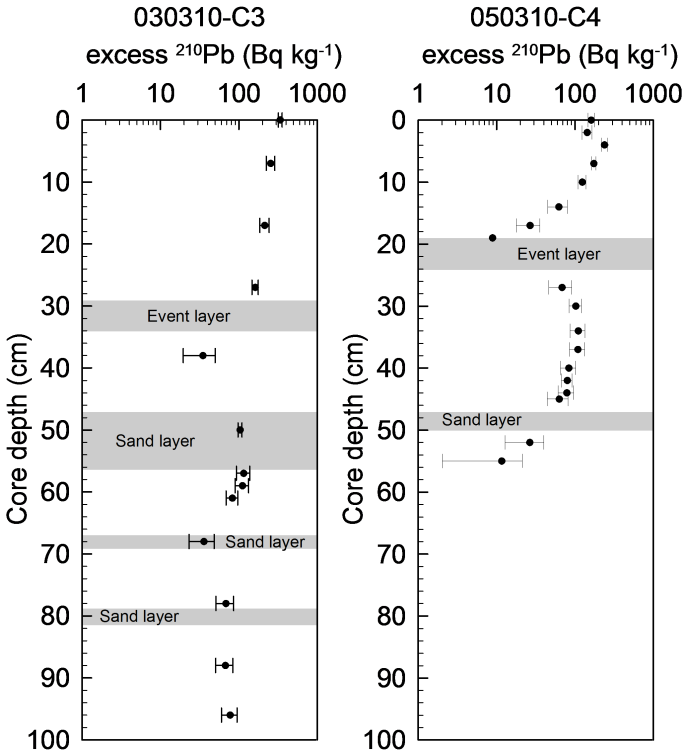


Figure 4. Excess ^{210}Pb activity profiles after mud correction with 2σ uncertainty ranges observed in the shallow water cores 030310-C3 and 050310-C4.

NHESSD
2, 7225–7267, 2014



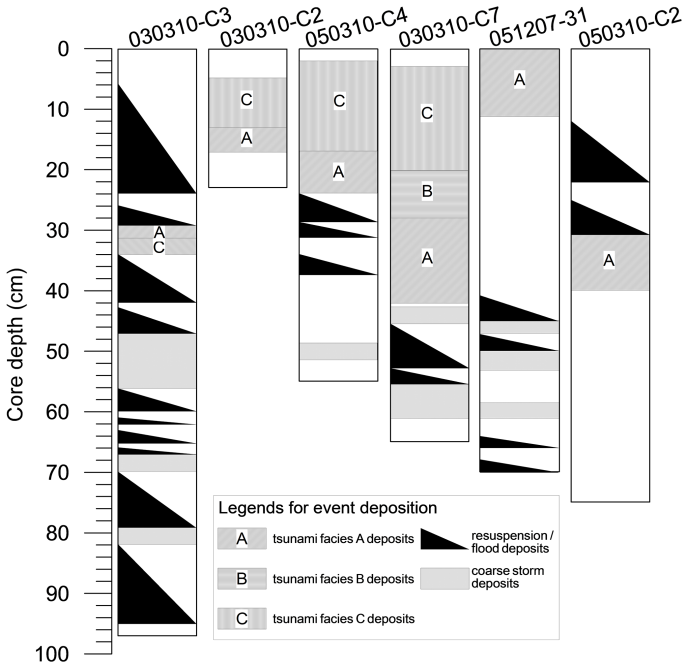


Figure 5. Event sequence log diagram for sediment cores taken in shallow water (< 16 m water depth).

NHESSD
2, 7225–7267, 2014

Internal structure of event layers preserved on the Andaman Sea

D. Sakuna-Schwartz et al.

CC BY

Hindawi Publishing Corporation
The Scientific World Journal
Volume 2014, Article ID 485068, 14 pages
http://dx.doi.org/10.1155/2014/485068

Research Article

Application of Binary Diagnostic Ratios of Polycyclic Aromatic Hydrocarbons for Identification of Tsunami 2004 Backwash Sediments in Khao Lak, Thailand

Siwatt Pongpiachan

NIDA Center for Research & Development of Disaster Prevention & Management, School of Social and Environmental Development, National Institute of Development Administration (NIDA), 118 Moo3, Sereethai Road, Klong-Chan, Bangkapi, Bangkok 10240, Thailand

Correspondence should be addressed to Siwatt Pongpiachan; pongpiajun@gmail.com

Received 3 April 2014; Revised 16 June 2014; Accepted 18 June 2014; Published 22 July 2014

Academic Editor: Gianluigi De Gennaro

Copyright © 2014 Siwatt Pongpiachan. This is an open access article distributed under the Creative Commons Attribution License, which permits unrestricted use, distribution, and reproduction in any medium, provided the original work is properly cited.

Identification of Tsunami deposits has long been a controversial issue among geologists. Although there are many identification criteria based on the sedimentary characteristics of unequivocal Tsunami deposits, the concept still remains ambiguous. Apart from relying on some conventional geological, sedimentological, and geoscientific records, geologists need some alternative "proxies" to identify the existence of Tsunami backwash in core sediments. Polycyclic aromatic hydrocarbons (PAHs) are a class of very stable organic molecules, which can usually be presented as complex mixtures of several hundred congeners; one can assume that the "Tsunami backwash deposits" possess different fingerprints of PAHs apart from those of "typical marine sediments." In this study, three-dimensional plots of PAH binary ratios successfully identify the Tsunami backwash deposits in comparison with those of global marine sediments. The applications of binary ratios of PAHs coupled with HCA are the basis for developing site-specific Tsunami deposit identification criteria that can be applied in paleotsunami deposits investigations.

1. Introduction

Polycyclic aromatic hydrocarbons (PAHs), usually acknowledged as a group of persistent organic pollutants (POPs), have been comprehensively investigated in the past decades because these congeners have a profound association with a wide range of adverse health effects and other respiratory diseases [1–3]. PAHs are widely detected in various types of environmental compartments including marine organisms [4–9]. It is well known that PAHs can be generated from both anthropogenic and natural sources [10–13]. According to recent studies, particulate PAHs are harmful to human health due to their responsibilities for cancer, endocrine disruption, and reproductive and developmental effects [14–17]. As a consequence of distress over its potential hazard to public health, numerous studies were conducted to investigate the impact of meteorological parameters on its temporal variation and spatial distribution [18, 19]. Further attempts on clarification of factors governing diurnal variation of PAHs have also been carried out in different countries [20–23].

PAHs and other semivolatile organic compounds (SVOCs) have also been applied as chemical tracers to discriminate marine deposits from terrigenous components [24–28]. In particular, binary diagnostic ratios of PAHs can be employed to categorize anthropogenic and biogenic sources in marine deposits [28–30]. The molecular diagnostic binary ratio method for PAH source identification involves comparing ratios between pairs of frequently found PAH compound characteristics of different sources. Stationary source combustion emissions from the use of coal, oil, and wood are low in Cor (coronene) relative to B[a]P, while mobile source combustion emissions from diesel and petroleum use are high in B[g,h,i]P and Cor relative to B[a]P [31]. The ratio of these PAHs can be used to distinguish between traffic dominated PAH profiles and other sources [32, 33]. The ratio of certain PAH species (diagnostic binary ratio) can provide some information about the impact of different sources of PAHs in ambient air [34, 35]. Fl/(Fl + Pyr), B[e]P/(B[e]P + B[a]P), B[b,j,k]F/B[g,h,i]P,

Ind/B[g,h,i]P, B[a]P/B[e]P, B[a]A/Chry, B[a]P/B[g,h,i]P, and Ind/(Ind + B[g,h,i]P) can be used as characteristic diagnostic parameters to identify their emission sources [30, 36]. For instance, Fl/(Fl + Pyr) and Ind/(Ind + B[g,h,i]P) ratios were used as indicators to discriminate fossil fuel from other modern biomass combustions, with low ratios (<0.40 and <0.20, resp.) signifying petroleum, intermediate ratios (0.40–0.50 and 0.20–0.50) indicating liquid fossil fuel (vehicle and crude oil) combustion whereas ratios higher than 0.50 can be considered as signals of wood or coal combustion [30].

Recently, Tipmanee et al. [37] used PAHs as "chemical proxy" to conduct source apportionment by using PCA technique in the Tsunami 2004 affected coastal area in the southern part of Thailand. They concluded that road dust and oil burning are two major sources of PAHs detected in marine surface sediments, indicating the importance of Tsunami backwash of terrestrial soils for coastal environments. However, in order to strengthen this conclusion, further investigations need to be performed. Without comparing the "fingerprint" of particulate PAH source profiles from various emission sources with those of marine deposits, it seems difficult to draw a conclusion by only relying on source apportionment technique. PCA offers the advantages of not requiring prior knowledge of the chemical composition and size distribution of emissions from specific sources (source profiles) but has the drawback of being mathematically indeterminate, allowing a wide range of possible solutions even when it is applied to relatively simple simulated data sets. The most difficult part of interpreting PCA is the explanation of negative correlations, which usually can be explained as contrast (when a parameter is growing in value the "negatively correlated one" is lowering its values). PCA has been applied to hundreds of environmental data matrices in order to interpret complex data structures on chemical pollution. Moreover, there are factorization techniques close to PCA that avoid this possible source of ambiguity as nonnegative matrix factorization, such as UNMIX and PMF. UNMIX is a multivariate receptor modeling package that inputs observations of particulate composition and seeks to find the number, composition, and contributions of the contributing sources or source types. This model also produces estimates of the uncertainties in the source compositions. UNMIX uses a generalization of the self-modeling curve resolution method developed by Henry, 1997 [38]. A major difference between UNMIX and PMF is that UNMIX does not make explicit use of errors or uncertainties in the ambient concentrations. This is not to imply that the UNMIX approach regards data uncertainty as unimportant, but rather that the UNMIX model results implicitly incorporate error in the ambient data.

In contrast to multivariate techniques such as PCA, visual comparison of PAH fingerprints and diagnostic binary ratios are preferable since they require no environmental insights of interpreting correlation coefficients of certain variables in each principal component and thus overcome the limitations of PCA. Overall, the main purposes of this study are to comprehensively investigate the fingerprints and diagnostic binary ratios of PAH aerosols from various emission sources in Songkhla province with marine deposits in Tsunami 2004 affected coastal area of Thailand. These findings will open a new window in applying PAHs as a "chemical proxy" to identify Tsunami backwash deposits and thus enhance the knowledge of Tsunami impacts on surficial sediment distribution in Khao Lak coastal area of the Andaman Sea.

2. Materials and Methods

2.1. Sampling Stations

2.1.1. Sediments from Marine Environment. The research area is governed by the northeast monsoon from mid-October until March and the southwest monsoon from May to September and the intermonsoon phases. This study was carried out offshore along the west coast of Phang Nga province, Thailand, which was heavily affected by the 2004 Tsunami [39, 40]. The research area covers approximately 1,000 km^2 between Thap Lamu and Pakarang Cape. The water depth of the surveyed area reached from 5 m down to 70 m. The sediment is built up by grain sizes from mud to gravel with a sediment thickness decreasing towards offshore (see Figures S1–S3 available online at http://dx.doi.org/10.1155/2014/485068). Details of the research area are described in Feldens et al. [41].

2.1.2. PM_{10} Monitoring Stations at Hat-Yai City. The first observatory station, Site-1, was placed at Novotel Centara Hat-Yai Hotel (7°00′20.65″N 100°28′15.65″E) at 30 m above the building basement and influenced mainly by transported pollution from traffic jams in the city center. Site-3 was positioned at Lee Gardens Grand Plaza Hotel (7°00′21.39″N 100°28′15.94″E) at 125 m above the ground level. Site-2, which was situated at Lee Gardens Grand Plaza Hotel at 60 m above the ground level, appears to be affected by a mixture of air masses including vehicular emissions, long-range transportation of aged particles and maritime aerosols. Intensive monitoring campaigns were conducted at all observatory stations simultaneously from December 17 to 20, 2007, in the relatively cold period. PM_{10} samples were collected every three hours continuously from 21:00 h December 17 to 21:00 h December 20 by using Graseby-Andersen.

2.1.3. Sampling Site Descriptions of Various Emission Sources at Songkhla Province. Population of Songkhla Province is about 1.32 million occupying an area of approximately 7,394 km^2. Songkhla is located 950 km south of Bangkok, situated on the eastern side of the Malayan Peninsula, bordering on Nakhon Sri Thammarat and Phatthalung to the north; Yala, Pattani, and States of Kedah (Sai Buri) and Perlis of Malaysia to the south; the Gulf of Thailand to the east; and Satun and Phatthalung to the west (Figure S4). Hat-Yai, a district of Songkhla, is better known than the provincial capital itself as an economic and tourism zone of Songkhla and thus many industrial factories and stores are located in this area. Sampling site descriptions are given in detail as follows.

Prince of Songkhla University (PSU). The site was situated at about 3 m above ground level at the Faculty of Environmental Management of Prince of Songkhla University and about

550 m away from the main traffic road that leads to the city center of Hat-Yai. It is important to note that PSU1 and PSU2 represent the sampling period of June (28–30 June, 2007) and October (24–26 October, 2007), respectively. This site is considered as an urban residential zone.

Traffic Intersection (TI). The station was located at the traffic intersection in front of the main gate of PSU. It is situated on the eastern side and approximately 2.5 km far away from the Hat-Yai city center. This station is regarded as a traffic area close to urban residential zone. The air samples were collected on 5–7 July, 2007.

Corpse Incinerator (CI). This station is a part of Kor-Hong temple, located at the northern side and about 1.5 km far away from TI. Since timbers and tires were generally used as fuel for corpse incineration, this site is considered as an emission source of both timbers and tires-burning. This site represents the sampling period of 19–21 July 2007.

Charoen Pokphand Factory (CPF). This site was situated inside the fish can manufacturing factory of Charoen Pokphand group, which is the largest business conglomerate in Thailand. As crude oil was used for the fish can production, this station can be regarded as an emission source of crude oil burning. The monitoring was conducted on 24–26 July 2007.

Songkhla Lake (SL). This station was located at the south of Songkhla Lake and approximately 13 km far away from the northern side of PSU. This site is also situated about 14 km away from the western side of the Gulf of Thailand. Since there are not many industrial and/or traffic emission sources including chemical and metallurgy factories and power plants in this district, we consider this site as a rural background sampling station. SL1 and SL2 represent the monitoring period of July (27–29 July, 2007) and October (20–22 October, 2007), respectively.

Rubber Sheet Manufacturing Factory 1 (RMF1). This monitoring site was located at Tumbol Tungwan, Hat-Yai district. As a part of the manufacturing process, the rubber sheet was treated with steam of high temperature and high pressure coupled with the purification by using sulfuric acid solution. Since Para rubber trees were used as fuel for this process, this site represents an emission of mixed Para rubber trees burning, latex fragments, and sulfuric acid aerosols. The air samples were collected from 30 July to 1 August 2007.

Rubber Sheet Manufacturing Factory 2 (RMF2). This station was situated at Tumbol Tachang, Banglum district. Both RMF1 and RMF2 are regarded as an emission of mixed Para rubber trees burning, latex fragments, and sulfuric acid aerosols. The air samples were collected from 2 to 4 August 2007.

Bus Terminal (BT). This site was located at the south-western side of PSU and approximately 1.4 km away from the campus. This station was selected as a source of diesel emission because the majority of these buses are diesel-fueled. The air sample collection was started from 5 to 7 August 2007.

Waste Incinerator (WI). This site was situated at the city center and belongs to the municipality of Hat-Yai city. Since the municipal waste incinerated is a heterogeneous mixture of solid wastes and burning fuels, this site can be recognized as a combination of solid waste burning and diesel exhaust emission. The air samples were collected from 28 to 30 August, 2007.

Barbeque Festival (BF). This site was located inside the PSU campus on the top roof of Faculty of Natural Resources. The barbeque festival has become an annual tradition that is held on the second week in August. The 40th Annual Barbecue Festival is set for Wednesday, August 15, 2007. This site can be considered as an emission of charcoal burning. The air samples were collected from 15 to 18 August, 2007.

Phetkasem Road (PR). This station was located at the heart of Hat-Yai city. The air mass collected at this area reflected the heaviest burden from traffic congestions with the mixture of diesel and benzene exhaust emissions. The monitoring was conducted on 27–29 August 2007.

Kor-Hong Hill (KHH). This site was situated at the radio station on the top of Kor-Hong hill with the elevation of 356 meters. The air mass passed over the station was considered as a mixture of all emission sources in urban area and thus can be regarded as an urban residential zone monitoring site. The sampling was conducted on 3–5 November 2007.

Rice Straw Burning (RSB). The rice straw burning has been the major practice for removing rice straw because it is fast, economical, and practical in removing disease organisms. Although the options for the disposition of rice straw are limited, this practice leads to unacceptable air pollution. The station was situated at rice field in Satingpra district, Songkhla Province, and considered as a representation of biomass burning. The sampling was conducted on 16 November 2007.

Biomass Burning (BB). As a part of soil preparation process, the biomass must be disposed of in order to make way for the plantation. The sampling site was adjacent to the unused land and located at Namom district, Songkhla Province. This site can be regarded as an emission source of biomass burning. The sampling was conducted on 17 November 2007.

Para Rubber Tree Burning (PTB). This station is located in Namom district, Songkhla Province, and can be recognized as an emission source of Para rubber tree burning. The air samples were collected on 18 November 2007.

2.2. Sampling Equipment

2.2.1. Filter Sample Collection and Meteorological Data. In this study, Graseby-Anderson high volume air sampler (PM10-TE6001) was used to collect PM_{10} samples every

3 h consecutively with the flow rate of 1.132 $m^3\ min^{-1}$. To avoid any contaminations, tweezers and aluminum foils were cleaned by dichloromethane (DCM) prior to use. All quartz fiber filters (47 mm Whatman quartz microfibre filters (QM/A)) were weighed gravimetrically on a microbalance Mettler Toledo AB204-S (Columbus, Ohio, USA) before and after sampling to quantify PM_{10} mass load. It is also worth mentioning that all filters were precleaned by DCM using Soxhlet extraction for 8 h prior to use to avoid any potential contamination. During the intensive monitoring campaign, all filters were kept in refrigerator at 4°C to minimize the loss of PAHs during sample preservation. Detailed description of sample collection has been published in Pongpiachan [42] and Pongpiachan et al. [43, 44].

2.2.2. Hydroacoustic Equipment and Sediment Sampling. During the research cruises in November-December 2007 with RV CHAKRATONG TONGYAI and November-December 2008 with RV BOONLERT PASOOK, approximately 1500 nautical miles of hydroacoustic profiles (side scan sonar, multibeam echo sounder, and shallow reflection seismic with a boomer system) were recorded offshore Pakarang Cape. Based on these data sediment distribution maps were compiled. The grab samples discussed in this study were taken with a Van-Veen-type grab sampler, which was used to collect 70 surface sediment samples during 1–8 December 2007. Sediment samples were wrapped in clean aluminum foil, placed in a glass bottle, and kept frozen at −20°C. They were freeze-dried prior to being grounded and sieved to homogenize the samples and then kept in the refrigerator at −4°C until analysis.

2.3. PAHs Analysis. All organic solvents (i.e., DCM and Hexane) are of HPLC grade and are purchased from Fisher Scientific. A cocktail of 15 PAHs as determined by Norwegian Standard (NS 9815: S-4008-100-T) (phenanthrene (Phe), anthracene (An), fluoranthene (Fluo), pyrene (Pyr), 11 h-benzo[a]fluorene (11H-B[a]F), 11 h-benzo[b]fluorene (11H-B[b]F), benz[a]anthracene (B[a]A), chrysene (Chry), benzo[b]fluoranthene (B[b]F), benzo [k]fluoranthene (B[k]F), benzo[a]pyrene (B[a]P), benzo[e]pyrene (B[e]P), indeno[1,2,3-cd]pyrene (Ind), dibenz[a,h]anthracene (D[a,h]A), benzo[g,h,i]perylene (B[g,h,i]P), each 100 $\mu g\ mL^{-1}$ in toluene: unit: 1 × 1 mL) and a mix of recovery internal standard PAHs (d_{12}-perylene (d_{12}-Per), d_{10}-fluorene (d_{10}-Fl), each 100 $\mu g\ mL^{-1}$ in xylene: unit: 1 × 1 mL) were supplied by Chiron AS (Stiklestadveien 1, N-7041 Trondheim, Norway). Standard stock solutions of 4 $\mu g\ mL^{-1}$ of deuterated PAHs (used as internal standard) and 100 $\mu g\ mL^{-1}$ of native PAHs were prepared in nonane. Working solutions were obtained by appropriate dilution in n-cyclohexane. All solutions were stored in amber colored vials at −20°C. Silica gel (0.040–0.063 mm) was purchased from Merck. All materials used (silica gel, glass, and cotton wool, etc.) were Soxhlet-extracted with DCM for 24 h and kept dry (in desiccator) until use. The fractionation/cleanup and blow-down process followed the method reported by Gogou et al. [45]. The samples were analyzed for PAHs using Varian GC/MS-MS system comprising a CP-3900 gas chromatograph (Walnut Creek, CA, USA) with a 1077 universal injector and a three-dimensional quadrupole ion-trap selected ion storage mass spectrometer (Varian Saturn 2200). The target compounds were separated on a 60 m length × 0.25 mm i.d. capillary column coated with a 0.25 μm film thickness. The chromatographic conditions coupled with the quantification and identification of PAHs were described in Pongpiachan et al. [43, 44]. Analysis of the congeners is based upon the principle of internal standard (IS) method. One of the essential requests of employing an IS is that it represents comparable physiochemical properties or the same type of substitution as the target compound. A relative response factor (RRF) for individual native congener was first analyzed. This is used for quantification, as the relative response between the IS and the native analyte should remain constant. It is an appropriate technique due to its recovery losses of the congener during extraction and analysis is expected to equal those of the IS. The computation of RRF can be explained as follows:

$$\mathrm{RRF} = \frac{A_{\mathrm{nat}}}{A_{\mathrm{is}}} \times \frac{C_{\mathrm{is}}}{C_{\mathrm{nat}}}, \tag{1}$$

where A_{nat} = peak area of the native compound in the standard; C_{nat} = concentration of the native compound in the standard; A_{is} = peak area of internal standard; C_{is} = concentration of the internal standard. The $\mathrm{RRF_{STD}}$ used for quantifying samples are the mean of those calculated for the two quantification standards run on the same day. Concentration (C) of analytes in sample extracts is calculated using the following formula:

$$C = \frac{A_{\mathrm{nat}}}{A_{\mathrm{is}}} \times \frac{1}{\mathrm{RRF_{STD}}} \times \frac{W_s}{W_{\mathrm{is}}}, \tag{2}$$

where W_{is} = weight of IS added to the sample and W_{s} = weight or volume of the sample analyzed. Where W_{is} = weight of IS added to the sample, W_s = weight or volume of the sample analysed. A recovery determination standard (RDS) was used for the calculation of both internal standard (IS) and the sampling efficiency standard (SES) of recoveries during sample preparation and extraction/purification. A known amount of RDS was added at the final stage prior to GC/MS analysis and was assumed to suffer zero loss:

$$\begin{aligned}\%\mathrm{Recovery} = &\left[\left(\frac{A_{\mathrm{is}}}{A_{\mathrm{RDS}}}\right)_{\mathrm{S}} \times \left(\frac{A_{\mathrm{RDS}}}{A_{\mathrm{is}}}\right)_{\mathrm{STD}}\right] \\ &\times \left[\left(\frac{C_{\mathrm{is}}}{C_{\mathrm{RDS}}}\right)_{\mathrm{STD}} \times \left(\frac{C_{\mathrm{RDS}}}{C_{\mathrm{is}}}\right)_{\mathrm{S}}\right] \times 100\%,\end{aligned} \tag{3}$$

where A_{RDS} is area of recovery determination standard and C_{RDS} is concentration of the recovery determination standard. Recoveries of IS were used as an indication of the analyte losses during extraction, preconcentration,

cleanup/fractionation, and blow-down stages. The calculation of the sampling efficiency by using the sampling efficiency standard (SES) is described as follows:

$$\%\text{Recovery of SES} = \left[\left(\frac{A_{is}}{A_{SES}}\right)_{STD} \times \left(\frac{A_{SES}}{A_{is}}\right)_{S}\right] \times \left[\left(\frac{C_{is}}{C_{SES}}\right)_{S} \times \left(\frac{C_{SES}}{C_{is}}\right)_{STD}\right] \times 100\%, \quad (4)$$

where A_{SES} = area of the sampling efficiency standard and C_{SES} = concentration of the sampling efficiency standard. Recoveries of SES were used as an indication of analyte losses during sampling as opposed to the analysis. Analytical precisions and accuracies were calculated using the standard SRM 1941b. Mean recovery (based on extraction of matrix-matched certified reference materials ($n = 8$)) was in range of 77–119%. The precision of the procedure, calculated as relative standard deviation on the duplicate samples, was less than 15%. All sample concentrations were calculated using standardized relative response factors run with each batch [43, 44].

2.4. The Representativity of Diagnostic Binary PAHs Ratios. Standard deviations of a data set comprised of triplicate PM_{10} bound PAH samples ($n = 3$) from 15 different sources at Songkhla province were employed to evaluate the representativity of collected atmospheric PAH patterns. The average percentage standard deviation of binary ratios (i.e., average of Fluo/Pyr, B[a]A/Chry, B[a]P/B[e]P, and Ind/B[g,h,i]P) was considerably low ranging from 9.30% to 39.1% with the average of 18.9%. As a consequence, it appears reasonable to assume that the diagnostic binary ratios can be applied for the representativity of PM_{10} bound PAHs profiles collected from various emission sources.

3. Results and Discussion

3.1. Levels and Distribution Patterns of PAHs in Khao Lak Marine Sediments. Table 1 and Figure 1 list the average concentration, minimum, maximum, and standard deviation of PAHs in the marine sediments of Khao Lak coastal area in comparison with those of other marine sediments around the world. The total concentrations of fifteen probably carcinogenic PAHs ranged from 12.58 ng g^{-1} to 278.10 ng g^{-1} with an arithmetic mean of 69.43 ± 70.67 ng g^{-1} as written in Table 2 and illustrated in Figures 2 and 3. In this study, the $\sum_{13}$ PAHs refers to the sum of analyzed Phe, An, Fluo, Pyr, B[a]A, Chry, B[b]F, B[k]F, B[a]P, B[e]P, Ind, D[a,h]A, and B[g,h,i]P. The observed $\sum_{13}$ PAHs were much lower than those values reported in harbor sediment of Boston (54,253 ng g^{-1}), coastal sediments of Barcelona Harbor (15,069 ng g^{-1}), riverine sediment of Guangzhou Channel (12,525 ng g^{-1}), mangrove sediment of Hong Kong (3,714 ng g^{-1}), coastal sediment of Cotonou (1,189 ng g^{-1}), and coastal sediment of Carteau (210 ng g^{-1}), but still higher than those values of coastal sediments in Rosas Bay (12 ng g^{-1}), Santa Ponsa Bay (26 ng g^{-1}), and Le Panier (34 ng g^{-1}) [46–52].

3.2. Diagnostic Binary Ratios of PAHs. As illustrated in Table 1, the diagnostic binary ratios of Ind/(Ind + B[g,h,i]P), B[a]A/Chry, B[a]P/B[g,h,i]P, Fluo/(Fluo + Pyr), B[k]F/Ind, and An/(Phe + An) of Khao Lak coastal sediments were calculated and compared with previous studies of PAH fingerprints from various emission sources. Since the mean value of B[a]P/B[g,h,i]P (0.41 ± 0.70) was in the range of 0.3–0.78, it denoted the impact of oil burnings on study sites [53]. This interpretation is further supported by the results of B[a]A/Chry (0.96 ± 1.91), Fluo/(Fluo + Pyr) (0.35 ± 0.41), and An/(Phe + An) (0.11 ± 0.11), highlighting the influence of oil combustions over Khao Lak sediment samples (see Table 2 [28, 53–56]). Obviously, these binary diagnostic ratios are quite useful and provide valuable information to identify the potential sources of PAHs. However, these diagnostic ratios alone, as well as source profiles, should be used with great caution as physiochemical processes such as UV-photolysis and heterogeneous reaction with trace gaseous species can alter PAH distribution pattern during their transport from the emission source to the receptor site. Furthermore, several studies report the biodegradation of PAHs in sediments, particularly occurring under aerobic, sulfate reducing, and denitrifying conditions [57–59]. The stabilities of diagnostic binary PAH ratios are questionable, especially in aquatic environment surrounded by PAH-degrading bacteria [59]. In order to minimize the above-mentioned uncertainties, the plots of three- dimensional diagnostic ratios can enhance the reliability of binary ratios and thus be used as a tool to characterize sediment samples based on its PAH emission profiles.

Six PAH congeners have been selected and categorized into three-dimensional plots of molecular diagnostic binary ratios of Fluo/(Fluo + Pyr), Ind/(Ind + B[g,h,i]P), and B[a]P/Chry, which represents x-axis, y-axis, and z-axis, respectively. The clearest features in all categories (see Figures 4(a) and 4(b)) are as follows: (i) three-dimensional (3D) plots of Non-Pakarang group and other global marine sediments were grouped together (see Figure 4(a)); (ii) there are very clear different sources in Pakarang group, plausibly indicating the effect of Tsunami backwash (see Figure 4(a)); (iii) 3D plots of Non-Pakarang group were located in similar positions as those of RMF, CPF, CI, PTB, and BB suggesting that PAHs were conveyed from emission sources in Songkhla province to Khao Lak coastal area, then consequently to sediments (see Figure 4(b)); and (iv) 3D plots of Pakarang group highly deviate from the majority of plot members in both figures (see Figures 4(a) and 4(b)), which can be explained by the deposition of terrestrial components triggered by Tsunami backwash in Pakarang area.

Further attempts were examined to investigate the reliability of binary ratios in order to characterize the origins of sediment samples. Statistical descriptions of six binary ratios were illustrated in Table 2. There are significant differences between average values of An/(An + Phe), B[a]A/(B[a]A + Chry), B[a]P/(B[a]P + B[e]P), Ind/(Ind + B[g,h,i]P), and

Table 1: Diagnostic binary ratios of PAHs, together with average, standard deviation, minimum and maximum of PAH concentrations (ng g^{-1} dry weight) in marine sediments collected at the study sites.

	Number of rings	Molecular formula	Molecular mass	Average (n =70)	Standard deviation	Minimum	Maximum	Percentage contribution
Phe	3	$C_{14}H_{10}$	178	15.77	6.19	4.33	37.17	22.71
An	3	$C_{14}H_{10}$	178	1.94	1.26	0.28	7.92	2.79
11H-B[a]F	4	$C_{17}H_{12}$	216	1.40	2.50	N.D.	12.82	2.02
11H-B[b]F	4	$C_{17}H_{12}$	216	0.82	1.31	N.D.	9.62	1.18
Fluo	4	$C_{16}H_{10}$	202	6.19	4.32	1.04	21.86	8.92
Pyr	4	$C_{16}H_{10}$	202	11.46	7.26	1.63	37.58	16.51
B[a]A	4	$C_{18}H_{12}$	228	0.69	0.86	0.13	4.84	0.99
Chry	4	$C_{18}H_{12}$	228	0.72	1.12	0.11	5.76	1.04
B[b]F	5	$C_{20}H_{12}$	252	2.10	3.28	0.05	16.06	3.02
B[k]F	5	$C_{20}H_{12}$	252	3.17	4.12	0.05	18.10	4.57
B[e]P	5	$C_{20}H_{12}$	252	2.93	4.33	0.05	20.55	4.22
B[a]P	5	$C_{20}H_{12}$	252	2.66	3.08	0.06	11.15	3.83
Ind	6	$C_{22}H_{12}$	276	3.30	5.21	0.04	22.32	4.75
D[a,h]A	5	$C_{22}H_{14}$	278	9.86	17.93	0.10	117.46	14.20
B[g,h,i]P	6	$C_{22}H_{12}$	276	6.42	7.90	0.15	48.02	9.25
$\sum$ PAH				**69.43**	**70.67**	**12.58**	**278.10**	**100.00**
Ind/(Ind + B[g,h,i]P)	Diesel: 0.35–0.70 [55]			0.34	0.87			
B[a]A/Chry	Coal: 1.0–1.2 [53], gasoline: 0.28–1.2 [53, 55]			0.96	1.91			
B[a]P/B[g,h,i]P	Coal: 0.9–6.6, vehicles: 0.3–0.78, oil burning: >2 [53]			0.41	0.7			
Fluo/(Fluo + Pyr)	Coal: 0.53 [55], gasoline: 0.40 [56]			0.35	0.41			
B[k]F/Ind	Diesel: 0.5 [60], wood combustion: 0.6 [60]			0.96	1.96			
An/(Phe + An)	Petroleum: <0.1, combustion: >0.1 [28, 54]			0.11	0.11			
B[a]P/$\sum$ PAH-$_{5rings}$ *				0.13	0.45			

* $\sum$ PAH-$_{5rings}$ is the sum of B[a]P, D[a,h]A, B[e]P, B[b]F, and B[k]F.

Table 2: Diagnostic binary ratios of PAHs in Andaman marine sediments in comparison with those of particulate PAHs from other emission sources.

	Andaman ($n = 70$)	Hat-Yai ($n = 72$)	Emission sources ($n = 17$)	t-test Andaman versus Hat-Yai	t-test Andaman versus emission sources
An/(An + Phe)	0.11 ± 0.11	1.16 ± 0.134	0.13 ± 0.11	S*	NS**
Fluo/(Fluo + Pyr)	0.35 ± 0.41	0.72 ± 0.120	0.50 ± 0.053	NS	S
B[a]A/(B[a]A + Chry)	0.96 ± 1.91	1.16 ± 0.053	0.51 ± 0.098	S	NS
B[a]P/(B[a]P + B[e]P)	0.48 ± 1.05	0.88 ± 0.13	0.41 ± 0.15	S	NS
Ind/(Ind + B[g,h,i]P)	0.34 ± 0.87	0.46 ± 0.13	0.46 ± 0.074	S	S
B[k]F/Ind	0.96 ± 1.96	0.68 ± 0.13	0.22 ± 0.16	S	S

*S: significant ($P < 0.05$), **NS.

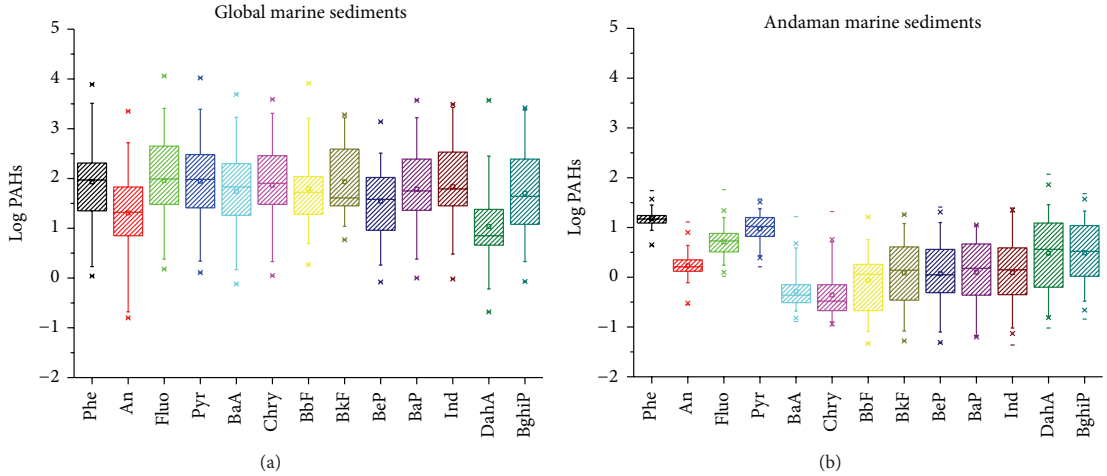


Figure 1: Box plots of PAHs in global marine and Andaman Sea sediments.

B[k]F/Ind in PM_{10} collected at Hat-Yai city and Khao Lak sediments. This can be explained by several reasons. Firstly, it can be postulated that urban aerosols from Hat-Yai city play a minor role in governing PAH distributions in Khao Lak sediments. Secondly, meteorological conditions can also alter particulate PAH profiles through UV-photolysis in fly ash particles [61, 62], aqueous phase [63], and heterogeneous reactions with ozone during the transport [64].

Thirdly, several studies report the importance of marine organisms for bioaccumulation of PAH compounds from dredged sediments [46, 65–67]. Hence, the differences of molecular diagnostic binary ratios of PAHs between Hat-Yai PM_{10} and Khao Lak sediments can be described as a consequence of bioaccumulation activities caused by marine organisms. Despite its varieties of emission sources, there are only three significant differences of average values of Fluo/(Fluo + Pyr), Ind/(Ind + B[g,h,i]P), and B[k]F/Ind observed in PM_{10} collected from 17 various emission sources and Khao Lak sediments. This finding reflects the fact that PAH contents in Khao Lak sediments were affected by more complicated emission sources rather than a single dominant point source.

3.3. Hierarchical Cluster Analysis (HCA). Cluster analysis (CA) seeks to identify homogeneous subgroups of cases in a population which both minimize within-group variation and maximize between-group variation. In this study, CA was conducted using SPSS 13.0 for Windows through Ward linkage on the correlation coefficient distance. Through the application of three diagnostic binary ratios, it seems reasonable to represent original PAHs data set in three dimensions and thus visualize key information that was hidden in the table, while working with only B[a]A/Chry, Fluo/(Fluo + Pyr), and Ind/(Ind + B[g,h,i]P) of the original data (see Figure 4). Cluster analysis can also assist in visualizing the data in two dimensions. It is also worth mentioning that HCA uses 100% of information available, whilst the applications of diagnostic binary ratios tend to rely on certain PAH congeners. In Figure 5, HCA of the PAH variables extracted from marine sediments and PM_{10} were examined through Ward linkage on the correlation coefficient distance. Figure 5(a) discloses a single dominant group, which comprises 90% of HCA members, highlighting that the distribution pattern of PAHs in Khao Lak sediments is similar to other world

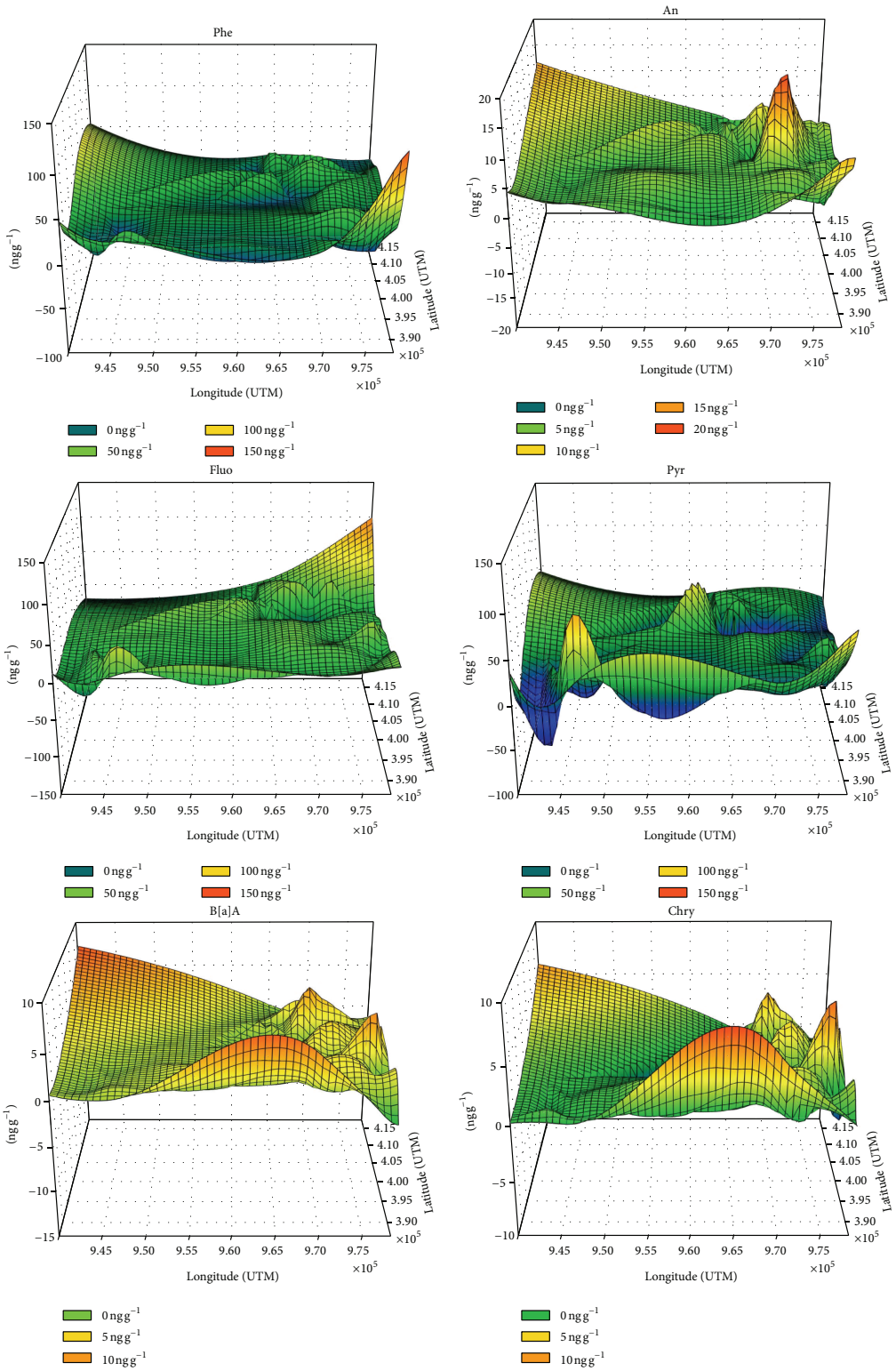


Figure 2: Continued.

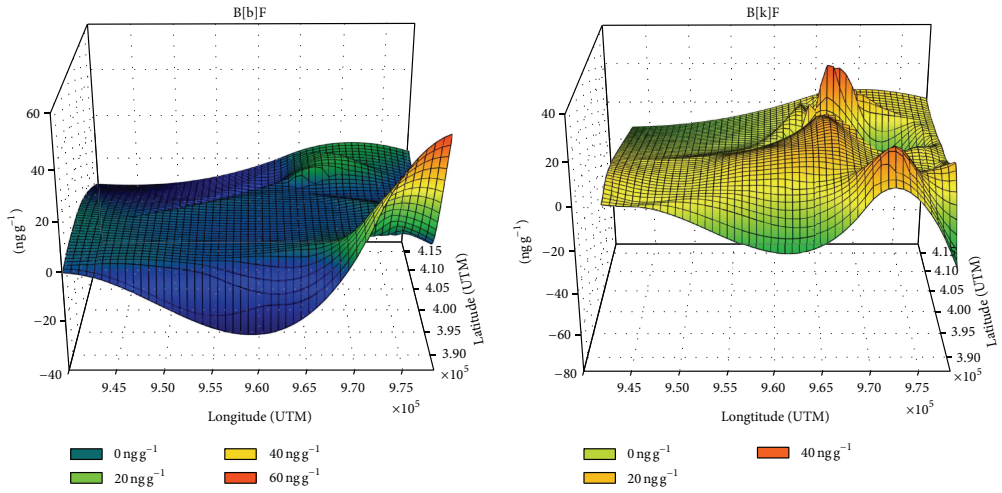


Figure 2: Distribution patterns of PAHs at the Tsunami affected coastal areas of Andaman Sea.

marine sediments to some degree. Apparently with no surprise, both "Pakarang group" and "Non-Pakarang group" are clustered next to each other and grouped with sediments collected from Spain and France (i.e., Figure 5(a), no. 17, no. 18, no. 21, and no. 22). For instance, "Non-Pakarang group" is grouped next to "Carteau, France (i.e., Figure 5(a), no. 17)," a highly nutrient-rich site located in the Gulf of Fos and subjected to chemical pollution from industrial and petrochemical complex at Fos [68]. Furthermore, most of the PAH contaminations observed in Santa Ponsa Bay (Figure 5(a), no. 20) and Rosas Bay (Figure 5(a), no. 21) are of pyrolytic origin [46]. This interpretation is in agreement with those of PCA results conducted by Tipmanee et al. [37], which conclude that 61.4% of PAHs are of pyrolytic origin (i.e., road dust). In Figure 5(a), "no. 19 (i.e., Barcelona Harbor, Spain)" is clearly a "*runt,*" at least in the single linkage dendrogram, because no. 19 does not join the main group until the last step of clusterizing process. This can be explained by another dominant source of PAHs in this coastal area. By plotting the ratios of ΣMP/P (sum of the methylphenanthrene concentrations/phenanthrene concentration) *versus* the isometric ratio of Fluo/Pyr for all the mussels sampled in the Mediterranean Sea, Baumard et al. [46] discovered an overimposition of petrogenic PAHs in Barcelona Harbor marine sediments. As a consequence, the convincing dissimilarity of no. 19 sample observed in dendrogram of Figure 5(a) can be attributed to the strong influence of either oil spill or petroleum leakage in Barcelona Harbor sediments.

Figure 5(b) demonstrates the HCA dendrogram of PAHs observed in Khao Lak marine sediments and PM_{10} collected from 17 various emission sources in Songkhla province. This analysis reveals three large differentiated clusters. One of these clusters groups together several of the particulate PAH emission sources in Songkhla province. In other two clusters appear the remaining variables. Within these clusters, other groupings appear such as those formed by "Pakarang group (no. 1)" and "Non-Pakarang group (no. 2)" observed in the second cluster. The third cluster reveals two members of PTB (no. 4) and RSB (no. 7), which are grouped next to "Pakarang group" and "Non-Pakarang group." Since PTB and RSB stand for "Para rubber tree burning" and "rice straw burning," respectively, these findings reflect the possible influence of biomass burnings on distribution of PAHs in Khao Lak sediments. It is also worth mentioning that no. 1 and no. 2 are close to no. 17 (WI) and no. 10 (BB), which are clusterized in the first cluster of dendrogram (see Figure 5(b)). Since WI and BB stand for "waste incinerator" and "biomass burning," one can assume some conceivable impacts of biomass burnings on PAH concentrations of Khao Lak coastal sediments in the Andaman Sea.

4. Conclusions

The Indian Ocean Tsunami of 2004 was only overshadowed by the 2011 Great East Japan Earthquake and Tsunami with more than 15,000 fatal casualties, but also the nuclear accidents and meltdowns in the Fukushima Daiichi Nuclear Power Plant. Apart from investigating significant concerns about the effect of PAH aerosols on human health, the comprehensive investigation of the "fingerprints" of PAH aerosols from marine deposits in 2004 Tsunami affected coastal areas of Thailand may contribute to the science leading to better Tsunami prediction.

Molecular diagnostic binary ratios of PAHs in Tsunami 2004 affected coastal sediments, Hat-Yai urban aerosols, and PM_{10} from various sources in Songkhla province were comprehensively investigated and compared. Three-dimensional plots of molecular diagnostic binary ratios successfully discriminate "Pakarang group" from other global marine sediment samples. Since hydroacoustic profiles show the impact of terrestrial deposits adjacent to "Pakarang Cape" coastal area [69, 70], it appears reasonable to ascribe Tsunami backwash 2004 to high deviations of "Pakarang group"

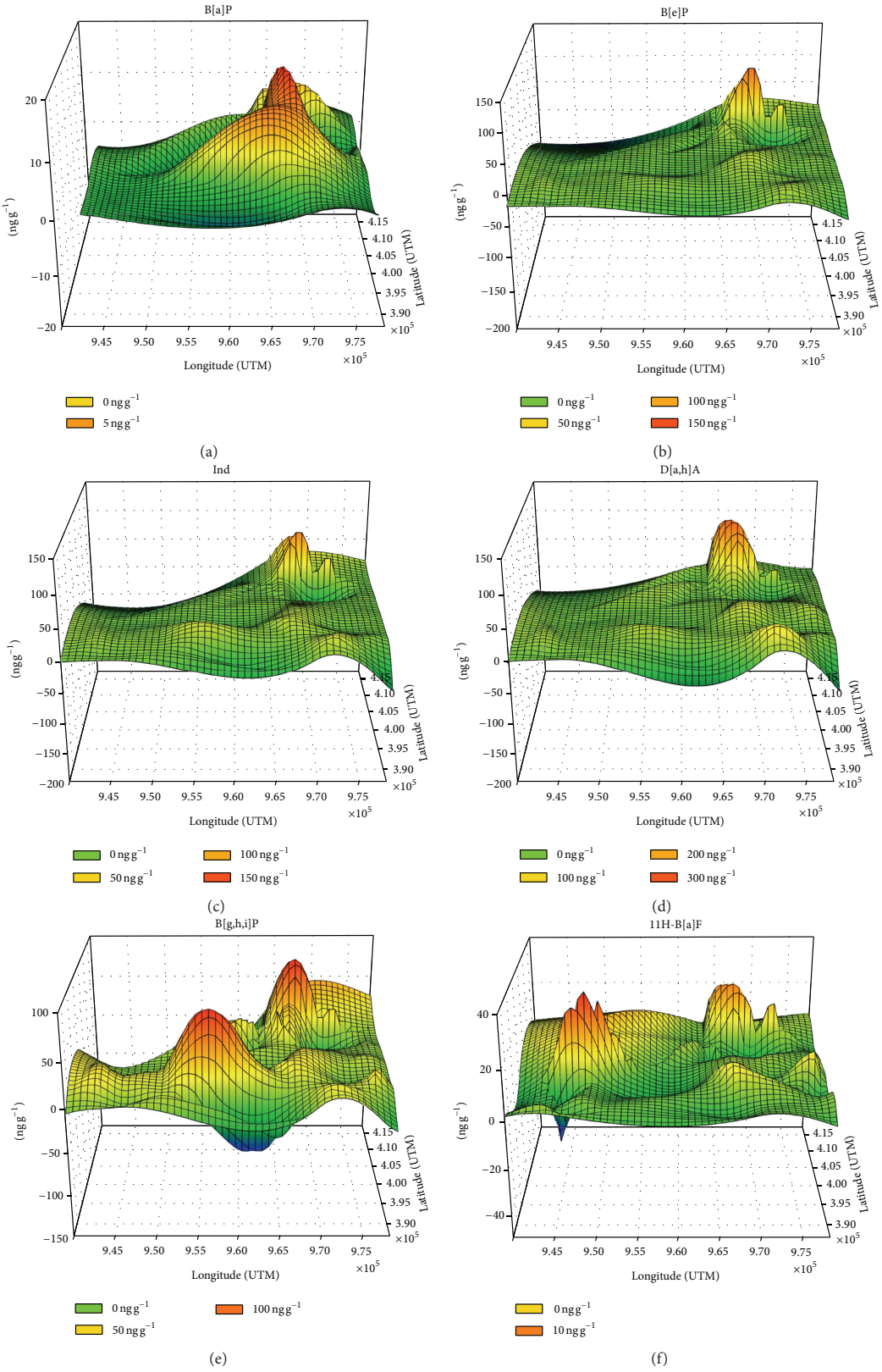


Figure 3: Continued.

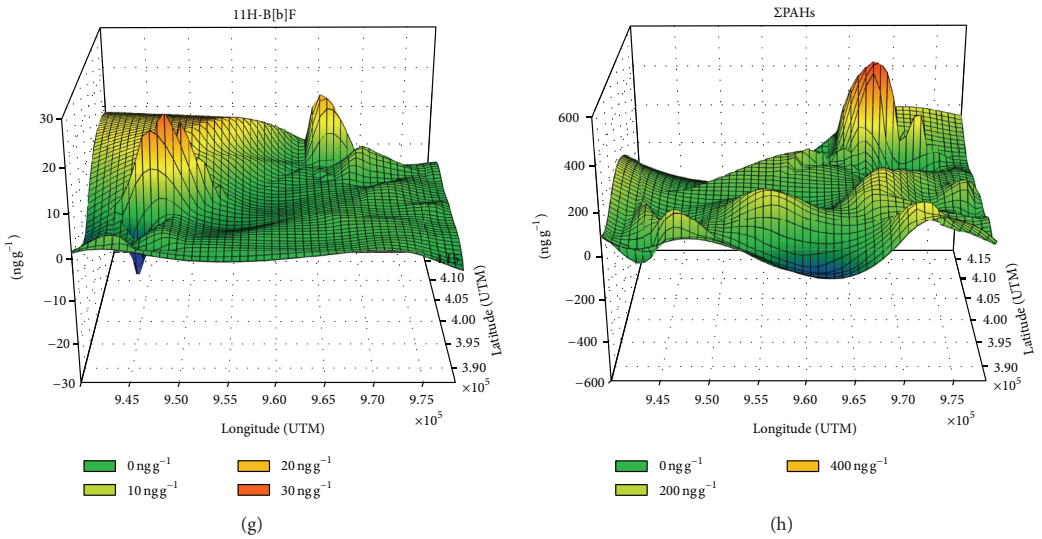
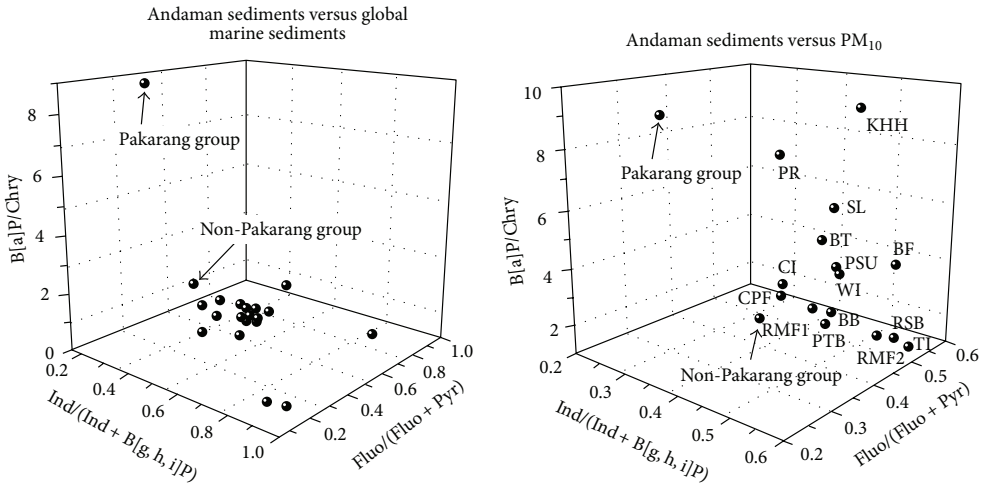


Figure 3: Distribution pattern of PAHs at the Tsunami affected coastal areas of Andaman Sea.



(a) Three-dimensional plots of molecular diagnostic binary ratios of B[a]P/Chry, Ind/(Ind + B[g,h,i]P), and Fluo/(Fluo + Pyr) of Pakarang group and Non-Pakarang group in comparison with those of other global marine sediments

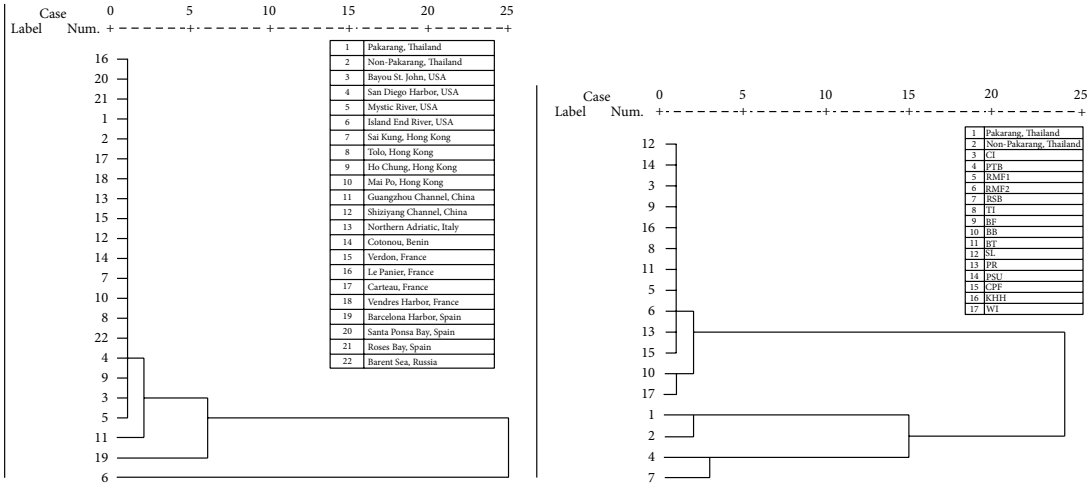
(b) Three-dimensional plots of molecular diagnostic binary ratios of B[a]P/Chry, Ind/(Ind + B[g,h,i]P), and Fluo/(Fluo + Pyr) of Pakarang group and Non-Pakarang group in comparison with those of PM$_{10}$ collected from various emission sources in Songkhla province

Figure 4: Diagnostic binary ratios of PAHs in Andaman Sea sediments and various types of PM$_{10}$ collected in Songkhla province, Thailand.

sediment samples observed in three-dimensional plots of binary ratios. Interestingly, five of six binary ratios were significantly different when comparing the average values of PAH contents in PM$_{10}$ collected at Hat-Yai city with Khao Lak sediments. This indicates that Khao Lak sediments have been influenced by more complicated emission sources rather than occupied by a long-range transportation of urban aerosols from Hat-Yai city. The application of HCA using PAH contents highlights the contribution of both pyrolytic combustions and biomass burning aerosols to distribution of PAH contents in Khao Lak coastal sediments. Overall, these findings may open a new window in using binary PAH ratios to investigate the paleotsunami from core sediments in other coastal regions and thus deeper insights into the science of Tsunami.

Conflict of Interests

The author declares that there is no conflict of interests regarding the publication of this paper.



(a) HCA of world marine sediments in comparison with those of Andaman Sea sediments

(b) HCA of PM_{10} from various emission sources in comparison with those of Andaman Sea sediments

Figure 5: Hierarchical dendrogram for PAHs using average linkage between groups.

Acknowledgments

This work was performed with the approval of National Institute of Development Administration (NIDA) and financial support from National Research Council of Thailand (NRCT). The author acknowledges Assistant Professor Dr. Charnwit Kositanont, Assistant Professor Dr. Surat Bualert, and Ms. Teeta Intasaen from Inter-Department of Environmental Science, Faculty of Graduate Studies, Chulalongkorn University, for their contributions to filed samplings and laboratory works. The author would like to express his deepest gratitude to Ms. Woranuch Deelaman, Ms. Jitlada Muprasit, Dr. Peter Feldens, and Dr. Klaus Schwarzer for their kind assistance.

References

[1] A. Bhargava, R. N. Khanna, S. K. Bhargava, and S. Kumar, "Exposure risk to carcinogenic PAHs in indoor-air during biomass combustion whilst cooking in rural India," *Atmospheric Environment*, vol. 38, no. 28, pp. 4761–4767, 2004.

[2] C. M. Chalbot, C. I. Vei, M. Lianou et al., "Environmental tobacco smoke aerosol in non-smoking households of patients with chronic respiratory diseases," *Atmospheric Environment*, vol. 62, pp. 82–88, 2012.

[3] L. D. Claxton and G. M. Woodall Jr., "A review of the mutagenicity and rodent carcinogenicity of ambient air," *Mutation Research: Reviews in Mutation Research*, vol. 636, no. 1–3, pp. 36–94, 2007.

[4] S. Pongpiachan, C. Choochuay, M. Hattayanone, and C. Kositanont, "Temporal and spatial distribution of particulate carcinogens and mutagens in Bangkok, Thailand," *Asian Pacific Journal of Cancer Prevention*, vol. 14, no. 3, pp. 1879–1887, 2013.

[5] S. Pongpiachan, D. Tipmanee, W. Deelaman, J. Muprasit, P. Feldens, and K. Schwarzer, "Risk assessment of the presence of polycyclic aromatic hydrocarbons (PAHs) in coastal areas of Thailand affected by the 2004 tsunami," *Marine Pollution Bulletin*, vol. 76, pp. 370–378, 2013.

[6] S. Pongpiachan, "Vertical distribution and potential risk of particulate polycyclic aromatic hydrocarbons in high buildings of Bangkok, Thailand," *Asian Pacific Journal of Cancer Prevention*, vol. 14, no. 3, pp. 1865–1877, 2013.

[7] S. Pongpiachan, "Diurnal variation, vertical distribution and source apportionment of carcinogenic polycyclic aromatic hydrocarbons (PAHS) in Chiang-Mai, Thailand," *Asian Pacific Journal of Cancer Prevention*, vol. 14, no. 3, pp. 1851–1863, 2013.

[8] C. B. Sette, T. D. A. Pedrete, J. Felizzola, A. H. Nudi, A. D. L. Scofield, and A. D. L. R. Wagener, "Formation and identification of PAHs metabolites in marine organisms," *Marine Environmental Research*, vol. 91, pp. 2–13, 2013.

[9] R. V. Yoshimine, R. S. Carreira, A. L. Scofield, and A. L. R. Wagener, "Regional assessment of PAHs contamination in SE Brazil using brown mussels (*Perna perna* Linnaeus 1758)," *Marine Pollution Bulletin*, vol. 64, no. 11, pp. 2581–2587, 2012.

[10] T. Lu, Z. Huang, C. S. Cheung, and J. Ma, "Size distribution of EC, OC and particle-phase PAHs emissions from a diesel engine fueled with three fuels," *Science of the Total Environment*, vol. 438, pp. 33–41, 2012.

[11] T. Okuda, H. Kumata, M. P. Zakaria, H. Naraoka, R. Ishiwatari, and H. Takada, "Source identification of Malaysian atmospheric polycyclic aromatic hydrocarbons nearby forest fires using molecular and isotopic compositions," *Atmospheric Environment*, vol. 36, no. 4, pp. 611–618, 2002.

[12] K. Slezakova, D. Castro, A. Begonha et al., "Air pollution from traffic emissions in Oporto, Portugal: health and environmental implications," *Microchemical Journal*, vol. 99, no. 1, pp. 51–59, 2011.

[13] H. Yang, S. Lai, L. Hsieh, H. Hsueh, and T. Chi, "Profiles of PAH emission from steel and iron industries," *Chemosphere*, vol. 48, no. 10, pp. 1061–1074, 2002.

[14] M. C. Liao, P. C. Chio, Y. W. Chen et al., "Lung cancer risk in relation to traffic-related nano/ultrafine particle-bound PAHs exposure: a preliminary probabilistic assessment," *Journal of Hazardous Materials*, vol. 190, no. 1-3, pp. 150–158, 2011.

[15] P. B. Hoyer, "Reproductive toxicology: current and future directions," *Biochemical Pharmacology*, vol. 62, no. 12, pp. 1557–1564, 2001.

[16] S. Matsui, "Endocrine disruptors," in *Encyclopedia of Ecology*, pp. 1259–1260, 2008.

[17] A. P. Wickramasinghe, D. G. G. P. Karunaratne, and R. Sivakanesan, "PM10-bound polycyclic aromatic hydrocarbons: Biological indicators, lung cancer risk of realistic receptors and 'source-exposure-effect relationship' under different source scenarios," *Chemosphere*, vol. 87, no. 11, pp. 1381–1387, 2012.

[18] M. Akyüz and H. Çabuk, "Meteorological variations of $PM_{2.5}/PM_{10}$ concentrations and particle-associated polycyclic aromatic hydrocarbons in the atmospheric environment of Zonguldak, Turkey," *Journal of Hazardous Materials*, vol. 170, no. 1, pp. 13–21, 2009.

[19] M. Amodio, M. Caselli, G. de Gennaro, and M. Tutino, "Particulate PAHs in two urban areas of Southern Italy: impact of the sources, meteorological and background conditions on air quality," *Environmental Research*, vol. 109, no. 7, pp. 812–820, 2009.

[20] T. Chetwittayachan, D. Shimazaki, and K. Yamamoto, "A comparison of temporal variation of particle-bound polycyclic aromatic hydrocarbons (pPAHs) concentration in different urban environments: Tokyo, Japan, and Bangkok, Thailand," *Atmospheric Environment*, vol. 36, no. 12, pp. 2027–2037, 2002.

[21] Z. Gu, J. Feng, W. Han et al., "Diurnal variations of polycyclic aromatic hydrocarbons associated with PM2.5 in Shanghai, China," *Journal of Environmental Sciences*, vol. 22, no. 3, pp. 389–396, 2010.

[22] J. Ringuet, A. Albinet, L. E. Garziandia, H. Budzinski, and E. Villenave, "Diurnal/nocturnal concentrations and sources of particulate-bound PAHs, OPAHs and NPAHs at traffic and suburban sites in the region of Paris (France)," *Science of the Total Environment*, vol. 437, no. 15, pp. 297–305, 2012.

[23] K. Zhang, B.-Z. Zhang, S.-M. Li, L.-M. Zhang, R. Staebler, and E. Y. Zeng, "Diurnal and seasonal variability in size-dependent atmospheric deposition fluxes of polycyclic aromatic hydrocarbons in an urban center," *Atmospheric Environment*, vol. 57, pp. 41–48, 2012.

[24] A. R. Mostafa, T. L. Wade, S. T. Sweet, A. K. A. Al-Alimi, and A. O. Barakat, "Distribution and characteristics of polycyclic aromatic hydrocarbons (PAHs) in sediments of Hadhramout coastal area, Gulf of Aden, Yemen," *Journal of Marine Systems*, vol. 78, no. 1, pp. 1–8, 2009.

[25] H. Takada, T. Onda, M. Harada, and N. Ogura, "Distribution and sources of polycyclic aromatic hydrocarbons (PAHs) in street dust from the Tokyo Metropolitan area," *Science of the Total Environment*, vol. 107, pp. 45–69, 1991.

[26] I. Tolosa, S. de Mora, M. R. Sheikholeslami, J. Villeneuve, J. Bartocci, and C. Cattini, "Aliphatic and aromatic hydrocarbons in coastal Caspian Sea sediments," *Marine Pollution Bulletin*, vol. 48, no. 1-2, pp. 44–60, 2004.

[27] M. B. Yunker, R. W. Macdonald, D. J. Veltkamp, and W. J. Cretney, "Terrestrial and marine biomarkers in a seasonally ice-covered Arctic estuary—integration of multivariate and biomarker approaches," *Marine Chemistry*, vol. 49, no. 1, pp. 1–50, 1995.

[28] M. B. Yunker, R. W. Macdonald, R. Vingarzan, R. H. Mitchell, D. Goyette, and S. Sylvestre, "PAHs in the Fraser River basin: a critical appraisal of PAH ratios as indicators of PAH source and composition," *Organic Geochemistry*, vol. 33, no. 4, pp. 489–515, 2002.

[29] M. Fang, W. Chang, C. Lee, and J. T. Liu, "The use of polycyclic aromatic hydrocarbons as a particulate tracer in the water column of Gaoping (Kaoping) Submarine Canyon," *Journal of Marine Systems*, vol. 76, no. 4, pp. 457–467, 2009.

[30] M. B. Yunker and R. W. Macdonald, "Petroleum biomarker sources in suspended particulate matter and sediments from the Fraser River Basin and Strait of Georgia, Canada," *Organic Geochemistry*, vol. 34, no. 11, pp. 1525–1541, 2003.

[31] U. Stenberg and T. Alsberg, "Capillary GC-MS analysis of PAH emissions from combustion of peat and wood in a hot water boiler," *Chemosphere*, vol. 8, no. 7, pp. 487–496, 1979.

[32] L. J. Brasser, "Polycyclic aromatic hydrocarbon concentrations in the Netherelands," VDI- Berichete Nr 348, 171-180, 1980.

[33] S. J. Mainwaring and D. M. Stirling, "A study of the size distribution and concentrations of polynuclear hydrocarbons in Melbourne air," in *Proceedings of 7th the International Clean Air*, 1981.

[34] X. Bi, G. Sheng, P. Peng, Y. Chen, Z. Zhang, and J. Fu, "Distribution of particulate- and vapor-phase n-alkanes and polycyclic aromatic hydrocarbons in urban atmosphere of Guangzhou, China," *Atmospheric Environment*, vol. 37, no. 2, pp. 289–298, 2003.

[35] H. Guo, S. C. Lee, K. F. Ho, X. M. Wang, and S. C. Zou, "Particle-associated polycyclic aromatic hydrocarbons in urban air of Hong Kong," *Atmospheric Environment*, vol. 37, no. 38, pp. 5307–5317, 2003.

[36] M. Tsapakis and E. G. Stephanou, "Occurrence of gaseous and particulate polycyclic aromatic hydrocarbons in the urban atmosphere: Study of sources and ambient temperature effect on the gas/particle concentration and distribution," *Environmental Pollution*, vol. 133, no. 1, pp. 147–156, 2005.

[37] D. Tipmanee, W. Deelaman, S. Pongpiachan, K. Schwarzer, and P. Sompongchaiyakul, "Using polycyclic aromatic hydrocarbons (PAHs) as a chemical proxy to indicate Tsunami 2004 backwash in Khao Lak coastal area, Thailand," *Natural Hazards and Earth System Science*, vol. 12, no. 5, pp. 1441–1451, 2012.

[38] R. C. Henry, "History and fundamentals of multivariate air quality receptor models," *Chemometrics and Intelligent Laboratory Systems*, vol. 37, no. 1, pp. 37–42, 1997.

[39] A. Siripong, "Andaman seacoast of Thailand field survey after the December 2004 Indian Ocean tsunami," *Earthquake Spectra*, vol. 22, no. 3, pp. S187–S202, 2006.

[40] W. Szczuciński, N. Chaimanee, P. Niedzielski et al., "Environmental and geological impacts of the 26 December 2004 tsunami in coastal zone of Thailand: overview of short and long-term effects," *Polish Journal of Environmental Studies*, vol. 15, no. 5, pp. 793–810, 2006.

[41] P. Feldens, K. Schwarzer, W. Szczuciński, K. Stattegger, D. Sakuna, and P. Somgpongchaiykul, "Impact of 2004 tsunami on seafloor morphology and offshore sediments, Pakarang Cape, Thailand," *Polish Journal of Environmental Studies*, vol. 18, no. 1, pp. 63–68, 2009.

[42] S. Pongpiachan, *Source apportionment of semi-volatile organic compounds in urban and rural air [Ph.D. thesis]*, University of Birmingham, Birmingham, UK, 2006.

[43] S. Pongpiachan, S. Bualert, P. Sompongchaiyakul, and C. Kositanont, "Factors affecting sensitivity and stability of polycyclic aromatic hydrocarbons," *Journal of Analytical Letters*, vol. 42, no. 13, pp. 2106–2130, 2009.

[44] S. Pongpiachan, K. Thamanu, K. F. Ho, S. C. Lee, and P. Sompongchaiyakul, "Predictions of gas-particle partitioning

coefficients (k_p) of polycyclic aromatic hydrocarbons at various occupational environments of Songkhla Province, Thailand," *The Southeast Asian Journal of Tropical Medicine and Public Health*, vol. 40, no. 6, pp. 1377–1394, 2009.

[45] A. Gogou, N. Stratigakis, M. Kanakidou, and E. G. Stephanou, "Organic aerosols in Eastern Mediterranean: components source reconciliation by using molecular markers and atmospheric back trajectories," *Organic Geochemistry*, vol. 25, no. 1-2, pp. 79–96, 1996.

[46] P. Baumard, H. Budzinski, Q. Michon, P. Garrigues, T. Burgeot, and J. Bellocq, "Origin and bioavailability of PAHs in the Mediterranean Sea from mussel and sediment records," *Estuarine, Coastal and Shelf Science*, vol. 47, no. 1, pp. 77–90, 1998.

[47] M. Bixian, F. Jiamo, Z. Gan et al., "Polycyclic aromatic hydrocarbons in sediments from the Pearl river and estuary, China: spatial and temporal distribution and sources," *Applied Geochemistry*, vol. 16, no. 11-12, pp. 1429–1445, 2001.

[48] A. P. Deshmukh, B. Chefetz, and P. G. Hatcher, "Characterization of organic matter in pristine and contaminated coastal marine sediments using solid-state 13C NMR, pyrolytic and thermochemolytic methods: a case study in the San Diego harbor area," *Chemosphere*, vol. 45, no. 6-7, pp. 1007–1022, 2001.

[49] H. W. Mielke, G. Wang, C. R. Gonzales, B. Le, V. N. Quach, and P. W. Mielke, "PAH and metal mixtures in New Orleans soils and sediments," *The Science of the Total Environment*, vol. 281, no. 1–3, pp. 217–227, 2001.

[50] H. H. Soclo, P. Garrigues, and M. Ewald, "Origin of polycyclic aromatic hydrocarbons (PAHs) in coastal marine sediments: case studies in Cotonou (Benin) and Aquitaine (France) areas," *Marine Pollution Bulletin*, vol. 40, no. 5, pp. 387–396, 2000.

[51] N. F. Y. Tam, L. Ke, X. H. Wang, and Y. S. Wong, "Contamination of polycyclic aromatic hydrocarbons in surface sediments of mangrove swamps," *Environmental Pollution*, vol. 114, no. 2, pp. 255–263, 2001.

[52] X. C. Wang, Y. X. Zhang, and R. F. Chen, "Distribution and partitioning of polycyclic aromatic hydrocarbons (PAHs) in different size fractions in sediments from Boston Harbor, United States," *Marine Pollution Bulletin*, vol. 42, no. 11, pp. 1139–1149, 2001.

[53] M. F. Simcik, S. J. Eisenreich, and P. J. Lioy, "Source apportionment and source/sink relationships of PAHs in the coastal atmosphere of Chicago and Lake Michigan," *Atmospheric Environment*, vol. 33, no. 30, pp. 5071–5079, 1999.

[54] H. Budzinski, I. Jones, J. Bellocq, C. Piérard, and P. Garrigues, "Evaluation of sediment contamination by polycyclic aromatic hydrocarbons in the Gironde estuary," *Marine Chemistry*, vol. 58, no. 1-2, pp. 85–97, 1997.

[55] W. F. Rogge, L. M. Hildemann, M. A. Mazurek, G. R. Cass, and B. R. T. Simoneit, "Sources of fine organic aerosol. 2. Noncatalyst and catalyst-equipped automobiles and heavy-duty diesel trucks," *Environmental Science and Technology*, vol. 27, no. 4, pp. 636–651, 1993.

[56] N. Tang, T. Hattori, R. Taga et al., "Polycyclic aromatic hydrocarbons and nitropolycyclic aromatic hydrocarbons in urban air particulates and their relationship to emission sources in the Pan-Japan Sea countries," *Atmospheric Environment*, vol. 39, no. 32, pp. 5817–5826, 2005.

[57] L. Lei, A. P. Khodadoust, M. T. Suidan, and H. H. Tabak, "Biodegradation of sediment-bound PAHs in field-contaminated sediment," *Water Research*, vol. 39, no. 2-3, pp. 349–361, 2005.

[58] T. Sayara, M. Pognani, M. Sarrà, and A. Sánchez, "Anaerobic degradation of PAHs in soil: Impacts of concentration and amendment stability on the PAHs degradation and biogas production," *International Biodeterioration and Biodegradation*, vol. 64, no. 4, pp. 286–292, 2010.

[59] Y. Tian, H. J. Liu, T. L. Zheng, K. K. Kwon, S. J. Kim, and C. L. Yan, "PAHs contamination and bacterial communities in mangrove surface sediments of the Jiulong River Estuary, China," *Marine Pollution Bulletin*, vol. 57, no. 6–12, pp. 707–715, 2008.

[60] C. K. Li and R. M. Kamens, "The use of polycyclic aromatic hydrocarbons as source signatures in receptor modeling," *Atmospheric Environment—Part A*, vol. 27, pp. 523–532, 1993.

[61] J. Niu, P. Sun, and K.-W. Schramm, "Photolysis of polycyclic aromatic hydrocarbons associated with fly ash particles under simulated sunlight irradiation," *Journal of Photochemistry and Photobiology A: Chemistry*, vol. 186, no. 1, pp. 93–98, 2007.

[62] J. Wilhelm, L. Stieglitz, E. Dinjus, and R. Will, "Mechanistic studies on the role of PAHs and related compounds in PCDD/F formation on model fly ashes," *Chemosphere*, vol. 42, no. 5–7, pp. 797–802, 2001.

[63] J. Sabaté, J. M. Bayona, and A. M. Solanas, "Photolysis of PAHs in aqueous phase by UV irradiation," *Chemosphere*, vol. 44, no. 2, pp. 119–124, 2001.

[64] Y. Bedjanian and M. L. Nguyen, "Kinetics of the reactions of soot surface-bound polycyclic aromatic hydrocarbons with O_3," *Chemosphere*, vol. 79, no. 4, pp. 387–393, 2010.

[65] M. C. Casado-Martínez, V. Branco, C. Vale, A. M. Ferreira, and T. A. DelValls, "Is Arenicola marina a suitable test organism to evaluate the bioaccumulation potential of Hg, PAHs and PCBs from dredged sediments?" *Chemosphere*, vol. 70, no. 10, pp. 1756–1765, 2008.

[66] E. Cortazar, L. Bartolomé, S. Arrasate et al., "Distribution and bioaccumulation of PAHs in the UNESCO protected natural reserve of Urdaibai, Bay of Biscay," *Chemosphere*, vol. 72, no. 10, pp. 1467–1474, 2008.

[67] D. Marinov, S. Dueri, I. Puillat et al., "Integrated modelling of polycyclic aromatic hydrocarbons in the marine environment: coupling of hydrodynamic, fate and transport, bioaccumulation and planktonic food-web models," *Marine Pollution Bulletin*, vol. 58, no. 10, pp. 1554–1561, 2009.

[68] N. Bodin, T. Burgeot, J. Y. Stanisière et al., "Seasonal variations of a battery of biomarkers and physiological indices for the mussel Mytilus galloprovincialis transplanted into the northwest Mediterranean Sea," *Comparative Biochemistry and Physiology C—Toxicology and Pharmacology*, vol. 138, no. 4, pp. 411–427, 2004.

[69] P. Feldens, K. Schwarzer, D. Sakuna, W. Szczuciński, and P. Sompongchaiyakul, "Sediment distribution on the inner continental shelf off Khao Lak (Thailand) after the 2004 Indian Ocean tsunami," *Earth, Planets and Space*, vol. 64, no. 10, pp. 875–887, 2012.

[70] D. Sakuna, W. Szczuciński, P. Feldens, K. Schwarzer, and S. Khokiattiwong, "Sedimentary deposits left by the 2004 Indian Ocean tsunami on the inner continental shelf offshore of Khao Lak, Andaman Sea (Thailand)," *Earth, Planets and Space*, vol. 64, no. 10, pp. 931–943, 2012.

Nat. Hazards Earth Syst. Sci., 13, 3113–3128, 2013
www.nat-hazards-earth-syst-sci.net/13/3113/2013/
doi:10.5194/nhess-13-3113-2013
© Author(s) 2013. CC Attribution 3.0 License.



Natural Hazards and Earth System Sciences
Open Access

Sediment transport on the inner shelf off Khao Lak (Andaman Sea, Thailand) during the 2004 Indian Ocean tsunami and former storm events: evidence from foraminiferal transfer functions

Y. Milker[1], M. Wilken[1], J. Schumann[1], D. Sakuna[2], P. Feldens[2,3], K. Schwarzer[2], and G. Schmiedl[1]

[1]Center of Earth System Research and Sustainability, University of Hamburg, Hamburg, Germany
[2]Institute of Geosciences, Coastal and Shelf Research, University of Kiel, Kiel, Germany
[3]GEOMAR Helmholtz Centre for Ocean Research Kiel, Kiel, Germany

Correspondence to: Y. Milker (yvonne.milker@uni-hamburg.de)

Received: 29 March 2013 – Published in Nat. Hazards Earth Syst. Sci. Discuss.: 29 May 2013
Revised: 29 October 2013 – Accepted: 2 November 2013 – Published: 5 December 2013

Abstract. We have investigated the benthic foraminiferal fauna from sediment event layers associated with the 2004 Indian Ocean tsunami and former storms that have been retrieved in short sediment cores from offshore environments of the Andaman Sea, off Khao Lak, western Thailand. Species composition and test preservation of the benthic foraminiferal faunas exhibit pronounced changes across the studied sections and provide information on the depositional history of the tsunami layer, particularly on the source water depth of the displaced foraminiferal tests. In order to obtain accurate bathymetric information on sediment provenance, we have mapped the distribution of modern faunas in non-tsunamigenic surface sediments and created a calibration data set for the development of a transfer function. Our quantitative reconstructions revealed that the resuspension of sediment particles by the tsunami wave was restricted to a maximum water depth of approximately 20 m. Similar values were obtained for former storm events, thus impeding an easy distinction of different high-energy events.

1 Introduction

The devastating tsunami of 26 December 2004 that originated from a 9.3 magnitude submarine earthquake off the northwest coast of the Indonesian island Sumatra (Stein and Okal, 2005) (Fig. 1) had severe impacts on the coastlines of southeastern Asia (Bell et al., 2005; Tsuji et al., 2006). The highly energetic tsunami wave resulted in major coastal changes and is documented in on- and offshore erosion phenomena and deposits. Detailed topographic, sedimentological and geochemical investigations documented the complex nature of erosion and deposition processes of the tsunami wave and its backflow along the western coast of Thailand (Choowong et al., 2007; Fagherazzi and Du, 2007; Hawkes et al., 2007; Jankaew et al., 2008; Mard Karlsson et al., 2009; Feldens et al., 2009; Sakuna et al., 2012). However, little is known on the exact provenance and transport dynamics of sediment particles in tsunamigenic offshore deposits. Specific sedimentological characteristics such as thickness of the high-energy layer, its grain size distribution and sorting have been studied by several authors in order to distinguish between storm and tsunami events (e.g., Morton et al., 2007; Kortegaas and Dawson, 2007; Dahanayake and Kulasena, 2008). These studies also revealed that it is often difficult to separate a storm layer from a tsunami layer from the sedimentological record alone.

Among other microfossils, benthic foraminifers are frequently found in tsunami deposits, providing information on the provenance of the sediment components (review by Mamo et al., 2009). Size distribution, shape and preservation of foraminiferal tests document the hydrodynamics of the tsunami wave but are also influenced by rapid post-depositional taphonomic processes (Yawsangratt et al., 2011). The occurrence of certain marine taxa in onshore tsunamites allowed for an assessment of the water depth range from which sediment particles have been resuspended and incorporated into the tsunami wave (e.g., Nanayama and

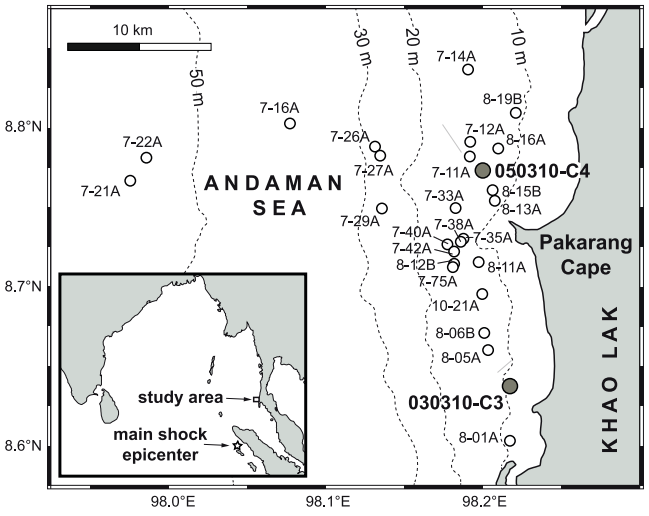


Fig. 1. Bathymetric map of the study area on the inner shelf of the eastern Andaman Sea off Cape Pakarang, Khao Lak, southwestern Thailand. Shown are the locations of the investigated surface sediment sites (small open circles) and the core sites (large grey circles) addressed in this study. See Table 1 for station details. The positions of the study area and the main shock of the 26 December 2004 earthquake are marked in the overview map of the northern Indian Ocean.

Shigeno, 2006; Uchida et al., 2010). Typically, the tsunamite assemblages contain open-shelf taxa, contrasting with lower diverse brackish faunas in under- and overlying marsh or other terrestrial sediments (Uchida et al., 2010). However, the published water depth estimates vary significantly, ranging from 30 m or shallower for a historical tsunami of southeastern India (Satyanarayana et al., 2007) up to 90 m for the 1992 tsunami of Hokkaido (Nanayama and Shigeno, 2006), and between 50 and 300 m for various tsunamites in Japan and southeastern Asia (Uchida et al., 2010). This compilation demonstrates that even tests from outer shelf to upper bathyal taxa have been documented in tsunamites (Dominey-Howes et al., 1998; Uchida et al., 2010). Sugawara et al. (2009) studied the foraminiferal content of offshore deposits of the southwest coast of Thailand related to the 2004 Indian Ocean tsunami on 4 stations from 4.5 m to 20.5 m water depth. The studied faunas reveal a significant backwash component but lack evidence for transport of particles from deeper to shallower water depth which might result from their sampling strategy. To date, all of these depth estimates have been based on qualitative information of bathymetric species ranges or hydrodynamic estimation of the tsunami wave and therefore remain relatively inaccurate.

In tropical and subtropical regions, the distribution of benthic shelf foraminifers depends on various factors, such as food availability and quality, substrate-type, bottom current velocity, temperature and salinity, vegetation and light penetration (e.g, Szarek et al., 2006; Murray, 2006; Parker and Gischler, 2011). The specific environmental setting is commonly reflected in a distinct depth zonation of shelf species. Of particular relevance are symbiont-bearing larger foraminifers that are adapted to limited depth intervals within the photic zone, depending on the specific light requirements of the algal symbiont and other habitat variables such as microscale environmental gradients within the substrate (Hohenegger et al., 1999; Beavington-Penney and Racey, 2004; Renema, 2006a, b). Different quantitative methods have been developed for water depth estimates, e.g, based on the ratio between benthic and planktonic foraminifers (Van der Zwaan et al., 1990), and the distribution patterns of certain faunas and benthic indicator taxa (Horton et al., 1999; Hohenegger, 2005; Milker et al., 2009). These methods have been successfully applied to paleobathymetric reconstructions in various sedimentary environments (e.g., Nelson et al., 2008; Rossi and Horton, 2009; Hawkes et al., 2010; Milker et al., 2011) and also bear a high potential for quantitative provenance studies of tsunami deposits.

The overall target of the present study is to generate quantitative data on the provenance of foraminiferal tests in high-energy event deposits from the inner shelf off Khao Lak, comprising layers of the 2004 tsunami and former storm events. For this, benthic foraminifers have been quantitatively analyzed from surface sediment samples and from two sediment cores retrieved from selected depositional systems of the inner shelf of the study area. The recent data set was used to establish a transfer function for water depth that was then applied to the fossil faunas. Our data will be particularly useful for sedimentological and modeling studies on hydrodynamics, wavelength and amplitude of tsunami waves. They will also contribute to the toolbox for distinguishing between storm and tsunami deposits.

2 Study area

The study area is situated 25 km off the Khao Lak region (Thailand) near Pakarang Cape (Andaman Sea) and covers an area of $\sim 1000\,km^2$ (Table 1, Fig. 1). The Andaman Sea is a marginal sea, separated from the Indian Ocean by the Nicobar and Andaman Islands. It is characterized by a relatively broad shelf region up to 200 km wide in the north, and a narrower shelf region in the south (Saidova, 2008). The absence of major riverine influence results in sedimentation of mixed siliciclastic–carbonate sediments, in many places dominated by coral–algal sand (Saidova, 2008; Feldens et al., 2009). The region is influenced by the monsoonal system with northeasterly winds during winter and southwesterly winds during summer. The monsoon system also accounts for the hydrologic properties of surface water masses. The summer monsoon results in stronger waves, influencing the coastal dynamics (Scheffers et al., 2012). In the southern Andaman Sea, the yearly range of surface water temperatures is 26–29 °C; surface salinities range between 31.5 and 33 psu (Levitus and Boyer, 1994; Varkey et al., 1996). The

Table 1. Surface sample and sediment core IDs, sampling year, longitude and latitude, and water depth of the investigated surface samples and sediment cores (see also Fig. 1).

Sample/core ID	Sampling period	Code in this study (RDA)	Type of material	Longitude	Latitude	Water depth (m)
021207-11A	12/2007	1	surface sample	08° 46.901	98° 11.512	20.1
021207-12A	12/2007	2	surface sample	08° 47.459	98° 11.528	20.1
021207-14A	12/2007	3	surface sample	08° 50.189	98° 11.433	18.7
021207-16A	12/2007	4	surface sample	08° 48.147	98° 04.652	44.7
031207-21A	12/2007	5	surface sample	08° 45.989	97° 58.549	63.4
031207-22A	12/2007	6	surface sample	08° 46.860	97° 59.166	61.8
031207-26A	12/2007	7	surface sample	08° 47.278	98° 07.884	33.6
031207-27A	12/2007	8	surface sample	08° 46.932	98° 08.094	26.5
031207-29A	12/2007	9	surface sample	08° 44.938	98° 08.154	25.1
051207-33A	12/2007	10	surface sample	08° 44.958	98° 10.965	17.0
051207-35A	12/2007	11	surface sample	08° 43.796	98° 11.270	15.2
051207-38A	12/2007	12	surface sample	08° 43.682	98° 11.168	15.1
051207-40A	12/2007	13	surface sample	08° 43.584	98° 10.655	17.8
051207-42A	12/2007	14	surface sample	08° 43.319	98° 10.908	15.7
081207-75A	12/2007	15	surface sample	08° 42.744	98° 10.866	16.5
061208-01A	12/2008	16	surface sample	08° 36.181	98° 13.044	10.3
061208-05A	12/2008	17	surface sample	08° 39.600	98° 12.217	13.0
061208-06II-B2	12/2008	18	surface sample	08° 40.250	98° 12.067	13.3
061208-11A	12/2008	19	surface sample	08° 42.917	98° 11.850	14.9
061208-12B	12/2008	20	surface sample	08° 42.860	98° 10.922	19.4
061208-13A	12/2008	21	surface sample	08° 45.233	98° 12.460	12.6
061208-15B	12/2008	22	surface sample	08° 45.639	98° 12.372	14.0
061208-16A	12/2008	23	surface sample	08° 47.200	98° 12.592	15.4
061208-19B	12/2008	24	surface sample	08° 48.548	98° 13.265	13.0
030310-21A	03/2010	25	surface sample	08° 41.720	98° 11.982	15.2
030310-C3	03/2010		sediment core	08° 38.708	98° 12.931	9.5
050310-C4	03/2010		sediment core	08° 46.659	98° 12.269	15.3

Andaman Sea is influenced by micro- to mesotidal semidiurnal tides with a tidal range from 1.1 to 3.6 m (Thampanya et al., 2006). This coastal region of the Andaman Sea is relatively unaffected by strong tropical cyclones. Typhoons can occur in the study area but their frequency is low (Kumar et al., 2008; Phantuwongraj and Choowong, 2012). The absence of larger riverine discharge (Feldens et al., 2009) as well as the absence of large storm events between the deposition of the 2004 tsunami deposits and the sampling campaigns from 2007 to 2010 (Regional Specialized Meteorological Centre (RMSC), New Delhi) allows for the investigation of depositional processes prior to, during and after the tsunami event in 2004.

3 Material and methods

3.1 Surface sediment samples and sediment cores

For this study, a total of 25 surface samples and two sediment cores, taken from the investigation area during three research cruises (November–December 2007, November–December 2008, February–March 2010), were investigated (Fig. 1, Table 1). The surface samples were collected with a grab sampler from water depth ranging from 10.3 to 63.4 m. The sites were selected based on detailed sea-floor mapping (Feldens et al., 2009, 2012) with high-resolution hydroacoustic systems (side-scan sonar, shallow seismic systems, multibeam echosounder) and an underwater video camera in order to cover a maximum variety of substrates and to get a clear picture of sediment distribution patterns and morphological features. The two sediment cores were recovered with a Rumohr gravity corer at 9.5 m water depth (core 030310-C3, length 97 cm) and 15.3 m water depth (core 050310-C4, length 56 cm) (Fig. 1; Table 1).

According to different lithological units of the cores, nine samples of 1 cm thickness were investigated from core 030310-C3 and eight samples from core 050310-C4 (for sampling position see Fig. 2). Six samples of core 030310-C3 and four samples of core 050310-C4 were taken from layers characterized by coarser-grained units. Three samples from core 030310-C3 and four samples from core 050310-C4 were taken from finer-grained layers deposited under normal background sedimentation. Two surface samples were taken onshore to investigate specimens redeposited during the 2004 tsunami.

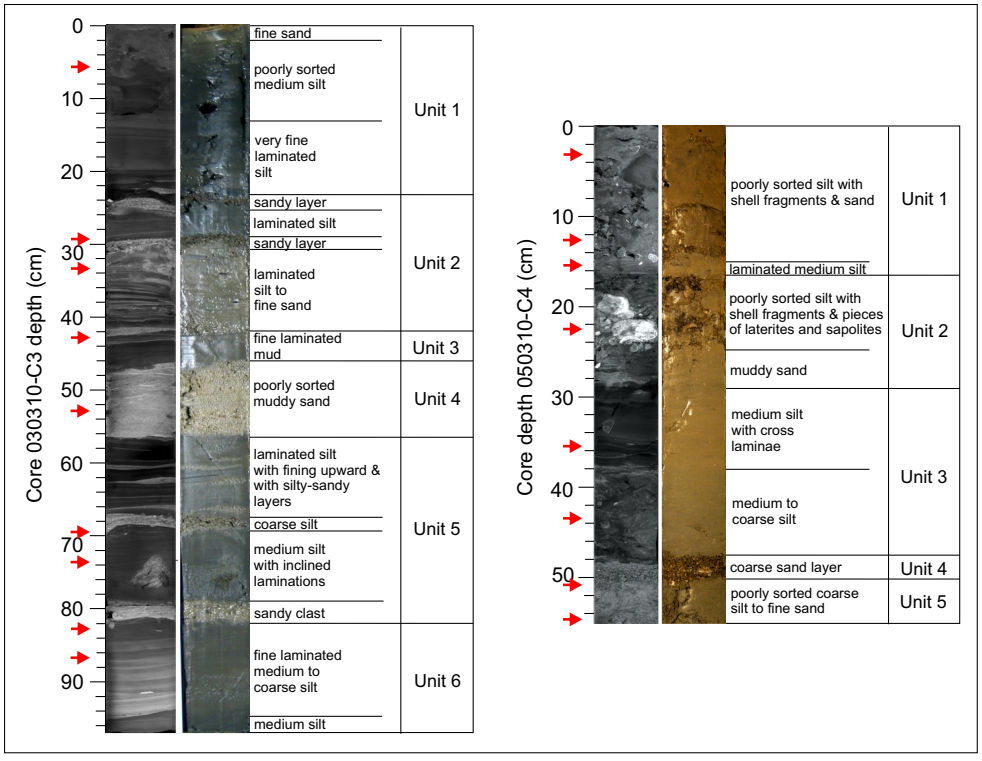


Fig. 2. Photographs, X-radiographs and definition of lithological units of sediment cores 030310-C3 and 050310-C4 versus core depth. The red arrows mark sample positions investigated in the frame of this study.

3.2 Foraminiferal and environmental data

Both the surface and core samples were wet-sieved with a 63 µm sieve. The fraction > 63 µm was dried at 40 °C for later foraminiferal analysis. The modern and fossil faunas were investigated from the > 125 µm fraction using representative splits containing approximately 300 benthic foraminiferal specimens. The identification of the foraminifera on the species level was mainly based on the studies of Hottinger et al. (1993), Jones (1994) and Hohenegger et al. (1999). Rare species or specimens that could not be identified on the species level were grouped into their genus or family. Potentially relocated benthic foraminifera (broken tests, tests fragments, and tests with yellowish-brown coloration) were counted separately.

In order to extract the dominant modern and fossil benthic foraminiferal assemblages, a principal component analysis (PCA) in Q-mode and with varimax rotation was carried out on the surface samples. A total of 53 modern foraminiferal taxa having relative minimum abundances of 0.5 % on the total fauna and being present in at least 3 samples were included into analysis. All potentially relocated specimens were excluded. The number of principal components (PCs) was selected based on eigenvalues > 1. PC loadings ≥ 0.4 for each axis were defined as significant (Malmgren and Haq, 1982; Backhaus et al., 2006).

In order to examine the relationship between the modern species in the data set of the surface samples and environmental parameters, a redundancy analysis (RDA) was carried out using Canoco (version 4.5) (Ter Braak and Smilauer, 2002; Leps and Smilauer, 2003). We selected the water depth and the percentages of silt and clay (< 63 µm), fine sand (63–125 µm) and coarser-grained sediment (> 125 µm) as environmental parameters. We used a reduced surface data set with 23 species having percentages exceeding 5 % in the total assemblage. Species counts were square-root-transformed and environmental parameters were standardized before analysis. Partial RDAs (with each environmental variable as the only variable) were calculated to evaluate the individual influence of the environmental parameters on the foraminiferal assemblages.

3.3 Development of foraminiferal-based transfer functions

We applied the detrended canonical correspondence analysis (DCCA) on the same reduced modern data set used for RDA (containing 23 species with percentages higher than 5 %) on the total fauna to analyze whether the species show a linear or unimodal distribution in relation to water depth (Birks, 1998, 1995). Birks (1995) suggests the use of linear regression methods for DCCA gradient lengths below 2 SD

standard deviation (SD) units, and unimodal methods for gradient lengths larger than 2 SD units. For this approach, we used the CANOCO software package (version 4.5) (Leps and Smilauer, 2003; Ter Braak and Smilauer, 2002).

For the development of the transfer function, the modern (training) data set was reduced to benthic foraminifera, identified on the species level, and with relative abundances of $> 0.5\,\%$ on the total dead assemblages. The fossil data sets were reduced to benthic species present in the surface data set. Potentially relocated specimens were removed from the training data set. The final modern data set consisted of 25 surface samples with a total of 49 dead species, ranging from 10.3 to 63.4 m water depth. In the fossil data sets, a total of 37 species from core 030310-C3 and 38 species from core 050310-C4 were used for reconstruction.

The modern analog technique (MAT) was applied to test whether the fossil samples provide good analogs for the modern samples by calculating dissimilarity coefficients (MinDC (minimum distance to closest analog) dissimilarity coefficients) (Birks, 1995). We selected the square chord distance as the dissimilarity coefficient (Overpeck et al., 1985) and the seven most similar modern samples. Coefficients lower than the 10th percentile have been defined as good analogs, coefficients between the 10th and 20th percentile have been considered as fair analogs and coefficients larger than the 20th percentile as poor analogs (Horton and Edwards, 2006; Birks, 1995; Kemp et al., 2009). For all calculations we used the C^2 software package (version 1.7.2) (Juggins, 2003).

We tested three methods for the paleo-water depth estimates in the sediment cores: the partial least squares (PLS) method that is based on a linear species–environment relationship, the weighted averaging (WA) that is based on a unimodal species–environment relationship and finally the combination of both methods, the WA-PLS method. The latter is presented here. The WA-PLS method creates new components from a data set by maximizing the covariance between the scores of the independent variable (water depth) and the dependent variables (species abundances) (Birks, 1998; Ter Braak and Juggins, 1993).

In order to obtain a normal distribution, species counts were square-root-transformed. In order to evaluate the performance of the transfer functions, we used the apparent coefficient of determination (R^2), allowing for an evaluation of the strength of the linear relationship between the observed and estimated water depths in the surface data set. In order to calculate the coefficient of determination of prediction (R^2_{jack}) and the root mean squared error of prediction (RMSEP) in the surface data set, we used the "jack-knifing" (leave one out) cross-validation technique (Horton and Edwards, 2006; Ter Braak and Juggins, 1993). Bootstrapping cross-validation (1000 cycles) was selected to evaluate the sample-specific errors of prediction in the fossil data sets (Birks et al., 1990; Horton and Edwards, 2006). The number of components for WA-PLS was selected according to the lowest RMSEP values if the reduction in prediction error exceeds 5 % for this component compared to the next lower component (Ter Braak and Juggins, 1993). All calculations were performed with the C^2 software, version 1.7.2 (Juggins, 2003).

4 Results

4.1 Lithology and sediment characteristics of sediment cores

The surface sediments are composed of a mixture of siliciclastic and carbonate particles of varying proportions and grain sizes. The biogenic components predominantly comprise coral and algal fragments, mollusc shells, echinoid fragments and benthic foraminifers. Differences are also characterized by the sand content ($> 63\,\mu$m) ranging from approximately 6 and to almost 100 % (Table S1). Most samples exhibit high sand contents exceeding 90 %. Local exceptions are restricted to several shallow mud-dominated sites (6–32 % sand) and the deepest sites (67–68 % sand).

The sediment cores were subdivided into different lithological units based on grain-size distributions and sedimentary structures, identified by visual inspection and/or by X-radiography images of the cores (Fig. 2).

Core 030310-C3 has been subdivided into six units (Fig. 2). Unit 6 consists of medium to coarse silt, with well-sorted medium silt in its lower part and finely laminated medium to coarse silt in its upper part. The contact to unit 5 is sharp and erosional. Unit 5 is mainly composed of very fine sand and silt. At its base a sandy clast, two cm in diameter, was found. The lower part of unit 5 consists of coarse silt followed by a subunit with medium silt showing some laminations, and a subunit of coarse silt. The upper part of unit 5 consists of laminated silt, showing a fining upward, and contains some mm-thick layers of coarse silt to very fine sand. Unit 4 is composed of a poorly sorted muddy sand layer and unit 3 consists of finely laminated mud. Unit 2 is composed of laminated clayey silt and contains two sand layers with laterites and shell fragments. The lower part of unit 2 consists of laminated silt to fine sand and the upper part is composed of slightly inclined laminated silt. The uppermost unit 1 consists of poorly sorted silt with a finely laminated silt subunit in the lower part and a medium silt subunit in the upper part.

Sediment core 050310-C4 has been subdivided into five units (Fig. 2). Unit 5 is composed of very poorly sorted coarse silt to fine sand and contains some shells. Unit 4 consists of a layer of coarse sand containing shell fragments. Unit 3 is composed of poorly sorted silt with medium-coarse silt in the lower part and medium silt in the upper part. The lower part of unit 2 is composed of muddy sand, while the upper part is an admixture of poorly to very poorly sorted silt, sand, gravels and shell fragments, clasts of sapolite, quartz and laterites. Unit 1, in the uppermost part of the core, consists of a laminated medium silt layer in the lowermost part followed by a subunit consisting of an admixture of poorly to very poorly sorted silt, sand, and shell fragments.

4.2 Distribution of foraminifera in the surface sediments

In the surface sediments, we identified a total of 59 different species. The shallow sites contain a significant amount of larger foraminifera with higher percentages of *Amphistegina radiata, Pararotalia stellata, Dentritina ambigua, Operculina ammonoides, Operculina complanata, Amphistegina lessonii, Amphistegina* sp. 1 and *Neorotalia calcar* (Fig. 3, Appendix A). Further dominant taxa include *Siphonaperta* sp. 2 (with a maximum of 32.1 %), *Quinqueloculina* sp. 1 (14.7 %), *Discorbinella bertheloti* (19.3 %), *Neoeponides praecinctus* (16.8 %),*Saidovina subangularis* (14.1 %), *Cibicidoides pseudoungerianus* (17.2 %) and *Quinqueloculina seminula* (9.1 %). Most of these taxa show a distinct bathymetric zonation, with species occurring with higher numbers at the shallower stations such as *P. stellata, Borelis schlumbergeri, A. lessonii, S. elliptica, D. ambigua* and *N. calcar*; at stations with intermediate water depths such as *A. radiata, O. ammonoides* and *N. praecinctus*; and at stations with higher water depths such as *S. subangularis* and *C. pseudoungerianus* (Fig. 3).

We observed relatively high amounts of potentially redeposited specimens with maximum percentages of 24 % (mean of 10.5 %) on the total assemblages at the shallower sites from approximately 10 to 30 m water depth, while the deeper sites contained lower amounts (mean of 3 %).

The PCA explains 89.1 % of the total variance in the surface data set for the first six principal components (PCs) (Table 2). The stations deeper than ∼ 45 m water depth are dominated by a *Neoeponides praecinctus–Operculina complanata* assemblage (PC2) with *S. subangularis, C. pseudoungerianus* and *D. bertheloti* as associated species (Fig. 4, Table 2). This assemblage explains 10 % of the total variance. The stations at intermediate water depths (between 16 and 34 m) are characterized by the *Amphistegina radiata* assemblage, containing *O. ammonoides* and *N. praecinctus* as associated taxa (PC1) (Fig. 4, Table 2). This PC explains 14.3 % of the total variance. The shallower stations, between 13 and 26 m water depth in the northern and middle part of the study area, are dominated by the *Siphonaperta* sp. 2 assemblage (PC3), with *A. radiata, Quinqueloculina* sp. 1 and *O. ammonoides* as associated species (Fig. 4, Table 2). This PC explains 38.5 % of the total variance. The shallowest stations in the study area, with water depths between 10 and 15 m, are characterized by three assemblages, each of them explaining almost 9 % of the total variance in the data set (Fig. 4, Table 2). The *Discorbinella bertheloti* assemblage (PC4) appears in the southern part of the study area and includes *Rosalina* spp., *Q. seminula, T. oblonga* and *A. tepida* as associated taxa. The *Operculina ammonoides–Dentritina ambigua* assemblage (PC5) occurs in the northern part of the study area and contains *A. lessonii* as the most important associated species. Finally, the *Pararotalia stellata* assemblage (PC6) occurs in the southernmost part of the study area (Fig. 4). Associated species of this assemblage are *A. radiata* and *B. schlumbergeri*.

Table 2. Results of the principal component analysis (see also Fig. 4) with the total variance explained by each principal component (PC) and the scores of the most important species. The species in bold, having the highest scores, are eponymous for the assemblages extracted from the surface samples.

PC axis	Explained variance (%)	Species	Scores
1	14.29	***Amphistegina radiata***	5.71
		Operculina ammonoides	1.31
		Neoeponides praecinctus	1.24
		Discorbinella bertheloti	0.89
		Amphistegina sp.	0.74
		Amphistegina lessonii	0.62
		Siphonaperta sp. 1	0.57
2	10.08	***Neoeponides praecinctus***	3.32
		Operculina complanata	3.03
		Saidovina subangularis	2.85
		Cibicidoides pseudoungerianus	2.78
		Discorbinella bertheloti	2.26
		Anomalinoides colligerus	0.89
		Reussella spinulosa	0.70
		Bolivina sp.	0.56
		Siphonaperta sp. 2	0.54
3	38.50	***Siphonaperta* sp. 2**	5.80
		Amphistegina radiata	2.80
		Quinqueloculina sp. 1	1.84
		Operculina ammonoides	1.11
4	8.86	***Discorbinella bertheloti***	4.28
		Rosalina spp.	3.88
		Quinqueloculina seminula	1.96
		Triloculina oblonga	1.65
		Ammonia tepida	1.05
5	8.86	***Operculina ammonoides***	3.49
		Dentritina ambigua	3.24
		Amphistegina lessonii	3.20
		Siphonaperta sp. 3	1.38
		Amphistegina sp.	1.24
		Borelis schlumbergeri	1.23
		Discorbinella bertheloti	1.02
		Pararotalia stellata	1.02
6	8.56	***Pararotalia stellata***	6.13
		Amphistegina radiata	1.89
		Borelis schlumbergeri	1.31
		Quinqueloculina sp. 1	0.95
		Elphidium craticulatum	0.65
		Quinqueloculina seminula	0.61

The results of the redundancy analysis (RDA) applied on the surface samples show that the water depth, explaining a total of 22 % of the variance ($p > 0.001$) in the data set, is the most important environmental parameter, followed by the proportion of silt and clay (pelite) (20.5 %, $p < 0.002$), fine sand (19.5 %, $p < 0.002$) and the coarser fraction (17.0 %,

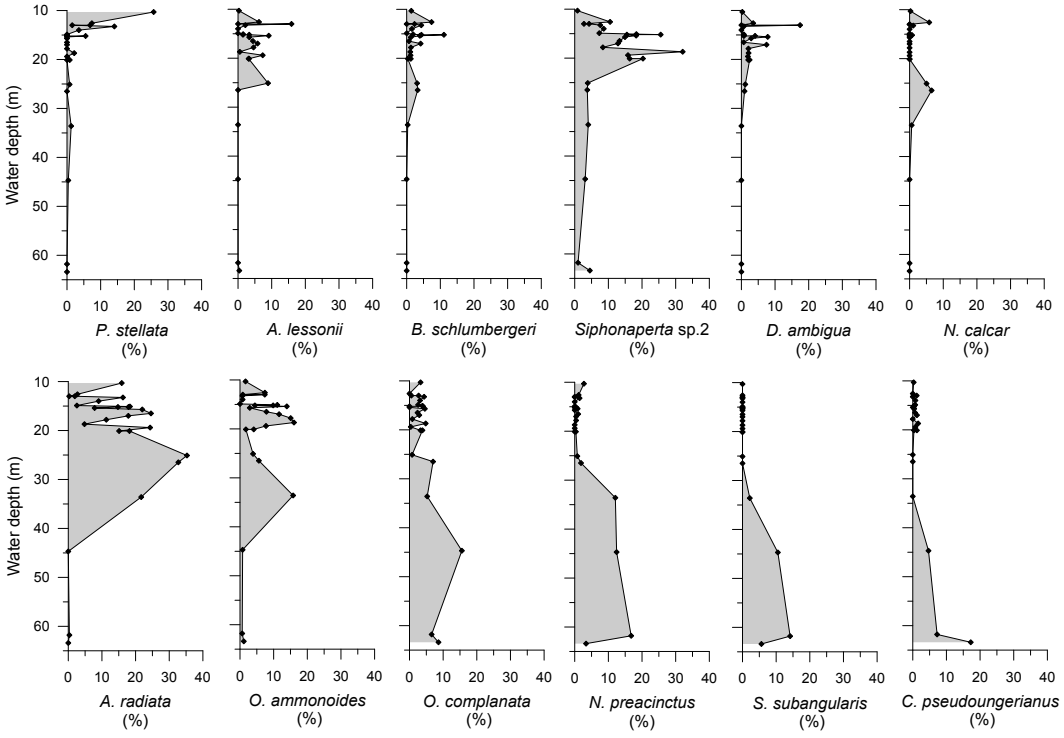


Fig. 3. Relative abundance of selected recent benthic foraminifera from surface sediments versus water depth, showing a distinct bathymetric zonation. Only species having a relative abundance of $> 5\,\%$ on the recent assemblages are presented.

Table 3. Results of the redundancy analysis (RDA).

Axes	1	2	3	4	Captured variance (%)	*p* value
Eigenvalues	0.296	0.135	0.068	0.014		
Species–environment correlations	0.905	0.945	0.802	0.529		
Cumulative percentage variance						
of species data	29.60	43.10	49.80	51.20		
of species–environment relation	57.80	84.10	97.30	100.00		
Correlation						
Water depth	0.685	−0.567	0.210	−0.001	22.2	<0.001
Fraction < 63 mum	0.699	0.245	−0.426	−0.123	20.5	< 0.002
Fraction > 125 mum	−0.627	−0.394	0.038	0.310	17.0	<0.001
Fraction 63–125 mum	0.643	0.438	0.398	0.098	19.5	<0.002

$p < 0.001$) (Table 3). Water depth, pelite and fine sand are positively correlated to the first RDA axis, while the content of coarser-grained sediment is negatively correlated to the first RDA axis (Fig. 5, Table 3). This axis explains a total of 29.6 % of the total variance in the data set (Table 3). Species of the PC2 assemblage, such as *S. subangularis*, *C. pseudoungerianus*, *Anomalinoides colligerus*, *N. praecinctus, and O. complanata*, show a clear correlation with increasing water depths, while other species, such as *B. schlumbergeri* and *N. calcar,* exhibit an association with lower water depths (Figs. 4 and 5). The species of the PC4 assemblage, such as *D. bertheloti*, *T. oblonga*, *Q. seminula* and *A. tepida,* show a correlation to finer-grained substrate. In contrast, *O. ammonoides*, *Siphonaperta* sp. 1 and *Siphonaperta* sp. 2 show a close relation to coarser-grained material. The species of the PC5 assemblage (*A. lessonii*, *D. ambigua* and *Siphonaperta* sp. 3) together with *A. radiata* and *Quinqueloculina* sp. 1 exhibit a relation both to shallow water and to coarser-grained material (Figs. 4 and 5).

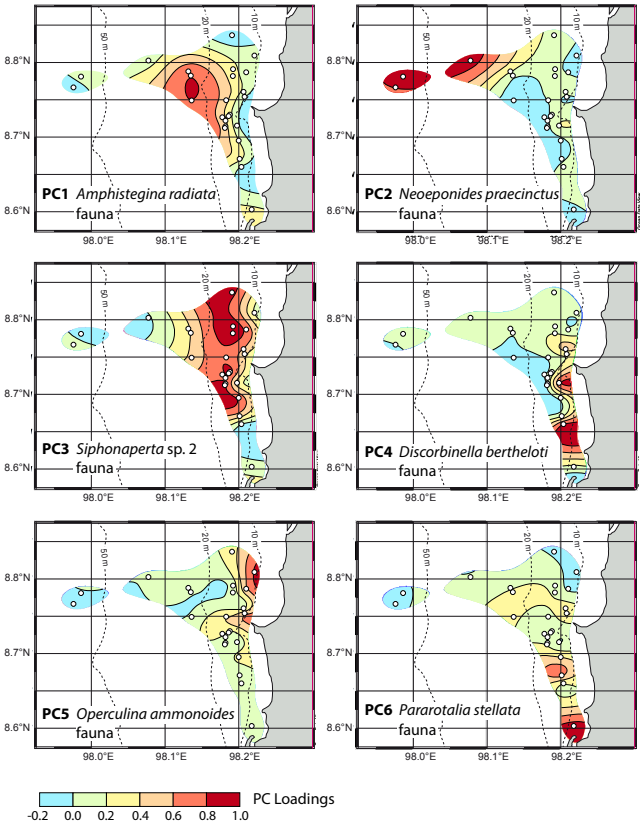


Fig. 4. Distribution of recent benthic foraminiferal assemblages extracted with Q-mode principal component analysis. Shown are PC loadings. Loadings > 0.4 indicate statistically significant influence of the respective fauna (Malmgren and Haq, 1984). Ocean Data View (Schlitzer, 2012) was used for data interpolation. For scale bar see Fig. 1.

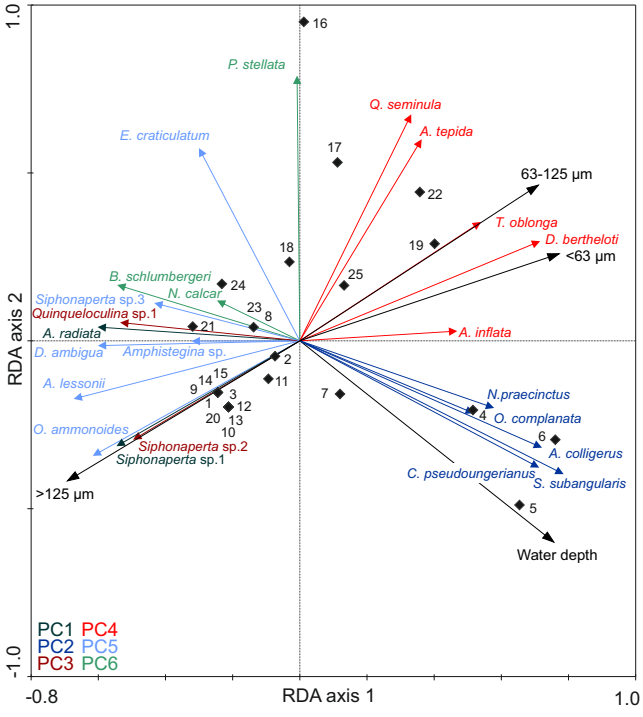


Fig. 5. Results of the redundancy analysis (RDA) applied on the surface samples (see also Table 3). The species arrows are colorized according to their membership to the principal components (PC) extracted from PCA (compare with Fig. 4). The distribution of recent foraminifers exhibits a strong relation to water depth but also to the grain size of the substrate. Species of the PC2 assemblage have a relation to deeper water depths and species of the PC6 assemblages occur more frequently at shallower water depths. For surface sample codes see Table 1.

4.3 Distribution of fossil foraminifera in the sediment cores

Sediment core 030310-C3 contains a total of 48 fossil species, each with percentages larger than 1 % on the total assemblages. The most abundant species in this core are *Amphistegina radiata* (with a maximum relative abundance of 21.4 %), *Siphonaperta* sp. 2 (19.4 %), *Discorbinella bertheloti* (17.8 %) and *Parrellina hispidula* (11.9 %) (Fig. 6a, Appendix A). In addition, species with percentages between 5 and 10 % include (in descending order) *Quinqueloculina* sp. 1, *Elphidium craticulatum*, *Quinqueloculina seminula* and *Borelis schlumbergeri* (Fig. 6a). Core 030310-C3 contains a very high content of redeposited tests with a mean value of 76 %. A maximum with 95 % redeposited specimens was found in the lowermost part of the core at 86.5 cm, and minimum values with 43–48 % redeposited specimens were observed in the upper part of the core at 5.5 and 33.5 cm (Fig. 8).

Sediment core 050310-C4 contains a total of 33 fossil species, each with percentages larger than 1 % on the total assemblages. The most dominant species in this core are *D. bertheloti* (with a maximum relative abundance of 21.2 %) and *Siphonaperta* sp. 2 (13.2 %) (Fig. 6b, Appendix A). Further species with relative abundances between 5 and 10 % are (in descending order) *Amphistegina* sp. 1, *A. radiata*, *Quinqueloculina* sp. 1, *Quinqueloculina seminula*, *Spiroloculina communis* and *Elphidium craticulatum* (Fig. 6b). The content of potentially relocated specimens in core 050310-C4 is lower than that observed in core 030310-C3, with a mean value of 48 % (Fig. 8).

4.4 Quantitative paleo-water depth reconstructions

The short gradient length of 1.74 SD for the first axis of the DCCA implies a more linear distribution of the species in relation to water depth (Table 4). This can be explained by the limited water depth range (approximately 10 to 63 m) included in this study, masking the common unimodal bathymetric species distributions. Although the weighted

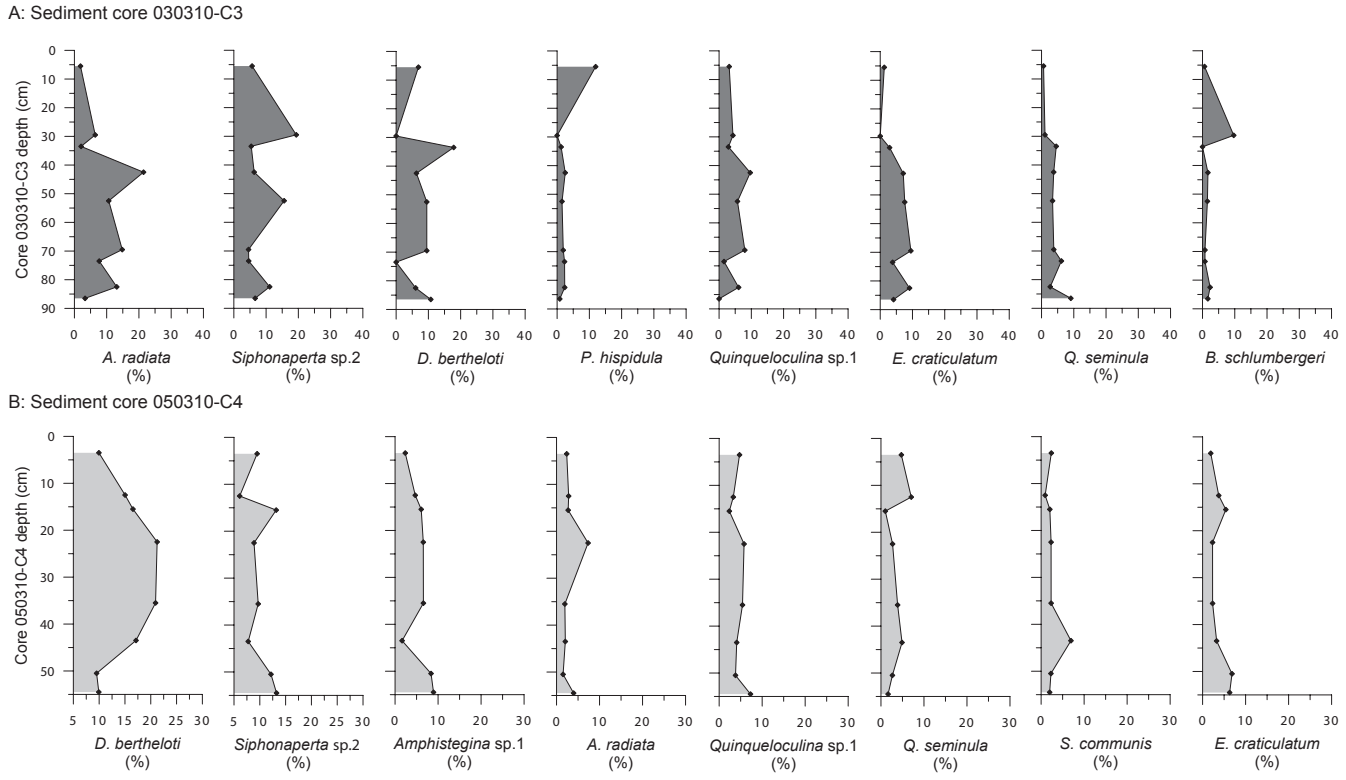


Fig. 6. Distribution of the most abundant fossil benthic foraminifera in sediment cores 030310-C3 **(A)** and 050310-C4 **(B)**. Only species with a relative abundance of $> 5\,\%$ on the fossil assemblages in the sediment cores are presented.

Table 4. Results of the detrended canonical correspondence analysis (DCCA). The short length of gradient for the first axis indicates a linear species–water-depth relationship in the surface samples.

	1	2	3	4
Eigenvalues	0.236	0.123	0.07	0.017
Lengths of gradient (SD)	1.738	1.723	1.112	0.706

averaging–partial least square (WA-PLS) method theoretically works better for gradient lengths of 2 and higher (Birks, 1998; Ter Braak et al., 1993), this method provided the best prediction potential from all methods applied. Moreover, this method can detect the influence of additional parameters such as substrate (Birks, 1998; Horton and Edwards, 2006).

The transfer function created by the WA-PLS method reveals a significant linear correlation ($R^2 = 0.97$ and cross-validated $R^2_{\text{jack}} = 0.92$) between the observed and the estimated water depths in the surface data set for the selected second component (Table 5, Fig. 7). The residuals in the surface data set range between -5.06 m and 2.71 m with a mean of 2.25 m (Fig. 8). The apparent root mean squared error (RMSE) and jack-knifed root mean squared error of prediction (RMSEP) for this component is ± 2.45 m and ± 4.09 m, respectively, showing a relatively good predictive potential of the transfer function (Table 5).

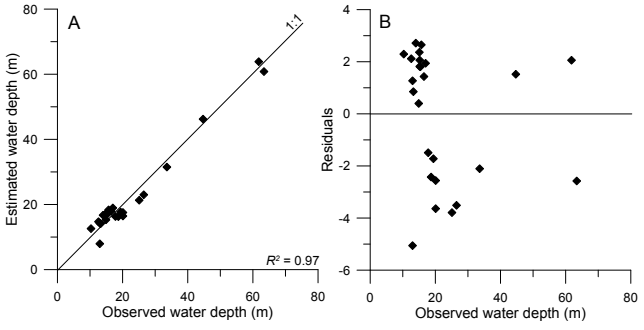


Fig. 7. Observed water depths versus estimated water depths by the WA-PLS transfer function in the surface samples **(A)** and their residuals **(B)**.

To test the robustness of the transfer function, the application of the MAT method showed that, in core 030310-C3, one good analog and four fair analogs, but also four poor analogs with MinDC values above the 20th percentile, were found (Fig. 8). In core 050310-C4, two samples have good analogs with MinDC values below the 10th percentile and the remaining six core samples have fair analogs with values between the 10th and 20th percentile (Fig. 8).

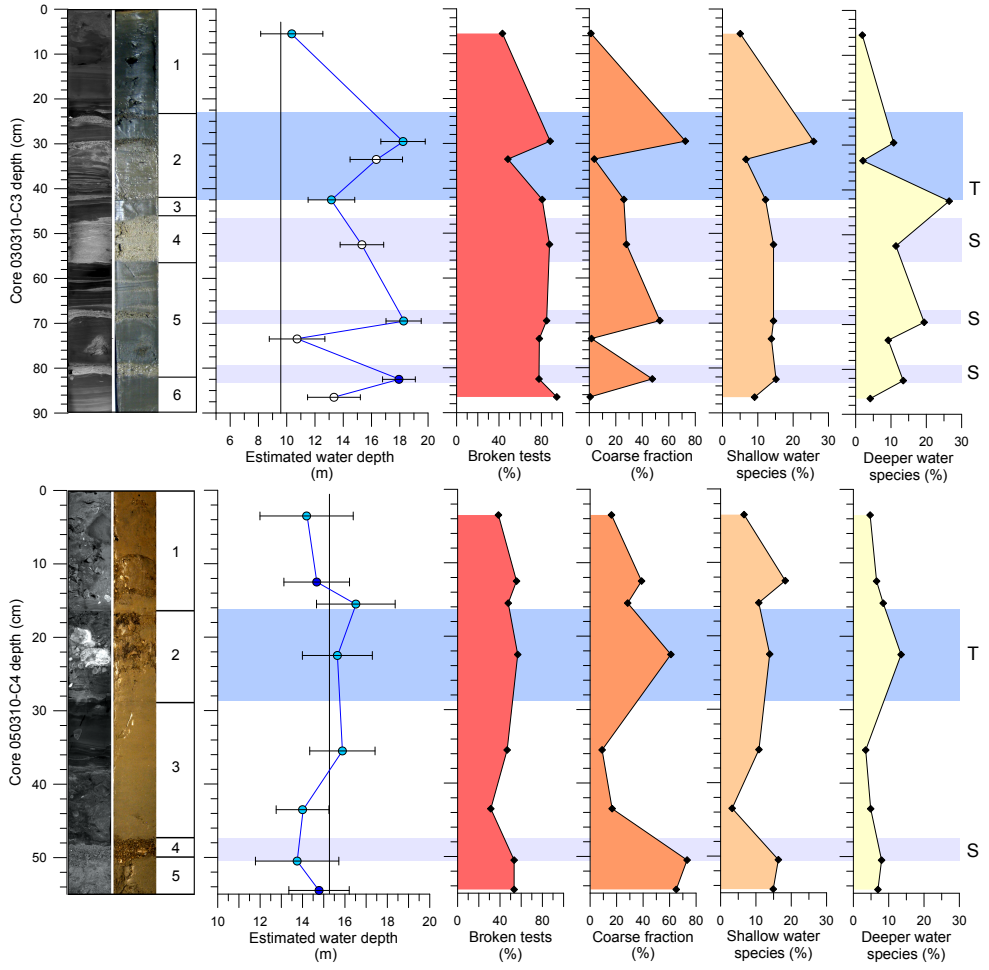


Fig. 8. Sediment core images with their lithological units (see also Fig. 2) and paleo-water depths in cores 030310-C3 and 050310-C4 estimated with the WA-PLS transfer function (open circles = bad analogs; light blue circles = fair analogs; blue circles = good analogs; calculated by modern analog technique). The vertical black lines mark the water depth where the sediment cores were taken. Further are shown the percentages of broken foraminiferal tests, proportion of the coarse fraction, and total relative abundances of species indicative for shallower water (*B. schlumbergeri, P. stellata, A. lessonii, N. calcar, D. ambigua* and *Amphistegina* sp.) and deeper water (*A. radiata* and *O. ammonoides*) in the study area (see also Figs. 3, 4 and 5). The shaded areas indicate storm layers (S) and the 2004 tsunami deposits (T).

Table 5. Results of the WA-PLS transfer function with the root mean squared error, the apparent coefficient of determination (R^2), the cross-validated coefficient of determination (R^2_{jack}), the root mean squared error of prediction (RMSEP) calculated by cross-validation, and the reduction in RMSEP (% change). The selected component for the paleo-water depth estimates in cores 030310-C3 and 050310-C4 is shown in bold.

Component	RMSE	R^2	R^2_{jack}	RMSEP	% change
1	4.50	0.90	0.85	5.46	
2	**2.45**	**0.97**	**0.92**	**4.09**	**25.12**
3	1.67	0.99	0.92	3.98	2.69
4	1.07	0.99	0.92	4.05	−1.65
5	0.79	1.00	0.92	3.94	2.63

The paleo-water depths estimated with the transfer function range from 10.36 (±2.54) m to 18.27 (±1.51) m for core 030310-C3 and from 14.40 (±1.91) m to 17.80 (±2.00) m for core 050310-C4 (Fig. 8). The mean sample-specific error, calculated by bootstrapping, is 1.88 m for core 030310-C3 and 1.59 m for core 050310-C4.

5 Discussion

5.1 Ecology of benthic foraminifera in the study area

Our results imply that both water depth and substrate act as relevant factors on the distribution of benthic foraminifers in the study area, explaining a large part of the observed faunal variability (Fig. 5). Similar relations have been reported from comparable environments of the lower photic zone on

a mixed siliciclastic–carbonate inner shelf (e.g., Renema, 2006a). Many species and the majority of the identified faunas exhibit a distinct bathymetric zonation (Figs. 3 and 4). All faunas except for PC 4 (*D. bertheloti* fauna) contain symbiont-bearing larger benthic foraminifers as dominant or associated components. The relative bathymetric zonation and habitats of larger foraminifers off Khao Lak are comparable to other areas of the Indo-Pacific realm and, thus, are likely controlled by various physical and biological factors, most of which are related to the requirements of the species-specific symbiotic algae (Hallock, 1981; Hohenegger et al., 1999; Beavington-Penney and Racey, 2004; Renema, 2006b). The main factors include water temperature, light penetration, nutrient concentration, food availability and transport, energy at the benthic boundary layer and substrate type and grain size.

In the shallowest environments of the study area, between approximately 10 and 15 m water depth, three distinctive faunas are observed: the larger foraminifers *O. ammonoides, D. ambigua* and *A. lessonii*, which dominate PC5 in the shallow northern parts of the study area (Fig. 4), are typically associated with strong to medium light intensity, moderate to low water energy, and sands or rubble with sand on the reef flat (Hohenegger et al., 1999; Renema, 2006b). The distribution maximum of *A. lessonii* commonly occurs between 10 and 20 m water depth (Renema, 2006b), which is consistent with its occurrence in our study area (Fig. 3). In contrast, *O. ammonoides* has been reported from a wider depth interval, including distribution maxima between 10 and 30 m (Renema, 2006a), in other areas between 40 and 60 m (Hohenegger, 2004). Further to the south, this fauna is replaced by PC4, dominated by the non-symbiont-bearing *D. bertheloti* and *Rosalina* spp. (Figs. 3 and 4). The cosmopolitan species *D. bertheloti* inhabits various shelf and deep-sea environments and has a clear preference for fine-grained substrates (Milker et al., 2009), where it likely profits from specific biogeochemical conditions and the availability of sufficient food particles on and below the sediment surface. In the study area, this fauna is confined to depressions in the reef flat that operate as sediment traps for muddy sediments (Feldens et al., 2012). To the south, this fauna is replaced by the *Pararotalia stellata* fauna. Little is known on the ecology of this species, but it seems to be associated with sandy substrates and has been reported as typical inner-shelf taxon in the study area (Hawkes et al., 2007; Yawsangratt et al., 2011).

The environments at intermediate water depths are dominated by the *Siphonaperta* sp. 2 fauna between 15 and 25 m, and the *Amphistegina radiata* fauna between 20 and 30 m water depth (Figs. 3 and 4). The larger foraminifer *A. radiata* is a characteristic taxon in both faunas and prefers firm substrates with maximum abundances between 20 and 40 m water depth, where it is adapted to variable light intensities and moderate to low water energy (Hohenegger et al., 1999; Hohenegger, 2004). This species commonly avoids the reef flat but is typical for rubble and macroalgal environments at the reef slope (Renema, 2006a). A similar adaption can be also inferred for the miliolid *Siphonaperta* sp. 2.

The deepest environments of the study area, below 30 m water depth, are characterized by *N. praecinctus* and *O. complanata*. The latter species typically replaces *O. ammonoides* at deeper sites and has been reported from sandy substrates between 30 and 90 m (in some areas down to 150 m) water depth, where it is likely adapted to low light intensities and low water energy (Hohenegger, 2004; Renema, 2006b).

5.2 Quantitative reconstruction of redeposition processes during the 2004 Indian Ocean tsunami

Our results demonstrate significant redeposition of sediment particles in the offshore sediments during the 2004 Indian Ocean tsunami, including site-specific uprush and back-wash processes (Fig. 8). Our results are in general agreement with previous observations documenting the severe impacts of the tsunami event on coastal and shallow-water environments from the study area and adjacent regions (Bell et al., 2005; Tsuji et al., 2006; Hawkes et al., 2007). The tsunami-induced run-up at Pakarang Cape reached more than 15 m in height and resulted in the deposition of a few-centimeter-thick sand-rich tsunamite layer (Szczucinski et al., 2005; Choowong et al., 2007; Hori et al., 2007, Jankaew et al., 2008, Brill et al., 2012). Goto et al. (2007) estimated that about 12 500 m^2 of Pakarang Cape were eroded by the 2004 Indian tsunami and a high amount of boulders were transported from offshore into the intertidal zone during the uprush. Hawkes et al. (2007) have shown that the shoreline of Thailand and Malaysia was influenced by up to three waves and a run-up of up to 2 km to the inland. Lay et al. (2005) reported inundation heights of up to 13 m for Sumatra, Thailand and Sri Lanka. On the inner shelf of the study area (9–15 m water depth), event layers of commonly 20–25 cm in thickness were identified as tsunami deposits (Sakuna et al., 2012). Based on the sedimentological observations and 210 Pb dating, assessing the decline in the excess of 210 Pb activities from the nearby area (Sakuna et al., 2012), the 2004 tsunami deposits are 18 cm thick in core 030310-C3 (lithological unit 2) and 13 cm thick in core 050310-C4 (lithological unit 2) (Figs. 2 and 8). Downcore, below the tsunami layers, we observed distinct sand layers in both cores, which were interpreted as storm layers. Core 030310-C3 contains three event layers, with one thicker layer in lithological unit 4 and two thinner layers in lithological unit 5. Core 050310-C4 contains one relatively thin event layer (lithological unit 4) (Figs. 2 and 8). The paleo-water depth estimates for core 030310-C3 indicate a sediment transport from deeper waters to the core location, similar for both the storm layers and the tsunamite (Fig. 8). The paleo-water depths estimated in the storm layers are 15.32 ± 1.54 m for the storm layer in lithological unit 4, and 17.94 ± 1.42 m and 18.27 ± 1.50 m for the lower and upper layer in lithological unit 5, respectively. In the tsunami layer,

we estimated paleo-water depths between 13.16 ± 1.90 m and 18.23 ± 1.68 m. Based on the modern water depth of 9.5 m at this site our results demonstrate a net transport from deeper to shallower environments but also limit the reworking and resuspension of particles to a maximum water depth of approximately 20 m. This result is supported by the low proportion of foraminifera (between two and four percent) in the core that in the present ocean occur in higher percentages at deeper water depths (~ 25 to ~ 60 m) (Fig. 3). Based on the regional seafloor topography (Fig. 1), particles have been transported over approximately 5 km distance. The reconstructed maximum water depth of 20 m is lower than most previous reconstructions based on foraminifers that inferred resuspension depths of 45–300 m (Dominey-Howes et al., 1998; Nanayama and Shigeno, 2006; Uchida et al., 2010). Obviously, the energies and depth impacts of tsunami waves can vary significantly, based on the distance to the source area and the specific coastal morphology (Rabinovich et al., 2011). On the other hand, the majority of existing reconstructions are simply based on general assumptions and observations of benthic foraminiferal distribution ranges, lacking regional reference data sets and a robust statistical assessment. As a consequence, at least some of the reported maximum water depths could be overestimated since many species from middle and deeper shelf environments can also inhabit inner-shelf ecosystems, depending on the local presence of suitable (fine-grained) substrates and related microhabitats (Milker et al., 2009; Mojtahid et al., 2010; Goineau et al., 2011).

Within the tsunami layer of core 030310-C3, changes to deeper paleo-water depths can be observed, likely representing changes in water energy and/ or an admixture of uprush and backwash events during successive tsunami waves (Fig. 8). The estimated deeper water depths in co-occurrence with a sand layer in the upper part of the tsunamite (around 30 cm) may represent a subsequent uprush event, i.e., during a subsequent tsunami wave reaching the coastal area around Cape Pakarang. Our interpretation is supported by frequent occurrences of various species, such as *O. complanata* and *A. radiata,* in the surface samples from deeper water depths. At present, these species preferentially occur between 10 and 45 m water depth, and reach their optima at around 25 m and 35 m water depth, respectively (Figs. 3 and 8). However, the coeval occurrence of species that commonly prefer shallower water depths in the present ocean (*B. schlumbergeri, N. calcar, P. stellata, D. ambigua, A. lessonii* and *Amphistegina* sp.) do not support a clear provenance signal for this potential uprush event in the core (Figs. 3 and 8). Similarly, Hawkes et al. (2007) concluded from microfossil distributions in the Pulau Penang region of northern Malaysia that uprush events related to the 2004 tsunami are indicated by specimens derived from the inner shelf, while backwash layers contain more specimens recently found in mangrove sediments. Furthermore, Nanayama and Shigeno (2006) observed higher percentages of redeposited benthic foraminifera from water depths shallower than 45 m in uprush deposits of the 1993 Hokkaido tsunami.

Our paleo-water depth estimates in core 030310-C3, retrieved from 9.5 m water depth, reveal a provenance of particles in the tsunami layer from approximately 13 to 18 m water depth (Fig. 8). This result is in accordance with existing studies demonstrating that, within 8 km distance to the shoreline, the occurrence of the 2004 tsunami layer was restricted to a maximum water depth of 9 to 18 m (Feldens et al., 2012; Sakuna et al., 2012). These studies also attributed different lithologies and structures within the tsunamite to various phases of the tsunami event; i.e., marine sand layers were related to uprush and intercalated muddy intervals to backwash phases.

Our paleo-water depth reconstructions of core 050310-C4 show that the particles within the tsunamite were derived from slightly deeper water depths of 16.94 ± 1.56 m (Fig. 8). However, our reconstructions show a higher variability for this core, hampering a straightforward reconstruction of redeposition processes from the paleo-water depth estimates alone. The higher variability in the estimated paleo-water depths in core 050310-C4 could be a consequence of the lower amount of larger foraminifera in this core. Larger foraminifera are particularly suitable for paleo-water depth estimations due to their stronger vertical zonation, which can be related to the light dependence of their symbionts and their dependence on hydrodynamic and trophic conditions, which can be linked to water depth (e.g., Hohenegger et al., 1999). In contrast, non-symbiont-bearing foraminifera occur over a wider depth range depending on the surrounding environmental conditions (Milker et al., 2009).

The sediments found in lithological unit 2, interpreted as the 2004 tsunami layer, contain terrestrial particles such as laterites, which indicates that this layer contains a mixture of particles derived from both uprush and backwash processes, inhibiting a clear distinction of the different phases of the tsunami event. The relatively high content of redeposited *A. radiata* and *O. ammonoides* in the middle part of the tsunami layer indicates sediment redeposition from water depths similar to that in core 030310-C3 (Fig. 8). The different percentages of redeposited specimens from deeper water in the two cores can be attributed to the different water depth of the core sites, representing different distances between source and deposition areas of the transported particles. This interpretation, however, is biased by the background redeposition processes that influence sedimentation of inner-shelf environments. The presence of bottom currents and wave action accounts for the overall significant percentages of relocated benthic foraminiferal tests in the recovered sediments of the study area (Fig. 8). Similar observations were also made by Yordanova and Hohenegger (2002) and Briguglio and Hohenegger (2011), indicating that downslope transport of larger benthic foraminifera due to normal wave activity can have significant influence on the accuracy of paleo-depth estimates because the real zonation of foraminifera can be

masked by such redeposition processes. More specifically, Yordanova and Hohenegger (2007) observed that the buoyancy and entrainment potential of larger foraminiferal tests varies depending on their test shape and density.

Based on preliminary datings, a storm layer has been identified in the lower part of the core (unit 4). This layer is characterized by sandy sediment, whose high content of coarse particles contrasts with the adjacent sediments (Fig. 2). Our paleo-water depth reconstruction indicates a sediment transport from slightly shallower to deeper water (14.04 ± 1.78 m). This result contrasts with observations from other areas, where sediment particles during comparable storm surges were preferentially transported from deeper to shallower water depths and where no backflow was observed (Nanayama et al., 2000).

Our data demonstrate that is not possible to distinguish tsunami deposits from background sedimentation based on the relative proportion of reworked particles. Instead, additional information on species composition is required for proper identification of high-energy events, particularly considering comprehensive data on the species distribution in the background sediment for comparison with the event layers.

6 Conclusions

For the first time, a transfer function for water depth reconstruction was developed on benthic foraminifers and applied to the reconstruction of redeposition processes and dynamics associated with the 2004 Indian Ocean tsunami. From our results we can extract the following conclusions:

- The distribution of recent benthic foraminifera on the inner shelf of the southeastern Andaman Sea off Khao Lak (Thailand) is typical for a tropical Indo-Pacific mixed siliciclastic–carbonate environment. The faunas exhibit not only a distinct bathymetric zonation but also a relation to the grain size of the substrate reflecting gradients in light intensity and water energy as well as specific microhabitats. A total of six assemblages have been distinguished, most of which including symbiont-bearing larger foraminifera as dominant and associated constituents. The shallowest sites, between 10 and 15 m, are inhabited by three assemblages, comprising the *Operculina ammonoides* fauna, the *Pararotalia stellata* fauna, and the *Discorbinella bertheloti* fauna. The last is associated with muddy sediments trapped in depressions on the reef flat. The sandy sediments at intermediate water depth are inhabited by the *Siphonaperta* sp. 2 fauna (between 15 and 25 m) and the *Amphistegina radiata* fauna (between 20 and 30 m). The deepest sites (below 30 m) are characterized by the *Neoeponides praecinctus* fauna adapted to low light intensities and low water energy.
- The distinct bathymetric zonation of most recent species allowed the development of a transfer function for quantitative water depth reconstructions with a high prediction potential. Our reconstructions for the 2004 Indian Ocean tsunami layer and pre-dating storm layers from two sites in the study area limit the maximum water depth of resuspension to approximately 20 m. This value is considerably lower than most previous estimates for various tsunami events in the Indo-Pacific realm. On the other hand, the differentiation between storm and tsunami layers in the study area based on foraminifera remains problematic because both events reveal similar characteristics and redeposition processes.

Appendix A

Species list

Ammonia tepida (Cushman, 1926) – Melis and Violanti (2006), p. 98, pl. 1, Figs. 1–2

Amphistegina lessonii (d'Orbigny, 1843) – Jones (1994), p. 109, pl. 111, Figs. 4–7; Hohenegger et al. (1999), p. 144, Fig. 19

Amphistegina radiata (Fichtel and Moll, 1798) – Hohenegger et al. (1999), p. 145, Fig. 20; Jones (1994), pl. 111, Fig. 3

Amphistegina sp. 1

Anomalinoides colligerus (Chapman and Parr, 1937) – Jones (1994), p. 98, pl. 94, Figs. 2–3

Borelis schlumbergeri (Reichel, 1937) – Hottinger et al. (1993), p. 68, pl. 75, Figs. 1–17

Cibicidoides pseudoungerianus (Cushman, 1922) – Cushman (1931), p. 123, pl. 22, Figs. 3–7; Milker and Schmiedl (2012), p. 106, Fig. 24.5–8

Dendritina ambigua (Fichtel and Moll, 1798) – Hohenegger et al. (1999), p. 131, Fig. 10

Discorbinella bertheloti (d'Orbigny, 1839) – Hottinger et al. (1993), p. 114, pl. 150, Figs. 1–4

Elphidium craticulatum (Fichtel and Moll, 1798) – Hottinger et al. (1993), p. 147, pl. 208, Figs. 1–10; Hawkes et al. (2007); p. 178, pl. 2, Fig. 8

Neoeponides praecinctus (Karrer 1868) – Jones (1994), p. 99, pl. 95, Figs. 1–3

Neorotalia calcar (d'Orbigny, 1839) – Hottinger et al. (1993), p. 140, pl. 199, Figs. 1–10; Hohenegger et al. (1999), p. 146, Fig. 21

Operculina ammonoides (Gronovius, 1781) – Hohenegger et al. (1999), p. 155, Fig. 28

Operculina complanata (Defrance, 1822) – Jones (1994), p. 110, pl. 112, Figs. 3–9

Pararotalia stellata (de Férussac, 1827) – Jones (1994), p. 107, pl. 108, Fig. 3; Hawkes et al. (2007), p. 176, pl. 1, Figs. 1–3

Parrellina hispidula (Cushman, 1936) – Melis and Violanti (2006), p. 98, pl. 1, Fig. 13; Berkeley et al. (2009), p. 84, pl. 3, Fig. 7a, b

Quinqueloculina seminula (Linné, 1758) – Jones (1994), p. 21, pl. 5, Fig. 6

Quinqueloculina sp. 1

Saidovina subangularis (Brady, 1881) – Jones (1994), p. 59, pl. 53, Figs. 30, 31

Siphonaperta sp. 1

Siphonaperta sp. 2

Siphonaperta sp. 3

Spiroloculina communis Cushman and Todd (1944) – Jones (1994), p. 25, pl. 9, Figs. 5–6

Triloculina oblonga (Montagu, 1803) – Berkeley et al. (2009), p.84, pl. 2, Fig. 5a, b, c

Supplementary material related to this article is available online at http://www.nat-hazards-earth-syst-sci.net/13/3113/2013/nhess-13-3113-2013-supplement.pdf.

Acknowledgements. For technical support during preparation of samples we thank Eva Vinx and Jutta Richarz at the Center of Earth System Research and Sustainability, Hamburg University. We further want to thank Johann Hohenegger and an anonymous reviewer for their constructive comments helping to improve the manuscript. The project from which the samples originate was funded by Deutsche Forschungsgemeinschaft (DFG) grant SCHW 572/11 and the National Research Council of Thailand (NRCT).

Edited by: H. Sterr
Reviewed by: J. Hohenegger and one anonymous referee

References

Backhaus, K., Erichson, B., Plinke, W., and Weiber, R.: Multivariate Analysemethoden, 11th Edn., Springer, Berlin, Heidelberg, New York, 2006.

Beavington-Penney, S. J. and Racey, A.: Ecology of extant nummulitids and other larger benthic foraminifera: applications in palaeoenvironmental analysis, Earth-Sci. Rev., 67, 219–265, 2004.

Bell, R., Cowan, H., Dalziell, E., Evans, N., O'Leary, M., Rush, B., and Yule, L.: Survey of impacts on the Andaman coast, southern Thailand following the great Sumatra-Andaman earthquake and tsunami of December 26, 2004, Bull. New Zealand Soc. Earth. Eng., 38, 124–148, 2005.

Berkeley, A., Perry, C. T., Smithers, S. G., Horton, B. P., and Cundy, A. B.: Foraminiferal biofacies across mangrove-mudflat environments at Cocoa Creek, north Queensland, Australia, Mar. Geol., 263, 64–86, 2009.

Birks, H. J. B.: Quantitative palaeoenvironmental reconstructions, in: Statistical Modelling of Quaternary Science Data, edited by: Maddy, D. and Brew, J. S., Cambridge, 161–254, 1995.

Birks, H. J. B.: Numerical tools in palaeolimnology – Progress, potentialities, and problems, J. Paleolimnol., 20, 307–332, 1998.

Birks, H. J. B., Line, J. M., Juggins, S., Stevenson, A. C., and Ter Braak, C. J. F.: Diatoms and pH reconstruction, Phil. Trans. R. Soc. Lond., B 327, 263–278, 1990.

Brill, D., Klasen, N., Jankaew, K., Brückner, H., Kelletat, D., Scheffers, A., and Scheffers, S.: Local inundation distances and regional tsunami recurrence in the Indian Ocean inferred from luminescence dating of sandy deposits in Thailand, Nat. Hazards Earth Syst. Sci., 12, 2177–2192, doi:10.5194/nhess-12-2177-2012, 2012.

Briguglio, A. and Hohenegger, J.: How to react to shallow water hydrodynamics: The larger benthic foraminifera solution, Mar. Micropalaeontol., 81, 63–76, doi10.1016/j.marmicro.2011.07.004, 2011.

Choowong, M., Murakoshi, N., Hisada, K., Charusiri, P., Daorerk, V., Charoentitirat, T., Chutakositkanon, V., Jankaew, K., and Kanjanapayont, P.: Erosion and deposition by the 2004 Indian Ocean tsunami in Phuket and Phang-nga provinces, Thailand. J. Coastal Res., 23, 1270–1276, 2007.

Cushman, J. A.: The foraminifera of the Atlantic Ocean, Part 8: Rotaliidae, Amphisteginidae, Calcarinidae, Cymbalporettidae, Globorotallidae, Anomalinidae, Planorbulinidae, Pupertidae and Homotremidae, Smithonian Institution, United States National Museum, Bulletin 104, Washington, 1931.

Dahanayake, K. and Kulasena, N.: Recognition of diagnostic criteria for recent- and paleo-tsunami sediments from Sri Lanka, Mar. Geol., 254, 180–186, doi:10.1016/j.margeo.2008.06.005, 2008.

Dominey-Howes, D., Dawson, A., and Smith, D.: Late Holocene coastal tectonics at Falasarna, western Crete: a sedimentary study, in: Coastal Tectonics, edited by: Stewart, I. and Vita-Finzi, C., Special Publications, Geological Society, London, 343–352, 1998.

Fagherazzi, S. and Du, X.,: Tsunamigenic incisions produced by the December 2004 earhquake along the coasts of Thailand, Indonesia and Sri Lanka, Geomorphology, 99, 120–129, doi:10.1016/j.geomorph.2007.10.015, 2007.

Feldens, P., Schwarzer, K., Szczuciński, W., Stattegger, K., Sakuna, D., and Somgpongchaiykul, P.: Impact of 2004 tsunami on seafloor morphology and offshore sediments, Pakarang Cape, Thailand, Polish J. Environ. Stud, 18, 63–68, 2009.

Feldens, P., Schwarzer, K., Sakuna, D., Szczucinski, W., and Sompongchaiyakul, P.: Sediment distribution on the inner continental shelf off Khao Lak (Thailand) after the 2004 Indian Ocean tsunami, Earth Planet. Space, 64, 875–887, 2012.

Goineau, A., Fontanier, C., Jorissen, F. J., Lansard, B., Buscail, R., Mouret, A., Kerhervé, P., Zaragosi, S., Ernoult, E., Artéro, C., Anschutz, P., Metzger, E., and Rabouille, C.: Live (stained) benthic foraminifera from the Rhône prodelta (Gulf of Lion, NW Mediterranean): Environmental controls on a river-dominated shelf, J. Sea Res., 65, 58–75, 2011.

Goto, K., Chavanich, S. A., Imamura, F., Kunthasap, P., Matsui, T., Minoura, K., Sugawara, D., and Yanagisawa, H.: Distribution, origin and transport process of boulders deposited by the 2004 Indian Ocean tsunami at Pakarang Cape, Thailand, Sediment. Geol., 202, 821–837, 2007.

Hallock, P.: Algal symbiosis: A mathematical analysis, Mar. Biol., 62, 249–255, 1981.

Hawkes, A. D., Bird, M., Cowie, S., Grundy-Warr, C., Horton, B. P., Tan Shau Hwai, A., Law, L., Macgregor, C., Nott, J., Eong Ong, J., Rigg, J., Robinson, R., Tan-Mullins, M., Tiong Sa, T., Yasin, Z., and Wan Aik, L.: Sediments deposited by the 2004 Indian Ocean Tsunami along the Malaysia–Thailand Peninsula, Mar. Geol., 242, 169–190, 2007.

Hawkes, A. D., Horton, B. P., Nelson, A. R., and Hill, D. F.: The application of intertidal foraminifera to reconstruct coastal subsidence during the giant Cascadia earthquake of AD 1700 in Oregon, USA, Quaternary Int., 122, 116–140, 2010.

Hohenegger, J.: Depth coenoclines and environmental considerations of western pacific larger foraminifera, J. Foramin. Res., 34, 9–33, 2004.

Hohenegger, J.: Estimation of environmental paleogradient values based on presence/absence data: a case study using benthic foraminifera for paleodepth estimation, Palaeogeogr. Palaeocl., 217, 115–130, 2005.

Hohenegger, J., Yordanova, E., Nakano, Y., and Tatzreiter, F.: Habitats of larger foraminifera on the upper reef slope of Sesoko Island, Okinawa, Japan, Mar. Micropalaeontol., 36, 109–168, 1999.

Hori, K., Kuzumoto, R., Hirouchi, D., Umitsu, M., Janjirawuttikul, N., and Patanakanog, B.: Horizontal and vertical variation of 2004 Indian tsunami deposits: An example of two transects along the western coast of Thailand, Mar. Geol., 239, 163–172, doi:10.1016/j.margeo.2007.01.005, 2007.

Horton, B. P. and Edwards, R. J.: Quantifying Holocene sea-level change using intertidal foraminifera: Lessons from the British Isles, Cushman Foundation for Foraminiferal Research, Special publication No. 40, 1–97, 2006.

Horton, B. P., Edwards, R. J., and Lloyd, J. M.: A foraminiferal-based transfer function: Implications for sea-level studies, J. Foramin. Res., 29, 117–129, 1999.

Hottinger, L., Halicz, E., and Reiss, Z.: Recent foraminiferida from the Gulf of Aqaba, Red Sea, Academia Scientarum et Artium Slovenica, Classis IV: Historia Naturalis, Lubljana, 179 pp., 1993.

Jankaew, K., Atwater, B. F., Sawai, Y., Choowong, M. Charoentitirat, T., Martin M. E., and Prendergast, A.: Mediveal forewarning of the 2004 Indian Ocean Tsunami in Thailand, Nature, 455, 1228–1231, 2008.

Jones, R. W.: The Challenger Foraminifera, 1st Edn., Oxford University Press Inc., New York, 149 pp., 1994.

Juggins, S.: Software for ecological and palaeoecological data analysis and visualisation, Tutorial Version 1.3, 1–24, 2003.

Kemp, A. C., Horton, B. P., Corbett, R., Culver, S. J., Edwards, R. J., and van de Plassche, O.: The relative utility of foraminifera and diatoms for reconstructing late Holocene sea-level change in North Carolina, USA, Quaternary Res., 71, 9–21, 2009.

Kortegaas, S. and Dawson, A. G.: Distinguishing tsunami and storm deposits: An example from Martinhal, SW Portugal, Sediment. Geol., 200, 208–221, doi:10.1016/j.sedgeo.2007.01.004, 2007.

Kumar, V. S., Babu, V. R., Babu, M. T., Dhinakaran, G., and Rajamanickam, G. V.: Assessment of storm surge disaster potential for the Andaman Islands, J. Coastal Res., 24, 171–177, doi:10.2112/05-0506.1, 2008.

Lay, T., Kanamori, H., Ammon, C. J., Nettles, M., Ward, S. N., Aster, R. C., Beck, S. L., Bilek, S. L., Brudzinski, M. R., Butler, R., DeShon, H. R., Ekström, G., Satake, K., and Sipkin, S.: The great Sumatra-Andaman Earthquake of 26 December 2004, Science, 308, 1127–1132, 2005.

Leps, J. and Smilauer, P.: Multivariate analysis of ecological data using CANOCO, Cambridge University Press, Cambridge, 269 pp., 2003.

Levitus, S., and Boyer, T. P.: World Ocean Atlas 1994, Volume 4. Temperature, National Environmental Satellite, Data, and Information Service, Washington, DC (United States), 1994.

Malmgren, B. A. and Haq, B. U.: Assessmant of quantitative techniques in paleobiogeography, Mar. Micropaleontol., 7, 213–230, 1982.

Mamo, B., Strotz, L., and Dominey-Howes, D.: Tsunami sediments and their foraminiferal assemblages, Earth-Sci. Rev., 96, 263–278, 2009.

Mard Karlsson, J., Skelton, A., Sandén, M, Ioualalen, M., Kaewbanjak, N., Pophet, N., Asavanant, J., and von Matern, A.: Reconstructions of the coastal impact of the 2004 Indian Ocean tsunami in the Khao Lak area, Thailand, J. Geophys. Res., 114, C10023, doi:10.1029/2009JC005516, 2009.

Melis, R. and Violanti, D.: Foraminiferal biodiversity and Holocene evolution of the Phetchaburi coastal area (Thailand Gulf), Mar. Micropalaeontol., 61, 94–115, 2006.

Milker, Y. and Schmiedl, G.: A taxonomic guide to modern benthic shelf foraminifera of the western Mediterranean Sea., Palaeontol. Electron., 15, 1–134, 2012.

Milker, Y., Schmiedl, G., Betzler, C., Römer, M., Jaramillo-Vogel, D., and Siccha, M.: Distribution of Recent benthic foraminifera in neritic carbonate environments of the Western Mediterranean Sea, Mar. Micropalaeontol., 73, 207–225, doi:10.1016/j.marmicro.2009.10.003, 2009.

Milker, Y., Schmiedl, G., and Betzler, C.: Paleobathymetric history of the Western Mediterranean Sea shelf during the latest glacial period and the Holocene: Quantitative reconstructions based on foraminiferal transfer functions, Palaeogeogr. Palaeocl., 307, 324–338, doi:10.1016/j.palaeo.2011.05.031, 2011.

Mojtahid, M., Jorissen, F., Lansard, B., and Fontanier, C.: Microhabitat selection of benthic foraminifera in sediments off Rhone river mouth (NW Mediterranean), J. Foram. Res., 40, 231–246, doi:10.2113/gsjfr.40.3.231, 2010.

Morton, R. A., Gelfenbaum, G., and Jaffe, B. E.: Physical criteria for distinguishing sandy tsunami and storm deposits using modern examples, Sediment. Geol., 200, 184–207, doi:10.1016/j.sedgeo.2007.01.003, 2007.

Murray, J. W.: Ecology and Applications of Benthic Foraminifera, Cambridge University Press, Cambridge, 2006.

Nanayama, F. and Shigeno, K.: Inflow and outflow facies from the 1993 tsunami in southwest Hokkaido, Sediment. Geol., 187, 139–158, 2006.

Nanayama, F., Shigeno, K., Satake, K., Shimokawa, K., Koitabashi, S., Miyasaka, S., and Ishii, M.: Sedimentary differences between the 1993 Hokkaido-nansei-oki tsunami and the 1959 Miyakojima typhoon at Taisei, southwestern Hokkaido, northern Japan, Sediment. Geol., 135, 255–264, 2000.

Nelson, A. R., Sawai, Y., Jennings, A. E., Bradley, L.-A., Gerson, L., Sherrod, B. L., Sabean, J., and Horton, B. P.: Great-earthquake paleogeodesy and tsunamies of the past 2000 years at Alsea Bay, central Oregon coast, USA, Quaternary Sci. Rev., 27, 747–768, 2008.

Overpeck, J. T., Webb III., T., and Prentice, I. C.: Quantitative interpretation of fossil pollen spectra: Dissimilarity coefficients and the method of Modern Analogs, Quaternary Res., 23, 87–108, 1985.

Parker, J. H. and Gischler, E.: Modern foraminiferal distribution and diversity in two atolls from the Maldives, Indian Ocean, Mar. Micropaleontol., 78, 30–49, 2011.

Phantuwongraj, S., and Choowong, M.: Tsunamis versus storm deposits from Thailand, Nat. Hazards, 63, 31–50, 2012.

Rabinovich, A. B., Candella, R. N., and Thomson, R. E.: Energy Decay of the 2004 Sumatra Tsunami in the World Ocean, Pure Appl. Geophys, 168, 1919–1950, 2011.

Renema, W.: Large benthic foraminifera from the deep photic zone of a mixed siliciclastoc-carbonate shelf off East Kalimantan, Indonesia, Mar. Micropaleontol., 58, 73–82, 2006a.

Renema, W.: Habitat variables determining the occurrence of large benthic foraminifera in the Berau area (East Kalimantan, Indonesia), Coral Reefs, 25, 351–359, 2006b.

Rossi, V. and Horton, B. P.: The application of subtidal foraminifera-based transfer function to reconstruct Holocene paleobathymetry of the Po Delta, northern Adriatic Sea, J. Foramin. Res., 39, 180–190, 2009.

Saidova, K. M.: Benthic foraminifera communities of the Andaman Sea (Indian Ocean), Oceanology, 48, 517–523, 2008.

Sakuna, D., Szczucinski, W., Feldens, P., Schwarzer, K., and Khokiattiwong, S.: Sedimentary deposits left by the 2004 Indian Ocean tsunami on the inner continental shelf offshore of Khao Lak, Andaman Sea (Thailand), Earth Planet. Space, 64, 931–943, 2012.

Satyanarayana, A., Nallapa Reddy, A., Jaiprakash, B. C., and Chidambaram, L.: A note on foraminifera, grain size and clay mineralogy of tsunami sediments from Karaikal-Nagore-Nagapattinam beaches, Southeast coast of India, J. Geol. Soc. India, 69, 70–74, 2007.

Scheffers, A., Brill, D., Kelletat, D., Brückner, H., Scheffers, S., and Fox, K.: Holocene sea levels along the Andaman Sea coast of Thailand, Holocene, 22, 1169–1180, 2012.

Stein, S. and Okal, E. A.: Speed and size of the Sumatra earthquake, Nature, 434, 581–582, 2005.

Sugawara, D., Minoura, N., Tsukawaki, S., Goto, K., and Imamura, F.: Foraminiferal evidence of submarine sediment transport and deposition by backwash during the 2004 Indian Ocean tsunami, Isl. Arc, 18, 513–525, 2009.

Szarek, R., Kuhnt, T., Kawamura, H., and Kitazato, H.: Distribution of recent benthic foraminifera on the Sunda Shelf (South China Sea), Mar. Micropaleontol., 61, 171–195, 2006.

Ter Braak, C. J. F. and Juggins, S.: Weighted averaging partial least squares regression (WA-PLS): an improved method for reconstructing environmental variables from species assemblages, Hydrobiologia, 269/270, 485–502, 1993.

Ter Braak, C. J. F. and Smilauer, P.: CANOCO Reference manual and CanoDraw for Windows User's guide (version 4.5), Microcomputer power Ithaka, NY, USA, 500 pp., 2002.

Ter Braak, C. J. F., Juggins, S., Birks, H. J. B., and Van der Voet, H.: Weighted Averaging Least Squares regression (WA-PLS): definition and comparison with other methods for species-environment calibration, in: Multivariate Environmental Statistics, edited by: Patil, G. P. and Rao, C. R., Elsevier Science Publishers B.V. (North Holland), Amsterdam, 525–560, 1993.

Thampanya, U., Vermaat, J. E., Sinsakul, S., and Panapitukkul, N.: Coastal erosion and mangrove progradation of Southern Thailand, Estuar. Coast. Shelf S., 68, 75–85, 2006.

Tsuji, Y., Namegaya, Y., Matsumoto, H., Iwasaki, S.-I., Kanbua, W., Sriwichai, M., and Meesuk, V.: The 2004 Indian tsunami in Thailand: Surveyed runup heights and tide gauge records, Earth Planet. Space, 58, 223–232, 2006.

Uchida, J.-I., Fujuwara, O., Hasegawa, S., and Kamataki, T.: Sources and depositional processes of tsunami deposits: Analysis using foraminiferal tests and hydrodynamic verification, Isl. Arc, 19, 427–442, 2010.

Van der Zwaan, G. J., Jorissen, F. J., and de Stigter, H. C.: The depth dependency of planktonic/benthic foraminiferal ratios: Constraints and applications, Mar. Geol., 95, 1–16, 1990.

Varkey, M. J., Murty, V. S. N., and Suryanarayana, A.: Physical oceanography of the Bay of Bengal and Andaman Sea, Oceanogr. Mar. Biol. Ann. Rev, 34, 1–70, 1996.

Yawsangratt, S., Szczucinski, W., Chaimanee, N., Chatprasert, S., Majewski, W., and Lorenc, S.: Evidence of probable paleotsunami deposits on Kho Khao Island, Phang Nga Province, Thailand, Nat. Hazards, 23, 1270–1276, doi:10.2112/05-0561.1, 2011.

Yordanova, E. K. and Hohenegger, J.: Taphonomy of larger foraminifera: Relationships between living individuals and empty tests on flat reef slopes (Sesoko Island, Japan), Facies, 46, 169–203, doi:10.1007/BF02668080, 2002.

Yordanova, E. K. and Hohenegger, J.: Studies on settling, traction and entrainment of larger benthic foraminiferal tests: implications for accumulation in shallow marine sediments, Sedimentology, 54, 1273–1306, doi:10.1111/j.1365-3091.2007.00881.x, 2007.

Tsunami deposits in near-shore and costal waters of Thailand (TUNWAT)

Grant-No. SCHW 572/11
Progress Report

Period: 27.09.2007 – 31.08.2009

K. Schwarzer, P. Feldens, D. Sakuna, K. Stattegger,
S. Pongpiachan, W. Szczuciński

Table of Contents

1. Introduction 3

2. Objectives 4

3. Investigation Area 5

4. Methods 7

4.1 Field Work 7

Cruise with RV CHAKRATONG TONGYAI in 2007 7

Cruise with RV BOONLERT PASOOK in 2008 8

4.2 Laboratory work 9

5. Results 10

5.1 Mud patches from 7 to 15 m depth 10

5.2 Channel system between -10 and -16 m 13

5.3 Morphological ridges starting at -15 m towards offshore 14

5.4 Further findings 17

5.4.1 Remnants of tin mining activities 17

5.4.2 Stone fields and small-scale depressions between 30 m and 35 m water-depth 17

5.4.3 Age control for a sediment core from 52 m water-depth 18

5.4.4 Observation from 60 m to 80 m water-depth 19

6. Interpretation 19

7. Conclusion 22

8. Future work 22

9. References 23

Appendix 28

List of Activities 28

Draft of a Research Article 29

1. Introduction

Tsunamis are among the largest catastrophic events in the world. Therefore they are recorded since historical times and numerous investigations have been done about their origin, wave distribution and energy release along coastlines. On December 26th, 2004 an M 9.3 submarine earthquake was generated off the northwest coast of the Indonesian Island Sumatra due to a complex tectonic activity between the Indo-Australian plate and the Sunda-Plate. This generated a giant tsunami which had an impact all over SE Asia coastlines, reaching till the East-coast of Africa (LAY et al. 2005, WEISS & BAHLBURG 2006).

Tsunamis have a strong potential for coastal changes as well as on deposits on- and offshore (BRYANT, 2001, WIEGEL, 2006 a, b and others, see Sedimentary Geology, Vol. 200 (2007), Marine Geology Vol. 242 (2007)). One of the most significant phenomena related to tsunami impacts is large scale sediment removal from the coast, followed by widespread deposition of marine sand on coastal lowlands (MINOURA & NAKAYA 1991). In addition, tsunami waves can resuspend, transport and redeposit sediments on the sea floor as a response to repeated incoming and returning flows. However, most of the knowledge about offshore, shallow marine tsunami deposits results from onshore outcrops of ancient lithified as well as well as not lithified strata (CANTALAMESSA & DI CELMA, 2005, FUJIWARA & KAMATAKI, 2007, DAWSON & STEWART 2008). A list of modern and paleotsunami indicators was compiled by MAMO ET AL. (2009). These indicators were mainly developed for onshore tsunami deposits and are partly of limited use for the investigation of offshore deposits. Some indicators, which might be of use in offshore areas, are given in Table 1.

Table 1. Selected tsunami indicators, modified and extended (from MAMO et al., 2009).

Tsunami deposit indicator	Description
Basal unconformity	Contact between base of tsunami deposit and underlying sequence may be sharp, unconformable or erosional.
Intraclasts	Lower/basal unit of tsunami deposit may contain rip-up or intraclasts or reworked underlying material.
Basal load structures	Lower/basal unit of tsunami-deposit may contain loading structures.
Fining upward sequence	Particle size of tsunami-deposit fines upward.
Cross bedding	Landward and seaward currents shown by imbrications of shells and/or low angled wedge shaped lamination and/or cross bedding.
Imbricated boulders	Stacks or lines or accumulations of imbricated boulders at the coast.
Biostratigraphy	Microfossil assemblages of diatoms and foraminifera. May be pelagic and/or benthic species in shallow water or coastal environments. Frustules/tests may be crushed or broken in significant percentages.
Debris from land based materials	Fragments of grass or plants derived from land; Laterite fragments, wood fragments.
Materials of anthropogenic origin.	Brick particles, cement.

Until now only poor knowledge exists about the deposition on the upper and lower shoreface and the shelf (definition of shoreface and shelf according to COWELL et al., 1999) which are induced by tsunami across-shelf backwash and which might produce sediment aprons, sand

bars or large sediment waves. Few investigations have been done on submerged unconsolidated young marine deposits (LE ROUX & VARGAS, 2005, VARGAS et al. 2005, NODA et al. (2007) and indicators specifically suited to offshore tsunami deposits, especially backwash deposits, have yet to be developed. FUJIWARA & KAMATAKI (2007) tried to develop a tsunami depositional model based on emerged Holocene tsunami deposits. WEISS (2008) follows a theoretical approach to determine tsunami impact on deep water sediments. HAWKES et al. (2007) and SUGAWARA et al. (2009) were using assemblages of foraminifera to distinguish between pre-tsunami deposits and tsunami deposits. SUGAWARA et al. (2009) could demonstrate clear evidence of a backwash transporting microfossils from the upper shoreface to the lower shoreface and the shelf.

In response to the devastating tsunami, which dramatically demonstrated the need for a better understanding of the dynamics of the seafloor and risk management, DFG and the National Research Council of Thailand (NRCT) jointly launched the programme TRIAS (Tracing Tsunami Impact in the Andaman Sea Region) for common research and capacity building. TUNWAT (Tsunami deposits in near-shore and coastal waters of Thailand), which is a subproject of TRIAS, is carried out jointly by

- Christian-Albrechts-Universität zu Kiel, Institute of Geosciences, Sedimentology, Coastal and Continental Shelf Research (IfG), Germany;
- Adam Mickiewicz University, Institute of Geology, Poland;
- International Atomic Agency, Marine Environment Laboratory, Monaco;
- Prince of Songkla University, Biogeochemical and Environmental Change Research Unit, Thailand;
- Phuket Marine Biological Center (PMBC), Oceanography and Environment Unit, Thailand;
- Chulalangkorn University, Southeast Asia START Regional Centre, Thailand.

2. Objectives

The December 2004 tsunami offered a unique opportunity to catalogue geomarine effects from a very well recorded series of events. Many of these effects have been unknown and have never been recorded until now. A modern deposit of unquestioned origin is invaluable for defining a palaeo-record. Up to now no systematically detailed study exists where geomorphological, sedimentological, geochemical and geological alterations offshore beyond the upper shoreface have been investigated after a tsunami has influenced a coastal area. This project was launched to assess for the first time the impact of tsunami waves on changes and/or offsets of large scale bedforms and on changes and/or offsets of nearshore and shelf sediment distribution patterns, to estimate the spatial extension of erosion as well as on deposition by the backwash.

The scientific questions of TUNWAT in detail are:

- How do incoming tsunami waves influence sediments and the seafloor topography in nearshore waters, on the upper and lower shoreface and on the shelf?
- How does backflow influence sediments, sediment distribution patterns and sea bottom topography in nearshore waters, on the shoreface and on the shelf?
- Are there distinguished conduits for the sediment backflow?
- How far offshore are sediments transported by the backflow?

- To which water-depth and to which offshore distance can tsunami-induced sedimentological and morphological alterations of the seafloor be observed?
- How do offshore tsunami deposits look like?
- How does an archive record of tsunami-affected shelf deposits look like?

Additionally to the scientific goals it is part of the project to support initiatives of our Thai partner organizations to build up capacities in coastal and shelf research by inviting and teaching their staff members in the application of highly sophisticated hydroacoustic systems by "training on the job" during common cruises and in data processing at Kiel University.

In this report project activities and first results of TUNWAT are presented.

3. Investigation Area

The continental shelf of the Andaman Sea adjacent to the Malay Peninsula is narrow and slightly inclined; the 50 m depth contour is reached approximately 7 km offshore Phuket and about 30 km offshore Phang Nha Province towards north. The coastal area is dominated by rocky cliffs altering with sandy lowlands and pocket beaches. This area is monsoon dominated with the NE-Monsoon active during winter (Oct. – March) and the SW-monsoon blowing during summer (May-Oct.). Strong storms are rare at this part of Thailand's coastal areas (cited in JANKAEW et al., 2008). The tide is mixed semidiurnal, ranging between 1.1 m and 3.6 m (THAMPANYA et al., 2006)

The present research area offshore Phank Ngha Province, between Thap Lamu and Phra Thong Island comprises approximately 1.000 km² (Fig. 1). It was selected for our investigations as it was severely hit by the 2004-tsunami (BELL et al., 2005, TSUJI et al., 2006, THANAWOOD et al. 2006). The wave run-up spiked at 15 m above the normal water level at Pakarang Cape (SIRIPONG, 2006) and up to 20 m at Phra Thong Island (JANKAEW et al., 2008). At Pakarang Cape an area of about 12.500m² was eroded by the tsunami waves (SYNOLAKIS & KONG, 2006). Hundreds of reef boulders were left and could be observed on the flat intertidal area after the coast was hit by the tsunami (GOTO et al., 2007).

In the past, extensive tin mining activities took place in the coastal area of Phang Nga Province on- and offshore up to – 50 m water depth, but ceased in the 1980s long before the tsunami hit the coastal area. Some sediment dispersion was created by the tin mining (SUWANWERAKAMTORN et al., 1990) Fluvial discharge is negligible in this area which increases the preservation potential of tsunamigenic features on the seafloor as they will not be mixed with land derived sediment during the rainy season.

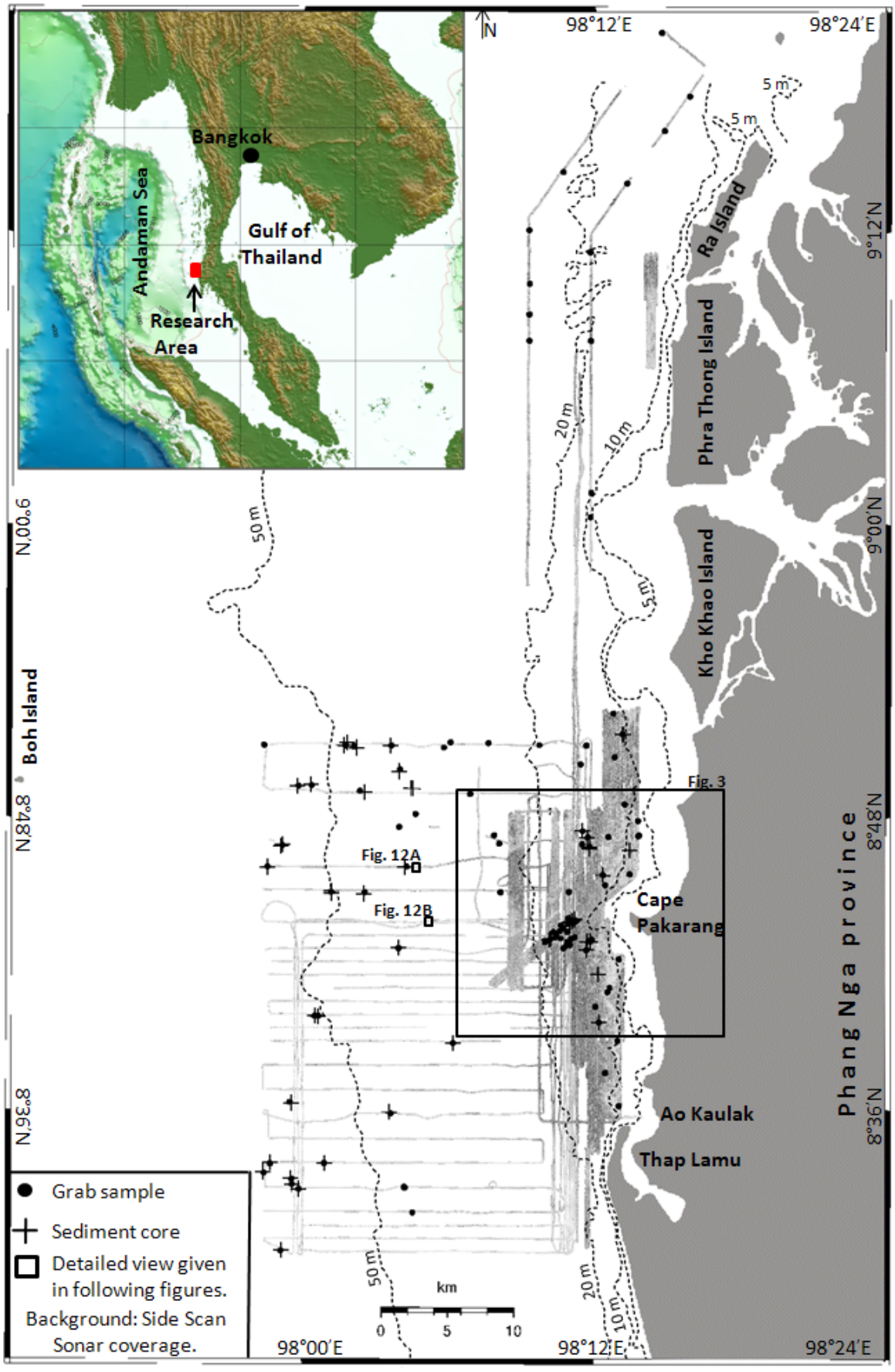


Fig. 1. The investigation area offshore Phang Nha Province. Included is the hydroacoustic survey grid carried out in 2007 and 2008, grab sampling stations and coring positions.

4. Methods

The literature is strongly focussed on multi-proxy sedimentary and stratigraphic evidence (e.g. DAWSON et al. 1996, NANAYAMA et al. 2000, GOFF et al., 2001, MOORE et al. 2005, LIU et al. 2005, SUGAWARA et al. 2009) to identify tsunami deposits, but sediment samples have often been taken without a precise sedimentological and bathymetrical pre-mapping. However, a detailed mapping of the seafloor is necessary to determine the spatial distribution of tsunami deposits. Our focus is on a very detailed, high resolution hydroacoustic mapping survey (multibeam echosounder, side-scan sonar, shallow reflection seismic) and underwater-video observations before taking sediment samples and sediment cores. This ensures to indentify unusual morphological and sedimentological patterns and to get sediment samples and cores even from small scale features which might be related to the tsunami.

4.1 Field Work

In the framework of TUNWAT, two research cruises have been carried out (see cruise reports of 2007 and 2008). The combined database of these cruises includes about 1500 nautical miles (nm) of hydroacoustic profiles, 112 surface sediment samples and 42 short sediment cores up to 2 m in length (see cruise reports for details).

4.1.1 Cruise with RV CHAKRATONG TONGYAI in 2007

The intention of the first cruise was to get an overview of the bathymetrical, sedimentological and geological/stratigraphical conditions in water depths between 10 and approximately 80 meter. Bathymetric mapping was carried out using a SeaBeam 1185 (L3 Communication / ELAC Nautik) multibeam echo sounder, with the transducer mounted to the starboard side of the vessel. Besides the transducers, which were provided by the project, all other components were supplied by the MASS-project of TRIAS. Side scan sonar data were collected using a KLEIN 595 towfish and control unit and digital data acquisition with the TRITON-software. Shallow water seismic reflection data were collected using an EG&G boomer system. Surface sediment samples were taken with a Van-Veen-Grab-Sampler. Each sample was photographed and subdivided into four parts for further laboratory analyses. To get detailed information about the architecture of the upper layers of the seafloor and to recognize unconformities, a small gravity corer (RUMOHR gravity corer) was used. Cores up to 2 m in length were recovered from the seafloor. Based on our knowledge about morphological and sedimentological conditions of numerous shelf areas in tropical environments, we could decide whether unusual structures appeared even three years after the event which could be related to the tsunami. In areas where potential tsunami influence was expected, based on the overview mapping results, detailed full coverage mapping was performed.

It was originally planned to run a 24 hours data acquisition program. Due to strong fishing activities in the investigation area especially during the nights, the cruise could not be carried out as originally planned. The towfish of the side scan sonar system as well as the transducers of the multibeam system had some physical contact with fishing nets several times. During some nights it was even not possible to head for sampling and coring positions as they were occupied by fishing boats or fishing nets. Approximately 2/3 of the nights could not be used for the research program. Some technical problems with RV CHAKRATONG TONGYAI reduced the amount of working time at sea as well (for details see cruise report).

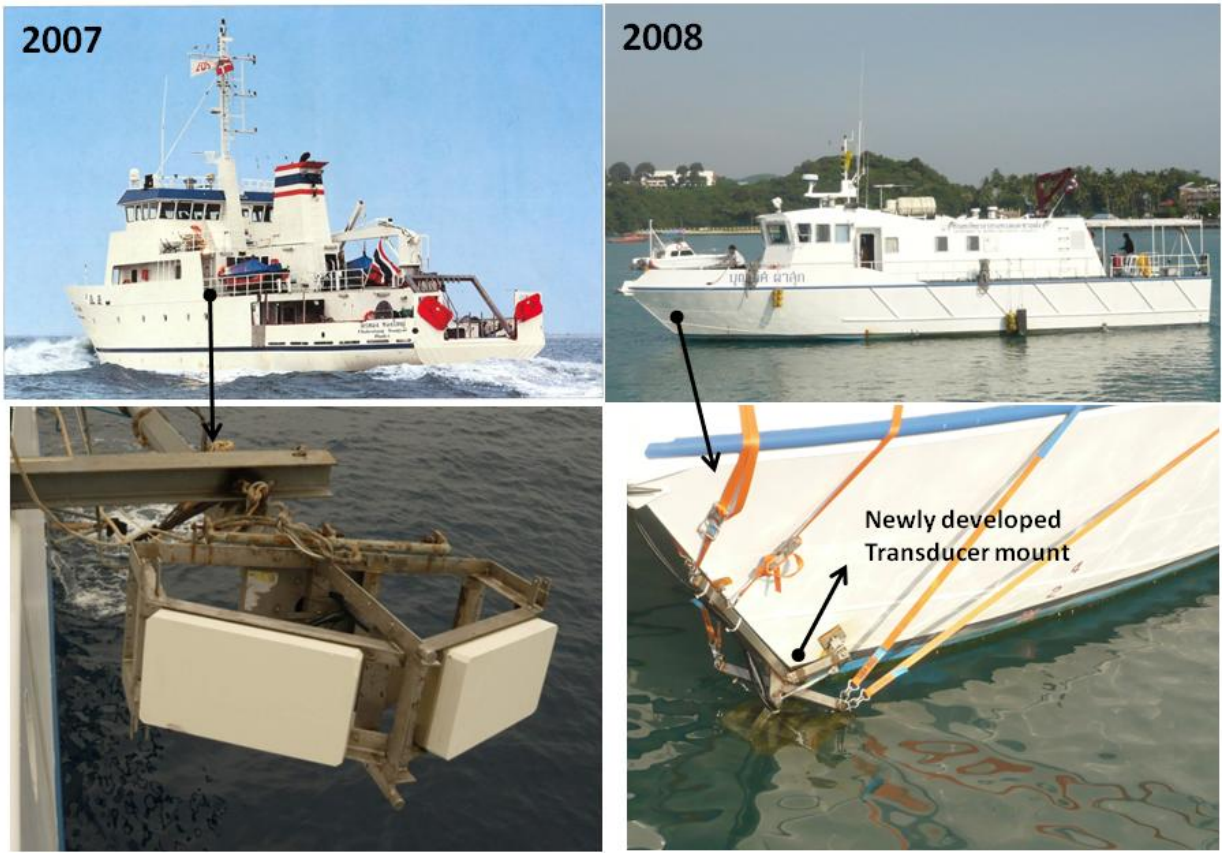


Fig. 2. Research vessels RV CHAKRATONG TONGYAI (right) and RV BOONLERT PASOOK (left) both belonging to Phuket Marine Biological Centre (PMBC). On RV CHAKRATONG TONGYAI multibeam transducers had to be welded to the port side of the ship, while on RV BOONLERT PASOOK the transducers were fixed at the bow of the ship using a special mount created by technicians of IfG.

4.1.2 Cruise with RV BOONLERT PASOOK in 2008

Based on analyzes of the data collected during the 2007-cruise, it was necessary to perform hydroacoustic mapping and sediment sampling towards north but as well in more shallow waters towards the 5 m contour line. Therefore we used RV BOONLERT PASOOK, a smaller vessel of PMBC with less draught but with less space in the laboratory and on the working-deck as well. Some adjustments and changes in the equipment were necessary. The Multibeam echosounder (SeaBeam 1185) was used again to record bathymetric data. The transducers were fixed to the bow of the ship using tension belts and a special mount developed by technicians of IfG (Fig. 2). A dual-frequency Benthos 1645 side scan sonar system with chirp technology was used to collect side scan sonar data. The chirp technology allows running profiles in shallow water by keeping high resolution data acquisition with a range of 100 m to both sides. Shallow seismic reflection data were collected using a low voltage Boomer system (C-Boom, C-Products Europe Ltd) which only needs 0,6 KV instead of 3,5 KV like the EG&G Boomer system. Therefore, no extra energy source was necessary. Underwater video observations were carried out by towing an underwater MARISCOPE camera. Surface sediments and short sediment cores were collected with the same devices which where used in 2007. As BOONLERT PASOOK is not equipped with an electrical winch to operate scientific equipment a hand winch was used for taking samples and sediment cores.

The main task during this cruise was to compile detailed and full-coverage morphological and sediment distribution maps of the seafloor offshore Phang Ngha Province and especially around Cape Pakarang, beginning at about 5 m water depth. Hydroacoustic mapping in shallow water is needed, as the influence of the tsunami, especially the backwash, seems to be stronger here. This could not be accomplished in 2007, as RV CHAKRATONG TONGYAI could not operate in waters shallower than 10 m. Several interesting, unusual sedimentary features, which were already observed in 2007, were recorded again to get more information about sediment dynamics, stability of observed structures and changes in the morphology. However, due to a lack of time during the cruise, the available repetitive measurements are still limited.

The investigation area was extended to offshore Phra Tong Island as it was proofed that this coastal area was as well strongly hit by the tsunami (JANKAEW et al., 2008). An overview mapping on a few selected profiles was carried out (see Fig. 1). These data are necessary, as we need to ensure our preliminary results by data from another area.

4.2 Laboratory work

While onshore tsunami deposits are supposed to contain organic and inorganic material of marine origin, offshore transported material should contain tracer-material indicating clearly sources from the mainland, depending on landforms and deposits which are exposed in those areas which were hit by the tsunami waves (ABRANTES et al., 2008, CHOOWONG et al., 2008, FUJIWARA, O. & KAMATAKI, T., 2007, HAWKES et al., 2007). The sediment surface samples have been first analysed for grain size, to calibrate data with Side-scan sonar images and to create sediment distribution maps.

A multi sensor core logger (MSCL), which is a non-destructive system for the acquisition of physical and acoustical properties of the sediments, e.g. gamma-ray attenuation, bulk-density, P-wave velocity and magnetic susceptibility was used. Measurements are carried out with a high spatial resolution, typically at 1 cm intervals along the length of a core (SCHULTTHEISS & WEAVER, 1992, BEST & GUNN, 1999). These properties are commonly used in paleooceanographic, paleoclimatic and stratigraphic studies for lithostratigraphic correlation (MIENERT et al., 1988, HERBERT & MEYER, 1991, SHACKLETON et al., 1995) but can be applied for tsunami studies to identify abrupt changes in sediment properties and bedding conditions (ABRANTES et al., 2008).

The XRF scanner is a non-destructive and high resolution method to determine relative element intensities in count per second (cps.), directly at the surface of a split sediment core. It can provide data about the elemental composition of the sediment which is then used in sediment provenance identification (JANSEN et al., 1998, PÄLIKE et al., 2001, WELTJI & TJALLINGII, 2008). Al, K, Si, Ti and Fe correspond to terrigenous content whereas Ca indicates $CaCO_3$, which is a marine representative. The correlation of element ratios (e.g. Fe/Ca, Ti/Ca) can help to identify marine deposits from deposits which have a high content of terrigenous material (LAMMY et al., 2001, BAHR, 2005, OHTA & ARAI, 2007). This helps to clearly distinguish tsunami deposits in the marine environment which contain terrestrial material. Problematic is the appearance of separate shells in mostly terrigenous deposits, as they shift the Ti/Ca ration towards Ca.

X-radiography images of thin slabs taken from the core surface were prepared to detect sedimentary structures that cannot be seen in any other way. It is recommended as a routine

procedure for preliminary study of unconsolidated sediments (AXELSSON, V. & HÄNDEL, S.K., 1972, JACKSON, P.D. et al., 1996).

In an innovative approach, sediment samples obtained during the TUNWAT cruises are analyzed for various polycyclic aromatic hydrocarbons (PAH) to determine sediment influx from land. A research article is currently prepared under the lead of Dr. Pongpiachan from our counterpart institution Prince of Songkla University, Biogeochemical and Environmental Change Research Unit (see appendix).

For dating purposes, Pb-210 analyses were conducted at the Institute of Geology, Adam Mickiewicz University in Poznań. The chosen sediment samples were dried, grounded, packed, silled and left in plastic containers for at least 3 weeks to allow complete ^{222}Rn decay. Gamma emitting radionuclides (^{210}Pb, ^{214}Pb, ^{214}Bi, ^{137}Cs) were measured using a high purity coaxial wide energy Germanium detector (Canberra GX2520 (relative efficiency 25%, resolution <2.0 keV) with remote detector chamber option (RDC-6 inches) for low energy background reduction. The detector end cap is composed of a low attenuated polycarbon window. The detector was placed in 10cm thick lead shield walls. Spectrums were acquired using a DSA1000 MCA with digital signal processing. The detector was commercially characterized by Canberra using the MCNP method called ISOCS/LabSOCS Characterization. Efficiencies for measured geometries were determined using LabSOCS code applying all corrections for sample geometry, matrix, and container type, for energy range 45 - 3000 keV. The results were analyzed with software GENIE 2000 with gamma analysis option. Precision and MDA (minimum detectable activity) of the measurements were determined using standard GENIE 2000 algorithms, which summarize all the analytical uncertainties and present them as 2sigma error. Due to low activities of measured isotopes the samples were measured for 155 hours (6.5 days) on average. The ^{210}Pb geochronology requires separation of ^{210}Pb supported (continuously produced in the sediment) and excess (delivered from the external sources). The supported ^{210}Pb was determined by measurement of ^{214}Pb, ^{226}Ra and ^{214}Bi. The excess ^{210}Pb activity was determined by subtracting supported ^{210}Pb (average of ^{214}Pb, ^{214}Bi activities) from total ^{210}Pb for each depth interval. Moreover ^{137}Cs and ^{40}K were measured.

5. Results

The description of the most important results presented in this chapter is given from the shallow to the deep water, starting in shallow water, as the observed structures are clearly limited to specific water depth intervals. The reference level for adjusting all multibeam echosounder measurements to produce reliable bathymetrical data is spring tide low water. Our data were corrected against this level of Ao Kaulak (Fig. 1) gauge by using the program Wxtide32 (www.wxtide32.com).

5.1 Mud patches from 7 m to 15 m water-depth

Close to the coast, a patchy cover of fine grained sediments (mud with small amount of sand) exists in water depths between -7 m to -15 m extending to a distance of 6 km from the coastline. These patches appear along north and south of Cape Pakarang. They cover an area of app. 6 km² south of Cape Pakarang and of app. 9 km² north of Cape Pakarang. The geomorphological setting and the extension of these patches perpendicular to the shoreline is different (Fig. 3).

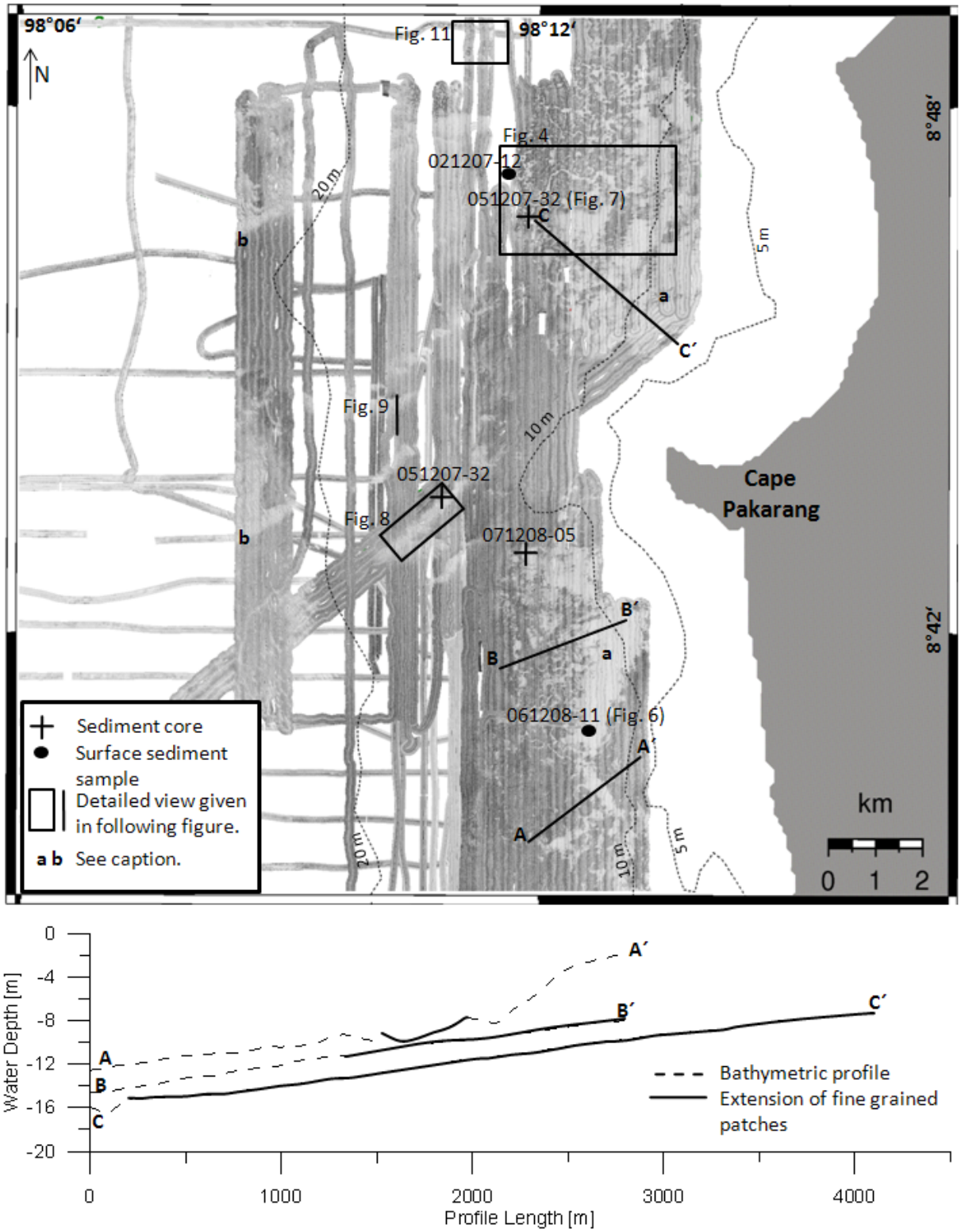


Fig. 3. Top: Mosaic of side scan sonar data showing the situation around Cape Pakarang (data were collected in 2008). Lighter colors represent patches of fine grained sediment (mud) (a). SW-NE striking features (b) are visible further offshore. Bottom: Bathymetric profiles showing the geomorphological position of the patches, indicated by a thick black line.

Some of the patches are located on the slope rising towards the shoreline with no discernible even small scale morphology of the patch area itself. Other patches, especially in the southern

part of the investigation area, are present in depressions up to 2 m deep. They are located in front of platforms, which are built up of carboniferous reef material or granitic outcrops.

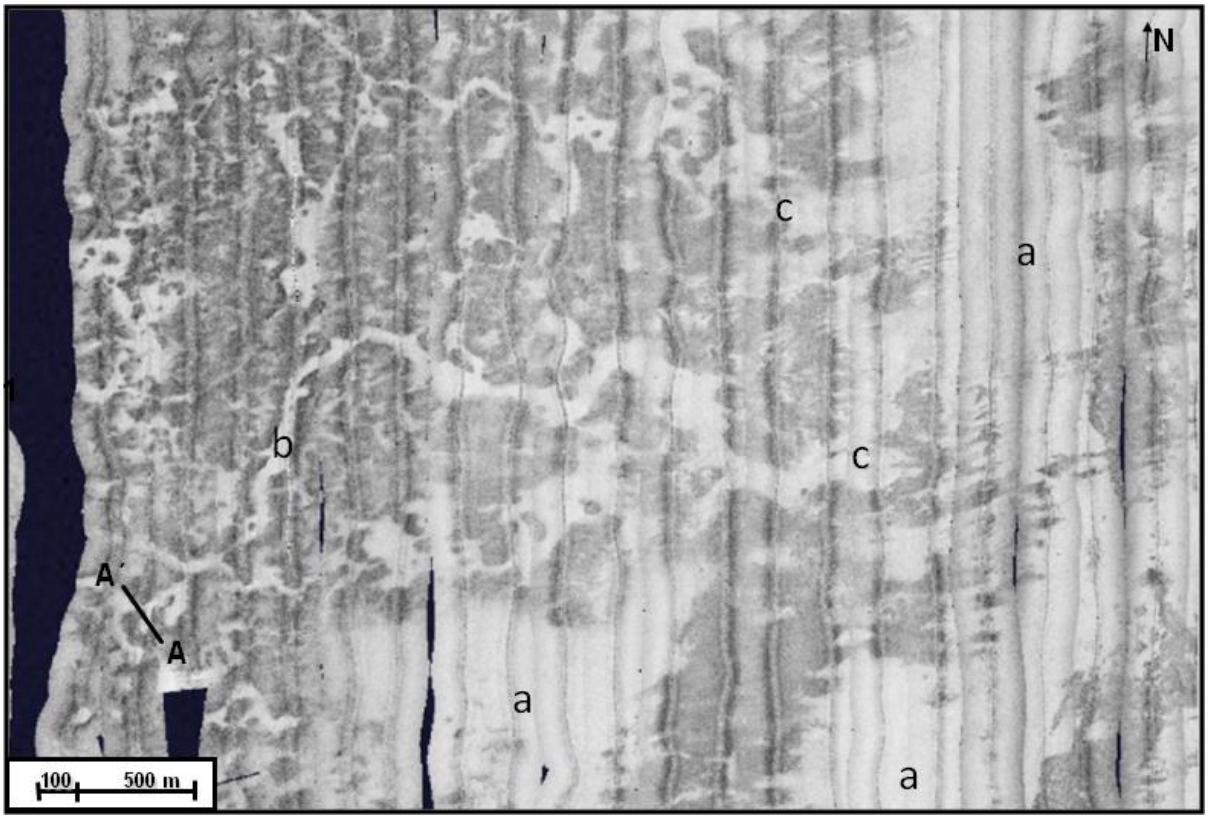


Fig. 4. Detailed view of patches of silty and muddy sediment, (a) 3 to 7 km offshore in water depth from 7 to 15 m. Further offshore small channels (b) are visible. They are connected (c) to the patches closer to the coastline. Profile A – A´ is shown in Fig. 5 (for position in investigation area see Fig. 3).

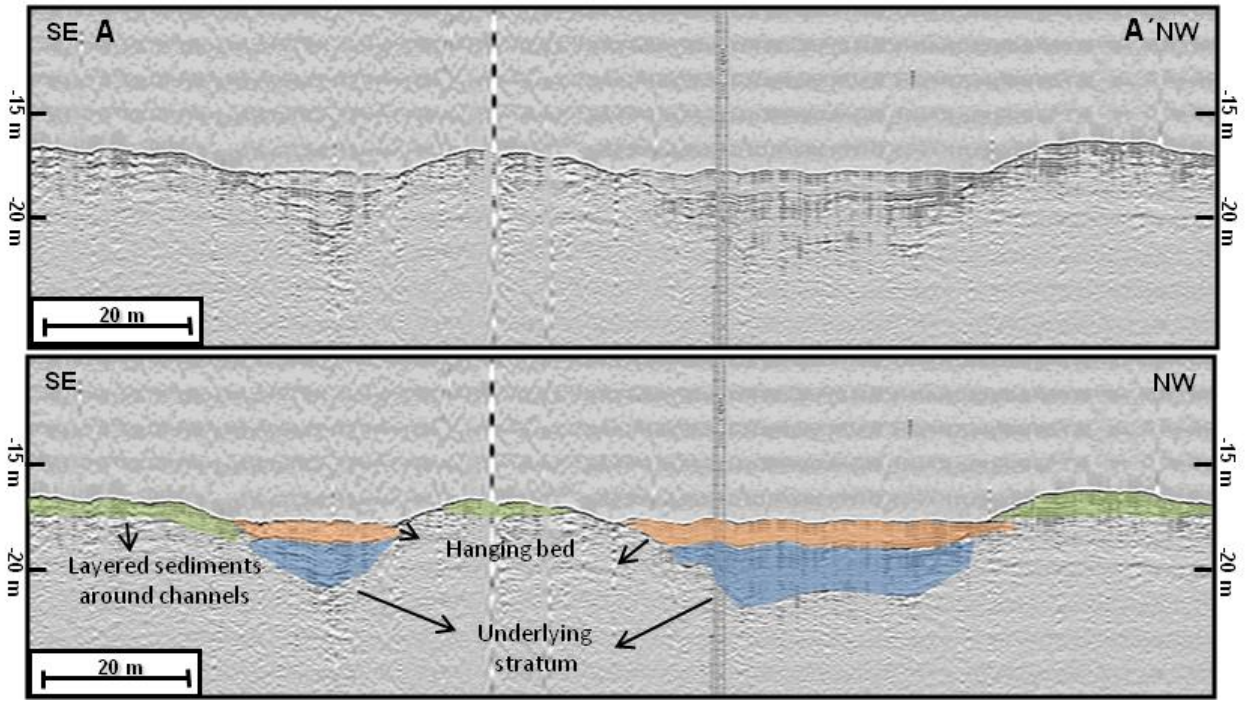


Fig. 5. Seismic profile crossing a channel (profile A-A´ in Fig. 4). Clearly visible are two generations of channel fillings (marked orange and blue). The structure of the seabottom surrounding the channels appears also stratified (marked green).



Fig. 6. Clasts of coarse sand with pieces of laterite. Sample 061208-11 taken 3.5 km offshore Cape Pakarang. For position of sample see Fig. 3.

In this area, both types of rocks are common close to the coastline (GERONIMO et al 2009). In most of the seismic profiles these patches are not discernable, as their thickness seems to be too small for being detected with the equipment which was used; however, when they could be distinguished, their thickness does not exceed 1.5 m at maximum. In sediment core 071208-05 taken in this area the thickness of the fine grained sediment was found to be only 15 cm. Below these layered, although partly disturbed fine grained sediments, coarser, non-stratified sand is found in core depths between 15 and 21 cm. At this core depth, another unconformity marks the change towards a different layer of coarse sand including shell fragments.

Sediment samples taken in the area of the patchy fine grained sediments are mainly composed of silt at the surface but contain clasts of sand and even gravel at their base. In grab sample 061208-11 (position see Fig. 3), numerous pieces of laterite (Fig. 6) were found inside the sandy intraclasts. The seafloor surrounding the patches is commonly composed of coarse sand.

5.2 Channel system from 10 m to 16 m water-depth

In water depths between -10 to -16 m, small-scale channel structures appear in the side-scan sonar mosaic (Fig. 4). The side scan images show that the channels commonly originate at the offshore boundary of the patches composed of fine grained deposits (Fig. 4). Their widths vary between 30 m and 150 m. According to the side scan sonar data, the surface sediment filling the channels is finer compared to the coarse seafloor sediments surrounding the channels. Towards offshore the incision depth of the channels increases up to 2 m, clearly visible in the bathymetric data. Towards onshore the channels are completely filled with sediment, but are still discernible in the seismic data. According to these data, the channel filling consists of two generations of layered sediment (Fig. 5). The seafloor surrounding the channels directly appears layered as well. Surface sediment sample 021207-12 taken in the vicinity of a channel contains grass originating from land. Core 051207-32 (Fig. 7) retrieved close to one of the channels in a water depth of 14.40 m contains a muddy layer, including

stiff mud clasts and wood fragments. This layer is covered by coarse sand and shell fragments. The element intensity ratios of Ti/Ca and Fe/Ca measured along this core (Fig. 7) show low values in sand layers and higher values in muddy layers. An x-radiography image reveals that the muddy layer contains shells fragments at its base.

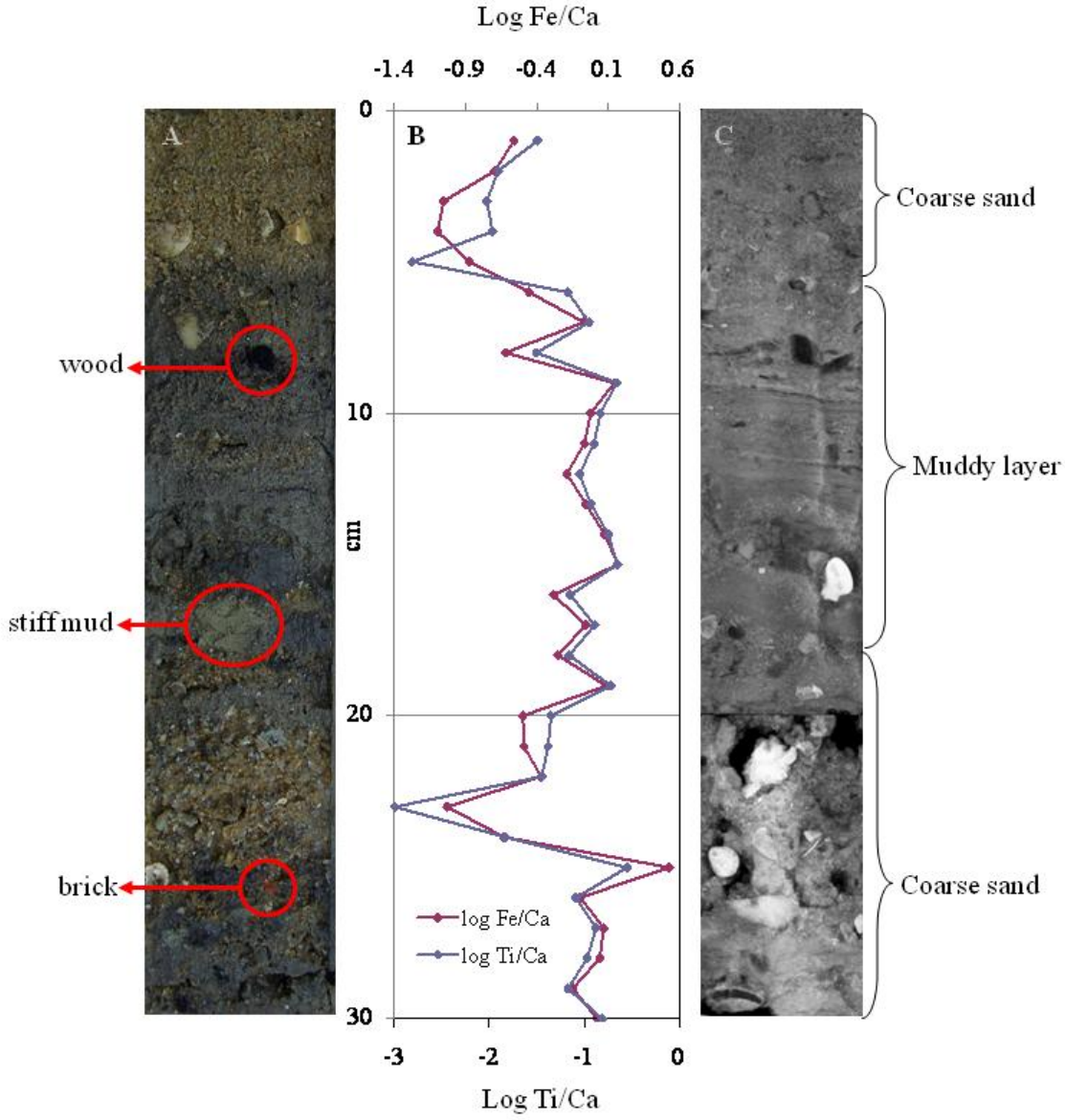


Fig. 7. Photo (A), diagram of Ti/Ca and Fe/Ca ratios (B) and (C) X-ray image of core 051207-32 which was taken in a channel structure at water depth 14.40 m. (position of core see Fig. 3.)

5.3 Morphological ridges starting at 15 m water-depth extending towards offshore

In deeper waters, elongated, SW-NE striking ridges are visible in the hydroacoustic and bathymetric data (Fig. 3, magnified view in Fig. 8). They are common between Thap Lamu and Cape Pakarang but appear as well in front of Phra Thong Island and Ra Islands in the northern part of the investigation area. No ridges have been found in front of the outlet between the islands of Kho Khao and Phra Thong (Fig. 1). Generally, the structures are first

observed in approximately 15 m water depth, while their continuation into water depth below 30 m is yet unknown. The ridges, with a steep NW and a gently dipping SE side reach heights of about 2 m above the seafloor, while their length exceeds several kilometers with a width of several hundred meters. The distance between two ridge crests varies between about one and five kilometers. In front of the steep north-eastern side of these ridges, small channels with incision depths up to 1 m are sometimes cut into the seafloor.

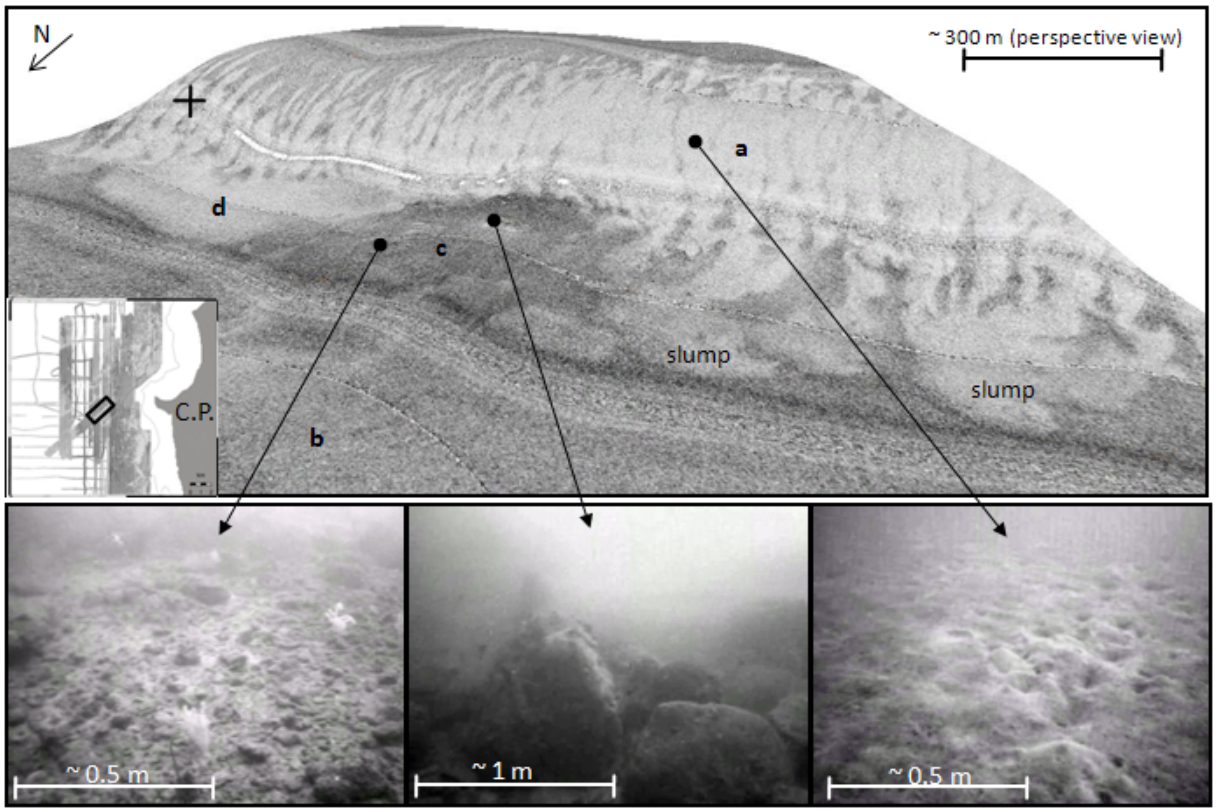


Fig. 8. Side scan sonar image of one of the ridges draped over the bathymetric dataset (vertical exaggeration = 50x).C.P.: Cape Pakarang (see also Fig. 3 for position in investigation area) a) flame-shaped sediment patches, consisting of fine to medium sand b) coarse sand c) gravel and boulders consisting of carbonate material (notice video images) d) sand at the surface, muddy material below Cross: position of short core 051207-37 (Fig. 10), showing sandy material on top and a fine grained layer 10 cm below the surface.

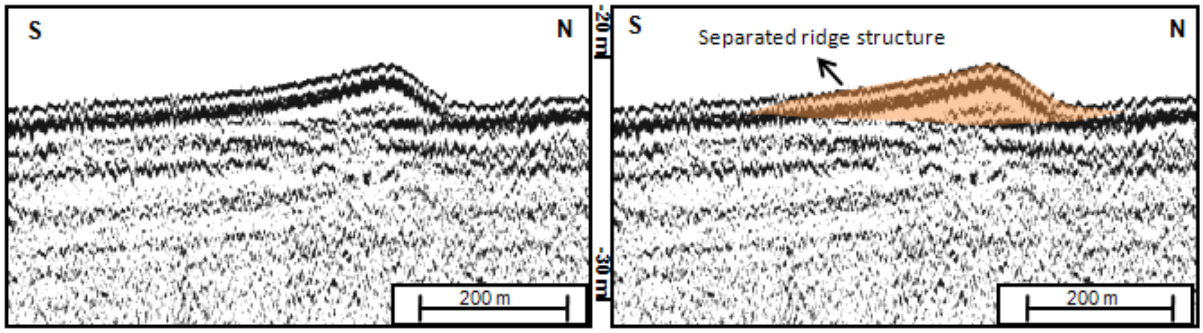


Fig. 9. Seismic profile crossing a ridge (position see Fig. 3). Clearly visible is the asymmetric form of the ridge which is indicating a transport direction from South to North. Additionally, the ridge is separated from the layers below by an unconformity.

For one ridge, a side scan sonar mosaic was draped over the bathymetric data (Fig. 8) to see correlations between sedimentary structures and morphology. A prerequisite for this type of image are detailed bathymetric data. Grab samples taken around the ridge (Fig. 8) reveal the presence of different sediment properties in a small area: Bright elongated, flame-shaped structures are deposited at the slope of the ridge and are composed of well sorted fine sand to medium sand. At the base of the slope, slump-like sedimentary structures are visible in the side scan sonar image. Here, the grab samples contain muddy material just a few centimetres below the seafloor which is composed of medium to fine sand. Core 051207-37 (Fig. 10) which was taken in this area on the slope of the ridge, also shows the presence of a muddy layer 10 cm below the surface. This layer also shows a higher Fe/Ca and Ti/Ca ratio compared to the rest of the core. Below this layer, coarse sand containing complete shells and shell fragments is deposited. Towards the base of the core, muddy sand with few shells is found.

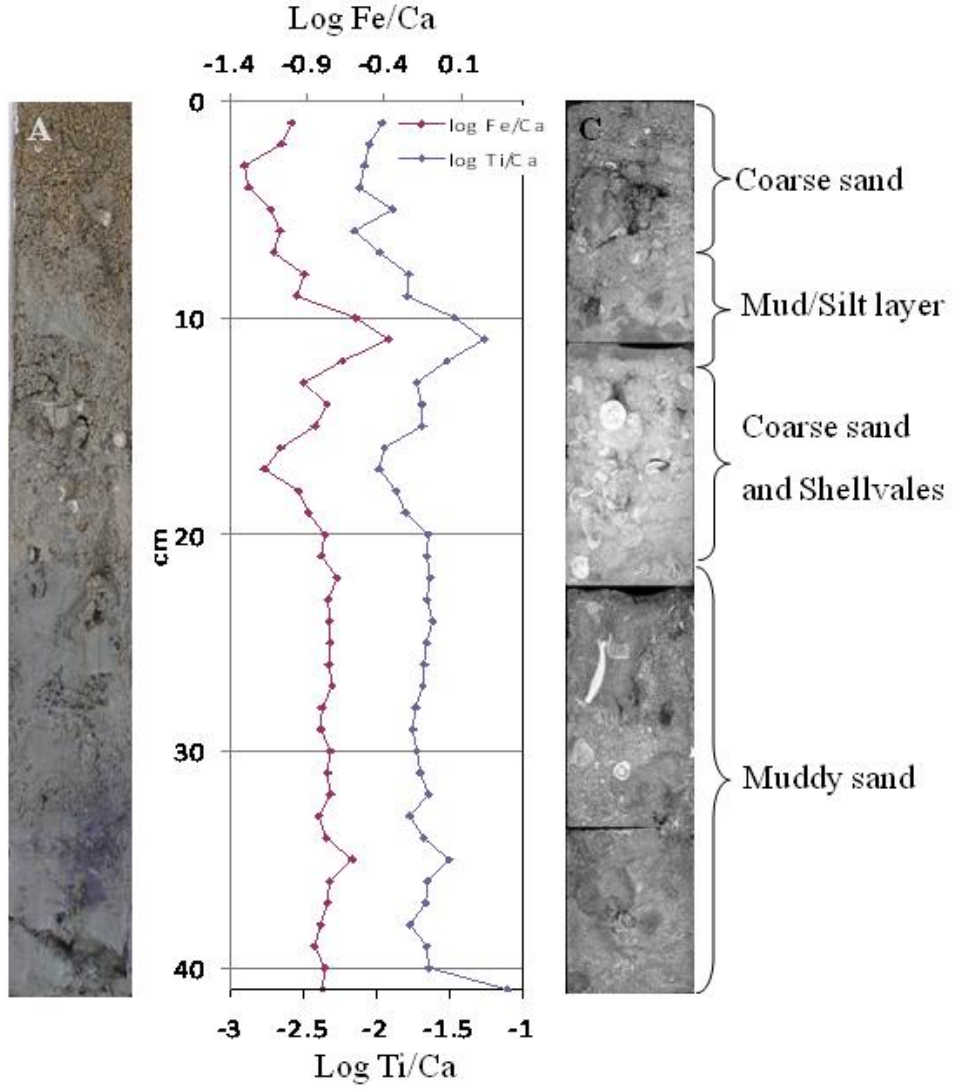


Fig. 10. Photography (A), diagram of Ti/Ca and Fe/Ca ratios (B) and (C) X-ray image of core 051207-37 (for position of core see Fig. 3).

In few places, carbonate reef fragments with a size from gravel to boulders are deposited at the base of the steep ridge slope (see underwater video screenshots in Fig. 8). According to seismic data, the ridges are not connected to subsurface structures, but are clearly separated from the sedimentological structures below by an unconformity (Fig. 9). Generally, the surface of the seafloor surrounding the ridge is composed of coarse sand.

5.4 Further findings

5.4.1 Remnants of tin mining activities

Remnants of tin mining activities can be found in water depths of about 20 to 25m north-west of Cape Pakarang, visible in form of up to 7 m deep holes. These holes can be easily detected in the side scan sonar images, as they appear lighter than the surrounding seafloor and are therefore probably filled with finer material. It is expected that the holes acted as traps for sediment transported offshore during the tsunami event.

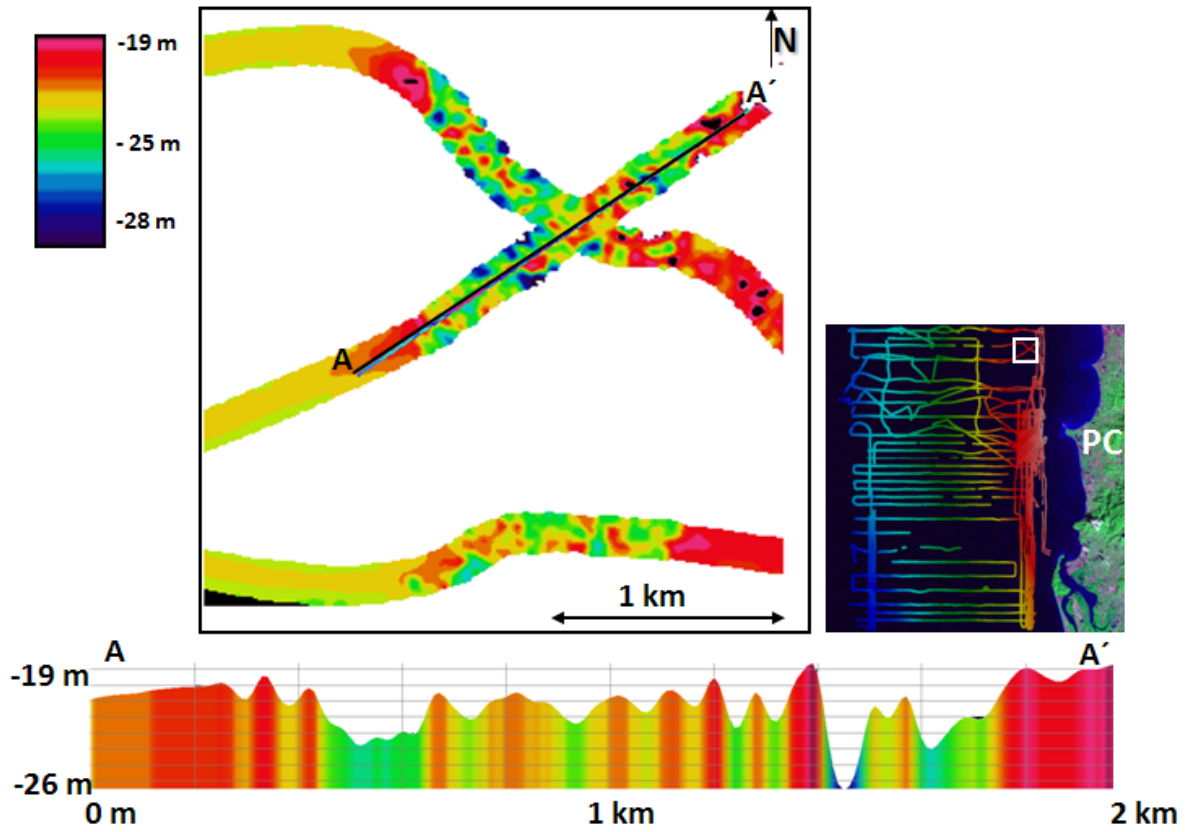


Fig. 11. Bathymetric data collected in 2007 (PC: Cape Pakarang). Remnants of tin mining activities can be seen as deep holes on the seafloor (for position see Fig. 3).

5.4.2 Stone fields and small-scale depressions between -30 and -35 m

In water depths between 30 and 35 meters, elongated fields of stones and boulders appear in the side scan sonar and boomer data (visible in Fig. 12A). Further offshore, several small circular features, with diameters about 10 m, are apparent in the side scan sonar data, commonly in water depths of around 35 m (Fig. 12B). These features are not visible in the bathymetric data, due to problems with the heave correction of the motion sensor during some days in 2007. Judging from their appearance in the side scan sonar images, they form holes in the seafloor. According to side scan sonar data, the filling of these holes is finer compared to the surrounding seafloor. However, due to the small size of the features, a direct sampling to retrieve sediment was not possible.

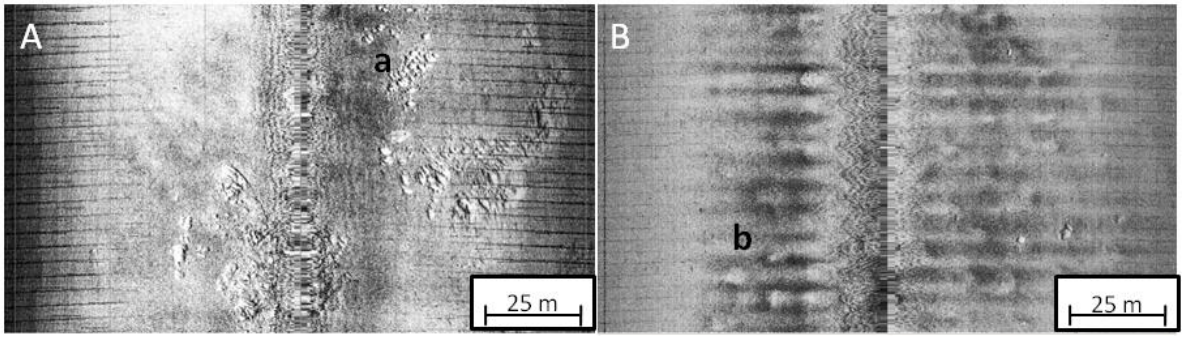


Fig. 12. A: Stone fields (a) in water depths of 30 to 35 m B: Numerous small depressions (b) in the seafloor in 35 m depth (for position see Fig. 1).

5.4.3 Age control for a sediment core from 52 m water-depth

The 210Pb dating method was applied for a core 02/12/07/18 collected from the mid shelf of Andaman Sea (52 m water depth). The core revealed distinct laminated surface sediment layers, up to about 8 cm in thickness (as visible in X-ray images), with two upward grain size fining trends (Fig.14). The 210Pb profile (Fig. 14) is composed of three segments. The upper segment (0-5 cm) shows a steady decrease of the activities with depth, the second unit (5-8 cm) has uniform, slightly increasing activities with depth, and the third unit (below 8 cm) is similar to the first one. Below 30 cm the excess 210Pb is not present.

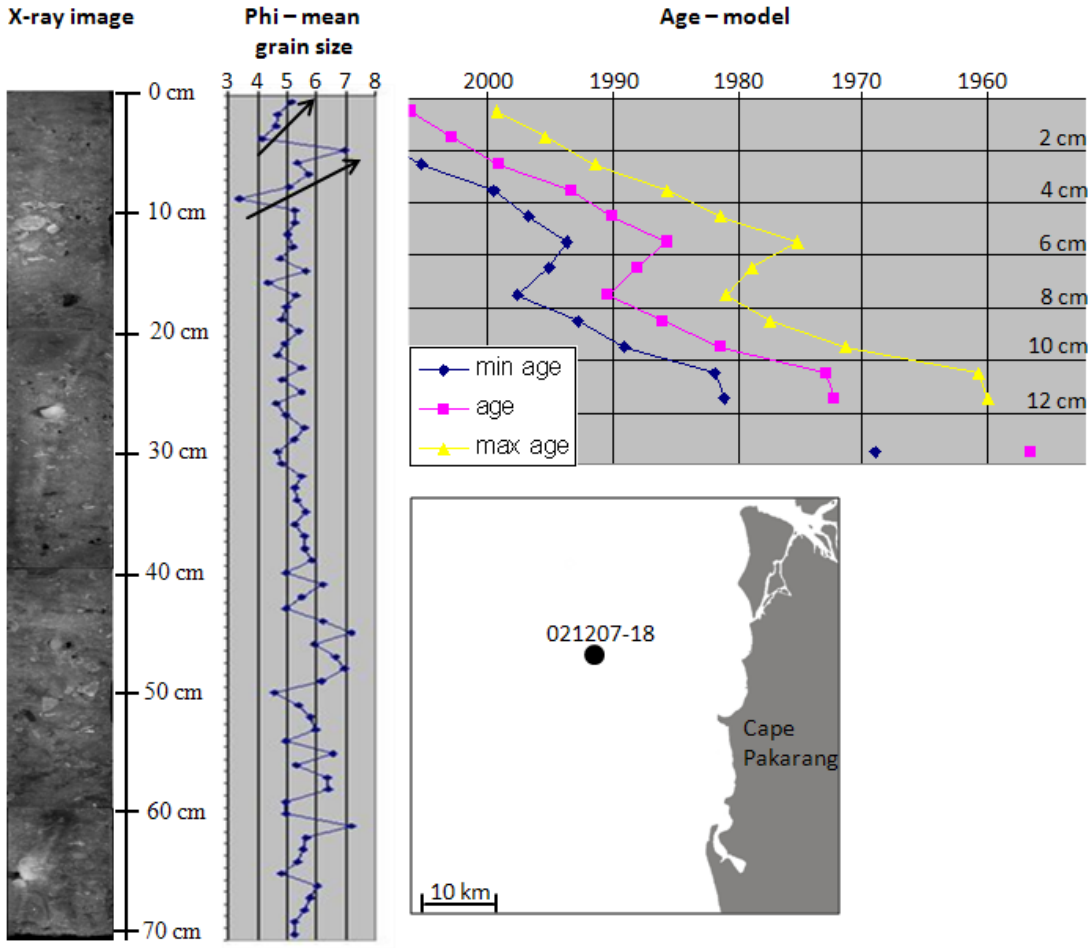


Fig. 13. X-ray-image, mean grain size and age model for core 021207-18, taken 24 km offshore from 52 m water depth. Two fining upward sequences are indicated by arrows.

The first and third segment are typical for more or less steady sediment accumulation - application of CIC (constant initial concentration) model reveals the accumulation rate in order of 0.3 cm y-1. The second unit is typical for rapid sedimentation and/or mixing. Its presence between two segments with profiles typical for steady accumulation suggests that it may be an event layer. The age ~1990 of the event was assessed from accumulation rate of the upper segment (0-5 cm). It is likely that the event layer was deposited by the largest typhoon recorded on Andaman Sea - Typhoon Gay in 1989.

5.4.4 Observation from 60 m to 80 m water-depth

Generally, the slope from water depths of about 30 m down to 80 m shows several N-S striking elevations which, according to the first data, seem to continue through the whole study area. Channelled incisions with a depth of several meters are visible in several profiles in the south-western part of the research area in water depths of about 80 m. Generally, first seismic data suggests that in water depths of 60 to 80 m, marine sediments form only a thin sheet above a buried paleomorphology (Fig. 14).

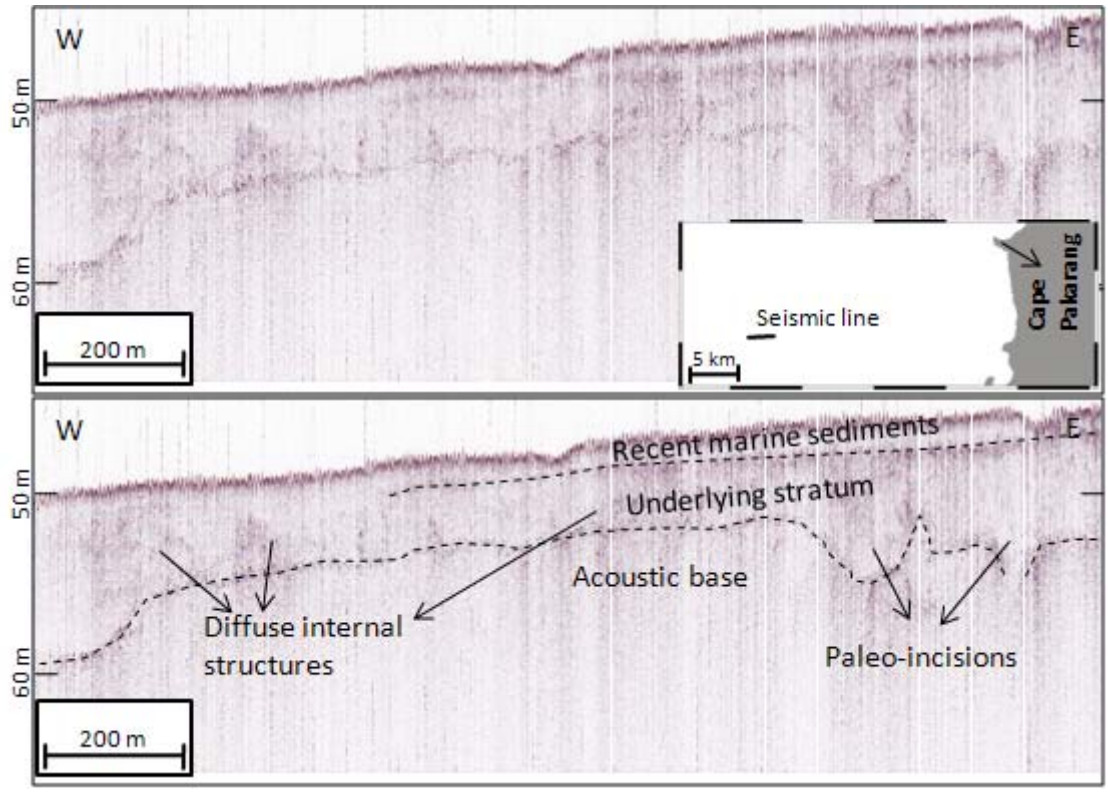


Fig. 14. In deeper waters, the recent marine sediments seem to form a thin cover above an underlying stratum and the acoustic base. In the layer below the marine sediments, diffuse internal structures of yet unknown origin are visible.

6. Interpretation

The general aim of TUNWAT is to identify the impact of the 2004 tsunami on the shoreface and the shelf. As not much about the pre-tsunami seafloor conditions offshore Khao-Lak was known, it is important to carefully differentiate between structures that existed before the tsunami (which were likely altered) and which were newly created due to the tsunami.

Furthermore, anthropogenic structures and their influence on the present seafloor conditions, especially widespread remnants of extensive tin mining activities have to be clearly defined, to avoid mixing them with tsunami induced structures. The interpretation of the hydroacoustic data so far focused up to now mainly on shallow water structures down to 30 m.

The muddy sediment patches between 5 and 15 m water-depth close to the coastline are unusual features for an open, wave dominated coastline, with coarse sand deposited both further on- and offshore. Additionally, it is unlikely that a thin cover of unconsolidated fine-grained material would not have been eroded during the tsunami run-up, which was powerful enough to transport large boulders on the intertidal flat.

Most of the fine-grained patches are not deposited in depressions, which would act as a shelter against currents and wave energy conditions. Despite, the deposition of these deposits happened directly on the exposed offshore inclined slope. Furthermore, pieces of laterite were commonly found in the grab samples. Usually laterite is formed in tropical environments onshore by chemical weathering of rocks (WANG 2002). This land based material was transported to its offshore position by currents. Pieces of grass found close to the Laterite particles further support the assumption of an on- offshore transport of different kinds of material.

Sediment core 07120805 shows presumably coarse sand as pre-tsunami seafloor sediment at its base, similar to the coarse sand commonly found at the seafloor surface in the investigation area. Above, separated coarse sediment clasts are deposited in a matrix of finer grained material. This sediment is assumed to be deposited during the tsunami, as intraclasts are a typical indicator for tsunami deposits (Table 1). Normally, intraclasts are also not found in storm deposits (KORTEKAAS & DAWSON 2007). Additionally, the unconformities visible in the cores support the deposition of these layers during a separate event. The fine grained material in the upper part of the core was therefore likely deposited during the tsunami backflow.

The possibility of muddy material deposited close to the coastline by the tsunami is supported by observations of SHI & SMITH (2003), who note that a large amount of clay and silt is removed from onshore sediment during tsunami run-up and backwash, but onshore tsunami sediments are typically composed of sandy material. The fine grained material is transported offshore and, according to our data, deposited close to the coastline. Mud drapes deposited onshore by the 2004 Indian Ocean tsunami are mentioned by CHOOWONG ET AL. (2008). Mud drapes deposited during a paleo-tsunami event are described by FUJIWARA & KAMATAKI (2007), although here the material derived from offshore. In contrast, the fine-grained sediment we found in front of Cape Pakarang likely originate from onshore. Altogether, the silty and muddy sediment patches offshore Cape Pakarang were most likely deposited by the 2004 tsunami.

The small scale channel system is obviously connected to the described patches of fine-grained sediment 4 to 5 km offshore, as the onset of these channels is located here. However, it is unlikely that the channels were created during the tsunami event. These channels show a meandering shape, which is an unlikely result of a high velocity-, probably hyperconcentrated density flow (LE ROUX & VARGAS 2005, NARAYANA et al. 2007). The seismic data clearly show two separate channel fillings. We assume that sediment transported offshore by the tsunami backflow was trapped within the channels. This is indicated by sediment core 051207-32 (Fig. 7); the coarse sand, typical for the seafloor around Pakarang Cape, in the upper 5 cm was likely deposited after the tsunami event. The material below, containing wood and brick fragments, was deposited during the backwash. A deposition of material by the

backwash in already existing channels would explain both, a) the connection to the patches with proposed tsunamigenic fine grained sediment more close to the coastline, and b) the decrease of channel infilling towards offshore.

The ridge system in about 20 m water depth was probably not created by the tsunami, but is interpreted as a system of sand ridges which existed prior to the tsunami. Ridge systems with comparable geomorphological characteristics and striking directions towards the shoreline are described e.g. by LI & KING (2007) for the Scotia Shelf or in the North Sea (ANTHONY & LETH 2002). Most probably these ridges are formed due to regular hydrodynamic processes (VAN DE MEENE & VAN RIJN 2000), although moribund ridges as remnants from times with a lower sea level are known (DYER & HUNTLEY 1999, KUBICKI 2008). The asymmetric appearance of the ridges off Pakarang Cape points to a transport direction from SE to NW. A SE-NW current direction is unlikely for both run-up and backwash of the tsunami in this area as indicated by satellite images (images of the IKONOS satellite) and models of the flow direction and current velocity around Pakarang Cape. The flame-shaped sediment patches on the steeper slope of the ridges are therefore likely connected to the normal evolution of the ridge system. However, several grab samples and core material (core 051207-37, Fig. 10) show muddy sediment close to the surface. Muddy layers in those kinds of ridge systems have not been described yet in the literature. The thin layer of muddy material in this core shows high ratios of Ti/Ca, and might therefore be of terrestrial origin. A deposition of this material during the monsoon is unlikely, as more layered structures would be expected. Additionally, riverine sediment input into the investigation area is very small. Therefore, we assume that the muddy material was deposited during the tsunami backwash, similar to the thicker fine grained sediments closer towards the coastline. The deposition of the coarse sand after the tsunami on this muddy layer could have triggered the observed small-scale slumps on the steep side of the ridges (Fig. 8).

Boulders located at the base of the ridge (Fig. 8) could be transported by the backwash: During the tsunami run-up, a lot of boulders were transported on the intertidal flat on Pakarang Cape (GOTO et al. 2007). The backwash at Pakarang Cape was modelled by GOTO et al. (2007). The authors show that the current speed of the backwash was in the order of 3m/s. This would be strong enough to move the observed boulders (GOTO et al. 2007, IMAMURA et al. 2008), which have a diameter of less than 1 meter according to underwater images. Furthermore, once boulders were moving, they would be transported downslope from Pakarang Cape towards offshore (GERONIMO et al. 2009).

Taking into account a channelized backwash (LE ROUX & VARGAS 2005, FAGHERAZZI & DU 2007), it is possible that in some areas the current speed was strong enough to transport boulders deposited at Pakarang Cape over a larger distance back towards the sea, while in most areas the speed was lower, leading to the deposition of a sequence of finer material. This could explain the presence of a sequence of sand and finer grained material close to coastline in front of Pakarang Cape.

Sediment cores, taken in water depths of more than 50 m, show only minor influences of the tsunami event, in form of a fining upward sequence in the first centimetres below the seafloor. The fining upward sequence could potentially be created with the tsunami wave passing by and suspending sediment. However, the influence of the passing wave would be minor, compared to theoretical computations of WEISS (2008), who showed that the 2004 tsunami should be able to move fine sand in water depths of 335 meter in the Indian Ocean.

The muddy layer incorporated into the sand ridge system is the most offshore situated indicator of tsunami backwash transport that we identified. This mud layer is only of minor thickness. Therefore, it is assumed that the backwash influence in water depths below 30 m was generally small, and most of the sediment transported by the backflow was deposited in more shallow waters. This is in agreement with concepts of COLEMAN (1968) who notes that most of the material transported by the backwash is either deposited a few km in front of the shoreline, or in the deeper offshore waters beyond the shelf.

6. Conclusion

The data analyzed so far indicate:

- Clear signals of tsunami backwash deposits are found up to 30 m water depth; mainly in form of fine grained sediments. These sediments are either deposited directly on the exposed slope, or in traps like small channels.

- The backwash deposits are recognized as fine-grained (clay and silt) deposits, in combination with land-based material like grass and laterite fragments deposited in intraclasts.

- The backwash deposits have clear lateral boundaries and are not present continuously in front of the whole coastline.

- Morphological structures existing prior to the tsunami were altered during the event.

- The sediment deposited during the tsunami backwash is partly of terrigenous origin.

- In front of Pakarang Cape, the backwash was strong enough to transport boulders downslope.

- The backwash appeared as a channelized, highly turbulent and high density flow.

- The influence of the backwash, as well as the run-up of the tsunami below 30 m water depth was probably small.

7. Future work

During the next cruise existing gaps in the hydroacoustic dataset need to be filled. Additionally the hydroacoustic survey will be extended into deeper waters, to determine the spatial distribution of observed features perpendicular to the shoreline. Especially in water depth below 30 m the available hydroacoustic data coverage does not allow statements about a continuation and spatial distribution of already observed structures, especially of the ridge system which was altered by the tsunami.

The research area will be extended to the north along the coastline, to find correlations of the offshore deposition of tsunami sediments against properties of the tsunami wave (e.g. run up height) and/or the onshore morphology.

Repeated hydroacoustic surveys in areas which already have been surveyed will allow to asses altering of structures and the preservation potential of tsunami deposits. These deposits should be out of equilibrium under normal conditions. They will be eroded or covered by sediment. This will determine whether the backwash deposits are available in the geological record.

Additional core samples are required to determine the geochemical background against which tsunami sediments can be surely recognized. Furthermore, as the hand-operated winch during the cruise in 2008 limited coring activities, many of our cores do not penetrate the assumed tsunami sediment layers. Longer cores taken with an electrical operated winch are needed to assess thickness and possible further layering of tsunami deposits. Eventually, an influence of the run-up close to the coastline was missed up to now, because sediment layers influenced by the run-up of the tsunami wave have not been sampled due to insufficient core length.

Planned laboratory works include the analysis of the < 63µm grain size distribution of the surface sediment samples. Additionally, detailed grain size distributions for most cores have to be continued. Analysis of clay mineral composition will give further insight into the origin of the sediments. Furthermore, core material will be analysed for different radio-nuclides. Depending on the assumed age of the sediments, dating by ^{14}C, ^{210}Pb and ^{137}Cs will be used in order to get precise information about the age of sediments, erosion-events and accumulation rates.

9. References

ABRANTES, F., ALT-EPPING, U., LEBREIRO, S., VOELKER, A., SCHNEIDER, R., 2008. Sedimentological record of tsunamis on shallow-shelf areas: The case of the 1969 AD and 1755 AD tsunamis on the Portugese Shelf off Lisbon. Marine Geology 249: 283-293.

ANTHONY, D., LETH, J.O. 2002. Large-scale bedforms, sediment distribution and sand mobility in the eastern North Sea off the Danish west coast. Marine Geology 182: 247-263

AXELSSON, V. & HÄNDEL, S.K., 1972. X-radiography of unextruded sediment cores. Geografiska Annaler. 54: 34-37.

BAHR, A., LAMY, F., ARZ, H., KUHLMANN, H., WEFER, G., 2005. Late glacial to Holocene climate and sedimentation history in the NW Black Sea. Marine Gelology 214: 309-322.

BEST, A.I. & GUNN, D.E., 1999. Calibration of marine sediment core loggers for quantitative acoustic impedance studies. Marine Geology 160: 137-146.

BELL, R., COWAN, H., DALZIELL, E., EVANS, N., O`LEARY, M., RUSH, B., YULE, L., 2005. Survey of impacts on the Andaman Coast, Southern Thailand following the great Sumatra-Andaman earthquake and tsunami of December 26, 2004. Bull. of The New Zealand Soc. For Earthquake Eng. 38(3), 123-148.

BRYANT, E. 2001. Tsunami. The Underrated Hazard: Cambridge, 320 p.

CANTALAMESSA, G., DI CELMA, C., 2005. Sedimentary features of tsunami backwash deposits in a shallow marine Miocene setting, Mejillones Peninsula, northern Chile. Sedimentary Geology, 178, 259 – 273.

CHOOWONG, M., MURAKOSHI N., HISADA K. 2008. 2004 Indian Ocean tsunami inflow and out flow at Phuket, Thailand. Marine Geology. 248: 179-192.

CHOOWONG, M., MURAKOSHI, N., HISIDA, K., CHAROENTITIRAT, T., CHARUSIRI, P., PHANTUWONGRAJ, S., WONGKOK, P., CHOOWONG, A., SUBSAYJUN, R., CHUTAKOSITKANON, V., JANKAEW, K., KANJANAPAYONT, P. 2008. Flow conditions of the 2004 Indian Ocean tsunami in Thailand, inferred from capping bedforms and sedimentary structures. Terra Nova 20, 141-149.

COLEMAN, P. J. 1968. Tsunamis as geological agents. J. Geol. Soc. Aust. 15: 267-273.

COWELL, P.J., HANSLOW, D.J., MELEO, J.F., 1999. The shoreface. In: SHORT, A.D. (ed.), Handbook of beach and shoreface morphodynamics, Chichester: Wiley, 39 – 71.

DAWSON, A.G., SHI, S., DAWSON, S., TAKAHASHI, T., SHUTO, N., 1996. Coastal sedimentation associated with the june 2nd and 3rd, 1994 tsunami at Rajegwesi, Java. Quat. Science Review, 15, 901 – 912.

DAWSON, A.G., STEWART, I. (2007) Tsunami deposits in the geological record. Sedimentary Geology 200: 166-183.

DAWSON, A.G., STEWART, I. (2008) Offshore tractive current deposition: The forgotten tsunami sedimentation process. In: Tsunamiites – Features and Implications. 153 – 160.

DYER, K.R., HUNTLEY, D.A., 1999. The origin, classification and modelling of sand banks and ridges. Continental Shelf Research 19 (10), 1285-1330.

FAGHERAZZI, S., DU, X., 2007. Tsunamigenic incisions produced by the December 2004 earthquake along the coasts of Thailand, Indonesia and Sri Lanka. Geomorphology 99: 120-129.

FELDENS, P., SCHWARZER, K., SZCZUCIŃSKI, W., STATTEGGER, K., SAKUNA, D., SOMGPONGCHAIYKUL, P., 2009. Impact of 2004 Tsunami on Seafloor Morphology and Offshore Sediments, Pakarang Cape, Thailand. Polish J. of Environ. Stud. 18 (1), 63-68.

FUJIWARA, O., KAMATAKI, T., 2007. Identification of tsunami deposits considering the tsunami waveform: An example of subaqueous tsunami deposits in Holocene sjallow bay on southern Boso Peninsula, Central Japan. Sedimentary Geology, 200, 295 – 313.

GERONIMO, I.D., CHOOWONG, M., PHANTUWONGRAJ, S., 2009. Geomorphology and superficial bottom sediments of Khao Lak coastal area (SW Thailand). Polish J. of Environ. Stud. 18(1).

GOFF, J., CHAGUÉ-GOFF, C., NICHOLS, S., 2001. Palaeotsunami deposits: a New Zealand perspective. Sediment. Geol., 143, 1 – 6.

GOTO, K. CHAVANICH, S.A., IMAMURA, F., KUNTHASAP, P., MATSUI, T., MINOURA, K., SUGAWARA, D., YANAGISAWA, H., 2007. Distribution, origin and transport process of boulders deposited by the 2004 Indian Ocean tsunami at Pakarang Cape, Thailand. Sed. Geol. 202, 821-837.

HAWKES, A.D., BIRD, M., COWIE, S., GRUNDY-WARR, C., HORTON, B.P., TAN SHAU HWAI, A., LAW, L., MACGREGOR, C., NOTT, J., ONG, J.E., RIGG, J., ROBINSON, R., TAN-MULLINS, M., TIONG SA, T., YASIN, Z., WAN AIK, L., 2007. Sediments deposited by the 2004 Indian Ocean Tsunami along the Malaysia – Thailand Peninsula. – Marine Geology, 242, 169 – 190.

HERBERT, T.D., MEYER, L.A., 1991. Long climatic time series from sediment physical property measurements. J. Sediment. Petrol., 61(7): 1089-1108.
IMAMURA, F., GOTO, K., OHKUBO, S., 2008. A numerical model for the transport of a boulder by tsunami. Journal of Geophysical Research 113, C01008, doi:10.1029/2007JC004170.

JACKSON, P.D., BRIGGS, K.B., FLINT, R.C., 1996. Evaluation of sediment heterogeneity using microresistivity imaging and X-radiography. Geo-Marine Latters 16: 219-225.

JANKAEW, K., ATWATER, B.F., SAWAI, Y., CHOOWONG, M., CHAROENTITIRAT, T., MARTIN, M.E., PRENDERGAST, A., 2008. Medieval forewarning of the 2004 Indian Ocean tsunami in Thailand. Nature 455, 1228-1231.

JANSEN, J.H.F., VAN DER GAAST, S.J., KOSTER, B., VAARS, A.J., 1998. CORTEX, a shipboard XRF-scanner for element analyses in split sediment cores. Marine Geology 151: 143-153.

KORTEKAS, S., DAWSON, A.G. 2007. Distinguishing tsunami and storm deposits: An example from Martinhal, SW Portugal. Sedimentary Geology 200; 208-221.

KUBICKI, A. 2008. Large and very large subaqueous dunes on the continental shelf off southern Vietnam, South China Sea. Geo-Mar Lett. 28; 229–238.

LAMMY, F., HEBBELN, D., RÖHL, U., WEFER, G., 2001. Holocene rainfall variability in southern Chile: a marine record of latitudinal shifts of the Southern Westerlies. Earth Planet. Sci. Lett. 185: 369-382.

LAY, T., KANAMORI, H., AMMON, J.C., NETTLES, M., 2005. The great Sumatra-Andaman earthquake of 26 December 2004. Science, 306, 1127 – 1133.

LE ROUX, J.P.,VARGAS, G., 2005. Hydraulic behaviour of tsunami backflows: insights from their modern and ancient deposits. Environ. Geol 49, 65-75.

LI, M.Z., KING, E.L., 2007. Multibeam bathymetric investigations of sand ridges and association bedforms and their relation to storm processes, SableBank, Scotian Shelf. Marine Geology 243, 200-228.

LIU, P.L.F., LYNETT, P., FERNANDO, P., JAFFE, H., FRITZ, B., HIGMAN, H., MORTON, B., GOFF, J., SYNOLAKIS, C. 2005.Observation by the international tsunami survey team in Sri lanka. Science 308, 1595.

MIENERT, J., CURRY, W.B., SARNTHEIN, M., 1988. Sonostratigraphic records from equatorial Atlantic deep-sea carbonates: paleoceanographic and climatic relatinships. Marine Geology 83: 9-20.

MINOURA, K., NAKAYA, S., 1991. Traces of Tsunami preserved in intertidal lacustrine and marsh deposits: some examples from northeast Japan. Journal of Geology, 99, 265 – 287.

MOORE, A., GELFENBAUM, G., TRIYONO, 2005. Sedimentary depositsof the 26th December 2004 tsunamion the northwest coast of Aceh, Indonesia. Earth Planets Space, 58, 253 – 258.

NANAYAMA, F., SHINEGO, K., SATAKE, K., SHIMOKAKA, K., KOITABASHI, S., MIYASAKA, S., ISHII, M., 2000. Sedimentary differences between the 1993 Hokkaido-nansei-oki tsunami and the 1959 Miyakijima typhoon at Taisei, southwestern Hokkaido, northern Japan. Sediment. Geol. 187, 139 – 158.

NARAYANA , A.C., TATAVARTI, R., SHINU, N., SUBEER, A., 2007. Tsunami of December 26, 2004 on the southwest coast of India: Post-tsunami geomorphic and sediment characteristics. Marine Geology 242, 155-168.

NODA A., KATAYAMA, H., SAGAYAMA, T., SUGA K., UCHIDA Y., SATAKE K., ABE K., OKAMURA Y., 2007. Evaluation of tsunami impacts on shallow marine sediments: An example from the tsunami caused by the 2003 Tokachioki earthquake, northern Japan. Sed. Geol. 200, 314-327.

OHTA, T., ARAI,H., 2007. Staatistical empirical index of chemical weathering in igneous rocks: A new tool for evaluating the degree of weathering. Chemical Geology 240: 280-297.

PÄLIKE, H., SHACKLETON, N.J., RÖHL, U., 2001. Astronomical forcing in Late Eocene marine sediments. Earth Planet. Sci. Lett. 193: 589-602.

SCHULTTHEISS, P.J.,WEAVER, P.P.E., 1992. Multi-Sensor Core Logging for Science and Industry. In: IEEE Xplore.

SHACKLETON, N.J., CROWHURST, S., HAGELBERG, T., PISIAS, N.G., SCHNEIDER, D.A., 1995. A New Late Neogene time scale: application to Leg 138 sites. In: N.G. Pisias, L.A. Mayer et al. (Editors), Proc. ODP Sci. Results 138: 73-101.

SHI, S., SMITH, D.E., 2003. Coastal tsunami geomorphological impacts and sedimentation processes: Case studies of modern and prehistorical events. International Conference on Estuaries and Coasts. November 9-11, 2003, Hangzhou, China.

SIRIPONG, A., 2006. Andaman Seacoast of Thailand Field Survey after the December 2004 Indian Ocean Tsunami. Earthquake Spectra 22 (S3), 187-202.

SUGAWARA, D., MINOURA, K., NEMETO, N., TSUKAWAKI, S., GOTO, K., IMAMURA, F., 2009. Foraminiferal evidence of submarine sediment transport and deposition by backwash during the 2004 Indian Ocean tsunami. Island Arc. doi: 10.1111/j.1440-1738.2009.00677.

SUWANWERAKAMTORN, R., PAIJITPRAPAPORN, A., DOWNREASNG, D., SUWANASING, P., 1990. Sediment dispersion from offshore TIN dredging along Andaman sea coast using satellite data. Proc. Asian Association on Remote Sensing.

SYNOLAKIS, C.E., KONG, L., 2006. Runup measurements of the December 2004 Indian Ocean Tsuanmi. Earthquake Spectra 22 (S3), 67-91.

SZCZUCIŃSKI, W. CHAIMANEE, N., NIEDZIELSKI, P., RACHLEWICZ, G., SAISUTTICHAI, D., TEPSUWAN, T., LORENC, S., SIEPAK, J., 2006. Environmental and Geological Impacts of the 26

December 2004 Tsunami in Coastal Zone of Thailand – Overview of Short and Long-Term Effects. Polish. J. of Environ. Stud. 15(5): 793-810.

THAMPANYA, U., VERMAAT, J.E., SINSAKUL, S., PANAPITUKKUL, N., 2006. Coastal erosion and mangrove progradation of Southern Thailand. Estuar., Coast. Shelf Sci. 68:75-85.

THANAWOOD, C., YONGCHALERMCHAI, C., DENSRISEREEKUL, O., 2006. Effects of the December 2004 tsunami and disaster management in southern Thailand. Science of Tsunami Hazards, 24, 206 – 217.
TSUJI, Y., NAMEGAYA, Y., MATSUMOTO, H., IWASAKI, S.I.., KANBUA, W., SRIWICHAI, M., MEESUK, V., 2006. The 2004 Indian tsunami in Thailand. Surveyed runup heights and tide gauge records. Earth Planets Space 58, 223-232.

VAN DEN BERGH G.D., BOER W., DE HAAS H., VAN WEERING TJ.C.E., VAN WIJHE R., 2003. Shallow marine tsunami deposits in Teluk Banten (NW Java, Indonesia), generated by the 1883 Krakatau eruption. Marine Geology 197, 13-34.

VAN DE MEENE, J.W.H., VAN RIJN, L.C. 2000. The shoreface connected ridges along the central dust coast – part 1: field observations. Continental Shelf Research 20:2295-2323.

VARGAS, G., ORTLIEB, L., CHAPRON, E., VALDES, J., MARQUARDT, C. 2005. Paleoseismic inferences from a high-resolution marine sedimentary record in northern Chile (23° S). Tectonophysics, 399, 381 – 398.

WANG, Y., 2002. Coastal laterite profiles at Po Chue Tam, Lantau Island, Hong Kong: the origin and implication. Geomorphology 52 (3-4), 335-346.

WEISS, R. 2007. Sediment grains moved by passing tsunami waves: Tsunami deposits in deep water. Marine Geology 250: 251-257.

WEISS, R., BAHLBURG, H. 2006. The Coast of Kenya Field Survey after the December 2004 Indian Ocean Tsunami. Earthquake Spectra 22 (S3), 235-240.

WELTJI, G.J., TJALLINGII, R., 2008. Calibration of XRF core scanners for quantitative geochemical logging of sediment cores: Theory and application. Earth Planet. Sci. Lett. 274: 423-438.

WIEGEL, R.L., 2006a. Tsunami information sources. Science of Tsunami Hazards, 24 (2), 58 p.

WIEGEL, R.L., 2006b. Tsunami information sources. Science of Tsunami Hazards, 25 (2), 67 p.

Appendix - List of Activities

Diploma-Thesis:

WISANUKORN POONCHAI: Geochemische und sedimentologische Untersuchungen an Sedimentproben aus dem vom Tsunami 2004 betroffenen Schelfbereich der Andaman-See vor der Küste Khao Laks (Thailand). – Diplomarbeit Inst. F. Geowissenschaften, Univ. Kiel gemeinsam mit Department Geowissenschaften, Univ. Hamburg.

Presentations.

K. SCHWARZER: Tracing Tsunami Impacts on- and offshore in the Andaman Sea Region (TRIAS). - The Celebration of the 30th Anniversary of Thai – German (NRCT – DFG) Cooperation 2008. 13 – 14 November 2008, Ciang Mai, Thailand

K. SCHWARZER: Tsunami Deposist in nearshore and coastal waters of Thailand. - Seminar at the Chulalongkorn University, Bangkok. December 16th, 2008.

P. FELDENS: Impact of the December 2004-Tsunami on Shelf Deposits in the Andaman Sea. First Results. – Environmental Impacts of Tsuanmi. September 2008, Slubice, Poland.

P. FELDENS: Tsunami deposits in near-shore and coastal waters of Thailand. – Arbeitskreis Küsten und Meere. 24 – 26. April, 2009, Kiel, Germany.

Publications:

FELDENS, P., SCHWARZER, K., SZCZUCIŃSKI, W., STATTEGGER, K., SAKUNA, D., SOMGPONGCHAIYKUL, P., 2009. Impact of the 2004 Tsunami on Seafloor Morphology and Offshore Sediments, Pakarang Cape, Thailand. Polish J. of Environ. Stud. 18 (1), 63-68.

FELDENS, P., SAKUNA, D., SCHWARZER, K., 2009 Shallow water sediment structures in a tsunami-affected area (Pakarang Cape, Thailand). Coastline Reports (accepted).

DAAD-Grant:

M.Sc. Daroonwan Sakuna is granted by a 3 years PhD - scholarship of the Deutscher Akademischer Austausch Dienst" (DAAD) to work within the TUNWAT-project.

Training activites:

A two week training course, focussing on multibeam data processing and interpretation, side scan sonar data processing and interpretation and geochemical analysis of sediment core material has been given in cooperation with the MASS project from February, 4th to February, 17th, 2008.
Participants: Daroonwan Sakuna, Suratta Bunsomboonsakul, Danai Tipmanee.

Draft of a Research Article

Assessment of Using Polycyclic Aromatic Hydrocarbons (PAHs) to Characterize Terrestrial Deposit in Tsunami-Affected Coastal Areas of Andaman Sea, Thailand

SIWATT PONGPIACHAN,[*,†,‡] PENJAI SOMPONGCHAIYAKUL, [†,‡] PETER FELDENS, [§] DAROONWAN SAKUNA, [§,□] WITOLD SZCZUCIŃSKI, [□] AND KLAUS SCHWARZER, [§]

Biogeochemical and Environmental Change Research Unit, Faculty of Environmental Management, Prince of Songkla University, Hat-Yai, Songkla, 90112, Thailand, National Center of Excellence for Environmental and Hazardous Waste Management-PSU Satellite Center, Prince of Songkla University, Hat-Yai, Songkla, 90112, Thailand, Institute of Geosciences Sedimentology, Coastal and Continental Shelf Research Otto-Hahn-Platz 1, D-24118 Kiel, Germany, Phuket Marine Biological Center, P.O. Box 60, Phuket 83000, Thailand, Institute of Geology Adam Mickiewicz University, Maków Polnych 16, 61-606 Poznań, Poland

Introduction

The 2004 Indian Ocean earthquake is widely acknowledged by the scientific community as one of the world's greatest natural disasters in modern times. Despite of a fairly large number of papers dealing with several impacts of the extreme event onshore, little is known about the geomorphological, sedimentological and geological alterations offshore. Since the offshore physical data is substantially crucial for the study of both the modern and past extreme event, it is therefore important to distinguish the difference between terrestrial deposit and background submarine sediment. In principle, there are several physical evidences to prove the existence of extreme event originated terrestrial deposits. It is well known that the enrichment of terrestrial plant debris in sediment can be considered as signatures of planetary records followed by the discovery of large boulders in the sedimentary dispositional environment (1-2). However, there are also several problems associated with the employment of these conventional proxies due to its low preservation potential in the submarine environment. Firstly as the plant fragments settle through the water column, several biogeochemical transformations such as remineralization, chemical decomposition and microbial degradation take place (3-4). Secondly, the power of wind-generated waves, hurricane/monsoon waves, daily tides, and even anthropogenic activities such as the clean-up of the contaminated sediments coupled with natural bioturbation can dramatically alter both the topographical and sedimentological features of tsunami deposit (5). Thirdly, there is no a single feature to categorize tsunami, hurricane, monsoon and other type of extreme event deposits except through the careful comprehensive investigation of variability in clast grain-size, shape, roundness, packing, sorting with the precise assessment of the lateral geometry of the entire sedimentary body (6). In the light of these difficulties, more alternative well-preserved terrestrial indicators are essentially required to enhance the reliability of data interpretation.

Polycyclic aromatic hydrocarbons (PAHs) have several advantages which may possibly be a promising alternative to the classical terrestrial proxies because i) they are composed of strong benzene ring and thus most likely to possess a higher degree of biogeochemical degradation persistence in comparison with other terrigenous proxies such as lignin (7-9), ii) they are widely distributed in terrestrial soils and marine sediments (10), and iii) they can be used as biomarkers for identifying sources (11). Traffic emissions, industrial activities, accidental oil spill and biomass burnings are generally considered as primary major sources of PAHs. Once released from primary sources into the atmosphere, they will persistently exist in the environment. As a consequence, PAHs is considered likely to remain a potential imprint in the depositional sedimentary environments. In this study, the authors hypothesize that the three dimensional binary ratio plots of PAHs coupled with various analogies of statistical

analysis assist in a better understanding of offshore terrestrial deposit distribution pattern, which can be subject to erosion by tsunami/monsoon waves and surface runoff by heavy rain in the tsunami-affected coastal areas of Andaman Sea, Thailand. Note that it is the purpose of this paper to illustrate the general principle of using PAHs as an innovative proxy to separate the terrestrial deposit from the background sediment for the first time in tsunami-affected coastal areas. Neither the source apportionment nor the analysis of spatial variation of PAHs is the main focus of this study. In addition, the risks and possibilities of applying PAHs as an alternative extreme event biomarker will be critically reviewed and discussed.

Methodology

All solvents are HPLC grade, purchased from Fisher Scientific. A cocktail of 15 PAHs Norwegian Standard (NS 9815: S-4008-100-T). After the freeze drying process is completed, the samples were carefully weighed and placed in pre-cleaned Thimber. The extraction of PAHs was conducted using 250 ml of Soxhlet extractors and spiked with a known amount of internal standard (d10-Fl: Phe, An, Fluo, Pyr, 11H-B[a]F, 11H-B[b]F, B[a]A, Chry; d12-Per: B[b]F, B[k]F, B[a]P, B[e]P, Ind, D[a,h]A, B[g,h,i]P) and extracted with DCM containing 1 g of copper powder for 8 h. The fractionation/cleanup process followed the conventional method using the difference in solvent polarity (12). After the extraction, the DCM solvent was concentrated to incipient dryness by a combination of rotary evaporation and blowing under a gentle nitrogen stream. The concentrated extract is then diluted in 10 ml of n-hexane before application to the top of a disposable silica gel column. The extract was then fractionated into individual compound classes by flash chromatography on silica gel as follows: The concentrate was applied to the top of a 30 × 0.7 cm diameter column, containing 1.5 g of silica gel (activated at 150 ºC for 3 h).

A mass spectrometer is an instrument that separates ions according to the mass-to-charge ratio (m/z) and measures their relative abundance. The instrument is calibrated against ions of known m/z. All mass spectrometers operate by separating gas phase ions in a low pressure environment by the interaction of magnetic or electrical fields on the charged particles. In this study, the analyses were performed using a Varian GC/MS-MS system comprising a CP-3900 gas chromatograph (Walnut Creek, CA, USA) with a 1077 universal injector and a three dimensional quadrupole ion-trap selected ion storage mass spectrometer (Varian Saturn 2200). The target compounds were separated on a 60 m length × 0.25 mm i.d. capillary column coated with a 0.25 μm film thickness (phase composition: cross-linked/surface bonded 5% phenyl, 95% methylpolysiloxane. Specified in EPA methods 207, 508, 515, 515.2, 524.2, 525, 548.1, 680, 1625, 1653, 8081, 8141, 8270 and 8280) stationary phase (Agilent JW Scientific DB-5 GC columns).

Results and Discussions

Concentrations of PAHs in marine sediment samples

In this study, we investigate the validity of PAHs for the first time as a proxy to investigate the impact of tsunami on the distribution of terrestrial sediments in the recent deposits of Andaman sea by collecting 71 sediment samples at the western coastal areas of Tublamu Navy Port, Phang-Nga Province, Thailand in December 2007. The averages and standard deviations of fifteen PAH congeners were presented as follows; Phenanthrene (16.33 ± 7.71 ng g^{-1}), Anthracene (2.09 ± 1.80 ng g^{-1}), Fluoranthene (6.90 ± 7.39 ng g^{-1}), Pyrene (11.61 ± 7.31 ng g^{-1}), 11H-Benzo[a]fluoranthene (1.67 ± 3.36 ng g^{-1}), 11H-Benzo[b]fluoranthene (1.09 ± 2.65 ng g^{-1}), Benzo[a]anthracene (0.92 ± 2.07 ng g^{-1}), Chrysene (1.02 ± 2.67 ng g^{-1}), Benzo[b]fluoranthene (2.10 ± 3.28 ng g^{-1}), Benzo[k]fluoranthene (3.17 ± 4.12 ng g^{-1}), Benzo[e]pyrene (3.27 ± 5.11 ng g^{-1}), Benzo[a]pyrene (2.99 ± 3.47 ng g^{-1}),

Indeno[g,h,i]perylene (3.61 ± 5.77 ng g^{-1}), Dibenzo[a,h]anthracene (10.14 ± 17.94 ng g^{-1}) and Benzo[g,h,i]perylene (6.85 ± 8.65 ng g^{-1}).

Comparison of the total PAHs in marine sediments around the world

In general, the ∑PAHs as defined by the sum of Phe, An, Fluo, Pyr, B[a]A, Chry, B[b]F, B[k]F, B[e]P, B[a]P, Ind, D[a,h]A, B[g,h,i]P found in this study were significantly lower than other sediment samples collected from riverine and coastal environments around the world. In addition, the average concentration of ∑PAHs (71 ± 77 ng g^{-1}: dry weight) was lower than the concentrations proposed by sediment quality guideline and the probable effects level for biological adverse effects by factors of 6 and 86 respectively.

Three dimensional plots of PAHs binary ratios

The concentrations of selected marker compounds and PAH ratios have been developed and used for the source identification of PAHs. The characteristics of PAH patterns in the coastal sediments are subject to different emission patterns from various sources, and thus a single ratio may not be enough to identify sources. Instead of using a single ratio, the combinations of two or more indicators provide more information for source identifications. However, these ratios should be used with caution because the PAHs profiles of different sources are often difficult to discriminate, and can be altered due to their reactivity with other atmospheric species, such as OH radical, NO_x, O_3, and subjected to photo-degradation by UV light during their transportation and destroyed by microbiological degradation after their deposits in marine sediments. In this study, two combinations of binary PAH ratios (X: Fluo/(Fluo+Pyr), Y: Ph/(Ph+An), Z:B[a]A/Chry) and (X: Ind/(Ind+B[g,h,i]P), Y:B[a]P/Phe, Z: Fluo/An) were plotted to identify the tsunami deposits in comparison with other riverine and coastal sediments around the world (Figure 1).

Hierarchical Cluster Analysis (HCA)

HCA can be a suitable statistical tool for differentiating between PAHs of anthropogenic and biogenic origin. To obtain more information on the origins of PAHs in coastal sediments, HCA had been conducted on the 13 variables (i.e. 13 PAHs). The cluster analysis revealed the presence of two different groups as displayed in the dendogram below. The first cluster (n = 8) consists of B[a]A, Chry, An, B[k]F, B[a]P, B[b]F, B[e]P and Ind. The PAHs present in this cluster are generally of biomass burning such as forest fire. However, it is important to stress that B[a]A, Chry and An are of both anthropogenic and biogenic origin. The second cluster can be divided into three subgroups; the first consists of Fluo, B[g,h,i]P, and the second is composed of Phe, Pyr, and the third contains D[a.h]A. According to literature findings, the PAHs present in the first, second, third subgroup can be considered to be of mainly "petroleum combustion origin", "diesel emission origin" and "wood combustion origin" respectively. PAHs concentrations found at the sampling sites, as mentioned previously, can be attributed to the fact that these collecting positions are closely related to both anthropogenic and natural emissions (Figure 2).

Principal Component Analysis (PCA)

Five components were identified from the principal component matrix each representing 41.80 %, 24.90 %, 15.17 %, 8.69 % and 3.80 % of the variance, thus accounting for 94.36 % of the total variance (Table 1). PC1 shows high loading on high molecular weight PAHs (i.e. B[b]F, B[k]F, B[e]P, B[a]P and Ind). These compounds are typical biomarkers of biomass burning. Thus, it is reasonable to assume that the forest fire govern the spatial distribution of PAHs in this coastal region and explained for 41.80 % source contribution. The relatively high loadings of D[a,h]A and B[g,h,i]P can be attributed to wood combustion in PC2. On the other hand, PC3 has high loading of Phe and An, followed by the relatively high abundances

of Fluo, B[a]A, Chry found in PC4 indicating the signature of “diesel emissions” and “oil combustions” plausibly delivered to the sampling sites via long range transportation and/or the “wash back” of terrestrial components triggered by tsunami.Three dimensional plots of PC1, PC2, PC3 successfully discriminated the potential tsunami deposit group from the typical marine sediment group as displayed in Figure 3. In this study, the typical marine sediment group (i.e. 5D, 7, 8D, 9D, 10D, 11D, 14D, 17D, 26D, 39D, 45D, 49D, 53D, 56, 2D, 65D, 74D, 75D) were observed as a “horizontal laid down position”, whereas the potential tsunami deposit group (i.e. 31A, 32, 32D, 34D, 35D, 36D, 41D, 42C, 44D, 69D, 70D, 71D, 72-2D, 72bD, 73D) were found as a “horizontal laid up position”. Other sediment samples laid down between these two layers were considered as mixture the typical marine sediments and tsunami deposits.

Conclusions

Three dimensional plots of binary ratios of PAHs coupled with the combination of PC1, PC2 and PC3 show promising results of using PAHs as a proxy to identify the tsunami deposit. HCA and PCA indicated the “forest fires” as a major source of PAHs in marine sediments. However, more data are required to validate this innovative approach.

Acknowledgement

This project was granted by DFG & NRCT. The authors would like to express special gratitude to Dr. Somkiat Khokiattiwong, Ms. Suratta Bunsomboonsakul & Dr. Anond Snidvongs for their contributions on collections of coastal sediments together with Chakrathong crews.

References

(1) Fujino, S.; Masuda, F.; Tagomori, S.; Matsumoto, D. Sed. Geol. 2006, 187 (3-4), pp. 127-138..
(2) Mastronuzzi, G.; Pignatelli, C.; Sansò, P.; Selleri, G. Mar. Geol. 2007, 242 (1-3), pp. 191-205.
(3) Lund-Hansen, L.C.; Pejrup, M.; Floderus, S. J. Sea Res. 2004, 52, pp. 87-98.
(4) Sanchez-Vidal, A.; Calafat, A.; Canals, M.; Frigola, J.; Fabres, J. Cont. Shelf Res. 2005, 25, pp. 609-628.
(5) Einsele, G.; Chough, S.K.; Shiki, T. Sed. Geol. 1996, 104, pp. 1-9.
(6) Dawson, A.G.; Shi, S. Pur Appl. Geophys. 2000, 157, pp. 875-897.
(7) Miltner, A.; Emeis, K.C.; Struck, U.; Leipe, T.; Voss, M. Chem. Geol. 2005, 216 (3-4), pp. 313-328.
(8) Tareq, S. M.; Tanaka, N.; Ohta, K. Sci. Total Environ. 2004, 324 (1-3), pp. 91-103.
(9) Ferella, N.; Lucotte, M.; Louchouarn, P.; Roulet, M. Org. Geochem. 2001, 32 (12), pp. 1143-1458.
(10) Curtosi, A.; Pelletier, E.; Vodopivez, C.L.; Mac Cormack, W. P. Sci. Total Environ. 2007, 383 (1-3), pp. 193-204.
(11) Zakaria, M. P.; Okuda, T.; Takada, H. Mar. Pollut. Bull. 2001, 42 (12), pp. 1357-1366.
(12) Gogou, A. I. ; Apostolaki, M.; Stephanou, G.E. *J Chromatogr A*. 1997. 799, pp.215-231.

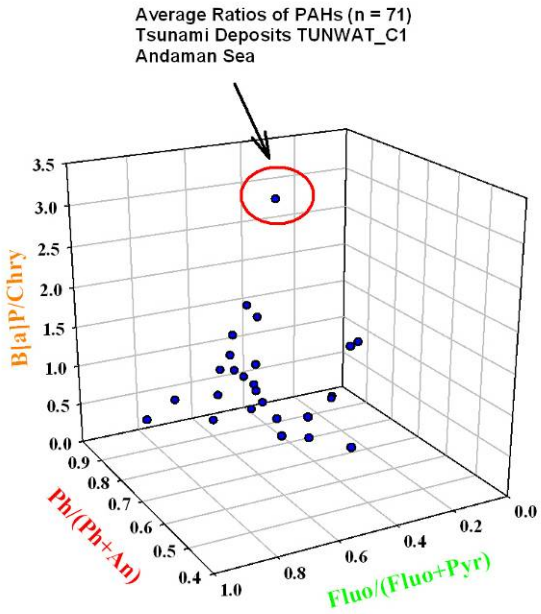


Fig 1. Three dimensional plots of PAH binary ratios

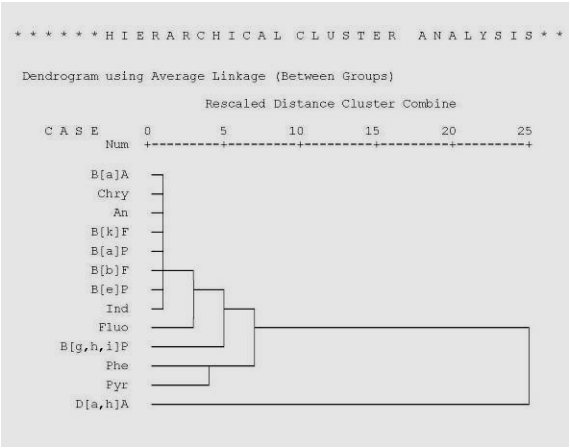
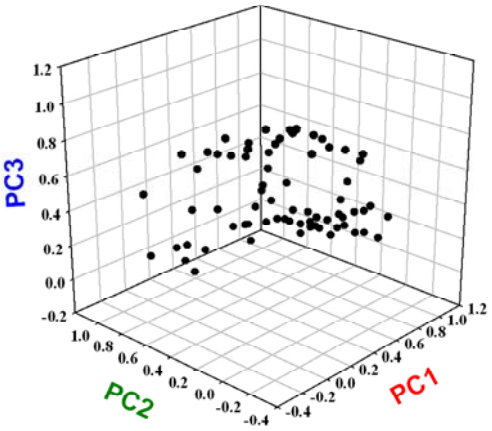


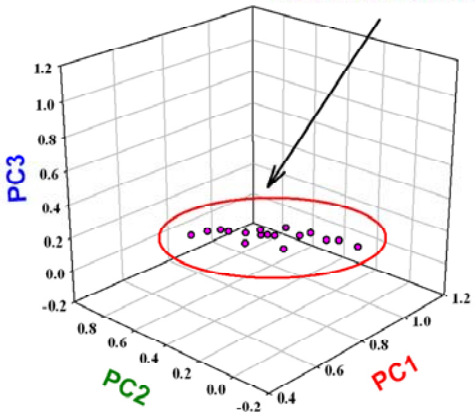
Fig 2. Hierarchical Cluster Analysis (HCA) of PAHs

Table 1. Source apportionment of PAHs in sediment samples

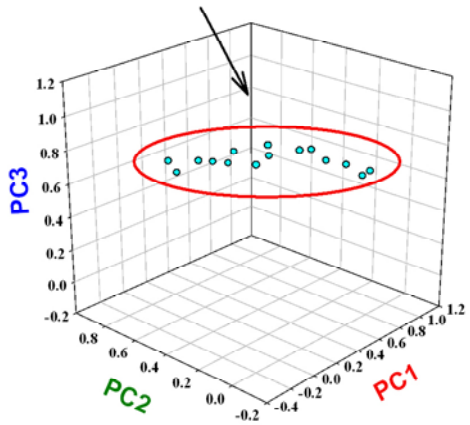
PAH Congeners	Principal Component (PC)				
	PC 1	**PC 2**	**PC 3**	**PC 4**	**PC 5**
Phe	0.031	0.080	**0.943**	0.234	-0.058
An	0.174	0.040	**0.927**	0.262	-0.111
Fluo	0.070	0.385	-0.191	**0.592**	**0.592**
Pyr	-0.029	0.011	-0.076	0.171	**0.973**
B[a]A	-0.091	-0.150	0.390	**0.867**	0.151
Chry	-0.065	-0.148	0.360	**0.893**	0.143
B[b]F	**0.880**	0.233	0.360	0.045	-0.054
B[k]F	**0.846**	0.210	-0.018	-0.252	0.088
B[e]P	**0.973**	0.011	-0.042	0.037	-0.059
B[a]P	**0.833**	0.486	0.111	0.004	0.031
Ind	**0.842**	0.483	0.018	-0.009	-0.015
D[a,h]A	0.299	**0.913**	0.038	-0.092	0.098
B[g,h,i]P	0.384	**0.889**	0.086	-0.105	0.015
Intitial Eigenvalues Total of Variance (%)	41.80 %	24.90 %	15.17 %	8.69 %	3.80 %
Probable Source Type	Biomass Burning	Wood Combustion	Diesel Emission	Oil Combustion	Fugitive Emission



5D, 7, 8D, 9D, 10D, 11D, 14D, 17D, 26D
39D, 45D, 49D, 53D, 56, 2D, 65D, 74D, 75D
Typical Marine Sediment Group



31A, 32, 32D, 34D, 35D, 36D, 41D, 42C, 44D
69D, 70D, 71D, 72-2D, 72bD, 73D
TSUNAMI DEPOSIT GROUP



2, 3D, 4D, 6D, 12AD, 12bD, 15C, 16, 18, 19D, 20D, 21D
22D, 23D, 24D, 25D, 27, 29D, 30D, 37D, 40D, 43D, 46D, 47B
48D, 50D, 51D, 52D, 55D, 56D, 57D, 61D, 62D, 63D, 64D, 66D
70_2D, 76D, 77D
Mixture Between Typical Marine Sediemnts and Tsunami Deposits

